Multi-scale study of rejuvenation mechanism and evaluation method for aged bitumen recycling

Ren, S.

Important note
To cite this publication, please use the final published version (if applicable).
Please check the document version above.

Multi-scale study of rejuvenation mechanism and evaluation method for aged bitumen recycling

Shisong REN

Multi-scale study of rejuvenation mechanism and evaluation method for aged bitumen recycling

Dissertation

for the purpose of obtaining the degree of doctor

at Delft University of Technology

by the authority of the Rector Magnificus, prof.dr.ir. T.H.J.J. van der Hagen,

chair of the Board for Doctorates

to be defended publicly on

Wednesday 10 April 2024 at 12:30 o'clock

by

Shisong REN

Master of Engineering in Chemical Engineering and Technology

China University of Petroleum (East China), China

born in Nantong, China

This dissertation has been approved by the

Promotor: Prof.dr.ir. S.M.J.G. Erkens

Copromotor: Dr. X. Liu

Composition of doctoral committee:

Rector Magnificus	Delft University of Technology, chairperson
Prof.dr.ir. S.M.J.G. Erkens	Delft University of Technology, promotor
Dr. X. Liu	Delft University of Technology, copromotor

Independent members:

Prof.dr.ir. E. Schlangen	Delft University of Technology
Prof.dr. B. Huang	University of Tennessee, United States
Prof.dr. A. Bhasin	The University of Texas at Austin, United States
Prof.dr. G. Airey	University of Nottingham, United Kingdom

Reserve member:

Prof.dr. H.M. Jonkers	Delft University of Technology

Dedicated to my family

Acknowledgements

As I stand at the culmination of my doctoral journey, I reflect on the passage of time, recognizing its fleeting yet enduring nature. Earning this PhD title posed considerable challenges, particularly considering the nearly two-year period dominated by the Covid-19 virus. Numerous individuals played diverse roles in contributing to this work. I seize this opportunity to publicly extend my sincere gratitude to all those who have been a part of this journey.

First and foremost, I extend my gratitude to my mentor, Prof. Sandra Erkens, for her ongoing guidance and nurturing support. In the role of a "driving instructor," she not only monitors the direction and advancement of my research but also allows ample space for scientific exploration and personal growth. Her insightful and invaluable suggestions and comments on both the research and doctoral thesis encompass a blend of scientific and practical perspectives. Crucially, I have gained significant knowledge in enhancing the rigor and logic of my research under her mentorship. It is truly my honor to have completed my doctoral research under her guidance.

I am indebted to Dr. Xueyan Liu, my co-promoter and daily supervisor. I vividly recall receiving his call five years ago while having lunch in my dormitory, offering support for my doctoral studies at TU Delft. Throughout my doctoral journey, Dr. Liu consistently aided me in resolving diverse challenges related to research topic determination, experimental characterizations, simulations, publications, and thesis writing. I appreciate his substantial assistance and unwavering support.

I also would like to express my gratitude to my committee members Prof. Erik Schlangen, Prof. Amit Bhasin, Prof. Baoshan Huang, Prof. Gordon Airey, and Prof. Henk Jonkers for their time, comments, and efforts. Meanwhile, many thanks to the Chairman Prof. Arjan Mol for hosting my defence.

I want to thank my previous supervisors in china Prof. Weiyu Fan and Prof. Yuzhen Zhang for their always support to my academia and life. Meanwhile, I want to give special thanks to Prof. Ming Liang, who took me into the asphalt research realm.

I extend my heartfelt appreciation to my colleagues in the pavement engineering section for their unwavering encouragement and support. Special thanks are due to Dr. Peng Lin for his steadfast backing throughout my research journey, particularly during the initial year when we engaged in numerous discussions on my research topic. Dr. Ruxin Jing deserves my gratitude for consistently assisting me in both research and life challenges. I express my thanks to Cor Kasbergen for translating the summary into Dutch. Dr. Katerina Varveri merits acknowledgment for her continuous academic support and valuable contributions to our collaborative work. I am grateful to Dr. Kumar Anupam for his invaluable advice on my research. Additionally, I would like to

I would also like to express my appreciation to my colleagues who have been instrumental in providing significant assistance in both my life and research: Yangming Gao, Lili Ma, Yi Zhang, Lu Zhou, Haopeng Wang, Dongyu Niu, Panos Apostolidis, Chen Wang, Hong Zhang, Shi Xu, Sheng Wang, Rui Wu, Zhaojie Sun, Daniel Akinmade, Yi Li, Mahmoud Khadijeh, Sadaf Khalighi, Ajay Jagadeesh, Avishreshth Singh, Eli A. Martinez-Streignard, Saranga Premarathna, and Mohammadjavad Berangi.

Over these 4.5 years, numerous events have unfolded, but my friends have consistently stood by me. I would like to express my gratitude to my friends: Weikang Feng, Pei He, Jiafang Chen, Yunlong Guo, Dan Ren, Haopeng Zhang, Zhanchong Shi, Chen Liu, George Pipintakos, Bowen Li, Junyan Zhang, Jin Huang, Xiuli Wang. In this foreign land, we have experienced numerous moments of food, joy, and concern, supporting each other in our studies, research, and daily lives. Special thanks go to my friend, Yabin Wang, for designing the cover.

Last but not least, I want to express my gratitude to my parents, who always give me selfless love and endless support. I am sorry that I haven't been able to go back to accompany you all more often in the past few years.

Shisong Ren

At Delft

2024.02

Contents

1

Introduction

This chapter aims to present the reader with the state of the art on the knowledge and application of reclaimed asphalt (RA) and the role of rejuvenation techniques. Several research questions and objectives are derived from the research background. In addition, the research guidelines, evaluation methodologies, and outline of this thesis are mentioned herein.

1.1 Recycling potential of reclaimed asphalt (RA)

Asphalt concrete, in flexible pavements, is one of the most widely used materials in the construction industry. Annual worldwide production of asphalt mixtures for paving operations has been estimated to be more than one billion tons [1, 2]. Asphalt pavement stands as a cornerstone of road infrastructure worldwide, playing a pivotal role in transportation systems [3-5]. Its widespread use extends to Europe, where it serves as the primary surfacing material for roads, highways, and urban thoroughfares [6, 7]. The durability and versatility of asphalt contribute to its prominence in various regions, addressing the demands of diverse climates and traffic conditions [8, 9].

As shown in **Figure 1.1**, despite its ubiquity, asphalt pavement is subject to degradation due to a multitude of loading and environmental factors. The combination of heavy traffic loads, fluctuating temperatures, freeze-thaw cycles, and exposure to environmental elements contributes to distress mechanisms, such as cracking and fatigue [10, 11]. Understanding and mitigating the impact of these factors are essential for maintaining the longevity and performance of asphalt pavements [12, 13]. Nevertheless, asphalt pavement inevitably experiences performance deterioration, necessitating maintenance and reconstruction, which leads to the generation of a significant amount of reclaimed asphalt (RA) materials [14, 15].
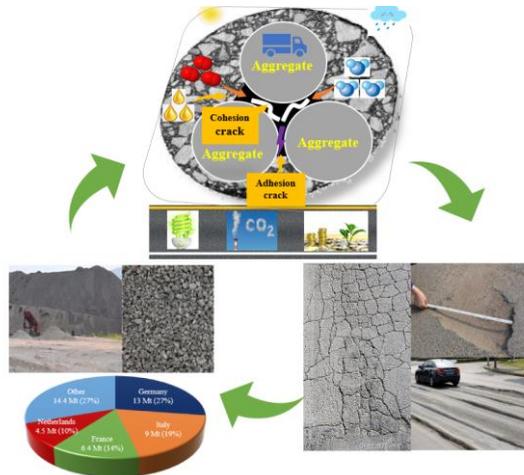
Figure 1.1 Recycling idea of reclaimed asphalt

The concept of recycling reclaimed asphalt (RA) materials has gained prominence due to its potential economic and environmental benefits [16-18]. Recycling allows for the reuse of existing materials, reducing the demand for virgin resources and minimizing the environmental footprint associated with asphalt production [19]. This sustainability-driven approach aligns with the broader goals of green infrastructure and circular [20]. In Europe, particularly in the Netherlands, there has been a notable emphasis on the recycling of RA materials in asphalt pavements [21]. Nowadays, many highway and transportation agencies adopt the use of RA in both plant recycling (up to 50%) and in-place recycling (up to 100%) due to the significant benefits in economic saving, environmental protection, and sustainable development [22, 23]. In the Netherlands, 71% of the RA is used in Hot Mixing Asphalt (HMA) and Warm Mixing Asphalt (WMA) [24].

However, the current state of RA recycling reveals practical challenges. Issues such as the variability in RA properties, concerns about material quality, and the need for consistent recycling practices pose hurdles to widespread and effective implementation [25, 26]. Based on the report from the European Asphalt Pavement Association (EAPA), covering 16 countries, it is observed that despite the generation of 47.6 million

tons of site-down asphalt materials in 2021, only 17.2 million tons of recycled asphalt (RA) pavement was accessible for utilization by the asphalt industry [27].

Numerous research endeavours have been undertaken to investigate the influence of RA on asphalt mixture performance [28-30]. These studies delve into the mechanical [31], rheological [32], and durability [33] aspects of asphalt mixtures containing varying percentages of RA. The findings contribute valuable insights into the potential advantages and challenges associated with integrating recycled materials into asphalt pavements. It was reported that using RA materials in asphalt mixtures could create durability concerns (e.g., moisture susceptibility increasing and deteriorating cracking and fatigue resistance) due to aged and stiff bitumen binders in RA materials [34, 35]. The asphalt mixtures with high RA content show satisfactory high-temperature deformation resistance, but their low-temperature flexibility and adhesion performance are much worse than conventional ones, leading to a limited RA percentage in new asphalt pavement in practice [36, 37].

Despite the positive strides in RA recycling, challenges emerge when considering high dosage RA in asphalt pavements. The increased use of recycled materials poses concerns regarding the potential impact on mixture performance, including issues related to stiffness [38], fatigue resistance [39], and long-term durability [40]. Achieving optimal performance with higher RA dosages requires careful consideration of mixture design and binder modification [41]. One critical aspect influencing the performance of RA mixtures is the aging of bitumen [16, 42]. The aged binder in reclaimed asphalt materials can contribute to suboptimal performance, including increased susceptibility to cracking and reduced mechanical properties [7, 9, 13, 43].

To address this, the use of rejuvenators becomes imperative [44]. Rejuvenators play a vital role in restoring the aged bitumen, enhancing its properties, and ensuring compatibility with RA, thereby contributing to the sustainable and efficient reuse of materials in asphalt pavements [45-47]. An assessment was conducted to examine the impact of three distinct rejuvenators on the characteristics of both binder and mixtures incorporating a significant proportion of reclaimed asphalt (RA) materials. The findings revealed that the use of rejuvenators led to an augmentation in the non-recoverable creep compliance of the bitumen. Moreover, when comparing the linear amplitude sweep (LAS) results, the rejuvenated binder exhibited improved fatigue properties in contrast to the virgin binder [48-50]. Notably, the application of a rejuvenator alleviated the cracking tendencies of asphalt mixture, although it was observed that the rutting and moisture susceptibility of the mixtures were adversely affected [51]. Nonetheless, it is noted that there are currently no widely accepted evaluation and classification standards for a diverse range of rejuvenators concerning their effectiveness in rejuvenating asphalt mixtures [26, 52].

1.2 Aging and rejuvenation of bitumen binder

The aging of bitumen consists of short-term aging during the mixing and construction and long-term aging during its service life. The key aspects of bitumen aging are considered to be the effect of oxidation and loss of volatiles, resulting in increased bitumen viscosity, making it stiffer and more brittle than a fresh binder [53]. Regarding the aging mechanism of bitumen, many studies focused on the aging effect on the change of chemical components and functional groups of bitumen [54-56]. During long-term aging, introducing polar oxygen-containing chemical functionalities increases molecular interactions and the content of high molecular weight components (asphaltenes) [57]. Consequently, gel-like structures may be formed, and two functional groups (carbonyl and sulfonyl groups) are prevalently formed. These changes lead to the hardening and performance loss of bitumen binder [58].

Several researchers found that during aging, a change in the different bitumen fractions could be observed [59-61]. The aging process initially causes a reduction in aromatic content, followed by an increase in resin content, accompanied by a higher dosage of asphaltene [62]. Consequently, there is a widely accepted notion that aromatics give rise to resin, which subsequently transforms into asphaltene [63-65]. Meanwhile, the alteration in saturate content is almost negligible, as evidenced by their low chemical reactivity [66].

These transformations collectively lead to a glass transition temperature that is slightly higher but remains nearly unchanged [67]. The impact of aged bitumen on mixture performance is a pivotal consideration in the sustainable evolution of asphalt construction, particularly as the industry strives to increase the levels of RA incorporation [68]. As bitumen undergoes aging, alterations in its chemical and rheological properties can affect the overall performance of asphalt mixtures [56, 69]. To navigate this challenge and advance sustainability goals, the industry is increasingly turning to higher levels of RA, presenting a dual challenge: achieving elevated RA content while preserving mixture performance [38, 70]. In this context, the use of rejuvenators becomes crucial [16, 32]. Rejuvenators play a vital role in restoring the aged bitumen, enhancing its workability, and ensuring compatibility with RA, thereby mitigating the potential loss of performance associated with aged binders [47, 71]. This holistic approach, combining increased RA levels with the judicious application of rejuvenators, represents a key strategy in overcoming the challenges posed by aged bitumen, paving the way for more sustainable and resilient asphalt mixtures.

Upon the addition of rejuvenators to the aged bitumen, the thermo-mechanical and rheological properties of the binder can be restored, leading to an improved service life of asphalt pavements [53, 72]. Many rejuvenators have been successfully added to the asphalt mixtures containing RA materials to reduce the stiffness of bitumen and provide the desired performance [29, 73]. In regular hot recycling of limited RA levels, a softer bitumen is added to the mixture and the combined aged and new binder realises the intended bitumen class [46, 74]. Rejuvenators usually are additives with a high proportion of light components that are added to the aged binder to improve its rheological and engineering properties by softening it [56-59]. The deterioration of asphalt pavement performance is influenced by the aging of bitumen [64, 65, 68]. When recycled, the diminished properties of aged material impact the quality of the new mixture [36]. The incorporation of rejuvenators is anticipated to rectify and enhance the chemical, rheological, and mechanical attributes of aged binders, ensuring that the use of recycled asphalt (RA) does not negatively impact the new mixture [8-11]. Achieving this objective necessitates the thorough assessment and effective restoration of the properties of aged bitumen [22, 30].

To this end, there is a growing interest in the study of bitumen-rejuvenator interactions to develop and identify highly efficient rejuvenators [51, 54, 57]. Previous research has considered various influencing factors, including the degree of bitumen aging, rejuvenator type, rejuvenator content, bitumen source, and more [56-59]. Another crucial aspect of rejuvenation technology is ensuring compatibility between the rejuvenator and aged bitumen [19, 31, 32]. This is essential to prevent the uneven distribution of the rejuvenator in the bitumen layer, which could lead to rapid rutting and cracking damage in recycled asphalt pavement [31, 38]. The ideal scenario involves the rapid and uniform diffusion of the rejuvenator into the aged bitumen layer surrounding RA particles, resulting in a new and homogeneous rejuvenated bitumen [31, 70]. The current challenge involves exploring kinetically-controlled diffusivity and thermodynamically-controlled compatibility as key research points [38, 47]. Most existing studies measured the blending levels between rejuvenators and aged bitumen through comparing the rheological and morphological features of different rejuvenated layers after blending [19, 32]. However, the experimental tests are time-consuming and the corresponding results strongly depend on the material characteristics and blending conditions [31, 75]. Establishing a methodology for predicting and verifying the diffusion and compatibility of a rejuvenator-aged bitumen system is essential. This involves inputting material components and blending conditions (such as mixing temperature and time).

Rejuvenators play a critical role in the revitalization of asphalt, and they can be sourced from various outlets [72, 74]. The careful selection of the appropriate rejuvenator type and dosage is essential for optimal results. Rejuvenators come in diverse forms, encompassing plant oils, waste-derived oils, engineered products, and both traditional and non-traditional refinery base oils [4, 75]. Effective rejuvenators should interact well with aged binders, yielding rejuvenated bitumen of high quality [76, 77]. However, there is limited information available on the specific functions of rejuvenators that enhance the properties of aged binders [52, 78]. Various rejuvenator types exert distinct effects on the restoration of aged bitumen performance [40, 47, 49]. Studies suggest that the use of vegetable oil-based rejuvenators is advantageous

when the asphaltene content is adequate, especially for in-place or in-plant cold mixture recycling [79]. Additionally, waste vegetable (WV) oil has been found to effectively rejuvenate aged binders, albeit with a potential increase in moisture susceptibility [12-14, 80]. It is advisable to incorporate an adhesion-promoting additive when using WV oil to mitigate this issue [81]. Furthermore, excessive rejuvenator dosage can lead to problems such as poor adhesion and the detachment of the bitumen film from the aggregate [72, 75]. Overall, the multitude of rejuvenator types/components and the varying states of aged bitumen make it challenging to establish critical evaluation indicators for rejuvenation efficiency.

Although it is recognized that understanding the rejuvenation mechanism of different rejuvenators in aged bitumen is of great importance [30], it is currently studied from the micro and macro-scale perspectives [34, 48], which lacks consideration of molecular interactions. The molecular dynamics (MD) simulation technique is a numerical method based on computer analysis, simulating the static characteristics (physical interaction) and movements of molecules by setting up a reasonable molecular model to define the chemical and physical properties of the microsystem [53]. It can output the molecular-scale thermodynamic properties, including static (e.g. density, glass transition temperature, energy, cohesive energy density, etc.) and dynamic indices (self-diffusion coefficient) [82, 83]. Meanwhile, the interfacial diffusion process between different layers, such as bitumen, rejuvenator, and moisture molecules can be observed [84-86]. Thus, the MD simulation method is useful for exploring the rejuvenation mechanism from the molecular scale to the microstructure scale and establishing the rejuvenation evaluation method [87], provided that representative models of both the rejuvenators studied and the aged bitumen are used. Nevertheless, advancements in MD simulation methodology are necessary for the comprehensive investigation of aging and rejuvenation in bitumen. **Chapter 2** provides an overview of the existing state of MD simulation applications in the realm of bituminous materials [88, 89]. Until now, molecular dynamics simulation has offered a means of molecular-scale assessment for the interaction between rejuvenators and aged bitumen. However, the lack of accurate or known molecular structures for various aged binders and rejuvenators, which are crucial input parameters, hampers the MD applications on rejuvenated bitumen research.

1.3 Research questions and objectives

Given the current state of research, comparing the outcomes of experiments and numerical analyses on rejuvenated binders from various studies proves challenging. This difficulty arises from the considerable diversity in material compositions, encompassing both aged bitumen and rejuvenating agents, as well as the range of indicators employed. Consequently, this diversity impedes the selection of suitable combinations of rejuvenating agents and the attainment of a comprehensive understanding of the rejuvenation process. Here are the main sub-questions involved in this thesis:

- How can we establish molecular models for both aged bitumen and rejuvenators using existing knowledge and contemporary material characterization tools?

- Is it possible to study and predict the diffusion and compatibility behaviors of different kinds of rejuvenators in aged bitumen using molecular dynamics simulations?

- What are the critical indicators for evaluating and distinguishing the rejuvenation effects of rejuvenators on performance recovery of aged bitumen?

- Can the combination of MD simulations and experimental testing be used to develop theories about the rejuvenation process and build an evaluation method for rejuvenator effectiveness?

For the aforementioned reasons, the main goal of this thesis is to explore the rejuvenation mechanism of aged bitumen and develop an evaluation method based on the chemo-thermo-rheological methodologies of rejuvenation efficiency assessment. To achieve the goal, the following research objectives will be accomplished:

- Establish and authenticate molecular models for both aged bitumen and rejuvenators by examining a range of chemical attributes, aiming to comprehend variations in nanoscale properties.

- Explore the diffusion capabilities and compatibility aspects of rejuvenators within aged bitumen to advance our understanding of the fundamental mechanisms underlying rejuvenation.

- Assess the rheological and thermodynamic characteristics of rejuvenated bitumen to propose essential evaluation criteria for determining the effectiveness of rejuvenating agents.

1.4 Thesis scope and methodology

The research scope is illustrated in **Figure 1.2**. This thesis focuses on understanding and evaluating the rejuvenation efficiency and mechanism of various rejuvenator-aged bitumen systems. It considers three key aspects—chemical composition, thermodynamic properties, and rheological behavior—that influence the rejuvenation process. Specifically, variations in chemical compositions, such as intermolecular interactions and the ratio of SARA fractions, impact the thermodynamic properties of rejuvenated bitumen. Additionally, the physical properties (e.g., density) are assumed to be closely linked to the rheological performance (e.g., modulus) of bituminous materials.
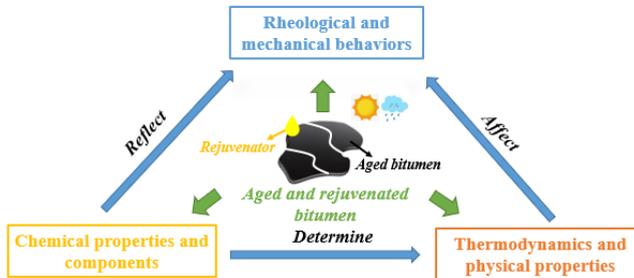
Figure 1.2 Research scope of this thesis
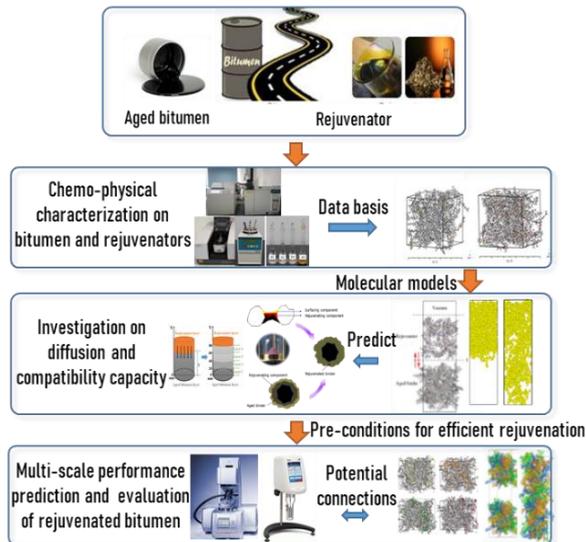
Figure 1.3 Research methodologies of this thesis

To this end, in this thesis, a multi-scale research approach will be performed to investigate the rejuvenation mechanism and evaluation methods of rejuvenated bitumen. **Figure 1.3** describes the research steps and methodologies throughout the thesis.

The chemical components and properties of aged bitumen and rejuvenators will be determined. Molecular models of aged bitumen and several types of rejuvenators will be built based on the chemical test results. Various molecular models are employed in simulations to predict thermodynamic and physical properties through molecular dynamics (MD) simulations. Subsequently, these properties are compared to experimental results to confirm the models' ability to capture essential distinctions among aging stages and various rejuvenator types.

The diffusion behavior of rejuvenators in aged bitumen will be investigated using numerical and experimental techniques. The MD simulation will establish the diffusion model and explore the diffusion behavior of rejuvenators in aged bitumen from a nanoscale perspective. Meanwhile, diffusion experiments in lab tests will validate the MD simulation results.

From the nanoscale, the MD simulation method will be used to predict the compatibility level between rejuvenator and bitumen components through different thermodynamic parameters, such as solubility parameter, Flory-Huggins factor, mixing free energy, binding energy, and radial distribution function. Moreover, the experimental storage stability tests will be implemented to validate the MD simulation findings.

The chemo-thermo-rheological performance of rejuvenated bitumen will be evaluated using experimental and MD simulation methods. A multi-scale understanding of the rejuvenation influence on the binder's high-and-low temperature performance will be investigated. The durability of rejuvenated bitumen will also be evaluated based on aging and fatigue. Lastly, the potential connections between the molecular-level thermodynamic parameters and critical rheological indices will be explored.

1.5 Thesis outline

This thesis comprises nine chapters that together describe the development of a multi-scale methodology for evaluating the rejuvenator efficiency and exploring the underlying mechanism of various rejuvenator-aged bitumen systems. In general, these nine chapters are divided into five parts to clarify the thesis structure:

Part I: Thesis background, objective, and preparation.

Part II: Experimental tests on and molecular models' determinations on aged bitumen and rejuvenators.

Part III: MD simulation predictions and experimental validations on prerequisites of bitumen-rejuvenator systems.

Part IV: Experimental characterizations and MD simulation predictions of the chemo-thermo-rheological performance of rejuvenated bitumen.

Part V: Summary.

The schematic flow diagram of the thesis chapters is shown in **Figure 1.4**, and a summary of each chapter is described as follows:

Part I is composed of **Chapter 1** and **Chapter 2**. The introductory chapter first highlights the definitions, research status, and challenges of rejuvenation technology of aged bitumen related to recycling reclaimed asphalt (RA) pavement materials. The main objectives and methodologies involved in this thesis will be stated, and the structure of the whole dissertation will be introduced.

The second chapter focuses on the literature review on the applications of molecular dynamics (MD) simulation methods in bituminous bitumen. This chapter will sum up the potential values of MD simulations

on performance evaluations and mechanism explanations of bituminous materials from the bulk and dynamic viewpoints.

Part I Thesis background, objective and preparation
Chapter 1: Introduction ┊ **Chapter 2:** Literature review

Part II Experimental tests and molecular models' determinations on aged bitumen and rejuvenators
Chapter 3: Chemical characterizations and MD simulations on long-term aging behaviors of bitumen
Chapter 4: Chemical characterizations and MD simulations on various rejuvenators

Part III MD simulation predictions and experimental validations on prerequisites of bitumen-rejuvenator systems
Chapter 5: Compatibility potential evaluation of different rejuvenator-aged bitumen blends
Chapter 6: Interfacial diffusion behaviors of rejuvenators in aged bitumen

Part IV Experimental characterizations and MD simulation predictions on chemo-thermo-rheological performance of rejuvenated bitumen
Chapter 7: Rejuvenation efficiency evaluation of rejuvenators in aged bitumen
Chapter 8: MD simulations on rejuvenation mechanism of rejuvenated bitumen

Part V Summary
Chapter 9: Conclusions and recommendations

Figure 1.4 Schematic flow diagram of thesis structure

The purpose of **Part II** of this thesis is to recognize the chemical characteristics and build representative molecular models of aged bitumen and rejuvenators for further investigating the rejuvenation efficiency and mechanism of various aged bitumen-rejuvenator systems at the atomic level. To this end, both **Chapter 3** and **Chapter 4** are implemented. The third chapter is dedicated to exploring the long-term aging behavior of the bitumen used in this thesis from the perspective of chemical characteristics. Thus, the molecular models of virgin and aged bitumen at various long-term aging levels will be determined. Afterward, the thermodynamic properties of bitumen as a function of aging time will be predicted by MD simulations, which will be further verified by experimental measurements.

Similarly, both average and multi-component molecular models of various rejuvenators will be proposed in **Chapter 4** based on their chemical characteristics and molecular compositions. The difference in the chemical and thermodynamic parameters between different rejuvenators will be detected and discussed. In addition, the MD outputs on established average and multi-component models are compared and used to optimize the final representative molecular models of rejuvenators for further MD simulations on aged bitumen-rejuvenator interaction systems.

Part III aims to multi-scale evaluate the prerequisites (compatibility and diffusion) of the aged bitumen-rejuvenator systems using a combined method of MD simulation and experimental validation. **Chapter 5** explores the compatibility potential between aged bitumen and rejuvenators at an atomic scale based on thermodynamic parameters outputted from MD simulations. At the same time, a thermal stability

test of rejuvenated bitumen will be carried out to verify the conclusions obtained from MD simulations qualitatively.

The diffusion behaviors of rejuvenators in aged binders will be studied in **Chapter 6.** Molecular dynamic simulations will be first implemented to predict the diffusion capacity of the rejuvenator in an aged bitumen matrix, considering the effects of rejuvenator type, aging degree of bitumen, and temperature. Moreover, the experimental diffusion tests on rejuvenator-aged bitumen bi-layer specimens will be performed to verify the MD simulation results.

Afterward, **Part IV** focuses on the rejuvenation efficiency and mechanism of rejuvenated bitumen using experimental characterizations and molecular dynamics simulations. **Chapter 7** investigates the coupling effects of rejuvenator type/dosage and aging level of bitumen on the chemical and rheological characteristics of rejuvenated bitumen. It is expected to propose several critical indicators for effectively evaluating and distinguishing the rejuvenation efficiency on the chemical and rheological (high-temperature rutting, low-temperature cracking, and fatigue resistance) properties of rejuvenated bitumen.

Chapter 8 explores the rejuvenation mechanisms between rejuvenators and aged bitumen aiming to explain the underlying reasons for the difference in the rejuvenation efficiency of various rejuvenators observed in **Chapter 7**. A series of thermodynamic parameters of rejuvenated binders will be obtained from molecular dynamics simulations, and their connections with critical rheological evaluation parameters proposed before will be analysed regarding high-temperature deformation, low-temperature flexibility, and cohesion cracking performance.

Chapter 9 will present the main findings, conclusions, and limitations of this thesis. The innovative rejuvenation evaluation methods and technologies from both aspects of experimental characterizations and MD simulations will be summarized. Meanwhile, some recommendations and suggestions for future work on further promoting the rejuvenation technology of aged bitumen will be discussed.

1.6 References

[1] R. Singh, R. Sharma, S. Akram, A. Gehlot, D. Buddhi, P. Malik, R. Arya. Highway 4.0: Digitalization of highways for vulnerable road safety development with intelligent IoT sensors and machine learning. Safety Science. 2021, 143, 105407.

[2] G. Valdes, F. Peres-Jimenez, R. Miro, A. Martinez, R. Botella. Experimental study of recycled asphalt mixtures with high percentages of reclaimed asphalt pavement. Construction and Building Materials. 2021, 25(3), 1289-1297.

[3] B. Huang, G. Li, D. Vukosavlievic, X. Shu, B. Egan. Laboratory investigation of mixing hot-mix asphalt with reclaimed asphalt pavement. Transportation Research Record: Journal of the Transportation Research Board. 2005, 1929, 37-45.

[4] X. Li, M. Marasteanu, R. Williams, T. Clyne. Effect of reclaimed asphalt pavement (proportion and type) and binder grade on asphalt mixtures. Transportation Research Record: Journal of the Transportation Research Board. 2008, 2051, 90-97.

[5] S. Zhao, B. Huang, X. Shu, M. Woods. Comparative evaluation of warm mix asphalt containing high percentages of reclaimed asphalt pavement. Construction and Building Materials. 2013, 44, 92-100.

[6] A. Shah, R. McDaniel, G. Huber, V. Gallivan. Investigation of properties of plant-produced reclaimed asphalt pavement mixtures. Transportation Research Record: Journal of the Transportation Research Board. 2007, 1998, 103-111.

[7] J. Shen, S. Amirkhanian, J. Miller. Effects of rejuvenating agents on superpave mixtures containing reclaimed asphalt pavement. Journal of Materials in Civil Engineering. 2007, 19(5), 376.

[8] M. Zaumanis, R. Mallick, R. Frank. 100% recycled hot mix asphalt: A review and analysis. Resources, Conservation and Recycling. 2014, 92, 230-245.

[9] V. Antunes, A.C. Freire, J. Neves. A review on the effect of RAP recycling on bituminous mixtures properties and the viability of multi-recycling. Construction and Building Materials. 2019, 211, 453-469.

[10] S. Magar, F. Xiao, D. Singh, B. Showkat. Applications of reclaimed asphalt pavement in India- A review. Journal of Cleaner Production. 2022, 335, 130221.

[11] F. Xiao, S. Yao, J. Wang, X. Li, S. Amirkhanian. A literature review on cold recycling technology of asphalt pavement. Construction and Building Materials. 2018, 579-604.

[12] W. Song, B. Huang, X. Shu. Influence of warm-mix asphalt technology and rejuvenator on performance of asphalt mixtures containing 50% reclaimed asphalt pavement. Journal of Cleaner Production. 2018, 192, 191-198.

[13] S. Kim, G. Sholar, T. Byron, J. Kim. Performance of polymer-modified asphalt mixture with reclaimed asphalt pavement. Transportation Research Record: Journal of the Transportation Research Board. 2009, 2126, 109-114.

[14] A. Yousefi, A. Behnood, A. Nowruzi, H. Haghshenas. Performance evaluation of asphalt mixtures containing warm mix asphalt (WMA) additives and reclaimed asphalt pavement (RAP). Construction and Building Materials. 2021, 268, 121200.

[15] R. Vidal, E. Moliner, G. Martinez, M. Rubio. Life cycle assessment of hot mix asphalt and zeolite-based warm mix asphalt with reclaimed asphalt pavement. Resources, Conservation and Recycling. 2013, 74, 101-114.

[16] N. Tapsoba, C. Sauzeat, H. Benedetto, H. Baaj. M. Ech. Behaviour of asphalt mixtures containing reclaimed asphalt pavement and asphalt shingle. Road Materials and Pavement Design. 2014, 15(2), 330-347.

[17] H. Jahanbakhsh, M. Karimi, H. Naseri, F. Nejad. Sustainable asphalt concrete containing high reclaimed asphalt pavements and recycling agents: performance assessment, cost analysis, and environmental impact. Journal of Cleaner Production. 2000, 244, 118837.

[18] Y. Wang, Z. Leng, X. Li, C. Hu. Cold recycling of reclaimed asphalt pavement towards improved engineering performance. Journal of Cleaner Production. 2018, 171, 1031-1038.

[19] B. Bowers, B. Huang, X. Shu, B. Miller. Investigation of reclaimed asphalt pavement blending efficiency through GPC and FTIR. Construction and Building Materials. 2014, 50, 517-523.

[20] F. Xiao, L. Xu, Z. Zhao, X. Hou. Recent applications and developments of reclaimed asphalt pavement in China, 2010-2021. Sustainable Materials and Technologies. 2023, 37, e00697.

[21] I. Fernandez, P. Gonzalez, I. Vego, D. Fresno. Recyclability potential of asphalt mixes containing reclaimed asphalt pavement and industrial by-products. Construction and Building Materials. 2019, 195, 148-155.

[22] A. Gedik. A review on the evaluation of the potential utilization of construction and demolition waste in hot mix asphalt pavements. Resources, Conservation & Recycling. 2020, 161, 104956.

[23] Federal Highway Administration report. User Guidelines for waste and byproduct materials in pavement construction. FHWA-RD-97-148.

[24] D. Bizarro, Z. Steinmann, I. Nieuwenhuijse, E. Keijzer, M. Hauck. Potential carbon footprint reduction for reclaimed asphalt pavement innovations: LCA methodology, best available technology, and near-future reduction potential. Sustainability. 2021, 13, 1382.

[25] F. Xiao, N. Su, S. Yao, S. Amirkhanian, J. Wang. Performance grades, environmental and economic investigations of reclaimed asphalt pavement materials. Journal of Cleaner Production. 2019, 211, 1299-1312.

[26] B. Hill, D. Oldham, B. Behnia, E. Fini, W. Buttlar, H. Reis. Low-temperature performance characterization of bio-modified asphalt mixtures that contain reclaimed asphalt pavement. Transportation Research Record: Journal of the Transportation Research Board. 2013, 2371, 49-57.

[27] European Asphalt Pavement Association (EAPA). Asphalt in figures 2021. 2021.

[28] J. Gao, J. Yang, D. Yu, Y. Jiang, K. Ruan, W. Tao, C. Sun, L. Luo. Reducing the variability of multi-source reclaimed asphalt pavement materials: A practice in China. Construction and Building Materials. 2021, 278, 122389.

[29] M. Wrobel, A. Woszuk, M. Ratajczak, W. Franus. Properties of reclaimed asphalt pavement mixture with organic rejuvenator. Construction and Building Materials. 2021, 271, 121514.

[30] L. Devulapalli, S. Kothandaraman, G. Sarang. A review on the mechanisms involved in reclaimed asphalt pavement. International Journal of Pavement Research and Technology. 2019, 12, 185-196.

[31] P. Kriz, D. Grant, B. Veloza, M. Gale, A. Blahey, J. Brownie, R. Shirts, S. Maccarrone. Blending and diffusion of reclaimed asphalt pavement and virgin asphalt binders. Road Materials and Pavement Design. 2014, 15(S1), 78-112.

[32] P. Shirodkar, Y. Mehta, A. Nolan, K. Sonpal, A. Norton, C. Tomlinson, E. Dubois, P. Sullivan, R. Sauber. A study to determine the degree of partial blending of reclaimed asphalt pavement (RAP) binder for high RAP hot mix asphalt. Construction and Building Materials. 2011, 25(1), 150-155.

[33] Q. Aurangzeb, I. Al-Qadi. Asphalt pavements with high reclaimed asphalt pavement content: economic and environmental perspectives. Transportation Research Record: Journal of the Transportation Research Board. 2014, 2456, 161-169.

[34] B. Bowers, D. Allain. B. Diefenderfer. Review of agency pavement recycling construction specifications. Transportation Research Record. 2020, 2674(8), 243-251.

[35] A. Abed, N. Thom, D. Presti. Design considerations of high RAP-content asphalt produced at reduced temperatures. Materials and Structures. 2018, 51, 91.

[36] W. Song, Z. Xu, F. Xu, H. Wu, J. Yin. Fracture investigation of asphalt mixtures containing reclaimed asphalt pavement using an equivalent energy approach. Engineering Fracture Mechanics. 2021, 253, 107892.

[37] L. Gao, H. Li, J. Xie, Z. Yu, S. Charmot. Evaluation of pavement performance for reclaimed asphalt materials in different layers. Construction and Building Materials. 2018, 159, 561-566.

[38] K. Roja, E. Masad, W. Mogawer. Performance and blending evaluation of asphalt mixtures containing reclaimed asphalt pavement. Road Materials and Pavement Design. 2021, 22(11), 2441-2457.

[39] J. Gao, Y. Yao, J. Yang, L. Song, J. Xu, L. He, W. Tao. Migration behavior of reclaimed asphalt pavement mastic during hot mixing. Journal of Cleaner Production. 2022, 376, 134123.

[40] A. Ali, Y. Mehta, A. Nolan, C. Purdy, T. Bennert. Investigation of the impacts of aging and RAP percentages on effectiveness of asphalt binder rejuvenators. Construction and Building Materials. 2016, 110, 211-217.

[41] Y. Chen, Z. Chen, Q. Xiang, W. Qin, J. Yi. Research on the influence of RAP and aged asphalt on the performance of plant-mixed hot recycled asphalt mixture and blended asphalt. Case Studies in Construction Materials. 2021, 15, e00722.

[42] Y. Qian, F. Guo, Z. Leng, Y. Zhang, H. Yu. Simulation of the field aging of asphalt binders in different reclaimed asphalt pavement (RAP) materials in Hong Kong through laboratory tests. Construction and Building Materials. 2020, 265, 120651.

[43] W. Ferreira, V. Branco, K. Vasconcelos, A. Bhasin, A. Sreeram. The impact of aging heterogeneities within RAP binder on recycled asphalt mixture design. Construction and Building Materials. 2021, 300, 124260.

[44] A. Forton, S, Mangiafico, C. Sauzeat, H. Benedetto, P. Marc. Properties of blends of fresh and RAP binders with rejuvenator: Experimental and estimated results. Construction and Building Materials. 2020, 236, 117555.

[45] J. Zhang, H, Sun, H. Jiang, X. Xu, M. Liang, Y. Hou, Z. Yao. Experimental assessment of reclaimed bitumen and RAP asphalt mixtures incorporating a developed rejuvenator. Construction and Building Materials. 2019, 215, 660-669.

[46] S. Pradhan, U. Sahoo. Influence of softer binder and rejuvenator on bituminous mixtures containing reclaimed asphalt pavement (RAP) material. International Journal of Transportation Science and Technology.

[47] W. Mogawer, A. Booshehrian, S. Vahidi, A. Austerman. Evaluating the effect of rejuvenators on the degree of blending and performance of high RAP, RAS, and RAP/RAS mixtures. Road Materials and Pavement Design. 2013, 14 (S2), 193-213.

[48] M. Zaumanis, R. Mallick. Review of very high-content reclaimed asphalt use in plant-produced pavements: state of the art. International Journal of Pavement Engineering. 2015, 16(1), 39-55.

[49] S. Im, P. Karki, F. Zhou. Development of new mix design method for asphalt mixtures containing RAP and rejuvenators. Construction and Building Materials. 2016, 115, 727-734.

[50] S. Casillas, A. Braham. Development of a performance-based approach to asphalt emulsion selection for cold in-place recycling applications. Transportation Research Record. 2022, 1-12.

[51] A. Behnood. Application of rejuvenators to improve the rheological and mechanical properties of asphalt binders and mixtures: A review. Journal of Cleaner Production. 2019, 171-182.

[52] A. Mansourkhaki, M. Ameri, M. Habibpour, B. Underwood. Chemical composition and rheological characteristics of binders containing RAP and rejuvenator. Journal of Materials in Civil Engineering. 2020, 32(4), 1-11.

[53] V. Loise, P. Calandra, A. Abe, M. Porto, C. Rossi, M. Davoli, P. Caputo. Additives on aged bitumens: What probe to distinguish between rejuvenating and fluxing effects? Journal of Molecular Liquids. 2021, 339, 116742.

[54] C. Li, A. Rajib, M. Sarker, R. Liu, E. Fini, J. Cai. Balancing the aromatic and ketone content of bio-oils as rejuvenators to enhance their efficacy in restoring properties of aged bitumen. ACS Sustainable Chemistry & Engineering. 2021, 9, 6912-6922.

[55] M. Guo, H. Liu, Y. Jiao, L. Mo, Y. Tan, D. Wang, M. Liang. Effect of WMA-RAP technology on pavement performance of asphalt mixture: A state-of-the-art review. Journal of Cleaner Production. 2020, 266, 121704.

[56] Z. Han, P. Cong, J. Qiu. Microscopic experimental and numerical research on rejuvenators: A review. Journal of Traffic and Transportation Engineering (English Edition). 2022, 9(2), 180-207.

[57] K. Schwettmann, N. Nytus, S. Weigel, M. Radenberg, D. Stephan. Effects of rejuvenators on bitumen ageing during simulated cyclic reuse: A review. Resources, Conservation and Recycling. 2023, 190, 106776.

[58] R. Ahmed, K. Hossain. Waste cooking oil as an asphalt rejuvenator: A state-of-the-art review. Construction and Building Materials. 2020, 230, 116985.

[59] H. Ziari, A. Moniri, P. Bahri, Y. Saghafi. The effect of rejuvenators on the aging resistance of recycled asphalt mixtures. Construction and Building Materials. 2019, 224, 89-98.

[60] Y. Li, P. Hao, M. Zhang. Fabrication, characterization and assessment of the capsules containing rejuvenator for improving the self-healing performance of asphalt materials: A review. Journal of Cleaner Production. 2021, 287, 125079.

[61] X. Xu, A. Sreeram, Z. Leng, J. Yu, R. Li, C. Peng. Challenges and opportunities in the high-quality rejuvenation of unmodified and SBS modified asphalt mixtures: State of the art. Journal of Cleaner Production. 2022, 378, 134634.

[62] S. Xu, H. Wu, W. Song, Y. Zhan. Investigation of the aging behaviors of reclaimed asphalt. Journal of Cleaner Production. 2022, 356, 131837.

[63] C. Yang, J. Zhang, F. Yang, M. Cheng, Y. Wang, S. Amirkhanian, S. Wu, M. Wei, J. Xie. Multi-scale performance evaluation and correlation analysis of blended asphalt and recycled asphalt mixtures incorporating high RAP content. Journal of Cleaner Production. 2021, 317, 128278.

[64] A. Abdelaziz, E. Masad, A. Martin, E. Mercado, A. Bajaj. Multiscale characterization of aging and rejuvenation in asphalt binder blends with high RAP contents. Journal of Materials in Civil Engineering. 2021, 33(10), 1-18.

[65] A. Mohamed, S. EI-Badawy, F. Xiao. Aging potential and its impact on the bonding strength of rubberized RAP asphalt binder. ACS Sustainable Chemistry & Engineering. 2023, 11, 751-765.

[66] F. Kaseer, A. Martin, E. Arambula-Mercado. Use of recycling agents in asphalt mixtures with high recycled materials contents in the United States: A literature review. Construction and Building Materials. 2019, 211, 974-987.

[67] M. Alae, L. Xu, Z. Cao, X. Xu, F. Xiao. Fatigue and intermediate-temperature cracking performance of rejuvenated recycled asphalt binders and mixtures: A review. Journal of Cleaner Production. 2023, 384, 135587.

[68] S. Tarbox, J. Daniel. Effects of long-term oven aging on reclaimed asphalt pavement mixtures. Transportation Research Record: Journal of the Transportation Research Board. 2012, 2294, 1-15.

[69] S. Huang, T. Turner, Aging characteristics of RAP blend binders: rheological properties. Journal of Materials in Civil Engineering. 2014, 26(5), 966-973.

[70] J. Wu, Q. Liu, S. Yang, M. Oeser, C. Ago. Study of migration and diffusion during the mixing process of asphalt mixtures with RAP. Road Materials and Pavement Design, 2021, 22(7), 1578-1593.

[71] B. Bowers, B. Huang, X. Shu. Refining laboratory procedure for artificial RAP: A comparative study. Construction and Building Materials. 2014, 52, 385-390.

[72] M. Nazzal, W. Mogawer, A. Austerman, L. Qtaish, S. Kaya. Multi-scale evaluation of the effect of rejuvenators on the performance of high RAP content mixtures. Construction and Building Materials. 2015, 101, 50-56.

[73] B. Anupam, U. Sahoo, A. Chandrappa. A methodological review on self-healing asphalt pavements. Construction and Building Materials. 2022, 321, 126395.

[74] D. Ganter, T. Mielke, M. Maier, D. Lupascu. Bitumen rheology and the impact of rejuvenators. Construction and Building Materials. 2019, 222, 414-423.

[75] Z. Xie, H. Rizvi, C. Purdy, A. Ali, Y. Mehta. Effect of rejuvenator types and mixing procedures on volumetric properties of asphalt mixtures with 50% RAP. Construction and Building Materials. 2019, 218, 457-464.

[76] G. Guduru, K. Kuna. Classification of reclaimed asphalt pavement (RAP) material using simple indicative tests. Construction and Building Materials. 2022, 328, 127075.

[77] G. Cuciniello, N. Mallegni, M. Cappello, S. Filippi, P. Leandri, G. Polacco, M. Losa. Classification and selection of exhausted oils for rejuvenating bituminous blends. Construction and Building Materials. 2021, 278, 122387.

[78] M. Cavalli, M. Zaumanis, E. Mazza, M. Partl, L. Poulikakos. Effect of ageing on the mechanical and chemical properties of binder from RAP treated with bio-based rejuvenators. Composites Part B: Engineering. 2018, 141, 174-181.

[79] M. Hugener, M. Partl, M. Morant. Cold asphalt recycling with 100% reclaimed asphalt pavement and vegetable oil-based rejuvenators. Road Materials and Pavement Design. 2014, 15(2), 239-258.

[80] Z. Zou, X. Gu, Q. Dong, F. Ni, Y. Jiang. Rutting and fatigue cracking performance of SBS-RAP blended binders with a rejuvenator. Construction and Building Materials. 2019, 203, 294-303.

[81] M. Zaumanis, R. Mallick, L. Poulikakos, R. Frank. Influence of six rejuvenators on the performance properties of reclaimed asphalt pavement (RAP) binder and So recycled asphalt mixtures. Construction and Building Materials. 2014, 71, 538-550.

[82] T. Moghaddam, H. Baaj. The use of rejuvenating agents in production of recycled hot mix asphalt: A systematic review. Construction and Building Materials. 2016, 114, 805-816.

[83] S. Yan, Q. Dong, X. Chen, C. Zhou, S. Dong, X. Gu. Application of waste oil in asphalt rejuvenation and modification: A comprehensive review. Construction and Building Materials. 2022, 340, 127784.

[84] Y. Ding. Blending and diffusion of recycled asphalt pavement and new approach to recycling asphalt shingle. PhD thesis. University of Tennessee.

[85] M. Mousavi, F. Pahlavan, EH. Fini. Multi-scale investigation of oxidative aging in biomodified asphalt binder. The Journal of Physical Chemistry C. 2016, 120, 17224-17233.

[86] Z. Chen, J. Pei, R. Li, F. Xiao. Performance characteristics of asphalt materials based on molecular dynamics simulation – A review. Construction and Building Materials. 2018, 189, 695-710.

[87] M. Zadshir, D. Oldham, EH. Fini. Investigation bio-rejuvenation mechanisms in asphalt binder via laboratory experiments and molecular dynamics simulation. Construction and Building Materials. 2018, 190, 392-402.

[88] S. Ren, X. Liu, P. Lin, Y. Gao, S. Erkens. Molecular dynamics simulation on bulk bitumen systems and its potential connections to macroscale performance: Review and discussion. Fuel. 2022, 328, 125382.

[89] S. Ren, X. Liu, P. Lin, Y. Gao, S. Erkens. Review on the diffusive and interfacial performance of bituminous materials: From a perspective of molecular dynamics simulation. Journal of Molecular Liquids. 2022, 366, 120363.

2

Literature review on applications of molecular dynamics simulation in bituminous materials

The molecular dynamics simulation (MD) method has been proven to be an efficient tool for explaining the atomic-level interaction mechanism and predicting the essential thermodynamic properties of different material systems (e.g. density, cohesive energy density, solubility parameters, glass transition temperature, free volume, etc.). The MD simulation technology has been used for bituminous materials for a very short time compared to experimental characterizations, and it is important to figure out the role of MD simulations in solving the scientific and engineering challenges in asphalt pavement materials. This chapter summarizes the application cases of MD simulation in bituminous materials and discusses the potential relationships between the nanoscale and macroscale characteristics. This review work can help us effectively evaluate the rejuvenation mechanism and efficiency from the perspective of atomic scale.

2.1 Introduction

2.1.1 MD simulation application and principle

Molecular dynamics simulation is a powerful computational technique used in various scientific disciplines to study the dynamic behavior of molecules and atoms at the atomic level. This method provides invaluable insights into the movement, interactions, and properties of complex molecular systems over time. At its core, molecular dynamics simulation works by numerically solving Newton's equations of motion for each atom or molecule in a simulated system. By tracking the positions and velocities of these particles at discrete time intervals, researchers can observe how the system evolves and gain a detailed understanding of its thermodynamic and kinetic properties. Molecular dynamics simulations have wide-ranging applications in fields such as chemistry, physics, materials science, and biology, enabling scientists to investigate phenomena ranging from protein folding to the behavior of materials under extreme conditions.

The MD simulation method is employed in different fields of food [1], medicine [2], energy and fuels [3], chemistry [4], and polymer [5]. As shown in **Figure 2.1**, the MD simulation method plays a vital role in multiscale studies in multidisciplinary materials engineering, chemical engineering, and physical and applied physics. In this review, the application fields of MD simulation will be introduced with the classification of the study perspective, including mass transition, mechanical response, reaction mechanism, and interfacial interaction. Although the MD simulation method involves all aspects, these four points are extensively researched in bituminous materials.

- Mass transition: The mass, energy, and momentum transitions are common are present in our lives and studies. Through the MD simulation, the mass transition process could be observed visually at an atom level.
- Mechanical response: The mechanical response is the inner structure change of materials under external force. The MD method can be employed to simulate the interaction between the atoms in different substances and reflect the mechanical response, which is the principle of the atomic force microscope.
- Reaction mechanism: The molecular interaction and reaction mechanism can be explored with MD simulation. Meanwhile, the transition state of matters during chemical reactions is easily captured, which is beneficial to understanding the reaction procedure and effectively controlling the chemical reaction rate and direction.
- Interfacial interaction: Interfacial interaction significantly affects the adhesion properties of a multiphase system. The MD simulation method can help researchers understand the interfacial phenomenon and find the right ways to enhance the interfacial macroscale mechanical behaviors from the perspective of molecular interaction.
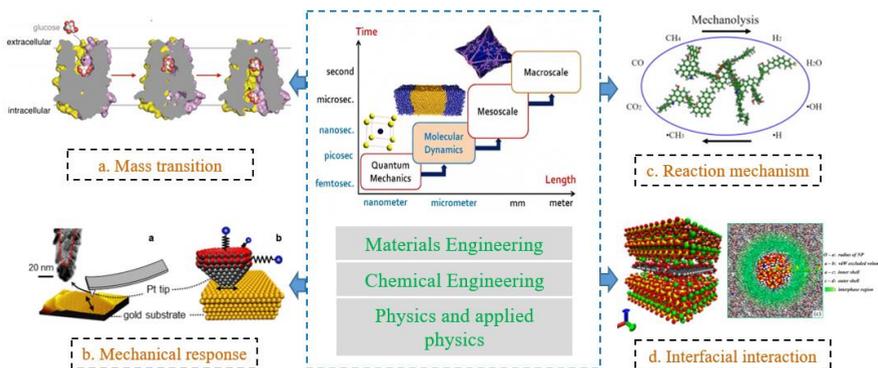
Figure 2.1 The application fields of MD simulation [1-5]

The MD simulation technology combines the theoretical knowledge of quantum mechanics and Newton's classical mechanics to study the material characteristics from the viewpoint of the molecular level [6, 7]. **Figure 2.2** illustrates the basic principle of MD simulation, and it includes the following steps:
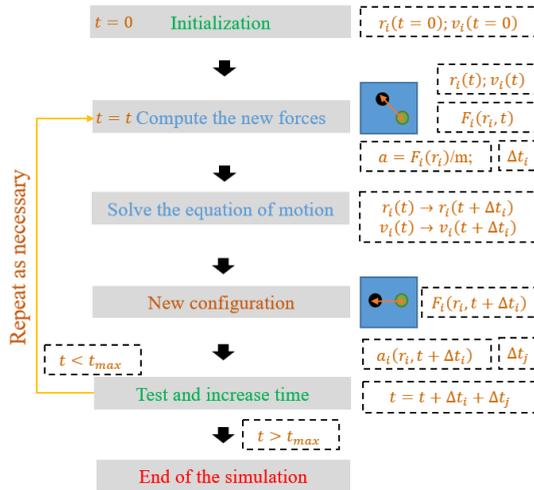
Figure 2.2 The basic principle of MD simulation

- Step 1-Initialization: Before conducting the MD simulation program (simulation time t=0), the target molecules are incorporated into the simulation system with an initiation position r_i (t=0) and velocity v_i (t=0).
- Step 2-Compute the new forces: The interaction forces F_i (r_i, t) between molecules are calculated under the influence of the applied forcefield (see **section 2.1.2**).
- Step 3-Solve the equation of motion: The acceleration value of the molecule is estimated using the Newton equation (a=F/m). When time elapses from t to t+Δt, the new position and velocity of the molecule change from r_i(t) and v_i(t) to r_i(t+Δt) and v_i(t+Δt), respectively.
- Step 4-Repeat steps 2 and 3: If the time t+Δt is lower than the fixed maximum simulation time t_{max}, steps 2 and 3 will be repeated to obtain the equilibrium system and relevant results. During this step, the interaction force will be recalculated, while the molecular velocity and position will be renewed.
- Step 5-End of the simulation. When the time t+Δt reaches the set value (t_{max}), the MD simulation will be ended. Meanwhile, the trajectories of configuration and energy during simulation are recorded, which can be further analysed to predict physical and thermodynamic properties of the simulated system, such as density, glass transition temperature, cohesive energy density, solubility parameter, self-diffusion coefficient, surface free energy, etc.

Given the benefits mentioned above, the MD simulation method has been employed in the field of bituminous materials to further understand the molecular interaction of different components in bitumen and predict the important physical, thermodynamic, and mechanical properties. The applications of MD simulation technology in the virgin bitumen systems without any additives and oxidation aging are introduced in **Figure 2.3**. During the preparation step, the selection of bitumen models and forcefield is the most important, which directly influences the quality of simulation results. After obtaining an optimized model by minimizing energy, the MD simulation programs could be conducted under different conditions of ensembles, temperature (e.g. Thermostat control), pressure (e.g. Barostat control), time step, and simulation time. Then, the equilibrium configuration of the bulk bitumen system and the trajectories are recorded to calculate the physical and thermodynamic properties. To validate the reliability of the selected molecular models and forcefield, it is necessary to compare the chemical and physical parameters outputted from MD

simulation with the corresponding experimental results. Lastly, more MD simulation procedures are implemented to predict the important indicators of bitumen systems, including the thermo-physical, thermo-dynamics, and structural characteristics. Based upon this, this thesis will explore the compatibility, diffusion, and rejuvenation efficiency of various rejuvenators in aged bitumen.

Molecular dynamics simulation study on the bulk bitumen system

| Preparation | Selection of bitumen models | | Forcefield optimization |
| | |

- Average molecular model;
- Three-components molecular model;
- Four-components molecular model;
- Six-components molecular model;
- Twelve-components molecular model;
- Twenty-components molecular model;

➢ OPLS forcefield;
➢ COMPASS forcefield;
➢ COMPASS II forcefield;
➢ PCFF forcefield;
➢ ACEFF forcefield;
➢ CHARMM forcefield;

| Operation | Implement of MD simulation programs |

Ensemble (NVT; NPT; NVE; NPH); Thermostat and Barostat; Time step; Simulation time

| Validation | Validation of molecular models and Forcefield |

✓ Chemical characteristics: SARA fractions; elemental compositions; functional groups;
✓ Physical properties: Density; Glass transition temperatures; Solubility parameters;

| Prediction | Performance prediction of bitumen system |

❑ Thermo-physical   ❑ Thermo-dynamics   ❑ Mechanical   ❑ Structural

Figure 2.3 The overall program of MD simulation of bulk bitumen system

2.1.2 Some Forcefields for MD simulations of bitumen

Choosing the right forcefield for a particular simulation model is crucial for the precision and trustworthiness of simulation results. Nevertheless, there is no definitive consensus on the ideal forcefield for MD simulations involving bituminous materials. This is because the available forcefields for bitumen are typically adaptations from those designed for other organic and inorganic substances, polymers, or metals. Consequently, the use of different forcefields in various MD simulation studies of bitumen systems has led to a lack of uniformity. **Table 2.1** provides an overview of the various types of forcefields employed in MD simulations of bulk bitumen systems.

In summary, the COMPASS (II) forcefield is the most popular selected in MD simulations of bitumen. However, the ACEFF, GAFF, PCFF, CVFF, and CHARMM forcefields are used in a few cases. It should be mentioned that the ReaxFF and MARTINI Forcefields are available in specific systems, such as the molecule oxidation reaction. In addition, the ReaxFF is useful for detecting the chemical reaction pathway in bitumen by calculating the chemical bond energy, like exploring the oxidative aging mechanism at an atomic scale (see **section 2.2.2**). In addition, You et al. [31] employed the ACEFF forcefield in an MD simulation on the 12-component bitumen model and found an excellent agreement between the MD simulation outputs and that from the OPLS forcefield. In detail, the density determined in this study at 298.15K was 0.988 g/cm^3, reflecting a 1.1% decrease compared to the reference [9]. However, a deviation between predicted density (0.968 g/cm^3) and measured value (1.032 g/cm^3) is still observed at 333.15K.

Similarly, Sonibare et al. [11] compared the MD simulation outputs with CHARMM and OPLS-aa forcefields on the three-component bitumen model, demonstrating that the density, diffusion coefficient, and RDF parameters from the two forcefields were very similar. Nevertheless, the CHARMM forcefield could predict the crystallization of n-docosane at 300K more accurately than the OPLS-aa forcefield. Overall, the

differences in MD simulation outputs with various Forcefields are still unclear, but the COMPASS (II) is a first choice for MD simulations of bituminous materials, which will also be utilized in this dissertation.

Table 2.1 Commonly-used Forcefield in MD simulations on bulk bitumen systems

Forcefield type	Abbreviation	Brief descriptions	References
Optimized Potential for Liquid Simulation (in all-atom version)	OPLS (-aa)	*The intermolecular interaction comprises the pairwise repulsive and attractive Lennard-Jones and Coulomb forces, which work significantly well on many organic functional groups and protein models.*	[8-11]
Condensed-phase Optimized Molecular Potential for Atomistic Simulation Studies Forcefield	COMPASS (II)	*It is the first forcefield derived from an ab initio calculation method and the most popular forcefield applied to bituminous materials models. It can be utilized to simulate well and predict the structure, conformation, vibration frequency, and thermodynamic properties of a single molecule or condensed matter in a wide range.*	[12-23]
Amber Cornell Extension Forcefield	ACEFF	*It is based on the Amber Cornell Force Field with some experimental parameters obtained from the General Amber Force Field (GAFF). Moreover, it is appropriate for different simulation systems with organic and biological molecules.*	[24, 25]
General Amber Forcefield	GAFF	*It is an extension of the AMBER force field, and it was parameterized for most of the organic molecules.*	[4]
Polymer Consistent Forcefield	PCFF	*It is a class II ab initio force field from CFF91 and is mainly used for organic systems and some metallic elements, which have been extensively parameterized and validated for application to polymers and organic materials.*	[26]
Consistent Valence Forcefield	CVFF	*It can describe the intra- and inter-molecular interactions in bitumen nanocomposite systems and is adopted to simulate de-bonding behavior between the bitumen and mineral powder filler.*	[27]
Chemistry at Harvard Macromolecular Mechanics	CHARMM	*It covers a wide range of organic groups, including bio-molecules and drug-like molecules, and is well used in modelling systems containing solvent and bio-molecules.*	[11]
Reaction Forcefield	ReaxFF	*It is a bond-order-dependent Force Field allowing for bond breaking and formation, which has been parameterized and implemented to various materials and processes, including polymers, metals, ceramics, and silicon, for chemical simulations.*	[28]
MARTINI Forcefield	MARTINI	*It is based on parametrizing a large library of molecular simulation models against experimental thermodynamic data for coarse-grained molecular dynamics.*	[29]
DREIDING Forcefield	DREIDING	*It is a simple but versatile and generic all-atom force field to predict the thermodynamic and structural properties of organic, biological, and main-group inorganic molecules.*	[30]

2.1.3 Validation parameters of MD simulations

Validation of the established molecular models and setup parameters in molecular dynamics (MD) simulations is essential to enhance the accuracy of the predicted outcomes in comparison to the actual measurements. In terms of molecular structures and the numbers of bitumen molecules, it is imperative to measure additional chemical characteristics, including elemental compositions, SARA fractions, and the distribution of functional groups (such as S=O), to ensure that the established bitumen model accurately represents real-world materials. Following the MD simulations, it is standard practice to compare various physical and mechanical parameters derived from these simulations with the values obtained through experimentation or prior research. **Table 2.2** presents a compilation of frequently utilized validation parameters in MD simulation studies focusing on bituminous materials.

In the realm of MD simulations focused on bulk bitumen systems, various validation parameters have been consistently employed. These parameters encompass density, glass transition temperature, cohesive energy density, solubility parameter, diffusion coefficient, radial distribution function, shear modulus, viscosity, surface free energy, maximum adhesion force, nano-hardness, and modulus.

Table 2.2 The commonly-used validation parameters in MD simulations on bituminous materials

Parameters	References	Parameters	References
Density (g·cm⁻³)	[8, 9, 14, 15, 23, 25, 31-40]	Radial distribution function (RDF)	[18, 22]
Glass transition temperature (K)	[18, 22, 25, 33, 34, 35, 39]	Shear modulus (GPa)	[31, 33]
Cohesive energy density (J·m³)	[18, 34, 35, 41]	Viscosity (Pa·s)	[25, 30, 31]
Solubility parameter (J·m³)⁰·⁵	[18, 22, 35, 36, 41]	Surface free energy / maximum adhesion force (nN)	[37, 40]
Diffusion coefficient (m²/s)	[42]	Nanohardness and modulus (MPa)	[43]

Among these parameters, the density, glass transition temperature, cohesive energy density, and solubility parameters are the most prevalent and widely used for validating the reliability of MD simulation results, as evidenced by their frequent inclusion in numerous references. The reason is that these thermodynamic parameters can be measured directly and easily.

In addition to these fundamental properties, the radial distribution function results of SARA fractions have been instrumental in validating the colloidal structures of bitumen. Furthermore, the assessment of surface free energy in bituminous materials can be carried out through the contact angle test, while atomic force microscopy (AFM) has been instrumental in evaluating the maximum adhesion force, nano-hardness, and modulus of bitumen.

2.2 MD simulations on virgin and aged bitumen

2.2.1 MD models of virgin bitumen

It is difficult to determine the integral model of each bitumen molecule due to a huge among of molecule databases. Initially, only one type of molecule was adopted to represent the bitumen. Because of the petrochemical experience, Jenning et al. [44] developed eight average molecular models of the core bitumen (see **Figure 2.4**) based on the Nuclear Magnetic Resonance (NMR) spectroscopy results.
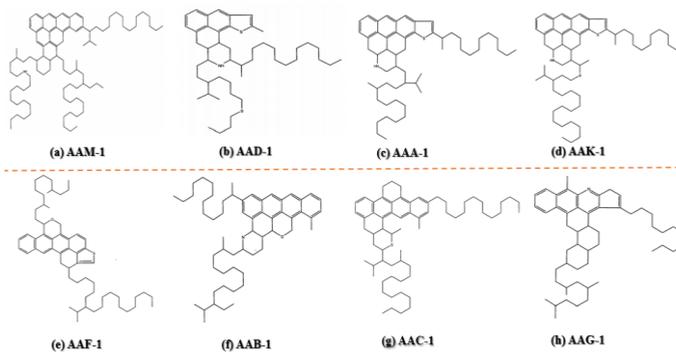
Figure 2.4 The average molecular models of eight SHAP core bitumen binders [44]

These average molecular structures comprise aromatic rings, naphthenic rings, and alkyl-branched chains, considering few heteroatoms. The bitumen source significantly influenced the average molecular structures in terms of molecular weight, functional group type, aromaticity, and branched-chain length. Although Pauli et al. concluded that it was possible to predict the density and surface energy of bitumen, these average models have been abandoned due to the negligence of the wide molecule region characteristic of bitumen [45].

According to the difference in molecular weight, aromaticity, polarity, and functional group distribution, the chemical components in bitumen are divided into four groups: saturate, aromatic, resin, and asphaltene. As shown in **Figure 2.5**, only saturate, resin, and asphaltene fractions were considered in the three-component model. The saturate and resin are represented by n-docosane and 1,7-dimethylnaphthalene, respectively. Meanwhile, two typical molecular structures of asphaltene are adopted as asphaltene molecules. Asphaltene I molecule is composed of many fused aromatic rings with short branches, while asphaltene II shows longer aliphatic chains surrounding a core of fewer aromatic rings. Zhang et al. [27] conducted an MD simulation on the three-component bitumen model with an Optimal Potential for Liquid Simulation (OPLS-aa) forcefield and validated that it could reasonably predict the density, thermal expansion coefficient, and isothermal compressibility of bitumen. The predicted and measured density at 330K was 0.93 and 1.03 g/cm^3, while the measured glass transition temperatures (-8.75 to -40.45°C) were lower than the simulated value (25°C).

(a) Saturate (n-Docosane)

(b) Resin
(1,7-Dimethylnaphthalene)

(c) Asphaltene I

(d) Asphaltene II
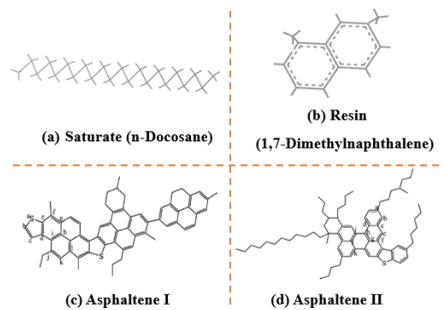
Figure 2.5 The molecular structures of each fraction in the three-component model [27]

Nevertheless, these three kinds of molecules are selected from different bitumen samples, leading to a difference between molecular components in the MD model with actual chemical components. Ding et al. [38] carried out a liquid chromatography (LC) transform combined with FTIR and GPC to separate and detect chemical components of virgin and aged bitumen into three groups based on molecular weight distribution. Afterward, the chemical and structural parameters of molecular weight, C/H ratio, and the number of aromatic carbons, aromatic rings, alkane carbons, branched-chain carbons, and the branched chains in the three fractions of virgin and aged bitumen could be calculated. The established three-component models of virgin and aged bitumen based on their results for this specific bitumen are illustrated in **Figure 2.6**, and the predicted density results revealed that their proposed models were more accurate than the previous model [27]. In detail, the predicted density value was about 1.025 g/cm^3, close to the measured value of 1.03 g/cm^3.

(a) Virgin bitumen model

(b) Aged bitumen model
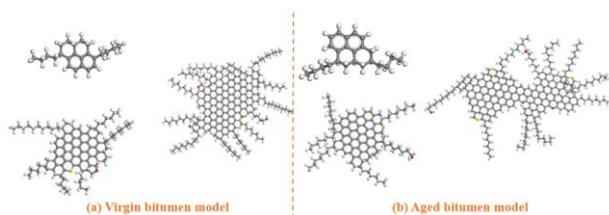
Figure 2.6 Three-component molecular models for virgin (a) and aged (b) bitumen [38]

The Four-component molecular model was built following the SARA separation theory of bitumen, and a sort of molecule represented each SARA fraction. Different four-component molecular models are shown in **Figure 2.7**. The four-component model 1 was adopted in many studies [20, 21, 25], in which the molecular formula for asphaltene, resin, saturate, and the aromatic molecule is $C_{53}H_{57}NOs$, $C_{100}H_{106}$, $C_{22}H_{46}$, and $C_{12}H_{12}$, respectively. In the meantime, the four-component model II is also popular [22, 46, 47]. The molecular formula (molecular weight) information is Asphaltene: $C_{150}H_{181}N_3O_2S_2$ (2122.24g/mol), Resin: $C_{59}H_{85}NOS$ (856.395g/mol), Aromatic: $C_{46}H_{50}S$ (634.966g/mol), and saturate: $C_{22}H_{46}$ (310.61g/mol).

The third four-component model for bitumen developed and employed [39, 48] is demonstrated in **Figure 2.7(c)**. In addition, Zeng et al. developed another four-component model of bitumen with the SARA molecular formula of $C_{51}H_{92}$ (saturate), $C_{103}H_{151}N$ (aromatic), $C_{95}H_{120}O_4$ (resin), and $C_{66}H_{80}S$ (asphaltene). Similarly, Ramezani and Rickgauer [49] built their four-component bitumen model by selecting each molecule from the 12-component molecular model recommended by Li and Greenfield [9].

(a) Four-component model I

(b) Four-component model II

(c) Four-component model III
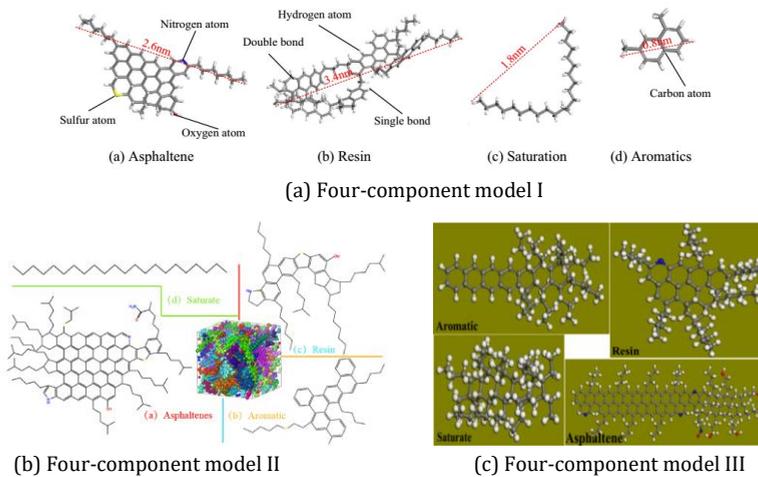
Figure 2.7 Molecular structure of each fraction in the four-component molecular model [20-22, 46-48]
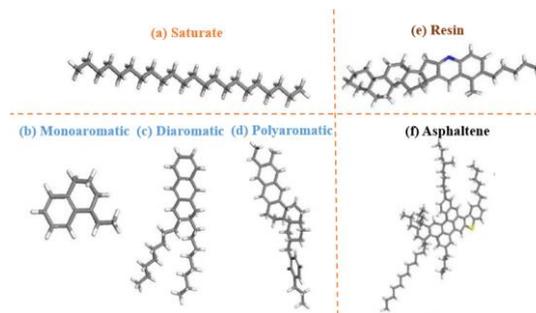
Figure 2.8 Molecular structure of each fraction in the six-component molecular model [13]

Based on the differences in molecular weight and aromaticity, Qu et al. subdivided the aromatic molecules into monoaromatic, diaromatic, and polyaromatic [13]. **Figure 2.8** illustrates their molecular structures, in which the n-docosane ($C_{22}H_{46}$) and 1,7-Dimethylnaphthalene ($C_{12}H_{15}$) refer to the saturate and monoaromatic molecules. Meanwhile, the Dioctyl-cyclohexane-naphthalene (DOCHN, $C_{30}H_{36}$) and Perhydrophenanthrene-naphthalene ($C_{35}H_{44}$) represent the diaromatic and polyaromatic molecules. In addition, the resin molecule is Quinolinohopane ($C_{34}H_{47}N$), and the asphaltene molecular formula is $C_{73}H_{100}S$.

It was reported that the predicted density and elastic modulus from MD simulation on the six-component model were closer to the experimental results than the 12-component model [40].

The twelve-component model proposed by Li and Greenfield [9] is the most popular for MD simulations on bitumen. The target bitumen was AAA-1, AAK-1, and AAM-1 from the Strategic Highway Research Program (SHRP). As displayed in **Figure 2.9**, the bitumen molecules are classified into four groups: saturates, naphthene aromatics, polar aromatics, and asphaltenes, and 2-5 molecules with different polarities and sizes are developed to represent these classes [10]. In detail, the squalene and hopane molecules are the saturate fraction, while the naphthene aromatics molecules are the perhydrophe-nanthrene-naphthalene (PHPN) and dioctyl-cyclohexane-naphthalene (DOCHN). Meanwhile, five molecules of quinolinohopane, pyridinohopane, thio-isorenieratane, trimethylbenzene-oxane, and benzobisbenzothiophene belong to the resin group. Three asphaltene molecules, named asphaltene-phenol, asphaltene-pyrrole, and asphaltene-thiophene were proposed by Mullins [50, 51]. The numbers of each molecule in three bitumen models were based on the solubility fractions and elemental compositions. After an MD simulation with an Optimized Potential for Liquids Simulation (OPLS) Forcefield, the predicted outputs in Hansen solubility parameters, density, thermal expansion coefficient, molecular rotational relaxation times, diffusion coefficients, and viscosity from the 12-component model agreed well with realistic values than the average and 3-component models. The predicted density of the 12-component model at 333K was 0.97 g/cm^3, closer to the experimental value of 1.03 g/cm^3 than the previous model (0.93 g/cm^3) [27].
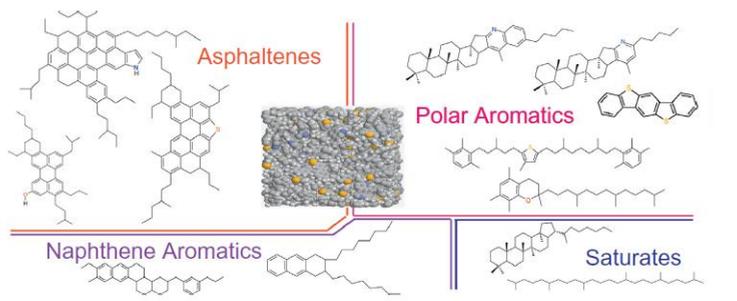
Figure 2.9 The molecular structures of each fraction in the twelve-component model [9]

2.2.2 MD models of aged bitumen

The organic molecules in bitumen are sensitive to oxidation during the pavement service life under the influence of temperature and the presence of oxygen. This oxidative aging of bitumen significantly affects the engineering properties of asphalt pavement, making the material more sensitive to low-temperature and fatigue cracking. Although it has been known that oxidative aging would form polar functional groups in bitumen, such as ketone and sulfoxide. However, the dynamic oxidation process and reaction products of each SARA fraction molecule are still unclear, which inhibits the establishment of the molecular structure of aged bitumen and investigation of aging influence on the thermodynamic properties from the nanoscale perspective.

Currently, a reaction molecular dynamic simulation (MD) method has been proposed to explore the chemical oxidation reaction of bitumen molecules and predict their potential reaction pathway. The atomistic-based chemo-physical forcefield environment ReaxFF was developed to solve the problem that the most common force field is only suitable for the system with no chemical reactions. The ReaxFF force field is based on the Density Functional Theory (DFT) [28, 52]. The interaction energy between different C-H-S-O atoms was calculated during the atomic-based MD simulation to determine the break and formation potential of old and new chemical bonds. Hence, the atomistic-level chemical oxidative kinetic characteristics and reaction pathway of bitumen molecules could be tracked, which is beneficial to explain the aging mechanism

and predict the chemical products of bitumen during the oxidation reaction. This section reviews previous studies using the reaction MD simulation in the oxidation reaction of bitumen molecules. **Table 2.3** lists the utilized molecular models of bitumen and simulation conditions in different studies, including the temperature and oxygen levels.

Table 2.3 The reactive MD simulation conditions in different studies

Bitumen model	Force field	Temperature	Oxygen level*	Ref
12-component AAA-1 bitumen model	ReaxFF force field	300, 400, 500, 600K	500 Molecular oxygen	[28]
		200, 300, 400, 500K	800 Atomic oxygen;	
		1200, 1400, 1600, 1800K	Molecular oxygen; Equivalent O_2 level of 0.25, 0.5, and 1*	[53]
3-component bitumen model		130°C	Molecular oxygen; One standard atmospheric pressure (1 ATM)	[54]
Average bitumen model				[55]

* The oxygen level is the ratio of the amount of oxygen to the amount of oxygen required to completely oxidize the bitumen molecules into CO_2, HO_2, SO_2, and NO_2.

(a)   (b)   (c)
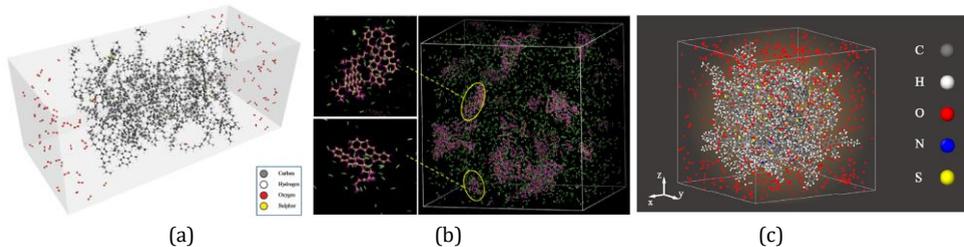
Figure 2.10 The oxygen-bitumen molecular models in reactive MD simulations
(a) [28], **(b)** [53], **(c)** [55]

Additionally, the simulation models in all studies were established by mixing the bitumen molecules and atomic or molecular oxygen, as shown in **Figure 2.10**. Under the interaction force, the oxygen molecule would approach and collide with the bitumen molecule. The potential energy is calculated with the ReaxFF force field to determine the break or formation of chemical bonds. Pan et al. [55] utilized the Reaction MD simulation and quantum chemistry theory to detect the oxidative aging of the saturate, resin, and asphaltene molecules as well as the average molecule of bitumen. The molecular models representing the different fractions of bitumen before and after oxidation aging are presented in **Figure 2.11**. The results revealed that the aromatic and asphaltene molecules were partially oxidized with sulfoxidation and ketonization, while the saturate molecule was quite resistant to oxidation. For these bitumen molecules, the saturated alkane chain would be separated into shorter chains, and sulfoxide formation was earlier than the carbonyl term [28]. Further, the ratio of sulfoxide to carbonyl functional groups depended on the sulfur dosage in bitumen.

The 12-component molecular model proposed by Li and Greenfield [9] (see **section 2.2.1**) has been validated to be more accurate than the previous three-component models, which will be used in this thesis. Based on the newly developed bitumen model, Yang [53] and Hu [28] applied the reaction MD simulation method to estimate the oxidative aging mechanism of the AAA-1 molecular bitumen for different simulation temperatures and oxygen content. Yang et al. [53] simulated the chemical reaction pathway between 12 types of bitumen molecules and aromatic or molecular oxygen, and the same finding could be observed that the ketones and sulfoxides were the main products of bitumen oxidation aging. It was also observed that atomic oxygen facilitated the cleavage of carbon-hydrogen bonds and the generation of hydroperoxides and

asphaltene polymerization. The ketones were more easily generated on the cyclic benzyl carbons than the branched ones.

Besides, the environmental temperature significantly affected the reaction thermodynamics and aging products of bitumen. When the temperature was lower than 300K, no reaction product could be observed, which was related to the fact that the collision possibility between reactant molecules was too low. The system energy was lower than the reaction activation energy. However, at the high temperature of 600K, the C-C, C-H, or C-S chemical bonds in bitumen molecules would be broken, and large amounts of harmful gases (such as SO_3, H_2O_2, CO, CO_2, and O_2) would be formed, and this is the pyrolysis and oxidative combustion of bitumen molecules.

Moreover, the sulfoxide groups were found to generate earlier than ketones because the sulfur atoms were easily connected with oxygen atoms and the stability of the S=O bond was high. In addition, the molecular or atomic oxygen was attached to the α-C atom to form the hydroperoxides, followed by the formation of sulfoxide and carbonyl functional groups. Hence, the hydroperoxides (C-O-O·) are the critical intermediate product to determine the occurrence of oxidative aging of bitumen molecules. The polymerization mechanism showed that it would occur when the aromatics and free radicals were formed by the "dehydrogenation" oxidation reactions to form asphaltenes [28].

(a)   (b)
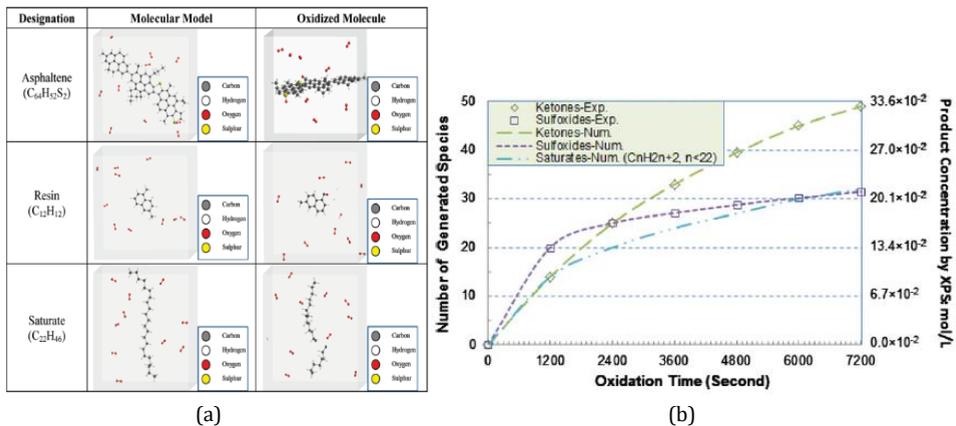
Figure 2.11 Molecular models of fractional bitumen molecules and average bitumen molecules before and after oxidative aging [55]
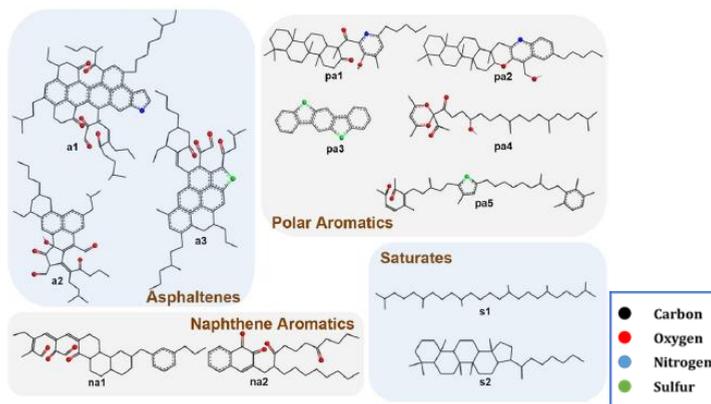
Figure 2.12 Representative molecular structures of the aged bitumen [28]

More recently, the influence of reaction temperature and oxygen level on the oxidative aging kinetics and pathway of AAA-1 bitumen molecules was studied by Hu et al. using reactive MD simulation with the ReaxFF [28]. During the oxidative reaction simulation, the yields of oxygen-containing functional groups in bitumen were accelerated as the increment in temperature and oxygen content. **Figure 2.12** illustrates the representative molecular structures of bitumen molecules after oxidative simulation. It was found that the aromatic rings decomposed, which resulted in the decreased aromaticity of aged bitumen. The reason is the high system temperature higher than 1200K, which allows the occurrence of ring-opening and condensation reactions. Although it was proved that the reactive MD simulation method was significantly effective in exploring the oxidative reaction process of bitumen molecules at the atomic scale, a few studies have been conducted. Hence, more work needs to be done to examine the oxidative aging mechanism and chemical products of bitumen, which could be beneficial to establishing molecular models of aged bitumen with different aging degrees. Meanwhile, more chemical characterization methods should be performed to validate the results from reactive MD simulations, such as the FTIR, GPC, NMR, XPS, and Elementary analysis [56].

2.2.3 MD simulations on aging influence on bitumen properties

Although many experimental methods could be employed to directly investigate the aging influence on the physical, rheological, and mechanical properties, they could not closely link the macroscale aging effects with the intrinsic molecular-level compositions and interaction changes. Additionally, the laboratory tests are time-consuming and depend on the availability of instruments, which significantly hinders the deep understanding of the aging behaviors of bitumen. As mentioned before, the MD simulation could potentially be used to predict the physical, thermodynamic, and mechanical properties of virgin and aged binders.
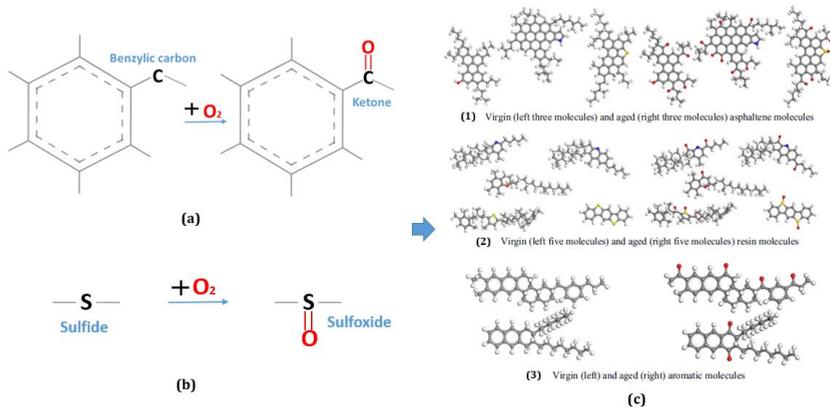
Figure 2.13 The formation of (a) ketone, (b) sulfoxide, and (c) SARA fractions in bitumen molecules during oxidative aging [23]
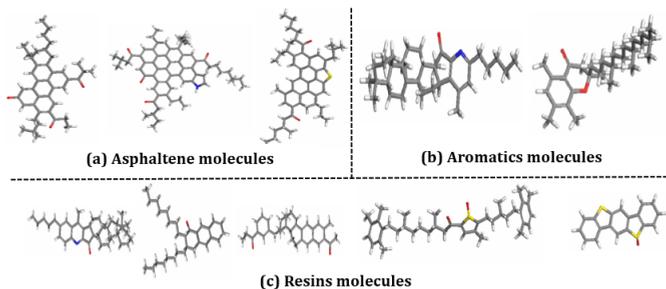
Figure 2.14 Molecular structures of SARA fractions for short-term aged bitumen [13]

Before the MD simulation runs, the most important issue is establishing an accurate molecular model of aged bitumen. Based on the aforementioned results from macroscale characterizations and microscale reactive MD simulation, it is believed that oxygen molecules would react with the benzyl carbon and sulfur atoms in bitumen molecules easily, and the main two functional groups (ketones and sulfoxides) are formed dramatically, which is illustrated in **Figure 2.13**. Hence, researchers established the representative oxidized molecular structure of SARA fractions of aged bitumen by fully creating the C=O and S=O at the potential benzyl carbon and sulfur positions in the molecular structure of virgin bitumen. **Figure 2.13(c)** lists the molecular structures of the 12-component bitumen model before and after aging. It is the common molecular model of an aged bitumen when the aging behavior is fundamentally studied through MD simulation [23]. However, this full-oxidized molecular model for aged bitumen does not consider the influence of aging degree on the molecular structures' variation of bitumen molecules. Hence, Qu et al. [13] tried to build the molecular structures of SARA fractions in short-term aged bitumen, in which the numbers of carbonyl and sulfoxide groups are between that in molecular molecules of virgin and full-oxidized bitumen models. The oxidized asphaltene, resin, and aromatic molecules for short-term aged bitumen are displayed in **Figure 2.14**.

Table 2.4 The input and output parameters of MD simulation in the aging effects of bitumen

Molecular models of SARA fractions in aged bitumen	Aided-Experimental tests	Selected force field	MD simulation output parameters
Fully-oxidized 12-component molecular model	SHRP AAA-1 bitumen model	DREIDING	Potential energy; Density; Bulk modulus (Isothermal compressibility); Viscosity; Compression and tension strength;
Fully-oxidized 12-component molecular model	SHRP AAA-1 bitumen model	COMPASSII	Density; Surface free energy; Viscosity; Cohesive energy density; Radial distribution functions; Mean square distance; Self-healing density; Diffusion coefficient; Energy ratio
Fully-oxidized 12-component molecular model	SHRP AAA-1 bitumen model	COMPASSII	Cohesive energy density; Glass transition temperature; Fractional free volume; Mean square distance; Adhesion energy; Energy ratio
Partial and fully-oxidized 12-component molecular model	Functional groups; SARA fractions	COMPASS	Density; Cohesive energy density; Surface free energy; Fractional free volume; Work of adhesion;
Fully-oxidized 12-component molecular model	SARA fractions; oxygen content	-	Density; Bulk modulus; Viscosity; Glass transition temperature

After determining the molecular structures of SARA fractions in virgin and aged bitumen, comparing different physical and thermodynamic properties of virgin and aged bitumen models could be conducted after the MD simulation. **Table 2.4** lists the detailed input parameters in various previous studies on the aging influence on the properties of bitumen, including the molecular models of aged bitumen utilized and the selected force field. Besides, the physical and thermodynamic properties obtained from MD simulation are also shown to investigate the difference in these properties between virgin and aged binders. Based on the MD simulation results, it was reported that the formation of polar oxidized functional groups (mainly C=O and S=O) would significantly increase the density, bulk modulus, and viscosity, which is related to the enhancement of intermolecular and intramolecular forces in aged bitumen. Hence, oxidative aging would increase the hardness and resistance to uniform compression or tension. Pan et al. found that the oxidized

bitumen was compressed and tensioned slower than virgin bitumen due to the stronger intermolecular bonds. Xu [23] and Luo [42] used the same molecular models of virgin and aged bitumen and the force field to evaluate the aging influence on the physical, thermodynamics, and interfacial adhesion properties of bitumen. It was revealed that the aged bitumen model exhibited higher cohesive energy density and glass transition temperature. At the same time, aging would deteriorate the surface free energy, mean square distance, self-healing rate, fractional free volume, and diffusion coefficient. It would be expected that the addition of polar functional groups enhanced the molecular interaction and accelerated the shrinkage of the bitumen system. The bitumen molecules' diffusion ability dropped because of the increased molecular size and the decreased free volume. However, limited work has studied the impact of aging degree on molecular-scale properties of bitumen, which will be investigated in this thesis considering the variable aging level of RA binders.

These conclusions were also obtained by Qu [13] and Farshad et al. [57], who established more accurate molecular models of virgin and aged binders with Rolling Thin Film Oven Test (RTFOT) and Pressure Aging Vessel (PAV) tests according to the experimental results of the functional groups, SARA fractions distribution, and oxygen dosage. Further, oxidative aging would significantly decrease the energy ratio and increase the moisture damage potential of the bitumen-aggregate system. Interestingly, although the surface free energy of aged bitumen was lower than virgin bitumen, Luo et al. [42] found the adhesion properties of aged bitumen were superior because the presence of polar groups would strengthen the bonding between bitumen and aggregates, which was the opposite to the results in a previous study [13]. The reason may be related to the different molecular models of aged bitumen utilized in MD simulation. Additionally, the adhesion strength of the bitumen-aggregate system was also affected by the aggregate type, bitumen composition, and moisture dosage.

2.3 MD simulations on bio-bitumen and rejuvenated bitumen

2.3.1 Bio-bitumen

To reduce the consumption of base bitumen and manufacture environmentally sound and sustainable binders, bio-bitumen is proposed by adding the bio-oils derived from the fast pyrolysis process of microalgae, waste wood, and swine manure. It has been verified that bio-oils could partially replace petroleum-based bitumen and restore and improve the rheological properties of oxidized bitumen [58-60]. The interaction mechanism between bio-oils and bitumen with MD simulations has been explored by using MD simulations. However, it is difficult to determine the exact molecular formula of bio-oil because of its complex components and different resource types.

(a) Molecular structure of cellulose   (b) Molecular structure of bio-oil   (c) Molecular structure of paraffin

(d) Molecular structures of the fatty acids (Linoleic acid, Palmitic acid, Oleic acid)
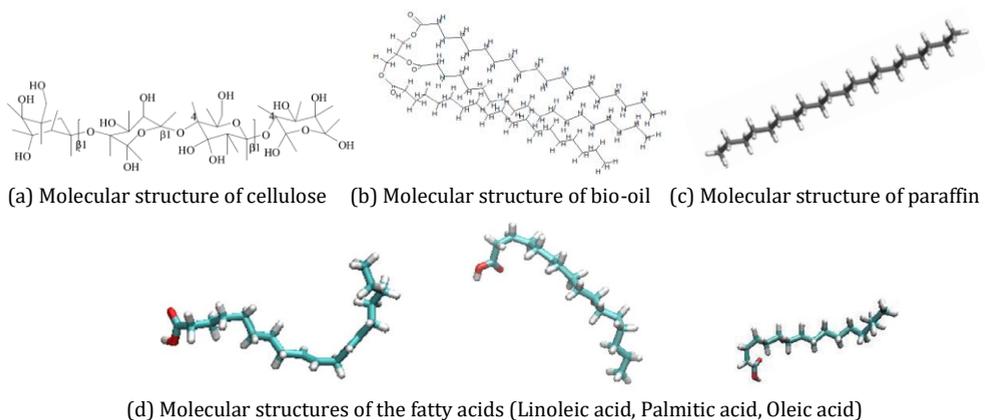
Figure 2.15 The representative molecular structures of bio-materials for bio-bitumen [58-61]

Several typical molecular structures of various bio-materials are summarized in **Figure 2.15**, such as cellulose(a), triglyceride(b), paraffin(c), and fatty acids(d). Although the molecular structures are different, the long-chain aliphatic hydrocarbons, carbonyl, ester, or amide groups are the main elements of bio-oil molecules. Hence, the molecular structures of bio-oils are similar to those of saturates, which would soften the bitumen and restore its rheological properties by changing the molecular interaction and colloidal structure of bitumen molecules.

The bio-oil effects on bitumen have been investigated using MD simulations to predict the thermodynamics and diffusion properties of bio-bitumen. Qu et al. [60] applied MD simulation (with COMPASS force field) to study the influence of bio-based waste cooking oil and paraffin (wax) molecules on the physical properties of bitumen. Compared to the virgin bitumen model, the bio-oil modified bitumen systems showed a lower density, surface free energy, and cohesive energy density, consistent with the low modulus and good fatigue resistance from experimental results. In addition, MD simulation results revealed that the addition of paraffin would deteriorate the stiffness and molecular mobility of bitumen, and that's why the wax adversely influenced the fatigue and low-temperature cracking resistance of the binder, and its dosage should be controlled.

Further, Sonibare et al. [58] established a representative molecular model of waste vegetable oil by mixing three types of fatty acids with the molar ratio of oleic acid to palmitic acid to linoleic acid as 7:6:2. The three-component molecular model of bitumen was utilized in this study. The structure, molecular interaction, and thermodynamic properties of vegetable oil modified bitumen were predicted based on the MD simulation trajectories with the OPLS-aa forcefield. Notably, the density, molecular diffusion behaviors, and thermal conductivity of vegetable oil molecular models were not dependent on the type of fatty acid. The reason may be related to the similar molecular structures of linoleic, palmitic, and oleic fatty acids when the incorporated vegetable oil molecules could enhance the density and relaxation of bitumen. Importantly, the influence of vegetable oil molecules on decreasing the viscosity of bitumen is significant at low temperatures, which converted to a negligible effect at high temperatures. Regarding the molecular structure, the fatty acid molecules could be uniformly distributed in bitumen and facilitate the molecular interactions between bitumen components. The dynamic mobility of bitumen was accelerated by adding vegetable oil molecules, which was attributed to its low molecular weight and high diffusion ability. Similar conclusions in terms of the dynamic properties of bio-bitumen were reported by Sun and Zhou [59]. They found that the diffusion coefficient of the bio-bitumen model improved with the increment in cellulose molecule content. The compatibility between bio-oil and saturate molecules was better than resin and asphaltene due to their similar chemical structures. Therefore, the bio-oil could be used as the saturate fraction of bitumen, which significantly strengthened the diffusion driving force and flexibility of bitumen. Additionally, no chemical reaction was observed while mixing waste wood bio-oil and bitumen. Due to the softening effect, the bio-oils are always used as rejuvenators to restore the colloidal structure and physio-rheological properties of aged bitumen by supplementing the light components. The rejuvenation function of bio-oil will be discussed in the following section. It could be speculated that the interaction mechanism of bio-oil should be the same, no matter the modification or rejuvenation cases. The only difference is the molecular variety of bitumen systems.

2.3.2 Rejuvenated bitumen

In addition to the loss of volatiles, aged bitumen is produced through the oxidation of bitumen molecules and the elevation of the heavy-to-light components ratio. This modification affects the molecular interaction and colloidal structure within the original bitumen systems. Theoretically, the oxidized molecules with large molecular weight in aged bitumen could be restored and transformed into the original bitumen molecules through deoxidization and deagglomeration [7, 36]. However, it is difficult for pavement engineers and researchers to realize the objective due to the high reaction energy [7]. Hence, most rejuvenation cases of aged bitumen are achieved by replenishing the light-weight oil fractions decreased during the aging process of bitumen, such as the saturates and aromatics.

According to previous experimental studies, different rejuvenators could be used to restore and improve the rheological and mechanical properties of aged bitumen, such as bio-oils (vegetable oils) [36, 58], paraffinic oil [61], naphthenic oil [33], and aromatic oil [61]. Although the rejuvenation effects depend on the rejuvenator type and dosage, it is expected that incorporating rejuvenators could improve the low-temperature cracking and fatigue resistance of aged bitumen. To understand the underlying rejuvenation mechanism and evaluate the rejuvenator effects on nanoscale properties of aged bitumen, molecular dynamic (MD) simulation technology has been proven to be effective [58-63]. However, it is challenging to determine the molecular models of different rejuvenators because most of them are composed of multiple types of molecules, especially those derived from petroleum-refining products. **Figure 2.16** lists the typical molecule models of rejuvenators. Considering the chemical characteristics of aromatic oil, naphthenic, and paraffinic oils, a single molecular formula $C_{12}H_{16}$ containing polar benzene ring, saturated naphthenic, and alkyl hydrocarbons is the common model used as the molecular structure of rejuvenator (see **Figure 2.16(a)**) [62]. The molecular structures of these actual rejuvenators will be determined in this thesis based on chemical characteristics.

As mentioned, the bio-oils are also an important rejuvenator, consisting of long-chain alkane, carbonyl, and ester functional groups. For instance, Shu et al. [63] established the molecular structure (shown in **Figure 2.16(b)**) of sunflower oil. The molecular structures of fatty acids discussed in a section on bio-bitumen were also applied to establish the molecular models of vegetable oil or waste cooking oil rejuvenated bitumen. Besides, other scholars found that the amide functional group also existed in rejuvenators. Xiao et al. [64] suggested the formula of $C_{13}H_{15}NO_3$ and $C_{11}H_{13}NO_2$ to represent the molecular structures of two rejuvenators used in their study. Meanwhile, the aromatic-based model with indole group (C_8H_9N) and alkyl-based model containing amide ($C_{16}H_{32}NO$) were built, which are shown in **Figures 2.16(c)** and **(d)**, respectively. From these molecular models, the polar aromatic cyclic and long-chain alkyl hydrocarbons are the main body of rejuvenator molecules, which connect with various polar functional groups, such as carbonyl, ester, indole, or amide. Thus, the hydrocarbon and functional group types should be the main components when building the molecular models of rejuvenators.

(a) $C_{12}H_{16}$ (b) $C_{10}H_{18}O_2$ (c) C_8H_9N (d) $C_{16}H_{32}NO$

(e) Saturate: $C_{15}H_{28}$ (Cyclic); $C_{14}H_{30}$ (Straight); Aromatic: $C_{15}H_{22}$ (Naphthene); $C_{11}H_{14}NO_2$ (Polar)
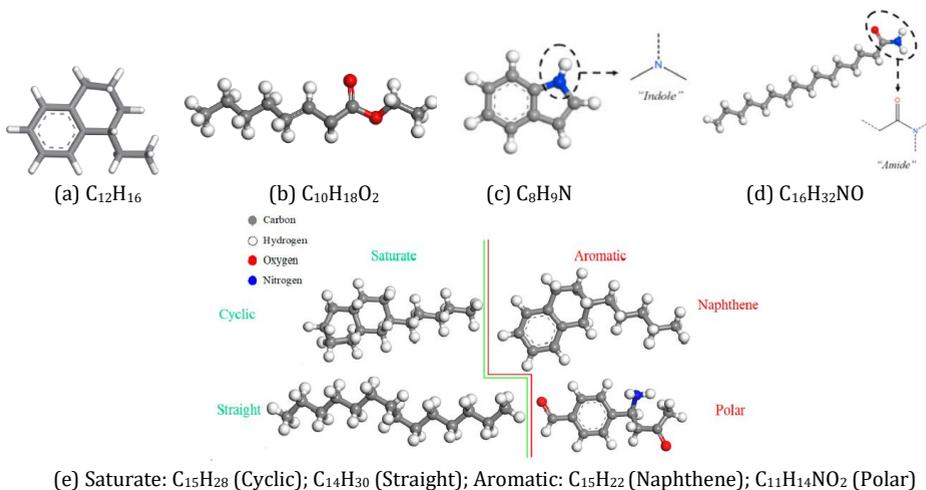
Figure 2.16 Typical molecular structures of rejuvenators [62-64]

Sun and Wang [65] divided the molecular structures of rejuvenators into four categories, cyclic saturates, straight saturates, naphthene aromatics, and polar aromatics. Their developed molecular models are displayed in **Figure 2.16(e)**. When establishing the rejuvenators' molecular structures, they concentrated on the types of main hydrocarbon bodies and functional groups. However, these four types of rejuvenator

molecules were proposed based on previous work without any experimental measurement for diffusion evaluation and comparison of different rejuvenators in aged bitumen. Hence, these molecular models should be further optimized to be close to the real rejuvenators based on their chemical properties.

Meanwhile, the rejuvenation mechanism of rejuvenated bitumen could be explained at the molecular and atomic scales using MD simulation. The combination of rejuvenation technology and MD simulation could be beneficial to designing effective rejuvenators of aged bitumen with different aging degrees and chemical properties. Cui et al. [62] conducted an MD simulation to investigate the impacts of rejuvenator ($C_{12}H_{16}$) dosage on restoring the thermodynamics, adhesion properties, and microstructure of aged bitumen considering the temperature and moisture factors with the classic 12-component bitumen model and COMPASSII forcefield. It showed that the rejuvenator molecules would improve the cracking resistance based on the increase of cohesion work while weakening the rutting resistance due to decreased modulus and viscosity of aged bitumen. Regarding the microstructure, the addition of a rejuvenator would hinder the self-agglomeration of asphaltenes and restore the colloidal structure to some extent, which could be fully close to that of virgin bitumen. Moreover, the moisture damage resistance of rejuvenated bitumen was better than aged bitumen. The temperature and moisture would also significantly affect the adhesion properties of bitumen on aggregates, which will be stated in the following bitumen-aggregate interfacial system. Yang et al. [66] studied the thermal-mechanical properties of bio-oil regenerated bitumen with a ternary rejuvenator model containing acetic acid, 1-carboxy-2-propanone, and methanol. The MD simulation demonstrated that incorporating bio-oil molecules could restore aged bitumen's thermal expansion coefficient, modulus, and ductility. However, the excessive bio-oil molecules would adversely influence the bitumen's high-temperature properties and thermal stability. Accurate representation of materials, be it bitumen or aged bitumen with rejuvenator, necessitates the inclusion of relevant molecules and force fields to capture essential characteristics. However, validation through laboratory tests remains the sole means of ensuring the model's representativeness.

The aged bitumen always presents higher viscosity due to the strong molecular interaction and low molecular mobility, which would lead to the inhomogeneity and high mixing temperature needed. The utilization of a rejuvenator aims to restore not only the thermodynamics and rheological properties of aged bitumen but also activate the diffusion ability of bitumen molecules. It is impossible to observe the function of the rejuvenator regarding increasing the dynamic nature of aged bitumen molecules for predicting the blending potential of rejuvenated bitumen. Hence, several researchers implemented MD simulations to capture the difference in diffusion behaviors between aged and rejuvenated binders. Xiao et al. [64] established the molecular models of rejuvenated binders to characterize the effects of rejuvenator type and bitumen aging degree on the actual movement of rejuvenators in aged binders. The simulation results of the mean square distance (MSD) and diffusion coefficient showed that rejuvenators diffused faster in long-term aged bitumen, which was also reported by Shu et al. [63] that the aging of bitumen would increase the diffusion rate of sunflower oil molecules in the bitumen model. Moreover, the sunflower oil diffusion process consisted of rapid contact and equilibrium diffusion stages. A similar MD simulation of rejuvenator diffusion in aged binders has also been performed by Xu et al. [67], and they found that apart from the thermal motion, the molecular interaction also contributed to the diffusion force between the rejuvenator and aged bitumen molecules. In conclusion, MD simulations offer the ability to anticipate and visualize the diffusion patterns of rejuvenators in aged bitumen at the molecular level, although the validation efforts remain relatively constrained. This thesis aims to investigate the diffusion capabilities of different rejuvenators by integrating MD simulation predictions with experimental validation.

The aforementioned studies all estimated the diffusion behaviors of rejuvenators and bitumen models in the molecular models of rejuvenated binders. Hence, the diffusion of a molecule results from its self-motion and molecular interaction. The concentration gradient has no driving force because the rejuvenated bitumen model is homogeneous. Thus, it is also called "self-diffusion". In practice, the rejuvenator is always incorporated into the reclaimed asphalt mixture (aged bitumen cover on aggregate), and the rejuvenator

diffuses into the aged bitumen gradually, which is influenced by mixing temperature, time, and intensity [68]. To observe and predict the diffusion process of rejuvenators in aged bitumen, the two-layer molecular model consisting of pure rejuvenator and aged bitumen layers was established. In addition, an MD simulation was run to measure the diffusion coefficient of rejuvenator molecules derived from a concentration gradient [69].

2.4 MD simulations on the diffusion of rejuvenator in aged bitumen

It is interesting to understand the transport/diffusion behaviors between rejuvenators and aged bitumen from the molecular-scale perspective for designing rejuvenators with high blending potential. The diffusion coefficient is the main parameter to evaluate the diffusion behaviors, but it is difficult to measure through the macroscale experimental tests [70]. The MD simulation has been proven to be an effective tool for measuring the diffusion coefficient index and observing the molecular-level diffusive process; thus, the diffusion coefficient values of different molecules in the multi-component substances are gauged.

Rejuvenators are incorporated to restore the physiochemical and mechanical properties of aged bitumen. Their ability to diffuse into the aged binder is a pre-requisite to guarantee their effectiveness and the homogeneity of rejuvenated bitumen. However, measuring the self-and-mutual diffusion parameters and observing the underlying interactive mechanism between the rejuvenators and bituminous materials is difficult. MD simulation can help researchers understand the diffusive behavior of rejuvenators in aged bitumen at the atomic level. **Figure 2.17** shows the self-diffusion **(I)** and inter-diffusion molecular models **(II-IV)** of rejuvenated bitumen systems, accompanied by the corresponding MD simulation results. The mixed rejuvenated bitumen model showed that the additional rejuvenator molecules could enhance the translational mobility of SARA fractions in bitumen [67]. Cui et al. also investigated the self-diffusion behavior of rejuvenator molecules in rejuvenated bitumen systems, considering the influence of temperature and rejuvenator dosage [62]. Compared to warm-mix temperatures, the self-diffusion coefficient of rejuvenators was 2-3 times larger at hot-mix temperatures, which was weakened as the rejuvenator dosage increased.

Most existing literature pays closer attention to the inter-diffusion characteristic of rejuvenators penetrating from the rejuvenator matrix to the bitumen layer. As shown in **Figure 2.17(II)**, Xu and Wang [67] first explored the inter-diffusion of rejuvenator molecules in a bi-layer rejuvenator-aged bitumen model with MD simulations and calculated the inter-diffusion coefficient of the rejuvenator based on the mass density profile in the z-direction, which agreed well with the experimental result. It was detected that the rejuvenator and bitumen molecules diffused mutually, and the diffusion rate of the rejuvenator was faster than bitumen molecules due to the smaller molecular size. It was proposed that the inter-diffusion process was related to not only the molecular parameters of both rejuvenator and bitumen molecules (molecular type and concentration) but also external environmental conditions (temperature and moisture dosage). Sun and Wang [65] developed bi-layered models to validate this hypothesis and compare the inter-diffusion coefficient of different rejuvenators into aged bitumen. The diffusion behavior of all rejuvenators followed Fick's second law and varied distinctly with various molecular structures of rejuvenators. The rejuvenator with polar aromatics showed the lowest inter-diffusion rate, while the naphthene aromatics showed the best. Additionally, the more oxygen-containing functional groups in long-term aged bitumen significantly hinder the diffusion of rejuvenators. Meanwhile, it was found that the diffusion driving force was affected by the molecular thermal motion and intermolecular force. Micro-voids in bituminous materials provided space conditions and promoted the diffusion capacity of rejuvenator molecules [71].

In practice, both bitumen and rejuvenator are incorporated into the RA mixtures to improve the aged binder's high-and-low temperature properties. A three-layered molecular model containing rejuvenator, virgin, and aged bitumen was proposed to investigate the influence of adding rejuvenator molecules on the inter-diffusion mobility between the new and aged binders (**Figure 2.17 IV**). The rejuvenator in the middle layer improved the diffusion speed of both fresh and aged bitumen molecules and increased their blending degree, which is more obvious at high temperatures. A similar conclusion was also reported by Ding et al. [72], who employed the rotational viscometer (RV), gel permeation chromatography (GPC), and MD

simulation methods to investigate the diffusion behavior between virgin and aged binders considering the rejuvenator effect. Moreover, in the process of inter-diffusion between pristine and aged bitumen, it was confirmed that the diffusion of large molecules within bitumen played a crucial role. Additionally, the diffusion coefficients of bitumen molecules were not solely determined by their diffusive capability but were also influenced by the characteristics of aged bitumen molecules, such as the free volume fraction and intermolecular interaction. Ding et al. [73] introduced and computed the volume diffusion coefficients for pristine-pristine, aged-aged, and bio-aged-aged bitumen layers. They concluded that the aging of bitumen binder resulted in a reduction in diffusion efficiency. The bio-rejuvenator was found to effectively restore the diffusive capability and dispersion of aged bitumen molecules. Although the diffusion coefficient parameters between rejuvenators and aged bitumen can be predicted, the validation work has not been done in previous work, and the investigation on coupling effects of rejuvenator type and aging degree of bitumen on diffusion behavior is limited.
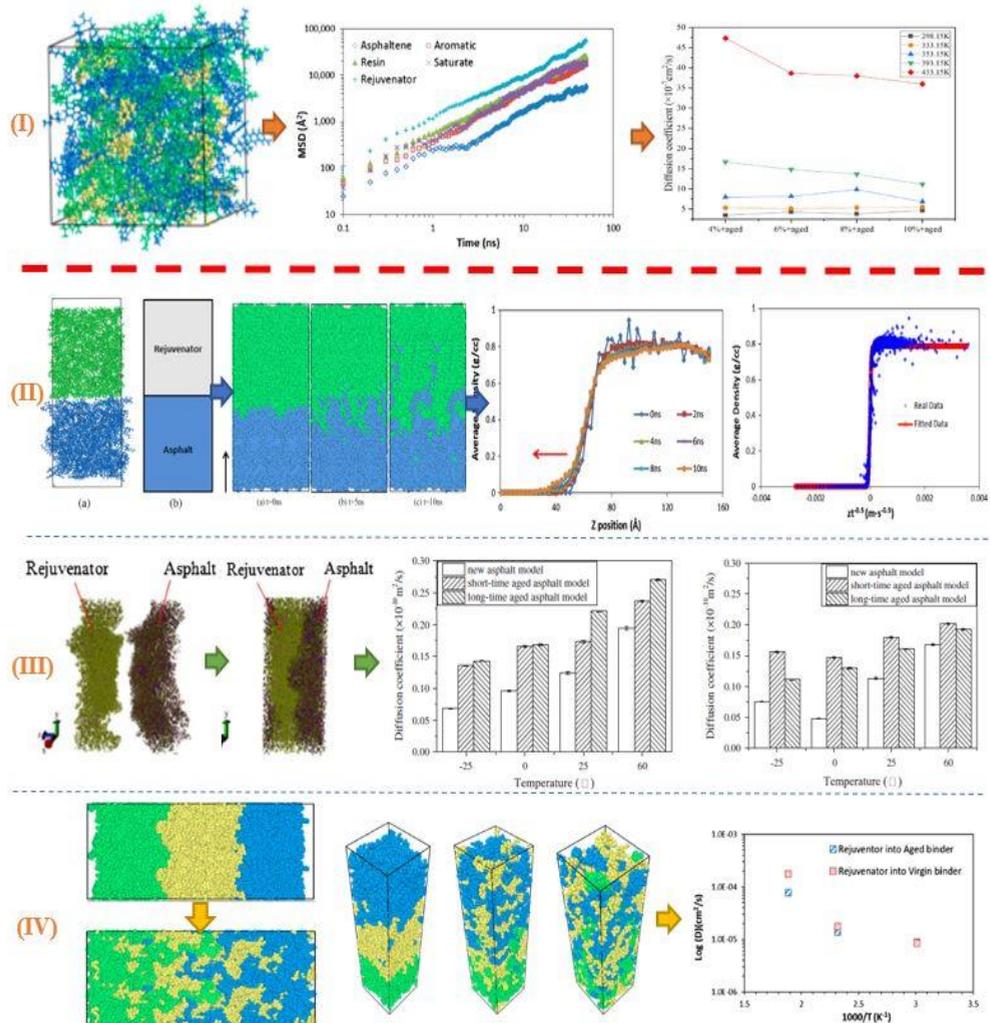
Figure 2.17 The diffusion behaviors of rejuvenators at the molecular level [65, 67, 71, 73]

2.5 Summary

This chapter summarizes the application cases of the molecular dynamics (MD) simulation method in the field of bituminous materials in bulk and dynamics systems. It can help us systematically understand the current functions of MD simulation and further develop its potential values in addressing the research issues in asphalt pavement engineering. The main conclusions are listed as follows:

- Different molecular models of bitumen have been developed, including the average, 3-component, 4-component, 6-component, and 12-component molecular models. Currently, the 12-component model is the most popular for its high accuracy.

- Although different forcefields are used during the MD simulation of bituminous materials, COMPASS (II) is the most commonly used. In addition, the general validation parameters contain the density, glass transition temperature, cohesive energy density, and solubility parameters. From MD simulations, different thermo-physical, thermo-dynamics, thermo-mechanical, and structural parameters of bitumen models can be predicted.

- MD simulation is an effective tool to investigate the influence of aging and rejuvenation on the molecular-scale properties of bituminous materials, as well as explain the underlying mechanism from the viewpoints of intermolecular interaction, molecular structure, and molecular mobility. However, it is still necessary to clear the molecular structures of aged bitumen, bio-oil, and rejuvenators to ensure the reliability of MD simulation outputs.

- The dynamic processes during the molecular diffusion phenomenon of bituminous materials can be visualized in MD simulations at an atomic level, and the corresponding diffusion coefficient parameters of rejuvenator and bitumen molecules can be predicted considering various influence factors of temperature, pressure, and humidity.

Based on this literature review, some points are recommended:

- Developing representative molecular models for virgin/aged bitumen and rejuvenators is crucial to enhance the logicality of MD simulation outcomes and facilitate validation. Instead of randomly selecting a generic model from past studies, it is essential to perform a series of chemical characterizations of bitumen before embarking on MD simulations.

- Although the basic parameters of density, glass transition temperature, and solubility parameter can be utilized to validate the reliability of MD simulation outcomes, more optimization and characterization work are required to explain and shorten the gaps between experimental values and MD simulation outputs.

- To study the effect of rejuvenation and design more efficacious rejuvenators for reclaimed asphalt pavements, the long-term aging reaction mechanism and their influence on the molecular structures of bitumen molecules should be further explored and used to establish a molecular model of aged bitumen.

- More validation work is required to verify the MD simulation outputs regarding the diffusion and compatibility prediction of rejuvenators in aged bitumen at variable temperatures and material components.

- The potential connections between the outputted parameters from MD simulations and macroscale properties from experiments should be further established, to reach the point where MD simulations play an important role in predicting the rheological and mechanical properties of bituminous materials without doing large amounts of laboratory tests.

2.6 References

[1] G. Chen, K. Huang, M. Miao, B. Feng, O.H. Campanella. Molecular dynamics simulation for mechanism elucidation of food processing and safety: state of the art. Comprehensive Reviews in Food Science and Food Safety. 2019, 18, 243-263.

[2] E.C. Neyts, P. Brault. Molecular dynamics simulations for plasma-surface interactions. Plasma Processes and Polymers. 2017, 14, 1600145.

[3] M. Seyyedattar, S. Zendehboudi, S. Butt. Invited review-Molecular dynamics simulations in reservoir analysis of offshore petroleum reserves: A systematic review of theory and applications. Earth-Science Reviews. 2019, 192, 194-213.

[4] M. Karplus, J.A. McCammon. Molecular dynamics simulations of biomolecules. Nature Structural Biology. 2002, 9, 9.

[5] J. Barrat, J. Baschnagel, A. Lyulin. Molecular dynamics simulations of glassy polymers. Soft Matter. 2010, 6, 3430-3446.

[6] Z. Chen, J. Pei, R. Li, F. Xiao. Performance characteristics of asphalt materials based on molecular dynamics simulation-A review. Construction and Building Materials. 2018, 189: 695-710.

[7] H. Yao, J. Liu, M. Xu, J. Ji, Q. Dai, Z. You. Discussion on molecular dynamics (MD) simulations of the asphalt materials. Advances in Colloid and Interface Science. 2021. https://doi.org/10.1016/j.cis.2021.102565

[8] L. Zhang, M.L. Greenfield. Analyzing properties of model asphalts using molecular simulation. Energy & Fuels. 2007, 21, 1712-1716.

[9] D.D. Li, M.L. Greenfield. Chemical compositions of improved model asphalt systems for molecular simulations. Fuel. 2014, 115, 347-356.

[10] D.D. Li, M.L. Greenfield. Viscosity, relaxation time, and dynamics within a model asphalt of larger molecules. The Journal of Chemical Physics. 2014, 140, 034507.

[11] K. Sonibare, L. Rathnayaka, L. Zhang. Comparison of CHARMM and OPLS-aa forcefield predictions for components in one model asphalt mixture. Construction and Building Materials. 2020, 236, 117577.

[12] Y. Feng, C. Yu, K. Hu, Y. Chen, Y. Liu, T. Zhang. A study of the microscopic interaction mechanism of styrene-butadiene-styrene modified asphalt based on density functional theory. Molecular Simulation. 2021, DOI: 10.1080/08927022.2021.1876874

[13] X. Qu, Q. Liu, M. Guo, D. Wang, M. Oeser. Study on the effect of aging on physical properties of asphalt binder from a microscale perspective. Construction and Building Materials. 2018, 187, 718-729.

[14] C. Bao, Y. Xu, C. Zheng, L. Nie, X. Yang. Rejuvenation effect evaluation and mechanism analysis of rejuvenators on aged asphalt using molecular simulation. Materials and Structures. 2022, 55:52.

[15] P. Wang, Z. Dong, Y. Tan, Z. Liu. Investigation the interactions of the saturate, aromatic, resin, and asphaltene four fractions in asphalt binders by molecular simulations. Energy & Fuels. 2015, 29, 112-121.

[16] M. Guo, Y. Huang, L. Wang, J. Yu, Y. Hou. Using atomic force microscopy and molecular dynamics simulation to investigate the asphalt micro properties. International Journal of Pavement Research and Technology. 2018, 11, 321-326.

[17] L. Zhu, X. Chen, R. Shi, H. Zhang, R. Han, X. Cheng, C. Zhou. Tetraphenylphenyl-modified damping additives for silicone rubber: Experimental and molecular simulation investigation. Materials and Design. 2021, 202, 109551.

[18] C. Yu, K. Hu, Q. Yang, Y. Chen. Multi-scale observation of oxidative aging on the enhancement of high-temperature property of SBS-modified asphalt. Construction and Building Materials. 2021, 313, 125478.

[19] M. Su, J. Zhou, J. Lu, W. Chen, H. Zhang. Using molecular dynamics and experiments to investigate the morphology and micro-structure of SBS modified asphalt binder. Materials Toady Communications. 2022, 30, 103082.

[20] X. Yu, J. Wang, J. Si, J. Mei, G. Ding, J. Li. Research on compatibility mechanism of biobased cold-mixed epoxy asphalt binder. Construction and Building Materials. 2020, 250, 118868.

[21] L. Wang, Y. Liu, L. Zhang. Micro/nanoscale study on the effect of aging on the performance of crumb rubber modified asphalt. Mathematical Problems in Engineering. 2020, 1924349.

[22] K. Hu, C. Yu, Q. Yang, Y. Chen, G. Chen, R. Ma. Multi-scale enhancement mechanisms of graphene oxide on styrene-butadiene-styrene modified asphalt: An exploration from molecular dynamics simulations. Materials & Design. 2021, 208, 109901.

[23] G. Xu, H. Wang. Molecular dynamics study of oxidative aging effect on asphalt binder properties. Fuel. 2017, 188, 1-10.

[24] Q. Qiu, J, Zhang, L. Yang, J. Zhang, B. Chen, C. Tang. Simulation of the diffusion behavior of water molecules in palm oil and mineral oil at different temperatures. Renewable Energy. 2021, 174, 909-917.

[25] H. Yao, Q. Dai, Z. You. Molecular dynamics simulation of physicochemical properties of the asphalt model. 2016, 164, 83-93.

[26] Y. Gao, Y. Zhang, C. Zhang, X. Liu, R. Jing. Quantifying oxygen diffusion in bitumen films using molecular dynamics simulations. Construction and Building Materials. 2022, 331, 127325.

[27] L. Zhang, M.L. Greenfield. Effects of polymer modification on properties and microstructure of model asphalt systems. Energy & Fuel. 2008, 22, 3363-3375.

[28] D. Hu, X. Gu, B. Cui, J. Pei, Q. Zhang. Modeling the oxidative aging kinetics and pathways of asphalt: a ReaxFF molecular dynamics study. Energy & Fuels. 2020, 34, 3601-3613.

[29] G. Li, M. Han, Y. Tan, A. Meng, J. Li, S. Li. Research on bitumen molecule aggregation based on coarse-grained molecular dynamics. Construction and Building Materials. 2020, 263, 120933.

[30] F. Nie, W. Jian, D. Lau. An atomistic study on the thermomechanical properties of graphene and functionalized graphene sheets modified asphalt. Carbon. 2021, 182, 615-627.

[31] L. You, T. Spyriouni, Q. Dai, Z. You, A. Khanal. Experimental and molecular dynamics simulation study on thermal, transport, and rheological properties of asphalt. Construction and Building Materials. 2020, 265, 120358.

[32] S. Ren, X. Liu, P. Lin, S. Erkens, Y. Xiao. Chemo-physical characterization and molecular dynamics simulation of long-term aging behaviors of bitumen. Construction and Building Materials. 2021, 302, 124437.

[33] S. Liu, X. Qi, L. Shan. Effect of molecular structure on low-temperature properties of bitumen based on molecular dynamics. Construction and Building Materials. 2022, 319, 126029.

[34] M. Li, Z. Min, Q. Wang, W. Huang, Z. Shi. Effect of epoxy resin content and conversion rate on the compatibility and component distribution of epoxy asphalt: A MD simulation study. Construction and Building Materials. 2022, 319, 126050.

[35] M. Wu, G. Xu, Y. Luan, Y. Zhu, T. Ma, W. Zhang. Molecular dynamics simulation on cohesion and adhesion properties of the emulsified cold recycled mixtures. Construction and Building Materials. 2022, 333, 127403.

[36] D. Hu, X. Gu, Q. Dong, L. Lyu, B. Cui, J. Pei. Investigating the bio-rejuvenator effects on aged asphalt through exploring molecular evolution and chemical transformation of asphalt components during oxidative aging and regeneration. Journal of Cleaner Production. 2021, 329, 129711.

[37] K. Shan, C. Bao, D. Li, C. Zheng. Microscopic analysis of the rejuvenation mechanism and rejuvenation effect of asphalt binders. Advances in Materials Science and Engineering. 2021, 1958968.

[38] Y. Ding, B. Huang, X. Shu. Investigation of functional group distribution of asphalt using liquid chromatgraphy transform and prediction of molecular model. Fuel. 2018, 227, 300-306.

[39] X. Zhou, X. Zhang, S. Xu, S. Wu, Q. Liu, Z. Fan. Evaluation of thermo-mechanical properties of graphene/carbon-nanotubes modified asphalt with molecular simulation. Molecular Simulation. 2017, 43(4), 312-319.

[40] X. Qu, Z. Fan, T. Li, B. Hong, Y. Zhang, J. Wei, D. Wang, M. Oeser. Understanding of asphalt chemistry based on the six-fraction method. Construction and Building Materials. 2021, 311, 125241.

[41] M. Su, C. Si, Z. Zhang, H. Zhang. Molecular dynamics study on influence of Nano-ZnO/SBS on physical properties and molecular structure of asphalt binder. Fuel. 2020, 263, 116777.

[42] L. Luo, L. Chu, T.F. Fwa. Molecular dynamics analysis of oxidative aging effects on thermodynamic and interfacial bonding properties of asphalt mixtures. Construction and Building Materials. 2021, 269, 121299.

[43] M. Xu, J. Yi, P. Qi, H. Wang, M. Marasteanu, D. Feng. Improved chemical system for molecular simulations of asphalt. Energy & Fuels. 2019, 33, 3187-3198.

[44] P. W. Jennings, J.A.S. Pribanic, M.A. Desando, M.F. Raub, S. Frederick, J. Hoberg. Binder characterization and evaluation by nuclear magnetic resonance spectroscopy. Report. 1993.

[45] A.T. Pauli, F.P. Miknis, A.G. Beemer, J.J. Miller. Assessment of physical property prediction based on asphalt average molecular structures. Preprints-American Chemistry Society. Division Petroleum Chemistry. 2005, 50, 255-259.

[46] L. Chu, L. Luo, T.F. Fwa. Effects of aggregate mineral surface anisotropy on asphalt-aggregate interfacial bonding using molecular dynamics (MD) simulation. Construction and Building Materials. 2019, 225, 1-12.

[47] M. Guo, Y. Tan, L. Wang, Y. Hou. Diffusion of asphaltene, resin, aromatic and saturate components of asphalt on mineral aggregates surface: molecular dynamics simulation. Road Materials and Pavement Design. 2017, 18(3), 149-158.

[48] X. Zhang, X. Zhou, W. Ji, F. Zhang, F. Otto. Characterizing the mechanical properties of Multi-layered CNTs reinforced SBS modified asphalt-binder. Construction and Building Materials. 2021, 296, 123658.

[49] M.G. Ramezani, J. Rickgauer. Understanding the adhesion properties of carbon nanotube, asphalt binder, and mineral aggregates at the nanoscale: a molecular dynamics study. Petroleum Science and Technology. 2020, 38(1): 28-

[50] O.C. Mullins. The modified Yen model. Energy & Fuels. 2010, 24, 2179-2207.

[51] O.C. Mullins, H. Sabbah, J. Eyssautier, A.E. Pomerantz, L. Barre, A.B. Andrews. Y. Ruiz-Morales, F. Mostowfi, R. McFarlane, L. Goual, R. Lepkowicz, T. Cooper, J. Orbulescu, R.M. Leblanc, J. Edwards, R.N. Zare. Advances in asphaltene science and the Yen-Mullins model. Energy & Fuels. 2012, 26, 3986-4003.

[52] L. Xue, Y. Shao, W. Zhong, H. Ben, K. Li. Molecular dynamic simulation on the oxidation process of coal tar pitch. Fuel. 2019, 242, 50-61.

[53] Y. Yang, Y. Wang, J. Cao, Z. Xu, Y. Li, Y. Liu. Reactive molecular dynamic investigation of the oxidative aging impact on asphalt. Construction and Building Materials. 2021, 279, 121298.

[54] R.A. Tarefder, I. Arisa. Molecular dynamic simulations for determining change in thermodynamic properties of asphaltene and resin because of aging. Energy & Fuels. 2011, 25, 2211-2222.

[55] J. Pan, R.A. Tarefder. Investigation of asphalt aging behaviour due to oxidation using molecular dynamics simulation. Molecular Simulation. 2016, 42(8), 667-678.

[56] T. Pan, Y. Lu, S. Lloyd. Quantum-chemistry study of asphalt oxidative aging: an XPS-aided analysis. Industrial & Engineering Chemistry Research. 2012, 51, 7957-7966.

[57] F. Fallah, F. Khabaz, Y.R. Kim, S.R. Kommidi, H.F. Haghshenas. Molecular dynamics modeling and simulation of bituminous binder chemical aging due to variation of oxidation level and saturate-aromatic-resin-asphaltene fraction. Fuel. 2019, 237, 71-80.

[58] K. Sonibare, G, Rucker, L. Zhang. Molecular dynamics simulation on vegetable oil modified model asphalt. Construction and Building Materials. 2021, 270, 121687.

[59] B. Sun, X. Zhou. Diffusion and rheological properties of asphalt modified by bio-oil regenerant derived from waste wood. Journal of Materials in Civil Engineering. 2018, 30(2), 04017274.

[60] X. Qu, Q. Liu, C. Wang, D. Wang, M. Oeser. Effect of co-production of renewable biomaterials on the performance of asphalt binder in macro and micro perspectives. Materials. 2018, 11, 244.

[61] X. Qu, D. Wang, Y. Hou, M. Oeser, L. Wang. Influence of paraffin on the microproperties of asphalt binder using MD simulation. Journal of Materials in Civil Engineering. 2018, 30(8), 04018191.

[62] B. Cui, X. Gu, D. Hu, Q. Dong. A multiphysics evaluation of the rejuvenator effects on aged asphalt using molecular dynamics simulations. Journal of Cleaner Production. 2020, 259, 120629.

[63] B. Shu, M. Zhou, T. Yang, Y. Li, Y. Ma, K. Liu, S. Bao, D.M. Barbieri, S. Wu. The properties of different healing agents considering the micro-self-healing process of asphalt with encapsulations. Materials. 2021, 14, 16.

[64] Y. Xiao, C. Li, M. Wan, X. Zhou, Y. Wang, S. Wu. Study of the diffusion of rejuvenators and its effect on aged bitumen binder. Applied Sciences. 2017, 7, 397.

[65] W. Sun, H. Wang. Molecular dynamics simulation of diffusion coefficients between different types of rejuvenator and aged asphalt binder. International Journal of Pavement Engineering. 2020, 21(8), 966-976.

[66] T. Yang, M. Chen, X. Zhou, J. Xie. Evaluation of thermal-mechanical properties of bio-oil regenerated aged asphalt. Materials. 2018, 11, 2224.

[67] G. Xu, H. Wang. Diffusion and interaction mechanism of rejuvenating agent with virgin and recycled asphalt binder: a molecular dynamics study. Molecular Simulation. 2018, 44(17), 1433-1443.

[68] J. Liu, Q. Liu, S. Wang, X. Zhang, C. Xiao, B. Yu. Molecular dynamics evaluation of activation mechanism of rejuvenator in reclaimed asphalt pavement (RAP) binder. Construction and Building Materials. 2021, 298,123898.

[69] M. Li, L. Liu, C. Xing, L. Liu, H. Wang. Influence of rejuvenator preheating temperature and recycled mixture's curing time on performance of hot recycled mixtures. Construction and Building Materials. 2021, 295, 123616.

[70] U. Muhlich, G. Pipintakos, C. Tsakalidis. Mechanism based diffusion-reaction modelling for predicting the influence of SARA composition and ageing stage on spurt completion time and diffusivity in bitumen. Construction and Building Materials. 2021, 267, 120592.

[71] M. Xu, J. Yi, D. Feng, Y. Huang. Diffusion characteristics of asphalt rejuvenators based on molecular dynamics simulation. International Journal of Pavement Engineering. 2019, 20(5), 615-627.

[72] Y. Ding, B. Huang, X. Shu, Y. Zhang, M.E. Woods. Use of molecular dynamics to investigate diffusion between virgin and aged asphalt binders. Fuel. 2016, 174, 267-273.

[73] H. Ding, H. Wang, X. Qu, A. Varveri, J. Gao, Z. You. Towards an understanding of diffusion mechanism of bio-rejuvenators in aged asphalt binder through molecular dynamics simulation. Journal of Cleaner Production. 2021, 126977.

3

Chemical characterization and molecular dynamics simulation of long-term aging behavior

The objective of this chapter is to establish a representative molecular model of aged bitumen for different long-term aging degrees based on several chemical characteristics. Molecular dynamics simulations were employed to estimate the thermodynamic parameter variations of bitumen during long-term aging. In addition, to predict the chemical component distribution (SARA fractions and functional groups) in long-term aged bitumen as a function of the aging time, two long-term aging kinetic models were developed to describe the evolutions of functional group distribution and SARA fraction composition of long-term aged bitumen.

3.1 Introduction

An asphalt pavement is exposed to a complex environment with changing atmospheric and loading conditions, causing the bitumen aging and making pavements more vulnerable to cracking and ravelling [1-3]. As such, aged pavements have a shorter service life under the same loading conditions, increasing the costs of maintenance [4]. Apart from external environmental factors, the aging process of bitumen constitutes an internal factor contributing to the decline in the performance of asphalt pavement [5, 6]. The rejuvenation technology was developed to restore and improve the chemo-rheological properties of aged bitumen by incorporating different light-weight bitumen-like fractions [7, 8]. However, there is no unified and effective method for rejuvenated bitumen evaluation because the chemical components and mechanical performance of bitumen in different RAP materials differ dramatically [9]. Furthermore, it was reported that the aging level of bitumen significantly affected the required rejuvenator type and dosage [10]. Therefore, before studying rejuvenation, it is necessary and meaningful to set up a reference framework for the aging of bitumen.

The aging behaviors of bitumen with mechanical measurements, microscale morphological analysis, and chemical and physical properties characterizations have been investigated [11, 12]. From the viewpoint of material components, the bitumen is composed of four-groups fractions in the line of the difference in molecular weight and polarity: Saturate (S), Aromatic (A), Resin (R), and Asphaltene (As) (named the SARA fractions). The aging reference frame is based on the following premises that these four fractions contributed to the colloidal structure of bitumen differently, and the asphaltene molecules acted as the colloidal core part dispersed in the maltene phase [13]. The ratio of SARA fractions significantly influenced the rheological and mechanical properties of bitumen [14]. During the aging process of bitumen, the lighter saturate and aromatic fractions decrease gradually, while the heavier resin and asphaltene components increase. At the same time, the asphaltene clusters in aged bitumen start to agglomerate due to the lower dispersion capacity of the maltene phase, related to the higher stiffness and viscosity of the bitumen [15]. In addition, the oxidation reaction of bitumen molecules was considered to be the main aging mechanism, leading to the formation of polar functional groups, such as carbonyl C=O and sulfoxide S=O chemical groups [16, 17]. To sum up, oxidative aging results in the ratio change of SARA compositions and microstructures of bitumen molecules, thus affecting the service life of asphalt pavements.

Currently, a multiscale way from the microscale to the macroscale to explore the effects of modification, aging, or rejuvenation on the properties of bitumen [18, 19] or bitumen-aggregate interfacial systems [20, 21] has attracted researchers' attention. Asphalt binders and mixtures are composed of many different types of molecules, and their macroscale performance is determined by their microstructure, thermodynamic behavior, and nanoscale molecular interaction [22]. Molecular dynamics (MD) simulations are an effective method to predict complex molecular systems' thermodynamic properties and interpret the experimental results from the viewpoints of molecular interactions and microstructures. Previous studies demonstrated that MD simulation was a useful supplementary technology to further insight into bituminous materials' modification and rejuvenation mechanisms [23-25]. Zhang et al. employed an MD simulation to verify the positive role of an anti-stripping agent in improving the cohesive, adhesive, and moisture damage resistance of bitumen and found that the improvement mechanism was due to the formation of hydrogen bonding between bitumen and anti-stripping agent molecules [26]. Su et al. investigated the effects of Nano-ZnO/SBS modifiers on the physical properties and molecular structures of bitumen through the MD simulation method. They clarified that nano-ZnO/SBS may alleviate the accumulation of strong polar components and reinforce the tightness of the asphalt molecular structure [27]. Besides, Cui et al. implemented the MD simulation to evaluate the rejuvenator effects on aged bitumen at the microscale level and concluded that the addition of a rejuvenator would not only be beneficial to improving the cracking and moisture resistance but also mitigating the self-aggregation of asphaltene molecules and restoring the colloidal structure of aged bitumen [28].

The MD simulation technology has been widely utilized to explore the aging mechanism and its influence on the molecular structures and thermodynamic properties of bitumen. Li and Greenfield proposed

the 12-component molecular model to represent the SARA fractions of bitumen, and the corresponding molecular model of virgin bitumen was utilized to predict its thermodynamic properties [29, 30]. Regarding the aging reaction mechanism, Hu et al. conducted a reactive MD simulation method to explore the potential oxidation reaction paths of bitumen molecules [31]. The results revealed that the aging oxidation accelerated the formation of polar functional groups, such as the ketones and sulfoxide groups. Yang et al. also observed these simulation results and mentioned that the sulfoxide was formed earlier than the ketone, and the high temperature and oxygen dosage would accelerate the formation of polar groups [32]. Liu et al. ran the MD simulation and validated the aging gradient along with the layer depth due to the oxygen concentration gradient in a bitumen layer [33]. Based on the chemical characteristics of the aging products and the basic 12-component molecular model of virgin bitumen, the molecular models of short-term and long-term aged bitumen were established to introduce oxygen atoms to form the polar carbonyl and sulfoxide groups, and the ratio of SARA molecules was modified following the SARA fractions obtained. The MD simulations could predict the aging effects on the thermodynamic properties and molecular structures of bitumen, indicating that aging would significantly increase the binder density, viscosity, modulus, and agglomeration potential of bitumen, which are associated with the strong molecular interactions between the additional polar molecules [34-36].

The chemical attributes in aged bitumen, such as functional groups and SARA fractions, serve as crucial inputs for creating molecular models that exhibit a strong correlation with the duration of aging. Regarding the kinetics model of bitumen aging, there were two periods with a declining fast-rate and a constant-rate. Jin et al. [37] recommended that the combined first-order, zero-order oxidation model was capable of modelling bitumen oxidation kinetics. Liu and Glover [38] utilized the combined model to study the oxidation kinetics of warm-mix asphalt and found that the warm-mix additives showed on great adverse effect on the oxidation kinetics of bitumen. Meanwhile, the oxygen diffusion model was also coupled with the reaction model of bitumen. Cui et al. [39] considered the process that oxygen molecules penetrated into the bitumen film and then reacted with the bitumen molecules to establish a diffusion-reaction balance oxidation model of bitumen. In the meantime, Zhang et al. developed new short-term and long-term aging models for bitumen binders to predict the viscosity of aged binders accurately [40, 41]. It should be mentioned that oxidation reaction models were mostly based on the functional group variation measured from the Fourier transform infrared (FTIR) spectroscopy results, such as the carbonyl and sulfoxide indices [42, 43]. The oxidation reactions between the oxygen and bitumen molecules include generating oxygen-containing functional groups and converting the chemical compositions (saturate S, aromatic A, resin R, and asphaltene A_s) [44]. The variation of SARA fractions during the aging process plays a vital role in determining aged bitumen's macroscale rheological and mechanical properties [44]. However, the oxidation reaction kinetics model of bitumen from the viewpoint of SARA fractions' conversion has not been studied yet, which obstructs the further understanding of the long-term aging mechanism of bitumen.

To study the effect of rejuvenators on the nano level, some research gaps regarding the application of MD simulation technology in the field of bituminous binders remain. For example, the commonly-used 12-component molecular models of SARA fractions for virgin bitumen do not consider the existence of the sulfoxide groups [44-46], while the formation of C=O and S=O groups was found to have a serious impact on the properties [16,17]. Moreover, the current molecular models for aged bitumen were established empirically, and the effects of long-term aging degree on the molecular structure and material composition have not been investigated systematically. To have a molecular frame work to assess the effectiveness of rejuvenators in the main body of this thesis, in this chapter MD models accounting for the aging of bitumen are developed. These will be validated experimentally for a limited number of conditions and used to study the rejuvenator effect.

3.2 Chapter objectives

This chapter aims to develop the molecular models of virgin and various aged bitumen stages according to their chemical characteristics for further MD simulations on rejuvenated bitumen systems. Meanwhile, the

long-term aging effects on the thermodynamic properties of bitumen will be understood. Lastly, the reaction kinetics models of functional groups and SARA fractions distribution in bitumen will be proposed to predict the chemical information for establishing aged bitumen models with variable long-term aging times.

To this end, the bitumen is firstly aged to various degrees: short-term aging (TFOT), long-term aging in standard (PAV), and extended PAV (40 and 80 hours, respectively). The chemical characteristics (SARA fractions, functional groups distribution, element compositions) of virgin and aged bitumen were measured. Secondly, the molecular models of the virgin and aged bitumen were built and validated through density tests. Afterward, the MD simulations were conducted on these models to predict and assess the influence of long-term aging on the thermodynamic properties of bitumen. Finally, the long-term aging reaction kinetics models for the chemical characteristics (functional groups and SARA fractions distribution) of bitumen were developed to provide basic data to establish the molecular models of long-term aged bitumen with different aging levels without continuously performing these chemical tests.

3.3 Materials and experimental methods

3.3.1 Virgin bitumen and its properties

This thesis uses a single PEN70/100 bitumen from Total Nederland N.V. as a reference bitumen material. The physical properties and chemical components of the bitumen are shown in **Table 3.1**.

Table 3.1 The physical properties and chemical components of PEN 70/100 virgin bitumen

Properties		Value	Test standard
25°C Penetration (0.1 mm)		91	ASTM D5 [47]
Softening point (°C)		48	ASTM D36 [48]
135°C Dynamic viscosity (Pa•s)		0.8	AASHTO T316 [49]
25°C Density (g/cm³)		1.017	EN 15326 [50]
60°C Density (g/cm³)		0.996	
	Saturate, S	3.6	ASTM D4124 [51]
Chemical	Aromatic, A	53.3	
fractions (wt%)	Resin, R	30.3	
	Asphaltene, As	12.8	
	Colloidal index, CII		
	Carbon, C	84.06	ASTM D7343 [52]
Element compositions	Hydrogen, H	10.91	
(wt%)	Oxygen, O	0.62	
	Sulfur, S	3.52	
	Nitrogen, N	0.9	
Complex shear modulus at 1.6 Hz & 60°C (kPa)		2.4	AASHTO M320 [53]
Phase angle at 1.6 Hz & 60°C (°)		84.5	

3.3.2 Preparation of long-term aged bitumen

To understand the aging influence on the chemical and thermodynamic properties of bitumen, the virgin bitumen was subjected to both short-term and long-term aging procedures with different aging durations. The short-term aged bitumen was prepared by using the thin film oven test (TFOT) at 163°C for 5 hours and transferred to the pressure aging vessel (PAV) device to manufacture the long-term aged binders under the temperature and pressure condition of 100°C and 2.1MPa. The long-term aging durations for the long-term aged bitumen were selected as 20, 40, and 80 hours considering the aging degrees of bitumen in reclaimed asphalt [54, 55]. For convenience, the virgin bitumen, short-term aged, and long-term aged bitumen binders for 20, 40, and 80 hours are abbreviated as the VB, SAB, LAB20, LAB40, and LAB80.

3.3.3 Chemical characterization methods

3.3.3.1 Thin-layer chromatography with flame ionization detection (TLC-FID)

In this thesis, the TLC-FID technology detected the SARA fractions distribution in virgin and aged bitumen (IP 469 2001). Firstly, a solution involving 0.1g bitumen and 10 ml toluene was manufactured and went through a silica chrome rod by three solvents: n-heptane, toluene/n-heptane (80:20), and dichloromethane/methanol (95:5). The saturate constituents were separated chromatographically in n-heptane, while the aromatic and resin were detached based on solubility difference in toluene/n-heptane and dichloromethane/methanol solvents. Lastly, the asphaltene components were the residual in the sampling spot. After the separation procedure, the chromatogram columns of the chrome rod were monitored using the FID device to determine the mass weight of SARA components in virgin and aged bitumen. See **section 3.4.1** for results.

3.3.3.2 Attenuated total reflectance-Fourier-transform infrared (ATR-FTIR) spectroscopy

The chemical functional group distributions in virgin and aged binders were measured using the ATR-FTIR spectrometer from the PerkinElmer with a single-point ATR fixture. The wavenumbers were set at the region of 600-4000 cm^{-1} to determine mostly increases in S=O and C=O. The bitumen sample was scanned 12 times with a fixed instrument resolution of 4 cm^{-1}. See **section 3.4.2** for results.

3.3.3.3 Elemental analysis

The aging effect on the element compositions of virgin and aged bitumen was estimated with an elemental analyser (Vario EL III, Elementar Corp., Germany). Before the test, the element distribution of the reference substance sulfanilamide was examined to calibrate the testing accuracy. A 5-10mg bitumen sample was put in tin capsules to measure the mass percentage of the carbon C, hydrogen H, oxygen O, nitrogen N, and sulfur S elements for all samples. See **section 3.4.3** for results.

3.4 Chemical characteristics of virgin and aged bitumen

3.4.1 Bitumen components

The mass weight values of the saturate, aromatic, resin, and asphaltene fractions in virgin and aged bitumen are displayed in **Figure 3.1(a)**. The total weight value of aromatic and resin fractions in virgin bitumen is larger than 80wt%, and the aging process has no obvious influence on saturate content in bitumen. The saturate molecule shows no heteroatom and has less reaction potential with oxygen molecules. Thus, the conversion ratio of saturate constitution in bitumen is still almost zero after 80h long-term aging. Meanwhile, as the aging degree increases, the aromatic dosage in bitumen declines dramatically. In contrast, the concentrations of both resin and asphaltene fractions increase gradually.

In addition, bitumen's aging level notably influences the mass weight of aromatic, resin, and asphaltene fractions. The aromatic dosage decreases by 1.7%, 9.4%, 14.5%, and 20.8% when the bitumen is subjected to short-term aging and long-term aging for 20, 40, and 80 hours, respectively (see **Figure 3.1(a)**). Hence, complementing aromatic composition is the main way during the rejuvenation process of aged bitumen. On the contrary, the asphaltene content rises by 1.8%, 5.8%, 7.9%, and 12.6%, respectively. The increment in asphaltene fraction could shorten the relative distance between asphaltene molecules and strengthen their molecular interactions, promoting the agglomeration level of asphaltene nanoparticles [56]. It is generally considered that bitumen exhibits a colloidal structure, where the asphaltene nanoparticle is regarded as the colloidal nucleus. Besides, the asphaltene molecules are surrounded by the resin fractions, playing a key role in stabilizing the colloidal structure and preventing an additional agglomeration of the asphaltene nucleus. **Figure 3.1(a)** illustrates that short-term aging seems to not influence the resin fractions in bitumen, while it enlarges distinctly as the long-term aging time. In detail, the mass weight of resin fraction in bitumen rises from 30.3% to 33.9%, 36.8%, and 38.4% when the long-term aging duration is 20, 40, and 80 hours,

respectively. In this thesis, the chemical fractions will be part of important input parameters for establishing molecular models of virgin and aged bitumen.
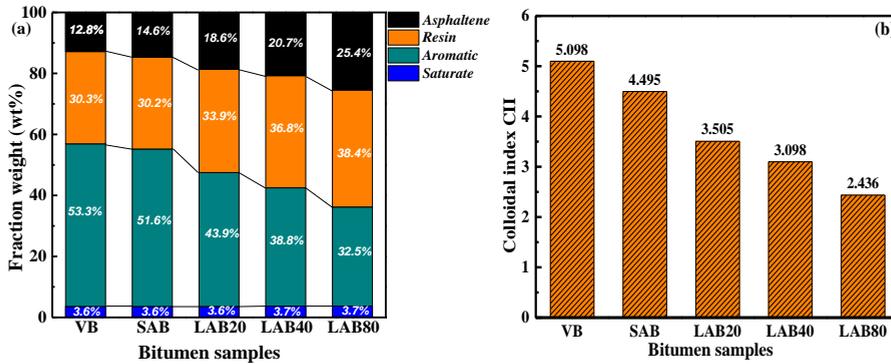
Figure 3.1 SARA fractions distribution (a) and colloidal index (b) of virgin and aged bitumen

The parameter of the colloidal index (CII) is normally utilized to evaluate the variation of the colloidal structure of bitumen, which is calculated as follows:

$$\text{Colloidal index CII} = \frac{R + A}{A_S + S} \tag{3.1}$$

where R, A, As, and S represent the mass fraction of resin, aromatic, asphaltene, and saturate, respectively.

The CII values of virgin and aged binders are demonstrated in **Figure 3.1(b)**, and the bitumen with a higher CII value exhibits a more stable colloidal structure. As the increment in aging degree, the colloidal index of bitumen markedly decreases and drops down to approximately half point when the long-term aging time is 80 h. Overall, the colloidal structure of bitumen tends to be more unstable during a long-term aging procedure.

3.4.2 Functional groups distribution

The FTIR spectra curves of virgin and aged bitumen samples are displayed in **Figure 3.2**. The main functional groups in bitumen are summarized in **Table 3.2**. Regarding the functional group distribution of fresh bitumen, the strong peak at 1030 cm^{-1} can be observed, indicating that the sulfoxide functional groups exist in the virgin bitumen. This finding will be considered while establishing a molecular model for virgin bitumen. Compared to virgin bitumen, aged bitumen presents strong absorption peaks at 1030 cm^{-1} and 1700 cm^{-1}, which refers to the sulfoxide and carbonyl functional groups.

To quantitatively assess the effect of long-term aging on the functional groups' distribution of bitumen, the carbonyl index (CI) and sulfoxide index (SI) is calculated as follows [14].

$$\text{Carbonyl index CI} = \frac{A_{1700}}{\sum A} \tag{3.2}$$

$$\text{Sulfoxide index SI} = \frac{A_{1030}}{\sum A} \tag{3.3}$$

$$\sum A = A_{(2952,2862)} + A_{1700} + A_{1600} + A_{1460} + A_{1375} + A_{1030} + A_{864} + A_{814} + A_{743} + A_{724} \tag{3.4}$$

where A_{1700} and A_{1030} refer to the area value of absorption peak at the wavenumber point of 1700 cm^{-1} and 1030 cm^{-1}, respectively. Besides, $\sum A$ represents the total area values of all absorption peaks.
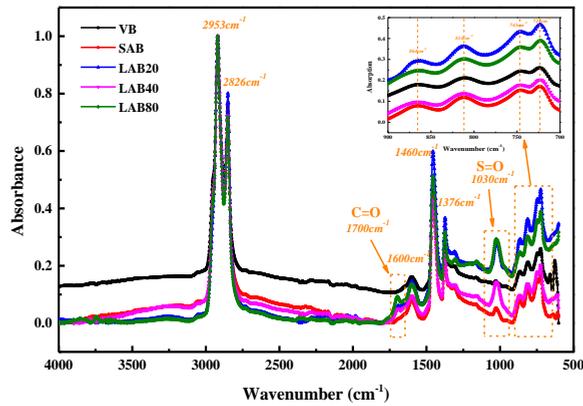
Figure 3.2 The detailed FTIR spectra of virgin and aged bitumen

Table 3.2 Main functional groups in virgin and aged bitumen [14]

Wavenumber (cm^{-1})	Chemical functional groups
2952 and 2862	Asymmetric and symmetric stretching vibrations of C-H on aliphatic hydrogen
1700	Stretching vibration of C=O group
1600	Stretching vibration of C=C on an aromatic ring
1460	Bending vibration of C-H on methylene
1375	Bending vibration of C-H on methyl
1030	Stretching vibration of S=O group
864, 814 and 743	Bending vibration of C-H on the substituents on aromatic rings (One, two, or three and four adjacent hydrogen atoms, respectively)
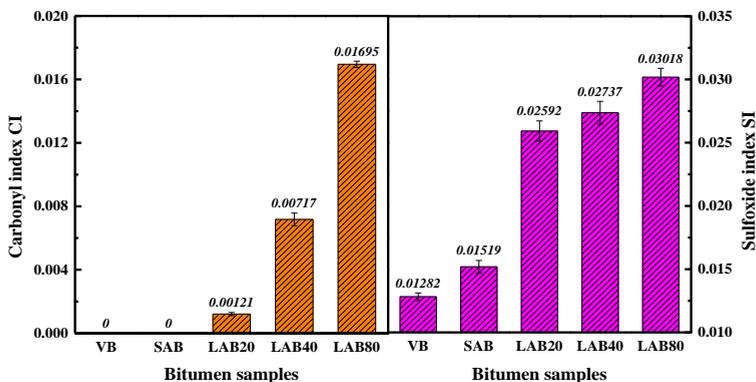
Figure 3.3 The carbonyl index CI and sulfoxide index SI of virgin and aged bitumen

The variations of carbonyl and sulfoxide indexes in virgin and aged bitumen with various aging conditions are shown in **Figure 3.3**. It is observed that no C=O is monitored in the fresh bitumen, denoting that the C=O is not sensitive to short-term aging. On the contrary, the S=O of virgin bitumen is detected and increases. It demonstrates that the S=O existing in the fresh bitumen should be considered in determining the molecular model of the virgin bitumen. Meanwhile, the sulfoxide index is invariably larger than the carbonyl index regardless of the aging degree, attributed to its characteristic of high sulfur concentration. This

assumption will be validated by elemental analysis results. Both carbonyl and sulfoxide index increase as the aging level deepens associated with the high possibility of oxidation and substitution reactions in bitumen molecules.

It is noticed that the sensitivity of CI and SI parameters to the aging time is significantly different. From **Figure 3.3**, the increasing rate of SI value is faster than CI during the short-term aging period. Moreover, the carbonyls start to form and increase during the long-term aging process. In other words, the sulfoxides are generated earlier than the carbonyls because the sulfur atom shows a higher reactivity than the bitumen carbon atom. On the contrary, carbonyl increment is continuous in a long-term aging stage, whereas the SI parameter stabilizes gradually due to the limitation of the sulfur amount in bitumen molecules. In conclusion, the sulfur oxidation reaction is easier than the carboxylation, which agrees with previous studies [14, 32].

The graphical illustration of the main oxidation reactions of a representative bitumen molecule is displayed in **Figure 3.4**, demonstrating the generation of C=O and S=O groups. Based on the chemical bonding theory, the bond energy of the sulfoxide group (522 kJ/mol) is lower than that of the carbonyl group (728 kJ/mol), so that explains why the formation of the S=O is easier than the C=O group.

On the other hand, from the viewpoint of electronic interaction theory, the sulfur atom exposes two long-pair electrons. In comparison, the carbon atom shows no long-pair electrons because all four electrons are occupied with forming the covalent bonds with the two adjacent hydrogen and carbon atoms. Thus, it is easy for the sulfur atoms to react with the oxygen molecules and form the peroxide radical, followed by creating the sulfoxide functional groups. That's why the S=O is easier to form than the C=O. This result is in line with the previous literature [14, 16, 32], which revealed that the sulfoxide formation would occur earlier than the ketone group. As a result, the aging behavior and mechanism are closely related to the chemical components of virgin bitumen, especially for the sulfur element concentration.
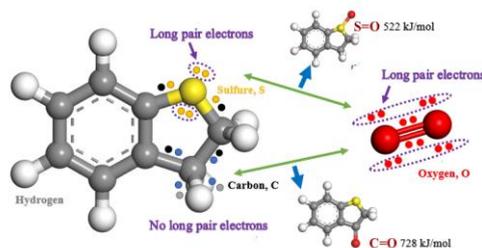
Figure 3.4 The graphical illustration of the main reaction during the aging of bitumen

3.4.3 Elemental analysis

The element compositions of virgin and aged bitumen are listed in **Table 3.3**. The carbon content (C%) is more than 80%. Furthermore, the hydrogen concentration H% is higher than 10% for all bitumen samples. Importantly, it should be mentioned that the sulfur dosage S% is about 3.5%, implying that the virgin bitumen selected in this thesis comes from a high-sulfur crude oil resource. This finding is consistent with the existence of a sulfoxide functional group in the fresh bitumen from FTIR results.

Table 3.3 The element compositions of virgin and aged bitumen

Bitumen samples	N (wt%)	C (wt%)	H (wt%)	S (wt%)	O (wt%)	H/C
VB	0.90	84.06	10.902	3.52	0.618	1.556
SAB	0.91	83.72	10.856	3.51	1.004	1.556
LAB20	0.92	83.26	10.748	3.49	1.582	1.549
LAB40	0.89	83.02	10.437	3.53	2.113	1.509
LAB80	0.91	82.14	10.098	3.54	3.312	1.475

Meanwhile, the aging of bitumen has no obvious influence on the nitrogen and sulfur concentration, significantly affecting the proportions of other elements (C, H, and O). With the increment in aging degree, the carbon and hydrogen element dosages reduce, while the oxygen concentration increases dramatically. It means that the oxidation degree of the binder deepens gradually as the aging time increases. To further assess the influence of aging on the molecular structure of bitumen, the ratio of H/C is calculated and shown in **Table 3.3**. Herein, the H/C value refers to the hydrogen atom number (N_H) ratio to carbon atom number (N_C), calculated as **Eq.3.5**.

$$\frac{H}{C} = \frac{N_H}{N_C} = \frac{\dfrac{H\%}{M_H}}{\dfrac{C\%}{M_C}} \tag{3.5}$$

where H% and C% are the mass fraction of hydrogen and carbon element in bitumen; and M_H and M_C represent the molar weight of C and H atoms, which are set as 1g/mol and 12g/mol, respectively.

The H/C ratio decreases remarkably with the increment in long-term aging time. Compared to virgin bitumen, the H/C ratio value reduces from 1.556 to 1.475. This phenomenon reveals that the aging of bitumen would strengthen the degree of unsaturation and aromaticity. On the one hand, during the aging of bitumen, light constituents (an aromatic fraction with low polarity) would transfer to the heavy components (resin and asphaltene fractions with high aromaticity). On the other hand, the oxidation reaction would result in the proportion enlargement of C=O and S=O groups, increasing the unsaturation degree. The FTIR results have validated the phenomena. Therefore, the aging mechanism of bitumen is composed of the synergistic effects of components transforming and oxidation reaction. These chemical characterization results provide the data support and theoretical basis for establishing the molecular models of virgin and aged binders.

3.5 Molecular dynamics simulations

3.5.1 Establishment of molecular model for virgin bitumen

In this chapter, the 12-component model established by Li and Greenfield [29] is adopted as the basis of molecular models for virgin and aged bitumen with different aging levels. As mentioned before, the S=O group exists in the selected bitumen. However, this characteristic was not considered during the establishment of the 12-component model. To accurately simulate the high-sulfur bitumen, one sulfoxide functional group is added to the molecular models of the resin fraction (Benzobisbenzothiophere and Thioisorenieratane). The detailed information on the sulfoxide functional group is illustrated in **Figure 3.5**. Meanwhile, the other ten molecular models of SARA fractions in the virgin bitumen remain the same as that in Greenfield's 12-component model.
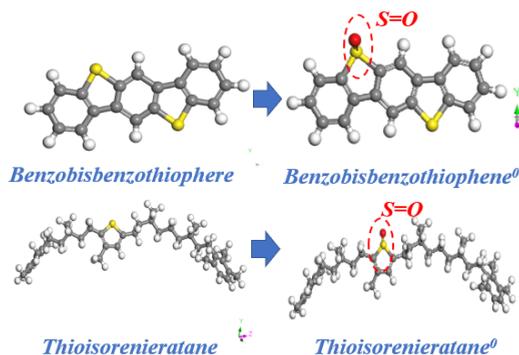
Figure 3.5 The generation of the S=O group in resin molecule models
Grey: Carbon; Yellow: Sulfur; White: Hydrogen; Red: Oxygen

The overall adopted molecular models of SARA fractions for the virgin bitumen in this thesis are shown in **Figure 3.6** shows. To distinguish the molecular models of SARA fractions in the fresh and aged binders with different aging levels, the superscript of "0" is remarked for each SARA molecule in virgin bitumen.
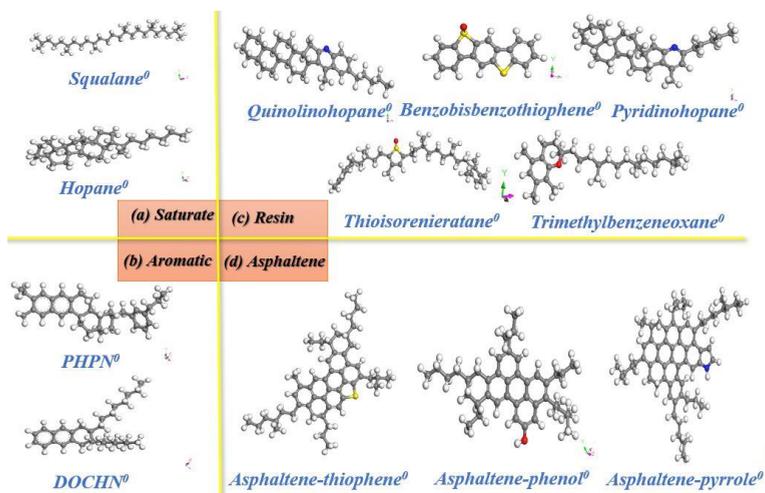
Figure 3.6 The molecule models of the SARA fractions for virgin bitumen
Grey: Carbon; Yellow: Sulfur; White: Hydrogen; Red: Oxygen; Blue: Nitrogen

3.5.2 Establishment of molecular models for various aged bitumen

3.5.2.1 Building aged molecule models

According to the FTIR and elemental analysis results presented in **Figure 3.3** and **Table 3.3**, it is noted that aging exhibits great effects on the functional groups and element components of bitumen. The oxidation aging of bitumen leads to an increment in C=O and S=O groups. Meanwhile, the amount of oxygen has an increasing trend with increased aging based on elemental analysis results. Previous studies [56, 57] also showed that ketone and sulfoxide are the two main products during the aging of bitumen. Researchers tried to attach the C=O and S=O groups to the molecular model of SARA fractions in virgin bitumen to form the corresponding molecular models for aged bitumen. However, in these aged bitumen models, the C=O and S=O groups were generated at all potential reaction positions of the original molecular structure without considering the influence of the long-term aging level [16, 36].

In this thesis, different amounts of oxygen atoms were introduced into molecule structures of the fresh aromatic, resin, and asphaltene fractions to build the molecular structures of aged bitumen. The formation of oxidized molecules of SARA fractions is shown in **Figure 3.7**, except for the saturate because it is insensitive to oxidation. Apart from the Benzobisbenzothiophene, Trimethylbenzeneoxane, and Thiophene molecules, each molecule shows two oxidized structures: a partial-oxidized one and a full-oxidized one. The superscripts of "1" and "2" distinguish the partial- and full-oxidized molecules. In addition, only one potential oxidation reaction point (the formation of S=O or C=O) exists in benzobisbenzothiophene and trimethylbenzeneoxane molecules, that's why they do not have a partially-oxidized molecule structure.

In a prior investigation [32], reactive MD simulations confirmed the early formation of S=O compared to C=O formation. This disparity is attributed to the oxygen atoms' greater affinity for sulfur atoms as opposed to carbon atoms. In the case of the thiophene molecule, the initial oxidation leads to the creation of S=O, followed by a gradual build-up of C=O groups. Differentiated oxidized thiophene molecules are denoted by subscripts ranging from "1" to "4," corresponding to varying degrees of oxidation aging.

(a) Virgin and oxidized aromatic molecules

(b) Virgin and oxidized resin molecules

(c) Virgin and oxidized asphaltene molecules
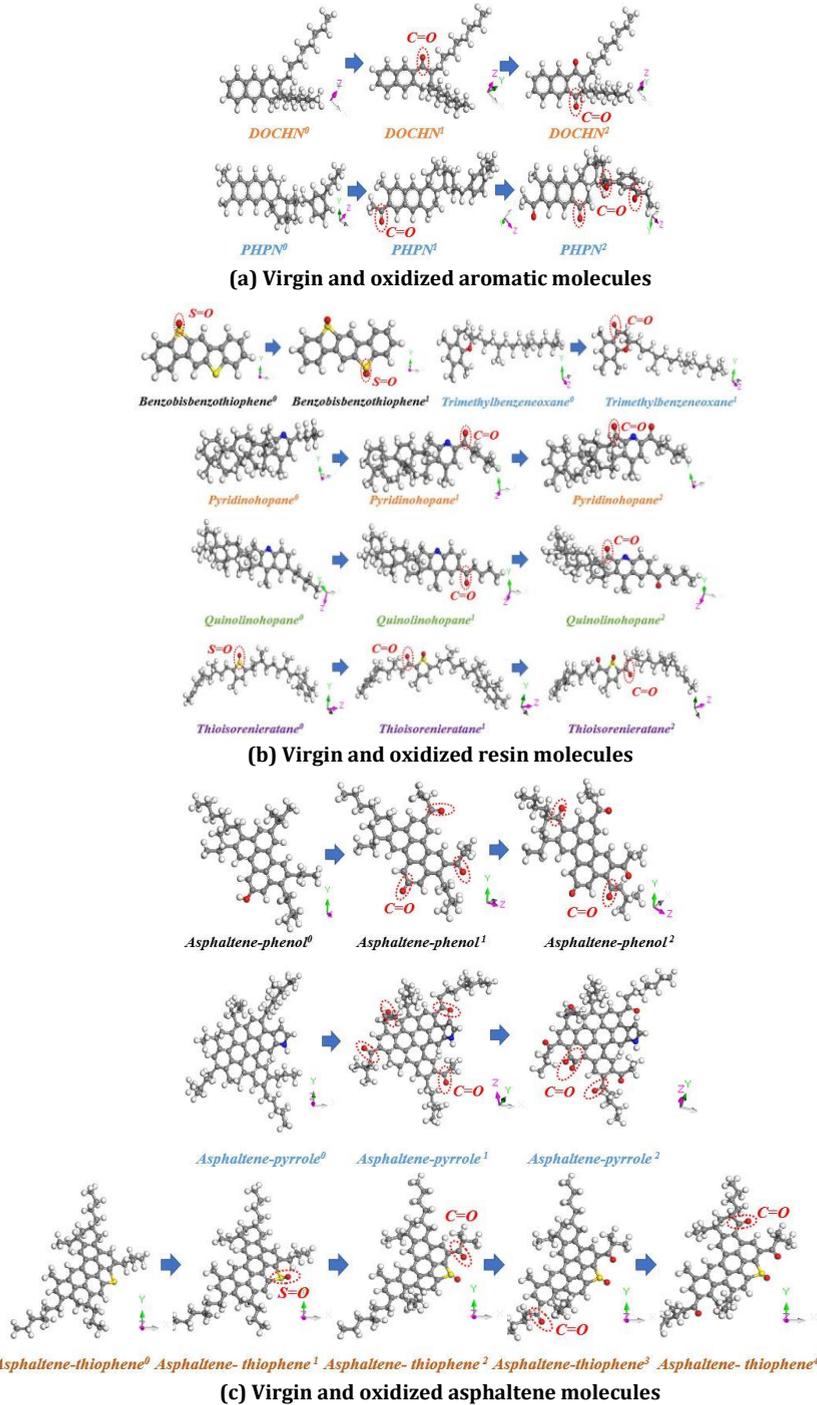
Figure 3.7 The virgin and oxidized molecules for aromatic (a), resin (b), and asphaltene (c)
Grey: Carbon; Yellow: Sulfur; White: Hydrogen; Red: Oxygen; Blue: Nitrogen
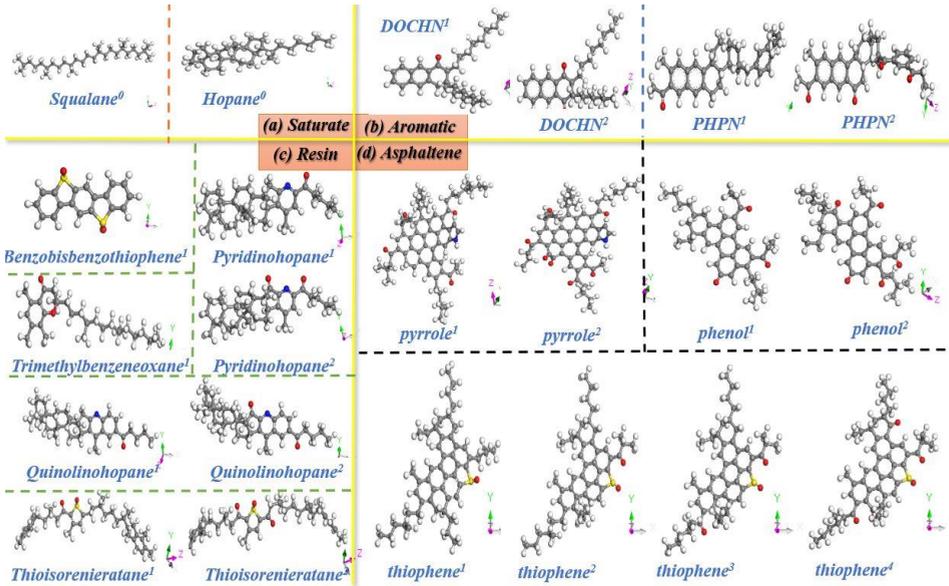
Figure 3.8 Twelve-component molecule models of SARA factions for aged bitumen
Grey: Carbon; Yellow: Sulfur; White: Hydrogen; Red: Oxygen; Blue: Nitrogen

All 12-component molecular models of SARA fractions in aged bitumen are summarized in **Figure 3.8**. **Table 3.4** lists the detailed molecular information of virgin and oxidized molecules for SARA fractions, including the molecular formula, molar mass, and the number of contained C=O and S=O groups. The construction of the fresh and aged molecular models of SARA fractions provides the essential elements for building the molecular models of the virgin and aged bitumen with variable aging levels.

Table 3.4 The molecular information on virgin and oxidized molecules of SARA fractions

Chemical fractions	Molecular structure	Chemical formula	Molar mass (g/mol)	Number of C=O	Number of S=O
Saturate	Squalane[0]	$C_{30}H_{62}$	422.9	0	0
	Hopane[0]	$C_{35}H_{62}$	483.0	0	0
Aromatic	PHPN[0]	$C_{35}H_{44}$	464.8	0	0
	PHPN[1]	$C_{35}H_{42}O$	478.8	1	0
	PHPN[2]	$C_{35}H_{36}O_4$	520.8	4	0
	DOCHN[0]	$C_{30}H_{46}$	406.8	0	0
	DOCHN[1]	$C_{30}H_{44}O$	420.8	1	0
	DOCHN[2]	$C_{30}H_{42}O_2$	434.8	2	0
Resin	Quinolinohopane[0]	$C_{40}H_{59}N$	554.0	0	0
	Quinolinohopane[1]	$C_{40}H_{57}NO$	568.1	1	0
	Quinolinohopane[2]	$C_{40}H_{55}NO_2$	582.0	2	0
	Thioisorenieratane[0]	$C_{40}H_{60}SO$	589.1	0	1
	Thioisorenieratane[1]	$C_{40}H_{58}SO_2$	603.1	1	1
	Thioisorenieratane[2]	$C_{40}H_{56}SO_3$	617.1	2	1
	Benzobisbenzothiophene[0]	$C_{18}H_{10}S_2O$	306.4	0	1
	Benzobisbenzothiophene[1]	$C_{18}H_{10}S_2O_2$	322.4	0	2

Pyridinohopane[0]	$C_{36}H_{57}N$	503.9	0	0
Pyridinohopane[1]	$C_{36}H_{55}NO$	517.9	1	0
Pyridinohopane[2]	$C_{36}H_{53}NO_2$	531.9	2	0
Trimethylbenzeneoxane[0]	$C_{29}H_{50}O$	414.8	0	0
Trimethylbenzeneoxane[1]	$C_{29}H_{48}O_2$	428.8	1	0
Asphaltene-phenol[0]	$C_{42}H_{54}O$	575.0	0	0
Asphaltene-phenol[1]	$C_{42}H_{48}O_4$	617.0	3	0
Asphaltene-phenol[2]	$C_{42}H_{44}O_6$	645.0	5	0
Asphaltene-pyrrole[0]	$C_{66}H_{81}N$	888.5	0	0
Asphaltene-pyrrole[1]	$C_{66}H_{73}NO_4$	944.5	4	0
Asphaltene-pyrrole[2]	$C_{66}H_{67}NO_7$	986.5	7	0
Asphaltene-thiophene[0]	$C_{51}H_{62}S$	707.2	0	0
Asphaltene-thiophene[1]	$C_{51}H_{62}SO$	723.2	0	1
Asphaltene-thiophene[2]	$C_{51}H_{60}SO_2$	737.2	1	1
Asphaltene-thiophene[3]	$C_{51}H_{58}SO_3$	751.2	2	1
Asphaltene-thiophene[4]	$C_{51}H_{54}SO_5$	779.2	4	1

(The "Asphaltene" row label spans the asphaltene block on the left side.)

3.5.2.2 Initial verification of the aged bitumen models

The aging behavior not only influences the molecular structures but also dramatically affects the proportion of the bitumen's chemical components. Due to the formation of polar functional groups and free radicals, the aromatic fractions transform into the resin and asphaltene components. The variation in material compositions would markedly result in a change in the physical and rheological properties of bitumen [56]. In this chapter, when the virgin and oxidized molecular structures of SARA fractions are determined, the molecular models of virgin and binders in different stages of aging can be constructed based on the chemical compositions found from the SARA analysis results. The detailed SARA fractions constitution in the molecular models of the virgin, short-term aged, as well as 20, 40, and 80h long-term aged bitumen, are summarized in **Tables 3.5-3.9**, respectively. The SARA fractions in molecular models of virgin and aged bitumen agree well with the experimental results.

Table 3.5 The SARA fractions in a molecular model of virgin bitumen

Chemical fractions	Molecular structure	Chemical formula	Molecule number	Fraction weight (in the model)	Fraction weight (in bitumen)
Saturate	Squalane[0]	$C_{30}H_{62}$	2	3.9wt%	3.60wt%
	Hopane[0]	$C_{35}H_{62}$	1		
Aromatic	PHPN[0]	$C_{35}H_{44}$	20	52.33wt%	53.30wt%
	DOCHN[0]	$C_{30}H_{46}$	21		
Resin	Quinolinohopane[0]	$C_{40}H_{59}N$	3	31.04wt%	30.30wt%
	Thioisorenieratane[0]	$C_{40}H_{60}SO$	3		
	Benzobisbenzothiophene[0]	$C_{18}H_{10}S_2O$	13		
	Pyridinohopane[0]	$C_{36}H_{57}N$	3		
	Trimethylbenzeneoxane[0]	$C_{29}H_{50}O$	4		
Asphaltene	Asphaltene-phenol[0]	$C_{42}H_{54}O$	2	12.73wt%	12.80wt%
	Asphaltene-pyrrole[0]	$C_{66}H_{81}N$	2		
	Asphaltene-thiophene[0]	$C_{51}H_{62}S$	2		

Table 3.6 The SARA fractions in a molecular model of short-term aged bitumen

Chemical fractions	Molecular structure	Chemical formula	Molecule number	Fraction weight (in the model)	Fraction weight (in bitumen)
Saturate	Squalane[0]	$C_{30}H_{62}$	2	3.86wt%	3.60wt%
	Hopane[0]	$C_{35}H_{62}$	1		
Aromatic	PHPN[0]	$C_{35}H_{44}$	20	50.60wt%	51.60wt%
	DOCHN[0]	$C_{30}H_{46}$	20		
Resin	Quinolinohopane[0]	$C_{40}H_{59}N$	3	30.73wt%	30.20wt%
	Thioisorenieratane[0]	$C_{40}H_{60}SO$	3		
	Benzobisbenzothiophene[0]	$C_{18}H_{10}S_2O$	13		
	Pyridinohopane[0]	$C_{36}H_{57}N$	3		
	Trimethylbenzeneoxane[0]	$C_{29}H_{50}O$	4		
Asphaltene	Asphaltene-phenol[0]	$C_{42}H_{54}O$	2	14.80wt%	14.60wt%
	Asphaltene-pyrrole[0]	$C_{66}H_{81}N$	2		
	Asphaltene-thiophene[1]	$C_{51}H_{62}SO$	3		

Table 3.7 The SARA fractions in a molecular model of 20h long-term aged bitumen

Chemical fractions	Molecular structure	Chemical formula	Molecule number	Fraction weight (in the model)	Fraction weight (in bitumen)
Saturate	Squalane[0]	$C_{30}H_{62}$	2	3.78wt%	3.60wt%
	Hopane[0]	$C_{35}H_{62}$	1		
Aromatic	PHPN[0]	$C_{35}H_{44}$	12	43.67wt%	43.90wt%
	PHPN[1]	$C_{35}H_{42}O$	6		
	DOCHN[0]	$C_{30}H_{46}$	17		
Resin	Quinolinohopane[0]	$C_{40}H_{59}N$	4	33.79wt%	33.90wt%
	Thioisorenieratane[1]	$C_{40}H_{58}SO_2$	3		
	Benzobisbenzothiophene[1]	$C_{18}H_{10}S_2O_2$	13		
	Pyridinohopane[0]	$C_{36}H_{57}N$	4		
	Trimethylbenzeneoxane[0]	$C_{29}H_{50}O$	4		
Asphaltene	Asphaltene-phenol[0]	$C_{42}H_{54}O$	3	18.76wt%	18.60wt%
	Asphaltene-pyrrole[0]	$C_{66}H_{81}N$	3		
	Asphaltene-thiophene[2]	$C_{51}H_{60}SO_2$	3		

Table 3.8 The SARA fractions in a molecular model of 40h long-term aged bitumen

Chemical fractions	Molecular structure	Chemical formula	Molecule number	Fraction weight (in the model)	Fraction weight (in bitumen)
Saturate	Squalane[0]	$C_{30}H_{62}$	2	3.68wt%	3.70wt%
	Hopane[0]	$C_{35}H_{62}$	1		
Aromatic	PHPN[1]	$C_{35}H_{42}O$	15	38.54wt%	38.80wt%
	DOCHN[1]	$C_{30}H_{44}O$	16		
Resin	Quinolinohopane[1]	$C_{40}H_{57}NO$	5	36.86wt%	36.80wt%
	Thioisorenieratane[1]	$C_{40}H_{58}SO_2$	3		
	Benzobisbenzothiophene[1]	$C_{18}H_{10}S_2O_2$	14		
	Pyridinohopane[1]	$C_{36}H_{55}NO$	4		
	Trimethylbenzeneoxane[0]	$C_{29}H_{50}O$	5		

	Asphaltene-phenol[1]	$C_{42}H_{48}O_4$	4		
Asphaltene	Asphaltene-pyrrole[1]	$C_{66}H_{73}NO_4$	3	20.92wt%	20.70wt%
	Asphaltene-thiophene[3]	$C_{51}H_{58}SO_3$	3		

Table 3.9 The SARA fractions in a molecular model of 80h long-term aged bitumen

Chemical fractions	Molecular structure	Chemical formula	Molecule number	Fraction weight (in the model)	Fraction weight (in bitumen)
Saturate	Squalane[0]	$C_{30}H_{62}$	2	3.48wt%	3.70wt%
	Hopane[0]	$C_{35}H_{62}$	1		
Aromatic	PHPN[2]	$C_{35}H_{36}O_4$	13	32.50wt%	32.50wt%
	DOCHN[2]	$C_{30}H_{42}O_2$	13		
Resin	Quinolinohopane[2]	$C_{40}H_{55}NO_2$	5	38.79wt%	38.40wt%
	Thioisorenieratane[2]	$C_{40}H_{56}SO_3$	3		
	Benzobisbenzothiophene[1]	$C_{18}H_{10}S_2O_2$	15		
	Pyridinohopane[2]	$C_{36}H_{53}NO_2$	5		
	Trimethylbenzeneoxane[1]	$C_{29}H_{48}O_2$	6		
Asphaltene	Asphaltene-phenol[2]	$C_{42}H_{44}O_6$	4	25.23wt%	25.40wt%
	Asphaltene-pyrrole[2]	$C_{66}H_{67}NO_7$	4		
	Asphaltene-thiophene[4]	$C_{51}H_{54}SO_5$	4		
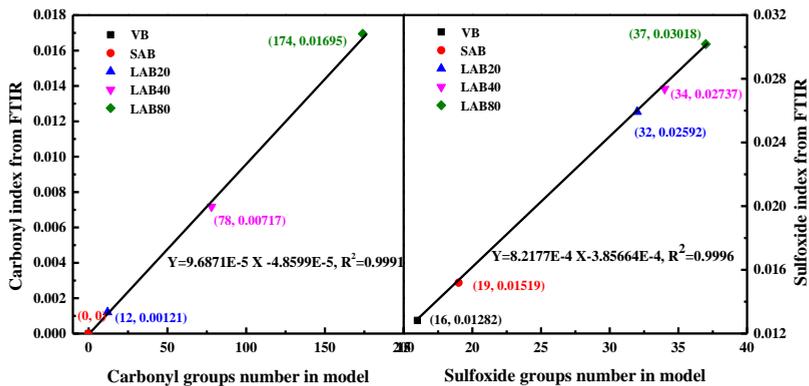
Figure 3.9 The correlations between functional group numbers in the MD model and FTIR results

Furthermore, the number of ketone and sulfoxide functional groups in the MD simulation systems is calculated to verify the model rationality of virgin and aged binders, demonstrated in **Figure 3.9**. Notably, for all bitumen systems, there are linear relationships between the number of C=O and S=O groups in molecular models and measured values from FTIR tests. It is expected that the change rate of ketone and sulfoxide functional groups from the MD simulation models should be the same as those measured values. However, the FTIR test results only provide the related intensity of the specific peaks, and it is difficult to figure out the exact number of functional groups. Hence, the numbers of ketone and sulfoxide in simulation models of aged binders are determined based on the C=O and S=O ratio to fresh bitumen. That's why the slope values of the correlation equations between the ketone or sulfoxide number in the MD simulation model and carbonyl or sulfoxide indices from FTIR (**Figure 3.9**) are not equal to 1.0. Using this linear correlation between the models and FTIR test results, the number of polar functional groups in the molecular models of aged bitumen with an unknown aging degree could be determined.

3.5.3 MD simulation protocols

The molecular dynamics simulation procedure for an initial condition contains two stages: energy minimization and pre-equilibrium process. First, the geometry optimization of each molecule is conducted to search for its most stable configuration with minimum energy [25, 28]. Afterward, the molecular models of virgin and aged binders are established with the COMPASSII forcefield, the commonly-used forcefield to describe the intermolecular interactions of bitumen molecules and exhibit advantages in precisely predicting the thermodynamic properties of bituminous materials. The detailed molecular interaction terms included in the COMPASSII forcefield could be found in previous literature [28, 36, 44]. Next, all molecules are involved in a cubic simulation box automatically and randomly to obtain an initial bituminous molecular model with an initial density of 0.1 g/cm^3, followed by an energy minimization to avoid overlapping atoms.

At the end of the energy minimization, the molecular dynamics simulation is performed to obtain the stable and condensed molecule models of virgin and aged bitumen under the isothermal-isobaric (NPT) and the canonical (NVT) ensembles at 25°C for 200 picoseconds (ps), respectively. The time step of 1 femtosecond (fs) is selected. Moreover, the Andersen barostat and the Nose thermostat are adopted to control the pressure and temperature conditions during the MD simulation, respectively. Regarding the non-bond molecular interaction, the Van der Waals and electrostatic forces are considered, and the Atom-based with a cut-off distance of 12.5 Å and Ewald method are implemented to calculate the van der Waals and electrostatics terms of potential energy. The MD simulation conditions of all bitumen models are the same and generally used in previous work [26-28, 34-36].

(a) Virgin bitumen   *(b) Short-term aged bitumen*   *(c) 20h Long-term aged bitumen*

(d) 40h Long-term aged bitumen   *(e) 80h Long-term aged bitumen*
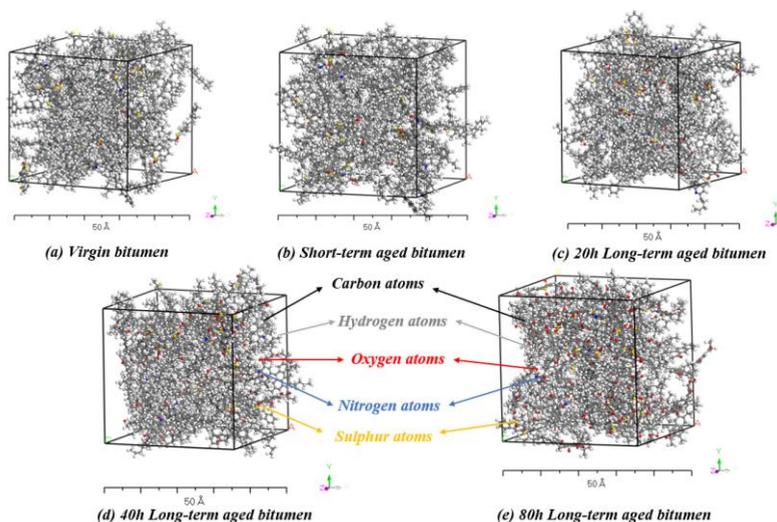
Figure 3.10 Molecular models of virgin and aged bitumen with various aging degrees

The final equilibrium configurations of the molecular models for the virgin, short-term aged, and different long-term aged bitumen after the MD simulation procedure with the NPT and NVT ensembles are illustrated in **Figure 3.10**. According to the FTIR result presented in **Figure 3.9**, the quantity of oxygen atoms (highlighted in red) in bitumen models exhibits an increase with the degree of aging. **Figure 3.11** demonstrates the density variations of the whole system as a function of MD simulation time at 293.15K. As the initial density of the simulation system is set as 0.1g/cm^3, the model volume shrinks under the combined influence of the external pressure and the molecular interaction, which compresses the system and enlarges the density. Thence, the density of the bitumen model rises dramatically at the beginning of the simulation. When the simulation time exceeds 50ps, the density values of all bitumen systems remain constant with slight fluctuations, considered to indicate the formation of molecular equilibrium models [28, 35]. The trajectory of

molecules in the entire molecular system during NVT equilibrium MD simulations lasting between 50 and 200ps can yield essential thermodynamic characteristics. These include cohesive energy density, energetic parameters, self-diffusion capacity, glass transition temperature, volumetric parameters, and surface free energy for both virgin and aged binders. These thermodynamic properties may have associations with the rheological and mechanical attributes of bitumen, such as rutting factor, relaxation parameters, fatigue life, and cracking width, which will be further investigated in **Chapter 8** through experimental exploration. Additionally, as the aging level increases, the density of bitumen also increases. That is due to the increment in heavy components with high molecular weights and the improvement of intermolecular interactions with the incorporation of polar groups (additional S=O and C=O).
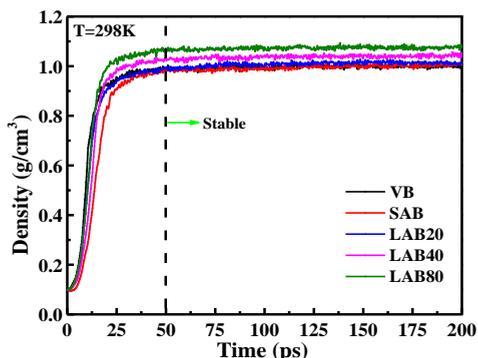
Figure 3.11 The density curves of bitumen samples at 298.15K (=25℃) during the NPT simulations

3.5.4 Validation of MD simulations

The reasonability of the MD simulation outputs is assessed through comparing the results from MD simulations and experiments. Density is one of the commonly-used parameters to verify the accuracy of simulation models and forcefield parameters. The capillary-stoppered pyknometer method was performed to measure the density values of bitumen at 25℃ and 60℃ according to EN 15326 [43]. The density results of virgin and aged bitumen at 25 and 60℃ are shown in **Figure 3.12**. The virgin bitumen's density at 25℃ measured from MD simulation and experiment is 0.999 and 1.017g/cm³, respectively. MD simulation and experimental results agree well with the values reported in previous studies, which revealed that the 25℃ density of virgin bitumen was close to 1.0g/cm³ [27, 28]. The slight difference in density between the experimental results and simulation predictions might come from system operation errors, such as the forcefield type and ensemble selection. It can be found that the density value of bitumen enlarges distinctly as the aging depth increases. As mentioned before, long-term aging could lead to increased asphaltene and resin fractions and decreased aromatic components in bitumen. The density values of asphaltene and resin are higher than those of aromatic and saturate ingredients because of their larger molecular weights and polarities. Interestingly, the increasing rate of density from MD simulation and experimental results is different. The rising rate of density from the experiment is slower than that from the MD simulation, which may be due to the difference in material components in aged bitumen between molecular models and realistic results.

From **Figure 3.12**, it shows that with an increase in temperature, the density values of virgin and aged bitumen all display a reduction tendency, which is attributed to the enlargement in the intermolecular distance and volume expansion of the whole system. The correction analysis between the density results from the experiment and MD simulation is performed, which is displayed in **Figure 3.12(c)**. It can be found that there is a strong linear relationship between the experimental and MD simulation results, which further validates the reasonability of the MD simulation program. Theoretically, the slope and intercept value of the correlation equation should be 1 and 0, respectively, when the experimental value is equal to the predicted

results from the MD simulation. However, a difference between the experimental results and simulation prediction is to be expected due to the use of a limited number of molecules to represent the whole material.
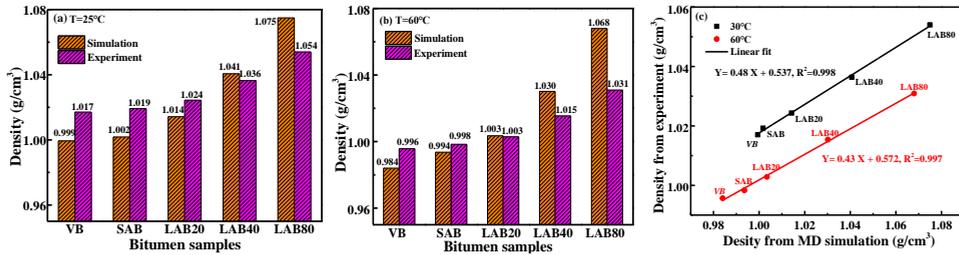
Figure 3.12 The result comparison of density parameter of virgin and different aged bitumen from experiments and MD simulation

3.6 MD simulation results and discussion

3.6.1 Bulk properties of virgin and aged bitumen

The physical characteristics of the bulk bitumen system significantly affect its rheological and mechanical performance due to the influence of the chemical composition and external conditions. In this thesis, the effects of short-term and long-term aging time on the cohesion energy density and solubility parameters of bitumen are studied through the MD simulation, which will be correlated with high-temperature rheological performance of bitumen in **Chapter 8**.

3.6.1.1 Cohesive energy density

The cohesion energy density (CED) is an important parameter to assess the molecular attraction interaction degree of the whole bulk system, which examines the mutual attraction of all molecules per unit volume. The mathematical expression of CED is presented as follows [28]:

$$E_{CED} = E_{vdw} + E_{ele} = E_{coh}/V \tag{3.6}$$

where E_{CED} represents the cohesive energy density (J/cm^3), E_{coh} refers to the total cohesive energy of the whole system (J), and V is the volume of the molecular system. In addition, the E_{vdw} and E_{ele} are the Van der Waals term and electrostatic term of cohesive energy density. It should be noted that the E_{coh} value is equal to the energy for separating all molecules from the system [36]. Hence, it is possible that the CED parameter has a correlation with the high-temperature stiffness and resistance to rutting in bitumen, and this hypothesis will be confirmed in **Chapter 8**.

The variation of the cohesive energy density of bitumen as a function of aging duration is displayed in **Figure 3.13(a)**. It can be detected that the cohesive energy density is composed of the Van der Waals and Electrostatic terms, and the non-bond interaction contributes to the intermolecular forces of the bitumen system. In this thesis, the measured CED value of virgin bitumen is $3.36*10^8$ J/cm^3, a little larger than the CED region of $3.19*10^8$-$3.22*10^8$ J/m^3 reported in previous studies [22, 25, 28]. This may be related to the addition of sulfoxide functional groups enhancing the polarity and molecular interaction between bitumen molecules. Moreover, the Van der Waals force contributes more to the cohesive energy of bitumen than the electrostatic interaction [58].

The aging duration significantly influences the cohesive energy density of bitumen, which increases gradually as the aging degree deepens, especially in the period of long-term aging. During the aging process of bitumen, more polar functional groups and high molecular-weight fractions are generated, promoting the improvement in molecular interaction. Therefore, the CED value and hardness of long-term aged binders are larger than that of virgin or short-term aged bitumen, consistent with previous literature's conclusions [28,

44]. It is worth mentioning that the increasing trend of the Van der Waals and electrostatic forces to the aging degree is distinctly different. When the long-term aging is more than 40 hours, the electrostatic interaction enhances more significantly than the Van der Waals force. Compared to the LAB40, the CED improvement of the LAB80 binder mainly comes from the increment in electrostatic interaction, associated with the distinct contents of polar functional groups, especially the C=O index in the LAB80 bitumen. To sum up, the Van der Waals interaction between the bitumen molecules is dominant in enhancing the cohesive energy and stiffness of virgin and aged bitumen. However, as the aging degree increases, the electrostatic force's contribution to the energy composition of bitumen models is more obvious. Regarding the case of 80 hours long-term aging, the Van der Waals force is still higher than the electrostatic interaction. Therefore, it can be deduced that the van der Waals force plays a dominating role in determining the CED value of all bitumen samples.
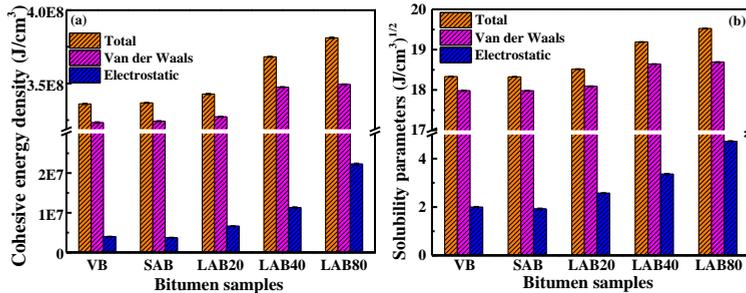
Figure 3.13 Influence of long-term aging time on the cohesive energy density(a) and solubility parameter (b) of bitumen

3.6.1.2 Solubility parameter

According to the Flory-Huggins theory, materials with similar solubility parameters are likely miscible [59, 60]. As such, a difference in the solubility parameters significantly affects the compatibility between different components in a compound blend. Therefore, it is important to understand the influence of long-term aging on the solubility parameter, to assess the compatibility between aged bitumen and other additives, such as rejuvenators and polymers [58-61]. The incompatibility of rejuvenators or polymers with bitumen would result in the phase separation of an inhomogeneous binder, negatively influencing the mechanical properties of asphalt pavement, including the resistance to rutting, fatigue, and thermal cracking [59]. The solubility parameter of bitumen can be measured by conducting a solubility test with several types of solvents. However, the experimental method is difficult to perform because of the required solvents, especially in a pavement engineering laboratory. Thus, employing the MD simulation to predict the solubility parameter of virgin, aged bitumen, or additives (rejuvenators and modifiers) is convenient.

$$\delta = (E_{CED})^{1/2} = (E_{vdw} + E_{ele})^{1/2} \tag{3.7}$$

During the MD simulation, the solubility parameter values of the virgin, short-term, and long-term aged binders are calculated following **Eq.3.7** [28]**,** and the results from the simulations in the previous section are illustrated in **Figure 3.13(b)**. It can be seen that the solubility parameter of the virgin bitumen is 18.33 $(J/cm^3)^{1/2}$. Based on previous studies [16, 28], the reported range of solubility parameter of bitumen is 13.30-22.50 $(J/cm^3)^{1/2}$. Thus, the reasonability of molecular models of bitumen and MD simulation programs has been further validated. Long-term aging enlarges the solubility parameter of bitumen, but short-term aging appears to have little effect. Similar to the CED parameter, the Van der Waals force exerts a significant influence on determining the solubility parameter of both virgin and aged bitumen. Moreover, the solubility parameter contributed from an electrostatic interaction becomes more distinct as the aging time prolongs, which is linked to the generation of polar functional groups during the oxidation aging of bitumen. To sum up, the solubility parameter values of aged binders with various aging levels are different, affecting their miscibility with rejuvenators. Therefore, the selection of rejuvenator type should consider the aging degree

of bitumen, which not only determines the optimum rejuvenator dosage but also influences the compatibility and diffusion characteristics of the rejuvenated bitumen. The compatibility and intermolecular interaction between different types of rejuvenators and aged bitumen will be explored in **chapter 5**.

3.6.2 Cohesive properties of virgin and aged bitumen

The asphalt mixture is composed of bitumen binder, aggregate, and filler. The interfacial performance between the aggregates and bitumen is of great value to guarantee the sufficient adhesive property and moisture resistance of asphalt pavement. Different mechanical and thermodynamics methods have been proposed to detect the interfacial adhesion of asphalt mixtures, such as the universal tension and contact angle tests [25, 35]. Nonetheless, conducting these experimental measurements invariably consumes both time and financial resources, and the resultant outcomes do not provide insights into the molecular-scale perspective of interfacial bonding mechanisms. In this thesis, the influence of long-term aging on the cohesive and adhesive properties of bitumen is investigated with the parameters of surface free energy and work of cohesion obtained from MD simulations. Simultaneously, film models for both virgin and aged bitumen were constructed, and it's worth noting that the film models lack periodic boundary conditions along the Z direction, unlike the bulk model. The MD simulations for these film models employ identical setup parameters as those used in the simulations for a bulk model. The surface free energy and work of cohesion values of virgin and aged bitumen systems can be calculated using **Eqs.3.8** and **3.9** [16, 28], respectively, and the results are presented in **Figure 3.14**.

$$\gamma = (E_{film} - E_{bulk})/2A \qquad (3.8)$$

$$W_{aa} = 2\gamma \qquad (3.9)$$

where γ and W_{aa} show the surface free energy and work of cohesion (mJ/m^2), E_{film} and E_{bulk} represent the potential energy of the confined bitumen film and bulk bitumen system (mJ), respectively. Besides, parameter A refers to the new surface area (mm^2).

Regarding the surface free energy, the value obtained from the MD simulations for the virgin bitumen is approximately 70 mJ/m^2, within the commonly-found range of 39.92-71.56 mJ/m^2 [60]. The aging of bitumen leads to a reduction in surface free energy, indicating that the required external energy for creating a new surface of bitumen decreases as the aging degree increases. Compared to the virgin and short-term aged bitumen, it is easier for long-term aged binders to crack. Moreover, long-term aging reduces the work of cohesion value of bitumen, denoting that fracture resistance of bitumen deteriorates with the increase in aging degree. Compared with unaged bitumen, surface free energy and work of cohesion of short-term, 20, 40, and 80h long-term aged binders decreases by 1.4%, 21.5%, 35.8%, and 58.3% (see **Figure 3.14**).
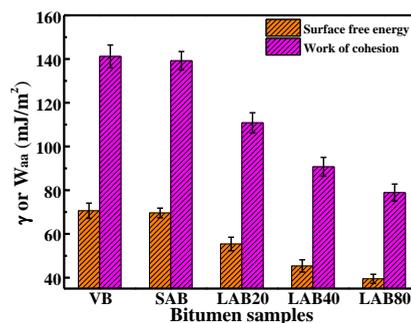
Figure 3.14 Influence of aging time on the surface free energy and work of cohesion of bitumen

3.6.3 Dynamic behavior of virgin and aged bitumen

The dynamic properties also play an important role in explaining the aging behavior of bitumen. The mobility of molecules has a significant influence on the thermodynamic and rheological properties of bitumen, as well as the mass exchange between the aged bitumen and rejuvenator, polymers, or moisture. However, it is difficult for conventional laboratory experiments to detect variations in the dynamic properties of bitumen molecules. As a result, the synergistic effects of long-term aging level and temperature on the self-diffusion capacity of bitumen molecules are still unclear. For this reason, MD simulation technology is used here to determine virgin and aged bitumen systems' mean square distance (MSD). It quantifies how a molecule's position deviates from a reference position as time progresses. The MSD values variation of bitumen models is recorded as the function of simulation time following **Eq.3.10** at different temperatures of 248, 273, 298, 333, and 393K (-25, 0, 25, 60, and 120°C). There is an obvious relationship between the diffusion coefficient D and the slope of the MSD curve, described in **Eq.3.11**. The diffusion behavior of molecules is determined by the Brownian self-movement (kinetic energy) and molecular interactions (potential energy) [19, 27, 28]; thus, it is also called the self-diffusion to distinguish it from the inter-diffusion resulting from the mass concentration difference.

$$MSD(t) = < \Delta r_i(t)^2 > = < [r_i(t) - r_i(0)]^2 > \qquad (3.10)$$

$$D = \frac{1}{6N} \lim_{t \to \infty} \frac{d}{dt} \sum MSD(t) = \frac{a}{6} \qquad (3.11)$$

where MSD(t) refers to the mean square distance of molecular systems at time t, $r_i(0)$ and $r_i(t)$ represent the initial and ultimate coordinate at time t, N means the total number of molecules, and a is the slope value of the correlation curve between MSD and simulation time.
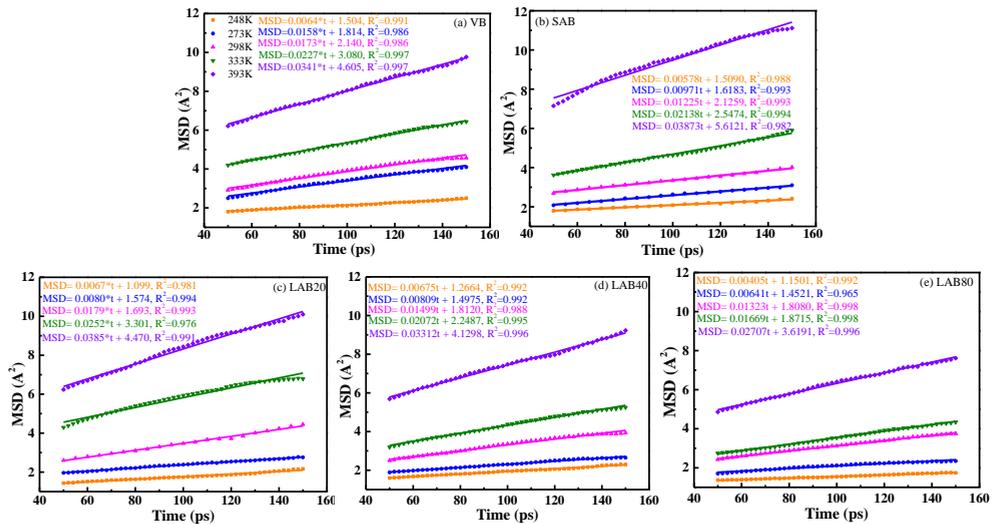
Figure 3.15 The relationship between mean square distance and simulation time for virgin and different aged bitumen

The MSD values of virgin and aged binders at different MD simulation durations and temperatures are displayed in **Figure 3.15**. It can be found that the MSD parameter of the bitumen system presents a positive linear correlation with the simulation time, indicating that the distance of molecules increases gradually during the MD simulation. Meanwhile, the MSD parameter of bitumen decreases as the aging degree increases, which is associated with the improvement in intermolecular interaction due to the formulation of polar groups and reduction of system free volume. Hence, long-term aging would significantly hinder molecules' mobility and deteriorate the bitumen's relaxation ability. Additionally, high temperature is beneficial to

increasing the MSD values and mobility of molecules, which contributes to the increment in molecular energy and results in a volume expansion of the bitumen system.

The slope ("a" value) variations of MSD values to the simulation time differ a lot at different temperatures, attributed to the rate of movement of molecules. The calculated diffusion coefficient D values of virgin and aged bitumen are listed in **Table 3.10**. Notably, the self-diffusion coefficient of the bitumen model reduces with aging and increases with higher temperatures, respectively. However, these D values are on the same order of magnitude (10^{-7} cm^2/s), except for the LAB80 bitumen at 248K (10^{-8} cm^2/s), which is consistent with the reported diffusion coefficient D value of bitumen from previous studies [20, 36, 45]. Further, it is interesting to mention that the influence of temperature on the diffusion coefficient of bitumen models is more apparent than that of the aging degree. That's why the workability of aged bitumen in RAP material could be improved by increasing the mixing and compaction temperature. However, this way is energy consuming and if the temperature gets too high, the RAP material can get damaged, that is why the rejuvenators are incorporated to enhance the mobility of bitumen molecules through weakening the intermolecular interactions and increasing the free volume fractions.

Table 3.10 The diffusion coefficient of virgin and different aged bitumen

Bitumen samples	D (393K) cm^2/s	D (333K) cm^2/s	D (298K) cm^2/s	D (273K) cm^2/s	D (248K) cm^2/s
VB	$5.73*10^{-7}$	$3.79*10^{-7}$	$2.88*10^{-7}$	$2.13*10^{-7}$	$1.57*10^{-7}$
SAB	$6.05*10^{-7}$	$3.98*10^{-7}$	$2.88*10^{-7}$	$2.19*10^{-7}$	$1.57*10^{-7}$
LAB20	$5.78*10^{-7}$	$3.65*10^{-7}$	$2.55*10^{-7}$	$1.89*10^{-7}$	$1.31*10^{-7}$
LAB40	$5.52*10^{-7}$	$3.45*10^{-7}$	$2.50*10^{-7}$	$1.72*10^{-7}$	$1.13*10^{-7}$
LAB80	$4.51*10^{-7}$	$2.78*10^{-7}$	$1.92*10^{-7}$	$1.07*10^{-7}$	$6.75*10^{-8}$

3.7 Long-term aging reaction kinetics models

As mentioned at the beginning of this chapter, although the aging mechanism of bitumen is complex, it is necessary to have a sufficient fundamental understanding and build the aging reaction kinetics models of bitumen to create and validate rejuvenation models. As shown in **sections 3.5.2.1** and **3.5.2.2**, the SARA fractions and functional group distribution are the two most important chemical characteristics for determining the molecular models of aged bitumen. In this thesis, three levels of long-term aged bitumen were prepared and characterized from experiments, and with the long-term aging reaction kinetics models created with the test results from these materials, we can predict the chemical components (functional group and SARA fraction distributions) in aged bitumen (Total 70/100) with different aging degrees (between 20- and 80-hours PAV) to establish their molecular models without complicated tests. In this chapter, the aging reaction kinetics models of bitumen are proposed following the variations of functional groups and SARA fractions in bitumen during the long-term aging procedure.

3.7.1 Functional groups-based models

The variations of carbonyl and sulfoxide indices as a function of long-term aging time are shown in **Figure 3.16**. As the aging time prolongs, the aging index differences such as ΔCI, ΔSI, and ΔCAI rise linearly. Meanwhile, previous literature reported that the increase rate of carbonyl and sulfoxide groups remained constant during the long-term aging process of bitumen [6, 14]. It means that functional group generation rates are independent of their initial concentrations. Thus, the Zero-order model is suitable for describing the long-term aging reaction kinetics of bitumen on the carbonyl and sulfoxide functional groups. The Zero-order models are listed as **Eqs.3.12-3.15**.

$$CI = CI + SI \tag{3.12}$$

$$\Delta CI = CI_t - CI_0 = k_{CI} \cdot t \tag{3.13}$$

$$\Delta SI = SI_t - SI_0 = k_{SI} \cdot t \tag{3.14}$$

$$\Delta CAI = CAI_t - CAI_0 = k_{CAI} \cdot t \tag{3.15}$$

where the CI_0, CI_t, SI_0, SI_t and CAI_0, CAI_t are the carbonyl, sulfoxide, and combined index at reaction time $t=0$ and $t=t$, respectively, while the k_{CI}, k_{SI}, and k_{CAI} refer to the corresponding reaction rate constants.

From **Figure 3.16**, it depicts that the Zero-order model can well fit the correlation curve between the functional-group based aging index difference and aging reaction time with a correlation coefficient R^2 higher than 0.994, listed in **Table 3.11**. The functional group-based reaction rate constants are located in the region of 0.7-$3.3*10^{-4}$ ($mol \cdot L^{-1} \cdot h^{-1}$). Besides, the k_{CI} and k_{CAI} values manifest the same magnitude, while the k_{SI} value is the lowest. Hence, the functional group-based aging reaction model of bitumen depends dramatically on the type of selected functional groups.
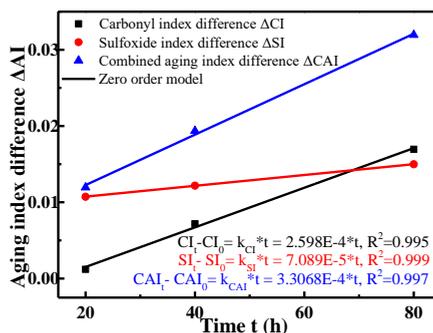
Figure 3.16 Overall reaction models of bitumen from FTIR test results

Table 3.11 The reaction rate constant of functional groups in bitumen

Aging index	CI	SI	CAI
k ($mol \cdot L^{-1} \cdot h^{-1}$)	2.598E-4	7.089E-5	3.307E-4
R^2	0.9947	0.9999	0.9965

3.7.2 SARA fractions-based models

The two-step consecutive reaction model is adopted to quantitatively describe the aging reaction kinetics of bitumen. During the aging of bitumen, the aromatic fraction would convert to the resin fraction, which further changes into the asphaltene components. There are different complex chemical reaction models with several-step reactions, including the chain reaction, opposing reaction, parallel reaction, and consecutive reaction [61-63]. By definition, during the consecutive reaction model, there are at least two-step reactions in which the reactant in the next reaction is the product of the previous step.

Herein, the aging mechanism of the transformation between the aromatics, resin, and asphaltene fractions in bitumen is assumed to belong to the consecutive reaction. It should be mentioned that the air pressure is constant at 2.1MPa during the whole PAV test, indicating a slight variation in oxygen concentration. To simplify the complex aging reaction, the oxygen reactant is omitted. Afterward, the influence of oxygen concentration on the reaction rate is considered in the reaction rate constant k_1 and k_2. The detailed consecutive reaction equation is shown as follows:

$$(\beta)A \xrightarrow{k_1} R \xrightarrow{k_2} (\gamma)A_S \tag{3.16}$$

$$t = 0 \qquad A_0 \qquad R_0 \qquad A_{S0}$$

$$t = t \qquad A_t \qquad R_t \qquad A_{St}$$
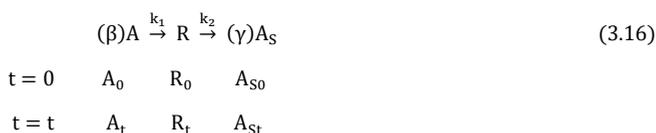
where A refers to the aromatic molecule, R represents the resin molecule, and A_S is the asphaltene molecule. The parameters of β and γ are the stoichiometric numbers. It means that when one resin molecule is generated, β aromatic molecules are consumed during the long-term aging reaction. Similarly, when one resin molecule is depleted, the number of new asphaltene molecules is γ. Moreover, k_1 and k_2 are the reaction rate constants of the first and second-step reactions.

Before conducting the aging process (at t=0), the aromatic, resin, and asphaltene fraction concentration values are A_0, R_0, and A_{S0}, respectively. When the aging reaction time is at t=t, the corresponding concentration is A_t, R_t, and A_{st}. The reaction order can be different from the sum of the stoichiometric number of reactants. To explore the aging reaction kinetics, the reaction order of the first and second reactions is assumed as n and m, respectively. Thus, the consumption rate of aromatic fraction and the generation rate of asphaltene components are calculated as **Eqs.3.17** and **3.18**.

$$\frac{dA}{dt} = -k_1 \cdot A^n \tag{3.17}$$

$$\frac{dA_S}{dt} = k_2 \cdot R^m \tag{3.18}$$

where A and A_s are the concentration of aromatic and asphaltene fractions, respectively; t refers to the reaction time; k_1 and k_2 are the corresponding reaction rate constants.

The integration formula of **Eq.3.17** can be rewritten as follows:

$$A_t^{(1-n)} - A_0^{(1-n)} = (n-1) \cdot k_1 \cdot t, (n \neq 1) \tag{3.19}$$

For the Zero-order reaction model, the reaction rate is independent on the initial concentration of reactants. **Eq.3.17** can be rewritten as follows:

$$\frac{dA}{dt} = -k_1 \cdot A^0 = -k_1 \tag{3.20}$$

By further simultaneous integration of both sides, **Eq.3.20** can be expressed as shown:

$$A_t = A_0 - k_1 \cdot t \tag{3.21}$$

In addition, when the reaction model is First-order, the integral form of **Eq.3.17** is as follows:

$$A_t = A_0 \cdot e^{(-k_1 \cdot t)} \tag{3.22}$$

Similarly, regarding the Second-order reaction model, the relationship between the reactant concentration and time can be described as:

$$\frac{1}{A_t} = \frac{1}{A_0} + k_1 t \tag{3.23}$$

To investigate the reaction kinetics rate k_1 from the aromatic to resin molecules, the molar concentration of aromatic fraction as a function of long-term aging time is demonstrated in **Figure 3.17**. With aging time prolonging, the aromatic molarity in bitumen decreases dramatically. Moreover, the decreasing rate seems to slow down gradually, which may be associated with the reduced reactant concentration and increased product dosage during the oxidative reaction procedure. The common reaction kinetics models, Zero-order, First-order, and Second-order, are first used to describe the relationship between the aromatic molarity and aging time. The correlation curves with different kinetics models are also shown in **Figure 3.17**. The reaction rate constant k_1 and correlation coefficient R^2 values can be obtained and listed in **Table 3.12**. It can be seen that the order of R^2 value is Second-order > First-order > Zero-order, indicating that the Second-order reaction model is more accurate in describing the oxidative aging kinetics of aromatic fractions. However, these reaction models are assumed to fit the reaction curve of aromatic molecules. In addition, the optimum reaction model is still unclear, although the Second-order model seems more reasonable.
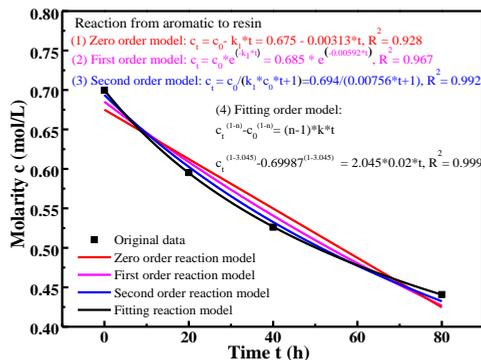
Figure 3.17 The molar concentration of aromatic fractions

Table 3.12 The parameters of aromatic oxidative reaction in different kinetics models

Kinetics models	Zero-order	First-order	Second-order	Third-order
k_1	0.00313	0.00592	0.0109	0.02
R^2	0.928	0.967	0.992	0.999

The general n-order reaction model (shown in **Eq.3.19**) is then adopted to fit the correlation curve between the aromatic molarity and reaction time, as illustrated in **Figure 3.17**. The correlation coefficient R^2 value is 0.999, and the reaction order of aromatic molecules is determined as 3.045. Hence, it can be deduced that the optimum kinetics model for aromatic fraction is the Third-order reaction model. **Table 3.12** displays the reaction rate constant k_1 of the aromatics with several different kinetics models during a long-term aging process. With the reaction order extending from zero to three, both the k_1 and R^2 values increase. When the Third-order reaction model is utilized, the calculated k_1 value is 0.02 $(mol \cdot L^{-1})^{-2}(h)^{-1}$, and the R^2 value is 0.999.

To estimate the second step reaction kinetics from the resin to asphaltene molecules, the asphaltene molarity as a function of long-term aging time is drawn in **Figure 3.18**. The linear correlation between the asphaltene molarity and reaction time is significant, and the Zero-order kinetics model is employed here to describe the generation rate k_2 of asphaltene molecules. In **Eq.3.24**, t is the aging time, A_{st} and A_{s0} are the asphaltene concentration at t=t and t=0, and k_2 represents the reaction rate constant regarding the conversion from resin to asphaltene fractions.

$$A_{st} = A_{s0} + k_2 \cdot t \tag{3.24}$$

It manifests that the generation rate of asphaltene molecules during the long-term aging process is constant and independent on the reactant concentration (resin molecules), which is similar to that of the aforementioned functional groups-based models. The reaction rate constant k_2 and correlation coefficient R^2 for the second step reaction is 3.85E-4 $mol \cdot (L \cdot h)^{-1}$ and 0.9987, respectively. It indicates that the Zero-order model can well fit the aging reaction kinetics of asphaltene molecules.

It is worth mentioning that the second step reaction rate constant k_2 is much lower than the k_1 in the first step of the consecutive reaction model. Hence, the reaction rate from resin to asphaltene is much slower than that from aromatic to resin, leading to the large consumption of aromatics and increased resin concentration. Moreover, the rate control step of the whole consecutive reaction is the second-step, and the reaction rate constant k of the whole consecutive reaction is near k_2. From the viewpoint of reaction kinetic knowledge, the increase in asphaltene fractions would be beneficial to hindering the aging reaction rate of bitumen. Interestingly, the reaction rate constant k_2 is very close to the k_{CI} and k_{CAI} values obtained from the FTIR test (see **Table 3.11**). It further validates that the transformation from the resin to asphaltene molecules is the control step of the whole consecutive reaction model. Further, the k_{SI} value calculated from the change

rate of sulfoxide functional groups is the lowest. Therefore, the parameters of k_{CI} and k_{CAI} are more appropriate than the k_{SI} to describe the long-term aging reaction kinetics of the whole bitumen.
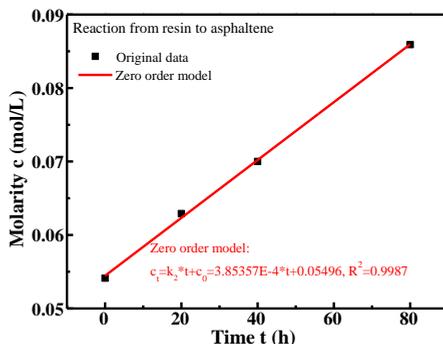
Figure 3.18 Reaction models from resin to asphaltene fractions of bitumen

3.7.3 Quantitative conversion relationship between aromatic, resin, and asphaltene

The final step of the consecutive reaction model is to determine the stoichiometric numbers β and γ, which is significant in figuring out the transformation relationships between the aromatic, resin, and asphaltene components during the artificial long-term aging process from a molecular scale. From **Eq.3.15**, when the aging time is t, the consumption of aromatic is (A_0-A_t), while the yield of asphaltene is ($A_{st}-A_{s0}$). According to the consecutive reaction model, the concentration difference of resin fraction at time t comes from two parts: the generation in the first step reaction and the consumption in the second step reaction. Thus, the concentration difference of resin fraction can be introduced as follows:

$$R_t - R_0 = \frac{A_0 - A_t}{\beta} - \frac{A_{st} - A_{s0}}{\gamma} \qquad (3.25)$$

where the R_0, A_0, and A_{s0} are the initial molarity of resin, aromatic, and asphaltene fractions at t=0, respectively; while the R_t, A_t, and A_{st} are their corresponding molarity value at reaction time t; β and γ are the stoichiometric numbers.

We assume that the first step is the Third-order reaction; thus, the reaction rate equation of aromatic fraction is described as:

$$\frac{1}{A_t^2} - \frac{1}{A_0^2} = 2 \cdot k_1 \cdot t \qquad (3.26)$$

Similarly, the second step reaction is assumed as the Zero-order model, and the reaction rate equation of the asphaltene fraction is:

$$A_{st} - A_{s0} = k_2 \cdot t \qquad (3.27)$$

By substituting **Eqs.3.26** and **3.27**, **Eq.3.25** can be rewritten as:

$$\Delta R = R_t - R_0 = \frac{A_0 - \dfrac{A_0}{\sqrt{1 + 2 \cdot k_1 \cdot t \cdot A_0^2}}}{\beta} - \frac{k_2 \cdot t}{\gamma} \qquad (3.28)$$

where ΔR refers to the molarity difference of resin fraction, and k_1 and k_2 are the reaction rate constant of the first and second-step reactions, respectively.

The relationship between the molarity difference of resin fraction ΔR and the long-term aging time t is introduced in **Eq.3.29**, used to fit the curve in **Figure 3.19**. It should be noted that the predicted value of A_0,

k_1, and k_2 is 0.694 mol·L^{-1}, 0.02(mol·L^{-1})$^{-2}$(h)$^{-1}$, and 3.85E-4 mol·(L·h)$^{-1}$. Meanwhile, the predicted values of β and γ are approximately 2.82 and 0.58, respectively, and the R^2 value is 0.992. To this end, the detailed consecutive reaction of bitumen during the long-term aging process is shown as follows:

$$(2.82) A \xrightarrow{k_1} R \xrightarrow{k_2} (0.58)A_S \tag{3.29}$$
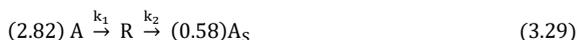
According to this consecutive reaction equation, it can be interpreted that when one resin molecule is generated, the consumption number of aromatic molecules is 2.82. At the same time, only 0.58 asphaltene molecules can be obtained when one resin molecule is consumed. A detailed illustration of the consecutive reaction model is presented in **Figure 3.19**. It should be mentioned that all aromatic, resin, and asphaltene fractions are component groups containing amounts of various molecule types. Due to the molecular interaction and existence of polar functional groups in aromatic, resin, and asphaltene molecules, intermolecular agglomeration would occur, increasing the difficulty in distinguishing the high-weight molecules from the aggregates of lightweight molecules. The chemical reaction and physical aggregation are both considered in the consecutive reaction model of bitumen during the long-term aging process.

$$\Delta R = R_t - R_0 = \frac{A_0 - \dfrac{A_0}{\sqrt{1 + 2 \cdot k_1 \cdot t \cdot A_0^2}}}{\beta} - \frac{k_2 \cdot t}{\gamma}$$

β=2.82, γ=0.58；
R^2=0.992

■ Original data
— Consecutive model fitting curve
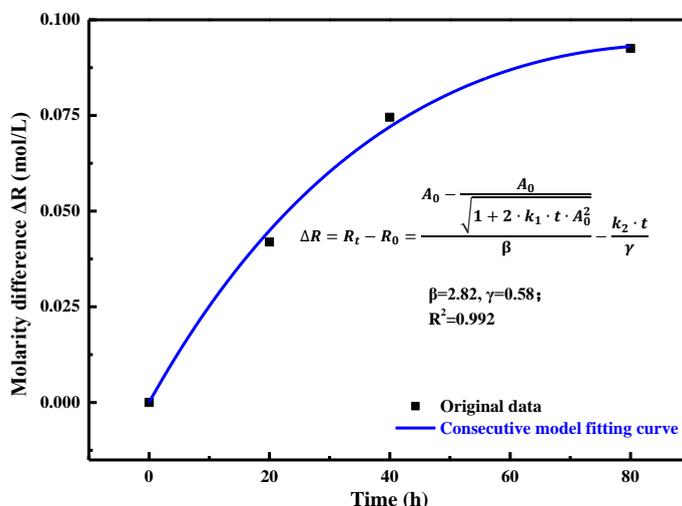
Figure 3.19 Reaction model of resin fraction

The long-term aging reaction kinetic models of bitumen based on the variation rate of functional groups (C=O or S=O) and chemical compositions (aromatic, resin, and asphaltene) are illustrated in **Figure 3.20**. From the viewpoint of functional groups, the average reaction rates of carbonyl, sulfoxide, and combined indices are calculated, which is the most common model of bitumen oxidative aging. Although the functional groups-based model can reflect the oxidative rate of bitumen molecules with oxygen to a certain degree, it fails to elaborate on the conversion law between SARA fractions in bitumen during the long-term aging process. Hence, one novel consecutive two-step model is established according to the conversion correlation between aromatic, resin, and asphaltene fractions. The reaction rate constants in SARA-based kinetics models are calculated, and the corresponding stoichiometric numbers of aromatic, resin, and asphaltene are determined. It should be mentioned that the increase in resin and asphaltene dosage is due to molecular transformation and molecular agglomeration. During the aging process, the bitumen molecules would aggregate together due to the high polarity and intermolecular attraction [44, 54], which is hard to separate by solvents in SARA fractions measurement and leads to the increased number of large-scale molecules (resins and asphaltenes) in SARA results. Hence, to truly verify this process, more work should be done to eliminate the influence of intermolecular agglomeration on the SARA fractions distribution with the help of functional solvents and effective separation methods.
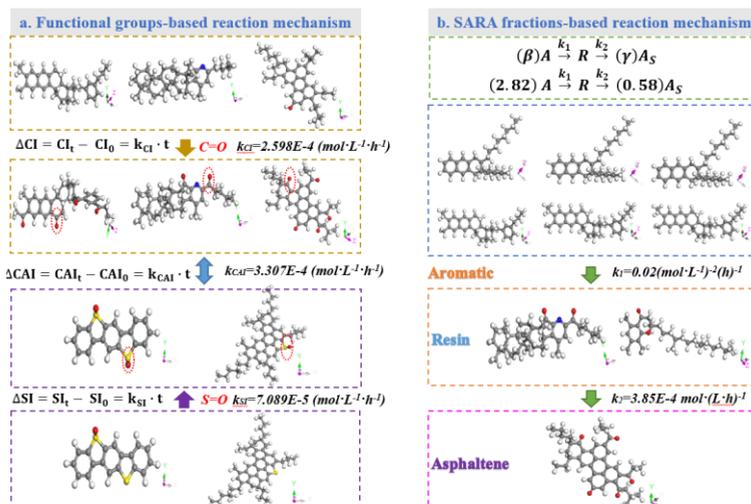
Figure 3.20 The illustration graph of long-term aging reaction kinetics models

3.8 Summary

This chapter aims to figure out the variations of chemical properties (SARA fractions, functional group distribution, element compositions) of bitumen in different short-term and various spans of long-term aging. Based on the chemical characteristics obtained from FTIR, SARA, and elemental analyses results, representative molecular models of the specific virgin bitumen used and the corresponding aged binders with various long-term aging levels were established. These molecule models were validated by comparing some physical parameters from experiments and MD simulation outputs. Afterward, the long-term aging effects on the thermodynamic properties of bitumen in terms of bulk, interfacial, and diffusive aspects were explored by MD simulations. Lastly, the long-term aging kinetics models of chemical components (functional groups and SARA fractions) in bitumen were developed and discussed to anticipate the chemical parameters of long-term aged bitumen with any aging level. Here are the main conclusions drawn from this chapter:

➢ **Chemical characterizations on virgin and aged bitumen**

- During the long-term aging of bitumen, the aromatic component decreased dramatically, while the resin and asphaltene fractions increased gradually. Besides, the sulfoxide and carbonyl functional groups would grow, and the sulfur oxidation reaction was easier than the carbon oxidation.

- The C%, H%, and H/C ratio values would decrease during the long-term aging of bitumen, which markedly increased the oxygen dosage due to the polymerization reaction of light fractions and agglomeration of heavy molecules.

➢ **Establishment and validation on molecular models of virgin and aged bitumen**

- The molecular models of virgin and different aged bitumen were established and validated. The sulfoxide functional groups were found in virgin bitumen and added to the molecular model of bitumen. In addition, the molecular models of aged bitumen could be built by introducing different dosages of oxygen-containing functional groups (C=O and S=O) and adjusting the mass ratio of SARA fractions.

- The functional groups and density outputs from MD simulations agreed well with the laboratory results.

➢ **MD simulations on long-term aging influence on thermodynamic properties of bitumen**

- The MD simulations could be successfully applied to predict and explore the long-term aging influence on the thermodynamic properties of bitumen, which would act as an important media in connecting the chemical components with the macroscale mechanical performance of bituminous materials.

- Apart from the chemical properties from experiments, the influence of long-term aging on the thermodynamics properties was predicted through the MD simulation method. The aging of bitumen significantly enhanced the cohesive energy density, solubility parameter, and activation energy. However, at the same time, it deteriorated the surface free energy, work of cohesion as well as molecular mobility of the bitumen system.

➢ **Long-term aging kinetics models of bitumen for predicting chemical input parameters of MD simulations**

- The Zero-order model was suitable to describe the long-term aging reaction kinetics of bitumen from the viewpoint of the carbonyl and sulfoxide functional groups. The functional group-based reaction rate constants were located in the region of $0.7\text{-}3.3*10^{-4}$ (mol·L^{-1}·h^{-1}). Besides, the k_{CI} and k_{CAI} values had the same magnitude, while the k_{SI} value was the lowest.

- The aromatic fraction would convert to the resin fraction and change into the asphaltene components. In the consecutive reaction model, there were at least two-step reactions, and the reactant in the next reaction was the product of the previous step. The Second-order reaction model described the oxidative aging kinetics of aromatic fractions more accurately than the Zero-order and First-order models. However, the most optimum kinetics model for aromatic fraction was the Third-order reaction model, with the corresponding k_1 value of 0.02 $(\text{mol·L}^{-1})^{-2}(\text{h})^{-1}$.

- The Zero-order model could well fit the aging reaction kinetics of asphaltene molecules, and the related reaction rate constant k_2 was 3.85E-4 mol·(L·h)$^{-1}$. The reaction rate from resin to asphaltene was much slower than that from aromatic to resin. Moreover, the transformation from the resin to asphaltene molecules was the control step of the whole consecutive reaction model.

- When one resin molecule was generated, the consumption number of aromatic molecules was about 2.82. At the same time, when one resin molecule was consumed, only 0.58 asphaltene molecules could be generated.

3.9 References

[1] C. Zheng, C. Shan, J. Liu, T. Zhang, X. Yang, D. Lv. Microscopic adhesion properties of asphalt-mineral aggregate interface in cold area based on molecular simulation technology. Construction and Building Materials. 2021, 268, 121151.

[2] S. Ren, X. Liu, M. Li, W. Fan, J. Xu. S. Erkens. Experimental characterization of viscoelastic behaviors, microstructure and thermal stability of CR/SBS modified asphalt with TOR. Construction and Building Material. 2020, 261, 120524.

[3] L. Ma, F. Wang, P. Cui, M. Yunusa, Y. Xiao. Effect of aging on the constitutive models of asphalt and their mixtures. Construction and Building Materials. 2021, 272, 121611.

[4] T.B. Moghaddam, H. Baaj. The use of rejuvenating agents in production of recycled hot mix asphalt: A systematic review. Construction and Building Materials. 2016, 114:805-816.

[5] M. Guo, H. Liu, Y. Jiao, L. Mo, Y. Tan, D. Wang, M. Liang. Effect of WMA-RAP technology on pavement performance of asphalt mixture: A state-of-the-art review. Journal of Cleaner Production. 2020, 266, 121704.

[6] X. Liu, B. Li, M. Jia, Z. Zhang, Z. Liu, H. Li. Influence of short-term aging on anti-cracking performance of warm modified asphalt at intermediate temperature. Colloids and Surfaces A. 2019, 582, 123877.

[7] T. Moghaddam, H. Baaj. The use of rejuvenating agents in production of recycled hot mix asphalt: A systematic review. Construction and Building Materials. 2016, 114, 805-816.

[8] A. Behnood. Application of rejuvenators to improve the rheological and mechanical properties of asphalt binders and mixtures: A review. Journal of Cleaner Production. 2019, 231, 171-182.

[9] V. Antunes, A. Freire, J. Neves. A review on the effect of RAP recycling on bituminous mixtures properties and the viability of multi-recycling. Construction and Building Materials. 2019, 211, 453-469.

[10] A. Behnood. Application of rejuvenators to improve the rheological and mechanical properties of asphalt binders and mixtures: A review. Journal of Cleaner Production. 2019, 231:171-182.

[11] L. Wang, Y. Liu, L. Zhang. Micro/Nanoscale study on the effect of aging on the performance of crumb rubber modified asphalt. Mathematical Problems in Engineering. 2020, 1924349: 1-10.

[12] R. Tauste, F. Moreno-Navarro, M. Sol-Sanchez, M.C. Rubio-Gamez. Understanding the bitumen ageing phenomenon: A review. Construction and Building Materials. 2018, 192: 593-609.

[13] J. Wang, T. Wang, X. Hou, F. Xiao. Modelling of rheological and chemical properties of asphalt binder considering SARA fraction. Fuel. 2019, 238, 320-330.

[14] R. Jing, A. Varveri, X. Liu, A. Scarpas, S. Erkens. Ageing effect of chemo-mechanics of bitumen. Road Materials and Pavement Design. 2019, 1-16.

[15] F. Pahlavan, A. Samieadel, S. Deng, E. Fini. Exploiting synergistic effects of intermolecular interactions to synthesize hybrid rejuvenators to revitalize aged asphalt. ACS Sustainable Chemistry & Engineering. 2019, 7, 18, 15514-15525.

[16] G. Xu, H. Wang. Molecular dynamics study of oxidative aging effect on asphalt binder properties. Fuel. 2017, 188: 1-10.

[17] B. Li, W. Huang, N. Tang, J. Hu, P. Lin, W. Guan, F. Xiao, Z. Shan. Evolution of components distribution and its effect on low temperature properties of terminal blend rubberized asphalt binder. Construction and Building Materials. 2017, 136: 598-608.

[18] M. Mohammadafzali, H. Ali, G. Sholar, W. Rilko. Effects of rejuvenation and aging on binder homogeneity of recycled asphalt mixtures. Journal of Transportation Engineering, Part B: Pavemens. 2019, 145, 1, 1-9.

[19] J. Xu, Z. Fan, J. Lin, P. Liu, D. Wang, M. Oeser. Study on the effects of reversible aging on the low temperature performance of asphalt binders. Construction and Building Materials. 2021, 295, 123604.

[20] Z. Fan, C. Du, P. Liu, D. Wang, M. Oeser. Study on interfacial debonding between bitumen and aggregate based on micromechanical damage model. International Journal of Pavement Engineering. 2020, DOI: 10.1080/10298436.2020.1745800.

[21] Z. Fan, J. Lin, Z. Chen, P. Liu, D. Wang, M. Oeser. Multiscale understanding of interfacial behavior between bitumen and aggregate: From the aggregate mineralogical genome aspect. Construction and Building Materials. 2021, 271, 121607.

[23] D. Sun, G. Sun, X. Zhu, F. Ye, J. Xu. Intrinsic temperature sensitive self-healing character of asphalt binders based on molecular dynamics simulation. Fuel. 2018, 211: 609-620.

[24] L. Xie, Y. Shao, W. Zhong, H. Ben, K. Li. Molecular dynamic simulation on the oxidation process of coal tar pitch. Fuel. 2019, 242: 50-61.

[25] Y. Gao, Y. Zhang, Y. Yang, J. Zhang, F. Gu. Molecular dynamics investigation of interfacial adhesion between oxidised bitumen and mineral surfaces. Applied Surface Science. 2019, 479: 449-462.

[26] H. Zhang, M. Huang, J. Hong, F. Lai, Y. Gao. Molecular dynamics study on improvement effect bis(2-hydroxyethyl) terephthalate on adhesive properties of asphalt-aggregate interface. Fuel. 2021, 285, 119175.

[27] M. Su, C. Si, Z. Zhang, H. Zhang. Molecular dynamics study on influence of Nano-ZnO/SBS on physical properties and molecular structure of asphalt binder. Fuel. 2020, 263, 116777.

[28] B. Cui, X. Gu, D. Hu, Q. Dong. A multiphysics evaluation of the rejuvenator effects on aged asphalt using molecular dynamics simulations. Journal of Cleaner Production. 2020, 259, 120629.

[29] D.D. Li, M.L. Greenfield. Chemical compositions of improved model asphalt systems for molecular simulations. Fuel. 2014, 115: 347-356.

[30] D.D. Li, M.L. Greenfield. Viscosity, relaxation time, and dynamics within a model asphalt of larger molecules. The Journal of Chemical Physics. 2014, 140, 034507.

[31] D. Hu, X. Gu, B. Cui, J. Pei, Q. Zhang. Modeling the oxidative aging kinetics and pathways of asphalt: A ReaxFF molecular dynamics study. Energy & Fuels. 2020, 34, 3: 3601-3613.

[32] Y. Yang, Y. Wang, J. Cao, Z. Xu. Reactive molecular dynamic investigation of the oxidative aging impact on asphalt. Construction and Building Materials. 2021, 121298.

[33] Q. Liu, J. Wu, L. Xie, Z. Zhang, X. Ma, M. Oeser. Micro-scale investigation of aging gradient within bitumen film around air-binder interface. Fuel. 2021, 286, 119404.

[34] L. Luo, L. Chu, T.F. Fwa. Molecular dynamics analysis of oxidative aging effects on thermodynamic and interfacial bonding properties of asphalt mixtures. Construction and Building Materials. 2020, 121299.

[35] Z. Long, L. You, X. Tang, W. Ma. Y. Ding, F. Xu. Analysis of interfacial adhesion properties of nano-silica modified asphalt mixtures using molecular dynamics simulation. Construction and Building Materials. 2020, 255, 119354.

[36] X. Qu, Q. Liu, M. Guo, D. Wang. M. Oeser. Study on the effect of aging on physical properties of asphalt binder from a microscale perspective. Construction and Building Materials. 2018, 187: 718-129.

[37] X. Jin, R. Han, Y. Cui, C. Glover. Fast-rate-constant-rate oxidation kinetics model for asphalt binders. Industrial & Engineering Chemistry Research. 2011, 50, 13373-13379.

[38] G. Liu, C. Glover. A study on the oxidative kinetics of warm mix asphalt. Chemical Engineering Journal. 2015, 280, 115-120.

[39] Y. Cui, C. Glovr, J. Braziunas, H. Sivilevicius. Further exploration of the pavement oxidation model-diffusion-reaction balance in asphalt. Construction and Building Materials. 2018, 161, 132-140.

[40] D. Zhang, B. Birgisson, X. Luo, I. Onifade. A new long-term aging model for asphalt pavements using morphology-kinetics based approach. Construction and Building Materials. 2019, 229, 117032.

[41] D. Zhang, B. Birgisson. X. Luo, I. Onifade. A new short-term aging model for asphalt binders based on rheological activation energy. Materials and Structures. 2019, 52, 68.

[42] Z. Zhao, M. Xuan, Z. Liu, Y. Cong, Y. Wei, K. Liao. A study on aging kinetics of asphalt based on softening point. Petroleum Science and Technology. 2003, 21(9&10), 1575-1582.

[43] Y. Wang, K. Zhao, C. Glover, L. Chen, Y. Wen, D. Chong, C. Hu. Effects of aging on the properties of asphalt at the nanoscale. Construction and Building Materials. 2015, 80, 244-254.

[44] F. Fallah, F. Khabaz. Y. Kim, S. Kommidi, H. Haghshenas. Molecular dynamics modeling and simulation of bituminous binder chemical aging due to variation of oxidation level and saturate-aromatic-resin-asphaltene fraction. Fuel. 2019, 237, 71-80.

[45] Y. Ding, B. Huang, X. Shu, Y. Zhang, M.E. Woods. Use of molecular dynamics to investigate diffusion between virgin and aged asphalt binders. Fuel. 2016, 174: 267-273.

[46] J. Pan, R.A. Tarefder. Investigation of asphalt aging behaviour due to oxidation using molecular dynamics simulation. Molecular Simulation. 2016, 42, 8: 667-678.

[47] ASTM D5-06. Standard test method for penetration of bituminous materials.

[48] ASTM D36-06. Standard test method for softening point of bitumen (ring and ball apparatus).

[49] AASHTO T316-13. Standard method of test for viscosity determination of asphalt binder using rotational viscometer.

[50] EN 15326. British standard for bitumen and bituminous binders-measurement of density and specific gravity-capillary-stoppered pycnometer method.

[51] ASTM D4124. Standard test method for separation of asphalt into four fractions.

[52] ASTM D7343. Standard practice for optimization, sample handling, calibration, and validation of X-ray fluorescence spectrometry methods for elemental analysis of petroleum products and lubricants.

[53] AASHTO M320. Standard specification for performance-graded asphalt binder.

[54] D. Oldham, X. Qu, H. Wang, E.H. Fini. Investigating change of polydispersity and rheology of crude oil and bitumen due to asphaltene oxidation. Energy & Fuels. 2020, 34: 10299-10305.

[55] D. Yu, Y. Gu, X. Yu. Rheological-microstructural evaluations of the short and long-term aged asphalt binders through relaxation spectra determination. Fuel. 2020, 265, 116953.

[56] F. Wang, Y. Xiao, P. Cui, J. Lin, M. Li, Z. Chen. Correlation of asphalt performance indicators and aging degrees: A review. Construction and Building Materials. 2020, 250, 118824.

[57] M. Xu, J. Yi, P. Qi, H. Wang, M. Marasteanu, D. Feng. Improved chemical system for molecular simulations of asphalt. Energy & Fuels. 2019, 33(4): 3187-3198.

[58] J. Wreczycki, Y. Demchuk, D. Bielinski, M. Bratychak, V, Gunka, R Anyszka, T. Gozdek. Bitumen binders modified with sulfur/organic copolymers. Materials. 2022, 15(5), 1774.

[59] Z. Long, S. Zhou, S. Jiang, W. Ma, Y. Ding, L. You, X. Tang, F. Xu. Revealing compatibility mechanism of nanosilica in asphalt through molecular dynamics simulation. Journal of Molecular Modeling. 2021, 27, 81.

[60] J. Howson, E. Masad, A. Bhasin, D. Little, R. Lytton. Comprehensive analysis of surface free energy of asphalts and aggregates and the effects of changes in pH. Construction and Building Materials. 2011, 25: 2554-2564.

[61] E. Leroy, A. Souid, R. Deterre. A continuous kinetics model of rubber vulcanization predicting induction and reversion. Polymer Testing. 2013, 32, 575-585.

[62] M. Tjahjono, C. Huiheng, E. Widjaja, K. Sa-ei, M. Garland. Combined online transmission FTIR measurements and BTEM analysis for the kinetics study of a consecutive reaction in aqueous-organic phase medium. Talanta. 2009, 79, 856-862.

[63] J. Guo, A. Lua. Kinetics study on pyrolytic process of oil-palm solid waste using two-step consecutive reaction model. Biomass & Bioenergy. 2001, 20, 223.

4

Chemical characterizations and MD simulations on various rejuvenators

*Apart from aged bitumen, it is necessary to probe the difference in chemical and thermodynamic properties between various rejuvenators to figure out the interaction efficiency and mechanism between aged bitumen and rejuvenators. In this chapter, a series of chemical characterizations of the four commonly-used types of rejuvenator will be presented to determine their proper representation in the average and multi-component molecular model as aged bitumen in **Chapter 3**. In addition, MD simulations are carried out using these average and multi-component models of rejuvenators to detect the difference in predicted outputs. Based on the results of these simulations, the average model was selected for the MD simulations on rejuvenator-aged bitumen systems.*

4.1 Introduction

Nowadays, numerous rejuvenators are developed and selected to reactivate the mechanical performance of aged bitumen by supplementing the saturates and aromatics fractions and diluting the generated polar products during aging. Different kinds of recycling agents from bio-resources (such as vegetable oils [1], waste cooking oils [2], and other bio-oils [3]) and petroleum-based products (like engine oils [4], naphthenic oils [5], aromatic oils [6], etc.) have proven to be efficient in improving the initial low-temperature cracking resistance, fatigue life, workability, and durability of aged bitumen and mixture [7-9]. The results are summarized in **Table 4.1**.

Table 4.1 Summary of experimental results of six rejuvenators on bitumen and mixture [7]

Property	Test method	Standard	Virgin	RAP	WV oil	WV Grease	Organic oil	Tall oil	Aromatic Extract	WEO
Rutting	High PG	≥64°C	√	√	√	√	√	√	√	√
	WTT rut depth	≤12.5 mm	×	√	√	√	√	√	√	√
Moisture	WTT inflection point	≥10,000 cycles	×	√	×	√	√	√	√	√
Aging	Loss of volatiles	≤1%	√	√	√	√	√	√	√	×
Workability	Rot. Viscosity	≤3Pa·s	√	×	√	√	√	√	√	√
	Mix workability	≤10 gyr	√	×						
Low temp. cracking	Low PG	≤-22°C	√	×	√	√	√	√	√	×
	Cracking temperature	≤-22°C	√	×				×	√	
Fatigue	G*sinδ	≤ 5,000kPa	√	×	√	√	√	√	√	√
	CAST, 50% stiffness loss	≥ 3E+09 cycles	√	√	√	√	√	√	√	×
Summary			3.0	1.0	3.0	5.0	5.0	4.5	5.5	2.0

To date, the American National Centre for Asphalt Technology (NCAT) categorized the rejuvenators into five groups based on their chemical characteristics and material resources, including the paraffinic-oils, naphthenic-oils, aromatic extracts, triglycerides/fatty acids, and tall oils [5], listed in **Table 4.2**. Paraffinic oils, aromatic extracts, and naphthenic oils are the by-products of petroleum processing, while triglycerides (fatty acids) and tall oils are both bio-based materials [10]. Generally, the chemical components of crude oil are complicated and strongly depend on the source. Based on the molecular distribution, crude oil is divided into the paraffinic, intermediate, and cycloalkyl groups [11]. Similarly, the chemical compositions in paraffinic oils, aromatic extracts, and naphthenic oils are significantly different [12]. The main components in paraffinic oils, like engine oil or lubricating oils, are the saturated long-chain alkane molecules, while the rejuvenators in the aromatic extracts group are rich in aromatic hydrocarbons [5].

Table 4.2 Classifications of different typical rejuvenators for aged bitumen recycling [5, 15]

Category	Examples	Description
Paraffinic oils	Waste engine oil or waste engine oil bottom	Refined used lubricating oils
Aromatic extracts	Commercial products	Refined crude oil products with polar aromatic oil components
Naphthenic oils	Commercial products	Engineered hydrocarbons for asphalt modification
Triglycerides & fatty acids	Waste vegetable oil Oleic acid	Derived from vegetable oils
Tall oils	Commercial products	Paper industry by-products; Same chemical family as liquid anti-strip agents and emulsifiers

Moreover, naphthene molecules with saturated aromatic rings are detected in naphthenic oils [13]. On the other hand, triglycerides and fatty acid molecules are the main components in vegetable and cooking oils [14]. Lastly, tall oils are the by-products of the paper industry, and it is separated from other bio-oils because there are many polar oxygen-containing functional groups in their molecular structures [10]. Hamzeh et al. detected the distinct difference in chemical properties between five recycling agents and found that the rejuvenation efficiency on mechanical properties and moisture susceptibility significantly depends on the recycling agents [8].

Although it can distinguish the difference in chemical characteristics of various rejuvenators, such as SARA components and functional group distribution, the underlying mechanism regarding the interactions (compatibility) between aged bitumen and rejuvenators is still unclear and difficult to monitor at the macroscale [16]. Molecular dynamics (MD) simulation is a powerful tool to help researchers understand molecular interactions and predict the essential thermodynamic properties of materials at the nanoscale [17]. **Figure 4.1** illustrates typical molecular structures of rejuvenators normally used in MD simulations [18-21]. A single molecular formula $C_{12}H_{16}$ containing a polar benzene ring, saturated naphthenic, and alkyl hydrocarbons is the simple model used for the molecular structure of a rejuvenator [18, 19]. However, this imagined structure does not correspond to the actual rejuvenator composition. Meanwhile, the molecular structure of $C_{10}H_{18}O_2$ was utilized to represent sunflower oil [20]. The aromatic-based model with indole group (C_8H_9N) and alkyl-based model containing amide ($C_{16}H_{32}NO$) were also built, in which the polar aromatic cyclic and long-chain alkyl hydrocarbons are the main body of rejuvenator molecules connected with the polar functional group of indole or amide [21]. Because of the many different models, Sun and Wang divided the molecular structures of rejuvenators, in line with the SARA fractions for bitumen, into four categories, cyclic saturate, straight saturate, naphthene aromatic, and polar aromatic only on a molecular level [22].

(a) $C_{12}H_{16}$ (b) $C_{10}H_{18}O_2$ (c) C_8H_9N (d) $C_{16}H_{32}NO$
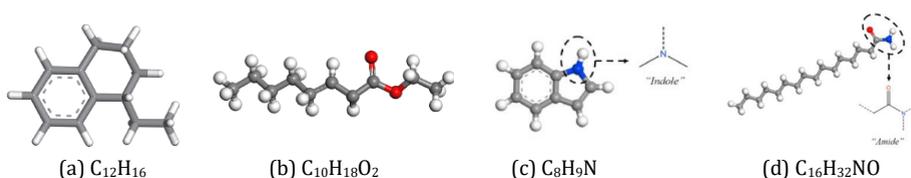
Figure 4.1 Typical molecular structures of rejuvenators used in MD simulations [18-21]

However, these existing molecular structures of rejuvenators are mostly empirical and based on limited chemical characterizations. This sketchy estimation led to a huge difference between MD simulation outputs and experimental results. Moreover, the authentic rejuvenation mechanism at an atomic scale is still unclear, which hinders the classification, optimization, and proper design of efficient rejuvenators for aged bitumen recycling. It is of great significance to systematically conduct the chemical characterizations on generic rejuvenators to determine the representative molecular models of different common rejuvenators for MD simulations. Furthermore, it is also necessary to fundamentally investigate and compare the chemical, physical, and thermodynamic properties of these generic rejuvenators. Additionally, it is found that the molecular structures of these rejuvenators in all MD simulation cases are the average model, in which only one sort of molecule is employed to represent one whole rejuvenator [22-24]. Investigating the impact of certain specific or characteristic molecules in the rejuvenator may become challenging.

4.2 Research objective and scheme

The main objective of this chapter is to develop representative average and multi-component molecular models of four commonly-used rejuvenators and compare their thermodynamics behaviors at an atomic level using MD simulations. **Figure 4.2** illustrates the research framework of this chapter. Firstly, the elemental composition, functional groups distribution, and average molecular weight of four basic commonly-used rejuvenators (bio-oil, engine-oil, naphthenic-oil, and aromatic-oil) were measured to provide the basis to

determine their average molecular structures. Meanwhile, the Gas chromatography-mass spectrometry (GC-MS) test (introduced in **section 4.3.2.4**) was performed to detect the molecular components in these rejuvenators and establish representative multi-component molecular models. Afterward, the MD simulations were adopted on both average and multi-component molecular models to fundamentally predict the thermodynamic properties (Energetic parameters, cohesive energy density, solubility parameter, diffusion behavior, volumetric and structural characteristics) of various rejuvenators, while experimental tests (density and glass transition temperature) were implemented to validate the reliability of the proposed molecular models of the rejuvenators. Lastly, the MD outcomes from average and multi-component models were compared with experimental results to determine the final molecular models of these rejuvenators to be used for further MD simulations on rejuvenated bitumen systems.
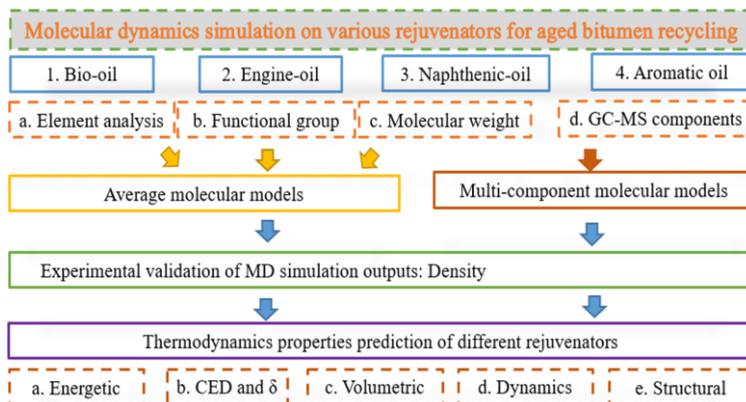
Figure 4.2 Research schemes and methodologies

4.3 Materials and experimental methods

4.3.1 Rejuvenators

In this thesis, four types of generic rejuvenators were selected: bio-oil (BO), engine-oil (EO), naphthenic-oil (NO), and aromatic-oil (AO). The bio-oil with a color of pale yellow is the rap-oil, while the engine oil (brown liquid), naphthenic oil (transparent liquid), and aromatic oil (dark-brown semisolid) are all petroleum-based products. **Table 4.3** lists the physical indices of these four rejuvenators. The declining order for their density values is AO > BO > NO > EO, while the magnitude for dynamic viscosity at 25°C is AO > NO > EO > BO. It should be mentioned that the AO rejuvenator exhibits a similar density as virgin bitumen (approximately 1.0 g/cm³) [25], and it presents a higher viscosity than the other three rejuvenators. In addition, the BO rejuvenator shows a higher density than the NO and EO, but its viscosity value is the lowest.

Table 4.3 The basic properties of various rejuvenators

Items	BO	EO	NO	AO
Color	Pale yellow	brown	transparent	Dark-brown
Density (25°C, g/cm³)	0.911	0.833	0.875	0.994
Density (60°C, g/cm³)	0.899	0.814	0.852	0.978
Viscosity (25°C, cP)	50	60	130	63100
Flash point (°C)	265-305	>225	>230	>210

4.3.2 Experimental methods

4.3.2.1 Element analysis

The elemental compositions of four rejuvenators, referring to the dosage of carbon (C), hydrogen (H), Sulfur (S), Nitrogen (N), and Oxygen (O) elements, were measured with an elemental analyser (Vario EL III) manufactured from the Elementar Corp., Germany. The machine was first calibrated by testing the element distribution of one reference substance (sulfanilamide). Afterward, about 10-mg rejuvenator was wrapped in a thin capsule and put into a sample tank for sufficient oxidization and combustion. The gas products were separated and detected to determine the content of different elements (C%, H%, S%, and N%). Lastly, the oxygen concentration (O%) was calculated by (100-C%-H%-S%-N%), assuming that no other element type existed in these rejuvenators. The results can be found in **section 4.4.1**.

4.3.2.2 Attenuated total reflectance-Fourier-transform infrared (ATR-FTIR) spectroscopy

The molecular structures of organic rejuvenators are composed of hydrocarbon chains and polar functional groups with heteroatoms [26]. In this chapter, the functional groups in the molecular structures of four rejuvenators were monitored using the ATR-FTIR device with a wavenumber region of 600-4000 cm^{-1} at room temperature. The scan number for each sample was 12, and at least three parallel tests were measured to ensure data accuracy. The results can be found in **section 4.4.2**.

4.3.2.3 Vapor Pressure Osmometry (VPO) test

In this thesis, the average molecular weights of rejuvenators were obtained using a Vapor Pressure Osmometry (VPO) test, a conventional way to measure the molecular weight values of different petroleum distillates [27]. The engine-oil, naphthenic-oil, and aromatic-oil rejuvenators were all petroleum-based products with molecular weight lower than 1000 g/mol, which is hardly detected by the Gel Permeation Chromatography (GPC) test. **Figure 4.3** illustrates the working principle, test device, and rejuvenator specimens of the VPO test, which estimates the average molecular weight according to the difference in Vapor pressure because of the incorporation of solute into a pure solvent. The results can be found in **section 4.4.3**.

The VPO device adopted here was a Knauer osmometer (Knauer, Berlin-Heidelberg, West Germany), shown in **Figure 4.3(b)**. Toluene was used as a solvent, while benzile was the calibration substance. Before testing, different benzile/toluene solutions with concentrations of 0.005, 0.01, 0.015, and 0.02 mol/kg were manufactured. The standard solution curve of the VPO response parameter v/c along the relative mass molarity c of solute could be drawn. Meanwhile, rejuvenator/toluene solutions with specific mass ratios were prepared (see **Figure 4.3(c)**), and the corresponding VPO response v/c values of rejuvenator solutions were measured. Lastly, the relative mass molarity of the rejuvenator in solution was determined in a standard curve, and the average molecular weight of the solvent (rejuvenator) could be calculated.
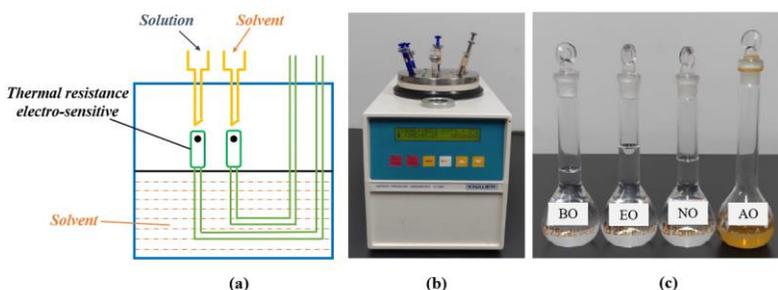
Figure 4.3 The working principle, test device, and rejuvenator samples in the VPO test

4.3.2.4 Gas chromatography-mass spectrometry (GC-MS) test

The GC-MS test is an efficient way to analyze tiny amounts of a substance, and previous work successfully detected the chemical compositions in bio-based rejuvenators [28, 29]. Hence, the chemical components in various rejuvenators were identified using the GC-MS method. The basic working principle of the GC-MS test

is displayed in **Figure 4.4**. First, the column retains the rejuvenator molecules and elutes as the retention time prolongs due to polarity and solubility differences [30]. Afterward, the separated molecules are captured, ionized, accelerated, and detected by a mass spectrometer by measuring the molecule mass. The GC-MS device utilized herein was Agilent 6890 N/5975 from the USA. About 1 mg of the rejuvenator sample was purged with inert gas (nitrogen) into an airtight chamber at room temperature. The pyrolysis temperature and time were set as 200°C and 15s with an increasing rate of 10 °C/ms [31]. Besides, the electron energy and scanning range employed in the system were selected as 70 eV and 30-1000 amu., respectively. Finally, the type and amount of substances in each rejuvenator could be outputted as a GC-MS curve using the substance library (see **Appendix A**). The results can be found in **section 4.4.4**.
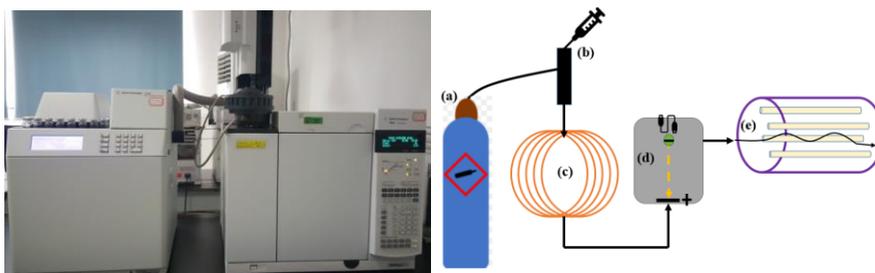
Figure 4.4 The basic working principle of the GC-MS method (a) Inert gas system; (b) injector; (c) gas chromatography column; (d) ionization room; (e) a mass spectrometry measurement system

4.3.2.5 Pycnometer density measurement

The density is the most popular parameter for validating the reasonability of molecular structures and MD simulation settings (Forcefield type, time step, energy summation method, etc.). In this chapter, the density values of four rejuvenators were tested with the capillary-stoppered pycnometer method at 25 and 60°C according to the standard of EN 15326 [25]. The results are shown in **section 4.6.3**.

4.3.2.6 Dynamic viscosity test

The dynamic viscosity values of four rejuvenators were measured with a rotational viscometer (RV) at different temperatures of 25, 40, 60, and 100°C following the AASHTO T316-13 standard. The rotor spinning rate was 20 rad/s, and the viscosity was recorded when the holding time was longer than 30 min. The results are shown in **section 4.7.5**.

4.4 Experimental results and discussion

4.4.1 Elemental compositions of rejuvenators

Element components are significant in determining the atom numbers, whole molecular formula, and molecular weight. **Table 4.4** displays the elemental compositions (N, C, H, S, and O) of four rejuvenators. As expected, these four rejuvenators are mainly composed of carbon and hydrogen elements (hydrocarbons). Besides, it is depicted that in all rejuvenators, the N and S element contents are markedly lower than C and H. Besides, the oxygen dosage in engine-oil, naphthenic-oil, and aromatic-oil is less than 0.5%. In comparison, a high oxygen content of 11.36% is detected in bio-oil rejuvenator. Herein, the oxygen-containing functional group exists in the molecular structure of bio-oil rejuvenator, and the chemical components in three petroleum-based rejuvenators are hydrocarbons without heteroatom functional groups.

The ratio of hydrogen to carbon element (H/C) is utilized to estimate the unsaturation degree of hydrocarbons. The higher the H/C ratio is, the larger the saturation degree is. Similarly, the ratio of oxygen to carbon element (O/C) is calculated to assess the concentration of oxygen-containing functional groups in

rejuvenators. **Table 4.4** also lists the H/C and O/C values of four rejuvenators. The engine-oil exhibits the highest H/C ratio, indicating that the molecular structure of the engine-oil presents the largest saturation degree. Meanwhile, the bio-oil and naphthenic-oil show a similar H/C value, while the H/C value of aromatic-oil is the lowest. It means that the aromatic oil presents the strongest degree of unsaturation, and there are plenty of unsaturated hydrocarbons in aromatic-oil, such as olefin, alkyne, and aromatic rings.

Table 4.4 Elemental compositions in various rejuvenators

Rejuvenators	N%	C%	H%	S%	O%	H/C	O/C
Bio-oil	0.15	76.47	11.96	0.06	11.36	1.88	0.1114
Engine-oil	0.23	85.16	14.36	0.13	0.12	2.02	0.0011
Naphthenic-oil	0.12	86.24	13.62	0.1	0.1	1.90	0.0009
Aromatic-oil	0.55	88.01	10.56	0.48	0.4	1.44	0.0034

4.4.2 Functional group distribution

The functional groups' distribution in different rejuvenators is demonstrated in **Figure 4.5**. It is manifested that these four rejuvenators have the same strong absorbance peaks at 2920 and 2853cm^{-1}, representing the C-H stretch of methylene (-CH$_2$-) and methyl (-CH$_3$) in alkanes, respectively. Moreover, the characteristic peaks at 1456 and 1376 cm^{-1} are observed in FTIR curves of all rejuvenators, which refer to the C-H bend of both -CH$_2$- and -CH$_3$ groups. Besides, the absorbance peak at 745 cm^{-1} resulted from the C-H bend of -CH$_2$- in alkanes with more than four methylene terms.
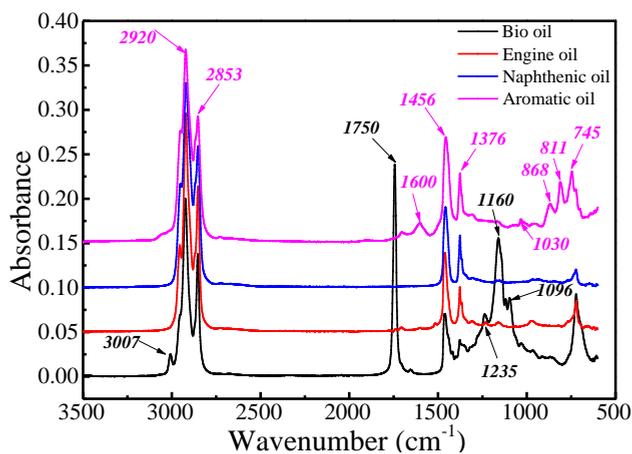
Figure 4.5 The FTIR results of different rejuvenators

It is depicted that the engine-oil and naphthenic-oil have no additional characteristic peak, indicating that their main chemical components are saturated hydrocarbons without heteroatom functional groups. However, the functional groups' distribution in bio-oil is significantly different from other petroleum-based rejuvenators. The strong characteristic peaks at 1750 and 1160 cm^{-1} are probed from the C=O and C-O-C stretch in esters, respectively. Therefore, the ester group exists in the molecular structure of bio-oil, and the same phenomenon was mentioned in previous studies [32, 33]. In addition, the weak peaks at 1235 and 1096 cm^{-1} are due to the C-C(O)-C stretch of acetates and the C-C stretch of ketone in esters.

Interestingly, a small peak at 3007cm^{-1} is observed and related to the -O-H stretch of hydroxyl in the molecular structure of the fatty acid in bio-oil. It is worth noting that the peak area of -OH is smaller than ester groups, indicating that the chemical component in bio-oil rejuvenator is mostly the ester with long-chain alkanes. Regarding the aromatic-oil, the specific absorbance peaks occur at 1600, 868, and 811 cm^{-1}. The characteristic peak at 1600cm^{-1} represents the C=C stretch of aromatic rings, while the peaks at 868 and

811 cm^{-1} are both from the C-H bend (meta and para) in aromatic rings. It can be summarized that the aromatic-oil is composed of hydrocarbons with aromatic rings, and no heteroatom functional group is observed in the aromatic-oil rejuvenator.

4.4.3 Average molecular weight

The VPO curve with a correlation equation describing a linear relationship between the v/c parameter and solute concentration is displayed in **Figure 4.6**. The v/c values of rejuvenator solutions with specific mass fractions (rejuvenator/solvent) were measured, and the corresponding results are summarized in **Table 4.5**. Based on the standard solution curve and v/c value, the related points of four rejuvenator solutions are found and marked in **Figure 4.6**. Afterward, the relative mass molarity of each rejuvenator in the corresponding solution is determined as 0.01026 (bio-oil), 0.00788 (engine-oil), 0.0157 (naphthenic-oil) and 0.01463 (aromatic-oil) mol·kg^{-1}. The average molecular weight of these rejuvenators can be calculated according to **Eq.4.1**.

$$M_n = \frac{m_r}{c * m_s} \tag{4.1}$$

where M_n is the average molecular weight of the rejuvenator, g/mol; m_r and m_s represent the mass of the rejuvenator phase and whole solution, g; while c refers to the mass molarity of rejuvenator in a solvent, mol/g.
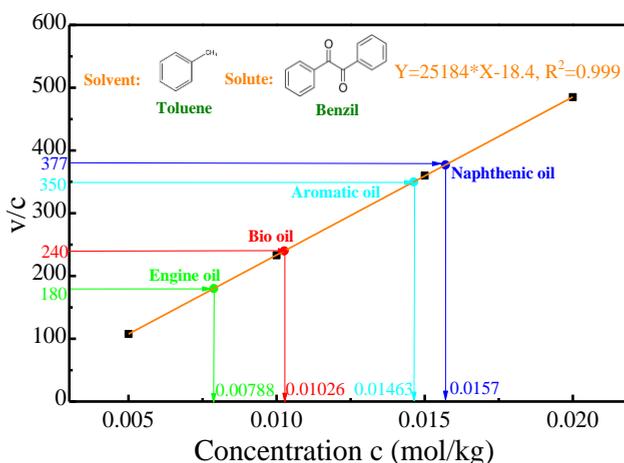
Figure 4.6 The VPO results of different rejuvenators

The average molecular weight values of the four rejuvenators are summarized in **Table 4.5**. For each rejuvenator solution, the v/c value was measured at least five times, and the M_n parameter of these rejuvenators is the average value for several parallel tests. It is found that the M_n values of all rejuvenators are lower than 500 g/mol, which is near the reported average molecular weight of saturate and aromatic fractions in bitumen [11]. It was also mentioned that the increased molecular weight was the key reason for the performance deterioration of bitumen during the aging process [25]. Hence, these oil products with light molecular weight are generally selected as rejuvenators to facilitate molecular weight distribution and restore the macroscale performance of aged bitumen [26]. Moreover, the ranking for the average molecular weight of four rejuvenators is BO < EO < NO < AO. In detail, the M_n value of bio-oil, engine-oil, naphthenic-oil, and aromatic-oil rejuvenator is 286.43, 316.48, 357.06, and 409.99 g/mol, respectively. Therefore, the average molecular weight plays an important role in determining the average molecular structures of rejuvenators, which will be detailed in **section 4.5**.

Table 4.5 The VPO parameters and average molecular weight of various rejuvenators

Rejuvenators	Bio-oil	Engine-oil	Naphthenic-oil	Aromatic-oil
m_r (g)	0.0654	0.0577	0.1234	0.0710
m_s (g)	21.8250	23.0800	22.4384	11.8334
v/c	240	180	377	350
c (mol/kg)	0.01026	0.00788	0.0157	0.01463
M_n (g/mol)	286.43	316.48	357.06	409.99

4.4.4 Chemical components distribution in different rejuvenators

Based on petroleum chemistry knowledge, both gasoline and diesel oil contain several types of alkanes with different carbon-chain lengths. Similarly, the generic rejuvenators from petroleum products are complicated and composed of numerous molecules. To understand the rejuvenation efficiency and mechanism between these rejuvenators and aged bitumen at the nanoscale, it is important to figure out the difference in chemical component distribution between various rejuvenators. In this chapter, the molecular compositions of rejuvenators are detected through the GCMS method, and the corresponding results are shown and discussed.

4.4.4.1 Chemical components in bio-oil rejuvenator

The GC-MS result of the bio-oil rejuvenator is displayed in **Figure 4.7**, and six characteristic peaks of chemical molecules with a retention time of 24.87, 30.87, 31.14, 31.33, 32.17, and 41.75 min are observed. On the basis of the chemistry library, these molecules are recognized as methyl palmitate, methyl linoleate, methyl oleate, methyl elaidate, methyl stearate, and methyl eicosenoate. Meanwhile, it can be found that oxygen-containing functional groups exist in all molecules of bio-oil, which is consistent with the previous studies [28, 29].
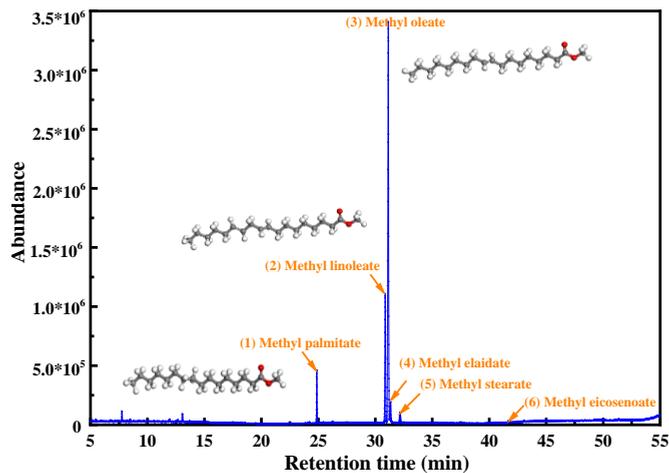
Figure 4.7 The GC-MS curve of bio-oil rejuvenator

Table 4.6 The main chemical components in bio-oil

No.	Retention time	Component	CAS	Mass fraction (wt%)
1	24.868	Methyl Palmitate	000112-39-0	5.30
2	30.8748	Methyl Linoleate	000112-63-0	20.19
3	31.1434	Methyl Oleate	000112-62-9	69.28
4	31.332	Methyl Elaidate	001937-62-8	3.11
5	32.1721	Methyl Stearate	000112-61-8	1.65
6	41.7453	Methyl Eicosenoate	003946-08-5	0.47

According to the peak area, the mass fraction of each component is calculated and listed in **Table 4.6**. The methyl oleate exhibits the maximum proportion of 69.28%, followed by the methyl linoleate (20.19%) and the methyl palmitate (5.30%), while the mass fractions of the other three molecules are lower than 5.0%. Hence, it is concluded that the bio-oil rejuvenator is mainly composed of methyl oleate, methyl linoleate, and methyl palmitate. Their molecular structures are also drawn in **Figure 4.7**. It is worth mentioning that the functional group in these three main molecules in bio-oil is identical, while the difference exists in the number of both carbon atoms and unsaturated double bond C=C in their body chains.

4.4.4.2 Chemical compositions in engine-oil rejuvenator

Apart from the bio-oil, the other three kinds of rejuvenators all come from petroleum refinery processing. As mentioned, engine-oil, naphthenic-oil, and aromatic-oil rejuvenators contain numerous molecules. **Figure 4.8(a)** illustrates the GC-MS curve of the engine-oil rejuvenator. Meanwhile, the complex chemical components in engine-oil can be found in **Table A.1** in **Appendix A**, which implies that the engine-oil rejuvenator is approximately composed of 56 different molecules. It significantly increases the difficulty in distinguishing the roles of these components in rejuvenation efficiency and mechanism when interacting with aged bitumen. Herein, these molecules in engine-oil rejuvenator are divided into four groups (alkane, monocyclic alkane, olefin, and other additives) with a similar separation principle to SARA fractions of bitumen [32].
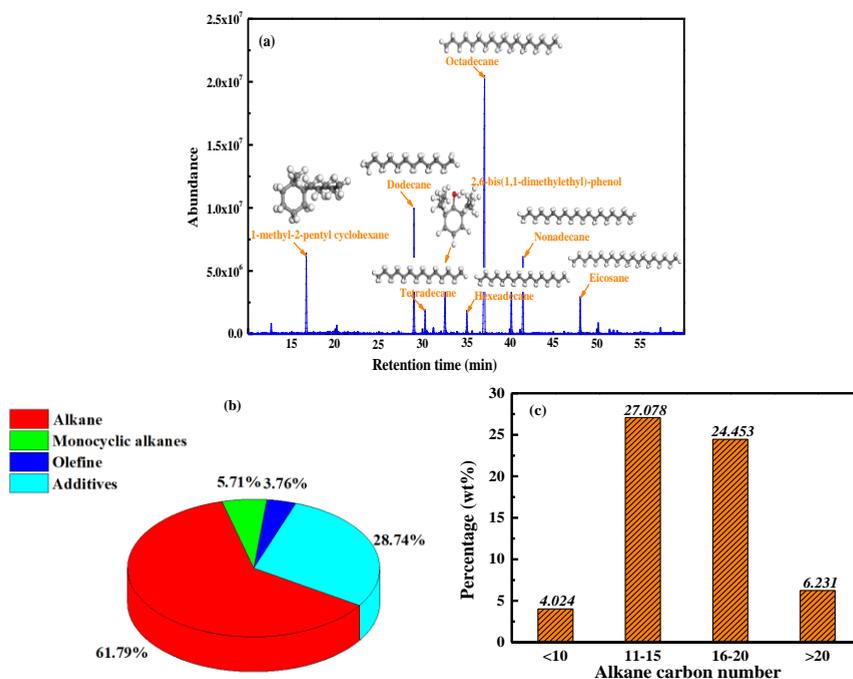
Figure 4.8 The components distribution and alkane classification in engine-oil rejuvenator

The dosages of four chemical component groups in the engine-oil rejuvenator are shown in **Figure 4.8(b)**. The alkane molecules present a percentage of 61.79%, which are the main components of engine-oil. Meanwhile, about 5.71% of monocyclic alkanes and 3.76% of olefins are detected. It should be mentioned that during the production of engine-oil, several additives were incorporated to improve its application performance, such as anti-aging and lubricity [10]. These additives molecules in engine-oil still occupy a distinct proportion of 28.74%, which cannot be ignored when determining the multi-component molecular

model of the engine-oil rejuvenator. Regarding the alkane group with a maximum dosage, **Figure 4.8(c)** displays the alkane molecules' classification and distribution according to the carbon atom's number of the main chain. It manifests that the alkane molecules in engine-oil exhibit disparate carbon-chain structures, which are always determined by the crude oil resources and the atmospheric distillation technologies [3]. Moreover, the carbon atom's number in molecular structures of most alkanes is in the region of 11-20. In detail, the percentage of alkanes with carbon numbers in the ranges of <10, 11-15, 16-20, and >20 is 4.0%, 27.1%, 24.5%, and 6.2%, respectively. From the GC-MS curve, it is depicted that the proportions of several molecules are more apparent, and their molecular structures are also marked in **Figure 4.8(a)**. The dominant molecules in alkanes are dodecane, tetradecane, hexadecane, octadecane, nonadecane and eicosane. Furthermore, the peak abundance of the octadecane is the strongest, followed by the dodecane and 1-methyl-2-pentyl cyclohexane, and the additive molecule of 2,6-bis (1,1-dimethylethyl)-phenol also shows an obvious peak.

4.4.4.3 Chemical compositions in naphthenic-oil rejuvenator

The GC-MS curve of the naphthenic-oil rejuvenator is demonstrated in **Figure 4.9**, and it denotes that almost 40 types of molecules exist in the naphthenic-oil. Detailed information on all molecules is listed in **Table A.2** in **Appendix A**. These chemical components in naphthenic-oil can be separated into an alkane, naphthenic, and other hydrocarbons (additives). It should be noted that the additive group contains those molecules without belonging to the alkane and naphthenic categories. The proportion of alkanes in the naphthenic-oil rejuvenator is approximately 17.85%, while the naphthenic concentration shows a maximum value of 59.79%. Thus, the main components in the naphthenic-oil rejuvenator are naphthenic molecules, followed by alkane molecules. Similar to the engine-oil, other impurity molecules are detected in the naphthenic-oil, which come from different additives added during petroleum processing to enhance its oxidative aging resistance [5, 9]. Due to the complexity and diversity, only the main additive molecules will be included in the multi-component molecular models of engine-oil, naphthenic-oil, and aromatic-oil.
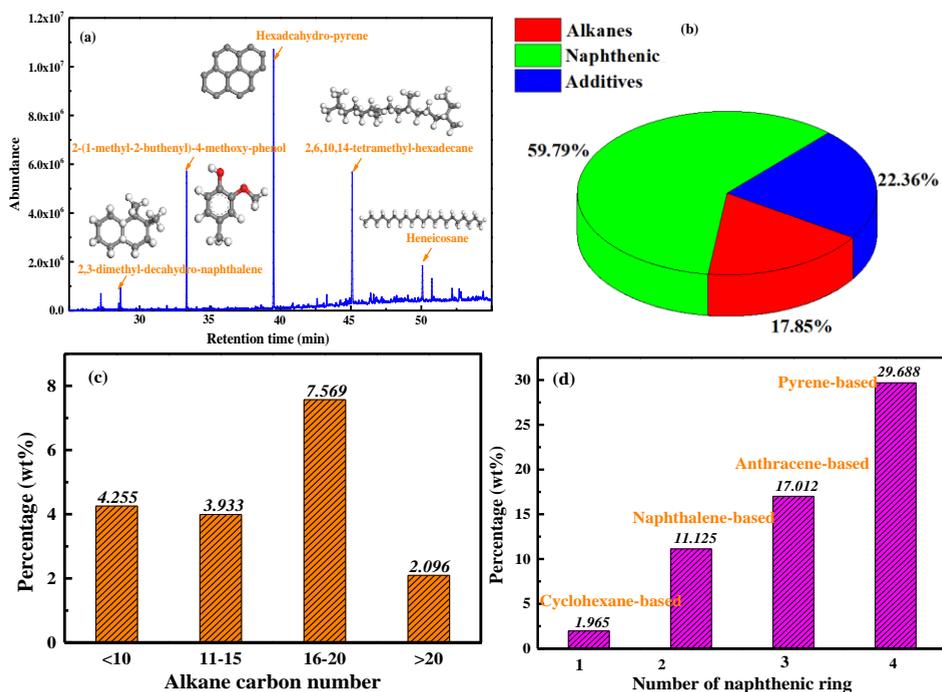
Figure 4.9 The components distribution, alkanes, and naphthenic classification in naphthenic-oil

For complete summarization and analysis, the alkanes and naphthenic molecules are further classified into several groups according to the number of carbon atoms in the alkane chain and naphthenic rings in the whole molecular structure. The corresponding results are illustrated in **Figures 4.9(c)** and **(d)**. Several kinds of alkane molecules with variable carbon-atom numbers in the body chain are observed in naphthenic-oil. The carbon number of most alkanes is lower than 20, and the related percentage is 15.76% in the naphthenic-oil rejuvenator. In addition, the alkanes' concentrations with the chain carbon number in the region of <10 and 11-15 are both 4% approximately, while the alkanes' proportion with the carbon number in 16-20 is 7.57%. Compared to the engine-oil, the alkane dosage in the naphthenic-oil rejuvenator is significantly lower, while the concentration of naphthenic molecules is much higher.

Additionally, the number of naphthenic rings in naphthenic molecules of naphthenic-oil differs from 1 to 4. According to the exact number of naphthenic rings, these naphthenic molecules are divided into four types: cyclohexane-based, naphthalene-based, anthracene-based, and pyrene-based molecules. It can be observed that the pyrene-based naphthenic molecules exhibit the largest proportion of 29.69%, followed by the anthracene-based (17.01%) and naphthalene-based (11.13%) naphthenic molecules, while the dosage of a cyclohexane-based naphthenic molecule is the lowest of 1.97%. From the GC-MS curve, some molecules show larger peaks, such as the 2,3-dimethyl-decahydro-naphthalene, 2-(1-methyl-2-butenyl)-4-methoxy-phenol, hexadcahydro-pyrene, 2,6,10,14-tetramethyl-hexadecane, and heneicosane. Their molecular structures are also displayed in **Figure 4.9(a)**. The hexadcahydro-pyrene molecule presents the strongest peak, followed by the 2-(1-methyl-2-butenyl)-4-methoxy-phenol and 2,6,10,14-tetramethyl-hexadecane. At the same time, the molecular concentrations of 2,3-dimethyl-decahydro-naphthene and heneicosane are similar but much lower than the other three molecules.

4.4.4.4 Chemical compositions in aromatic-oil rejuvenator

The GC-MS result of the aromatic-oil rejuvenator is illustrated in **Figure 4.10(a)**. Numerous peaks are monitored, proving that the aromatic-oil is a complicated material containing various types of molecules. The complicated chemical components in aromatic-oil are summarized in **Table A.3** in **Appendix A**, and they are categorized into four groups (alkane, olefin, aromatics, and additives). The dosage of these four groups of molecules is presented in **Figure 4.10(b)**. It is found that the aromatic-oil is mainly composed of alkane, olefin, aromatic molecules, as well as other hydrocarbons. The alkane content (13.74%) in aromatic-oil is markedly lower than that in the engine-oil (61.79%) and naphthenic-oil (17.85%) rejuvenators. Nevertheless, the concentration of aromatics molecules in aromatic-oil is significant at 53.91%, which is hardly detected in the other three rejuvenators. Moreover, about 2.16% of olefin molecules and 30.19% of other hydrocarbons are monitored in the aromatic-oil.

The alkanes molecules are distinguished in the light of the carbon-atom number in the body chain of molecular structure, and the results are illustrated in **Figure 4.10(c)**. It is manifested that the carbon-atom number in most alkane molecules is 11-20. In contrast, only 0.27% and 2.05% of alkane molecules have a carbon atom number lower than 10 and higher than 20, respectively. Moreover, the dosage of alkanes with a carbon atom number of 16-20 is almost 3.5 times than total concentration of alkanes from undecane to pentadecane. On the other hand, the type of aromatic molecules in aromatic-oil is not unique. In this chapter, these aromatic molecules are assorted following the number of aromatic rings in their molecular structures, including the benzene-based (single-ring), naphthalene-based (double-rings), and fluorene/indene (multi-rings). The concentration of each aromatics molecular group is shown in **Figure 4.10(d)**.
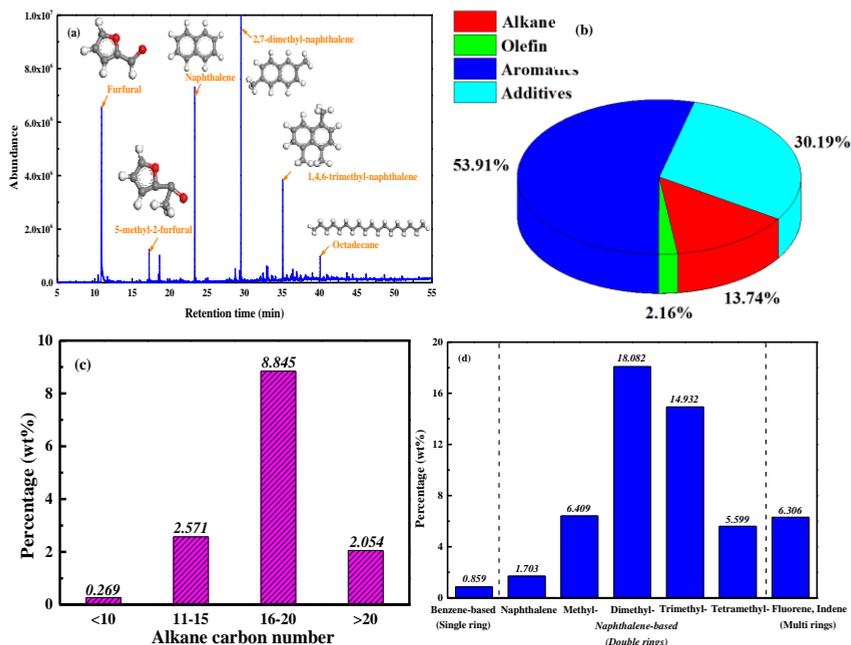
Figure 4.10 The components distribution, alkanes, and aromatics classification in aromatic-oil

It can be found that most aromatics molecules are naphthalene-based with a high dosage of 46.73%, while benzene-based and fluorene/indene only account for 0.86% and 6.31%, respectively. In the meantime, the naphthalene-based aromatics molecules are classified into five items based on the difference in the number of methyl substituents in aromatic rings, which varies from 0 to 4. Thence, the five groups of naphthalene-based aromatics molecules are named naphthalene, methyl-naphthalene, dimethyl-naphthalene, trimethyl-naphthalene, and tetramethyl-naphthalene. The dosage of naphthalene molecules is the lowest at 1.70%, indicating that almost all aromatic-oil naphthalene molecules have more or fewer substituents. Interestingly, the concentration of naphthalene-based molecules and the methyl substituents amount present the Gaussian distribution. The methyl-naphthalene and tetramethyl-naphthalene molecules are 6.4% and 5.6%, respectively. In addition, dimethyl-naphthalene and trimethyl-naphthalene show a large dosage of 18.1% and 14.9%. Thus, about 33% of naphthalene-based aromatic molecules present 2 or 3 methyl substituents. It provides the data basis for determining the molecular components of a multi-component molecular model of the aromatic-oil rejuvenator.

According to the GC-MS curve, the dosage of each molecule in the aromatic-oil rejuvenator is obtained, and the main components with apparently large content can be detected. Six strong peaks are seen in the GC-MS curve of the aromatic-oil rejuvenator, and the related molecular structures are also shown in **Figure 4.10(a)**. As the retention time prolongs, these six chemical components are furfural, 5-methyl-2-furfural, naphthalene, 2,7-dimethyl naphthalene, 1,4,6-trimethyl naphthalene, and octadecane. It further validates that the aromatic-oil rejuvenator mainly comprises alkenes, aromatics, and additives (solvents) molecules. The furfural and 5-methyl-2-furfural are the solvents used during the extraction process of aromatic oils. Moreover, the naphthalene, 2,7-dimethyl naphthalene, and 1,4,6-trimethyl naphthalene molecules are the mainly monitored chemical components in aromatic-oil. In addition, octadecane denotes the existence of alkane molecules in an aromatic-oil rejuvenator. In the following MD simulation section, some of these main components will be chosen to represent the different molecular groups for building the multi-component molecular model of the aromatic-oil rejuvenator.

4.5 Determining the molecular structure of different rejuvenators

4.5.1 Average molecular structure

Currently, the commonly-adopted molecular structures of rejuvenators are not accurate due to the lack of experimental evidence, strongly depending on the rejuvenators' resource and type [8]. This chapter determines the average molecular structures of four rejuvenators according to several chemical characteristics. First, the element compositions and average molecular weights are utilized to recognize the number of different atoms (C, H, S, N, and O) in the molecular formula of each rejuvenator. The basic principle for calculating the number is described in **Eq.4.2.**

$$n(X) = \frac{M_n \cdot X\%}{M(X)} \tag{4.2}$$

where $n(X)$ represents the number of atoms X, and X refers to carbon (C), hydrogen (H), oxygen (O), sulfur (S), or nitrogen (N), respectively; M_n is the average molecular weight of rejuvenator, g/mol; X% shows the mass fraction of element X from element analysis, and M(X) is the relative atomic mass of atom X.

The calculated numbers of different atoms in various rejuvenators are listed in **Table 4.7**. The relative concentrations of elements S and N are limited in each rejuvenator, which is attributed to the desulfurization and denitrification procedures of light-weight oil products (including gasoline, diesel fuel, engine-oil, and aromatic-oil) through the physical atmosphere/vacuum distillation and chemical hydrofining methods [33]. Most heteroatoms (S, N, and O) are in heavy oil or bitumen molecules. Moreover, the high oxygen content in the bio-oil rejuvenator is observed because of its biological resource. Thus, the heteroatoms are not considered during the establishment of average molecular structures for all rejuvenators except for the oxygen atoms in the bio-oil rejuvenator.

From **Table 4.7**, carbon and hydrogen account for the most elements in all rejuvenators, and that's why these rejuvenators are also called "hydrocarbons". The number of carbon atoms in rejuvenators differs from 18.8 to 30.07, while the number of hydrogen atoms is 35.28 to 40.30. Meanwhile, the H/C ratio and saturation degree in various rejuvenators are different, which leads to the difference in the chemo-mechanical properties of these corresponding rejuvenated bitumen. Considering atom number is an integer, the average chemical formula of bio-oil, engine-oil, naphthenic-oil, and aromatic-oil rejuvenator is $C_{19}H_{36}O_2$, $C_{22}H_{44}$, $C_{26}H_{48}$, $C_{30}H_{40}$, respectively.

Table 4.7 The calculated number of different atoms in various rejuvenators

Rejuvenators	n(C)	n(H)	n(O)	n(S)	n(N)
Bio-oil	18.80	35.28	2.09	0.0055	0.032
Engine-oil	22.21	44.95	0.023	0.013	0.051
Naphthenic-oil	25.66	48.62	0.022	0.011	0.031
Aromatic-oil	30.07	40.30	0.103	0.062	0.161

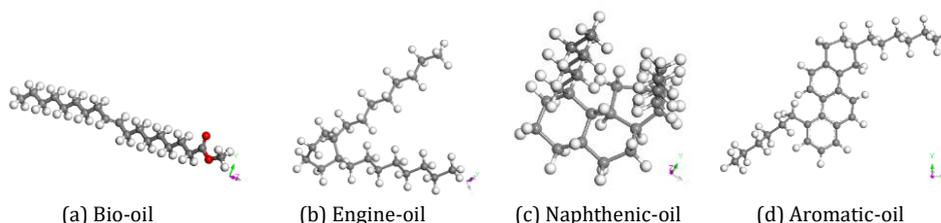| (a) Bio-oil | (b) Engine-oil | (c) Naphthenic-oil | (d) Aromatic-oil |

**Figure 4.11 The average molecular structure of various rejuvenators
(Carbon atoms: black; Hydrogen atoms: white; Oxygen atoms: red)**

However, the detailed molecular structures of rejuvenators cannot be determined because the existing forms and positions of these elements in different functional groups are still unknown. Previous studies employed the FTIR and Nuclear Magnetic Resonance Spectroscopy (C^{13}- or H^1-NMR) methods to distinguish the positions of the carbon, hydrogen atoms, and heteroatoms in specific functional groups [11, 34]. This dissertation implemented FTIR tests to identify the functional groups in the four rejuvenators. In addition, the position of the ester functional group in the molecular structure of bio-oil was decided [22].

The molecular structures of four rejuvenators are illustrated in **Figure 4.11**, in which the black color represents the carbon atoms. In contrast, the white and red color refer to the hydrogen and oxygen atoms, respectively. The bio-oil rejuvenator exhibits a characteristic ester with a straight-chain monoalkene of 19 carbon atoms. Meanwhile, the average molecular structure of the engine-oil rejuvenator consists of one cyclohexane and two saturated n-octane chains. For naphthenic oil, the main body in its chemical structure is the saturated tricyclic alkanes, which are connected with the n-hexane and n-heptane alkyl substituents. Furthermore, the aromatic-oil rejuvenator shows a distinct polycyclic aromatic hydrocarbon structure linked with the saturated straight-chain and monocyclic alkanes. Overall, the molecular structures of these four rejuvenators are significantly different in terms of molecular weight, saturation degree, aromaticity, and polarity, which would be related to their differentiated rejuvenation mechanism and efficiency during the aged bitumen recycling [5-8].

4.5.2 Multi-component molecular structures

The chemical component distribution in four rejuvenators was detected and analysed using the GC-MS method regarding the main molecular groups and molecules with high dosages. However, the molecular components in all rejuvenators are complex and diverse, especially the petroleum-based ones (engine-oil, naphthenic-oil, and aromatic-oil). It significantly brings huge difficulties in finding and establishing representative molecular models of these rejuvenators. Besides, it is unrealistic to consider all molecules in building the multi-component molecular models of pure rejuvenators and rejuvenated bitumen. It is found that there are 3 or 4 molecular groups included in these petroleum-based rejuvenators, while only six kinds of molecules are included in bio-oil rejuvenators. Generally, the molecules representing the saturate, aromatic, resin, and asphaltene fractions are selected to establish the multi-component molecular model of bitumen. Therefore, 3-5 molecules that were shown to be present in high dosage in the GC-MS curve are chosen to represent the main chemical molecular groups and establish the representative multi-component molecular models of four rejuvenators.

4.5.2.1 Bio-oil rejuvenator

From the GC-MS results, the sum content of methyl palmitate, methyl linoleate, and methyl oleate is 94.77%, and methyl oleate has the highest dosage of 69.28%. Hence, these three molecules are considered to build the multi-component model of bio-oil rejuvenator, and their molecular structures are illustrated in **Figure 4.12**. It can be seen that these three molecules present a similar main-chain structure (aliphatic hydrocarbons) and functional group (ester), and the difference is in the number of carbon atoms and double bonds in the main-chain structure.

(a) Methyl palmitate   (b) Methyl linoleate   (c) Methyl oleate
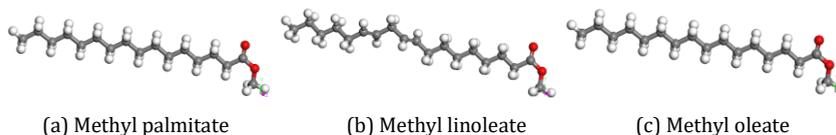
Figure 4.12 Three molecular elements in the bio-oil rejuvenator

In addition, the methyl elaidate (3.1%), methyl stearate (1.7%), and methyl eicosenoate (0.5%) molecules are not considered during the construction of a multi-component model of bio-oil rejuvenator because of their low molecular dosages. **Table 4.8** lists the dosage and the molecular number of these three

molecules in the bio-oil rejuvenator. Due to the omission of methyl elaidate, methyl stearate, and methyl eicosenoate molecules, the content of methyl palmitate, methyl linoleate, and methyl oleate in a multi-component model of bio-oil is calibrated as 5.6%, 21.3%, 73.10%, and the corresponding molecule numbers are 13, 44 and 151, respectively. The model dosage of these three molecules is not the same as the real value because the molecular number should be an integer. However, the difference in molecular dosage between calibrated and model values is small at 0.1%. This means that the multi-component model of the bio-oil rejuvenator should be accurate enough.

Table 4.8 The molecular components in a multi-component molecular model of bio-oil

Components	Measured dosage (wt%)	Calibrated dosage (wt%)	Chemical formula	Molecule number	Molecule dosage (wt%)
Methyl Palmitate	5.30	5.60	$C_{17}H_{34}O_2$	13	5.70
Methyl Linoleate	20.19	21.30	$C_{19}H_{34}O_2$	44	21.20
Methyl Oleate	69.28	73.10	$C_{19}H_{36}O_2$	151	73.10

4.5.2.2 Engine-oil rejuvenator

The engine-oil rejuvenator is mainly composed of alkanes, monocyclic alkanes, and additive molecules. In this thesis, the tetradecane molecule is selected to represent the alkanes molecular group, and the 1-methyl-2-pentyl-cyclohexane molecule refers to the monocyclic alkanes. Regarding the additives group, the high dosage of 28.7% demonstrates their key role in determining the chemo-physical and thermodynamics properties of the engine-oil rejuvenator. Herein, the additive molecules with a dosage higher than 3% are taken into consideration in the multi-component molecular model of engine-oil rejuvenators. These three additive molecules are 2,6-bis (1,1-dimethylethyl)-phenol, 1-pentanol, and butyl benzoate. **Figure 4.13** manifests five molecules' molecular structures in a multi-component engine-oil model. It is found that all three additive molecules show oxygen-containing functional groups, such as the phenolic, hydroxyl, and ester groups. These additive molecules with polar functional groups were incorporated in engine-oil to enhance their anti-aging and performance stability, which was also detected in previous studies [12, 33].

(a) Tetradecane	(b) 1-methyl-2-pentyl-cyclohexane	(c) 2,6-bis(1,1-dimethylethyl)-phenol

(d) 1-pentanol	(e) Butyl benzoate
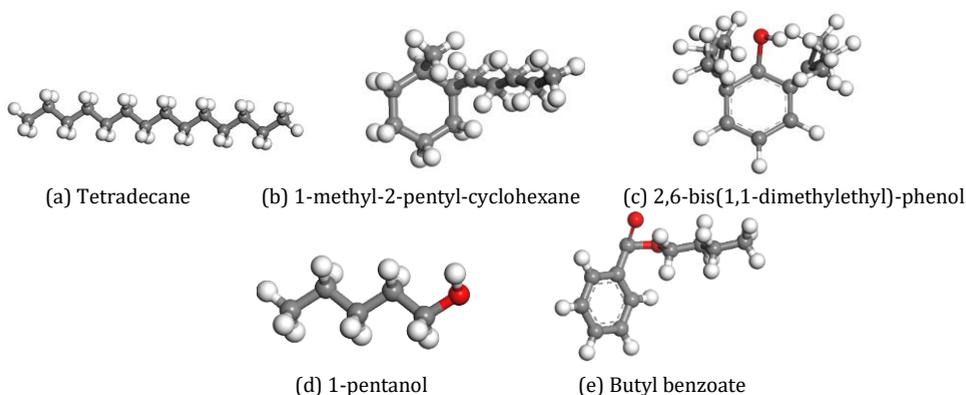
Figure 4.13 The molecular elements of engine-oil rejuvenator

In the multi-component model of engine-oil, five main molecules are included, and their measured and modelled dosages are summarized in **Table 4.9**. It should be mentioned that the measured dosage of tetradecane and 1-methyl-2-pentyl molecule comes from the concentration of alkanes and monocyclic alkanes molecular groups to balance the simplicity and accuracy of the engine-oil molecular model. Meanwhile, most additive molecules with low concentrations are ignored. Thus, the measured dosages of five

molecular elements are calibrated as 67.91%, 6.29%, 13.87%, 8.01%, and 3.92%, respectively. In addition, it should be noted that the total number of molecules in different rejuvenators maintains an approaching level. Accordingly, molecule number of tetradecane, 1-methyl-2-pentyl-cyclohexane, 2,6-bis(1,1-dimethylethyl)-phenol, 1-pentanol, and butyl benzoate molecule is 127, 14, 25, 34 and 8, respectively. Further, the molecule dosages of these five molecules in the model are much closer to the calibrated values.

Table 4.9 The material components in a multi-component molecular model of engine-oil

Components	Measured dosage (wt%)	Calibrated dosage (wt%)	Chemical formula	Molecule Number	Molecule dosage (wt%)
Tetradecane	61.79	67.91	$C_{14}H_{30}$	127	67.9
1-methyl-2-pentyl-cyclohexane	5.72	6.29	$C_{12}H_{24}$	14	6.3
2,6-bis(1,1-dimethylethyl)-phenol	12.62	13.87	$C_{14}H_{22}O$	25	13.9
1-pentanol	7.29	8.01	$C_5H_{12}O$	34	8.1
Butyl benzoate	3.57	3.92	$C_{11}H_{14}O_2$	8	3.8

4.5.2.3 Naphthenic-oil rejuvenator

The molecules in the naphthenic-oil rejuvenator belong to different chemical groups of alkanes, naphthenic, and other hydrocarbons. Based on the concentration distribution of various alkanes and naphthenic molecules with different carbon-chain lengths and the number of naphthenic rings, the tetradecane and hexadecahydro pyrene molecule is utilized to represent the molecular group of alkanes and naphthenic, respectively. In addition, the 2-methoxy-4-methyl phenol molecule with a high content of 14.49% is also selected as the additives molecular group. **Figure 4.14** shows the molecular structures for three types of molecules in the multi-component molecular model of the naphthenic-oil rejuvenator. Similar to additive molecules in engine-oil, the 2-methoxy-4-methyl phenol molecule has the aromatic ring and oxygen-containing functional groups (phenolic and methoxy) to improve performance stability and aging resistance of the naphthenic-oil rejuvenator.

(a) Tetradecane   (b) Hexadecahydro pyrene   (c) 2-methoxy-4-methyl phenol

Figure 4.14 The molecular elements in the naphthenic-oil rejuvenator

Table 4.10 The molecular components in naphthenic-oil

Components	Measured dosage (wt%)	Calibrated dosage (wt%)	Chemical formula	Molecule Number	Molecule dosage (wt%)
Tetradecane	17.85	19.37	$C_{14}H_{30}$	39	19.2
Hexadecahydro pyrene	59.79	64.90	$C_{16}H_{26}$	120	65.0
2-methoxy-4-methyl phenol	14.49	15.73	$C_8H_{10}O_2$	46	15.8

From **Table 4.10**, the measured dosage of tetradecane, hexadecahydro pyrene, and 2-methoxy-4-methyl phenol molecule is 17.85%, 59.79%, and 14.49%, respectively. Meanwhile, about 7.87% of molecules

(mainly in the additives group) are not considered in the multi-component molecular model of the naphthenic-oil rejuvenator. To eliminate that influence, the molecular number of the tetradecane, hexadecahydro pyrene, and 2-methoxy-4-methyl phenol is determined according to the normalized dosage of 19.37%, 64.90%, and 15.73%, which is 39, 120, and 46, respectively. It can be found the model dosages of these three molecules are similar to the experimental values, which guarantees the efficiency and reliability of predicted thermodynamics properties for a multi-component molecular model of naphthenic-oil rejuvenator outputted from MD simulations at the nanoscale level.

4.5.2.4 Aromatic-oil rejuvenator

According to the GCMS result, the aromatic-oil rejuvenator mainly contains alkanes, aromatics, and additives (like solvents). In this thesis, one molecule with maximum dosage in each group is selected to represent the alkanes, aromatics, and solvents molecules, which are the octadecane, 2,7-dimethyl naphthalene, and furfural. Their molecular structures are shown in **Figure 4.15**. Meanwhile, **Table 4.11** lists the measured dosage, calibrated dosage, and chemical formula of these three molecules. The chemical formula of octadecane, 2,7-dimethyl naphthalene, and furfural molecule is $C_{18}H_{38}$, $C_{12}H_{12}$, and $C_5H_4O_2$, respectively. Octadecane is a saturated alkane molecule with an 18-carbon chain, and 13.74% octadecane is detected in aromatic-oil.

Moreover, 53.91% 2,7-dimethyl naphthalene is found in aromatic-oil, which contains two aromatic rings connected with counterpoint methyl. About 26.13% of furfural molecules are monitored in the GCMS test of aromatic-oil, which is related to the processing process of aromatic oils with the furfural solvent [15, 34]. To eliminate the influence of other additives molecules, the content of octadecane, 2,7-dimethyl naphthalene, and furfural molecules is calibrated as 14.65%, 57.49%, and 27.86%, respectively. Based on the molecular formula and calibrated dosage, the number of octadecane, 2,7-dimethyl naphthalene, and furfural molecules is determined as 22, 140, and 110. Further, it is found that the dosage of each molecule in the model is close to measured values, and it ensures the reasonability of the multi-component model of aromatic-oil rejuvenator.

(a) Octadecane   (b) 2,7-dimethyl naphthalene   (c) Furfural
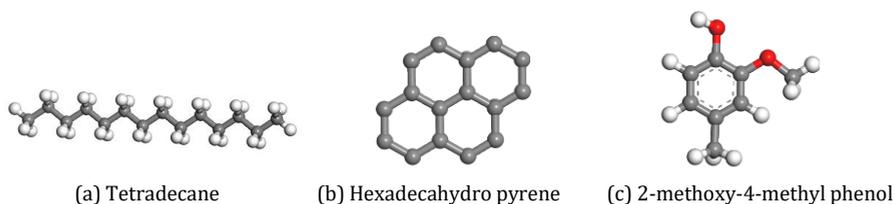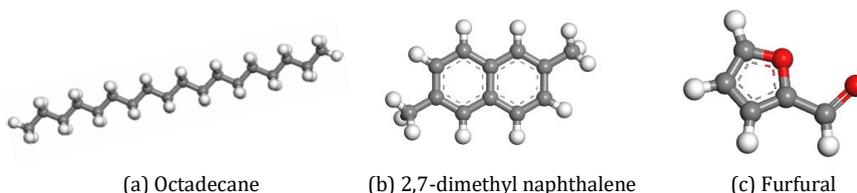
Figure 4.15 The molecular elements in aromatic-oil rejuvenator

Table 4.11 The molecular components in aromatic-oil

Components	Measured dosage (wt%)	Calibrated dosage (wt%)	Chemical formula	Molecule number	Molecule dosage (wt%)
Octadecane	13.74	14.65	$C_{18}H_{38}$	22	14.7
2,7-Dimethyl Naphthalene	53.91	57.49	$C_{12}H_{12}$	140	57.5
Furfural	26.13	27.86	$C_5H_4O_2$	110	27.8

4.6 MD simulations and validations

4.6.1 Average molecular models of rejuvenators

In this chapter, the average molecular models of four rejuvenators are built by randomly incorporating 200 rejuvenator molecules into a cubic simulation box with periodic boundary conditions. The initial molecular models of rejuvenators are shown in **Figure 4.16**, subjected to a geometry optimization procedure to

minimize the system energy and avoid overlapping rejuvenator atoms. The COMPASSII forcefield is adopted throughout the establishment and MD simulations of these molecular models of all rejuvenators, which was implemented to efficiently predict the thermodynamic parameters of various organic compounds [19]. In addition, the density values of all initial models were controlled at $0.1 g/cm^3$. Afterward, the MD simulations were conducted on these initial molecular models of pure rejuvenators with an isothermal-isobaric (NPT, constant molecular number, external pressure, and temperature) ensemble to achieve the equilibrium status at 298K and one-atmosphere pressure. The time step of 1 femtosecond (fs) was selected, and the total simulation time was 200 picoseconds (ps). Moreover, the Nose thermostat and Andersen barostat were chosen to control the temperature and pressure of these rejuvenator systems. The summation method for van der Waals and the electrostatic term was the Ewald with the accuracy of 0.001 kcal/mol and Atom-based with a cut-off distance of 15.5 Å, respectively.
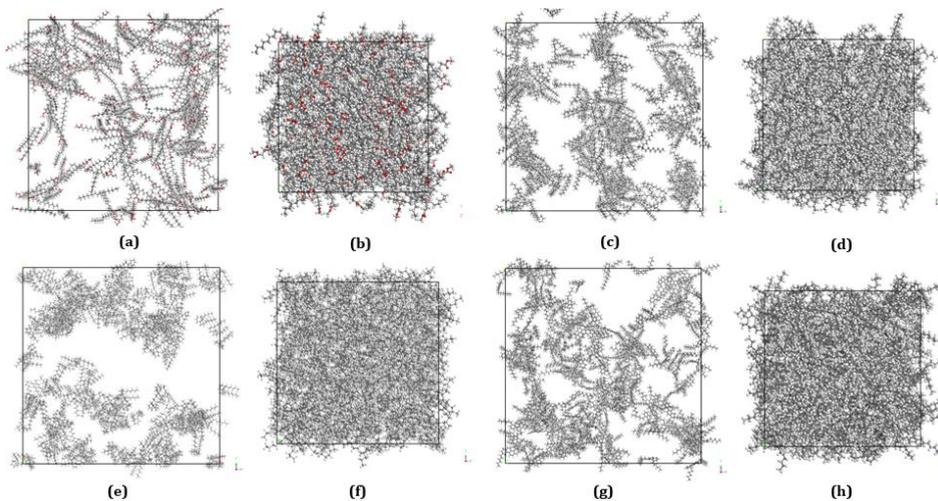
**Figure 4.16 The initial and final molecular models of rejuvenators during MD simulations
(a)(b) bio-oil; (c)(d) engine-oil; (e)(f) naphthenic-oil; (g)(h) aromatic-oil**

After the NPT equilibrium procedure, the canonical ensemble (NVT, constant atom number, system volume, and temperature) was performed to ensure those rejuvenator molecules were more relaxed and the whole rejuvenator model was more thermodynamically stable. The NVT simulation parameters were consistent with the previous NPT procedure. The incremental steps were 200000, and the Nose thermostat was used. The final equilibrium configurations of pure rejuvenator models are also illustrated in **Figure 4.16.** Under external pressure and temperature conditions, the rejuvenator molecules assemble due to the intermolecular interaction, and the whole model shrinks to a stable state. **Table 4.12** lists the main parameters of the equilibrium molecular models of four rejuvenators at 298K. It is worth noting that the amount of rejuvenator molecules in each molecular model is the same (200), but the cell volume (or cubic length) is significantly different with a magnitude order of BO < EO < NO < AO. The difference in cell volume between molecular models of various rejuvenators is attributed to the discrepancy in molecular volumes and interaction levels of rejuvenator molecules. The rejuvenator model with a smaller molecular volume and stronger intermolecular attraction would present a lower cell volume [22].

Regarding the aromatic-oil rejuvenator, the polyaromatic structure extends the model volume significantly. Compared to the bio-oil molecule, the engine-oil and naphthenic-oil molecules display the saturated cycloalkane rings, contributing to enlarging the model volume. Meanwhile, the existence of the polar ester group in bio-oil molecules plays a crucial role in enhancing the attractive intermolecular force, which is also proved by its larger net charge.

Table 4.12 The calculated number of different atoms in various rejuvenators

Parameters	BO	EO	NO	AO
Cell volume (Å^3)	112945	125339	134996	137206
Length (Å)	48.3381	50.0451	51.2988	51.5772
Vector velocity	-0.433643	0.04906	0.21837	-0.35461
Chemical formula	$C_{19}H_{36}O_2$	$C_{22}H_{44}$	$C_{26}H_{48}$	$C_{30}H_{40}$
Net charge	-2.4331E-8	7.4506E-9	7.4506E-9	7.4506E-9
Net mass	296.495	308.594	360.670	400.640

4.6.2 Multi-component molecular models of rejuvenators

The establishment and MD simulations running for multi-component models of four rejuvenators are the same as the average model systems. **Figure 4.17** illustrates the initial and equilibrium molecular configurations of four rejuvenators before and after the MD simulations. Different kinds of molecules in each rejuvenator model are displayed with distinguishable colours to observe the molecular distribution and agglomeration levels. During the MD simulations, the molecules in a multi-component model of rejuvenator gather together owing to intermolecular force under the external pressure and temperature, resulting in the volume shrinkage of the whole molecular model. Due to the difference in the number of atoms and molecules, the cell volume and length of various rejuvenators are not compared here. However, it is interesting to discuss the molecular distribution of different molecules in multi-component molecular models of rejuvenators.

(a) Bio-oil rejuvenator   (b) Engine-oil rejuvenator

(c) Naphthenic-oil rejuvenator   (d) Aromatic-oil rejuvenator
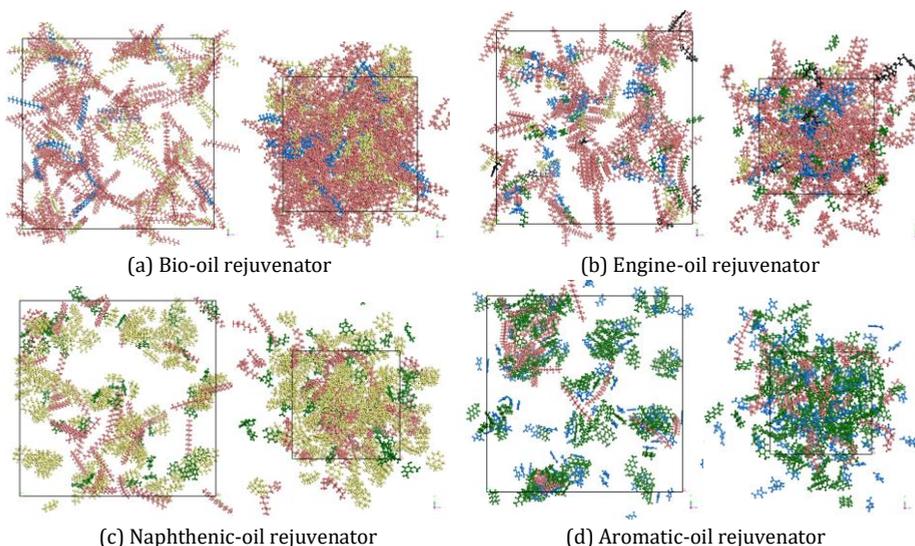
Figure 4.17 The initial and equilibrium molecular models of various rejuvenators

4.6.3 Experimental validation

The density values of various rejuvenators at 25°C and 60°C measured from experiments and MD simulations are illustrated in **Table 4.13**. As expected, the increase in temperature declines the density values of rejuvenators, which is associated with enhanced molecular mobility, enlarged intermolecular distance, and volume expansion at high temperatures [35]. This section compares the difference in density parameters from MD simulations and experimental results to validate the reliability of the proposed molecular structures of rejuvenators and the MD simulation settings (Forcefield, time step, simulation duration, etc.). It is illustrated that the predicted density values of all rejuvenators significantly approach the experimental

results at both 25°C and 60°C, indicating that the established average and multi-component molecular models of four rejuvenators are reasonable and the MD simulation outputs are credible.

Table 4.13 Density comparison of experimental results and MD simulation outputs

Rejuvenators	BO	EO	NO	AO
25°C density (g·cm⁻³) (Experiment)	0.911	0.833	0.875	0.994
25°C density (g·cm⁻³) (Average MD simulation)	0.868	0.821	0.886	0.971
25°C density (g·cm⁻³) (Multi-component MD simulation)	0.871	0.800	0.933	0.987
60°C density(g·cm⁻³) (Experiment)	0.899	0.814	0.852	0.978
60°C density(g·cm⁻³) (Average MD simulation)	0.842	0.802	0.865	0.955
60°C density (g·cm⁻³) (Multi-component MD)	0.841	0.774	0.906	0.954

From both average and multi-component models of four rejuvenators, the ranking order of predicted density is AO > NO > BO > EO. The influence factors may include molecular structure, molecular weight, and functional group distribution [8]. Compared with other rejuvenators, the aromatic-oil molecules have polar aromatic rings, which remarkably strengthen the intermolecular attractive force and tightness because of the stronger intermolecular agglomeration with Π-Π stacking [19, 22]. However, there is still a little difference between the tested and predicted density of rejuvenators, especially for the bio-oil rejuvenator. It should be noted that these differences are limited and inevitable. On the one hand, an average model cannot completely understand the chemical compositions in these rejuvenators, leading to the difference between experimental and MD simulation results. On the other hand, several components with low dosages in rejuvenators are ignored when determining their multi-component molecular models.

4.7 Thermodynamic properties prediction of rejuvenators

The fundamental understanding of the physical and thermodynamics properties of various rejuvenators is limited due to the difficulty of experimental measurement at the macroscale level. In this chapter, MD simulations are performed on both average and multi-component molecular models to predict the nanoscale performance of rejuvenators in terms of potential energy, cohesive energy density, solubility parameters, volumetric parameters, dynamics behaviors (mean square distance and diffusion coefficient), viscosity, and activation energy.

4.7.1 Potential energy

The MD simulations are implemented based on the variations in different energy parameters of a simulation model, which results in instantaneous molecular mobility that changes due to the molecular interactions till reaching an equilibrium state. The potential energy of rejuvenators depends on the intermolecular interactions and plays a vital role in determining the thermodynamic properties of the simulation system. In this section, the potential energy of the four rejuvenators, using the average and multi-component models, are discussed and compared.

The potential energy of both average and multi-component models of rejuvenators is illustrated in **Figure 4.18** at temperatures of 213K, 298K, and 363K. It should be noted that the positive values result from a regulation that the potential energy at infinity distance is equal to 0. When two molecules approach each other from the infinity point, the attractive intermolecular force does the positive work. Thus, the potential energy is lower than the infinity point (0) and shows a negative value till reaching the most stable state with the lowest potential energy. Afterward, as the molecules continue to get closer, the intermolecular repulsive force dominates, and the potential energy rises to overcome the repulsion. As the intermolecular distance decreases, the potential energy increases, even to a positive value.

As the temperature increases from 213K to 363K, the potential energy values of the four rejuvenators increase from 298K to 363K. Regarding the average models, when the temperature is constant, the potential energy values of bio-oil, engine-oil, and naphthenic-oil rejuvenators are negative, while the aromatic-oil

exhibits the highest positive potential energy. The reason is that the existence of condensed aromatic rings promotes the Π-Π stacking interaction between aromatic-oil molecules and the corresponding intermolecular distance reduces dramatically [19]. Meanwhile, both high polarity and molecular weight intensify the intermolecular attractive force. The aromatic-oil molecules with a small distance would exhibit high positive energy to overcome the huge repulsion. In addition, the potential energy of bio-oil is higher than engine-oil and naphthenic-oil, which is associated with the potential hydrogen-bond in polar ester groups. The higher molecular weight and poly-cycloalkane structure in the naphthenic-oil lead to larger potential energy than engine-oil. The potential energy results of multi-component models for rejuvenators are displayed in Figure **4.18(b)**. The overall ranking for the potential energy of four rejuvenators in the multi-component simulation case is the same as average models. However, the potential energy values of rejuvenators depend on the type of molecular models. For the BO, EO, and NO rejuvenators, the potential energy values of their multi-component models are slightly higher than the average models, but the multi-component model of aromatic-oil is much lower than its average model.
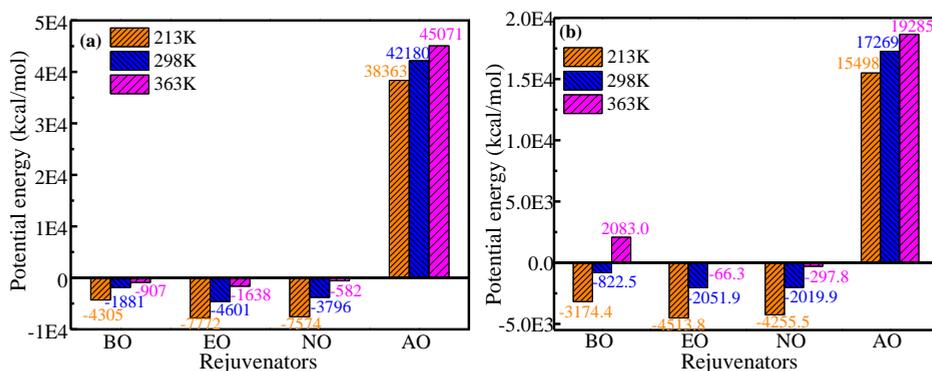
Figure 4.18 The potential energy of average (a) and multi-component (b) models of rejuvenators

4.7.2 Cohesive energy density and solubility parameter

The cohesive energy density (CED) and solubility parameters (δ) of various rejuvenators are outputted from MD simulations following **Eqs.4.7** and **4.8** [25].

$$CED_{total} = \frac{E_{coh}}{V} = \frac{E_{vdw} + E_{ele}}{V} \tag{4.7}$$

$$\delta_{total} = (CED_{total})^{0.5} = (\delta_{vdW}^2 + \delta_{ele}^2)^{0.5} \tag{4.8}$$

where E_{coh} and V refer to the total cohesion energy and volume of the whole rejuvenator model; E_{vdw} and E_{ele} are the van der Waals and electrostatic cohesion energy; δ is the total solubility parameters, composed of the van der Waals term δ_{vdW} and electrostatic one δ_{ele}.

The outputted CED and δ values of average models of rejuvenators at 298K are shown in **Figure 4.19**. The total CED parameter is composed of van der Waals and electrostatic terms. The van der Waals interaction plays a crucial role in determining the total CED value of each rejuvenator, which shows two orders of magnitude higher than the electrostatic one. The aromatic-oil rejuvenator exhibits the largest CED value of 3.406E8 J/cm³, followed by bio-oil (3.190E8 J/cm³) and naphthenic-oil (2.723E8 J/cm³). The engine-oil rejuvenator has the lowest CED (2.170E8 J/cm³), but it is close to the naphthenic-oil.

Meanwhile, the sequence of van der Waals CED for four rejuvenators is the same as the total term: AO > BO > NO > EO. It suggests that it is the most difficult for aromatic-oil molecules to evaporate from the main body. In contrast, the required energy for the evaporation of engine-oil and naphthenic-oil molecules is much lower. The evaporation degree of the rejuvenator molecules may be related to the thermal aging performance

of rejuvenated bitumen [7, 32]. The reason for the CED difference is that the aromatic-oil molecules own the fused aromatic rings with the strongest polarity, strengthening the intermolecular attraction force through the Π-Π stacking. Meanwhile, the polar ester group in the bio-oil molecule enlarges the attractive intermolecular interaction, which may be further enhanced by forming hydrogen bonds [20]. However, the average molecular structures of engine-oil and naphthenic oil are both composed of saturated cycloalkanes and straight alkanes with less polarity. Thus, the total, Van der Waals and electrostatic CED values of engine-oil and naphthenic-oil rejuvenators are lower than bio-oil and aromatic-oil rejuvenators. Interestingly, the electrostatic CED value of bio-oil is slightly higher than aromatic-oil, which may be explained through the larger charge value or smaller intermolecular distance between bio-oil molecules [20].
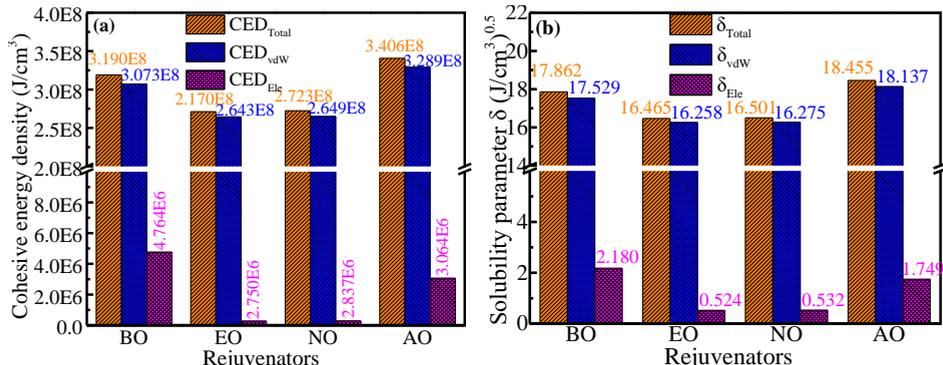
Figure 4.19 CED and solubility parameter of average models at 298K

The comparison in solubility parameters between various rejuvenators demonstrates a similar law to the CED parameter. The aromatic-oil rejuvenator presents the largest δ value of 18.455, followed by bio-oil (17.862). Besides, the engine-oil and naphthenic-oil exhibit lower δ values of 16.465 and 16.501, respectively. Meanwhile, the electrostatic δ values of aromatic-oil and naphthenic-oil are approximately 3-4 times larger than that of engine-oil and naphthenic-oil rejuvenators. From **Chapter 3**, it was mentioned that the δ values of aged bitumen after laboratory pressure aging vessel (PAV) long-term aging processes for 20h, 40h, and 80h were located in 18.5-19.5 [25], larger than four rejuvenators. According to solubility theory, the smaller the solubility parameter difference (Δδ) is, the better the compatibility between different phases is. Thence, the δ value of the aromatic-oil rejuvenator is the closest to the aged bitumen, followed by bio-oil and naphthenic-oil rejuvenators. And the Δδ value between the engine-oil and aged bitumen is the largest. In other words, the compatibility order of four rejuvenators with aged bitumen may be as follows: AO > BO > NO > EO, which will be further investigated and validated in **Chapter 5**.
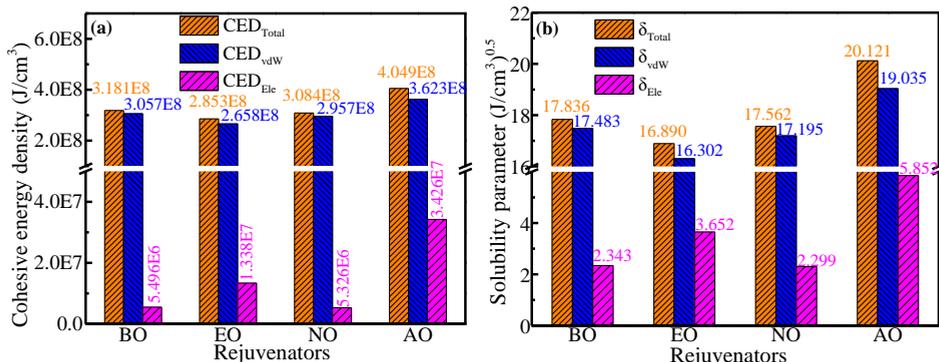
Figure 4.20 The CED and solubility parameter values of multi-component models at 298K

The CED and solubility parameter values of multi-component models of these four rejuvenators with the total, van der Waals, and electrostatic terms at 298K are displayed in **Figure 4.20**. Like the average models, the van der Waal force is the dominant intermolecular interaction in multi-component molecular models of all rejuvenators. Regarding the CED and solubility parameter, the magnitude order of multi-component models is the same as average cases following AO > BO > NO > EO. The aromatic-oil rejuvenator still exhibits the largest CED value, indicating that the intermolecular force in the multi-component molecular model of aromatic-oil is the strongest. The reason herein is related to the high aromaticity and polarity characteristics of 2,7-dimethyl naphthene molecules that existed in the aromatic-oil model with a high concentration. Meanwhile, the Π-Π conjugations between condensed aromatic rings in 2,7-dimethyl naphthene significantly enhance the intermolecular interactions of the aromatic-oil model. In addition, the furfural molecules with furan ring and aldehyde group also contribute to the improved intermolecular force of the whole aromatic-oil system.

In the multi-component molecular model of bio-oil rejuvenator, all kinds of molecules belong to the fatty acid esters combined with the unsaturated alkyl chain and an ester group. The polar ester group (-C=O-O-C-) in methyl palmitate, methyl linoleate, and methyl oleate molecules initiate the formation of hydrogen bonds, which are stronger than the van der Waals and electrostatic intermolecular forces but lower than Π-Π conjugations [19, 34]. That's why the CED and solubility parameter values of the bio-oil molecular model are smaller than aromatic-oil but higher than that of naphthenic-oil and engine-oil. Further, it is found that the naphthene-oil multi-component model has higher CED and solubility parameter values than the engine-oil model. The multi-component molecular model of naphthenic-oil is composed of hexadecahydro pyrene (65.0%), tetradecane (19.2%), and 2-methoxy-4-methyl (15.8%), while the multi-component model of engine-oil contains the tetradecane (67.9%), 1-methyl-2-pentyl-cyclohexane (6.3%), 2,6-bis (1,1-dimethyl ethyl)-phenol (13.9%), 1-pentanol (8.1%), and butyl benzoate (3.8%). Considering the main molecular compositions, the hexadecahydro pyrene molecules in the naphthenic-oil model show larger polarity and stronger intermolecular force from conjugate effects between the polycyclic cycloalkane structures than the tetradecane molecules in engine-oil [4, 5].

On the other hand, the aromatic-oil model also presents the highest electrostatic-based CED and solubility parameter values, followed by the engine-oil, while the bio-oil and naphthenic-oil are at a similar level. The high concentrations of 2,7-dimethyl naphthene and furfural molecules result in the large electrostatic energy in the multi-component molecular model of aromatic oil. Meanwhile, the high electrostatic-based CED and solubility parameter values of the engine-oil model are related to the hydrocarbons in the additives group with significant polarity and aromaticity. Overall, the predicted CED and solubility parameter values of the multi-component model of bio-oil rejuvenator are close to its average model, while the results of multi-component models of engine-oil, naphthenic-oil, and aromatic-oil are slightly larger than their corresponding average models.

4.7.3 Volumetric parameters

The nanoscale microstructure of bitumen was related to its macroscale relaxation and low-temperature cracking performance. **Figure 4.21** displays the volumetric parameters of average models of rejuvenators at 298K. The difference in molecular structures makes the volumetric parameters of the four rejuvenators variable. It is found that the bio-oil rejuvenator exhibits the lowest total volume and occupied volume, followed by the engine-oil and naphthenic-oil rejuvenators. Moreover, both total and occupied volumes of aromatic-oil rejuvenator are the maximum. It should be mentioned herein that the molecule number in all rejuvenators' average models is the same as 200, and the difference in volumetric indices may be ascribed to the molecule type and molecular interaction as well as the external factors (temperature and pressure).

As shown in **Figure 4.11**, the main structures in average models of bio-oil, engine-oil, naphthenic-oil, and aromatic-oil are the straight-chain alkane with an ester group, mono-cycloalkane, polycyclic alkanes, and polycyclic aromatic hydrocarbons, respectively. The increment in cycloalkane and aromatic rings' number leads to the enlargement of intrinsic molecular volume. Meanwhile, the molecular steric hindrance is

improved accordingly, extending the total volume of rejuvenator models. Regarding the free volume, the bio-oil rejuvenator has the lowest value, while the engine-oil rejuvenator shows the highest value, followed by the naphthenic-oil and aromatic-oil rejuvenators. The free volume is the most important index to determine the volume variation of the rejuvenator system [36, 37]. However, it is difficult to directly compare the free volume values of different rejuvenator models because of the huge difference in molecular structures, resulting in the variable occupied and total volumes. Herein, an effective index, fractional free volume (FFV), is introduced to quantitatively compare the free volume terms of various rejuvenators, calculated as follows:

$$FFV = \frac{V - 1.3V_{vdW}}{V} = \frac{V - V_0}{V} \tag{4.9}$$

where FFV is the fractional free volume, %; V refers to the total volume of the rejuvenator system, $Å^3$; V_{vdW} and V_o represent the van der Waals volume and occupied volume, $Å^3$, respectively.

The FFV parameters of the average models of four rejuvenators are calculated and displayed in **Figure 4.21(b)**. The FFV values of all rejuvenators' average models are lower than 25% and strongly depend on the molecular structure and type of rejuvenators. The engine-oil presents the largest FFV value of 20.30%, while the aromatic-oil has the lowest FFV (17.08%). Meanwhile, the FFV parameter of the bio-oil (18.54%) is slightly higher than the naphthenic-oil (18.51%). Furthermore, the total volume (the whole cubic), occupied volume (red color), and free volume (blue color) of the four rejuvenators are demonstrated in **Figure 4.22**. It is observed that the occupied volume of rejuvenator molecules is the continuous phase, while the free volume is distributed in an island-like form.
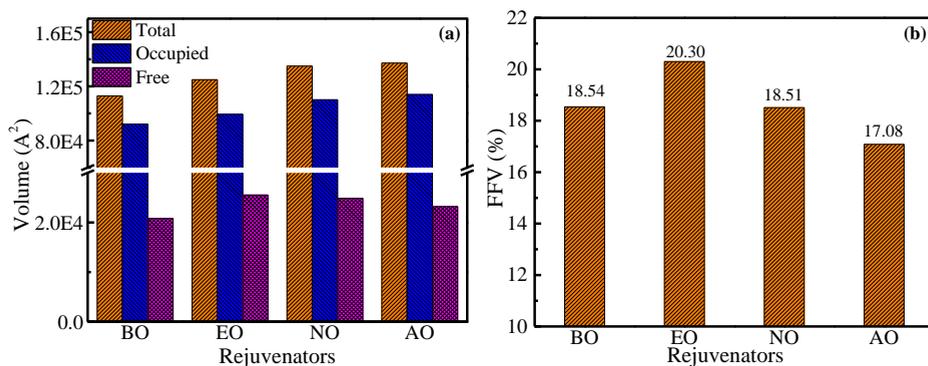
Figure 4.21 The volumetric parameters of average molecular models of rejuvenators at 298K

(a) Bio-oil   (b) Engine-oil   (c) Naphthenic-oil   (d) Aromatic-oil
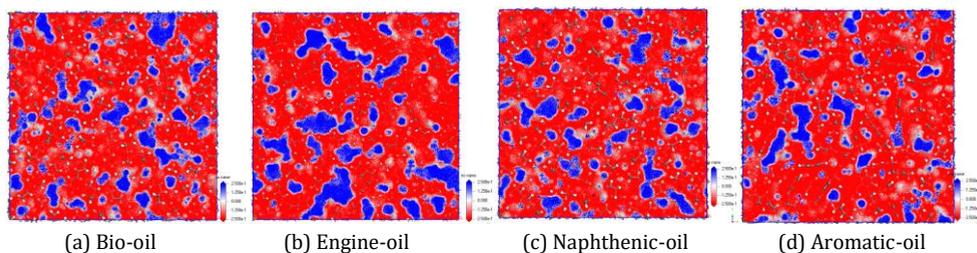
Figure 4.22 The schematic diagram of free volume in average molecular models of rejuvenators (The red color represents the occupied volume, and the blue one is the free volume)

At the same time, the volumetric indicators of multi-component molecular models of rejuvenators are explored, and **Figure 4.23** visualizes these volumetric characteristics of equilibrium multi-component molecular models of bio-oil, engine-oil, naphthenic-oil and aromatic-oil rejuvenators at 298 K. Different color

represent the various kinds of molecules in multi-component models of rejuvenators. It demonstrates that the total volume refers to the volume of the whole cubic simulation unit. Meanwhile, the occupied volume shows the sum of molecular volumes in multi-component models of rejuvenators. Further, the difference between the total volume and occupied volume is defined as the free volume, which is the sum of intermolecular space in one cubic simulation unit. Due to the periodic boundary condition, the volumetric parameters from each simulation unit of multi-component molecular models of rejuvenators are the same. To be more vivid, the free volume spaces in all equilibrium multi-component molecular models of rejuvenators are marked with grey-blue shapes.

(a) Bio-oil   (b) Engine-oil   (c) Naphthenic-oil   (d) Aromatic-oil
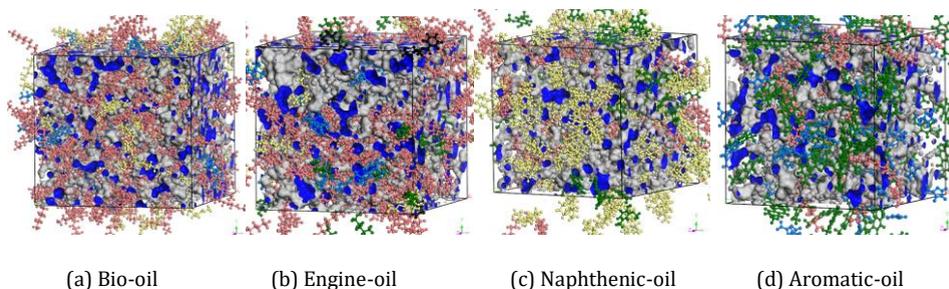
Figure 4.23 The free volume calculations on equilibrium molecular models of rejuvenators

The quantitative volumetric parameters of multi-component molecular models of four rejuvenators are shown in **Figure 4.24(a)**. As expected, the occupied volumes in multi-component molecular models of all rejuvenators are much larger than the free volumes. When the molecular number in each rejuvenator model is the same, the molecular volume mainly determines the occupied volume of the whole rejuvenator model. However, there is a huge difference in volumetric parameters between various rejuvenators. It is found that the multi-component model of the bio-oil rejuvenator exhibits the largest total, occupied, and free volumes, followed by the engine-oil and naphthenic-oil. At the same time, the aromatic-oil shows the lowest volumetric parameters. The reason can be explained from the viewpoint of molecular volume and configuration. In the multi-component model of bio-oil rejuvenator, the fatty acid ester molecules show a large molecular size and intermolecular distance because of the long-alkane chain in their molecular structures. For the tetradecane as the main molecule in the multi-component model of engine-oil, there are 14 carbon atoms in its main molecular body, which is shorter than the alkane chain of bio-oil molecules.
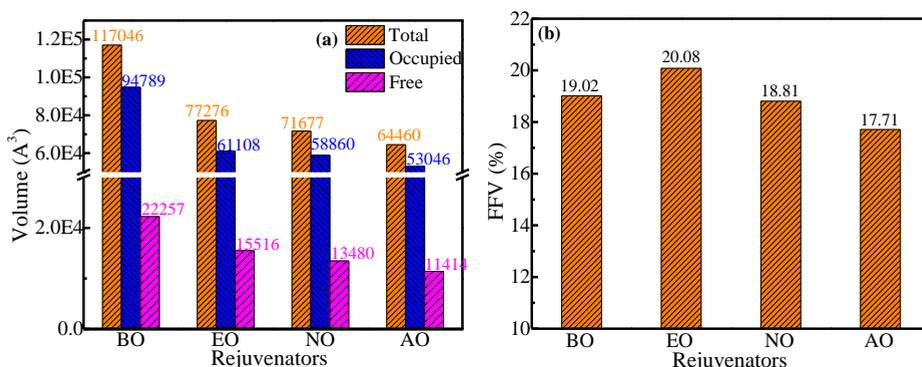
Figure 4.24 The volumetric parameters and FFV of different rejuvenators at 298K

Regarding the multi-component molecular models of naphthenic-oil and aromatic-oil rejuvenators, their lower volumetric parameters are not only related to the smaller molecular volume but also the stronger intermolecular forces. The polycyclic cycloalkanes structure in hexadecahydro pyrene as the main molecule

of the naphthenic-oil model leads to its smaller molecular size. Moreover, the 2,7-dimethyl naphthalene and furfural molecules in the multi-component model of aromatic-oil show the smallest molecular size due to the aromatic and furan rings with a short side chain. On the other hand, compared to bio-oil and engine-oil rejuvenators, the naphthenic-oil and aromatic-oil have more polar molecules, resulting in stronger intermolecular interaction and a narrower intermolecular space.

The FFV values of multi-component models of these four rejuvenators at 298K are illustrated in **Figure 4.24(b)**, which are in the region of 17-21% and distinctly approach the average models' results. Besides, the FFV order for the multi-component molecular models of rejuvenators is EO > BO > NO > AO, which is consistent with the conclusion in average models' simulations. The engine-oil rejuvenator exhibits the highest FFV value of 20.08%, followed by the bio-oil (19.02%) and naphthenic-oil (18.81%). Besides, the FFV value of the multi-component molecular model of aromatic-oil is the lowest at 17.71%. This is because the polar ester groups in bio-oil molecules enhance the intermolecular interaction and reduce the free volume concentration by forming hydrogen bonds. The high polarity and low molecular size of aromatic-oil molecules contribute to the low fractional free volume of the multi-component molecular model.

On the other hand, the influence of temperature on the FFV parameters of rejuvenators is also investigated. **Figure 4.25** illustrates the variations of occupied and free volumes in multi-component molecular models of rejuvenators as a function of temperature. The space with red color is the occupied volume, while the blue part refers to the free volume. For all rejuvenators, the free volume enlarges significantly with the temperature increasing. As the temperature rises from 173K to 393K, the free volume distribution changes from a sporadic state to island-like, which provides more free space for rejuvenator molecules to flow and relax at high external stress.
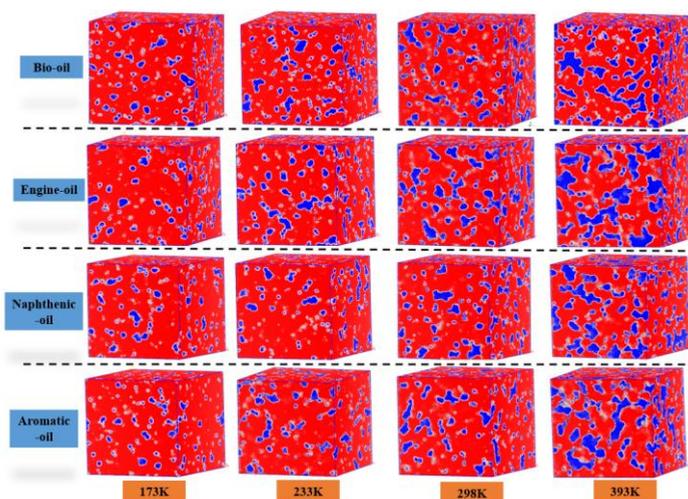
Figure 4.25 Influence of temperature on free volume distributions of four rejuvenators (Red color: Occupied volume; Blue color: Free volume)

The FFV values of average models as a function of temperature are displayed in **Figure 4.26(a)**. The FFV values of rejuvenators enlarge along with the increased temperature. Moreover, the increasing rate of the FFV parameter within a high-temperature region is more significant than that in the low-temperature range. When the temperature exceeds 273K, the magnitude of the FFV value for four rejuvenators follows EO > BO > NO > AO. This sequence is opposite to the density result, in which the engine-oil rejuvenator shows the lowest density while the aromatic-oil exhibits the highest density. From the viewpoint of the rejuvenator's average molecular structure, the engine-oil molecules with long alkane chains could stretch easily, while the polar ester functional group in bio-oil molecules shortens the intermolecular space. In addition, the

cycloalkane rings in the naphthenic-oil rejuvenator enlarge the molecular orientation and tightness, while the condensed aromatic rings in aromatic-oil molecules significantly promote the intermolecular stacking degree. However, when the temperature is lower than 213K, the FFV order changes into NO > AO > EO > BO. At extremely low temperatures, the bio-oil molecules with polar ester groups start to agglomerate [6], and the engine-oil molecules with long alkane chains show a crystallization trend [5], which remarkably reduces the free volume fraction. At the same time, the molecular interaction in naphthenic-oil is much smaller than that in aromatic-oil due to a strong Π-Π stacking between condensed aromatic rings.
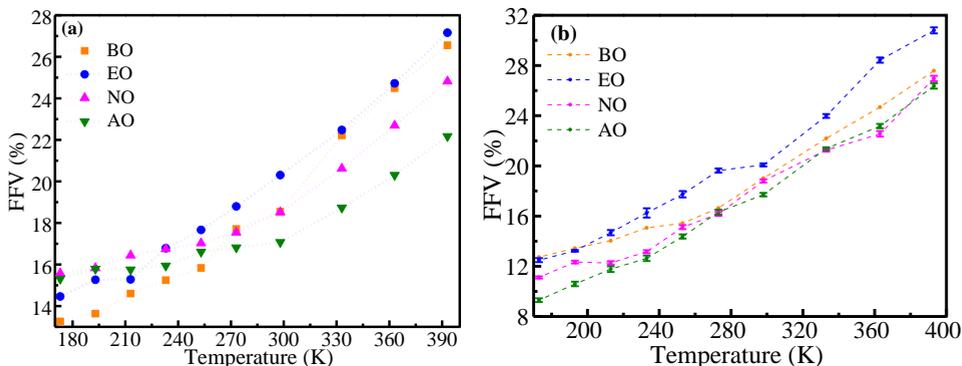
Figure 4.26 Influence of temperature on FFV of average (a) and multi-scale model (b)

At the same time, **Figure 4.26(b)** draws the variation of FFV values of multi-component models as a function of simulation temperature. When the temperature rises from 173K to 393K, the FFV values of bio-oil, engine-oil, naphthenic-oil, and aromatic-oil rejuvenators increase from 12.7%, 12.5%, 11.1%, and 9.3% to 27.6%, 30.8%, 27.0%, and 26.4%, respectively. In addition, the FFV parameters of the multi-component molecular models of four rejuvenators follow the decreasing order of EO > BO > NO > AO, which agrees well with the average models.

4.7.4 Mean square displacement and diffusion coefficient

The molecular mobility and dynamic behavior of various rejuvenators are predicted and compared. It was reported that molecular mobility was associated with low-temperature relaxation and self-healing capacity, as well as the diffusion rate of rejuvenators in aged bitumen [19]. The mean square displacement (MSD) of rejuvenator molecules is recorded, representing the movement distance relative to the initial position. The MSD results at 25°C of average models of rejuvenators are calculated with **Eq.4.10** and plotted in **Figure 4.27(a)**. The MSD value increases gradually as the simulation time prolongs, implying the self-movement of rejuvenator molecules. Various rejuvenators display different dynamic behaviors dramatically. The increasing trend of MSD values for bio-oil molecules is the most significant, followed by the engine-oil and naphthenic-oil rejuvenators. Meanwhile, when the simulation time is the same, the MSD value of the aromatic-oil rejuvenator is the smallest. It implies that the bio-oil molecules show the largest mobility. Aromatic-oil molecules are most difficult to move around because of the strong intermolecular force between condensed aromatic rings.

$$MSD(t) = <\Delta r_i(t)^2> = <[r_i(t) - r_i(0)]^2> \tag{4.10}$$

where MSD(t) is the mean square displacement of rejuvenator molecules at simulation time t (ps), Å^2; $r_i(0)$ and $r_i(t)$ refers to the initial and current coordinate, Å.

From **Figure 4.27(a)**, the MSD values of all rejuvenators present a linearly increasing trend as a function of simulation time after 50ps. To quantitatively collate the dynamic performance of various rejuvenators, the diffusion coefficient indicator is proposed using **Eq.4.11** [23, 24].

$$D = \frac{1}{6N} \lim_{t \to \infty} \frac{d}{dt} \sum MSD(t) = \frac{a}{6} \qquad (4.11)$$

where D refers to the self-diffusion coefficient of rejuvenator molecules, m^2/s; N is the total number of rejuvenator molecules; MSD represents the mean square displacement, $Å^2$; t is the simulation time, s; and a is the slope value in MSD-time curves.
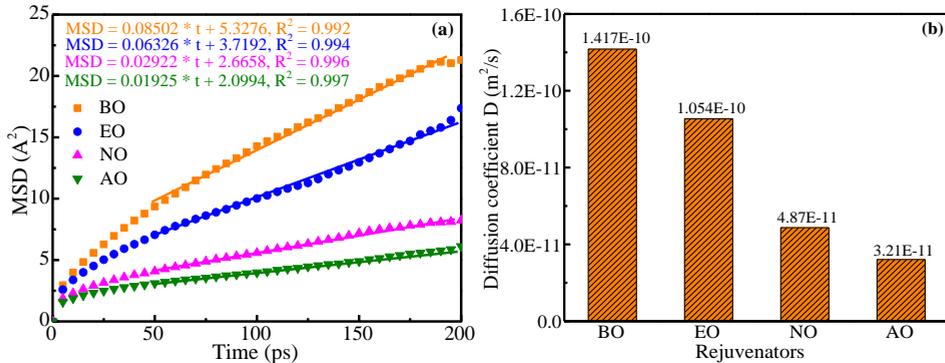
Figure 4.27 The MSD and self-diffusion coefficient of average models of rejuvenators at 298K

The calculated diffusion coefficient values of average models at 298K are listed in **Figure 4.27(b)**. The magnitudes of self-diffusion coefficient values for different rejuvenators at 298K vary from 3.21E-11 to 1.42E-10 (m^2/s), higher than that of virgin and aged bitumen (1.92E-11-2.88E-11 m^2/s) [25]. The rejuvenators exhibit a much greater dynamic performance than virgin and aged binders [10, 38]. Besides, the bio-oil rejuvenator shows the highest self-diffusion coefficient of 1.417E-10 m^2/s, while the aromatic-oil molecule displays the lowest self-diffusion coefficient of 3.21E-11 m^2/s. Meanwhile, the self- diffusion coefficient of engine-oil (1.054E-10 m^2/s) is almost two times larger than that of naphthenic-oil (4.87E-11 m^2/s).
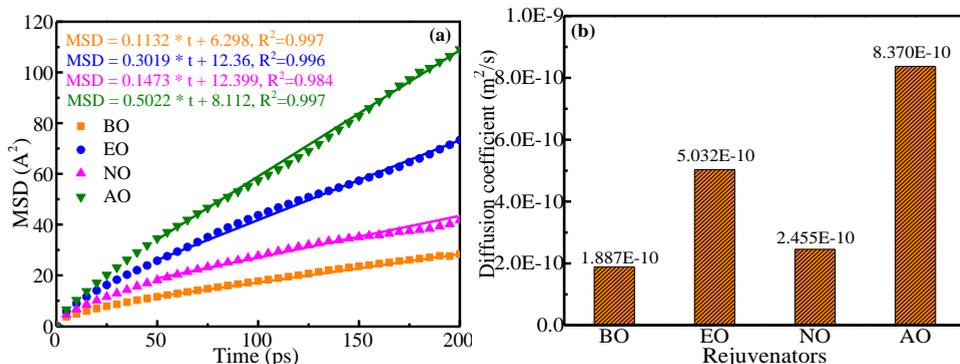
Figure 4.28 The MSD and diffusion coefficient of multi-component models of rejuvenators at 298K

Similarly, the MSD values of multi-component models of different rejuvenators as a function of simulation time at 298K are monitored and shown in **Figure 4.28(a)**. When the simulation time remains constant, the magnitude order of MSD values for the multi-component models of four rejuvenators is as follows: AO > EO > NO > BO. Meanwhile, the self-diffusion coefficient values of rejuvenators are calculated and presented in **Figure 4.28(b)**. The aromatic-oil rejuvenator exhibits the highest self-diffusion coefficient of 8.37E-10 m^2/s, followed by engine-oil (5.032E-10 m^2/s) and naphthenic-oil (2.455E-10 m^2/s), while the D value of the bio-oil rejuvenator is the smallest of 1.887E-10 m^2/s. The result completely conflicts with the finding from the average models' case (the magnitude order of MSD and D is BO > EO > NO > AO). It is out of

expectation that the aromatic-oil rejuvenator should exhibit the lowest dynamic performance due to its large molecular weight and intermolecular forces.

The GC-MS test can explain the reason for the unexpected phenomenon. The 2,7-dimethyl naphthene molecule is detected as the main molecule of aromatic-oil, but it is challenging to monitor the aromatic molecules with more than two fused aromatic rings because of their heavy molecular weight. It leads to the negligence of these large aromatic molecules in the multi-component molecular model of aromatic-oil rejuvenator. Meanwhile, incorporating furfural molecules with a high dosage of 57.5% plays a crucial role in enhancing the molecular mobility of the 2,7-dimethyl naphthalene. It is concluded that the GC-MS method is not able to measure all chemical components in aromatic-oil rejuvenators, and the large aromatic molecules should be considered in the multi-component molecular model of aromatic-oil.

For the other three rejuvenators, the diffusion coefficient of naphthenic-oil is expected to be lower than engine-oil. It is because more alkane molecules (tetradecane) exist in engine-oil than in naphthenic-oil. Moreover, the diffusion coefficient of the hexadecahydro pyrene as the main molecule of naphthenic-oil is much lower than the tetradecane alkane molecule. Regarding the bio-oil rejuvenator, the long carbon chain in fatty acid esters hinders the molecular diffusive ability. Besides, the formation of hydrogen bonds increases the intermolecular force and reduces the mobility of molecules in bio-oil. It should be mentioned that the MSD values of rejuvenators are the sum of the MSD of each molecule in their multi-component molecular models. It is still difficult to explain the underlying reason for the difference in MSD and D values between the multi-component molecular models of various rejuvenators. Due to the inaccurate MD simulation outputs of dynamic parameters, the multi-component models of these rejuvenators are not recommended and should be further improved in future work.

4.7.5 Viscosity and activation energy

The viscosity is the basic and crucial parameter to assess the rejuvenator's fluidity. It was reported that the rejuvenator with low viscosity exhibited a higher rejuvenation capacity for restoring the mechanical properties of aged bitumen [39, 40]. Herein, the viscosity values of four rejuvenators at different temperatures are predicted from MD simulations. At the same time, the rotational viscometer is employed to measure the realistic viscosity of rejuvenators. In the thesis, the expected viscosity values of four rejuvenators are determined through the Einstein-Stokes equation:

$$D = \frac{kT}{6\pi\eta r} \tag{4.14}$$

where D is the diffusion coefficient, m^2/s; T (K) and η (Pa·s) show the temperature and viscosity; k represents the Boltzmann constant, 1.38065E-23 J/K; and r is the radius of gyration for rejuvenator molecule, m.

The correlation curves between the inverse of testing temperatures (1/T) and dynamic viscosity values (η) of rejuvenators are drawn in **Figure 4.29**. As expected, the increased temperature weakens the intermolecular friction and reduces the viscosity values of rejuvenators. There is a linear relationship between the (1/T) and (Lnη), and it can be described with the Arrhenius equation as follows:

$$Ln\eta = \frac{E_{vis}}{R} \cdot \frac{1}{T} + LnA \tag{4.15}$$

where η refers to the dynamic viscosity value of the tested rejuvenator specimen, Pa·s; T is the temperature, K; E_{vis} is the flow activation energy, J/mol; while A and R is the pre-exponential parameter and gas constant, 8.314 J/(mol·K), respectively.

The predicted and measured viscosity values of four rejuvenators at different temperatures are shown in **Figure 4.29**. For MD simulation and experimental results, there is a linearly increasing trend for the (Lnη) parameter of all rejuvenators with the increase of (1/T) value. In the average models, the bio-oil rejuvenator shows the lowest viscosity, and the engine-oil rejuvenator has a similar viscosity with bio-oil regardless of

the testing temperatures. It implies that the bio-oil and engine oil rejuvenators exhibit the best fluidity and softening capacity. Compared with bio-oil and engine-oil rejuvenators, the naphthenic-oil presents a higher viscosity. It is related to the larger molecular weight and movement resistance. It should be mentioned that the aromatic-oil rejuvenator behaves the highest viscosity than other rejuvenators, which is associated with the largest molecular weight and strongest molecular interaction due to the distinctive aromaticity and polarity. Importantly, the magnitude order of viscosity for four rejuvenators from average models' simulations and experiments is the same: AO > NO > EO > BO. It further validates the reasonability of established average models and MD simulation settings. However, the difference between the predicted and measured viscosity values is still observed, and the predicted viscosity is lower than the real value. The reasons may due to the existing scale gap and negligence of heavy-weight molecules in the average molecular model, especially for the aromatic-oil.

At the same time, the predicted viscosity values of multi-component models of rejuvenators are also measured, and the correlation curves between the Ln(η) and 1/T are plotted in **Figure 4.29 (b)**. When the temperature is the same, the predicted viscosity of the naphthenic-oil is the largest, while there is no significant difference in the predicted viscosity of the other three rejuvenators. From the experimental results, the aromatic-oil exhibits the highest viscosity, followed by the naphthenic-oil, while the engine-oil and bio-oil show similar viscosity values. It relies on the fact that the predicted viscosity ranking of multi-component models of four rejuvenators agrees well with experimental results except for the aromatic-oil.
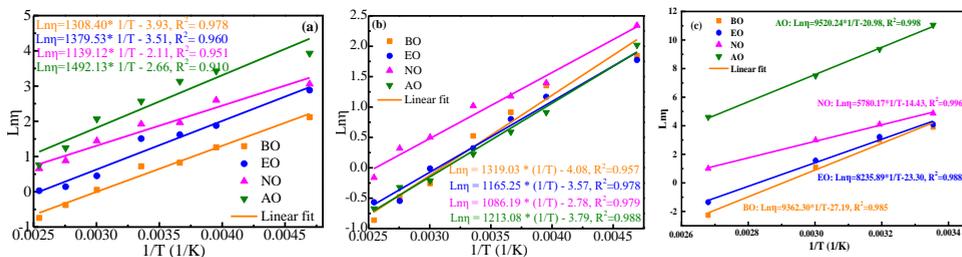
Figure 4.29 The predicted viscosity of average models (a) and multi-component models (b), and measured viscosity (c) of rejuvenators at different temperatures

The flow activation energy and pre-exponential factor values from MD simulations (E_{MD} and A_{MD}) and experiments (E_t and A_t) are summarized in **Table 4.14**. It is found that the simulation outputs present lower E_{vis} and higher A values than the experimental results. For both MD simulation and experimental results, the aromatic-oil has the highest flow activation energy, while the naphthenic-oil exhibits the lowest value. It manifests that the flow ability of aromatic-oil is worse than other rejuvenators. Besides, the sequence of pre-exponential factors for four rejuvenators from simulations and tests is the same as NO > AO > EO > BO. Hence, it is concluded that the MD simulation outputs are reliable but need to be further optimized to obtain the viscosity results of rejuvenators more approaching measured values.

Table 4.14 The E_{vis} and A values of four rejuvenators from MD simulations and tests

Rejuvenators	BO	EO	NO	AO
E_t (Experiment) (J/mol)	77838.2	68473.2	48056.3	79151.3
E_{MD} (Average model) (J/mol)	10878.04	11469.41	9470.64	12405.57
E_{MD} (Multi-component model) (J/mol)	10066.4	9687.9	9030.6	10285.5
A_t (Experiment)	1.55E-12	7.60E-11	5.41E-7	7.74E-10
A_{MD} (Average model)	1.17E-4	3.09E-4	7.76E-3	2.19E-3
A_{MD} (Multi-component model)	1.69E-2	2.82E-2	6.20E-2	3.26E-2

4.8 Summary and conclusion

The molecular structures of rejuvenators are highly important to enhance the accuracy of MD simulation outputs and fundamentally understand the underlying rejuvenation mechanism between aged bitumen and different rejuvenators. This chapter first shows the results of chemical tests to determine the chemical composition of four generic rejuvenators. Based on those compositions, representative average and multi-component molecular models of these rejuvenators are established and validated, based on density. Further, the MD simulations on rejuvenators' models are performed to predict and compare the thermodynamic properties of average and multi-component models of rejuvenators. Based on the comparison of the results of the simulation with chemistry principles, the average molecular models of rejuvenators are recommended for following MD simulations on the interactions between rejuvenators and aged bitumen, rather than the multi-component models. This is based on the following main findings:

➢ **Chemical characterizations of four rejuvenators**

- The oxygen-containing functional group exists in bio-oil, and the other three petroleum-based rejuvenators (engine-oil, naphthenic-oil, and aromatic-oil) are mainly composed of hydrocarbons with less heteroatom group. Moreover, the engine-oil and aromatic-oil present the smallest and largest unsaturation degree, and the bio-oil and naphthenic-oil exhibit similar H/C values. In addition, the FTIR test further denotes that the ester group is included in a bio-oil molecule, while the aromatic-oil comprises hydrocarbons with aromatic rings. Further, the average molecular weight of bio-oil, engine-oil, naphthenic-oil, and aromatic-oil rejuvenator is 186.43, 316.48, 357.06, and 409.99 g/mol, respectively.

- The GC-MS results reveal that the chemical components of petroleum-based rejuvenators are more complex than the bio-oil. The alkane, naphthenic, and aromatic molecules are the main chemical components of EO, NO, and AO rejuvenators, which differ in the carbon-chain length, the number of naphthenic rings, and aromatic rings. In detail, bio-oil rejuvenator mainly comprises methyl oleate, linoleate, and methyl palmitate. Meanwhile, the engine-oil rejuvenator is composed of approximately 56 different molecules, of which the alkane molecules present a percentage of 61.79%, which are engine-oil components. These alkanes molecules in engine-oil exhibit disparate carbon-chain structures, and the carbon atom's number in molecular structures of most alkanes is in the region of 11-20.

- From GC-MS tests, almost 40 types of molecules are detected in the naphthenic-oil rejuvenator. The proportion of alkanes in the naphthenic-oil rejuvenator is approximately 17.85%, while the naphthenic concentration shows a maximum value of 59.79%. Therefore, the main components in the naphthenic-oil rejuvenator are naphthenic molecules, followed by alkane molecules. Compared to the engine-oil, the alkane dosage in the naphthenic-oil rejuvenator is significantly lower, while the concentration of naphthenic molecules is much higher.

- The aromatic-oil rejuvenator is mainly composed of alkane, olefin, aromatic molecules, and other hydrocarbons. The alkane content (13.74%) in aromatic-oil is markedly lower than that in the engine-oil (61.79%) and naphthenic-oil (17.85%) rejuvenators. Nevertheless, the concentration of aromatics molecules in aromatic-oil is significant at 53.91%, which is hardly detected in the other three rejuvenators. Further, most aromatics molecules are naphthalene-based, with a high dosage of 46.73%, while benzene-based and fluorene/indene only account for 0.86% and 6.31%, respectively.

➢ **Determination of the average and multi-component molecular models of rejuvenators**

- The average chemical formula of bio-oil, engine-oil, naphthenic-oil, and aromatic-oil is derived as $C_{19}H_{36}O_2$, $C_{22}H_{44}$, $C_{26}H_{48}$, and $C_{30}H_{40}$. The bio-oil exhibits the straight-chain monoalkene of 19 carbon atoms with one ester group, and the engine-oil molecule consists of one cyclohexane and two saturated n-octane chains. Moreover, the main body in naphthenic-oil is the saturated tricyclic alkanes connected

with n-hexane and n-heptane alkyl substituents. Further, the aromatic-oil shows the polycyclic aromatic hydrocarbon structure as a centre linked with saturated straight-chain and monocyclic alkanes.

- In the multi-component bio-oil molecular model, the molecule numbers of methyl palmitate, methyl linoleate, and methyl oleate are 13, 44, and 151. Meanwhile, the molecular number of tetradecane, 1-methyl-2-pentyl-cyclohexane, 2,6-bis(1,1-dimethylethyl)-phenol, 1-pentanol, and butyl benzoate molecule in the multi-component molecular model of engine-oil is 127, 14, 25, 34 and 8, respectively.

- The molecular number of the tetradecane, hexadecahydro pyrene, and 2-methoxy-4-methyl phenol in the multi-component model of naphthenic-oil is 39, 120, and 4. At the same time, the number of octadecane, 2,7-dimethyl naphthalene, and furfural molecules in the multi-component model of aromatic-oil is determined as 22, 140, and 110.

> **MD simulation predictions on average and multi-component molecular models of rejuvenators**

- The overall ranking for the potential energy of four rejuvenators in the multi-component simulation cases is the same as average models: AO > BO > NO > EO. However, the potential energy values of rejuvenators depend on the type of molecular models.

- From both average and multi-component models, the sequence of CED and δ for four rejuvenators is the same as AO > BO > NO > EO, while the results of multi-component models of engine-oil, naphthenic-oil, and aromatic-oil are slightly larger than their corresponding average models.

- In addition, the fractional free volume (FFV) parameters of the multi-component molecular models of four rejuvenators follow the decreasing order of EO > BO > NO > AO, which is consistent with the finding in average models.

- In the average models, the bio-oil rejuvenator shows the highest diffusion coefficient of 1.417E-10 m^2/s, while the aromatic-oil molecule displays the lowest diffusion coefficient of 3.21E-11 m2/s. However, in the multi-component models, the aromatic-oil rejuvenator exhibits the highest diffusion coefficient of 8.37E-10 m^2/s, while the diffusion coefficient of the bio-oil rejuvenator is the smallest at 1.887E-10 m^2/s.

- The magnitude order of viscosity for four rejuvenators from average models' simulations and experiments is the same: AO > NO > EO > BO. Nevertheless, the predicted viscosity ranking of multi-component models of four rejuvenators agrees well with experimental results except for the aromatic-oil.

> **Comparison and determination of molecular models of rejuvenators for further MD simulations on rejuvenated bitumen systems**

- From the viewpoint of molecular compositions, the average models consider all chemical components of rejuvenators. However, only part of the molecules in rejuvenators are included in the multi-component molecular models. On the other hand, the average models lump all properties together by taking only the most common molecule, whereas the multi-component model allows for some specific/characteristic molecules.

- The average and multi-component molecular models of these rejuvenators are efficient to some extent, according to the validation results. In addition, the MD simulation outputs from average and multi-components models are the same in terms of positive energy, cohesive energy density, solubility parameter, and fractional free volume. However, most thermodynamic parameters strongly depend on the molecular structures of simulation models.

- The unexpected values of the self-diffusion coefficient D and viscosity manifest that the multi-component molecular model of aromatic-oil based on the GC-MS method is not accurate because the polycyclic aromatic molecules with heavy weight are not detected and considered. New chemical

separation and detection methods should be developed to measure the chemical composition distribution of polycyclic aromatic molecules in an aromatic-oil rejuvenator.

- Overall, the average molecular models are more accurate than the multi-component models and will be employed in following MD simulations on rejuvenated bitumen systems. However, the average model is not a complete representation due to the gap between experimental results and MD simulation outputs.

4.9 References

[1] K. Yan, H. Lan, Z. Duan, W. Liu, L. You, S. Wu, M. Milijkovic. Mechanical performance of asphalt rejuvenated with various vegetable oils. Construction and Building Materials. 2021, 293, 123485.

[2] D. Sun, G. Sun, Y. Du, X. Zhu, T. Lu, Q. Pang, S. Shi, Z. Dai. Evaluation of optimized bio-asphalt containing high content waste cooking oil residues. Fuel. 2017, 202, 529-540.

[3] M. Gong, J. Yang, J. Zhang, H. Zhu, T. Tong. Physical-chemical properties of aged asphalt rejuvenated by bio-oil derived from biodiesel residue. Construction and Building Materials. 2016, 105, 35-45.

[4] A. Chen, Z. Hu, M. Li, T. Bai, G. Xie, Y. Zhang, Y. Li, C. Li. Investigation on the mechanism and performance of asphalt and its mixture regenerated by waste engine oil. Construction and Building Materials. 2021, 313, 125411.

[5] H.F. Haghshenas, R. Rea, G. Reinke, D.F. Haghshenas. Chemical characterization of recycling agents. Journal of Materials in Civil Engineering. 2020, 32(5), 06020005.

[6] X. Yu, M. Zaumanis, S. Santos, L.D. Poulikakos. Rheological, microscopic, and chemical characterization of the rejuvenating effect on asphalt binders. Fuel. 2014, 135, 162-171.

[7] M. Zaumanis, R.B. Mallick, L. Poulikakos, R. Frank. Influence of six rejuvenators on the performance properties of reclaimed asphalt pavement (RAP) binder and 100% recycled asphalt mixture. Construction and Building Materials. 2014, 71, 538-550.

[8] G. Nsengiyumva, H.F. Haghshenas, Y.R. Kim, S.R. Kommidi. Mechanical-chemical characterization of the effects of type, dosage, and treatment methods of rejuvenators in aged bituminous materials. Transportation Research Record. 2020, 2674(3), 126-138.

[9] A. Rajib, F. Pahlavan, E. Fini. Investigating molecular-level factors that affect the durability of restored aged asphalt binder. Journal of Cleaner Production. 2020, 270, 122501.

[10] D. Hu, X. Gu, Q. Dong, L. Lyu, B. Cui, J. Pei. Investigating the bio-rejuvenator effects on aged asphalt through exploring molecular evolution and chemical transformation of asphalt components during oxidative aging and regeneration. Journal of Cleaner Production. 2021, 329, 129711.

[11] D. Li, M. Greenfield. Chemical compositions of improved model asphalt systems for molecular simulations. Fuel. 2014, 115, 347-356.

[12] C. Chen, D. Mira, X. Jiang. A molecular simulation study on transport properties of FAMEs in high-pressure conditions. Fuel. 2022, 316, 123356

[13] E. Fini, A. Samieadel, A. Rajib. Moisture damage and its relation to surface adsorption/desorption of rejuvenators. Industrial & Engineering Chemistry Research. 2020, 59, 30, 13414-13419.

[14] C. Bao, Y. Xu, C. Zheng, L. Nie, X. Yang. Rejuvenation effect evaluation and mechanism analysis of rejuvenators on aged asphalt using molecular simulation. Materials and Structures. 2022, 55, 52.

[15] NCAT. NCAT Researchers Explore Multiple User of rejuvenators asphalt technology news. 2014, 26 (NO.1 Spring), 1-16.

[16] M. Lin, J. Shuai, P. Li, X. Kang, Y. Lei. Analysis of rheological properties and micro-mechanism of aged and reclaimed asphalt based on multi-scales. Construction and Building Materials. 2022, 321, 126290.

[17] Z. Chen, J. Pei, R. Li, F. Xiao. Performance characteristics of asphalt materials based on molecular dynamics simulation-A review. Construction and Building Materials. 2018, 189: 695-710.

[18] J. Liu, Q. Liu, S. Wang, X. Zhang, C. Xiao, B. Yu. Molecular dynamics evaluation of activation mechanism of rejuvenator in reclaimed asphalt pavement (RAP) binder. Construction and Building Materials. 2021, 298, 123898.

[19] B. Cui, X. Gu, D. Hu, Q. Dong. A multiphysics evaluation of the rejuvenator effects on aged asphalt using molecular dynamics simulations. Journal of Cleaner Production. 2020, 259, 120629.

[20] X. Zhang, Y. Ning, X. Zhou, X. Xu, X. Chen. Quantifying the rejuvenation effects of soybean-oil on aged asphalt-binder using molecular dynamics simulations. Journal of Cleaner Production. 2021, 317, 128375.

[21] F. Pahlavan, A. Hung, E. Fini. Evolution of molecular packing and rheology in asphalt binder during rejuvenation. Fuel. 2018, 222, 457-464.

[22] W. Sun, H. Wang. Molecular dynamics simulation of diffusion coefficients between different types of rejuvenator and aged asphalt binder. International Journal of Pavement Engineering. 2020, 21(8), 966-976.

[23] Xu G., Wang H. Diffusion and interaction mechanism of rejuvenating agent with virgin and recycled asphalt binder: a molecular dynamics study. Molecular Simulation. 2018, 44(17), 1433-1443.

[24] M. Xu, J. Yi, D. Feng, Y. Huang. Diffusion characteristics of asphalt rejuvenators based on molecular dynamics simulation. International Journal of Pavement Engineering. 2019, 20(5), 259, 120629.

[25] S. Ren, X. Liu, P. Lin, S. Erkens, Y. Xiao. Chemo-physical characterization and molecular dynamics simulation of long-term aging behaviors of bitumen. Construction and Building Materials. 2021, 302, 124437.

[26] S. Ren, X. Liu, P. Lin, R. Jing, S. Erkens. Toward the long-term aging influence and novel reaction kinetics models of bitumen. International Journal of Pavement Engineering. 2022, https://doi.org/10.1080/10298436.2021.2024188

[27] L. Zhang, Q. Shi, C. Zhao, N. Zhang, K. Chung, C. Xu, S. Zhao. Hindered stepwise aggregation model for molecular weight determination of heavy petroleum fractions by vapor pressure osmometry (VPO). Energy & Fuels. 2013, 27, 3, 1331-1336.

[28] C. Li, A. Rajib, M. Sarker, R. Liu, E. Fini, J. Cai. Balancing the aromatic and ketone content of bio-oils as rejuvenators to enhance their efficacy in restoring properties of bitumen. ACS Sustainable Chemistry & Engineering. 2021, 9, 20, 6912-6922.

[29] R. Zhang, Z. You, H. Wang, X. Chen, C. Si, C. Peng. Using bio-based rejuvenator derived from waste wood to recycle old asphalt. Construction and Building Materials. 2018, 189, 568-575.

[30] F. Pahlavan, E. Fini. Phenolic compounds to hinder sulfur crystallization in sulfur-extended bitumen. Resources, Conversation & Recycling. 2022, 180, 106184.

[31] Y. Xiao, B. Yan, X. Zhang, X. Chang, M. Li. Study the diffusion characteristics of rejuvenator oil in aged asphalt binder by image thresholding and GC-MS tracer analysis. Construction and Building Materials. 2020, 249, 118782.

[32] F. Fallah, F. Khabaz, Y.R. Kim, S.R. Kommidi, H.F. Haghshenas. Molecular dynamics modeling and simulation of bituminous binder chemical aging due to variation of oxidation level and saturate-aromatic-resin-asphaltene fraction. Fuel. 2019, 237, 71-80.

[33] C. Hu, G. You. J. Liu, S. Du, X. Zhao, S. Wu. Study on the mechanisms of the lubricating oil antioxidants: Experimental and molecular simulation. Journal of Molecular Liquids. Journal of Molecular Liquids. 2021, 324, 115099.

[34] G. Li, Y. Tan. The construction and application of asphalt molecular model based on quantum chemistry calculation. Fuel. 2022, 308, 122037.

[35] M. Li, L. Liu, C. Xing, L. Liu, H. Wang. Influence of rejuvenator preheating temperature and recycled mixture's curing time on performance of hot recycled mixtures. Construction and Building Materials. 2021, 295, 123616.

[36] S. Ren, X. Liu. P. Lin, S. Erkens, Y. Gao. Chemical characterizations and molecular dynamics simulations on different rejuvenators for aged bitumen recycling. Fuel. 2022, 324, 124550.

[37] S. Ren, X. Liu, S. Erkens, P. Lin, Y. Gao. Multi-component analysis, molecular model construction, and thermodynamics performance prediction on various rejuvenators of aged bitumen. Journal of Molecular Liquids. 2022, 360, 119463.

[38] M. Wrobel, A. Woszuk, M. Ratajczak, W. Franus. Properties of reclaimed asphalt pavement mixture with organic rejuvenator. Construction and Building Materials. 2021, 271, 121514.

[39] P. Cong, X. Guo, L. Mei. Investigation on rejuvenation methods of aged SBS modified asphalt binder. Fuel. 2020, 279, 118556.

[40] S. Ren, X. Liu, H. Wang, W. Fan, S. Erkens. Evaluation of rheological behaviors and anti-aging properties of recycled asphalts using low-viscosity asphalt and polymers. Journal of Cleaner Production. 2020, 253, 120048.

5

Compatibility potential evaluation of different rejuvenator-aged bitumen blends

The interaction between aged bitumen and rejuvenators plays a crucial role in determining the blend quality and thermal stability of rejuvenated bitumen. This compatibility hinges largely on their chemical compositions, making it imperative to establish a predictive method for assessing rejuvenator compatibility in aged binders. In this chapter, we delve into the compatibility potential of rejuvenator-aged bitumen mixtures, employing molecular-level thermodynamic parameters. Furthermore, the quantitative compatibility predictions generated through molecular dynamics simulations are corroborated by qualitative findings from macroscopic thermal storage tests.

5.1 Introduction

As discussed in **Chapter 3**, the aging of bitumen is complicated [1-3] and rejuvenators can soften the material [4], which has positive and negative effects [5-8]. All of these evaluations are based on a hypothesis that the rejuvenators have been completely blended with aged bitumen, and a homogeneous rejuvenated bitumen is fabricated [9]. In practical engineering, the rejuvenators are directly incorporated into an asphalt mixture containing RAP with a mechanical mixing process for a blending duration at high temperatures [10, 11]. It is expected that the RAP aggregates are fully and evenly covered by rejuvenators, which can diffuse quickly and disperse uniformly in aged bitumen to ultimately form a homogeneous rejuvenated bitumen layer outside of all RAP aggregates [12]. However, it is difficult to achieve this goal within a limited period, and partial blending does exist in recycled mixtures, which are strongly dependent on the rejuvenator type, RAP content, aging degree of bitumen, mixing temperature, and time [13-15]. The non-homogeneous dispersion of rejuvenators in recycled asphalt pavement increases both the rutting and cracking potential due to the excessively high and low dosage of rejuvenators in various locations [16, 17]. Thence, it is essential to be able to assess blending potential as part of the selection of a rejuvenator.

Currently, the blending degree between the fresh and aged bitumen has been evaluated by different methods, such as stage extraction [18], microscopic observation [19], and Fourier transform infrared (FTIR) microscopy [20]. Moreover, the improvement effects of rejuvenators on the blending level between fresh and RAP binders have been proved, which strongly depends on the rejuvenator type [21]. The degree of blending of rejuvenators with aged bitumen is always estimated through a diffusion coefficient parameter [22, 23]. The ultimate blending level is attributed to the diffusive rate and compatibility behavior between the rejuvenator and aged bitumen. Bad compatibility would result in the inhomogeneous dispersion and phase separation of rejuvenators in aged bitumen, thus increasing the risk of local rutting or cracking of recycled asphalt roads [24, 25]. However, few studies focus on the compatibility issue between the rejuvenator and aged bitumen. The variety of rejuvenator types also makes it difficult to determine the connections between their chemical components and compatibility with RAP bitumen. On the other hand, although the glass transition temperature, rheological indices, solubility parameter, and storage stability index have been adopted to evaluate the compatibility level between the aged bitumen and rejuvenators, the underlying mechanism is still unclear from the viewpoint of intermolecular interactions.

The molecular dynamics (MD) simulation method is successfully employed in estimating the compatibility of polymer blend systems [26, 27]. Similarly, Zhang et al. qualified the compatibility between soybean-oil and aged bitumen using MD simulations and thermal storage tests. It was found that the soybean-oil rejuvenated bitumen exhibited excellent storage stability and compatibility potential [28]. However, the compatibility between rejuvenators in different categories and aged binders with variable aging levels has not been studied yet. Meanwhile, it is necessary to estimate the efficiency of MD simulations in quantitatively predicting the compatibility degree of rejuvenators in aged binders, which should then be validated and connected with several indicators from laboratory tests. Therefore, this study proposes a multi-scale method for evaluating the compatibility between rejuvenators and aged binders. To this end, the effects of rejuvenator types, the aging degree of bitumen, and temperature on the compatibility degree have been investigated. Lastly, the underlying mechanism of compatibility difference between different rejuvenator-aged bitumen systems has been fundamentally explored and discussed from an intermolecular interaction viewpoint, molecular mobility, and molecular dispersion levels.

5.2 Research methodology and protocol

The detailed research methodology is illustrated in **Figure 5.1**. It should be mentioned that steps i-iii is based on **chapter 3** and **chapter 4**.

(i) After determining and validating the molecular models of aged binders and rejuvenators, an MD simulation was adopted to predict the cohesive energy density (CED) and solubility parameter values.

(ii) At the same time, the elemental analysis results are used to calculate the solubility parameters of aged bitumen and rejuvenators, which are compared with MD simulation outputs.

(iii) Afterward, three thermodynamic parameters of solubility parameter difference (ΔS), Flory-Huggins factor (χ), and mixing free energy (ΔG_m) between various aged bitumen and rejuvenators are calculated using MD simulations outputs and validated through experimental results to assess their compatibility and blending possibility from the viewpoint of polymer science theory.

(iv) In addition, the molecular models of rejuvenated bitumen are established to measure the binding energy and intermolecular force between rejuvenator and aged bitumen molecules. Meanwhile, the molecular distribution and mobility of rejuvenator molecules in rejuvenated bitumen models are predicted from MD simulations to estimate the compatibility between rejuvenators and aged bitumen from the molecular scale.

(v) Lastly, the corresponding rejuvenated binders are manufactured and tested by using a thermal storage test to evaluate the compatibility of rejuvenators in aged bitumen.
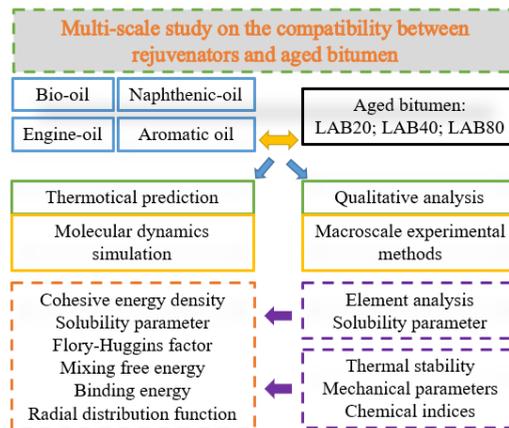
Figure 5.1 Research scheme for this chapter

5.3 Sample preparations and characterizations

5.3.1 Preparation of rejuvenated bitumen

The rejuvenated bitumen was prepared manually by mixing the aged bitumen and rejuvenators [29]. The 70g aged bitumen was heated firstly in an oven with 160°C for 30min to ensure sufficient flowability and workability. Afterward, the 7g (10% by weight) rejuvenator is incorporated and mixed with aged bitumen for 15min to guarantee a sufficient-blending state. It should be mentioned that the rejuvenated binder is heated during the blending process to hinder the inhomogeneous condition due to the temperature reduction. Twelve rejuvenated binders consisting of rejuvenators (BO, EO, NO, and AO) and aged bitumen (LAB20, LAB40, and LAB80) are manufactured for further thermal storage stability tests.

5.3.2 Experimental methods

5.3.2.1 Thermal storage test

In this section, the thermal storage test, performed to examine the compatibility between the rejuvenator and aged bitumen, is discussed. This thermal storage test is a standard and commonly-used method to assess the compatibility of polymer-modified bitumen [30, 31]. 50g rejuvenated bitumen was encased in a cylindrical aluminium tube and stored vertically in an oven at a temperature of 163°C for 48 hours. After that, the tube

specimens are placed in a refrigerator at -20°C for at least 4 hours for rapid cooling and conserving the molecular distribution [32]. The cooled tube was then cut into three equally large sections for further rheological and chemical characterization. It should be noted that each piece is heated and blended further to ensure homogeneous states before tests.

5.3.2.2 Dynamic shear rheometer (DSR) test

To quantitatively evaluate the separation degree of rejuvenator from aged bitumen, the evenly-divided rejuvenated bitumen specimens (top, middle, and bottom sections) after standardized thermal storage procedure are all characterized in terms of rheological and chemical properties. Herein, the DSR measurements consist of the frequency sweep (FS), steady-state flow, and multiple stress creep and recovery (MSCR) tests with a parallel plate geometry of 25mm diameter and 1mm gap to evaluate the homogenous degree of rejuvenated binders after thermal storage from the viewpoint of diverse rheological indexes.

During the FS test, two temperatures of 30 and 60°C are selected, with the frequency varying from 0.1 rad/s to 100 rad/s (AASHTO M320 [33]). According to the standard of AASHTO TP70 [34], the temperature and stress levels of the MSCR test herein are 52°C and 0.1/3.2 kPa, respectively. In addition, the steady-state flow test was conducted at 60 °C with the shear rate increasing from 10^{-3} to 10^{2} s^{-1}.

5.3.2.3 Attenuated reflectance-Fourier transfer infrared (ATR-FTIR) spectroscopy

The difference in chemical characteristics of three separated sections of rejuvenated binders after thermal storage is detected. Each specimen was scanned 12 times with the wavenumber scope of 600-4000 cm^{-1} and a fixed instrument resolution of 4 cm^{-1}. It should be mentioned that all samples have the DSR and FTIR tests at least three times to ensure data reliability.

5.4 MD simulations on compatibility evaluation

5.4.1 Molecular models of bitumen and rejuvenators

The final equilibrium molecular models of virgin and aged bitumen (as presented in **Chapter 3**) and four rejuvenators (**Chapter 4**) are illustrated in **Figure 5.2**, used for further analysis regarding thermodynamic parameters, structural characteristics, and dynamic behaviors.

Figure 5.2 Molecular models of the virgin, aged bitumen, and rejuvenators
(VB: virgin bitumen; SAB: short-term aged bitumen; LAB20, LAB40, and LAB80: 20-hours, 40-hours, and 80-hours aged bitumen; BO: bio-oil; EO: engine-oil; NO: naphthenic-oil; AO: aromatic-oil)
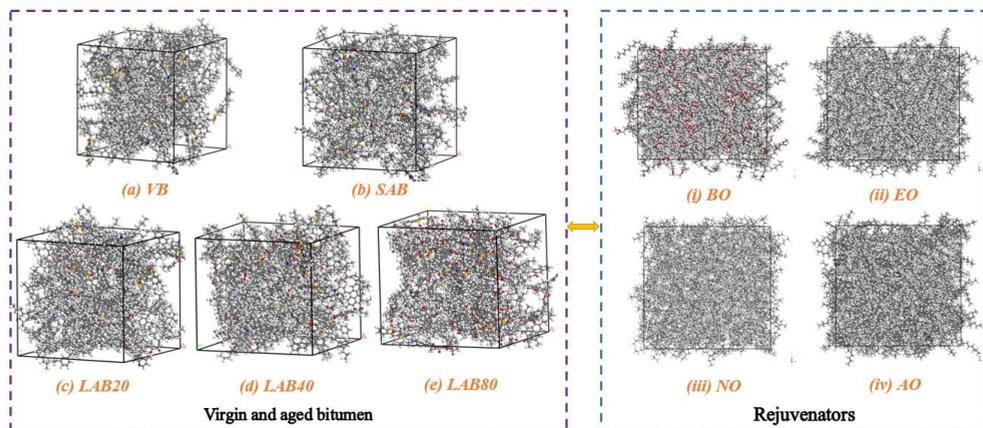
5.4.2 Thermodynamic properties of aged bitumen and rejuvenators

5.4.2.1 Cohesive energy density and solubility parameter

From the viewpoint of composite material, the solubility parameter is an essential indicator to evaluate the compatibility between various components [35]. Furthermore, a well-known principle is that two materials with similar solubility parameter values would behave with greater compatibility [36]. Therefore, the compatibility potential between rejuvenators and aged binders is first evaluated through their solubility parameter (δ), strongly related to the cohesive energy density (CED). Both the CED and δ values of bitumen and rejuvenators can be predicted from MD simulations, as shown in **Eqs.5.1** and **5.2**.

$$CED = \frac{E_{coh}}{V} = \frac{E_{vdw} + E_{ele}}{V} \tag{5.1}$$

$$\delta = \sqrt{CED} = \sqrt{\delta_{vdw}^2 + \delta_{ele}^2} \tag{5.2}$$

where CED and δ are the total cohesive energy density ($J \cdot cm^{-3}$) and solubility parameter (($J \cdot cm^{-3}$)$^{0.5}$), respectively; E_{coh} and V are the total cohesive energy and volume of simulation models; E_{vdw} and E_{ele} are the van der Waals and electrostatic term cohesive energy; δ_{vdw} and δ_{ele} are the van der Waals and electrostatic solubility parameter.

The cohesive energy in a molecular model comes from the non-bond intermolecular force, mainly consisting of van der Waals and electrostatic terms. Hence, the CED and δ parameters present van der Waal terms and electrostatic values. **Table 5.1** displays the CED and δ parameters of the virgin, aged bitumen, and rejuvenators in terms of total, van der Waals, and electrostatic terms, which can be directly calculated and outputted by MD simulations after obtaining the representative equilibrium models. With the increment in an aging degree, all CED and δ values of bitumen show an increasing trend. The involvement of polar functional groups in aged bitumen molecules would enhance the intermolecular force and cohesive energy. That's why the aged bitumen with a higher aging level would show a larger stiffness.

Table 5.1 Cohesive energy density and solubility parameters of aged bitumen and rejuvenators

Samples	CED ($J \cdot cm^{-3}$)	CED$_{vdw}$ ($J \cdot cm^{-3}$)	CED$_{ele}$ ($J \cdot cm^{-3}$)	δ ($J \cdot cm^{-3}$)$^{0.5}$	δ_{vdw} ($J \cdot cm^{-3}$)$^{0.5}$	δ_{ele} ($J \cdot cm^{-3}$)$^{0.5}$
VB	3.357E8	3.229E8	4.126E6	18.322	17.968	2.029
SAB	3.360E8	3.236E8	3.624E6	18.331	17.989	1.901
LAB20	3.425E8	3.266E8	6.989E6	18.507	18.072	2.642
LAB40	3.675E8	3.474E8	1.074E7	19.171	18.638	3.276
LAB80	3.804E8	3.486E8	2.231E7	19.504	18.670	4.723
BO	3.190E8	3.073E8	4.764E6	17.862	17.529	2.180
EO	2.711E8	2.643E8	2.750E5	16.465	16.258	0.524
NO	2.723E8	2.649E8	2.837E5	16.501	16.275	0.532
AO	3.406E8	3.289E8	3.064E6	18.455	18.137	1.749

The CED and δ values of all rejuvenators are smaller than those of virgin and aged bitumen, which further verifies that it is feasible to rehabilitate the CED and δ parameters of aged bitumen to the virgin level using these rejuvenators. However, these rejuvenators exhibit different CED and δ values, indicating a difference in restoration capacity on aged bitumen between these rejuvenators. This finding agrees well with the previous conclusion that the rejuvenation efficiency of the rejuvenator is influenced by the rejuvenator type and chemical components [37]. The sequence of CED and δ parameters for four rejuvenators is the same as AO> BO> NO > EO. It means that the CED and δ values of the aromatic-oil rejuvenator are the closest to virgin and aged bitumen, followed by bio-oil, but the naphthenic-oil and engine-oil rejuvenator show a large

gap in CED and δ values with virgin and aged binders. So, while the EO has a large capacity to lower the CED and δ of the aged bitumen, the very difference between its own CED and δ and that of aged bitumen limits its compatibility. The electrostatic CED and δ values are much lower than the van der Waals ones, indicating that intermolecular interactions of bitumen and rejuvenator molecules are dominated by the van der Waals force.

5.4.2.2 Validation from elemental analysis

The experimental elemental results of aged bitumen and rejuvenators are shown in **Table 5.2**. The elemental compositions of the bitumen models (AAA-1, AAK-1, and AAM-1) proposed by Li and Greenfield [38] are also listed herein.

Table 5.2 The elemental compositions of bitumen and rejuvenators

Bitumen	N%	C%	H%	S%	O%
VB	0.90	84.06	10.90	3.52	0.62
AAA-1*	0.40	85.60	10.00	3.60	0.40
AAK-1*	0.50	85.80	10.00	3.60	0.40
AAM-1*	0.70	86.90	11.00	1.40	0.40
SAB	0.91	83.72	10.86	3.51	1.00
LAB20	0.92	83.26	10.75	3.49	1.58
LAB40	0.90	83.02	10.44	3.53	2.11
LAB 80	0.91	82.14	10.10	3.54	3.31
Rejuvenators	N%	C%	H%	S%	O%
BO	0.15	76.47	11.96	0.06	11.36
EO	0.23	85.16	14.36	0.13	0.12
NO	0.12	86.24	13.62	0.10	0.10
AO	0.55	88.01	10.56	0.48	0.40

*AAA-1, AAK-1, and AAM-1 are the virgin bitumen models proposed by Li and Greenfield [38].

Compared with virgin bitumen, the aged binders exhibit a smaller carbon and hydrogen dosage due to the increase of oxygen content during the aging oxidation process, which tends to be more severe as the aging level increases. Meanwhile, the aging level does not influence the concentration of nitrogen and sulfur elements. Concerning the elemental compositions of rejuvenators, the bio-oil displays an apparent characteristic of high oxygen dosage, which is reflected by the ester group in its average molecular structure. Besides, the elemental compositions in the other three petroleum-based rejuvenators are mainly composed of carbon and hydrogen atoms, which present hydrocarbon characteristics [34]. Various rejuvenators exhibit different carbon and hydrogen element distributions. The engine-oil shows the lowest C% and highest H% values, followed by the naphthenic-oil rejuvenator, while the aromatic-oil has the opposite characteristic of the largest C% and smallest H% values.

The solubility parameter (δ) values of rejuvenators and bitumen can be calculated using an empirical formula developed on heavy oils based on the relationship between the δ value and elemental composition. Previous studies revealed that the correlation equation is efficient in predicting the δ values of petroleum distillates, which are similar to the results from a solvent titration method [35, 39, 40]. In addition, the titration method is cumbersome and not environmentally friendly, with different chemical solvents involved. **Eq.5.3** lists the empirical formula connecting the δ parameter with elemental compositions.

$$\delta = \frac{7.0 + 63.5f_a + 63.5\frac{H}{C} + 106\frac{O}{C} + 51.8\frac{N+S}{C}}{-10.9 + 12f_a + 13.9\frac{H}{C} + 5.5\frac{O}{C} - 2.8\frac{N+S}{C}} \tag{5.3}$$

where H, C, O, N, and S are the element concentrations in bitumen and rejuvenators, and f_a refers to the aromaticity, which is calculated as follows:

$$f_a = 1.132 - 0.560 * \left(\frac{H}{C}\right) \tag{5.4}$$

The measured H/C ratio, f_a, d, O%, and δ values of virgin and aged bitumen and different rejuvenators are listed in **Table 5.3**. It suggests that the aging degree decreases the H/C ratio but shows an increasing influence on the f_a, ρ, O%, and δ values of bitumen. The aromatic-oil has the lowest H/C ratio and highest f_a, ρ, and δ values, while the engine-oil shows the largest H/C ratio and smallest f_a, ρ, and δ parameters. In addition, the V_B indicator is the reference volume of the "average repeat unit" of bitumen samples proposed by Painter [40], calculated as follows:

$$V_B = \frac{V_m}{O} = \frac{1600}{O'd} \tag{5.5}$$

where O′ and d represent the oxygen concentration and specific gravity of bitumen samples. It demonstrates that the V_B value of bitumen reduces gradually as the aging degree increases.

Table 5.3 The structural parameters of aged bitumen and pure rejuvenators

Samples	H/C	f_a	ρ (g·cm⁻³)	O%	V_B.	δ (($J·cm^{-3})^{0.5}$)
VB	1.556	0.260	1.017	0.618	2546	18.340
SAB	1.556	0.261	1.019	1.004	1564	18.373
LAB20	1.549	0.265	1.024	1.582	988	18.456
LAB40	1.509	0.287	1.036	2.113	731	18.723
LAB80	1.475	0.306	1.054	3.312	458	19.016
BO	1.877	0.081	0.912	11.36	-	17.427
EO	2.023	0.001	0.833	0.120	-	16.083
NO	1.895	0.071	0.875	0.100	-	16.530
AO	1.440	0.326	0.994	0.400	-	18.779

The solubility parameter values of rejuvenators, virgin, and aged binders from both MD simulations prediction and experimental data calculation are presented side by side in **Figure 5.3** to assess the application potential of using MD simulations to predict the δ values of rejuvenators and aged binders, which is beneficial to preliminary judge their compatibility level without any laboratory test and design more efficient molecular structures of rejuvenators with excellent compatibility with aged bitumen. It is worth noting that the temperature would greatly influence the δ values, and here only presents the result at 25℃. **Figure 5.3** demonstrates that the total δ values of all bitumen and rejuvenators predicted from MD simulations are close to the calculated values based on elemental analysis results. The finding further confirms the feasibility of MD simulations on bitumen and rejuvenator materials.
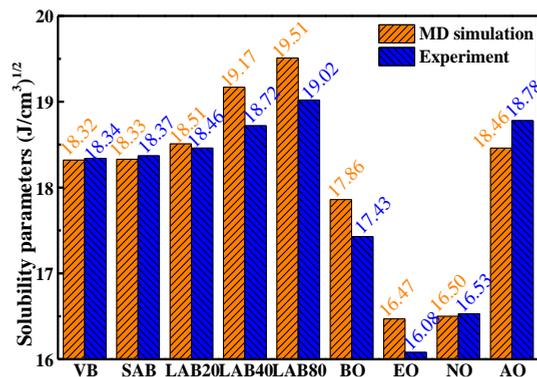
Figure 5.3 Solubility parameters of the virgin, aged bitumen, and rejuvenators

5.4.2.3 Solubility parameter difference Δδ

The solubility parameter difference Δδ at 298K between four rejuvenators (BO, EO, NO, AO) and aged binders with different aging degrees (LAB20, LAB40, LAB80) are calculated to assess their compatibility levels. The higher the Δδ value is, the worse the compatibility. The Δδ results from MD simulations and experiments are shown in **Figure 5.4**. It can be found that all Δδ values from both experiments and MD simulations are strongly dependent on the rejuvenator type and bitumen aging degree. When the aged bitumen is the same, the increasing sequence of total and van der Waals Δδ values for four rejuvenators is AO < BO < NO < EO, while the order of electrostatic Δδ values follows BO < AO < NO < EO. It suggests that the aromatic-oil rejuvenator exhibits the best compatibility with aged bitumen regardless of the aging level, followed by the bio-oil and naphthenic-oil. At the same time, the engine-oil shows the worst compatibility with aged binders. It should be mentioned that the conclusion from the MD simulations output is consistent with the experimental result, which further verifies the efficiency of MD simulations on compatibility prediction of rejuvenators in aged bitumen.
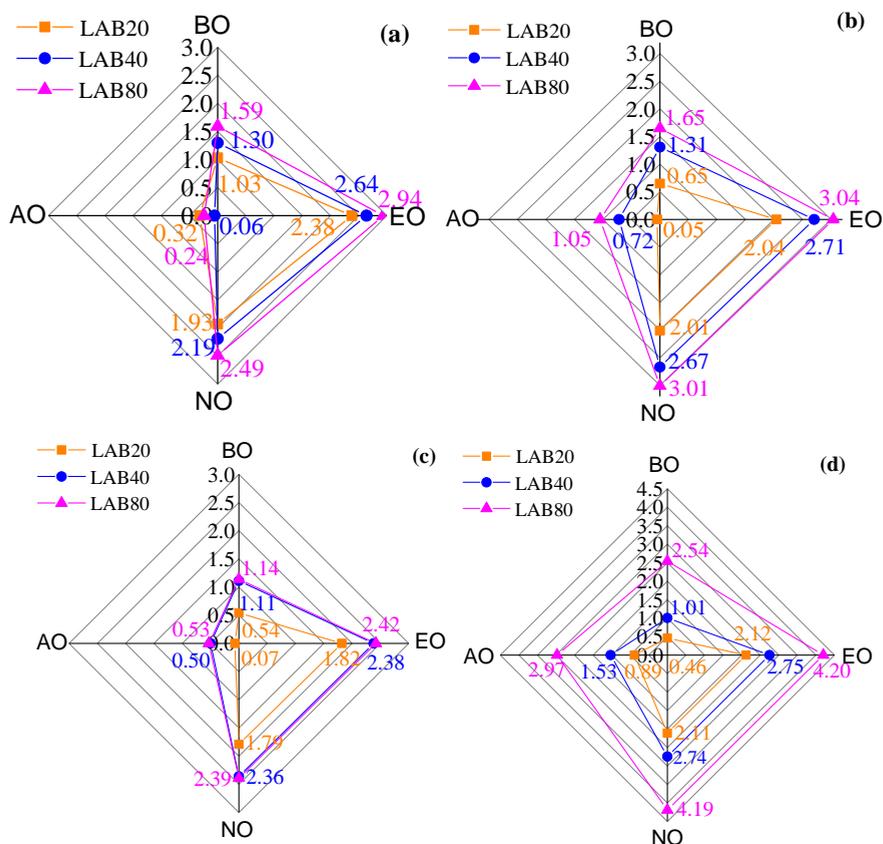
Figure 5.4 The solubility parameter difference Δδ between rejuvenators and aged binders (a) Experimental total δ; (b) MD simulation total δ; (c) MD simulation van der Waals δ; (d) MD simulation electrostatic δ

On the other hand, when the aging degree of bitumen increases, the total, van der Waals, and electrostatic Δδ values from MD simulations and experiments all show an increasing trend. It was already mentioned that the δ parameters of rejuvenators are lower than virgin and aged bitumen. The increment of

the δ value for aged bitumen because of the increasing aging level would enlarge the difference in the δ parameter between the rejuvenator and aged bitumen, reducing the compatibility. This is considered to be caused by the fact that the increased aging level significantly enhances the intermolecular force between the bitumen molecules, making it harder for rejuvenator molecules to break the strong interaction between the bitumen molecules to be compatible with them. Thus, the compatibility potential between the rejuvenator and aged bitumen is reduced as the aging degree of bitumen increases. It is worth noting that the aromatic-oil rejuvenator still presents a much lower Δδ value and best compatibility with long-term aged bitumen for 80 hours, which is least affected by the aging degree of bitumen. Interestingly, when the long-term aging duration of bitumen rises from 20 hours to 80 hours, the increment levels of Δδ values for bio-oil, engine-oil, and naphthenic-oil are similar. In addition, it is manifested that the total Δδ values between rejuvenators and aged binders are not a simple combination of van der Waals and electrostatic terms. The total Δδ values from both MD simulations and experiments are closer to the van der Waals Δδ than the electrostatic ones.

5.4.2.4 Flory-Huggins interaction parameter and mixing free energy

The Flory-Huggins theory is a classic principle for evaluating the compatibility of compatibility level and blending potential between various types of polymers and additives in composites [41]. Bituminous material behaves with viscoelastic characteristics, and it is assumed that the Flory-Huggins theory can be adopted herein to assess the compatibility between rejuvenators and aged bitumen. Therefore, two crucial parameters, Flory-Huggins parameter χ and mixing free energy ΔG_m, are utilized and calculated as follows:

$$\chi = \frac{V_B}{RT.}(\delta_B - \delta_R)^2 \tag{5.6}$$

where χ is the Flory-Huggins interaction factor; δ_B and δ_R are the solubility parameter value of aged bitumen and rejuvenator; V_B refers to the reference volume of the "average repeat unit" of bitumen; T and R show the temperature (K) and gas constant (8.314 $J \cdot K^{-1} \cdot mol^{-1}$), respectively.

$$\frac{\Delta G_m}{RT.} = \frac{\emptyset_R}{x_R}\ln\emptyset_R + \frac{\emptyset_B}{x_B}\ln\emptyset_B + \emptyset_R\emptyset_B\chi \tag{5.7}$$

where ΔG_m is the mixing free energy; $\emptyset_R$ and $\emptyset_B$ represent the volume fraction of rejuvenator and aged bitumen in rejuvenated binder; χ refers to the Flory-Huggins parameter; X_R and X_B are the polymerization degree of rejuvenator and bitumen molecules.

From **Eqs.5.6** and **5.7**, both χ and ΔG_m depend on the temperature T, indicating that the compatibility potential between rejuvenators and aged bitumen varies with temperature. Herein, the temperature is fixed at 25°C, and the temperature factor will be considered in the last section. Meanwhile, the mixing free energy ΔG_m is related to the volume fraction of the rejuvenator ($\emptyset_R$) and aged bitumen ($\emptyset_B$). The ΔG_m parameter represents the energy required when two materials are mixed completely. The negative ΔG_m values indicate that energy will be released from the mixing system to the environment, showing that the mixing process is thermodynamically spontaneous. In this case, the more negative/lower the ΔG_m value, the better the compatibility potential. When the temperature and volume fraction are constant, the ΔG_m value is exclusively influenced by the Flory-Huggins parameter χ. Besides, a low χ value reduces the ΔG_m value and enhances the compatibility extent between the rejuvenator and aged bitumen based on the correlation in **Eq.5.7**.

According to **Eq.5.6**, apart from the temperature and aged bitumen type, the Flory-Huggins parameter χ value is determined by the solubility parameter difference Δδ between the rejuvenator and aged bitumen. Overall, the more similar the δ values of rejuvenator and aged bitumen are, the lower the χ and ΔG_m values are, and the stronger the compatibility potential exhibits.

The Flory-Huggins interaction parameter χ values in various blending systems of rejuvenators and bitumen are calculated following **Eq.5.6**. Herein, the solubility parameter δ values of rejuvenators, virgin, and aged bitumen from both experiments and MD simulations are utilized to show the difference in χ between

measured and predicted values, which are listed in **Table 5.4** and **Table 5.5**, respectively. Compared with the virgin and short-term aged bitumen, the χ values between bio-oil, engine-oil, and naphthenic-oil rejuvenators and long-term aged binders are higher. It implies that long-term aging weakens the compatibility level between these rejuvenators and bitumen. However, it is interesting to note that the χ values between the aromatic-oil rejuvenator and long-term aged bitumen are even lower than a virgin binder. The reason may be related to the enhanced intermolecular force through a Π-Π interaction. After long-term aging, more asphaltene molecules with polyaromatic structures are generated, which results in a stronger Π-Π interaction between the polyaromatic rings in asphaltene and aromatic-oil molecules [42].

Various rejuvenators show different χ values with the same aged bitumen. Regardless of the aged bitumen type, the χ values between the aromatic-oil rejuvenator and aged binders are the lowest, indicating that the aromatic-oil exhibits the best compatibility potential with aged binders. In contrast, the engine-oil rejuvenator shows higher χ values and the worst compatible capacity with aged binders. The χ values of bio-oil and naphthenic-oil systems are in the middle, and the former displays better compatibility with aged bitumen than the latter. Overall, the ranking of χ values for four rejuvenators from both experiments and MD simulations is the same as AO < BO < NO < EO. Nevertheless, it should be mentioned that there is still little difference in χ values between experimental results and MD simulation outputs, mainly from the difference between established average structure and realistic multi-components characteristics of rejuvenators and aged binders. On the other hand, the aging degree of bitumen also affects the χ values and compatibility level between rejuvenators and aged bitumen, and its influence degree on various rejuvenators is different.

Table 5.4 Flory-Huggins parameters of different rejuvenated binders from experiments

χ value	VB	SAB	LAB20	LAB40	LAB80	Ranking
BO	0.246	0.264	0.422	0.496	0.468	2
EO	1.503	1.547	2.246	2.056	1.590	4
NO	0.967	1.002	1.479	1.419	1.142	3
AO	0.057	0.049	0.042	0.001	0.010	1

Table 5.5 Flory-Huggins parameters of different rejuvenated binders from MD simulations

χ value	VB	SAB	LAB20	LAB40	LAB80	Ranking
BO	0.063	0.065	0.168	0.506	0.502	2
EO	1.019	1.027	1.668	2.161	1.715	4
NO	0.979	0.987	1.609	2.102	1.673	3
AO	0.005	0.0046	0.001	0.151	0.206	1

The mixing free energy ΔG_{mix} values between rejuvenators and aged binders calculated with experimental data and MD simulation results are demonstrated in **Tables 5.6** and **5.7**. As mentioned above, the ΔG_{mix} value is affected by the Flory-Huggins interaction parameter (or solubility parameter difference) between rejuvenators and aged bitumen. It is also related to the temperature and volume fraction. This study aims to evaluate and compare the compatibility between different rejuvenators with aged binders. Thus, the temperature, volume fraction of the rejuvenator, and aged bitumen are fixed as 298K, 0.1, and 0.9. It is found that all ΔG_{mix} values between various rejuvenators and aged binders are negative, indicating that the system energy is released when rejuvenators and aged binders are mixed. This mixing process is spontaneous, and a stable blend with lower energy can be obtained. Nonetheless, when distinct rejuvenators are mixed with aged bitumen under consistent temperature and fixed volume fraction, the ΔG_{mix} values vary. It means that the rejuvenator type shows a great influence on compatibility between the rejuvenator and aged bitumen.

The order of ΔG_{mix} values for four rejuvenators is the same as that of the χ parameter and δ. To all aged binders, the aromatic-oil rejuvenator shows the lowest ΔG_{mix} and the largest compatible capacity with aged bitumen. Compared to the naphthenic-oil, the bio-oil exhibits lower ΔG_{mix} values and better compatibility behavior, while the engine-oil presents the highest ΔG_{mix}, and there is bad compatibility between the engine-

oil rejuvenator and aged bitumen. This conclusion is consistent with the experimental findings in the previous study [63].

Table 5.6 Mixing free energy of different rejuvenated binders from experiments

ΔG_{mix} (J·mol^{-1})	T (K)	$\varnothing_R$	$\varnothing_B$	VB	SAB	LAB20	LAB40	LAB80	Ranking
BO	298	0.1	0.9	-0.326	-0.324	-0.304	-0.309	-0.310	2
EO	298	0.1	0.9	-0.210	-0.205	-0.152	-0.131	-0.204	4
NO	298	0.1	0.9	-0.260	-0.257	-0.216	-0.208	-0.247	3
AO	298	0.1	0.9	-0.325	-0.326	-0.334	-0.328	-0.337	1

Table 5.7 Mixing free energy of different rejuvenated binders from MD simulations

ΔG_{mix} (J·mol^{-1})	T (K)	$\varnothing_R$	$\varnothing_B$	VB	SAB	LAB20	LAB40	LAB80	Ranking
BO	298	0.1	0.9	-0.351	-0.351	-0.313	-0.343	-0.320	2
EO	298	0.1	0.9	-0.261	-0.261	-0.141	-0.193	-0.193	4
NO	298	0.1	0.9	-0.254	-0.254	-0.144	-0.193	-0.191	3
AO	298	0.1	0.9	-0.331	-0.332	-0.326	-0.335	-0.328	1

5.4.3 Intermolecular binding energy

The compatibility potential between rejuvenators and aged binders has been evaluated through different thermodynamic parameters of $\Delta\delta$, χ, and ΔG_{mix}. However, all of these parameters come from two separate systems: bitumen and rejuvenator, and the compatibility mechanism from the viewpoint of intermolecular interaction is still unclear. Therefore, molecular models of various rejuvenated bitumen are established. The intermolecular energy between the rejuvenator and aged bitumen molecules is calculated to estimate their compatibility levels in this way.

The model establishment and MD simulation procedures of all rejuvenated binders are the same as the aged bitumen and rejuvenators, discussed in **Chapters 3** and **4**. The introduction of representative rejuvenator molecules makes the rejuvenated bitumen model 10% denser than the original bitumen model. The number of rejuvenator molecules in different aged bitumen is listed in **Table 5.8**. To simplify, the short name of the rejuvenated binder model is composed of bitumen aging degree, rejuvenator dosage, and type. For instance, the rejuvenated bitumen composed of LAB20 aged bitumen and 10% bio-oil rejuvenator is called "1P10B". It should be noted that the LAB20, LAB40, and LAB80 aged binders are also named 1P, 2P, and 4P, respectively. **Figure 5.5** illustrates the molecular equilibrium models of all rejuvenated binders with different rejuvenators and aged binders after the geometry optimization and MD simulation processes with NPT and NVT ensembles. This section focuses on the intermolecular energy between the rejuvenator and aged bitumen molecules. The following section will discuss the structural parameters regarding the molecular dispersion level.

Table 5.8 The molecular numbers of rejuvenators in different aged bitumen

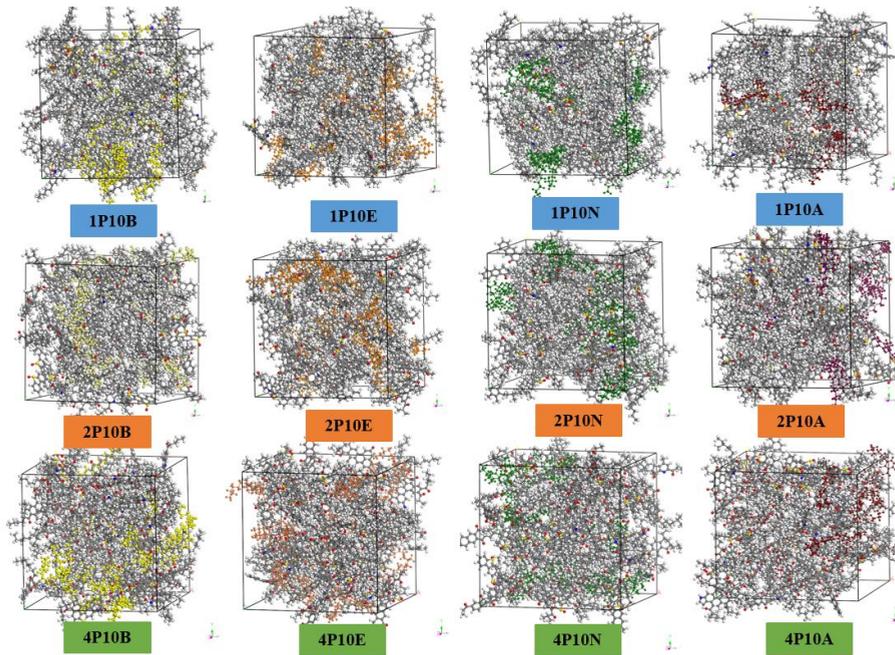| Aged bitumen	BO.	EO	NO	AO
LAB20	13	13	10	9
LAB40	13	13	11	10
LAB80	14	13	11	10

Figure 5.5 Molecular models of various rejuvenated binders
(Grey: bitumen molecules; Yellow: bio-oil molecules; Orange: engine-oil molecules; Green: naphthenic-oil molecules; Brown: aromatic-oil molecules)

In general, a hybrid system exhibits lower energy than the combined energies of its components, releasing energy to maintain greater thermodynamic stability. In this thesis, the binding energy $E_{binding}$ was utilized to assess the molecular interaction strength and compatibility level between the rejuvenator and aged bitumen molecules, which is calculated as follows:

$$E_{binding} = -E_{inter} = -(E_{total} - E_B - E_R) \tag{5.8}$$

where E_{total}, E_B, and E_R are the potential energy of the whole rejuvenated bitumen, aged bitumen phase, and rejuvenator phase, respectively.

The binding energy is a negative value of the interaction energy, representing the energy required to overcome the intermolecular force and separate the hybrid system into several independent phases. Therefore, the higher the binding energy value is, the stronger the intermolecular interaction between various molecules in different phases shows. Herein, the increased $E_{binding}$ suggests that the intermolecular interaction between the rejuvenator and aged bitumen molecules is enhanced, indicating greater compatibility between the rejuvenator and aged bitumen molecules.

The total, van der Waals and electrostatic $E_{binding}$ values between the rejuvenator and aged bitumen molecules are depicted in **Figure 5.6**. The electrostatic $E_{binding}$ values are notably lower than the van der Waals terms, highlighting the dominant role of van der Waals interactions in the force between rejuvenator and aged bitumen molecules. Regardless of the aging level of bitumen, the potential, van der Waals, and electrostatic $E_{binding}$ values of aromatic-oil rejuvenated bitumen are the largest, followed by the bio-oil rejuvenated binder. In addition, the naphthenic-oil rejuvenated binders show higher $E_{binding}$ values than the engine-oil rejuvenated bitumen. It suggests that the intermolecular interaction between the aged bitumen and aromatic-oil molecules is the strongest, accelerating their blending degree. This occurs because the

polyaromatic structure in aromatic-oil rejuvenators can establish strong Π-Π interactions with polar aromatic, resin, and asphaltene molecules in aged bitumen that still possess aromatic rings [43, 44].

On the other hand, the intermolecular interaction of bio-oil and aged bitumen molecules is superior to the naphthenic-oil and engine-oil rejuvenators. It may be related to the polar ester group in bio-oil molecular structure (see **Chapter 4**), which could form the hydrogen bond with aged bitumen molecules [45, 46]. From the viewpoint of intermolecular interaction strength, the compatibility potential ranking for these four rejuvenators is AO> BO> NO > EO, which is consistent with the previous conclusions from the thermodynamic parameters of $\Delta\delta$, χ, and ΔG_{mix}. At the same time, it is shown that the compatibility level between the aged bitumen and various rejuvenators can be predicted and compared through thermodynamic parameters and intermolecular binding energy. The $E_{binding}$ energy values of rejuvenated binders with the same rejuvenator and varying bitumen aging degrees are more tightly clustered compared to those of rejuvenated binders with different rejuvenators but at the same level of bitumen aging. In the case of both bio-oil and aromatic-oil rejuvenators, the Ebinding values steadily decrease as bitumen aging intensifies, whereas the engine-oil rejuvenator exhibits the opposite pattern. This observation may be attributed to the lower impact of the aging level on the saturated fraction of aged bitumen, which shares similar characteristics with the engine-oil rejuvenator.
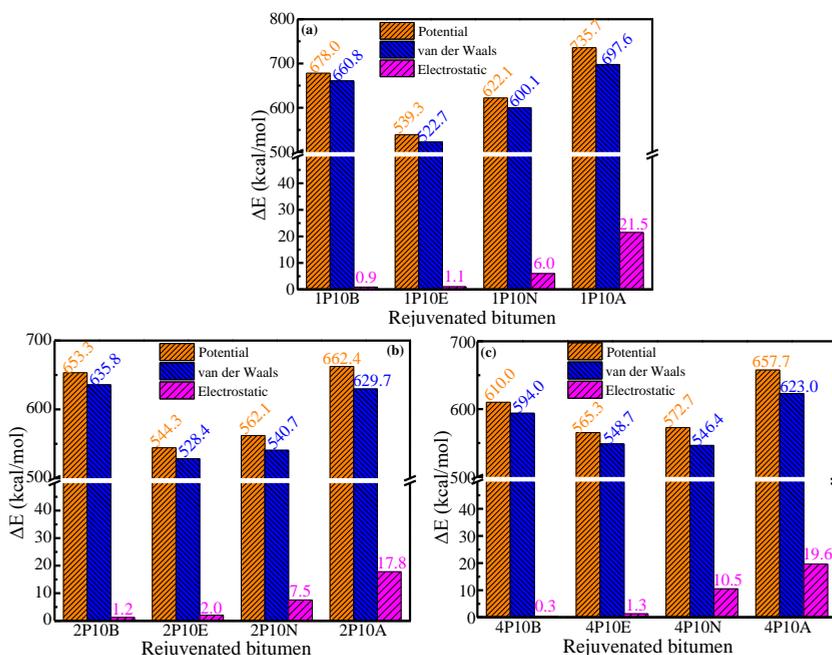
Figure 5.6 The binding energy E_binding values of various rejuvenated bitumen at 298K
(a) LAB20, (b) LAB40, (c) LAB80

5.5 Experimental results and discussion

In this chapter, the compatibility levels between various rejuvenators and aged binders with different aging degrees are investigated through the thermal storage stability test, the most general method for compatibility evaluation of polymer-modified bitumen [47, 48] and bio-bitumen [49, 50]. After a thermal storage process, both DSR and FTIR tests are performed to evaluate the homogeneity of rheological and chemical parameters between different sections of the rejuvenated bitumen samples after a thermal storage procedure. The

rheological indices of complex modulus G*, phase angle δ, rutting factor G*/sinδ, and fatigue factor G*sinδ from the frequency sweep tests, the zero-shear viscosity ZSV from the flow tests, and the recovery percentage R% and non-recoverable creep compliance J_{nr} values from the MSCR tests, of the homogenized bottom, middle, and top sections of each specimen are measured. Additionally, the carbonyl index C=O and sulfoxide index S=O of these specimens are calculated in **Chapter 3**. To assess the thermal storage stability of different rejuvenated binders, an efficient parameter of separation index SI based on various rheological and chemical properties is calculated as follows:

$$SI = \frac{P_{max} - P_{min}}{P_{ave}} * 100\% \tag{5.9}$$

where SI shows the separation index (%); P represents one of the rheological and chemical parameters; P_{max}, P_{min}, and P_{ave} are the maximum, minimum, and average values of parameter P among the bottom, middle, and top sections of each rejuvenated bitumen after the thermal storage process. Hence, the closer to zero the SI value is, the better the thermal phase stability of rejuvenated bitumen is shown.

5.5.1 Separation index based on G*, δ, G*/sinδ, and G*sinδ

The frequency sweep tests output the rheological parameters of G*, δ, G*/sinδ, and G*sinδ of the bottom, middle, and top sections of rejuvenated binders. **Figure 5.7** illustrates these rheological indices of 2P10B, 2P10E, 2P10N, and 2P10A rejuvenated binders at 30℃. When the rejuvenator dosage is 10wt%, compared to other rejuvenated binders, bio-oil rejuvenated bitumen exhibits lower G*, G*/sinδ, and G*sinδ values. On the other hand, the aromatic-oil rejuvenated bitumen has the largest G*, G*/sinδ, and G*sinδ. In addition, the phase angle δ values of bio-oil and aromatic-oil rejuvenated bitumen are larger than the engine-oil and naphthenic-oil ones. Hence, the rejuvenation capacity of engine-oil and naphthenic-oil rejuvenators on the ratio of viscous and elastic performance of aged bitumen is limited.
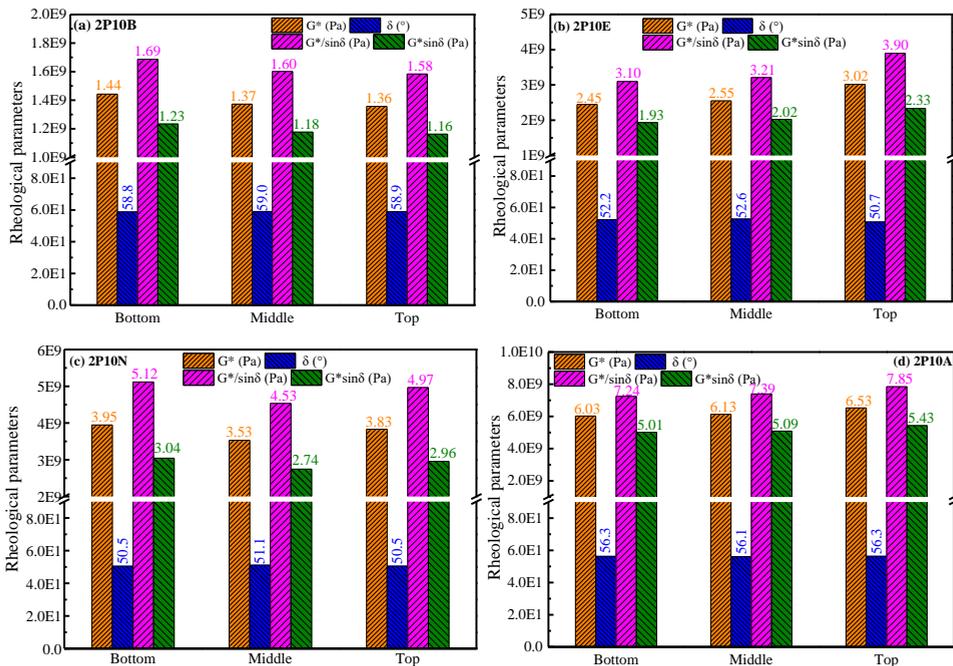

Figure 5.7 The rheological parameters of the bottom, middle, and top sections in rejuvenated binders
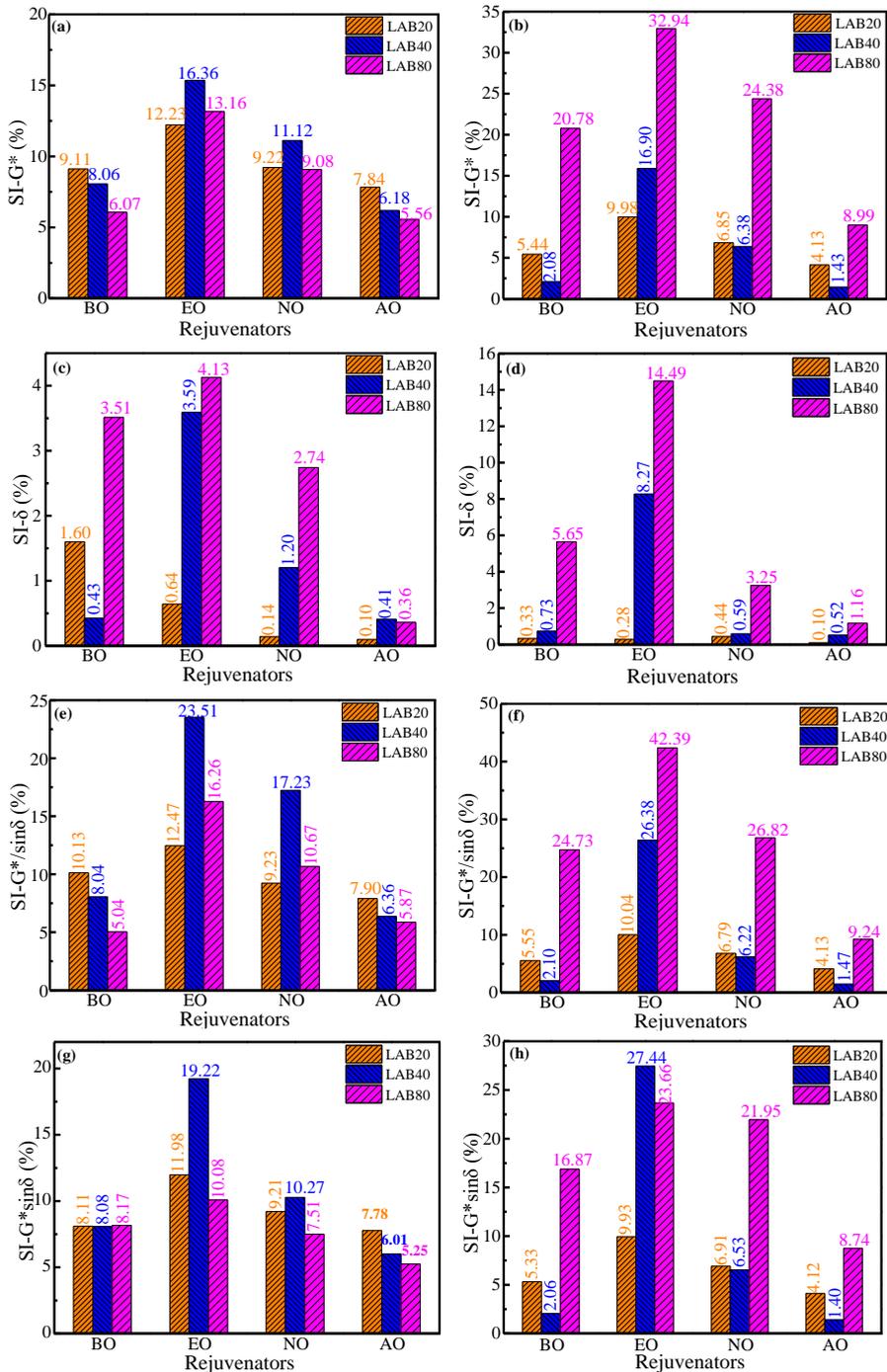
Figure 5.8 The separation index SI values of rejuvenated binders based on G*(a)(b), δ (c)(d), G*/sinδ (e)(f), and G*sinδ (g)(h)

To directly assess and compare the thermal storage stability and compatibility between various rejuvenators and aged binders, the separation indices based on these rheological parameters are calculated following **Eq.5.9**, and the corresponding results are displayed in **Figure 5.8**. It should be mentioned that two temperatures of 30°C (a)(c)(e)(g) and 60°C (b)(d)(f)(h) are selected for all FS tests to ensure the reliability of conclusions.

The SI values of all rejuvenated binders depend on the rheological parameter type and testing temperature. For all kinds of rejuvenators, the SI values of rejuvenated binders with LAB40 and LAB80 aged bitumen measured at 60°C are much larger than that at 30°C, while the rejuvenated binders with LAB20 aged bitumen show the opposite trend. In addition, the SI values based on the G*/sinδ and δ parameters of all rejuvenated binders are the highest and lowest, while SI parameters calculated from the G* and G*sinδ are similar regardless of the rejuvenator types, aging degree of bitumen, and testing temperatures. Thence, the G*/sinδ parameter is the most sensitive to evaluate the separation level of rejuvenated bitumen during the thermal storage process, while the δ parameter shows minimal sensitivity.

When the aging level of aged bitumen and testing temperature is fixed, the SI values based on all rheological indices of engine-oil rejuvenated bitumen are the highest, followed by the naphthenic-oil and bio-oil rejuvenated binders, while the aromatic-oil rejuvenated bitumen present the lowest SI values. The separation potential of engine-oil in rejuvenated bitumen is the largest during the thermal storage process, while the aromatic-oil rejuvenated binder exhibits the most stable blending level. Meanwhile, the SI values of bio-oil and naphthenic-oil rejuvenated binders are in the middle, and the former is lower than the latter. It denotes that the order of separation potential for four rejuvenators is AO < BO < NO < EO, which is consistent with the compatibility sequence from both MD simulations and experiments. The separation index SI values of rejuvenated binders with the LAB20, LAB40, and LAB80 aged bitumen are significantly different, indicating that the separation potential of rejuvenators is also affected by the aging level of aged bitumen in rejuvenated binders. However, the influence of the aging degree on the separation index values of various rejuvenated binders is not consistent, which agrees well with the MD simulation results regarding the role of aging degree on the compatibility between different rejuvenators and aged bitumen.

5.5.2 Separation index based on zero-shear viscosity

The steady-state flow tests are conducted to detect the difference in flow behaviors and zero-shear viscosity between the bottom, middle, and top sections of rejuvenated binders after a thermal storage stage. **Figure 5.9** illustrates the flow curves of three pieces in 2P10B, 2P10E, 2P10N, and 2P10A rejuvenated binders at 60°C. On the whole, the flow behaviors of all specimens are composed of the Newtonian flow region and shear-thinning range. It agrees well with the previous studies, which reported that the bituminous material exhibits the Newtonian flow characteristic, in which its viscosity values are independent of the shear rate. However, when the shear rate exceeds a crucial point, bitumen's viscosity values reduce as the shear rate increments dramatically, indicating a shear-thinning behavior. **Figure 5.9** demonstrates a difference in viscosity values and flow behaviors between the bottom, middle, and top sections of various rejuvenated binders after the thermal storage process.

The correlation curves between the shear rate and complex viscosity values of three sections in rejuvenated binders are fitted by the Carreau model:

$$\frac{\eta_0}{\eta} = [1 + (\frac{\gamma}{\gamma_c})^2]^s \qquad (5.10)$$

where η and γ are the complex viscosity (Pa·s) and shear rate (s^{-1}); η_0 represents the zero-shear viscosity, Pa·s; γ_c refers to the key shear rate related to the turning point before the shear-thinning region, s^{-1}, and s shows the slope value of the shear-thinning behavior range. It should be noted that the η_0 parameter is the critical viscosity when the shear rate reaches zero, which was proved to be an important indicator associated with the bitumen deformation resistance.
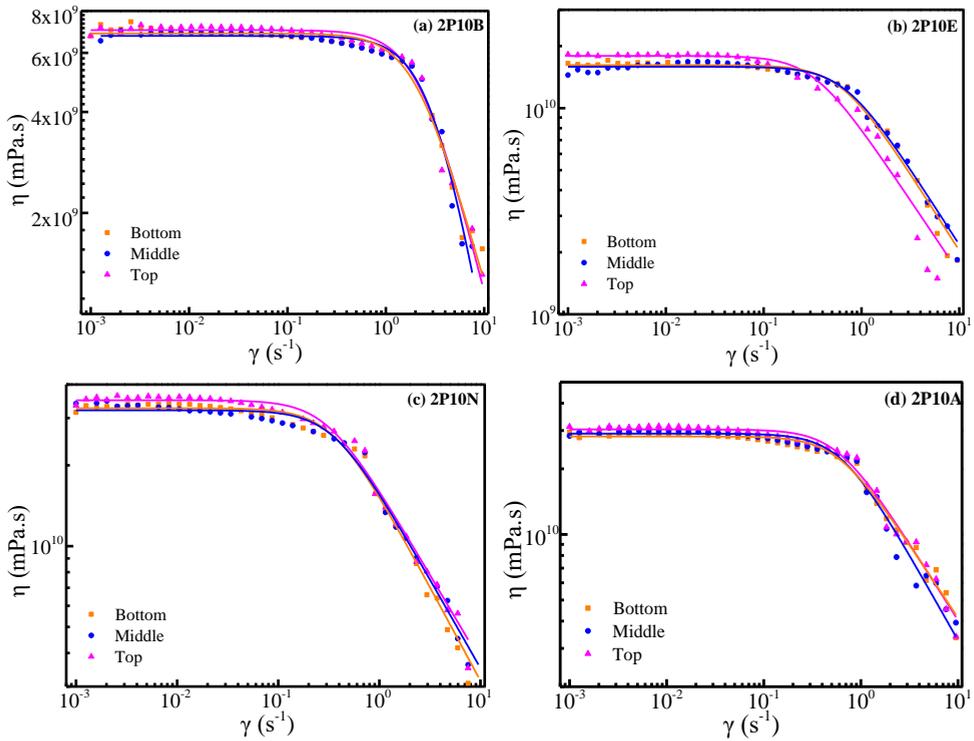
Figure 5.9 Flow curves of the bottom, middle, and top samples in rejuvenated binders after the thermal storage

According to **Eq.5.10**, the zero-shear viscosity (ZSV) of each section in rejuvenated binders can be outputted. The results are summarized in **Figure 5.10(a)-(c)**, considering the effects of rejuvenator type and the aging degree of aged bitumen in rejuvenated bitumen. Overall, the ZSV values of rejuvenated binders with various rejuvenators are significantly different. Regardless of the aging level of bitumen, the bio-oil rejuvenated binders have the lowest ZSV values, followed by the engine-oil and naphthenic-oil rejuvenated binders, while the aromatic-oil rejuvenated bitumen shows the highest ZSV values. It implies that the ranking for these four rejuvenators on the restoration level of ZSV values of aged bitumen follows BO> EO> BO> AO Furthermore, with the same rejuvenator dosage and aging degree of bitumen, aromatic-oil and naphthenic-oil rejuvenated binders exhibit stronger deformation resistance than the bio-oil and engine-oil rejuvenated bitumen.

Due to the constant rejuvenator dosage, the ZSV values of rejuvenated binders increase remarkably as the aging degree of bitumen deepens. It can be found that the thermal storage procedure leads to the difference in ZSV values between the bottom, middle, and top sections in rejuvenated bitumen. The separation index SI values based on the ZSV parameters of all rejuvenated binders are calculated using **Eq.5.9**, and these SI values are shown in **Figure 5.10(d)**. The SI values based on ZSV parameters of different rejuvenated binders also present the increasing law of AO < BO < NO < EO. It further validates that the aromatic-oil and bio-oil rejuvenators display better thermal phase stability and compatibility with aged bitumen than the naphthenic-oil and engine-oil. Moreover, the ZSV-based SI values of all rejuvenated binders are lower than those based on G*, G*/sinδ, and G*sinδ but higher than the δ-based ones. Interestingly, the role of the bitumen aging level in determining the separation potential of rejuvenators from aged bitumen can be evaluated according to the ZSV-based SI values. As the aging level of bitumen increases, the ZSV-based SI parameter of

all rejuvenated binders increases gradually. It manifests that the thermal storage stability of rejuvenated binders with the same rejuvenator type and dosage shows a worse trend as the bitumen aging becomes more severe.
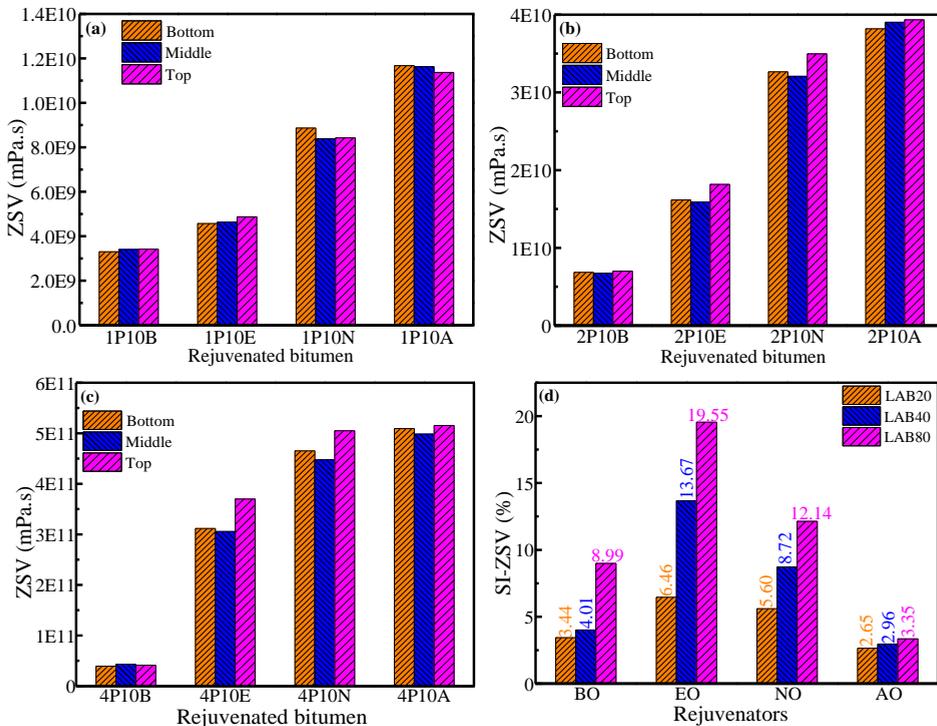
Figure 5.10 Zero-shear viscosity and SI values of rejuvenated binders at 60°C after a thermal storage process

5.5.3 Separation index based on R% and J_{nr}

The multiple stress creep and recovery (MSCR) tests are performed on all rejuvenated binders after the thermal storage process at 52°C. The crucial parameters, recovery percentage R and non-recoverable creep compliance J_{nr} are measured at the stress of 0.1kPa ($R_{0.1}$ and $J_{nr0.1}$) and 3.2kPa ($R_{3.2}$ and $J_{nr3.2}$). **Figure 5.11** displays the MSCR parameters of the bottom, middle, and top sections in various rejuvenated binders with LAB40-aged bitumen.

From **Figure 5.11**, the rejuvenated binders composed of aged bitumen and various rejuvenators exhibit different R% and J_{nr} values at both stress levels of 0.1 and 3.2kPa. When the rejuvenator dosage is the same, the bio-oil rejuvenated bitumen presents the lowest $R_{0.1}$ and $R_{3.2}$ but the highest $J_{nr0.1}$ and $J_{nr3.2}$ values. However, the aromatic-oil rejuvenated binder has the largest R% and smallest J_{nr} values. The R% and J_{nr} values of engine-oil and naphthenic-oil rejuvenated binders are in the middle. Meanwhile, the naphthenic-oil rejuvenated bitumen shows higher R% and lower J_{nr} values than the engine-oil rejuvenated binder. In general, the aging of bitumen increases the R% but reduces the J_{nr} values, indicating that the aged bitumen owns a larger elastic component ratio and stronger deformation recovery capacity than the virgin bitumen. The rejuvenators are incorporated into aged bitumen to recover all chemical and rheological properties to the virgin bitumen level. The bio-oil rejuvenator displays the most prominent effects on restoring the R% and J_{nr} values of aged bitumen, while the aromatic-oil rejuvenator shows minimal recovery capacity. It further

verifies that the rejuvenator efficiency on aged bitumen's rheological and mechanical performance strongly depends on the rejuvenator type and chemical components.
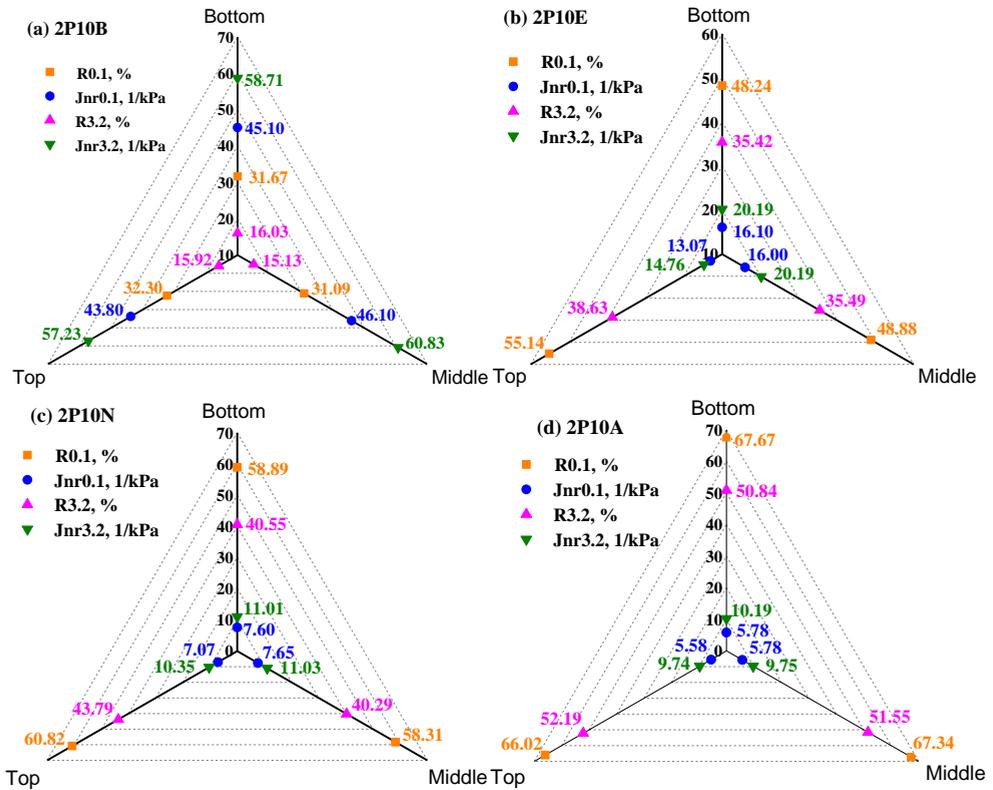
Figure 5.11 MSCR results of the bottom, middle, and top samples in rejuvenated binders after the thermal storage at 52°C

The separation index values based on MSCR parameters of the bottom, middle, and top sections in various rejuvenated binders are calculated and shown in **Figure 5.12**. The SI values depend on the MSCR parameter selected, and the R%-based SI values are lower than J_{nr}-based SI. No matter which MSCR parameter is selected, the SI values of engine-oil rejuvenated binders are the largest, followed by the naphthenic-oil and bio-oil rejuvenated bitumen, while the aromatic-oil rejuvenated binders show the lowest SI values. The same conclusion is drawn that the sequence of SI values based on all rheological indices for four rejuvenators is AO < BO < NO < EO, which agrees well with the finding of their compatibility ranking from both MD simulations and experimental results. Therefore, the thermal storage test combined with rheological characterizations can be adopted to validate the compatibility behaviors of various rejuvenators in aged binders predicted from MD simulations. However, the SI values of rejuvenated binders are sensitive to the selected parameter type, and it is necessary to find the effective rheological index for evaluating the compatibility potential of all rejuvenated binders.

On the other hand, the thermal storage stability of rejuvenated bitumen is also influenced by the aging degree of bitumen. With the long-term aging level increases, both R%-based and J_{nr}-based SI values of all rejuvenated binders show an increasing trend. For instance, the SI-$R_{3.2}$ values of BO, EO, NO, and AO rejuvenated binders increase by 3%, 12%, 6%, and 0.5%, while the SI-$J_{nr3.2}$ values enlarge by 10%, 34%, 24%,

and 7% when the aged bitumen varies from LAB20 to LAB80. Therefore, the thermal phase stability of engine-oil and naphthenic-oil rejuvenated binder are more sensitive to the aging degree variation of bitumen than the bio-oil and aromatic-oil rejuvenated bitumen.
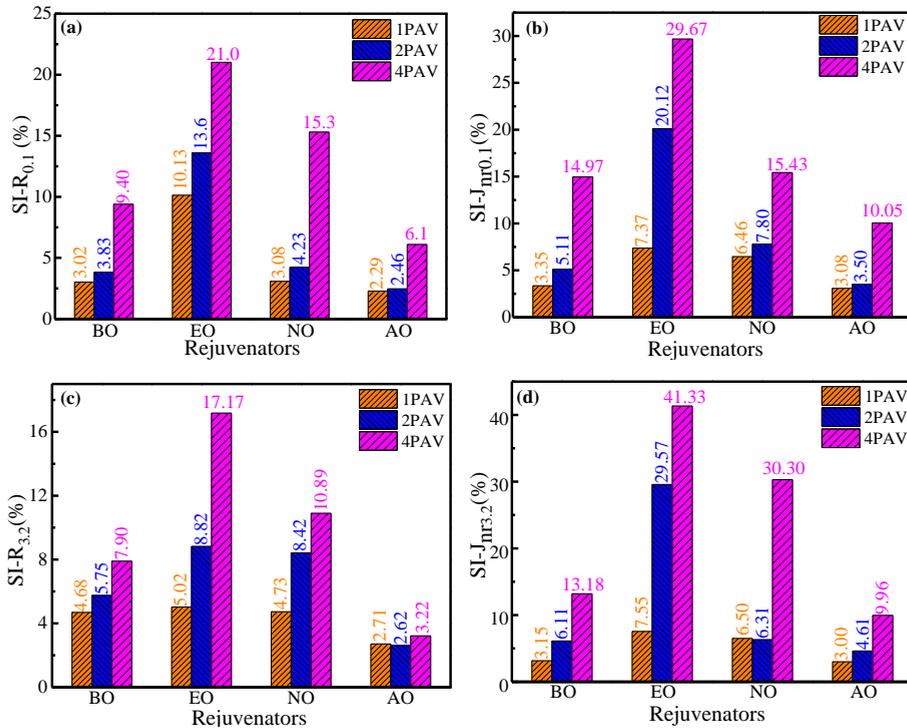
Figure 5.12 The separation index SI values of rejuvenated binders based on MSCR parameters of (a) $R_{0.1}$, (b) $J_{nr0.1}$, (c) $R_{3.2}$, and (d) $J_{nr3.2}$

5.5.4 Separation index based on chemical characteristics

Apart from the rheological indexes, the difference in chemical characteristics between different sections of rejuvenated binders is monitored through the FTIR test after thermal storage. **Figure 5.13** shows the FTIR curves of the bottom, middle, and top specimens in various rejuvenated bitumen. In different rejuvenated binders, most of the characteristic peaks are the same when the aging level of bitumen is kept constant. The peaks at 2952 and 2862 cm^{-1} are related to alkanes' C-H stretch of methylene (-CH$_2$-) and methyl (-CH$_3$). Moreover, two characteristic peaks at 1460 and 1375 cm^{-1} come from a C-H bend of the -CH$_2$- and -CH$_3$ groups. It is worth noting that these common peaks in rejuvenated bitumen are both from the bitumen and rejuvenator molecules. In addition, there is still a difference in FTIR curves between different rejuvenated binders due to the difference in molecular structures of these rejuvenators. Compared to aged bitumen, there is no specific peak observed in engine-oil and naphthenic-oil rejuvenated binders, indicating that the chemical structures of engine-oil and naphthenic-oil are similar to that of the bitumen. However, two strong peaks at 1750 and 1160 cm^{-1} are detected in FTIR curves of bio-oil rejuvenated bitumen, which is related to the C=O and C-O-C stretch in the ester group. The peaks at 1030, 1600, and 1700 cm^{-1} are found in FTIR curves of all rejuvenated binders, which refer to the aromatic structure, carbonyl, and sulfoxide functional groups in aged bitumen after the oxidative aging process. It is manifested that the absorbance strength of the 1600 cm^{-1} peak in aromatic-oil rejuvenated binders is stronger than the others, which is the result of the polyaromatic structure in aromatic-oil molecules.
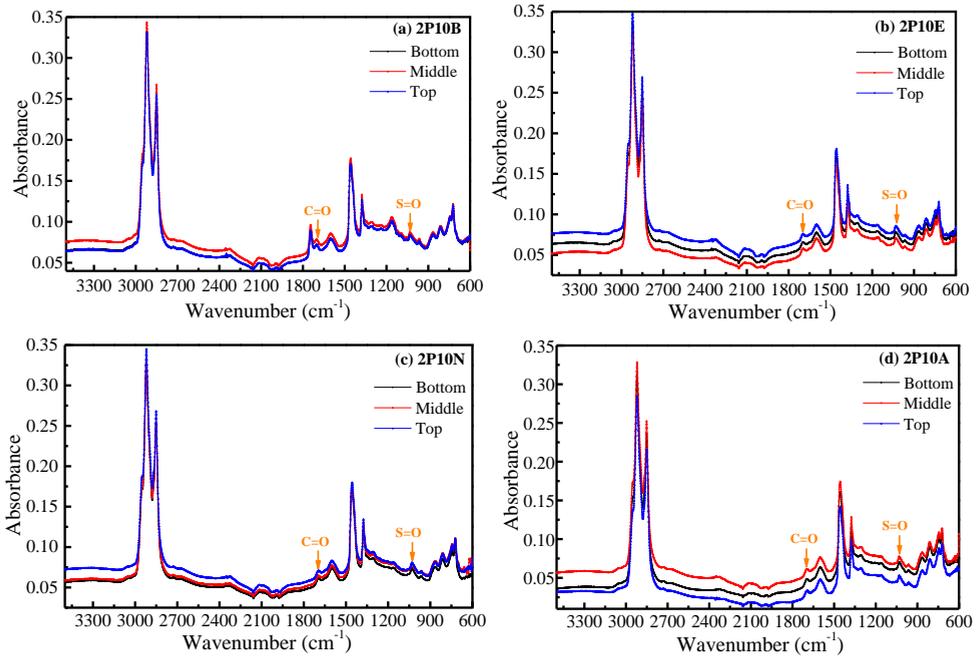
Figure 5.13 The FTIR curves of the bottom, middle, and top sections of different rejuvenated binders after the thermal storage process
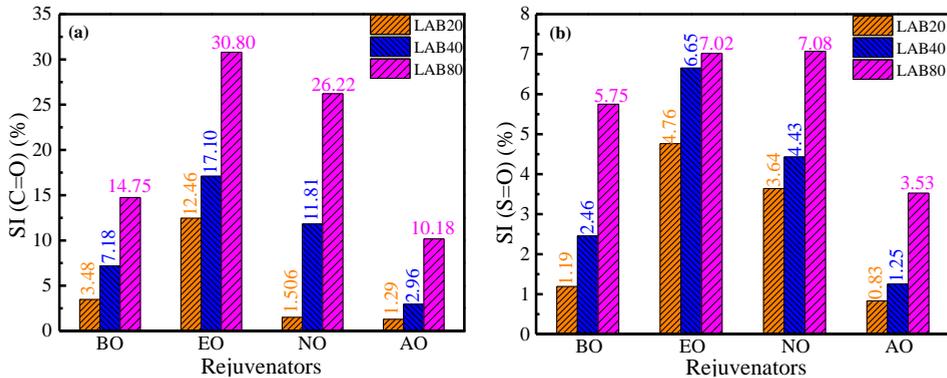
Figure 5.14 The separation index SI values of rejuvenated bitumen based on FTIR parameters of carbonyl index C=O and sulfoxide index S=O

The carbonyl index (C=O) and sulfoxide index (S=O) are the most popular chemical signals to evaluate the influence of aging and rejuvenation on the chemical characteristics of bituminous materials. In this thesis, the difference in carbonyl index and sulfoxide index between the bottom, middle, and top parts of rejuvenated binders after the thermal storage stage and the corresponding separation index values are obtained in **Eq.5.9** and displayed in **Figure 5.14**. The SI values based on the C=O index are much larger than the S=O index, indicating the former is more sensitive to the phase variation of rejuvenator molecules in aged bitumen during the thermal storage process. According to the SI parameters based on both C=O and S=O indices, the aromatic-oil rejuvenated bitumen shows the lowest SI values and the best thermal storage stability. On the

contrary, the engine-oil exhibits the largest separation potential from aged bitumen. Except for SI(C=O) in the LAB20 case, the ranking of thermal phase stability among these four rejuvenators based on chemical indices aligns with the results derived from rheological parameters. This finding further confirms the difference in phase stability and compatibility between various rejuvenators in aged binders. Likewise, the negative impacts of the aging level of aged bitumen on the thermal storage stability and compatibility potential between the rejuvenators and aged binders are observed through the SI parameters based on chemical indices.

5.6 Summary

The compatibility and thermal phase stability issues of rejuvenators in aged bitumen are complicated, especially at the molecular scale. In this chapter, different evaluation parameters in terms of thermodynamic parameters, intermolecular binding energy, molecular distribution, and molecular mobility of various rejuvenator molecules are predicted from MD simulations to assess and compare the compatibility behaviors of rejuvenators in aged binders. In addition, the experimental thermal storage tests are implemented on rejuvenated binders to detect the difference in thermal storage stability and compatibility between various rejuvenators in aged binders and to assess if these results are in line with the MD simulation results. Furthermore, the influence of bitumen aging degrees on the compatibility and thermal phase stability of various rejuvenated bitumen systems are discussed. The main conclusions from this study are listed as follows:

- The thermodynamic parameters of $\Delta\delta$, χ, and ΔG_m are efficient in estimating the compatibility potential of various rejuvenators with aged bitumen, and the compatibility of rejuvenators follows AO > BO > NO > EO.
- The intermolecular binding energy $E_{binding}$ values of rejuvenated bitumen are calculated. The aromatic-oil and engine-oil molecules display the strongest and weakest interaction strength with aged bitumen molecules.
- From experimental results (separation index SI values) from both rheological and chemical indices, the sequence of thermal storage stability of four rejuvenators follows AO > BO > NO > EO. In general, the thermal parameters ($\Delta\delta$, χ, ΔG_m, $E_{binding}$) obtained from MD simulations align closely with storage stability findings, a correlation not directly mirrored by kinetic (D) and structural indices (RC and g(r)).
- The increment in the aging degree of bitumen results in the increase of $\Delta\delta$ and SI values, as well as the intermolecular attraction level, while the molecular distribution uniformity and diffusive mobility of rejuvenator molecules are weakened. It suggests that the compatibility and thermal phase stability of rejuvenated bitumen tend to be worse when severely-aged bitumen is reused.
- High temperature adversely influences the compatibility between rejuvenators and aged binders. A high construction temperature suits aromatic-oil rejuvenated bitumen with a low diffusion coefficient but a high compatibility level. On the contrary, concerning the engine-oil rejuvenator showing large diffusive capacity but low capacity, a low blending temperature is the first choice.

5.7 References

[1] R. Tauste, F. Moreno-Navarro, M. Sol-Sanchez, M.C. Rubio-Gamez. Understanding the bitumen ageing phenomenon: A review. Construction and Building Materials. 2018, 192, 593-609.

[2] P. Apostolidis, X. Liu, C. Kasbergen, A. Scarpas. Synthesis of asphalt binder aging and the state of the art of anti-aging technologies. Transportation Research Record: Journal of the Transportation Research Board. 2017, 2633, 147-153.

[3] S. Zhang, Y. Cui, W. Wei. Low-temperature characteristics and microstructure of asphalt under complex aging conditions. Construction and Building Materials. 2021, 303, 124408.

[4] F. Li, Y. Wang, K. Zhao. The hierarchical structure of bitumen of different aging states at the molecular level and nanoscale. Fuel. 2022, 319, 123791.

[5] A. Behood. Application of rejuvenators to improve the rheological and mechanical properties of asphalt binders and mixtures: A review. Journal of Cleaner Production. 2019, 231, 171-182.

[6] X. Han, S. Mao, S. Xu, Z. Cao, S. Zeng, J. Yu. Development of novel composite rejuvenators for efficient recycling of aged SBS modified bitumen. Fuel. 2022, 318, 123715.

[7] S. Xu, X. Liu, A. Tabakovic, P. Lin, Y. Zhang, S. Nahar, B.J. Lommerts, E. Schlangen. The role of rejuvenators in embedded damage healing for asphalt pavement. Materials & Design. 2021, 202, 109564.

[8] M. Guo, A. Motamed, Y. Tan, A. Bhasin. Investigating the interaction between asphalt binder and fresh and simulated RAP aggregate. Materials & Design. 2016, 105, 25-33.

[9] A. Sreeram, Z. Leng, R. Hajj, W.L.G. Ferreira, Z. Tan, A. Bhasin. Fundamental investigation of the interaction mechanism between new and aged binders in binder blends. International Journal of Pavement Engineering. 2020, DOI: 10.1080/10298436.2020. 1799208.

[10] B. Cui, X. Gu, D. Hu, Q. Dong. A Multiphysics evaluation of the rejuvenator effects on aged asphalt using molecular dynamics simulations. Journal of Cleaner Production. 2020, 259, 120629.

[11] S. Vassaux, V. Gaudefroy, L. Boulange, L.J. Soro, A. Pevere, A. Michelet, V. Barragan-Montero, V. Mouillet. Study of remobilization phenomena at reclaimed asphalt binder/virgin binder interphases for recycled asphalt mixtures using novel microscopic methodologies. Construction and Building Materials. 2018, 165, 846-858.

[12] F. Kaseer, E. Arambula-Mercado, A.E. Martin. A method to quantify reclaimed asphalt pavement binder availability (effective RAP binder) in recycled asphalt mixes. Transportation Research Record. 2019, 2673(1), 205-216.

[13] M. Oreskovic, G.M. Pires, S. Bressi, K. Vasconcelos, D.L. Presti. Quantitative assessment of the parameters linked to the blending between reclaimed asphalt binder and recycling agent: A literature review. Construction and Building Materials. 2020, 234, 117323.

[14] C. Castorena, S. Pape, C. Mooey. Blending measurements in mixtures with reclaimed asphalt. Transportation Research Record: Journal of the Transportation Research Board. 2016, 2574, 57-63.

[15] S. Zhao, B. Bowers. B. Huang, X. Shu. Characterizing rheological properties of binder and blending efficiency of asphalt paving mixtures containing RAS through GPC. Journal of Materials in Civil Engineering. 2014, 26(5), 941-946.

[16] D.L. Presti, K. Vasconcelos, M. Oreskovic, G.M. Pires, S. Bressi. On the degree of binder activity of reclaimed asphalt and degree of blending with recycling agents. Road Materials and Pavement Design. 2020, 21(8), 2071-2090.

[17] S. Zhao, B. Huang, X. Shu, M.E. Woods. Quantitative evaluation of blending and diffusion in high RAP and RAS mixtures. Materials and Design. 2016, 89, 1161- 1170.

[18] P. Shirodkar, Y. Mehta, A. Nolan, K. Sonpal, A. Norton, C. Tomlinson, E. Dubois, P. Sullivan, R. Sauber. A study to determine the degree of partial blending of reclaimed asphalt pavement (RAP) binder for high RAP hot mix asphalt. Construction and Building Materials. 2011, 25, 150-155.

[19] M. Mohajeri, A.A.A. Molenaar, M.F.C. Van de Ven. Experimental study into the fundamentally understanding of blending between reclaimed asphalt binder and virgin bitumen using nanoindentation and nano-computed tomography. Road Materials and Pavement Design. 2014, 15(2), 372-384.

[20] A. Margaritis, G. Tofani, G. Jacobs, J. Blom, S. Tavernier, C. Vuye, W. Van den bergh. On the applicability of ATR-FTIR microscopy to evaluate the blending between neat bitumen and bituminous coating of reclaimed asphalt. Coatings. 2019, 9, 240.

[21] P. Shirodkar, Y. Mehta, A. Nolan, E. Dubois, D. Reger, L. McCarthy. Development of blending chart for different degrees of blending of RAP binder and virgin binder. Resources, Conservation and Recycling. 2013, 73, 156-161.

[22] F.Y. Rad, N.R. Sefidmazgi, H. Bahia. Application of diffusion mechanism: degree of blending between fresh and recycled asphalt pavement binder in dynamic shear rheometer. Transportation Research Record: Journal of the Transportation Research Board. 2014, 2444, 71-77.

[23] P. Kriz, D.L. Grant, B.A. Veloza, M.J. Gale, A.G. Blahey, J.H. Brownie, R.D. Shirts, S. Maccarrone. Blending and diffusion of reclaimed asphalt pavement and virgin asphalt binders. Road Materials and Pavement Design. 2014, 15(S1), 78-112.

[24] Y. Ding, B. Huang, X. Shu. Characterizing blending efficiency of plant produced asphalt paving mixtures containing high RAP. Construction and Building Materials. 2016, 126, 172-178.

[25] W.S. Mogawer, A. Booshehrian, S. Vahidi, A.J. Austerman. Evaluating the effect of rejuvenators on the degree of blending and performance of high RAP, RAS, and RAP/RAS mixtures. Road Materials and Pavement Design. 2013, 14(S2), 193-213.

[26] A. Jarray, V. Gerbaud, M. Hemati. Polymer-plasticizer compatibility during coating formulation: A multi-scale investigation. Progress in Organic Coatings. 2016, 101, 195-206.

[27] A. Takhulee, Y. Takahashi, V. Vao-soongnern. Molecular simulation and experimental studies of the miscibility of polylactic acid/polyethylene glycol blends. Journal of Polymer Research. 2017, 24, 8.

[28] X. Zhang, Y. Ning, X. Zhou, X. Xu, X. Chen. Quantifying the rejuvenation effects of soybean-oil on aged asphalt-binder using molecular dynamics simulations. Journal of Cleaner Production. 2021, 317, 128375.

[29] D. Oldham, A. Rajib, K.P.R. Dandamudi, Y. Liu, S. Deng, E.H. Fini. Transesterification of waste cooking oil to produce a sustainable rejuvenator for aged asphalt. Resources, Conservation & Recycling. 2021, 168, 105297.

[30] H. Wang, X. Liu, S. Erkens, A. Skarpas. Experimental characterization of storage stability of crumb rubber modified bitumen with warm-mix additives. Construction and Building Materials. 2020, 249, 118840.

[31] S. Ren, X. Liu, M. Li, W. Fan, J. Xu, S. Erkens. Experimental characterization of viscoelastic behaviors, microstructure and thermal stability of CR/SBS modified asphalt with TOR. Construction and Building Materials. 2020, 261, 120524.

[32] S. Ren, M. Liang, W. Fan, Y. Zhang, C. Qian, Y. He, J. Shi. Investigating the effects of SBR on the properties of gilsonite modified asphalt. Construction and Building Materials. 2018, 190, 1103-1116.

[33] AASHTO M320. Standard specification for performance-graded asphalt binder.

[34] AASHTO TP70. Standard method of test for multiple stress creep recovery (MSCR) test of asphalt binder using a Dynamic Shear Rheometer (DSR), American Association of State Highway and Transportation Officials, Washington (DC), 2009.

[35] A. Sceeram. Z. Leng. R. Hajj, A. Bhasin. Characterization of compatibility between aged and unaged binders in bituminous mixtures through an extended HSP model of solubility. Fuel. 2019, 254, 115578.

[36] Y. Luo, R. Wang, W. Wang, L. Zhang, S. Wu. Molecular dynamics simulation insight into two-component solubility parameters of graphene and thermodynamic compatibility of graphene and styrene butadiene rubber. The Journal of Physical Chemistry C. 2017, 121, 10163-10173.

[37] H.F. Haghshenas, R. Rea, G. Reinke, M. Zaumanis, E.H. Fini. Relationship between colloidal index and chemo-rheological properties of asphalt binders modified by various recycling agents. Construction and Building Materials. 2022, 318, 126161.

[38] DD Li, M.L. Greenfield. Chemical compositions of improved model asphalt systems for molecular simulations. Fuel. 2014, 115, 347-356.

[39] M. Elkashef, D. Jones, L. Jiao, R.C. Williams, J. Harvey. Using thermal analytical techniques to study rejuvenators and rejuvenated reclaimed asphalt pavement binders. Energy & Fuels. 2019, 33, 2651-2658.

[40] P. Wang, Z. Dong, Y. Tan, Z. Liu. Investigating the interactions of the saturate, aromatic, resin, and asphaltene four fractions in asphalt binders by molecular simulations. Energy & Fuels. 2015, 29, 112-121.

[41] J. Zhang, X. Gong, G. Wang. Compatibility and mechanical properties of BAMO-AMMO/DIANP composites: A molecular dynamics simulation. Computational Materials Science. 2015, 102, 1-6.

[42] G. Li, Y. Tan. The construction and application of asphalt molecular model based on the quantum chemistry calculation. Fuel. 2022, 308, 122037.

[43] H.F. Haghshenas, R. Rea, G. Reinke, D.F. Haghshenas. Chemical characterization of recycling agents. Journal of Materials in Civil Engineering. 2020, 32(5), 0602005.

[44] H. Ding, H. Wang, X. Qu, A. Varveri, J. Gao, Z. You. Towards an understanding of diffusion mechanism of bio-rejuvenators in aged asphalt binder through molecular dynamics simulation. Journal of Cleaner Production. 2021, 299, 126927.

[45] G. Xu, H. Wang. Molecular dynamics study of oxidative aging effect on asphalt binder properties. Fuel. 2017, 188, 1-10.

[46] D. Hu, X. Gu, B. Cui, J. Pei, Q. Zhang. Modeling the oxidative aging kinetics and pathways of asphalt: A ReaxFF molecular dynamics study. Energy & Fuels. 2020, 34(3), 3601-3613.

[47] M. Su, J. Zhou, J. Lu, W. Chen, H. Zhang. Using molecular dynamics and experiments to investigate the morphology and micro-structure of SBS modified asphalt binder. Materials Today Communications. 2022, 30, 103082.

[48] C. Yu, K. Hu, Q. Yang, D. Wang, W. Zhang, G. Chen, C. Kapyelata. Analysis of the storage stability property of carbon nanotube/recycled polyethylene-modified asphalt using molecular dynamics simulations. Polymers. 2021, 13, 1658.

[49] M. Li, Z. Min, Q. Wang, W. Huang, Z. Shi. Effect of epoxy resin content and conversion rate on the compatibility and component distribution of epoxy asphalt: A MD simulation study. Construction and Building Materials. 2022, 319, 126050.

[50] X. Yang, J. Mills-Beale, Z. You. Chemical characterization and oxidative aging of bio-asphalt and its compatibility with petroleum asphalt. Journal of Cleaner Production. 2017, 142, 1837-1847.

6

Interfacial diffusion behaviors of rejuvenators in aged bitumen

A rapid diffusion rate of rejuvenators in aged bitumen is expected to speed up the generation of the intended homogenously rejuvenated bitumen layer with improved mechanical performance on the aggregate surface. However, the quantitative evaluation method of the diffusion capacity of rejuvenators in aged bitumen is challenging and complicated. This is because the diffusion behaviors of rejuvenators in aged bitumen are affected by the rejuvenator type, aging level of bitumen, diffusion temperature, and time. This chapter aims to predict the diffusion coefficient parameters of four types of rejuvenators in aged bitumen with different aging levels using molecular dynamics (MD) simulations and explain the difference in diffusive capacity of various rejuvenator-aged bitumen systems at an atomic scale. Experimental diffusion tests are conducted to verify the MD simulation outputs.

6.1 Introduction

In an ideal rejuvenation procedure, the rejuvenator first attaches to the surface of aged bitumen, covering the RAP aggregates, then gradually diffuses into the aged bitumen layer until reaching a concentration equilibrium point and forming a homogenous rejuvenated bitumen [1]. However, previous studies mentioned that partial blending between the rejuvenator and aged bitumen was observed in most RAP recycling cases [2, 3]. This is an issue, because the blending level significantly affects the rejuvenation efficiency, and the heterogeneous distribution of rejuvenators in aged bitumen could result in a high potential of cracking and rutting distresses [4]. Therefore, it is crucial to establish a high blending level between rejuvenators and aged bitumen in a short period. This can be a challenge because the blending degree is influenced by many material and environmental factors, such as the rejuvenator type, aging level of bitumen, and mixing temperature and time [5, 6].

The blending degree of rejuvenated bitumen is strongly associated with the diffusive capacity of rejuvenators in aged bitumen, which is generally evaluated by a diffusion coefficient parameter based on Fick's diffusion law [7]. Different experiments were conducted to measure the diffusion coefficient value of the rejuvenator in aged bitumen. Karlsson and Isacsson [8] employed Fourier transform infrared spectroscopy by attenuated total reflectance (FTIR-ATR) to detect the diffusion rate of the rejuvenator considering the influence of temperature, bitumen film thickness, bitumen type, and components. The findings demonstrated that the FTIR-ATR is an effective measurement for determining the diffusion coefficient values of rejuvenators in an aged bitumen matrix. The diffusion characteristics of rejuvenators observed agreed well with Fick's Law, and the Arrhenius formula was appropriate to describe the temperature effect on the diffusion rate of rejuvenators in various aged binders when the temperature was above 30°C. Giacomo et al. [9] performed FTIR and dynamic shear rheometer (DSR) tests to monitor the diffusivity of rejuvenators in aged bitumen at 25°C and 140°C after a series of diffusion tests in tubes. The results revealed that the diffusion capacity strongly depended on the rejuvenator type and temperature. Fang et al. [10] also adopted a tube test to examine the diffusion coefficient (D) values of rejuvenators with variable temperatures and permeation times based on the viscosity variations during a diffusion process. It was reported that the increment in temperature and permeation time enlarged the permeation level of rejuvenators in aged bitumen. Moreover, the D values presented a decreasing trend with the increase in permeation time, which might be associated with reducing the permeation channel of rejuvenator molecules in aged bitumen. Ma et al. [11] performed a solvent extraction method to investigate the rejuvenator diffusion and distribution in various aged bitumen layers together with the penetration and DSR tests. The diffusive rate of rejuvenators in aged bitumen was remarkably attributed to the viscosity, components, and thermal stability. In addition, it was difficult for a rejuvenator to diffuse into the aged bitumen entirely within a short blending time.

Nowadays, the molecular dynamics (MD) simulation method has been successfully employed in the diffusion measurement of rejuvenators in aged bitumen. Xu et al. [12] investigated the molecular diffusive behaviors of rejuvenators in neat, short-term, and long-term aged bitumen with an MD simulation. They found that micro-voids between bitumen molecules and increased temperature benefited the fusion level of rejuvenator molecules. Meanwhile, Xu and Wang [13] also performed MD simulation to explore the diffusion and interaction mechanisms of rejuvenator molecules in virgin and aged bitumen using the Optimised Potentials for Liquid Simulation (OPLS) force field. The outputted diffusion coefficient values revealed that the rejuvenator diffused faster into virgin bitumen than aged bitumen layer and improved the blending level between new and aged bitumen, contrary to a previous conclusion [12]. Based on MD simulation outputs, Sun and Wang [14] found that the diffusion capacity of rejuvenator molecules in the aged bitumen model distinctly relied on the rejuvenator's molecular structure. The polar aromatic exhibited the worst diffusive capacity, while naphthene aromatic showed a faster diffusion rate than saturate-based rejuvenators. The positive effect of bio-rejuvenators on accelerating the fusion process between virgin and aged bitumen was also reported in an MD simulation research [15].

6.2 Objectives and outlines

This chapter predicts and compares the diffusion behavior of commonly-used rejuvenators in aged binders at variable aging levels at different temperatures. **Figure 6.1** illustrates the primary research protocol. First, the molecular models of aged bitumen and four different rejuvenators (bio-oil, engine-oil, naphthenic-oil, and aromatic-oil) are built based on their chemical characteristics. Afterward, four rejuvenator-aged bitumen bi-layer diffusion molecular models are established for MD simulations at different temperatures of 25, 60, 120, 140, 160, 180, and 200°C. Next, the molecular-scale diffusion phenomena of various rejuvenators in aged bitumen are observed and compared. Finally, analysing the mass density profile of rejuvenators in aged bitumen layers, the diffusion coefficient (D) values of four rejuvenators at different temperatures are predicted. In addition, the activation energy (Ea) and pre-exponential factor (A) parameters are derived based on these predicted D parameters.
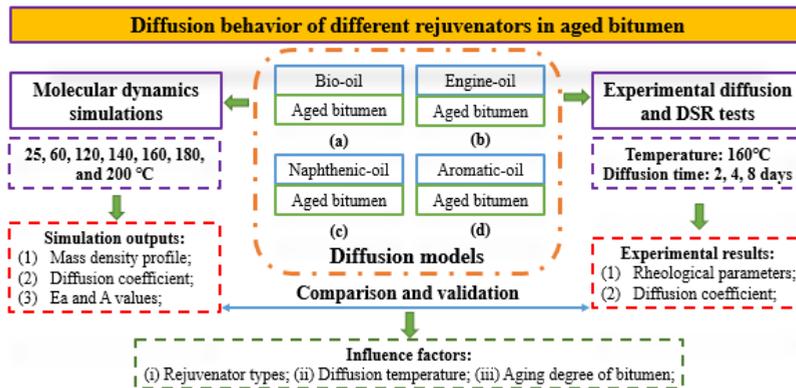
Figure 6.1 Research scheme and structure

In parallel, the diffusion tube tests with these four rejuvenators in aged bitumen (described in following **section 6.3.2**) are conducted at 160°C. The concentration distributions of rejuvenators are determined using the standard curves between the rheological parameters and rejuvenator concentration from the dynamic shear rheometer (DSR) tests. The experimental results of D, Ea, and A are compared with MD simulation outputs to estimate the application potential of the MD simulation method in predicting the diffusive capacity of various rejuvenators in an aged binder. Finally, the influence of rejuvenator type, diffusion temperature, and aging degree of bitumen on the diffusion behaviors of rejuvenators in aged binders are investigated.

6.3 Diffusion tests

6.3.1 Preparation of rejuvenated bitumen

In this chapter, calibration curves for the rheological indices and rejuvenator dosage were first developed to allow the determination of the concentration distribution of rejuvenators in the different aged bitumen layers in the tube test. From this, the corresponding diffusion coefficient values are then determined [9, 10]. To this end, rejuvenated bitumen was prepared homogeneously for different rejuvenator types and dosages. The LAB40-aged bitumen from **Chapter 3** was heated at 140°C for 10min to a flow state and blended with a rejuvenator manually for 15 minutes to prepare the homogenous rejuvenated binders. The rejuvenator dosages were 2.5, 5.0, 7.5, 10.0, 12.5, and 15.0 wt%. The types used are the same as in the rest of this thesis: bio-oil, engine-oil, naphthenic-oil, and aromatic-oil, and the rejuvenated binders are designated as BORB, EORB, NORB, and AORB, respectively. The prepared rejuvenated binders were preserved at low temperatures (5°C) for rheology tests.

6.3.2 Experimental diffusion assessment

The experimental values for four types of rejuvenators were determined using the tube test [9, 10], shown in **Figure 6.2**. About 40g of aged bitumen was poured into a cylindrical aluminium foil tube with a diameter of 13mm and a height of 100mm. When the aged bitumen sample was cooled to room temperature, 4g of rejuvenator (10 wt% of aged bitumen) was added on top of the aged bitumen. Afterward, the nozzle was sealed with foil tape to avoid the evaporation and oxidation of the rejuvenator during the test. Twelve samples (three replicates were performed for every rejuvenator-aged bitumen blend, each tested under varying diffusion durations) were prepared and vertically placed in an oven at 160°C [8, 10, 11], with the rejuvenator at the top. Each rejuvenator-aged bitumen case was represented by three parallel samples, each subjected to diffusion times of 2, 4, and 8 days, respectively.

At those times, the sample was removed from the oven to a freezer at -20°C for 24 hours to discontinue the diffusion process and solidify the diffusion state for further analyses. After removing it from the fridge, the aluminium foil tube was ripped off manually. As illustrated in **Figure 6.2**, the diffused sample was marked and cut into four layers with a height of 20mm. It should be mentioned that the tube bottom was set as the origin point. It was challenging to distinguish the rejuvenator phase from bitumen at an interface zone because the interfacial diffusion was bidirectional. The bottom aged bitumen layer, where the rejuvenator content was the lowest was still hard at room temperature. Each of the three layers was placed on an aluminium plate, heated at 160°C, and homogenized carefully by hand (10 min) for rejuvenator concentration determination using rheological calibration done before.
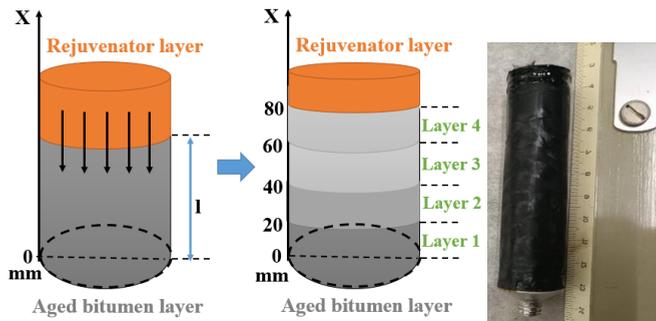
Figure 6.2 The schematic graph of the diffusion process of rejuvenator in aged bitumen

In line with the previous study [9], Fick's Second Law describes the relationship between the rejuvenator concentration with diffusion time and distance, as shown in **Eq.6.1**. It is assumed that the surface concentration C_1 is constant with time. The initial concentration C_0 of the rejuvenator in the sample equals zero.

$$\frac{C(t) - C_0}{C_1 - C_0} = 1 - \frac{4}{\pi} \sum_{n=0}^{\infty} \left[\frac{(-1)^n}{2n+1} \exp\left\{ \frac{-D(2n+1)^2 \pi^2 t}{4l^2} \right\} \cos\frac{(2n+1)\pi x}{2l} \right] \tag{6.1}$$

where C(t) refers to the rejuvenator concentration at diffusion time t, wt%; C_0 and C_1 are the initial and final concentrations of the rejuvenator, which are assumed to be 0 and 100 wt%; D represents the diffusion coefficient, m^2/s; t (s) and l (m) shows the diffusion time and the tube length filled with bitumen; the x denotes the abscissa where the rejuvenator concentration C(t) is calculated. Moreover, n is a positive integer increasing from 0 to ∞.

When an assumption is adopted that the C_0 is equal to zero, as stated above, **Eq.6.1** can be simplified as follows:

$$C(t,x) = C_1 - \frac{4}{\pi}C_1 \sum_{n=0}^{\infty}\left[\frac{(-1)^n}{2n+1}\exp\left\{\frac{-D(2n+1)^2\pi^2t}{4l^2}\right\}\cos\frac{(2n+1)\pi x}{2l}\right] \qquad (6.2)$$

From **Eq.6.2**, it is found that the rejuvenator concentration C(t) varies as a function of diffusion time (t) and position (x). Thus, the diffusion coefficient D values can be derived by fitting these correlation curves.

6.3.3. Dynamic shear rheometer (DSR) test

The rheological properties of each diffusion layer were measured through a DSR device with a plate diameter of 8mm and thickness of 2mm [16]. All rejuvenated bitumen and diffused samples were subjected to a frequency sweep test and linear amplitude sweep (LAS) test. The frequency sweep tests were conducted at 20°C with the frequency rising from 0.1 rad/s to 100 rad/s. Moreover, the G-R parameter was measured at 15 °C and 0.005 rad/s. Besides, all LAS tests were carried out at 20°C to obtain the life cycles at 2.5% and 5.0% strain levels according to AASHTO TP101 [17].

6.4 Molecular dynamics simulations on interfacial diffusion

6.4.1 Confined molecular models

The confined molecular models of aged bitumen and rejuvenators are established and equilibrated like the MD simulations on bulk systems described in **Chapters 3** and **4**. The only difference between the confined and bulk models is the boundary condition, and the periodic boundary condition is adopted in bulk models. For confined models, a periodic boundary condition is applied in both the x and y directions, while the non-periodic boundary condition is selected in the z-direction.

The confined molecular models of aged bitumen and rejuvenator after the isothermal-isobaric (NPT) and canonical (NVT) equilibrium MD simulations are shown in **Figure 6.3**. In the meantime, the bi-layer rejuvenator-aged bitumen diffusion model is established [13, 14]. A vacuum layer of 5 Å is added on the top of the diffusion model to block up the molecular interaction between adjacent simulation cells at the z-direction, as illustrated in **Figure 6.3**, with a dimension of 40 Å × 40 Å × 107 Å [27, 28]. It should be noted that all MD simulations on bulk, confined, and bi-layer molecular models are performed with a Polymer Consistent Force Field (PCFF), which has been widely employed and validated in polymers, organic, and bituminous materials [18].
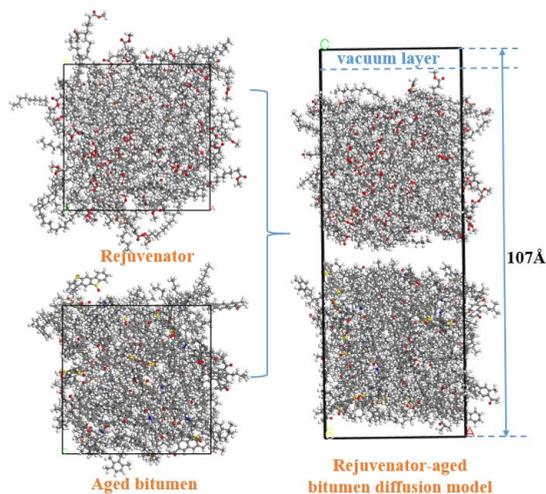
Figure 6.3 The rejuvenator-aged bitumen interfacial diffusion molecular model

6.4.2 Molecular models of rejuvenator-aged bitumen diffusion systems

All rejuvenator-aged bitumen diffusion models in this chapter are built using Materials Studio [10, 13]. **Figure 6.4** displays the BO-aged bitumen, EO-aged bitumen, NO-aged bitumen, and AO-aged bitumen interfacial models. The MD simulations on all diffusion models are completed in a Large-scale Atomic/Molecular Massively Parallel Simulator (LAMMPS) with an isothermal-isochoric (NVT) ensemble and Nose thermostat, introduced in **Chapter 3**. Meanwhile, the time step and simulation duration are 1 fs and 10 ns, which are sufficient to observe the diffusion behavior of rejuvenators towards aged bitumen. The atomic trajectories of the rejuvenator molecules in diffusion models are viewed through a visualization tool OVITO.
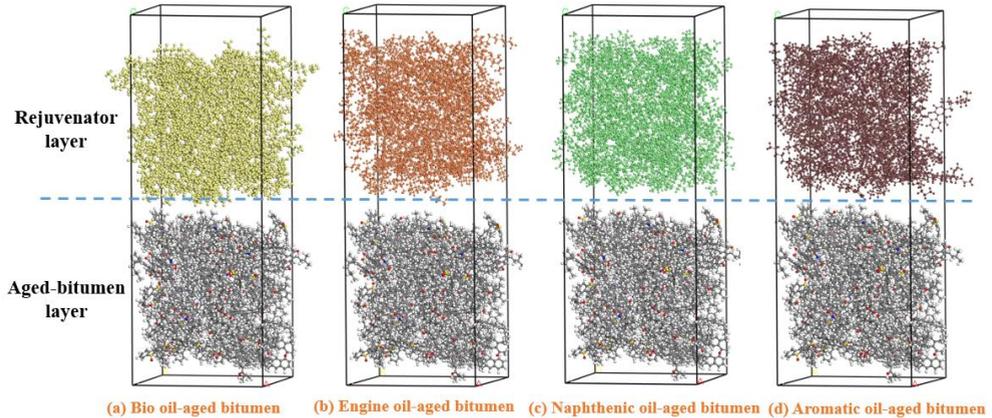
Figure 6.4 Different rejuvenator-aged bitumen diffusion molecular models
(Yellow: Bio-oil; Orange: Engine-oil; Green: Naphthenic-oil; Brown: Aromatic-oil)

6.4.3 Basic theory for calculating the diffusion coefficient parameter

The diffusion behavior is a material transfer process from a high-concentration region to another low-concentration phase until an equilibrium state is attached, characterized by a concentration gradient index [19]. Fick's Second Law generally describes the inter-diffusion behavior and quantitatively derives the diffusion rate between different material phases, assuming no volume change during a diffusion process.

$$\frac{\partial c}{\partial t} = \frac{\partial}{\partial z}\left(D(c) \cdot \frac{\partial c}{\partial z}\right) \tag{6.3}$$

where c refers to a mass concentration in g/cm^3; t is the diffusion time in ns; z represents the position of a thin layer in Å; and D(c) is the diffusion coefficient in m^2/s.

If we consider $D(c)=D_0$ as a constant, **Eq.6.3** offers a straightforward solution. In this thesis, we embraced this assumption and utilized **Eq.6.4** to determine the inter-diffusion coefficient of the rejuvenator into aged bitumen.

$$c(z,t) = c_0\left(1 - \mathrm{erf}\left(\frac{z}{2\sqrt{D_0 t}}\right)\right) \tag{6.4}$$

where c (z, t) is the concentration distribution of diffusive substances (rejuvenator molecules); c_0 represents the equilibrium rejuvenator concentration; erf is an error function, and D_0 is the constant inter-diffusion coefficient, m^2/s. Moreover, t and z show the diffusion time (ns) and a position point (Å).

6.5 MD simulation predictions and discussion

6.5.1 Molecular configurations of interfacial diffusion models

The molecular configurations at 160°C of different rejuvenator-aged bitumen diffusion models at the diffusion times of 0, 2, 4, 8, and 10ns are illustrated in **Figure 6.5**. It should be mentioned that bitumen molecules are hidden to monitor the diffusion trajectories of rejuvenator molecules. As the diffusion time is longer, all rejuvenator molecules gradually diffuse into the aged bitumen layer. When the diffusion time is at 10ns, part of the rejuvenator molecules could reach the bottom of the aged bitumen layer. However, the diffusion time of 10ns is still insufficient to form a homogenous rejuvenated bitumen, which agrees well with the previous finding that the partial blending between the rejuvenator and aged bitumen was observed during the recycling of asphalt mixtures [6]. In addition, the blank space in the rejuvenator layer refers to the bitumen molecules, indicating that the interfacial diffusion phenomenon between the rejuvenator and aged bitumen molecules is mutual, which was also observed by microscopic morphologies [2, 3].

Interestingly, no aromatic-oil molecule reached the bottom side of the aged bitumen layer even though the diffusion time was 10ns. It implies that the diffusion rate of aromatic-oil molecules is the lowest among these four rejuvenators, which is related to its high molecular weight, polarity, and the resulting intermolecular interaction with aged bitumen molecules [20]. Moreover, the amount of aged bitumen molecules in the aromatic-oil layer is the least and a longer blending time is required to obtain a homogeneous aromatic-oil rejuvenated bitumen. On the contrary, the bio-oil molecules can reach the bottom surface of the aged bitumen layer at 4ns, and the corresponding molecular amount at 10ns is the largest. Therefore, it suggests that the bio-oil molecules exhibit the highest diffusion capacity in aged bitumen. It may be associated with its lowest molecular weight and strongest molecular mobility characteristics [21], which also affects the compatibility behaviors shown in **Chapter 5** (AO > BO > NO > EO). In addition, the diffusion levels of engine-oil and naphthenic-oil molecules are in the middle, while the former displays a greater diffusion rate than the latter. In summary, when the diffusion time and temperature are fixed, the magnitude of the molecular concentration for four rejuvenators in aged bitumen is BO > EO > NO > AO.

(1-a) 2PB-160°C-0ns   (1-b) 2PB-160°C-2ns   (1-c) 2PB-160°C-4ns   (1-d) 2PB-160°C-6ns   (1-e) 2PB-160°C-8ns   (1-f) 2PB-160°C-10ns

(2-a) 2PE-160°C-0ns   (2-b) 2PE-160°C-2ns   (2-c) 2PE-160°C-4ns   (2-d) 2PE-160°C-6ns   (2-e) 2PE-160°C-8ns   (1-f) 2PE-160°C-10ns

(3-a) 2PN-160°C-0ns   (3-b) 2PN-160°C-2ns   (3-c) 2PN-160°C-4ns   (3-d) 2PN-160°C-4ns   (3-e) 2PN-160°C-8ns   (3-f) 2PN-160°C-10ns

(4-a) 2PN-160°C-0ns   (4-b) 2PN-160°C-2ns   (4-c) 2PN-160°C-4ns   (4-d) 2PN-160°C-6ns   (4-e) 2PN-160°C-8ns   (4-f) 2PN-160°C-10ns
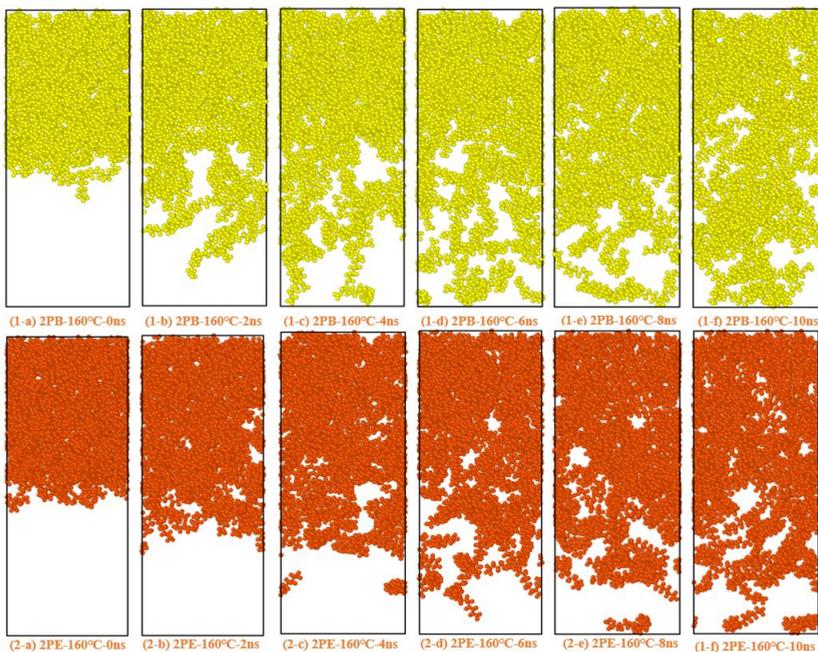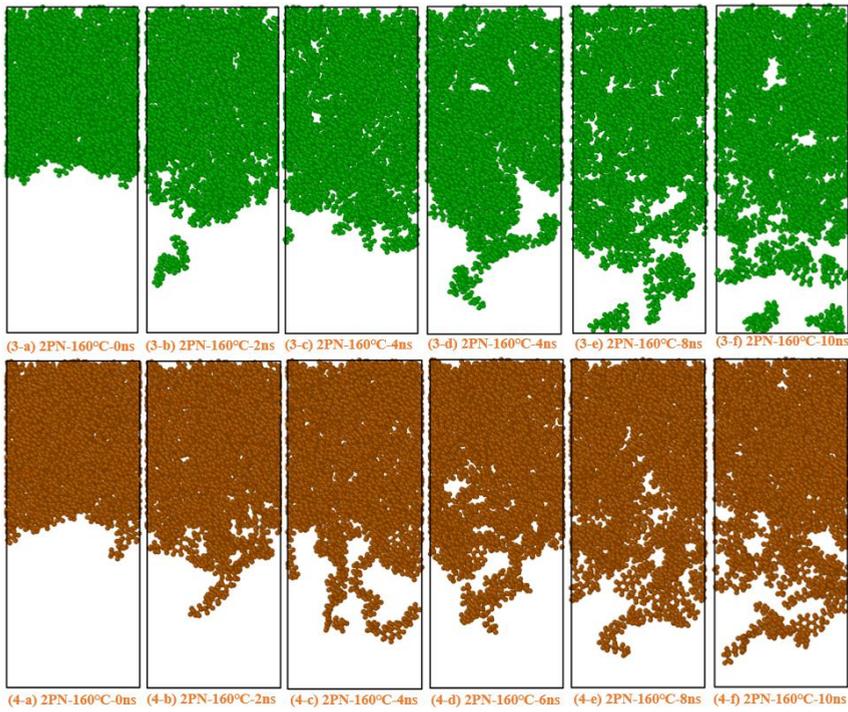
Figure 6.5 The snapshots of rejuvenator-aged bitumen models after MD diffusion simulations (Bio-oil: Yellow; Engine-oil: Red; Naphthenic-oil: Green; Aromatic-oil: Brown)

To predict and explore the temperature influence on diffusion behaviors of rejuvenators in aged bitumen at an atomic scale, the molecular configurations of four rejuvenators at 10 ns and different diffusion temperatures of 25, 60, 120, 160, and 200°C. The representative results are illustrated in **Figure 6.6**. The rejuvenator and aged bitumen molecules are displayed herein to observe the intermolecular diffusion and distribution level. All rejuvenator molecules show a deeper penetrating trend when the temperature increases, denoting that a high temperature promotes the diffusion rate of rejuvenator molecules. At the same time, more bitumen molecules penetrate the rejuvenator layer at high temperatures. However, at both 25 and 60°C, the amount of rejuvenator molecules in the aged bitumen layer is minimal, especially for the engine-oil, naphthenic-oil, and aromatic-oil rejuvenators.

On the other hand, the diffusion behavior of rejuvenator molecules in aged bitumen strongly depends on the rejuvenator type and component. At all simulation temperatures, the penetrating levels of bio-oil and aromatic-oil molecules are the largest and smallest, respectively. Compared to naphthenic-oil, more bitumen and engine-oil molecules are blended. It means that the penetrating capacity of engine-oil molecules is more substantial than naphthenic-oil. The molecular distribution of rejuvenators in aged bitumen varies remarkably after an MD diffusion simulation. Compared to other rejuvenators, bio-oil molecules are dispersed more homogeneously in aged bitumen, especially at 200°C. However, it should be mentioned that the molecular-scale distribution of rejuvenators in aged bitumen is still heterogeneous, even though the rejuvenator molecules are entirely blended in aged bitumen. At the same time, the agglomeration phenomenon of rejuvenator molecules is still apparent. In addition, the partial diffusion characteristic of engine-oil, naphthenic-oil, and aromatic-oil molecules in aged bitumen are observed at all temperatures. It indicates that the diffusion time of 10ns is insufficient for these rejuvenator molecules to diffuse in the aged bitumen layer entirely due to a low diffusion rate.
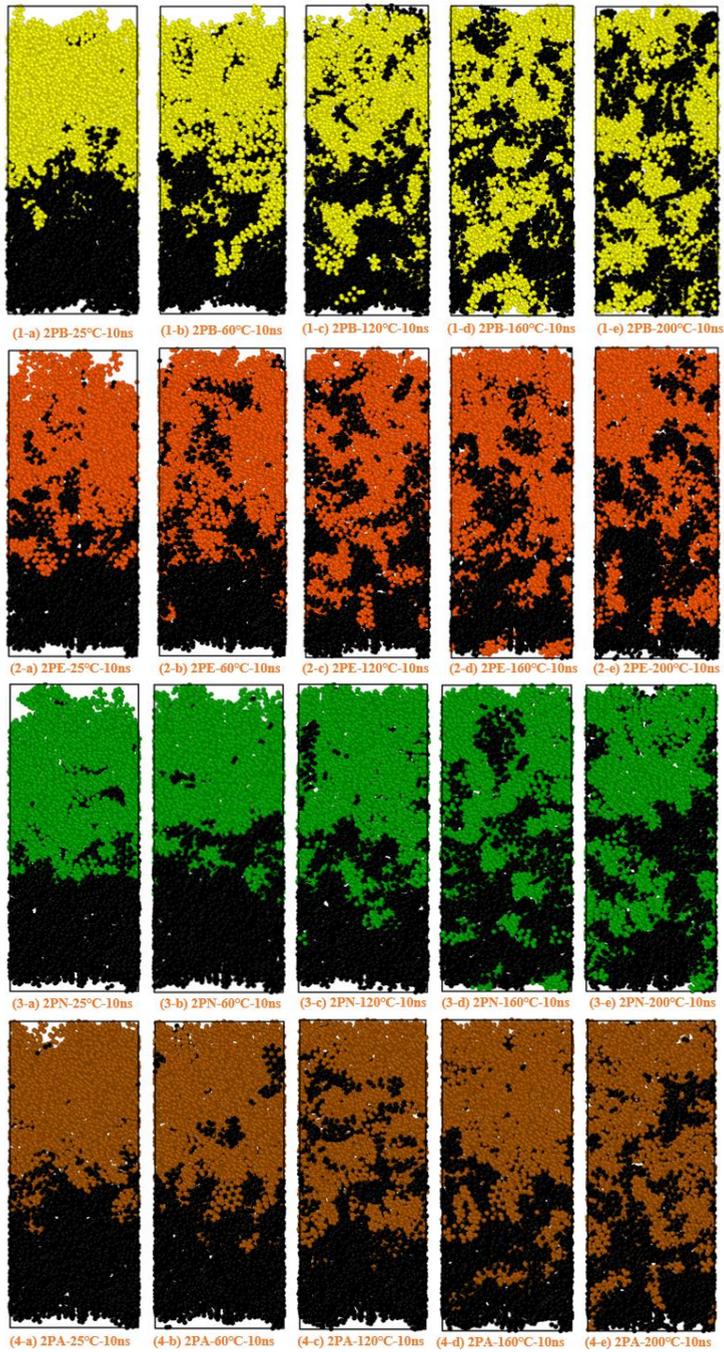
Figure 6.6 The snapshots of rejuvenator-aged bitumen molecular models at different temperatures (Bio-oil: Yellow; Engine-oil: Red; Naphthenic-oil: Green; Aromatic-oil: Brown; Bitumen: Black)

6.5.2 Mass density distribution of rejuvenators

The mass density distribution of rejuvenator molecules in aged bitumen is monitored as a function of the diffusion time. The mass density curves of different rejuvenators at 160°C with variable diffusion times of 2, 4, 6, 8, and 10 ns are extracted and drawn in **Figure 6.7**. For simplicity, these corresponding results at different temperatures of 25, 60, 120, 140, 180, and 200°C are not displayed herein. The mass density values of rejuvenator molecules in a rejuvenator phase are much higher than those in the aged bitumen phase, regardless of the rejuvenator type and diffusion duration. It implies that the diffusive equilibrium points of these rejuvenator-aged bitumen models have not been reached yet because of insufficient simulation time. Moreover, the mass density of rejuvenator molecules in the rejuvenator layer is not constant and decreases as the distance to the interface reduces. It reveals that the interfacial diffusion behavior of a rejuvenator-aged bitumen layer is bidirectional, and several bitumen molecules also diffuse into the rejuvenator layer. In the aged bitumen layer, the mass density of rejuvenator molecules shows a decreasing trend as the distance from the interface increases. It means that the distribution of diffused rejuvenator molecules in aged bitumen is in a stepped form, which can be observed from the snapshots of molecular diffusion models in **Figures 6.5** and **6.6**.

In addition, the mass density of the rejuvenator molecules in the aged bitumen phase gradually increases with increasing diffusion time, while the mass density in the rejuvenator phase decreases. It implies that the increment in diffusion time enlarges the blending level between the rejuvenator and aged bitumen molecules, which agrees well with the reported experimental results in previous studies [22, 23]. When the aging degree of bitumen and diffusion time are both fixed, the mass curves of rejuvenator molecules in the aged bitumen matrix depend on the rejuvenator type. It is associated with the difference in diffusion capacity and density between these four rejuvenators.
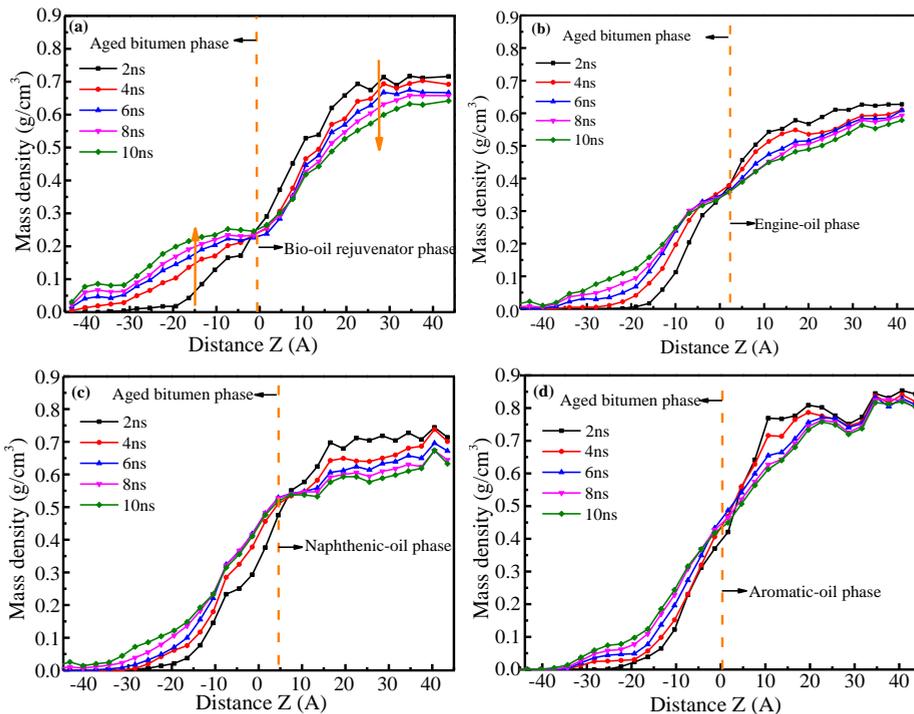
Figure 6.7 Mass density profile of rejuvenators in bi-layer systems
(a) Bio-oil; (b) Engine-oil; (c) Naphthenic-oil; (d) Aromatic-oil

6.5.3 Correlation curves of mass density versus diffusion distance and time

The diffusion coefficient parameters of four rejuvenators in aged bitumen at different temperatures are calculated according to Fick's Second Law (see **Eq.6.4**), and the correlation curves between mass density and $(z/t^{0.5})$ parameter are summarized in **Figure 6.8**. When the diffusion time and depth are the same, the mass density values of rejuvenator molecules in the aged bitumen phase significantly enlarge as the temperature rises, which decreases correspondingly in the rejuvenator layer due to the reduction in rejuvenator molecular amount and increase in bitumen molecules. It is consistent with the previous finding that a high temperature accelerated the blending degree between rejuvenators and aged bitumen in reclaimed asphalt pavement (RAP) materials [24].

The correlation curves between the mass density C of rejuvenator molecules and the $(z*t^{-0.5})$ parameter are fitted using **Eq.6.4**, and these fitting curves are also displayed in **Figure 6.8**. Meanwhile, all related fitting parameters are listed in **Table 6.1**. According to R^2 values higher than 0.97, the fitting efficiency of Fick's Second Law on diffusion characteristics of all rejuvenators is satisfactory. The parameter C_0 represents the equilibrium mass density of pure rejuvenator phase. The C_0 values of all reduce with increasing temperature, which is attributed to the decreased density of rejuvenators at high temperatures. When the temperature is at the same level, the magnitude of C_0 values for four rejuvenators is AO > NO > BO > EO. Moreover, parameter b ($b=1/(2*D^{0.5})$) shows a negative relationship with the diffusion coefficient (D) values of rejuvenators. With the diffusion temperature rising, the b values in these correlation curves decrease, particularly when the temperature rises from 25°C to 60°C. It denotes that the diffusion rates of rejuvenators in aged bitumen enlarge distinctly at high temperatures.

Figure 6.8 Density profiles for rejuvenator molecules scaled with $zt^{-0.5}$ in aged bitumen
(a) Bio-oil; (b) Engine-oil; (c) Naphthenic-oil; (d) Aromatic-oil

Table 6.1 The parameters in fitting curves of different rejuvenator-aged bitumen models

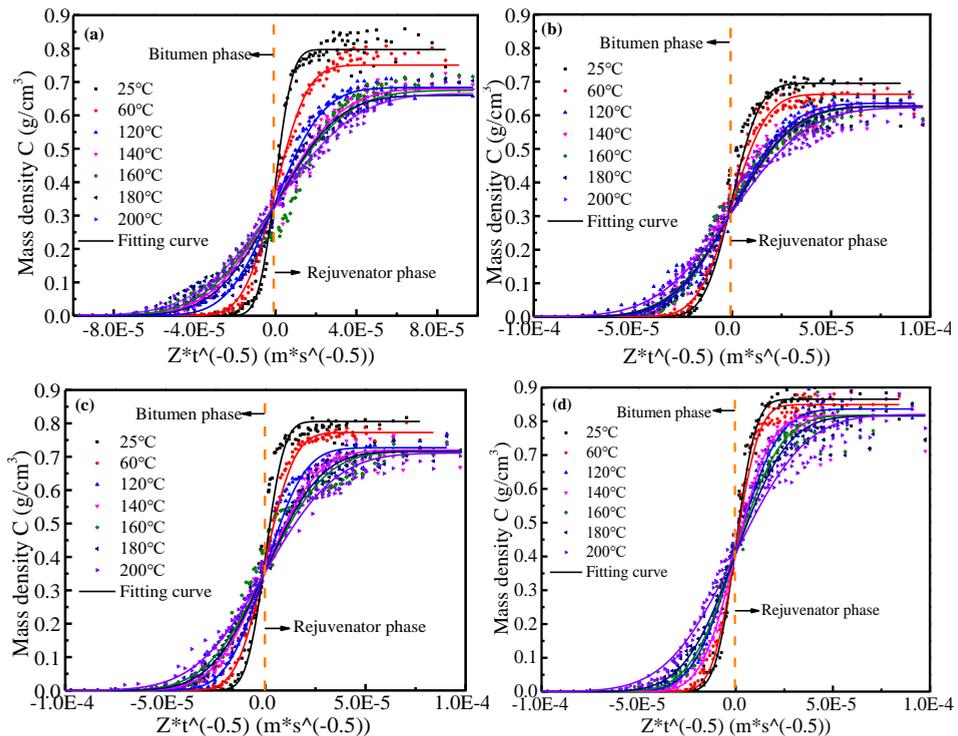| Model	T (°C)	-b	C_0 (g·cm³)	R^2	Model	-b	C_0 (g·cm³)	R^2
	25	107414	0.399	0.995		61202	0.355	0.988
(a)	60	55692	0.378	0.995	(b)	50911	0.331	0.988
BO and	120	37954	0.342	0.994	EO and	38065	0.318	0.986
Aged	140	27609	0.340	0.992	Aged	29465	0.314	0.986
bitumen	160	25585	0.337	0.974	bitumen	28551	0.313	0.987
system	180	24133	0.330	0.983	system	25767	0.314	0.995
	200	22648	0.333	0.993		23638	0.312	0.976
	25	96059	0.403	0.987		86351	0.433	0.993
(c)	60	62323	0.386	0.995	(d)	74818	0.425	0.996
NO and	120	46346	0.363	0.992	AO and	48172	0.418	0.994
aged	140	35102	0.360	0.994	aged	45471	0.408	0.993
bitumen	160	29983	0.358	0.979	bitumen	37847	0.409	0.989
system	180	27387	0.358	0.994	system	33390	0.408	0.988
	200	25328	0.356	0.987		25023	0.410	0.986

6.5.4 Diffusion coefficient prediction of different rejuvenators in aged bitumen

To directly evaluate and compare the diffusion capacity of various rejuvenators in aged bitumen at different temperatures, the diffusion coefficient (D) values are calculated according to the procedure described in section 6.4.3 and plotted in **Figure 6.9**. It can be seen that the magnitude for D parameters of four rejuvenators varies from 10^{-11} to 10^{-10} m²/s, which depends on both rejuvenator type and temperature dramatically. All D values of rejuvenators enlarge remarkably as the diffusion temperature rises. This is as expected since the enhanced molecular mobility of rejuvenator molecules at high temperatures would promote the permeation level of rejuvenators into the aged bitumen layer [14, 15]. Additionally, the increased temperature would enlarge the free volume ratio in aged bitumen and create more spatial volume for further diffusion of rejuvenator molecules [13]. The aromatic-oil rejuvenator exhibits the lowest diffusion coefficient D value in the whole diffusion temperature region. Polar aromatic rings strongly reduce the molecular mobility of aromatic-oil molecules.

In addition, the D values of bio-oil and engine-oil rejuvenators are higher than the naphthenic-oil. This is because the high molecular weight characteristic of the naphthenic-oil molecule negatively affects its molecular mobility. Interestingly, the comparison results regarding the diffusion coefficient values of bio-oil and engine-oil rejuvenators depend on the diffusion temperature. At low temperatures (25°C and 60°C), the engine-oil rejuvenator displays higher D values than the bio-oil, while the latter shows the largest diffusion coefficient at high temperatures (120-200°C).

At low temperatures, a polar ester functional group in bio-oil molecules improves the intermolecular interaction with aged bitumen molecules, which blocks the diffusion potential of bio-oil molecules due to insufficient molecular mobility. As a result, the intermolecular interactions between engine-oil and aged bitumen molecules are much lower than bio-oil, and that's why the engine-oil molecules exhibit a higher diffusion coefficient than the bio-oil at low temperatures. However, as reported in our previous work, bio-oil molecules' molecular mobility and self-diffusion capacity are higher than the engine-oil molecules at high temperatures [20]. Therefore, the bio-oil rejuvenator shows a faster diffusion rate than the engine-oil at high temperatures.

It is summarized that the rejuvenator type significantly influences the diffusion capacity of rejuvenators in aged bitumen. For instance, the D value of engine-oil molecules in aged bitumen at 60°C is 1.20, 1.50, and 2.16 times larger than that of bio-oil, naphthenic-oil, and aromatic-oil rejuvenators. Meanwhile,

the D value of bio-oil rejuvenator at 160°C is 1.24, 1.37, and 2.18 times higher than engine-oil, naphthenic-oil, and aromatic-oil molecules. Therefore, compared to bio-oil and engine-oil rejuvenators, a higher blending temperature is needed for both naphthenic-oil and aromatic-oil to diffuse and disperse in aged bitumen homogenously. Furthermore, during the mixing and compaction processes, the bio-oil rejuvenator would diffuse faster than engine-oil due to the high temperature (>120°C), but the latter would show a higher diffusion capacity than the former when the temperature of recycled asphalt pavement is lower than 60°C.
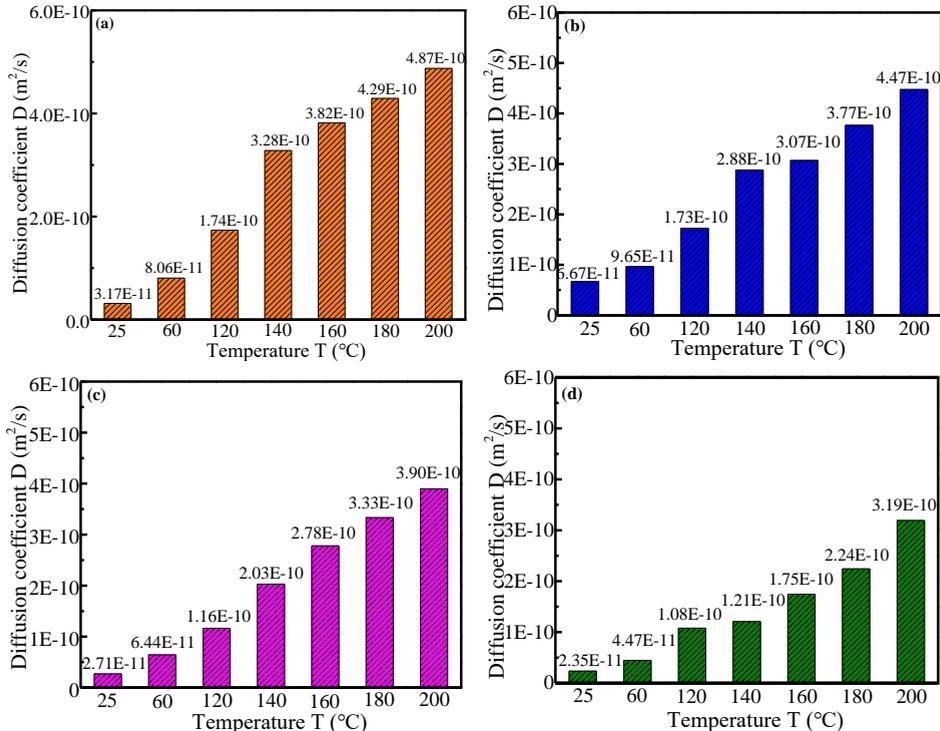
Figure 6.9 Diffusion coefficient of rejuvenators in aged bitumen versus temperatures
(a) Bio-oil; (b) Engine-oil; (c) Naphthenic-oil; (d) Aromatic-oil

6.5.5 Influence of temperature on D values of different rejuvenators in aged bitumen

To further explore the influence of temperature on the diffusion behaviors of various rejuvenators in aged bitumen, the Arrhenius equation is utilized to describe the relationship between the diffusion coefficient and temperature, which is expressed as follows:

$$LnD = \frac{-E_a}{R} * \frac{1}{T} + LnA \qquad (6.5)$$

where D is the diffusion coefficient, m^2/s; T shows the diffusion temperature, K; R refers to the universal gas constant (8.314 $J/mol \cdot K^{-1}$), E_a and A represent the activation energy (J/mol) and pre-exponential factor (m^2/s). It is worth noting that the E_a parameter relates to the critical energy for rejuvenator molecules to diffuse into the aged bitumen layer. In contrast, the A parameter herein means the maximum diffusion coefficient point of rejuvenator molecules when the diffusion temperature is infinite.

The correlation curves between the (LnD) of four rejuvenators and the (1/T) values are demonstrated in **Figure 6.10**. The correlation coefficient R^2 values are all higher than 0.90, indicating that the Arrhenius

formula could fit the LnD-1/T curves of all rejuvenators well. Moreover, the LnD values present a linear relationship with a reciprocal diffusion temperature. It can be found that the D values of four rejuvenators exhibit diverse temperature sensitivity. The magnitude of slope values (E_a/R) for four rejuvenators is BO > AO > EO > NO. It implies that the diffusion capacity of bio-oil molecules in aged bitumen presents the highest sensitivity to temperature variation, followed by aromatic-oil and engine-oil, while the naphthenic-oil shows less temperature sensitivity. The E_a and A values of the four rejuvenators are listed in **Table 6.2**. The order of pre-exponential factor (A) and activation energy (E_a) values for four rejuvenators is the same as BO > NO > AO > EO. When the temperature tends to the infinity point, the diffusion rate of engine-oil molecules is the smallest, while the bio-oil molecules exhibit the most considerable diffusion potential. In addition, the activation energy required for engine-oil molecular diffusion is the lowest, indicating that it is easiest for engine-oil molecules to have enough molecular mobility to penetrate an aged bitumen layer due to its lower molecular weight and absence of a polar functional group. On the contrary, the E_a value of bio-oil is higher than that of aromatic-oil and engine-oil rejuvenators. Although the bio-oil molecule has the smallest molecular weight and largest molecular mobility, the potential hydrogen bonds between the ester function group (-COO-) in bio-oil molecules and hydrogen atoms in bitumen molecules would hinder the deep diffusion process of bio-oil molecules in aged bitumen, which agrees well with previous findings [15, 25].
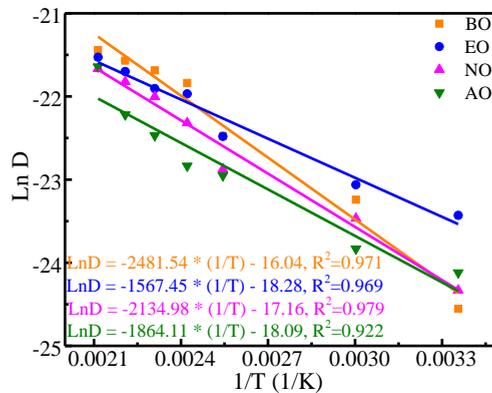
Figure 6.10 Correlations between temperature and diffusion coefficient of rejuvenators in aged bitumen

Table 6.2 The Ea and A parameters of various rejuvenators in LAB40-aged bitumen

Rejuvenator	BO	EO	NO	AO
E_a (J/mol)	18968.72	15256.02	13030.91	15498.21
A (m^2/s)	1.08E-7	1.15E-8	3.52E-8	1.39E-8

6.6 Experimental validations

6.6.1 Establishing standard curves of rheological indices

In view of the high similarity in physical and chemical characteristics, it is difficult to distinguish the rejuvenator from an aged bitumen matrix. In the previous studies [9, 10, 26], the variation of rheological indices of aged bitumen layers was measured to monitor the concentration distribution of rejuvenators in aged bitumen after different diffusion tests. Similarly, the calibration curves of different rheological parameters (G^*, δ, $G^*/sin\delta$, and $G^* sin\delta$), G-R parameter, and fatigue life N_f of rejuvenated bitumen as a function of rejuvenator dosage are shown in **Figures 6.11-6.13**.
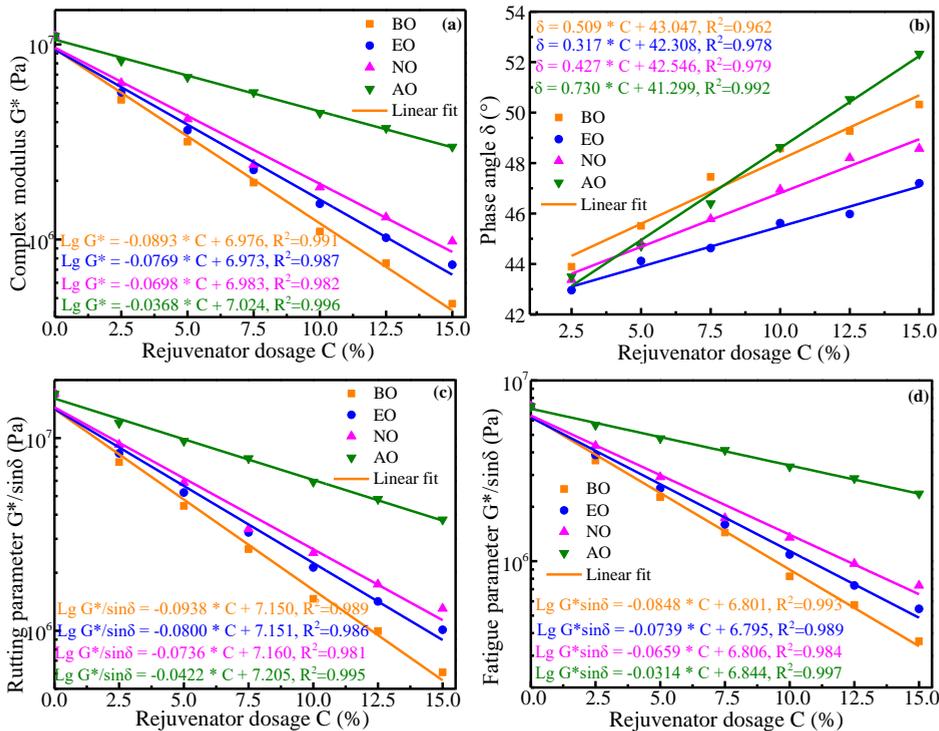
Figure 6.11 Correlation curves between different rheological indices with rejuvenator dosage

For the same rejuvenator dosage, the ranking of the rejuvenators for the values of G*, G*/sinδ, and G*sinδ is AO > NO > EO > BO. It suggests that the bio-oil rejuvenator has the largest effect on reducing the stiffness, rutting resistance, and fatigue resistance of aged bitumen. On the contrary, the rejuvenation effect of an aromatic-oil rejuvenator is the smallest as a result of its considerable molecular weight, polarity, and viscosity. Further, the rejuvenation efficiency on rheological performance restoration of engine-oil and naphthenic-oil rejuvenators is in the middle, with the former performing better than the latter.

The variable rates of these rheological indices of rejuvenated bitumen with four rejuvenators as a function of the rejuvenator dosage differ dramatically. Based on the absolute slope values in correlation equations, the order of rejuvenator dosage dependence level for the G*, G*/sinδ, and G*sinδ parameters of rejuvenated bitumen with four rejuvenators follows BO > EO > NO > AO. Meanwhile, the aromatic-oil rejuvenator shows the strongest influence on increasing the δ values of aged bitumen, followed by the bio-oil and naphthenic-oil rejuvenators. In contrast, engine-oil rejuvenated bitumen displays the lowest δ values regardless of the rejuvenator dosage.

Similarly, the correlation curves between the G-R values with the rejuvenator dosage are illustrated in **Figure 6.12**. It was reported that the G-R parameter is strongly associated with the cracking potential of bitumen, and a high G-R value represented a lower cracking resistance [30]. The aged bitumen exhibits the highest G-R value, which reduces significantly with an increase in rejuvenator content no matter the rejuvenator type. This suggests that applying rejuvenators can distinctly enhance the cracking resistance of aged bitumen. When the rejuvenator dosage is higher than 5%, the order of four rejuvenators for an improvement effect on G-R values is BO > EO > NO > AO.
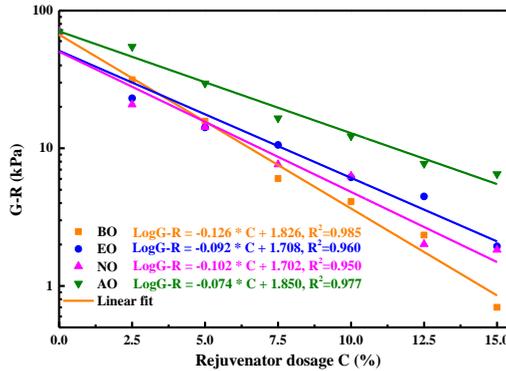
Figure 6.12 Correlation curves between the G-R parameter with rejuvenator dosage
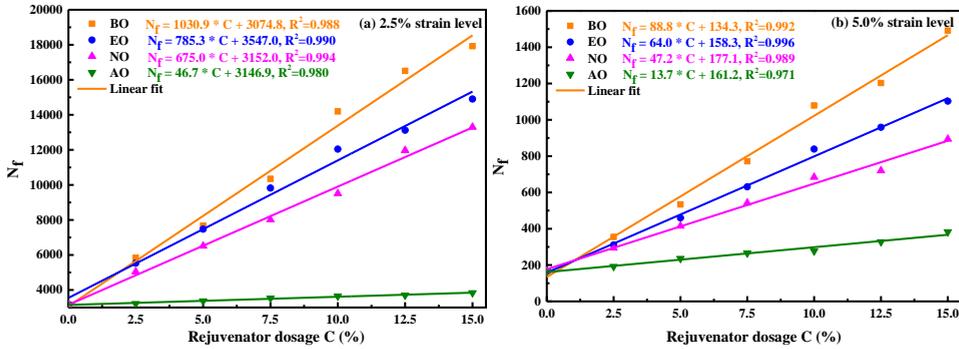
Figure 6.13 Correlation curves between the service life N_f with rejuvenator dosage

From the LAS tests, the fatigue life N_f values at 2.5% and 5.0% strain levels of rejuvenated binders with variable rejuvenator dosages are demonstrated in **Figure 6.13**. The N_f values of all rejuvenated bitumen increase linearly as an increment in rejuvenator content. Thence, adding these four rejuvenators can enhance the fatigue resistance of aged bitumen. However, the enhancement effect of the aromatic-oil rejuvenator is limited due to its large molecular weight and viscosity [20, 21]. The bio-oil rejuvenated binders show the highest N_f values, followed by the engine-oil and naphthenic-oil rejuvenated bitumen. The influence of rejuvenator content on the N_f values is more significant at a lower fatigue strain, depending on the rejuvenator type.
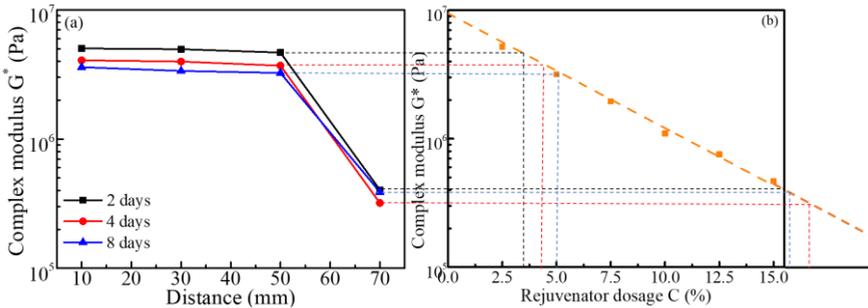
Figure 6.14 Correlation curves between the service life N_f with rejuvenator dosage

The diffused samples are equally divided into four parts, and each of them is subjected to rheological tests to determine the concentration distributions of rejuvenators in diffused specimens. **Figure 6.14** shows how to determine the rejuvenator dosage (C) in different layers after diffusion based on measured rheological properties (e.g. Complex modulus G*) and the corresponding G*-C correlation curve.

6.6.2 Comparison of the diffusion coefficient values of rejuvenators

In this thesis, the diffusion coefficient D values of four rejuvenators in aged bitumen are derived using MATLAB with **Eq.6.2** [27, 28]. The measured and predicted D values are plotted together in **Figure 6.15** to validate the MD simulation outputs. The measured D values depend on the characterization index type. For each rejuvenator, the difference in measured D values based on the rheological parameters of G*, G*/sinδ, G*sinδ, $N_{f2.5}$, and $N_{f5.0}$ is slight, but the D values based on G-R and δ are smaller than others. Thus, the G-R and δ parameters are not appropriate for measuring the concentration distribution of rejuvenators in aged bitumen. However, the magnitude of all measured D values of four rejuvenators is in the region of 10^{-11}-10^{-10} m^2/s, which agrees with previous studies [9, 11, 14, 26]. One rheological index (such as G* or N_f) is sufficient to determine the concentration distribution of rejuvenators in aged bitumen after a diffusion process.

From **Figure 6.15**, the predicted D values of all rejuvenators from MD simulations are higher than the experimental results. In detail, the estimated D values of bio-oil, engine-oil, naphthenic-oil, and aromatic-oil rejuvenator in aged bitumen are almost 3.4, 2.9, 4.3, and 5.9 times larger than the corresponding experimental results. Meanwhile, the DSR test and concentration determination based on standard curves would also cause deviations to some extent. The predicted D values are directly derived from a density distribution profile of rejuvenator molecules in an aged bitumen model. which may be more accurate by preventing a concentration conversion procedure. On the other hand, there are still differences between MD simulation molecular models of aged bitumen and rejuvenators with their realistic chemical components and molecular structures.
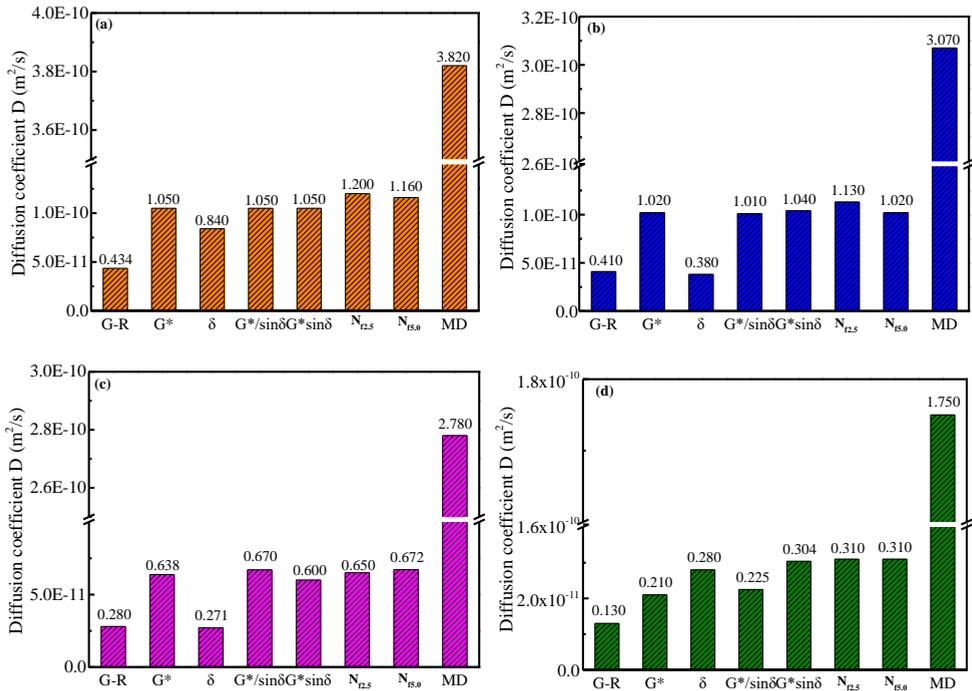
Figure 6.15 Comparison of D values from MD outputs and experimental results

All D values of four rejuvenators in aged bitumen from MD simulations and experimental tests are plotted in **Figure 6.16**. The measured and predicted D values show the same trend for four rejuvenators as BO > EO > NO > AO. Moreover, it can be seen that the difference in D values between measured and predicted D values is dependent on the rejuvenator type. However, there is no apparent relationship between the measured and predicted D values for all rejuvenators. The measured D values based on G-R and δ parameters are far from the predicted D values. These four rejuvenators show diverse molecular structures, molecular weight and polarity, and intermolecular interaction with aged bitumen molecules. Therefore, the difference between the measured and predicted D values is inconsistent for all rejuvenators. It is worth noting that these rejuvenators come from different categories, resulting in different degrees of difference between predicted and measured D values. Given this, it is recommended to compare the diffusion coefficient D values of various rejuvenators belonging to the same category (such as bio-oils, engine-oils, naphthenic-oils, or aromatic-oils) and establish a potential relationship between the predicted and measured D values of different rejuvenator groups. Afterward, a more efficient rejuvenator with a high diffusion capacity could be optimized from a molecular-scale perspective without any tedious experiment and trial process.
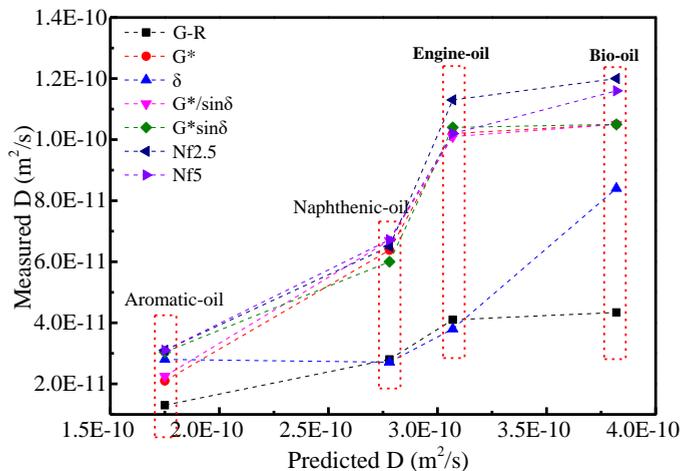
Figure 6.16 Influence of rejuvenator type on the diffusion coefficient values

6.7 Influence of aging degree and temperature on the D values of rejuvenators

According to the similarity in diffusion coefficient values, the MD simulation outputs are reliable and can accurately predict the diffusion behaviors of various rejuvenators in aged binders. The rejuvenator type, aging degree of bitumen, and temperature are considered in this MD simulation to study the diffusion characteristics of rejuvenator molecules in the aged bitumen model.

The significant influence of aging level on the D parameters of rejuvenators at various temperatures is reflected in **Figure 6.17**. As the aging degree of aged bitumen deepens, the D values of bio-oil, engine-oil, and naphthenic-oil molecules decrease, while the aromatic-oil exhibits an opposite behavior. For non-polar (engine-oil) and low-polar rejuvenators (naphthenic-oil), the increased aging level has little effect on their intermolecular force with aged bitumen molecules, but the reduction of free volume in aged bitumen presents a significantly negative influence on their diffusion behaviors. On the other hand, the D values of aromatic-oil molecules in aged bitumen rise gradually with the increment in aging level, indicating that the aromatic-oil rejuvenator diffuses faster in aged bitumen with a higher aging degree. Although bitumen aging reduces its free volume fraction, the enlarged polarity of bitumen molecules enhances the intermolecular interaction between the polar rejuvenator and aged bitumen molecules. That's why the aging level positively affects the diffusive capacity of the aromatic-oil rejuvenator. It should be mentioned that the adverse influence of aging

level on the free volume fraction in the aromatic-oil diffusion model still exists, but the effect of enlarged intermolecular force on the diffusion rate is more significant than the reduced free volume factor. However, the D value of the aromatic-oil rejuvenator at 160℃ decreases with the aging level changes from LAB40 to LAB80. It means that the positive role of aging level on the diffusive capacity of aromatic-oil molecules due to the enhanced intermolecular force mainly occurs at low temperatures, and its adverse impacts on free volume fraction and diffusion coefficient value become more apparent as the temperature rises.
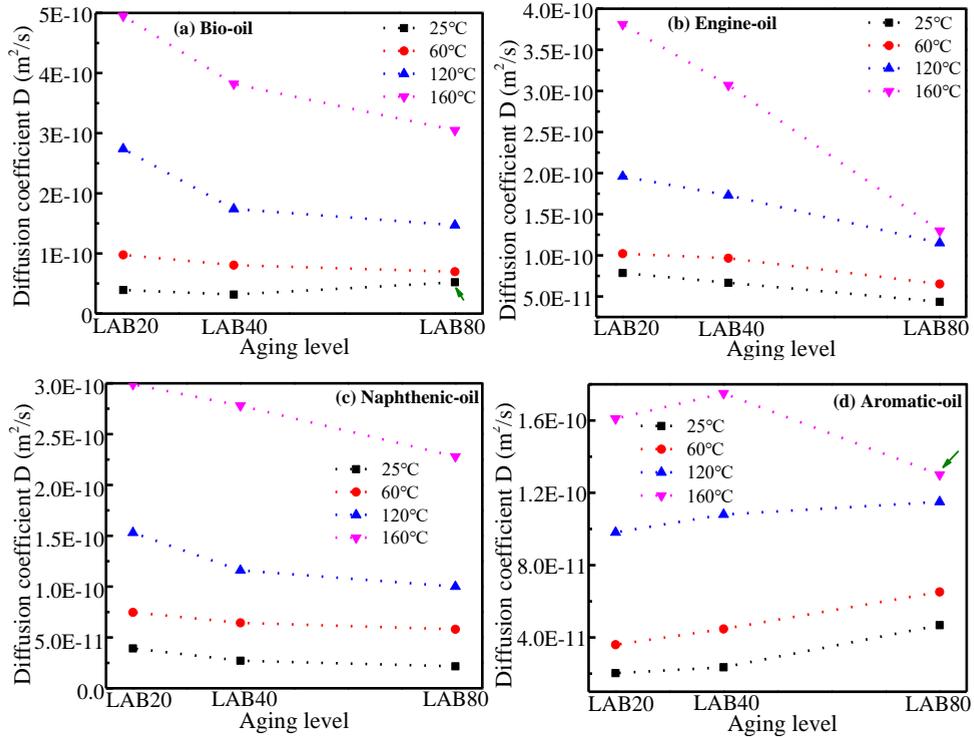
Figure 6.17 Influence of aging level on the D values of four rejuvenators at different temperatures

For bio-oil molecules, the aging level mainly adversely affects their diffusion behavior because of the reduction of free volume reduction. However, the D value at 25℃ increases as the aging level changes from LAB40 to LAB80, indicating that the high aging degree improves the diffusive rate of bio-oil molecules in aged bitumen at low temperatures. Furthermore, there is a polar ester (O-C=O) functional group in the molecular structure of bio-oil, and the enlarged intermolecular force between the bio-oil and aged bitumen molecules at 25℃ contributes more to improving its diffusion behavior than the negative effect of reduced free volume fraction. Lastly, it can be found that the aging level on the D parameters of rejuvenators in aged bitumen is also affected by the temperature and rejuvenator type. According to the downward or upward trend, the effects of the aging level on the D values of all rejuvenators are more significant at high temperatures. In addition, the influence level of the aging degree on D values of aromatic-oil molecules at low temperatures (25 and 60℃) is the maximum. At 120 and 160℃, the aging level shows a similar and most robust effect on D values of bio-oil and engine-oil, followed by the naphthenic-oil case, while this influence on aromatic-oil diffusion is the smallest.

6.8 Summary

This chapter aims to observe the diffusion behaviors of four rejuvenators in aged bitumen at an atomic level and predict their diffusive parameters at various temperatures using the MD simulation method. Moreover, experimental diffusion measurements and rheological characterizations are conducted to validate the simulation outputs. Further, the synergetic effects of rejuvenator type, aging level of bitumen, and temperature on the diffusive capacity of the rejuvenator-aged bitumen interfacial model are explored and discussed. Some main findings are listed as follows:

- At an atomic scale, the mutual but partial interfacial diffusion behaviors between the rejuvenators and the aged bitumen molecules are observed. Meanwhile, high temperature and long diffusion time promote the diffusion level of all rejuvenators in the aged bitumen.
- Fick's Second Law fits the concentration distribution of rejuvenator molecules in the aged bitumen matrix during various diffusion processes. Moreover, the diffusion coefficient D of four rejuvenators varies from 10^{-11} to 10^{-10} m^2/s, which strongly depends on the rejuvenator type, temperature, and bitumen aging levels.
- In most cases, the order for the diffusive capacity of four rejuvenators is BO > EO > NO > AO. However, the engine-oil displays a higher D value than the bio-oil at low temperatures (25 and 60 °C), which may be related to the strong surface adsorption between the polar bio-oil and aged bitumen molecules at low temperatures. In addition, the diffusion behavior of bio-oil in the aged bitumen presents a higher temperature sensitivity than the other three rejuvenators.
- The experimental results in both the magnitude and order of D parameters agree well with the MD simulation outputs, but the predicted D values at 160°C of all rejuvenators are about 3-6 times larger than the measured values. Moreover, one rheological index (G* or N_f, but no G-R and δ parameters) is sufficient to determine the concentration distribution of the rejuvenator in the aged bitumen after a diffusion process.
- Based on MD simulation outputs, the increased aging degree negatively affects the diffusion capacity of bio-oil, engine-oil, and naphthenic-oil rejuvenators in the aged bitumen, but the D value of the aromatic-oil molecule increases as the aging level deepens.

6.9 References

[1] Y. Xiao, B. Yan, X. Zhang, X. Chang, M. Li. Study the diffusion characteristics of rejuvenator oil in aged asphalt binder by image thresholding and GC-MS tracer analysis. Construction and Building Materials. 2020, 249, 118782.

[2] M. Mohajeri, A.A.A. Molenaar, M.F.C. Van de Ven. Experimental study into the fundamental understanding of blending between reclaimed asphalt binder and virgin bitumen using nanoindentation and nano-computed tomography. Road Materials and Pavement Design. 2014, 15(2), 372-384.

[3] S.N. Nahar, M. Mohajeri, A.J.M. Schmets, A. Scarpas, M.F.C. van de Ven, G. Schitter. First observation of blending-zone morphology at interface of reclaimed asphalt binder and virgin bitumen. Transportation Research Record: Journal of the Transportation Research Board. 2013, 2370, 1-9.

[4] G. Zou, J. Zhang, Y. Li, Z. Lin. Quantitative characterize binder blending and diffusion in recycled asphalt mixture: An environmental-friendly solution using wooden cube and 3D fluorescence image technology. Journal of Cleaner Production. 2021, 193, 126204.

[5] S. Vassaux, V. Gaudefroy, L. Boulange, L. Jean Soro, A. Pevere, A. Michelet, V. Barragan-Montero, V. Mouillet. Study of remobilization phenomena at reclaimed asphalt binder/virgin binder interphases for recycled asphalt mixtures using novel microscopic methodologies. Construction and Building Materials. 2018, 165, 846-858.

[6] J. Xu, P. Hao, D. Zhang, G. Yuan. Investigation of reclaimed asphalt pavement blending efficiency based on micro-mechanical properties of layered asphalt binders. Construction and Building Materials. 2018, 163, 390-401.

[7] Y. He, Z. Alavi, J. Harvey, D. Jones. Evaluating diffusion and aging mechanisms in blending of new and age-hardened binders during mixing and paving. Transportation Research Record: Journal of the Transportation Research Board. 2016, 2574, 64-73.

[8] R. Karlsson, U. Isacsson. Application of FTIR-ATR to characterization of bitumen rejuvenator diffusion. Journal of Materials in Civil Engineering. 2003, 15(2), 157-165.

[9] G. Cuciniello, N. Mallegni, M. Cappello, S. Filippi, P. Leandri, G. Polacco, M. Losa. Classification and selection of exhausted oils for rejuvenating bituminous blends. Construction and Building Materials. 2021, 278, 122387.

[10] Y. Fang, Z. Zhang, J. Shi, X. Yang, X. Li. Insights into permeability of rejuvenator in old asphalt based on permeation theory: Permeation behaviors and micro characteristics. Construction and Building Materials. 2022, 325, 126765.

[11] T. Ma, X. Huang, Y. Zhao, Y. Zhang. Evaluation of the diffusion and distribution of the rejuvenator for hot asphalt recycling. Construction and Building Materials. 2015, 98, 530-536.

[12] M. Xu, J. Yi, D. Feng, Y. Huang. Diffusion characteristics of asphalt rejuvenators based on molecular dynamics simulation. International Journal of Pavement Engineering. 2019, 20(5), 615-627.

[13] G. Xu, H. Wang. Diffusion and interaction mechanism of rejuvenating agent with virgin and recycled asphalt binder: a molecular dynamics study. Molecular Simulation. 2018, 44(17), 1433-1443.

[14] W. Sun, H. Wang. Molecular dynamics simulation of diffusion coefficients between different types of rejuvenator and aged asphalt binder. International Journal of Pavement Engineering. 2020, 21(8), 966-976.

[15] H. Ding, H. Wang, X. Qu, A. Varveri, J. Gao, Z. You. Towards an understanding of diffusion mechanism of bio-rejuvenators in aged asphalt binder through molecular dynamics simulation. Journal of Cleaner Production. 2021, 126977.

[16] AASHTO M 320. Standard Specification for Performance-graded Asphalt Binder.

[17] AASHTO TP 101. Standard Method of Test for Estimating Fatigue Resistance of Asphalt Binders Using the Linear Amplitude Sweep.

[18] Y. Gao, Y. Zhang, C. Zhang, X. Liu, R. Jing. Quantifying oxygen diffusion in bitumen films using molecular dynamics simulations. 2022, 331, 127325.

[19] Y. Ding, B. Huang, X. Shu, Y. Zhang, M.E. Woods. Use of molecular dynamics to investigate diffusion between virgin and aged asphalt binders. Fuel. 2016, 174, 267-273.

[20] S. Ren, X. Liu, P. Lin, S. Erkens, Y. Gao. Chemical characterizations and molecular dynamics simulations on different rejuvenators for aged bitumen recycling. Fuel. 2022, 324, 124550.

[21] S. Ren, X. Liu, S. Erkens, P. Lin, Y. Gao. Multi-component analysis, molecular model construction, and thermodynamics performance prediction on various rejuvenators of aged bitumen. Journal of Molecular Liquids. 2022, 119463.

[22] R. Karlsson, U. Isacsson. Bitumen rejuvenator diffusion as influenced by ageing. Road Materials and Pavement Design. 2002, 3(2), 167-182.

[23] W.S. Mogawer, A. Booshehrian, S. Vahidi, A.J. Austerman. Evaluating the effect of rejuvenators on the degree of blending and performance of high RAP. RAS, and RAP/RAS mixture. Road Materials and Pavement Design. 2013, 14(2), 193-213.

[24] BF. Bowers, B. Huang, X. Shu, B.C. Miller. Investigation of reclaimed asphalt pavement blending efficiency through GPC and FTIR. Construction and Building Materials. 2014, 50, 517-523.

[25] M. Li, L. Liu, C. Xing, L. Liu, H. Wang. Influence of rejuvenator preheating temperature and recycled mixture's curing time on performance of hot recycled mixtures. Construction and Building Materials. 2021, 295, 123616.

[26] M. Xu, Y. Zhang. Study of rejuvenators dynamic diffusion behavior into aged asphalt and its effects. Construction and Building Materials. 2020, 261, 120673.

[27] Y. Gao, Y. Zhang, Y. Yang, J. Zhang, F. Gu. Molecular dynamics investigation of interfacial adhesion between oxidized bitumen and mineral surfaces. Applied Surface Science. 2019, 479, 449-462.

[28] Y. Gao, Y. Zhang, F. Gu, T. Xu, H. Wang. Impact of minerals and water on bitumen-mineral adhesion and debonding behaviours using molecular dynamics simulations. Construction and Building Materials. 2018, 171, 214-222.

[29] S. Ren, X. Liu, P. Lin, S. Erkens, Y. Xiao. Chemo-physical characterization and molecular dynamics simulation of long-term aging behaviors of bitumen. Construction and Building Materials. 2021, 302, 124437.

[30] M. Ishaq, F. Giustozzi. Correlation between rheological tests on bitumen and asphalt low temperature crack tests. Construction and Building Materials. 2022, 320, 126109.

[31] S. Ren, X. Liu. Y. Gao, R. Jing, S. Erkens, P. Lin, H. Wang. Molecular dynamics simulation and experimental validation on the interfacial diffusion behaviors of rejuvenators in aged bitumen. Materials & Design. 2023, 226, 111619.

7

Rejuvenation efficiency evaluation of rejuvenators in aged bitumen

This chapter aims to comprehensively study how the type and quantity of rejuvenators, along with the extent of bitumen aging, impact rheological rutting, cracking, and fatigue resistance of rejuvenated bitumen. We develop a selection program for crucial rheological evaluation indicators to gauge their sensitivity to rejuvenator type, dosage, and bitumen aging level. Ultimately, we recommend specific critical indicators for evaluating the efficiency of rejuvenation, encompassing chemical properties, rheological traits, high-temperature rutting performance, low-temperature cracking susceptibility, and fatigue resistance in various rejuvenator-aged bitumen blends.

7.1 Background, research objective and scheme

Apart from the compatibility (**chapter 5**) and diffusion (**chapter 6**) issues between the rejuvenators and aged bitumen, the performance evaluation of rejuvenated bitumen is the research hotspot when the recycling of RAP materials is studied. Due to the complicated service environment, a series of rheological and mechanical properties of bituminous material should be sufficient to meet the requirements in terms of the resistance to high-temperature rutting, low-temperature cracking, and fatigue failure under variable heat, loading, moisture, and oxygen conditions [1-3]. Previous studies revealed that adding a rejuvenator could improve the low-temperature cracking and fatigue performance of aged bitumen [4-6], but the high-temperature anti-deformation would deteriorate due to its softening effect [7, 8]. Thus, the balancing principle between high-temperature rutting and cracking potential due to the low-temperature shrinkage and fatigue damage is always adopted to determine the rejuvenator content [9-11].

Currently, different influence factors (e.g., rejuvenator type, dosage, aging degree of bitumen, bitumen/RAP source, polymer type, aging protocol) on the rejuvenation effectiveness of rejuvenators on chemical and rheological performance of aged binder have been studied [12-15]. However, it is difficult to compare the conclusions obtained from various studies due to the variation of material components and evaluation methods [16, 17]. Although the restoration ratio of aged bitumen performance before and after adding the rejuvenator is the main quantitative parameter to assess the rejuvenator's efficiency [18-20], the result strongly depends on the type of selected chemical and rheological properties. The inconsistent evaluation method and parameters on the rejuvenation efficiency of rejuvenated bitumen hinder the further understanding of bitumen-rejuvenator interactions and rejuvenator components optimization.

---

1. Rejuvenated bitumen preparation

(i)   Rejuvenator type: Bio-oil, Engine-oil, Naphthenic-oil, Aromatic-oil
(ii)   Rejuvenator dosage: 0, 1.25%, 2.5%, 3.75%, 5%, 7.5%, 10% (LAB20); 0, 2.5%, 5%, 7.5%, 10%, 12.5%, 15% (LAB40 and LAB80)
(iii)   Aging degree of bitumen: LAB20, LAB40, LAB80

---

2. High-temperature performance of rejuvenated bitumen

(i)   Linear viscoelastic test: Rutting parameter ($G^*/\sin\delta$), Rutting failure temperature (RFT)
(ii)   Flow test: Zero-shear viscosity (ZSV), Carreau model parameters (b and c)
(iii)   Multiple stress creep and recovery test: Strain-time curve, Recovery percentage ($R_{0.1}$ and $R_{3.2}$), Creep compliance ($J_{nr0.1}$ and $J_{nr3.2}$), Stress sensitivity parameters (R_{diff} and $J_{nrslope}$)

---

3. Low-temperature cracking potential of rejuvenated bitumen (Relaxation behavior)

Shear stress (τ_{0s}, τ_{50s}, τ_{100s}), Relaxation time ($t_{75\%}$, $t_{50\%}$, $t_{25\%}$), Stress ratio (R_{50s}, R_{100s}), Relaxation model parameters (A and n)

---

4. Fatigue resistance of rejuvenated bitumen

(i)   Linear viscoelastic test: Fatigue parameter ($G^*\sin\delta$), Fatigue failure temperature (FFT), G-R parameter
(ii)   Linear amplitude test: Strain-stress curve parameters (ε_{sr}, E, f_{se}, f_{sr}, G_{se}, G_{sl}, G_{st}), S-VECD model parameters (C_1, C_2, α, k, S_f, A, B), Fatigue life ($N_{f2.5}$, N_{f5})
(iii)   Time sweep test: G*-N curve, Phase angle peak (δ_{peak}), Fatigue life ($N_{p50\%}$, N_{p20}), Dissipated energy (W_0), Crack width (C_{500}, C_{1500}, C_{3000})

---

5. Critical indicators for effectively evaluating rejuvenation efficiency
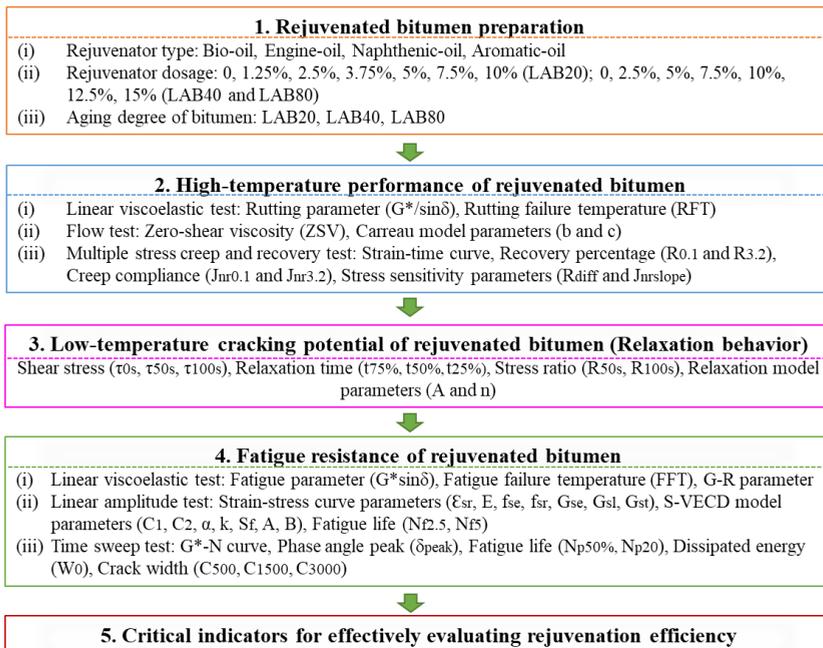
Figure 7.1 Research scheme and methodology of this chapter

To achieve our objectives, this chapter aims to:

(a) Investigate the combined effects of rejuvenator type, dosage, and the aging degree of bitumen on the chemical and rheological properties of rejuvenated bitumen.

(b) Identify potential correlations between the chemical and rheological parameters of rejuvenated bitumen.

(c) Evaluate the performance of rejuvenated binders in terms of high-temperature rutting, low-temperature relaxation, and fatigue, considering variations in rejuvenator type, dosage, and bitumen aging level.

(d) Propose critical indicators to effectively assess the rejuvenation efficiency of various rejuvenators in restoring the high-temperature rutting performance, low-temperature cracking potential, and fatigue resistance of aged bitumen.

The main research structure of this chapter is illustrated in **Figure 7.1**. Different rejuvenated binders are prepared with variable rejuvenator types, rejuvenator dosage, and the aging degree of bitumen. The Linear viscoelastic, flow, and MSCR tests are performed to estimate the high-temperature performance of rejuvenated bitumen. Different high-temperature parameters ($G^*/\sin\delta$, RFT, ZSV, b, c, $R_{0.1}$, $R_{3.2}$, $J_{nr0.1}$, $J_{nr3.2}$, R_{diff}, and $J_{nrslope}$) are considered. Moreover, the relaxation parameters (τ, t, R, A, and n) are utilized to evaluate the low-temperature cracking potential of rejuvenated bitumen. Various fatigue tests (LVE, LAS, and TS) are carried out to assess the fatigue resistance of rejuvenated binders. Finally, the key indicators that effectively assess and differentiate the rejuvenation capabilities of various rejuvenators on rutting, relaxation and fatigue performance of aged bitumen are proposed.

7.2 Preparation of rejuvenated bitumen

The full-mixing method was adopted to prepare rejuvenated bitumen, as described in **Chapter 5**. The rejuvenator dosages for all rejuvenators are the same [21]. When dealing with LAB20, the rejuvenator dosage levels vary from 1.25% to 10%, increasing in increments of 2.5%. These dosage levels also apply to both LAB40 and LAB80 binders due to their high aging degrees. It's important to clear that the nomenclature for a particular rejuvenated bitumen specifies the bitumen's aging level and the type/dosage of the rejuvenator. For instance, 2P10B signifies rejuvenated bitumen by mixing 10% bio-oil into LAB40-aged bitumen.

7.3 High-temperature performance evaluation

7.3.1 Introduction

It is well-agreed that the aging of bitumen is beneficial to enhancing the high-temperature rutting and deformation resistance because of the strengthened intermolecular molecules of bitumen [22, 23]. However, adding rejuvenators composed of light components always softens the aged bitumen and weakens its high-temperature performance [24]. The common principle during rejuvenation is to balance high-and-low temperature properties of rejuvenated bitumen [25, 26]. The rejuvenator type and dosage must be optimized to enhance the cracking resistance and adhesion performance and reserve the high-temperature property of aged bitumen [27, 28, 29]. The maximum content of rejuvenators was always controlled based on the high-temperature indices [30, 31].

Nevertheless, different evaluation methods and indicators were adopted to assess the high-temperature properties of bitumen, leading to difficulty directly comparing the rejuvenation effectiveness of various rejuvenators on the high-temperature behavior of aged bitumen [32, 33]. The rutting parameter ($G^*/\sin\delta$) and corresponding rutting failure temperature proposed by the SHRP project are the commonly-used indicators for estimating the rutting performance of bituminous materials [34]. Recently, some researchers proved that the multiple stress creep and recovery (MSCR) could better distinguish between complex bitumen than conventional indicators [35]. However, Skronka et al. found that the MSCR test overestimated the positive effects of elasticity on the high-temperature rutting performance of asphalt mixtures [36]. Further, Sharma et al. mentioned a good connection between the zero-shear viscosity measured from the flow test with the high-temperature rutting performance of asphalt bitumen and mixture [37, 38].

Based on the literature review, there are some limitations to the high-temperature performance evaluation of rejuvenated bitumen: (a) There is no unified evaluation method and indicator for assessing the high-temperature properties of bituminous materials. (b) The difference in material components of rejuvenator-aged bitumen blends significantly affects the high-temperature performance. There is limited research on systematically investigating and comparing the rejuvenation efficiency of various rejuvenators on the high-temperature behavior of aged bitumen. (c) The potential connections between different high-temperature rheological indicators of rejuvenated bitumen are still unclear.

7.3.2 High-temperature indices

The temperature sweep test measures the variation trend of the rutting parameter in the linear viscoelastic (LVE) region. The temperature rises from 30°C to 70°C, with an interval of 10°C. The frequency during the LVE test is constant at 10 rad/s. All experimental measurements were conducted with at least two replicates to achieve reliable results.

The zero-shear viscosity (ZSV) is closely related to the rutting potential of the asphalt binder and mixture [39]. The flow test at different temperatures of 40°C, 50°C, and 60°C was implemented with DSR to measure the difference in flow behavior and ZSV index of various rejuvenated binders. The shear rate of all flow tests varies from $10^{-3}s^{-1}$ to $10^{2}s^{-1}$.

The MSCR tests were performed at two stress levels of 0.1 kPa and 3.2 kPa at different temperatures of 52°C, 58°C, 64°C, and 70°C, respectively [40]. Two rheological indices (non-recoverable creep compliance J_{nr} (kPa^{-1}) and recovery percentage R (%)) can be calculated as follows:

$$J_{nr}(\sigma, N) = \frac{\varepsilon_r - \varepsilon_c}{\sigma} \tag{7.1}$$

$$R(\sigma, N) = \frac{\varepsilon_c - \varepsilon_r}{\varepsilon_c - \varepsilon_0} \times 100 \tag{7.2}$$

where σ and N refer to the applied stress (kPa) and the creep/recovery cycles; ε_c (%) and ε_r (%) are the shear strain values measured at the end of creep and recovery steps, respectively; ε_0 (%) represents the initial shear strain in the creeping stage. The J_{nr} parameter is related to the deformation potential of bituminous material, while the R index reflects the resilience. The R and J_{nr} parameters at both 0.1 kPa and 3.2 kPa stress levels are calculated as follows:

$$R_{0.1} = \frac{\sum_{N=11}^{20} R(0.1, N)}{10} \tag{7.3}$$

$$J_{nr0.1} = \frac{\sum_{N=11}^{20} J_{nr}(0.1, N)}{10} \tag{7.4}$$

$$R_{3.2} = \frac{\sum_{N=1}^{10} R(3.2, N)}{10} \tag{7.5}$$

$$J_{nr3.2} = \frac{\sum_{N=1}^{10} J_{nr}(3.2, N)}{10} \tag{7.6}$$

The MSCR results are strongly sensitive to the stress level, and two parameters ($J_{nrslope}$ and R_{diff}) are calculated to assess the dependence of virgin, aged, and rejuvenated bitumen on the stress applied as below:

$$J_{nrslope} = \frac{dJ_{nr}}{d\sigma} = \frac{J_{nr3.2} - J_{nr0.1}}{3.1} \times 100 \tag{7.7}$$

$$R_{diff} = \frac{R_{3.2} - R_{0.1}}{R_{0.1}} \times 100 \tag{7.8}$$

where stress differential dσ equals 3.1 kPa; $J_{nr3.2}$ and $J_{nr0.1}$ are the creep compliance of bitumen at the stress of 3.2kPa and 0.1kPa, while the $R_{3.2}$ and $R_{0.1}$ are the corresponding recovery percentages.

7.3.3 Rutting resistance from LVE test

The rutting parameter G*/sinδ of virgin and aged bitumen is displayed in **Figure 7.2(a)**. The G*/sinδ value of bitumen tends to decrease as the temperature rises, indicating that the rutting potential is larger at higher temperatures. The aging degree of bitumen significantly reduces the absolute slope values of G*/sinδ-T curves, showing that a high aging level decreases the temperature sensitivity of rutting performance. Meanwhile, the linearly increasing correlations between the G*/sinδ and long-term aging time are detected, regardless of the temperature. It implies that the rutting resistance of bitumen remarkably improves during the long-term aging process. Moreover, the influence of aging time on G*/sinδ becomes more obvious at high temperatures.

Based on the SHRP recommendation, the rutting failure temperature (RFT) index is proposed as the temperature when the G*/sinδ is 1kPa [41]. The RFT results of virgin and aged bitumen are shown in **Figure 7.2(b)**. As the long-term aging time is prolonged, the RFT value of bitumen increases significantly and linearly.
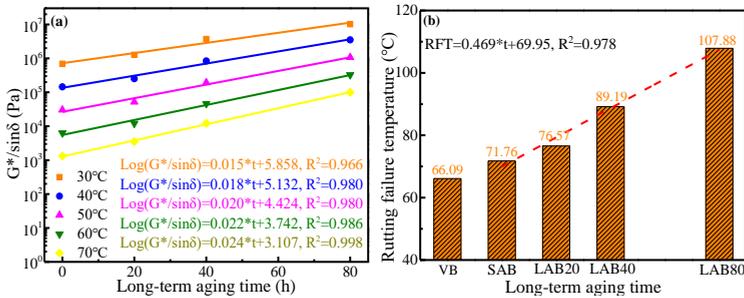
Figure 7.2 Rutting characteristics of virgin and aged bitumen

To quantitively estimate the rejuvenation effect of rejuvenators on the high-temperature performance of aged bitumen, the rejuvenation percentage parameter is proposed based on different high-temperature indices:

$$PR = \frac{P_{aged} - P_{rejuvenated}}{P_{aged} - P_{virgin}} * 100 \tag{7.9}$$

where PR is the rejuvenation percentage, and P represents the high-temperature indices. Moreover, the P_{virgin}, P_{aged}, and $P_{rejuvenated}$ are the high-temperature indices of the virgin, aged, and rejuvenated bitumen.

The G*/sinδ-based rejuvenation percentage (RPR) of rejuvenated bitumen at 60°C is displayed in **Figure 7.3**. Regardless of rejuvenator type and aging degree of bitumen, the RPR parameter rises linearly as the increased. It implies that incorporating rejuvenators weakens the high-temperature rutting resistance of aged bitumen because of their softening effects. The ranking of RPR of rejuvenated bitumen is AORB < NORB < EORB < BORB. Thus, the bio-oil rejuvenator has the highest reduction effect on the rutting resistance of aged bitumen, while the aromatic-oil can maximally reserve its high-temperature performance advantage. It is observed that the RPR values of all rejuvenated binders are lower than 100%, indicating that the anti-rutting performance of rejuvenated bitumen is still better than virgin bitumen. However, the rejuvenator dosage has to be controlled to ensure sufficient rutting resistance at high temperatures, especially for bio-oil and engine-oil rejuvenators. It is worth mentioning that the rejuvenation effect of these four rejuvenators on the rutting performance can be effectively evaluated and distinguished by the G*/sinδ result, depending on the temperature.
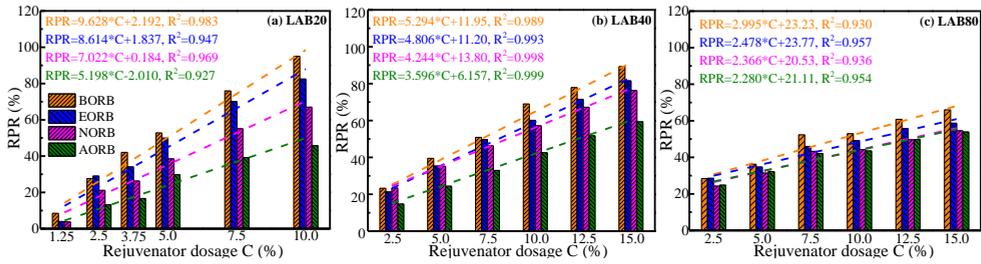
Figure 7.3 The G*/sinδ-based rejuvenation efficiency (RPR) of rejuvenated bitumen at 60°C

The rutting failure temperature (RFT) index is calculated with the G*/sinδ=1.0kPa criteria [42], and the RFT-based rejuvenation percentage (RFTR) is displayed in **Figure 7.4**. Similar to RPR, the RFTR shows a linearly increasing trend as the rejuvenator dosage rises. Regardless of rejuvenator dosage and bitumen aging level, the difference in RFTR values of rejuvenated binders is observed. The RFTR order of rejuvenated binders (BORB > EORB > NORB > AORB) is independent of rejuvenator type and aging degree of bitumen. Thus, the RFT index is recommended as an effective LVE indicator to characterize the high-temperature performance of rejuvenated bitumen.
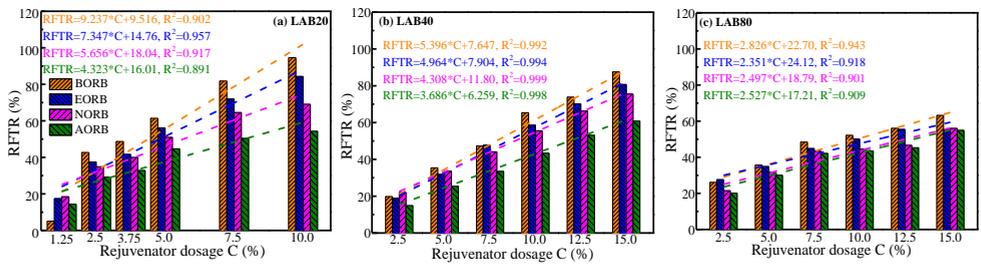
Figure 7.4 RFT-based rejuvenation efficiency (RFTR) of rejuvenated bitumen

7.3.4 Shear resistance from flow test

The strain level is small and no realistic deformation is involved in the whole LVE region [43]. The flow test is performed to examine the shear resistance of bitumen. The flow curves of virgin and aged bitumen are illustrated in **Figure 7.5(a)**. As observed, the flow behavior of bitumen strongly depends on the shear rate. Due to the Newtonian-flow characteristic, the complex viscosity remains constant at a low shear rate (<1 s^{-1}). As the shear rate exceeds the critical point, the bitumen is a non-Newtonian fluid. The Carreau model is adopted to quantitatively describe the flow curves of all binders, as described in **section 5.5.2** of **Chapter 5**.
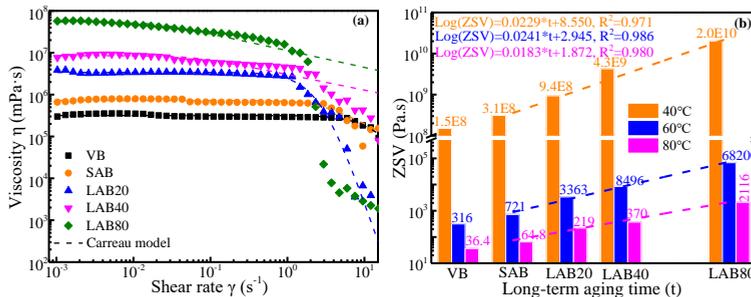
Figure 7.5 Flow behavior and ZSV values of virgin and aged bitumen

The ZSV values of virgin and aged bitumen are presented in **Figure 7.5(b)** at different temperatures. The Log(ZSV) value of bitumen has a linear relationship with the long-term aging time. The increased aging level results in a higher ZSV value of bitumen, which tends to decrease as the temperature rises.

The ZSV-based rejuvenation percentage (ZSVR) of rejuvenated bitumen is plotted in **Figure 7.6**, increasing exponentially as a function of rejuvenator content. When more rejuvenators are added, the recovery percentage on ZSV of aged bitumen presents a convergence close to 100%. Thus, it is difficult to clearly distinguish the rejuvenation effect of these rejuvenators on ZSV of aged binder with high rejuvenator dosages. The difference in ZSVR values of BORB and AORB binders is significant, but EORB and NORB show similar ZSVR parameters, especially when the aged bitumen is LAB40 or LAB80. Compared to $G^*/\sin\delta$, the ZSV parameter has a limitation in differentiating the rejuvenation efficiency of engine-oil and naphthenic-oil rejuvenators in aged bitumen with severe aging degrees.
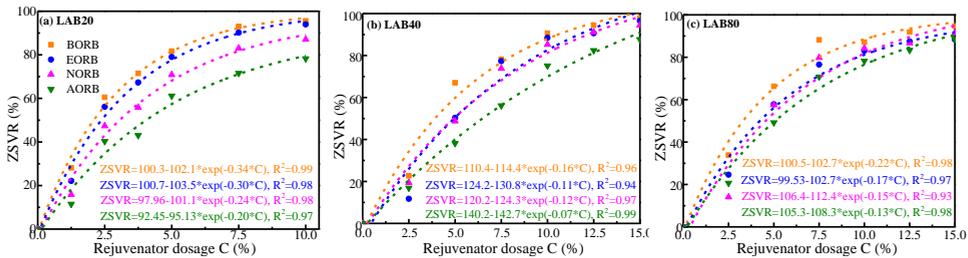
Figure 7.6 Influence of rejuvenator dosage on ZAVR values of rejuvenated bitumen

7.3.5 Anti-deformation capacity from MSCR test

7.3.5.1 Influence of aging on the MSCR indices of bitumen

The MSCR parameters of virgin and aged bitumen are plotted in **Figure 7.7**. The $R_{0.1}$ and $R_{3.2}$ values of bitumen exhibit exponential growth as the aging degree deepens. Simultaneously, prolonged aging leads to an exponential reduction in the parameters $J_{nr0.1}$, $J_{nr3.2}$, R_{diff}, and J_{nrdiff}.
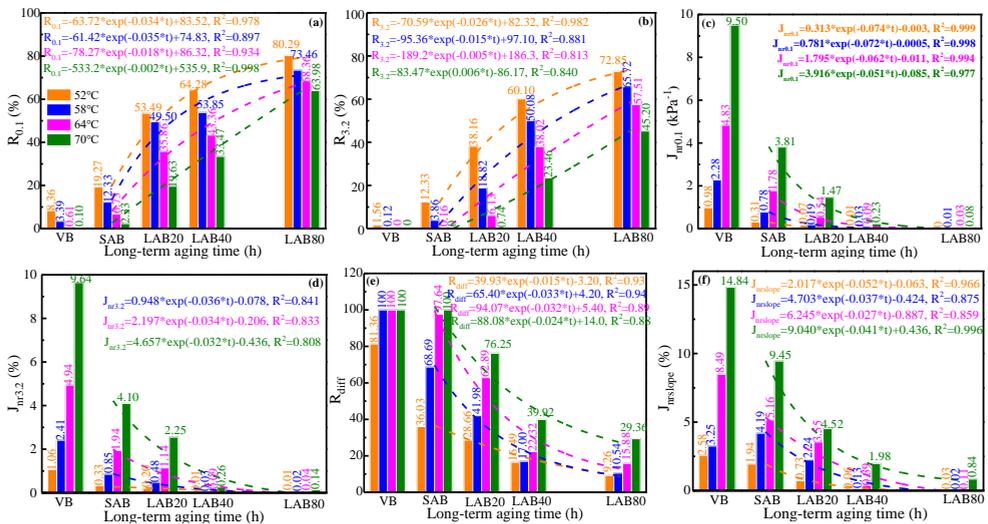
Figure 7.7 Influence of aging on the MSCR indices of bitumen

Moreover, temperature exerts a great influence on bitumen's elastic recovery and creep potential. With increasing temperature, the R-value decreases while J_{nr}, R_{diff}, and J_{nrdiff} increase. This implies that elevated temperatures diminish the elastic recovery and enhance the deformation level and stress sensitivity of bitumen. As the stress level rises from 0.1 kPa to 3.2 kPa, the R-value decreases, while J_{nr} increases. Consequently, the effects of aging on the MSCR parameters of bitumen are contingent on both temperature and stress level.

7.3.5.2 $R_{0.1}$-based rejuvenation percentage ($RR_{0.1}$)

The $RR_{0.1}$ values of rejuvenated bitumen are plotted in **Figure 7.8**. Regardless of rejuvenator type and temperature, the $RR_{0.1}$ value enlarges linearly as a function of rejuvenator dosage. At all temperatures, the $RR_{0.1}$ value of the BORB binder is the maximum, indicating bio-oil rejuvenator maximally weakens the elastic recovery capacity of aged bitumen. Interestingly, the $RR_{0.1}$ of AORB is higher than EORB and NORB due to the low-stress level. This result does not agree with both RPR and flow ZSVR conclusion (BO > EO > NO > AO). Thus, the $R_{0.1}$ parameter is inappropriate for distinguishing the rejuvenation efficiency.
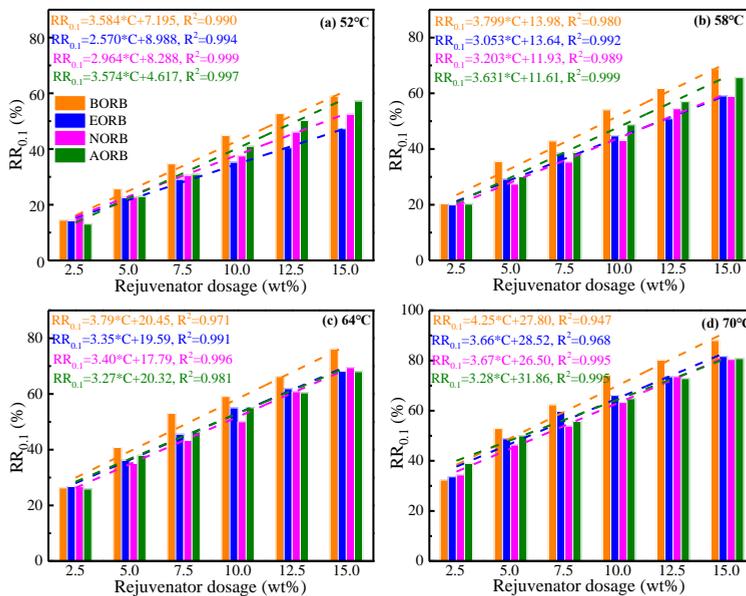
Figure 7.8 Influence of rejuvenator dosage on $RR_{0.1}$ value of rejuvenated bitumen

7.3.5.3 $R_{3.2}$-based rejuvenation percentage ($RR_{3.2}$)

The $R_{3.2}$ and $RR_{3.2}$ values of rejuvenated binders are illustrated in **Figure 7.9**. With the increase in rejuvenator dosage, the $RR_{3.2}$ tends to increase linearly or exponentially. The $RR_{3.2}$ values of various rejuvenated bitumen can be differentiated as a ranking of BORB > EORB > NORB > AORB, the same as the LVE rutting parameter and flow results. Hence, the $R_{3.2}$ parameter serves as a reliable metric for assessing the elastic recovery performance of rejuvenated binders, particularly under high-temperature conditions. However, it's important to note that temperature exerts a significant influence on the changing patterns of $RR_{3.2}$ values in rejuvenated binders. At lower temperatures (52°C and 58°C), $RR_{3.2}$ demonstrates a linear correlation with rejuvenator dosage, whereas this relationship becomes exponential at higher temperatures (64°C and 70°C). When investigating the impact of various rejuvenators on the elastic recovery properties of aged bitumen, it's crucial to consider the temperature factor.
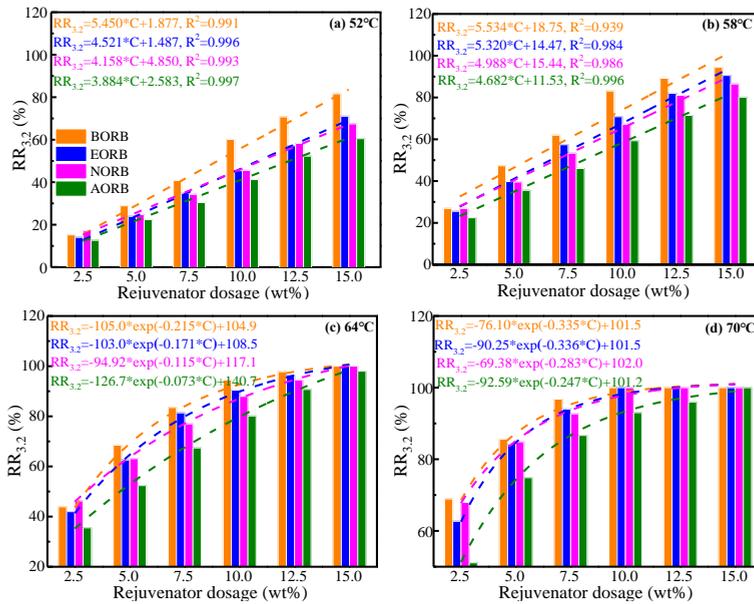
Figure 7.9 Influence of rejuvenator dosage on RR$_{3.2}$ value of rejuvenated bitumen

7.3.5.4 J$_{nr0.1}$-based rejuvenation percentage (J$_{nr}$R$_{0.1}$)

The relationship between J$_{nr}$R$_{0.1}$ values of rejuvenated binders and the dosage of the rejuvenator is illustrated in **Figure 7.10**.
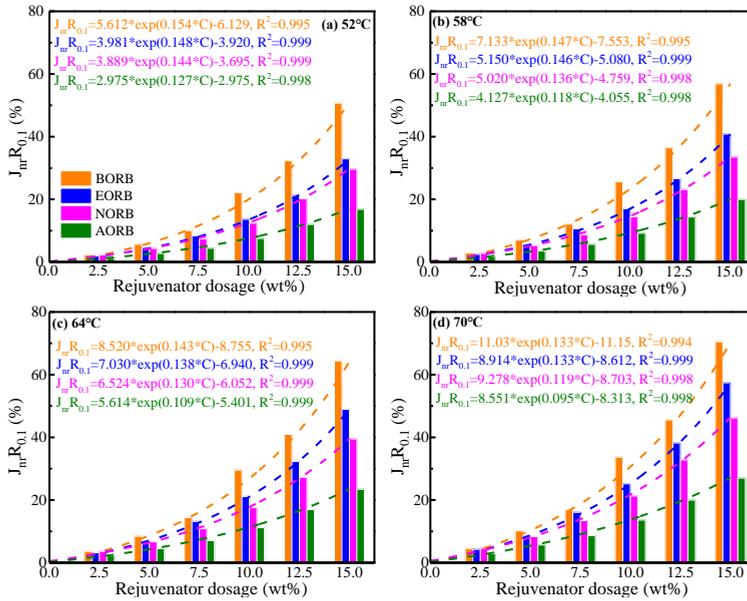
Figure 7.10 The influence of rejuvenator dosage on the J$_{nr}$R$_{0.1}$ value of rejuvenated bitumen

As the content of the rejuvenator increases, the $J_{nr}R_{0.1}$ for all rejuvenated binders exhibits a pronounced exponential increase. Regardless of the temperature and rejuvenator content, the ranking of $J_{nr}R_{0.1}$ value for rejuvenated binders follows the order BORB > EORB > NORB > AORB. This hierarchy implies that bio-oil rejuvenated bitumen has the highest creep potential, while aromatic-oil rejuvenated bitumen exhibits the least susceptibility to creep. Higher temperatures accelerate the rise in $J_{nr}R_{0.1}$ for rejuvenated bitumen due to increased molecular mobility. In summary, the $J_{nr0.1}$ parameter effectively assesses and distinguishes the impacts of these rejuvenators on the high-temperature creep potential of aged bitumen, but the $J_{nr0.1}$-based rejuvenation efficiency is contingent on temperature.

7.3.5.5 $J_{nr3.2}$-based rejuvenation percentage ($J_{nr}R_{3.2}$)

The $J_{nr}R_{3.2}$ curves versus rejuvenator dosages of different rejuvenated bitumen are shown in **Figure 7.11**. The $J_{nr}R_{3.2}$ values of rejuvenated binders increase exponentially as rejuvenator content increases. Meanwhile, the ranking of $J_{nr}R_{3.2}$ is BORB > EORB > NORB > AORB, the same as $J_{nr}R_{0.1}$. Thus, both $J_{nr0.1}$ and $J_{nr3.2}$ can be effective indicators for assessing the rejuvenation effects of various rejuvenators on the high-temperature creep performance of aged bitumen. Compared to $J_{nr}R_{0.1}$, the $J_{nr}R_{3.2}$ values are slightly higher when the rejuvenator type/dosage and aging degree of bitumen are the same. Measuring both $J_{nr0.1}$ and $J_{nr3.2}$ indices of rejuvenated bitumen is unnecessary, but the stress level and temperature should be kept constant when comparing the rejuvenation efficiency of different rejuvenators.
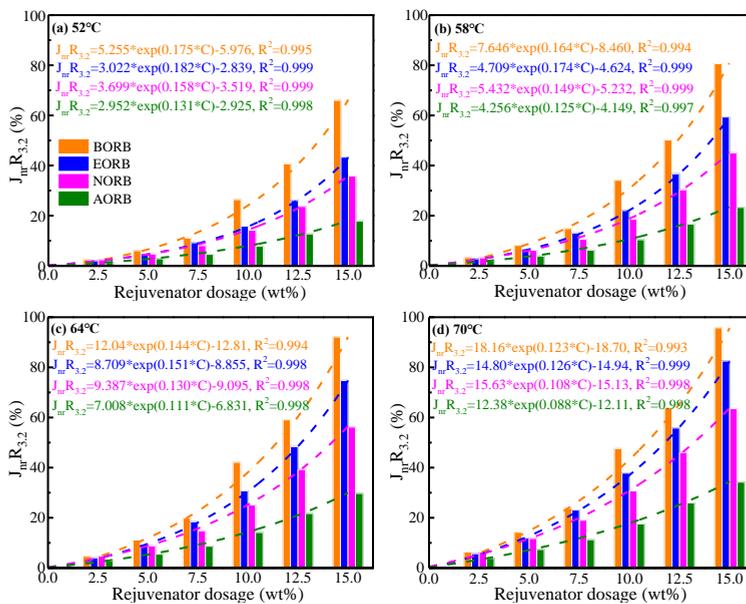
Figure 7.11 Influence of rejuvenator dosage on the $J_{nr}R_{3.2}$ value of rejuvenated bitumen

7.3.5.6 R_{diff}-based rejuvenation percentage ($R_{diff}R$)

The stress sensitivity of rejuvenated binders is estimated with parameters R_{diff} and $J_{nrslope}$. **Figure 7.12** shows the influence of rejuvenator type/dosage and temperature on aged bitumen's $R_{diff}R$ values. The order of $R_{diff}R$ values of rejuvenated binders is BORB > EORB > NORB > AORB. Nevertheless, the temperature affects the $R_{diff}R$ values of rejuvenated binders. When the temperature is 70°C, and the rejuvenator dosage exceeds 10%, the $R_{diff}R$ values of BORB, EORB, and NORB binders converse to 100%. Hence, the temperature should be lower than 64°C to effectively assess the influence of rejuvenator content on the $R_{diff}R$ value and differentiate the rejuvenation efficiency of different rejuvenators.
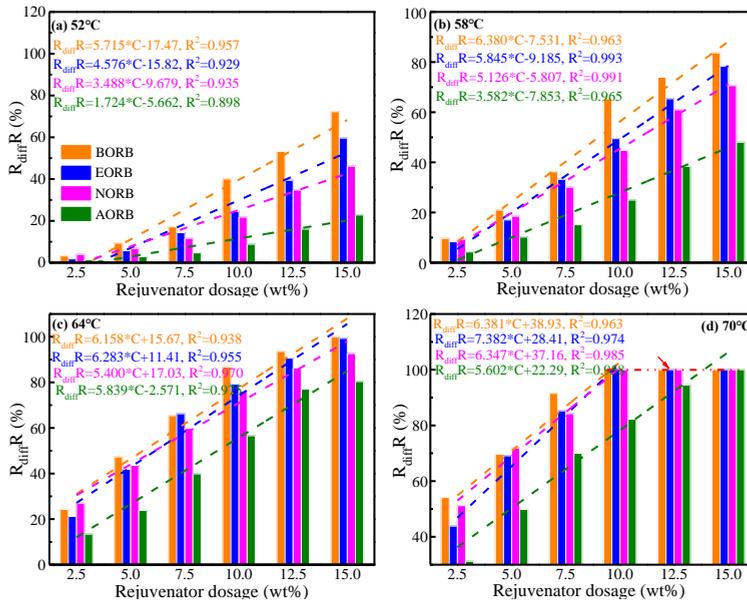
Figure 7.12 Influence of rejuvenator dosage on the $R_{diff}R$ value of rejuvenated bitumen

7.3.5.7 $J_{nrslope}$-based rejuvenation percentage ($J_{nrslope}R$)

The $J_{nrslope}R$ parameters of rejuvenated binders are presented in **Figure 7.13**. As rejuvenator content increases, the $J_{nrslope}R$ values enlarge exponentially, and high temperature promotes the improvement.
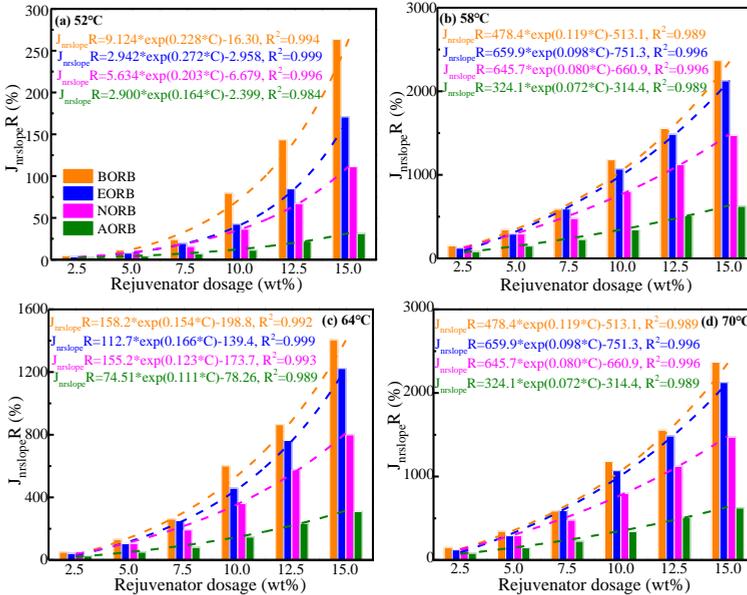
Figure 7.13 Influence of rejuvenator dosage on the $J_{nrslope}$ value of rejuvenated bitumen

When the temperature and rejuvenator content remain constant, the ranking of $J_{nrslope}R$ of rejuvenated binders is the same as $R_{diff}R$ (BORB > EORB > NORB > AORB). Additionally, the difference in $J_{nrslope}R$ values of different rejuvenated binders is significant. Thus, the $J_{nrslope}$ parameter can be an effective indicator for evaluating the rejuvenation efficiency of various rejuvenators on the stress sensitivity of aged bitumen.

7.3.6 Critical indicators recommendation and their potential connections

A scheme for the selection of effective and crucial evaluation indicators is outlined in **Figure 7.14(a)**. Initially, the process involves identifying potential indicators for evaluating rejuvenation efficiency and analysing their corresponding experimental outcomes. Subsequently, the feasibility of these chosen potential indicators in assessing rejuvenation effectiveness is verified, and any unsuitable indices with negative rejuvenation percentages are eliminated from consideration. To develop and optimize the components of the rejuvenator, the proposed evaluation criteria must be responsive to the variations induced by the rejuvenator type. This aspect is addressed in Step iii. Similarly, the selection of evaluation indicators must consider the impact of rejuvenator dosage, with any indicators that fail to gauge the effects of both the rejuvenator type and dosage on rejuvenation efficiency being discarded. Step v is designed to assess the sensitivity of potential evaluation indicators to the aging level of bitumen. The objective here is to ensure that the influence of rejuvenator type and dosage on the rejuvenation percentages remains consistent regardless of the bitumen's aging stage, while the effect of aging level is appropriately reflected. Indicators that do not meet the criteria of this step are considered sensitive indices. In Step vi, the indicators that still meet the criteria are examined concerning the range of rejuvenation percentages. In most cases, the ultimate goal of adding rejuvenators is to restore the properties of aged bitumen to a level comparable to virgin bitumen. Therefore, the expected range of rejuvenation percentages typically falls within 0-100%, with some allowance for slightly higher values in cases where rejuvenation demonstrates exceptional efficiency. This step eliminates any erratic indices displaying abnormal rejuvenation percentage results, ultimately identifying the parameters that can be considered effective evaluation indicators.
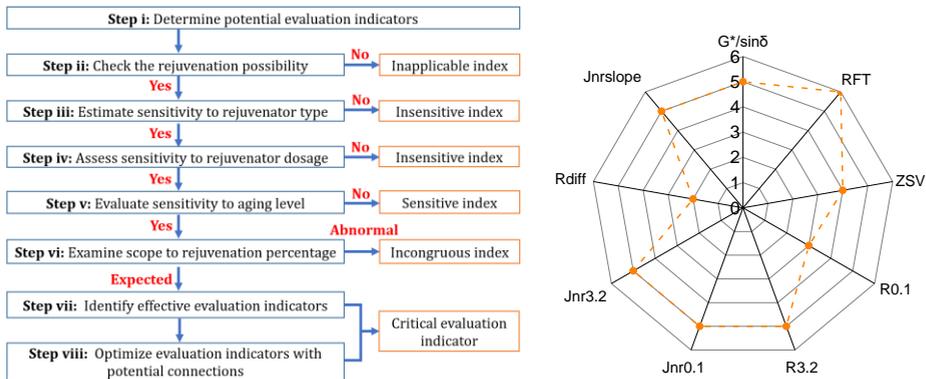
(a) The selection program for critical evaluation indicators   (b) Score for critical high-temperature indicators

Figure 7.14 Selection of critical high-temperature indicators

The sensitivity levels of different indicators from the LVE rutting, flow, and MSCR tests are calculated and compared in **Figure 7.14(b)**. The LVE test yields a score of 5 for both $G^*/\sin\delta$ and RFT parameters, while the ZSV index receives a slightly lower score of 4. In terms of the MSCR parameters, $R_{3.2}$, $J_{nr0.1}$, $J_{nr3.2}$, and $J_{nrslope}$ all earn a score of 5, indicating their consistent performance. However, $R_{0.1}$ and R_{diff} fall short with scores of 3 and 2, respectively. These scores suggest that RFT and ZSV can serve as effective indicators based on the LVE and flow tests, while $R_{3.2}$, $J_{nr0.1}$, $J_{nr3.2}$, and $J_{nrslope}$ are recommended for assessing the elastic behavior, creep potential, and stress sensitivity of rejuvenated bitumen.
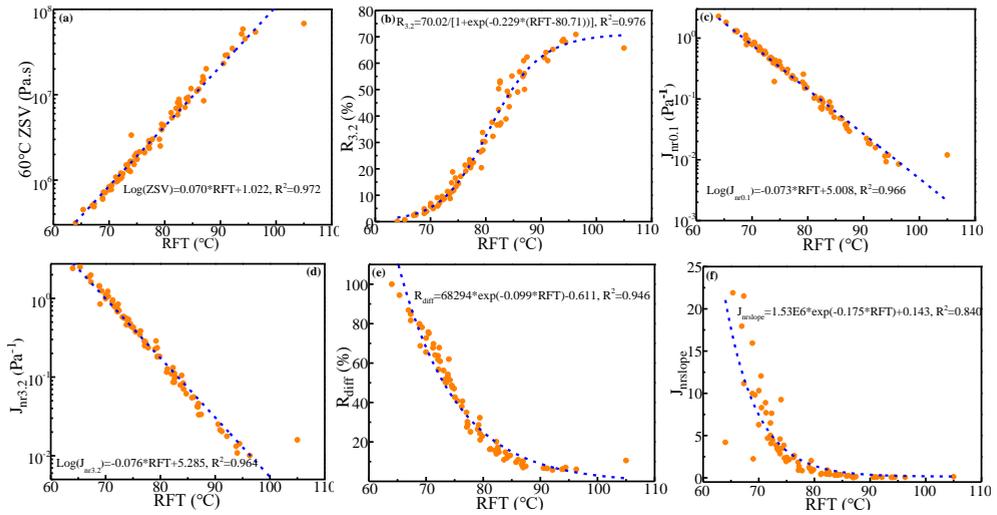
Figure 7.15 Correlations between the RFT with other critical evaluation indicators

In addition, the RFT index exhibits the highest score than ZSV and MSCR parameters, indicating that the RFT parameter is the first choice to evaluate and differentiate the high-temperature performance of various rejuvenator-aged bitumen systems. However, the flow and MSCR tests reflect the deformation capacity of bituminous materials. It is meaningful to correlate the RFT index with other parameters plotted in **Figure 7.15**. The RFT index is observed to correlate well with other effective high-temperature indicators. Regardless of rejuvenation conditions (rejuvenator type/dosage and aging degree of bitumen), the RFT parameter shows a positive linear relationship with the ZSV index but has a negative linear correlation with the $J_{nr0.1}$ and $J_{nr3.2}$. Moreover, the $R_{3.2}$ value of rejuvenated bitumen tends to increase exponentially as a function of the RFT parameter. The stress sensitivity parameters, R_{diff} and $J_{nrslope}$, decrease exponentially as the RFT value rises. Thus, the RFT index from the LVE test can be measured first, and the flow and MSCR parameters will be further predicted based on these correlations.

7.3.7 Summary

This subchapter aims to systematically investigate the complex effects of rejuvenator type/dosage and the aging degree of bitumen on the high-temperature performance of rejuvenated bitumen. The variations of rutting, flow, and elastic/creep parameters of rejuvenated binders are compared to propose the critical indicators for evaluating and distinguishing the rejuvenation efficiency of different rejuvenators on the high-temperature property of bitumen. The main findings are listed as follows:

(i) The bio-oil rejuvenator maximally weakens the high-temperature performance of aged bitumen, followed by the engine-oil and naphthenic -oil, while the aromatic-oil rejuvenated bitumen exhibits the best rutting, flow, and creep resistance.

(ii) Based on the score result, the parameters RFT and ZSV can be effective indicators from LVE and flow test, whereas $R_{3.2}$, $J_{nr0.1}$ or $J_{nr3.2}$, and $J_{nrslope}$ parameters are recommended to estimate the elastic performance, creep potential, and stress sensitivity of rejuvenated bitumen.

(iii) The RFT parameter is recommended as the critical indicator for effectively evaluating and differentiating the rejuvenation effectiveness of various rejuvenators on the high-temperature performance of aged bitumen. Moreover, the RFT index correlates well with other effective high-temperature indicators.

7.4 Low-temperature performance evaluation

7.4.1 Introduction

To date, various chemo-physical and rheological properties have been utilized to quantitatively assess the impact of material factors (aging, rejuvenation, and modification) and testing conditions (temperature) on the low-temperature performance of bituminous materials. A summary of low-temperature rheological evaluation parameters is presented in **Table 7.1**.

Table 7.1 Low-temperature performance evaluation of bituminous binder

	Rheological tests	Rheological indicators	Influence factors	Chemo-physical tests	Ref
1	BBR, 4mm DSR	S, m-value; ΔT_c G^*, δ	Temperature; Bitumen type	ATR-FTIR, SARA fractionation	[44]
2	BBR, Fraass breaking point	S, m, $T_{s=300}$, $T_{m=0.3}$, Fraass breaking point;	RAP binder dosage; rejuvenator; polybutadiene rubber	SARA fractionation; DSC	[47]
3	BBR	S, m-value	SARA ratio	SARA and DSC fractionation	[48]
4	DSR relaxation	G-R, residue stress	Rejuvenator type/dosage	DSC	[45]
5	BBR, Single Edge Notched Beam	S, m-value, fracture load, fraction deflection, fracture toughness, fracture energy	Bio-based and refined waste oil content	DSC	[49]
6	BBR, Asphalt binder cracking device (ABCD)	$T_{s=300}$, $T_{m=0.3}$, ΔT_c, ΔT_f	Binder source, compositional chemistry, crude oil processing, modification type, thermal properties	SARA, DSC	[50]
7	Ex-BBR, cone penetration test (CPT)	Critical grading temperature, cone penetration depth	Different modifiers, reversible aging level	Atomic force microscopy (AFM)	[51]
8	DSR relaxation, BBR	Shear stress, percentual stress relaxation at 30min and 60min, m-value	Bitumen type, temperature,	-	[52]
9	DSR relaxation	Shear stress, residue stress, relaxation time	Aging time, temperature, and pressure	-	[53]
10	Ductility, Creep, and relaxation test	Shear stress	Layer double hydroxides (LDHs)/crumb rubber modified bitumen and UV aging level	FTIR	[54]
11	DSR relaxation, BBR, SENB	Shear stress, stress ratio, relaxation time, S, m-value, fracture energy, maximum fracture displacement	Asphalt binder and mastic type	DSC	[55]
12	DSR relaxation	Shear stress, residue stress, relaxation model parameters	limestone particle size	-	[56]
13	DSR Relaxation	Percentage stress relaxation after 60min	Rejuvenator type, dosage,	-	[57]

The bending beam rheometer (BBR) test is the most commonly used method of estimating the low-temperature cracking potential of bitumen based on stiffness (S), m-value, ΔT_c, $T_{s=300}$, and $T_{m=0.3}$ parameters. Other rheological tests include the Fraass breaking point test, the single-edge notched beam (SENB), the asphalt binder cracking device (ABCD), the cone penetration test (CPT), and the ductility test. Additionally, chemo-physical methods, such as SARA fractionation, Fourier-transform infrared (FTIR) spectroscopy, differential scanning calorimetry (DSC), and atomic force microscopy (AFM) are utilized to explain why binders' low-temperature properties differ [44]. It has been reported that FTIR spectroscopy and SARA fractionation can provide information about the low-temperature behavior of bitumen. Furthermore, the glass transition temperature T_g is closely related to low-temperature rheological parameters [45, 46]. However, there is no general guideline on selecting testing methods and evaluation indices for determining the low-temperature performance of bitumen.

As measured from DSR tests, the relaxation performance of bitumen is highly correlated with its low-temperature cracking resistance from stress accumulation, as noted by Jing et al. [53]. Buchner et al. [52, 57] argued that the BBR test falls short in comprehensively estimating the low-temperature property of bitumen since it is a creep test and not a relaxation test. Bitumen and mastic relaxation behaviors have been characterized to analyze the effects of aging and rejuvenation on their cracking resistance. Regarding rejuvenation efficiency, it is essential to consider the low-temperature relaxation behaviors of rejuvenated bitumen [58]. However, the numerous variations in material characteristics, such as rejuvenator type/dosage and aging degree of bitumen, and relaxation parameters (i.e., shear stress, relaxation time, residue stress) considerably hinder the creation of an evaluation system for rejuvenation efficiency and the advancement of effective rejuvenators [59-61]. The reason for the difference in rejuvenation efficiency in different rejuvenator-aged bitumen systems is still vague, despite diverse randomized studies being conducted [62-64].

7.4.2 Low-temperature relaxation indices

The relaxation test was performed with a dynamic shear rheometer (DSR) at 0, 10, and 20°C. The geometry of the parallel plate was set as 2mm in thickness and 8mm in diameter. Moreover, the relaxation test was conducted with a strain-control model (a fixed strain of 1%). As shown in **Figure 7.16**, two steps were involved in the relaxation procedure: increasing-strain loading (0-0.1s) and constant-strain loading (0.1-100s). The strain rose from 0% to 1% during the first step, which was 1% in a relaxation time of 100s. The residue shear stress (τ), relaxation time (t), and shear stress ratio (R) were used to evaluate the relaxation performance of bituminous materials. Three residue shear stress at 0s, 50s, and 100s (τ_{0s}, τ_{50s}, τ_{100s}), three relaxation time with 75%, 50%, and 25% stress reduction ($t_{75\%}$, $t_{50\%}$, $t_{25\%}$), and stress ratio at 50s and 100s (R_{50s}, R_{100s}) were selected to evaluate the rejuvenation efficiency of various rejuvenator-aged bitumen blends systematically.
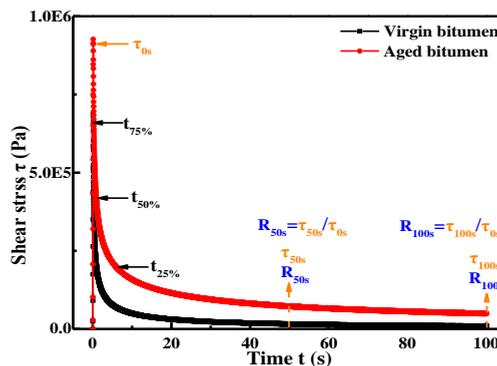
Figure 7.16 The representative relaxation curves of virgin and aged bitumen

7.4.3 Long-term aging effect on relaxation performance

The aging effect on the relaxation behaviors of bitumen is reflected with shear stress τ, relaxation time t, and stress ratio R parameters. The corresponding results are displayed in **Figure 7.17**. With the extension of long-term aging time, bitumen exhibits linear increases in Log(τ) and Log(t) values, while the R parameter at 0 and 10°C experiences exponential growth. This amplified stiffness and heightened intermolecular interaction contribute to the augmentation of τ, t, and R parameters in bitumen. Furthermore, the impact of long-term aging on the relaxation characteristics of bitumen varies based on the evaluation index type and testing temperature, as reflected in the different correlation equations. As both temperature and relaxation time increase, the slope and intercept values in the Log(τ)-t equations expand and diminish, respectively. This suggests that aging has a more pronounced effect on bitumen shear stress at elevated temperatures and extended relaxation times, leading to reduced τ values. Simultaneously, the influence of relaxation time surpasses that of temperature variation, particularly as the relaxation time extends from 50s to 100s.
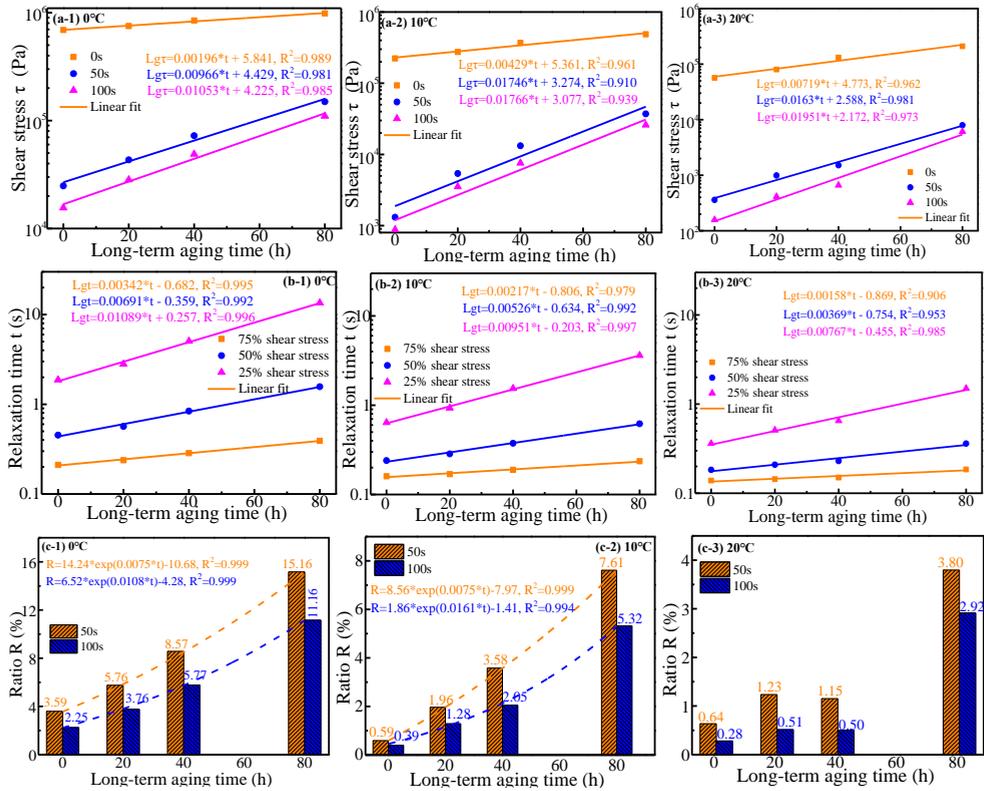
Figure 7.17 Relaxation parameters of virgin and aged bitumen at different temperatures

The severe-aging level leads to an obvious increment in relaxation time t of bitumen, rising as the residue stress ratio declines from 75% to 25% and decreasing as the temperature grows. A high temperature would promote the enlargement in molecular mobility and reduction in intermolecular interactions between bitumen molecules, and thus a shorter relaxation time is required for molecular relaxation [54]. The low residue stress ratio increases the slope value, which drops as the temperature rises. Moreover, the influence of the residue stress ratio on the sensitivity of relaxation time to long-term aging time is greater than the temperature. The aged bitumen exhibits a higher R% value at a longer relaxation time and a lower temperature. Similar to the τ parameter, the long relaxation time and high-temperature result in a low R-

value of bitumen, influencing the variation trend of equation parameters of R-t correlation curves. As the relaxation time and temperature increase, the R-value and its sensitivity to long-term aging time reduce gradually. When the temperature is 20°C, there is no clear relationship between the R-value and aging time.

7.4.4 Rejuvenation effect on relaxation performance

7.4.4.1 Shear stress-based rejuvenation percentage (τR)

The effect of rejuvenator dosage on the τR of LAB40 rejuvenated binders is displayed in **Figure 7.18**. The τR$_{50s}$ and τR$_{100s}$ of rejuvenated bitumen are extremely similar, and thus it is not necessary to measure both for rejuvenation efficiency evaluation. In addition, the τR$_{0s}$ values are greatly larger than the τR$_{50s}$ and τR$_{100s}$. For BORB, EORB, and NORB binder, the τR$_{0S}$ scope is 0-400%, which is 140% for AORB with 15% AO dosage. Meanwhile, all τR$_{50s}$ and τR$_{100s}$ values of rejuvenated binders are lower than 150%. The magnitude of τR parameters of rejuvenated bitumen is BORB > EORB > NORB > AORB. It suggests that the bio-oil rejuvenator shows the largest rejuvenation efficiency on the τR value of aged bitumen, while the aromatic-oil exhibits the weakest effectiveness. All τR parameters of BORB, EORB, and NORB binders increase exponentially as the rejuvenator dosage rises, while the AORB shows a linear relationship. Thus, the rejuvenator type affects the restoration level and the variation trend of τ parameter of rejuvenated bitumen to rejuvenator content.
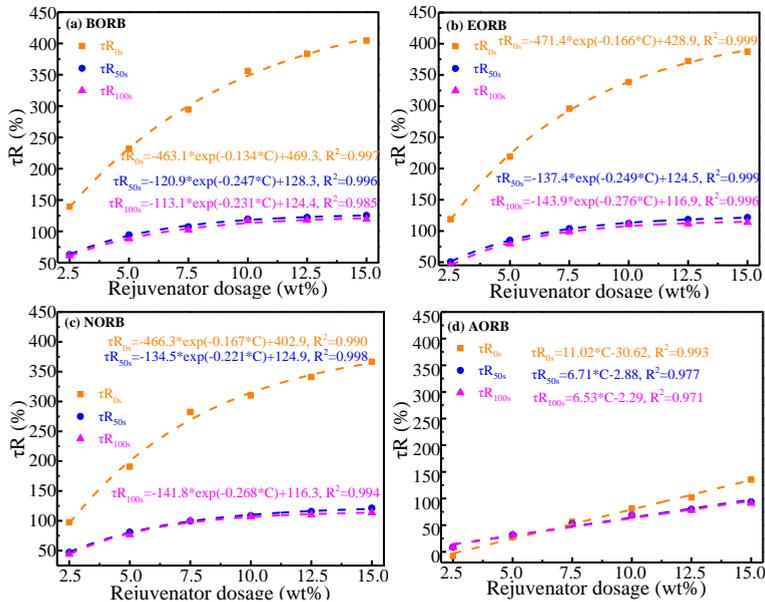
Figure 7.18 Influence of rejuvenator dosage on τR value of LAB40 rejuvenated bitumen

The aging degree of bitumen influences the τR value and its sensitivity to rejuvenator dosage, but the ranking of rejuvenation efficiency on τ value for four rejuvenators remains constant. Meanwhile, the variation trends (exponentially or linearly) of τR values of rejuvenated bitumen to rejuvenator dosage are independent of the aging degree of bitumen. The difference in τR$_{50s}$ and τR$_{100s}$ values of LAB20 rejuvenated bitumen is apparent, which cannot be detected in LAB40 and LAB80 cases. The increased aging degree reduces the τR values of rejuvenated binders but enlarges its sensitivity level to rejuvenator dosage based on the parameters of correlation equations shown in **Table 7.2**. Although these three τ parameters can reflect the rejuvenation effects of various rejuvenators, the scope of τR$_{0s}$ (0-700%) and τR$_{100s}$ (-150-150%) deviates from the complex modulus G*-based rejuvenation percentages (0-150%). Therefore, the τ$_{50s}$ is preferred as the most effective

parameter for rejuvenation efficiency evaluation on the shear stress of rejuvenated bitumen during the relaxation process.

Table 7.2 The correlation equations of τR-C curves of various rejuvenated binders

Samples		τR_{0s}	τR_{50s}	τR_{100s}
BORB	LAB20	-733*exp(-0.200*C) +738	-155*exp(-0.371*C) +153	-503*exp(-0.409*C) +238
	LAB40	-463*exp(-0.134*C) +469	-121*exp(-0.247*C) +128	-113*exp(-0.231*C) +124
	LAB80	-277*exp(-0.127*C) +302	-86*exp(-0.218*C) +111	-84*exp(-0.204*C) +110
EORB	LAB20	-765*exp(-0.166*C) +793	-153*exp(-0.271*C) +158	-396*exp(-0.279*C) +231
	LAB40	-471*exp(-0.166*C) +429	-137*exp(-0.249*C) +125	-144*exp(-0.276*C) +117
	LAB80	-265*exp(-0.147*C) +280	-88*exp(-0.194*C) +108	-85*exp(-0.201*C) +105
NORB	LAB20	-716*exp(-0.161*C) +689	-159*exp(-0.286*C) +141	-445*exp(-0.328*C) +179
	LAB40	-466*exp(-0.167*C) +403	-135exp(-0.221*C) +125	-142*exp(-0.268*C) +116
	LAB80	-284*exp(-0.085*C) +310	-89*exp(-0.146*C) +109	-85*exp(-0.150*C) +106
AORB	LAB20	16.51*C+58.75	9.00*C+16.71	25.27*C-162.2
	LAB40	11.02*C-30.62	6.71*C-2.88	6.53*C-2.29
	LAB80	4.61*C+27.39	3.38*C+33.23	3.35*C+33.31

7.4.4.2 Relaxation time-based rejuvenation percentage (tR)

The rejuvenation percentages based on relaxation times tR of rejuvenated bitumen are displayed in **Figure 7.19**. The increased rejuvenator dosage promotes the enlargement of tR values, and exponential relationships are observed. The BORB and AORB exhibit the largest and smallest tR parameters, respectively. It means that the bio-oil shows the greatest potential to restore the relaxation performance of aged bitumen, while the aromatic-oil has the lowest effect, which agrees well with the τR results.
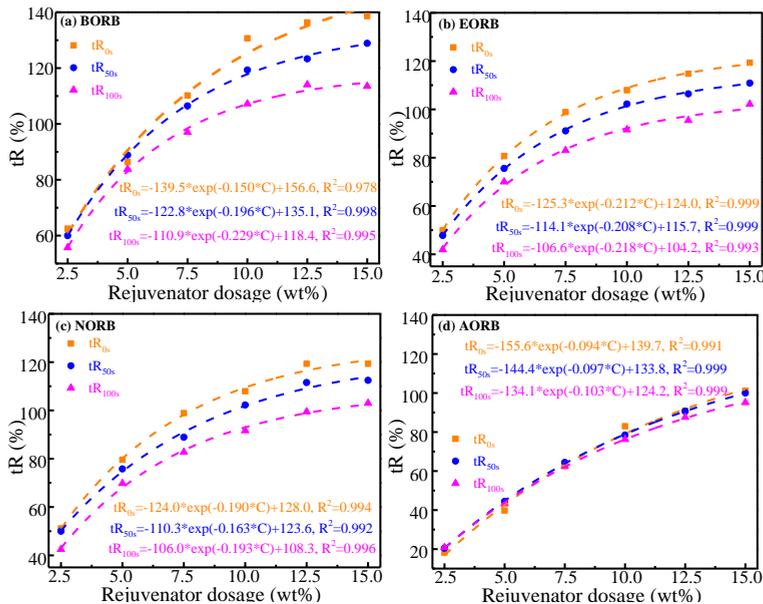
Figure 7.19 Influence of rejuvenator dosage on tR value of LAB40 rejuvenated bitumen

Moreover, the tR values of EORB and NORB binders are between BORB and AORB. The tR values of all rejuvenated bitumen tend to decrease as the residue stress ratio reduces, especially at high rejuvenator dosage. However, the difference in tR$_{75\%}$, tR$_{50\%}$, and tR$_{25\%}$ of AORB binders is insignificant. Further, the rejuvenator type and residue stress ratio affect the sensitivity level of the tR parameter to rejuvenator dosage

based on the exponential parameters in correlation equations. For BORB and AORB binder, the influence degree of rejuvenator dosage on tR values shows a decreasing trend with a reduction of residue stress ratio, which first increases and then declines for EORB and NORB. Additionally, this phenomenon is more obvious for BORB. Interestingly, the AORB binder exhibits the lowest tR but the highest dependence on rejuvenator dosage. Meanwhile, the residue stress ratio affects the sensitivity level of tR to rejuvenator content for BORB, EORB, and NORB.

Table 7.3 The correlation equations of tR-C curves of various rejuvenated binders

Samples		$tR_{75\%}$	$tR_{50\%}$	$tR_{25\%}$
BORB	LAB20	-790*exp(-0.189*C) +504	-607*exp(-0.239*C) +392	-461*exp(-0.291*C) +250
	LAB40	-140*exp(-0.150*C) +157	-123*exp(-0.198*C) +135	-111*exp(-0.229*C) +118
	LAB80	-89*exp(-0.186*C) +112	-75*exp(-0.196*C) +105	-65*exp(-0.197*C) +101
EORB	LAB20	-549*exp(-0.261*C) +328	-492*exp(-0.267*C) +268	-412*exp(-0.289*C) +189
	LAB40	-125*exp(-0.212*C) +429	-114*exp(-0.208*C) +116	-107*exp(-0.218*C) +104
	LAB80	-65*exp(-0.182*C) +92	-60*exp(-0.174*C) +90	-55*exp(-0.176*C) +88
NORB	LAB20	-569*exp(-0.194*C) +354	-522*exp(-0.245*C) +262	-409*exp(-0.249*C) +176
	LAB40	-124*exp(-0.190*C) +128	-110*exp(-0.170*C) +124	-106*exp(-0.193*C) +108
	LAB80	-81*exp(-0.156*C) +98	-73*exp(-0.163*C) +93	-70*exp(-0.161*C) +92
AORB	LAB20	-529*exp(-0.099*C) +318	-509*exp(-0.115*C) +279	-429*exp(-0.123*C) +212
	LAB40	-156*exp(-0.094*C) +261	-144*exp(-0.097*C) +134	-134*exp(-0.130*C) +124
	LAB80	-219*exp(-0.014*C) +141	-88*exp(-0.056*C) +126	-66*exp(-0103*C) +98

All the correlation equations for tR-C curves are listed in **Table 7.3**. Irrespective of the bitumen's aging degree, the order of the tR parameter for rejuvenated bitumen follows BORB > EORB ≈ NORB > AORB. However, the aging level significantly influences the tR value and its variation concerning the content of the rejuvenator. As the bitumen's aging deepens from LAB20 to LAB40 and LAB80, the restorative impact of all rejuvenators on relaxation time weakens, and the tR values become more responsive to changes in the rejuvenator dosage. It's worth noting that the three parameters ($tR_{75\%}$, $tR_{50\%}$, $tR_{25\%}$) can reasonably reflect the efficiency of various rejuvenators in restoring relaxation times in aged bitumen. Although there are differences, especially with AORB, these three relaxation time parameters can effectively gauge the evaluation of rejuvenation efficiency in terms of relaxation behavior.

The order of rejuvenation efficiency for relaxation time recovery remains constant across all relaxation time parameters for the four rejuvenators. Thus, it is advisable to select a relaxation time parameter with a single residue stress ratio to assess rejuvenation efficiency. In this thesis, the $t_{25\%}$ index is chosen as the most effective evaluation indicator because it encapsulates the majority of relaxation behavior in rejuvenated bitumen. It's important to emphasize that the relaxation time parameter should remain consistent to discern variations in the rejuvenation efficiency of relaxation performance in blends of various rejuvenator-aged bitumen while accounting for the influence of residue stress ratio.

7.4.4.3 Stress ratio-based rejuvenation percentage (RR)

The increasing variations of RR values at relaxation times of 50 and 100s as a function of rejuvenator dosage are observed in **Figure 7.20**. The RR parameter and its variation trend of rejuvenated bitumen depend on the rejuvenator type/dosage and relaxation time. The RR_{50s} values of rejuvenated bitumen enlarge linearly as the rejuvenator content rises. Moreover, the RR_{100s} parameter of BORB and AORB also show a linearly increasing trend, while the EORB and NORB binders present exponential relationships. However, the difference in RR_{50s} and RR_{100w} indices of rejuvenated bitumen is not tremendous, particularly for BORB and EORB binders. Within the whole rejuvenator dosage scope, the BORB has the highest RR value, indicating that the bio-oil rejuvenator can maximally restore the relaxation stress ratio of aged bitumen. Additionally, the RR_{50s} values of EORB and NORB are larger than the AORB, and the former is slightly smaller. Nevertheless, the RR_{100s} of

AORB with high rejuvenator content are higher than those of NORB and EORB binders. In other words, the magnitude of RR_{100s} for four rejuvenators depends on the rejuvenator dosage. Thus, it is not appropriate to use the R_{100s} parameter to estimate the rejuvenation efficiency of various rejuvenators on the relaxation performance of aged bitumen, and the R_{50s} index is more effective. Further, the magnitude of the increasing rate of RR_{50s} is AORB > NORB > BORB > EORB. It also will change the RR_{50s} ranking of various rejuvenated bitumen when the rejuvenator dosage breaks through a certain value.
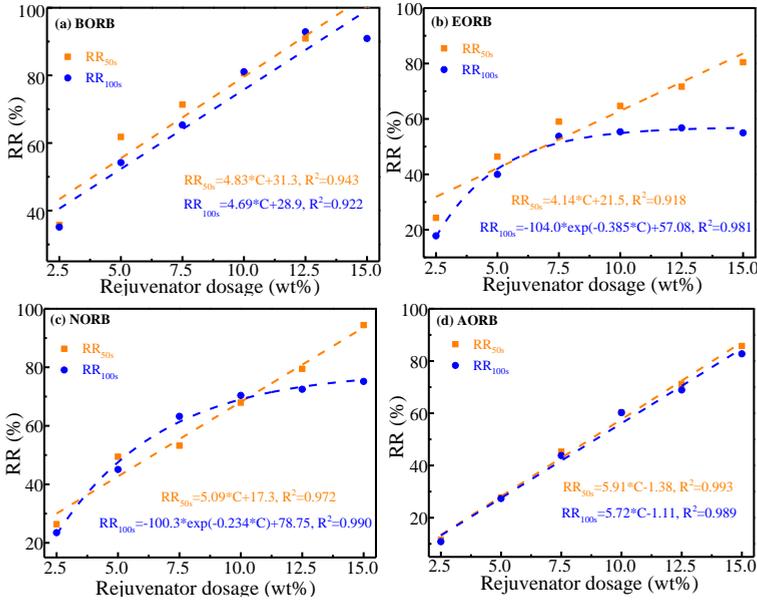
Figure 7.20 Influence of rejuvenator dosage on RR value of LAB40 rejuvenated bitumen

Table 7.4 The correlation equations of RR-C curves of various rejuvenated binders

Samples		RR_{50s}	RR_{100S}
BORB	LAB20	30.95*C-112.6	-514*exp(-0.234*C) +258
	LAB40	4.83*C+31.3	4.69*C+28.9
	LAB80	3.49*C+32.56	3.93*C+29.83
EORB	LAB20	30.26*C-155.6	-240*exp(-0.503*C) +14
	LAB40	4.14*C+21.5	-104*exp(-0.385*C) +57
	LAB80	2.62*C+23.50	2.78*C+22.65
NORB	LAB20	22.82*C-170.0	21.93*C-165.2
	LAB40	5.09*C+17.3	-100*exp(-0.234*C) +79
	LAB80	2.64*C+20.47	2.75*C+19.78
AORB	LAB20	24.9*C-185.4	-316*exp(-0.177*C) +90
	LAB40	5.91*C-1.38	5.72*C-1.11
	LAB80	3.57*C+21.15	3.53*C+21.18

Irrespective of the aging degree, the RR_{50s} of all rejuvenated binders increase linearly versus the rejuvenator content. However, the variation law (linearly or exponentially) of RR_{100s} depends on the aging level and rejuvenator type. When the aged bitumen is LAB80, the RR_{50s} and RR_{100s} parameters show a linearly increasing trend to rejuvenator dosage, while the difference in RR_{50s} and RR_{100s} values is limited. It indicates that the influence of relaxation time on the RR parameter of aged bitumen has disappeared at a high aging

level. Because of the consistency to variation law, the R_{50s} is more appropriate to effectively evaluate the rejuvenation efficiency of different rejuvenator-aged bitumen blends than the R_{100s} parameter. The correlation equations of RR-C curves are listed in **Table 7.4**. As the aging level increases, the RR_{50s} values and relative sensitivity to rejuvenator dosage of rejuvenated bitumen tend to decrease significantly. The order of RR_{50s} of rejuvenated bitumen (BORB > NORB > EORB > AORB) remains constant as the change of aging level, which affects the magnitude of slope values. It may result in an order variation of RR_{50s} values of rejuvenated binders at a higher rejuvenator dosage. This phenomenon is not observed in the aforementioned τR and tR cases.

7.4.5 Influence of aging and rejuvenation on the relaxation model of bitumen

It was reported [56, 65] that the relaxation behavior of bitumen can be described by the stress relaxation model based on thermodynamic theory as below:

$$\tau = \frac{ut^{1-n}}{\epsilon m(1-n)} = \frac{At^{1-n}}{\epsilon} \tag{7.10}$$

where A and n are the material parameters, τ and ε are shear stress and strain, and t denotes relaxation time.

As shown in **Figure 7.21**, the parameters A and n relaxation model of bitumen increase and decrease linearly as the long-term aging time extends. In addition, the magnitude and sensitivity of the A parameter to aging time are greater than the parameter n. The correlation equations between aging time t with parameters A and n can be utilized to predict the relaxation curves of aged bitumen with other long-term aging degrees.
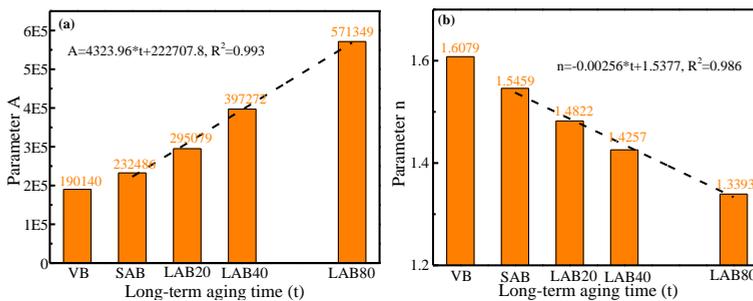
Figure 7.21 Influence of long-term aging time on parameters A and n
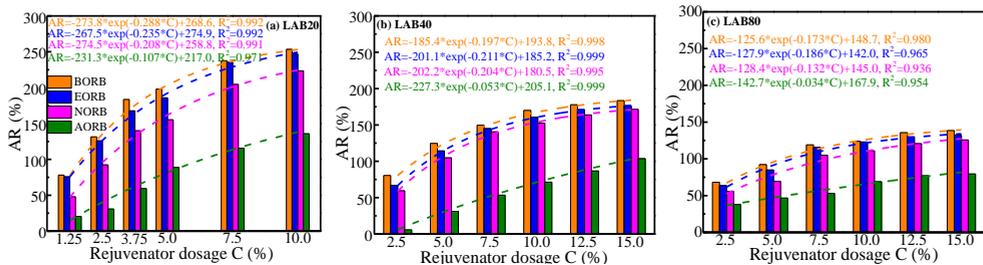
Figure 7.22 Influence of rejuvenator dosage on AR value of rejuvenated bitumen

The A-based rejuvenation percentage (AR) of rejuvenated bitumen is illustrated in **Figure 7.22**. The AR values present exponentially increasing trends as a function of rejuvenator content. The BORB exhibits the largest AR values for all aged binders, followed by the EORB and NORB, and the AORB shows the lowest AR parameter. It implies that the bio-oil rejuvenator can maximally restore the A value in the relaxation model equation of aged bitumen, whereas aromatic-oil displays the smallest rejuvenation efficiency on the A

parameter. Additionally, the rejuvenation effectiveness of engine-oil and naphthenic-oil rejuvenators is in the middle, and the former has a greater value. As the aging level deepens, the AR values of rejuvenated binders remarkably decrease, indicating that the rejuvenation efficiency of rejuvenators on the A parameter is lower in an aged bitumen with a higher aging degree. It should be mentioned that rejuvenators can restore the A parameter with increased sensitivity to rejuvenator type/dosage and aging level of bitumen. Therefore, the A parameter can be an effective index for evaluating the rejuvenation efficiency of various rejuvenator-aged bitumen blends.
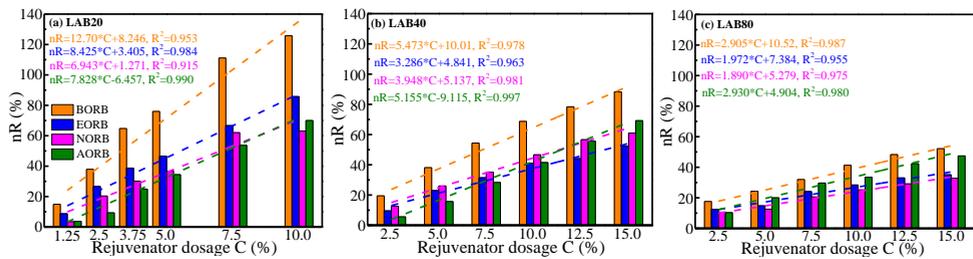
Figure 7.23 Influence of rejuvenator dosage on nR value of rejuvenated bitumen

The correlation curves between rejuvenator dosage and nR values of various rejuvenated binders are plotted in **Figure 7.23**. It is observed that the nR values increase linearly as the rejuvenator dosage rises. The bio-oil rejuvenated bitumen has the largest nR value. In contrast, the magnitude of the nR parameter for engine-oil, naphthenic-oil, and aromatic-oil rejuvenated binders significantly depends on the rejuvenator content and aging level of bitumen. Overall, the n parameter can effectively differentiate the rejuvenation efficiency of bio-oil from the others, but it fails to distinguish the engine-oil, naphthenic-oil, and aromatic-oil rejuvenators because of the high dependence of nR value to the aging state of bitumen.

7.4.6 Further discussion on critical relaxation parameters

The main goal of this study is to propose the reprehensive and effective parameters for evaluating the rejuvenation efficiency on relaxation behavior of various rejuvenator-aged bitumen blends. The sensitive level of different parameters to rejuvenator type/dosage and aging level is assessed and compared to determine the effective evaluation indicators for changeable rejuvenation conditions.

Table 7.5 Analysis of critical relaxation indicators for rejuvenation efficiency evaluation

Items	τ_{0s}	τ_{50s}	τ_{100s}	$t_{75\%}$	$t_{50\%}$	$t_{25\%}$	R_{50s}	R_{100s}	A	n
Recovery possibility	O	O	O	O	O	O	O	O	O	O
Sensitivity to rejuvenator-type	O	O	O	O	O	O	X	X	O	X
Sensitivity to rejuvenator dosage	O	O	O	O	O	O	O	O	$\odot^{1}$	O
Sensitivity to aging level	O	O	O	O	O	O	X	X	O	X
Recovery percentage region	0-700	0-200	-150-200	0-400	0-350	0-200	0-200	0-200	0-250	0-140

A screening program (shown in **Figure 7.14(a)**) is developed to select the critical evaluation indicators, considering the rejuvenation possibility, sensitivity degree to rejuvenator type/dosage and aging level, and the scope estimation of rejuvenation percentages. **Table 7.5** lists the assessment results of different relaxation parameters in this thesis. The O and X represent the satisfied and unsatisfied results of these parameters to requirements. In addition, one specific symbol $\odot$ is shown in the sensitivity of parameter A to rejuvenator dosage. The A-based rejuvenation percentages of rejuvenated binders have an exponentially

increasing trend as rejuvenator content rises, which shows a convergence at high rejuvenator dosage. Thus, the influence level of rejuvenator content on the A parameter restoration becomes insignificant as the rejuvenator dosage extends a certain value.

It can be found all relaxation parameters can be restored by adding rejuvenators. Interestingly, all shear stress τ and relaxation time t parameters meet the sensitivity requirements to rejuvenator type/dosage and aging level of bitumen, regardless of the relaxation time and residue stress state. However, their rejuvenation percentage regions are significantly different, which are 0-700%, 0-200%, -150-200%, 0-400%, 0-350%, and 0-200% to parameters τ_{0s}, τ_{50s}, τ_{100s}, $t_{75\%}$, $t_{50\%}$, and $t_{25\%}$. The high rejuvenation percentages of τ_{0s}, $t_{75\%}$, and $t_{50\%}$ are unexpected, and the minus value of τ_{100s} is nonpreferred. Moreover, the R_{50s} and R_{100s} parameters fail to be sensitive to rejuvenator type and aging level of bitumen. The relaxation model parameter A shows a great assessment result with a rejuvenation percentage scope of 0-250%, while the order of parameter n of rejuvenated bitumen strongly depends on the rejuvenator type and aging stage of bitumen. Therefore, the parameters τ_{50s}, $t_{25\%}$, and A are recommended as effective indicators for evaluating and comparing the rejuvenation efficiency of various rejuvenators on the relaxation performance recovery of aged bitumen

7.4.7 Summary

This subchapter aims to investigate the relaxation behavior of rejuvenated bitumen and propose the critical indicators for evaluating the rejuvenation efficiency of various rejuvenators. The main conclusions and some recommendations are provided as follows:

(i) Extended periods of aging cause an increase in shear stress (τ), relaxation time (t), and residue stress ratio (R) values in bitumen, all of which tend to decrease when rejuvenators are introduced. The τ and t values in rejuvenated bitumen exhibit a linear correlation with the dosage of the rejuvenator, whereas the R-value experiences exponential growth. In terms of rejuvenation efficiency, bio-oil proves to be the most effective, followed by engine oil and naphthenic oil, with aromatic oil demonstrating the lowest effectiveness. Additionally, higher aging levels of bitumen diminish the rejuvenation effectiveness of rejuvenators in restoring the relaxation performance of aged bitumen.

(ii) The proposed relaxation model can well describe the relaxation curves of the virgin, aged, and rejuvenated binders. The magnitude of AR values for rejuvenated bitumen is BORB > EORB > NORB > AORB, but the order of nR values is not constant relying on the rejuvenator dosage and aging degree of bitumen.

(iii) All relaxation parameters of aged bitumen can be regenerated by adding rejuvenators. The τ and t parameters meet the requirements for sensitivity to rejuvenator type/dosage and aging level of bitumen with the different rejuvenation percentage scopes. However, the magnitudes of R_{50s} and R_{100s} for rejuvenated bitumen vary based on the rejuvenator type and aging degree. In addition, the rejuvenation effectiveness of various rejuvenators can be distinguished with the relaxation model parameter A but not by parameter n. Thus, the parameters τ_{50s}, $t_{25\%}$, and A are recommended as critical indicators for evaluating the rejuvenation efficiency on relaxation performance of different rejuvenator-aged bitumen blends.

7.5 Fatigue performance evaluation

7.5.1 Introduction

The main reason for the short fatigue life of reclaimed asphalt material is the internal aged bitumen with high stiffness and less relaxation capacity [66]. To address this issue, various rejuvenators have been developed to restore the chemo-rheological properties of aged bitumen, and thus its fatigue behavior would be enhanced to some extent [67]. For instance, Cao et al. [68] found that waste vegetable oil could significantly improve the workability and fatigue resistance of aged binders. Similarly, other recycling agents (such as bio-oil,

paraffinic-oil, aromatic extract, tall-oil, etc.) positively affected the fatigue life of asphalt binders and mixtures [69].

Nevertheless, the rejuvenation efficiency on fatigue properties is significantly affected by the rejuvenator types and dosages, RAP sources, and percentages [70, 71]. Santos et al. [72] mentioned that the bio-oil rejuvenator in aged bitumen showed more mass loss after aging than other rejuvenators, shortening the fatigue life of bio-rejuvenated bitumen. Meanwhile, the conclusions regarding the aging influence on the fatigue life of bitumen from different studies are still inconsistent, resulting from the difference in material characteristics, aging protocol, and fatigue strain level [73]. To develop more high-quality rejuvenators with sufficient rejuvenation effectiveness on fatigue performance recovery, evaluating and comparing the rejuvenation efficiency of different rejuvenator-aged bitumen blends is necessary. Only in this way can we improve the macroscale fatigue performance of rejuvenated bitumen by adjusting rejuvenators' physiochemical characteristics.

Table 7.6 Fatigue evaluation indices of various bituminous materials

Virgin/aged bitumen	Rejuvenator type/dosage	Fatigue indices	Ref
An extracted RAP binder (Iowa, USA)	Soybean-based rejuvenator with a dosage of 12%	$G^*\sin\delta$ and G-R	[76]
RAP/VG40 blends with R/T=0.5 and 0.7	Waste vegetable oil with dosages of 5.5% and 11.3%	Failure strain, A, B, C parameters, $N_{f2.5\%}$	[77]
SBS-modified bitumen blended with RAP (Yanjin, China)	A rejuvenator with dosages of 2%, 4%, and 6%	Fatigue failure temperature; C_1, C_2, A, B, α, τ_{max}, $N_{f2.5\%}$ and $N_{f5\%}$	[78]
RAP mixture varying from 20 to 40% (Tehran, Iran)	Date seed oil (DSO) with a 5% dosage	G^* and N_f	[79]
Aged bitumen after 20h and 40h PAV tests	Aromatic extract and waste cooking-oil with dosage varies from 3.3% to 9.2%	D_f, α, $N_{f2.5\%}$, $N_{f5\%}$, a	[80]
RAP binder (Chongqing, China)	A rejuvenator with 2%, 4%, 6%, and 8% dosages	N_{f50}, N_{DR}, N_p, N_{p20}	[81]
Polymer modified bitumen and virgin bitumen	-	$G^*\sin\delta$, G-R, ΔT_c, A and B	[82]
PG 64-22 base bitumen	Bio-oil with 1%, 3%, and 5% dosages	$G^*\sin\delta$, R, ω_c, G-R, and N_f	[83]
70# bitumen, short-term aged, and asphalt mastic with 50% mineral powder content	-	D_R and N_f	[84]
PG 58-22 bitumen modified by bio-oil, natural rock, EVA, SBS, and crumb rubber	-	Elastic recovery (ER), $G^*_{50\%}$, PA peak; S×N peak, DER, $N_{f5\%}$, $N_{f10\%}$, $N_{f15\%}$	[85]

However, the variations of rejuvenation conditions and characterization tests result in many discrepancies in the literature about rejuvenators' effectiveness in enhancing the fatigue performance of RAP binder and mixture [74, 75]. **Table 7.6** lists some cases containing variable material components and fatigue evaluation indices. Until now, various fatigue tests have been adopted to assess the fatigue performance of bitumen blends, including linear viscoelastic measurements, time sweep, linear amplitude sweep, and elastic recovery tests. For each fatigue method, different evaluation indicators are proposed to quantitatively estimate the fatigue property change of bitumen due to aging, rejuvenation, and modification. The Superpave fatigue parameter ($G^*\sin\delta$), Glover-Rowe (G-R), fatigue failure temperature, rheological index (R), and

crossover frequency (ω_c) are used as LVE fatigue indices. Moreover, the TS parameters contain fatigue life N_{f50}, N_{DR}, N_p, N_{p20}, Fatigue damage factor D_R, 50% modulus $G^*_{50\%}$, PA peak, and S×N peak. The viscoelastic continuum damage (VECD) model is always utilized to analyze the LAS results, and different parameters (like A, B, C_1, C_2, α, τ_{max}, $N_{f2.5\%}$, and $N_{f5\%}$) were chosen randomly. Furthermore, the crack width derived from LAS and TS results was also calculated as a fatigue index. It is important and expected to introduce the universal indicators for evaluating the fatigue behavior of rejuvenated binders, considering the influence factors of bitumen components, rejuvenator types/dosages, and aging levels of bitumen.

7.5.2 Fatigue evaluation methods and indices

7.5.2.1 Linear viscoelastic (LVE) measurements

The linear viscoelastic properties of both aged and rejuvenated bitumen are evaluated using a dynamic shear rheometer (DSR) in a frequency sweep test. The DSR apparatus features plates with an 8mm diameter and a 2mm gap between them. The frequency of the test ranges from 0.01 to 100 rad/s, and it is conducted at various testing temperatures, specifically 0, 10, 20, and 40°C. The strain level is held constant at 0.1% to ensure that the bitumen exhibits a linear viscoelastic (LVE) response. The test generates the fatigue parameter G*sinδ, and the value at 10 rad/s is selected to determine the temperature at which fatigue failure occurs (G*sinδ=5000 kPa). Additionally, the G-R value is calculated as:

$$G-R = \frac{|G^*|(\cos\delta)^2}{\sin\delta} \tag{7.11}$$

where G* and δ are the complex shear modulus and phase angle at 15°C and 0.005 rad/s.

7.5.2.2 Linear amplitude sweep (LAS) test

The graph illustration of applied strain variation and sample dimension of the LAS test is displayed in **Figure 7.24(a)**. The diameter and height of the bitumen specimen are 8mm and 2mm, respectively. The applied strain increases linearly from 0.1% to 30%. The temperature and frequency are selected as 20°C and 10Hz. The total loading cycle number and test time are 3100 cycles and 310s.
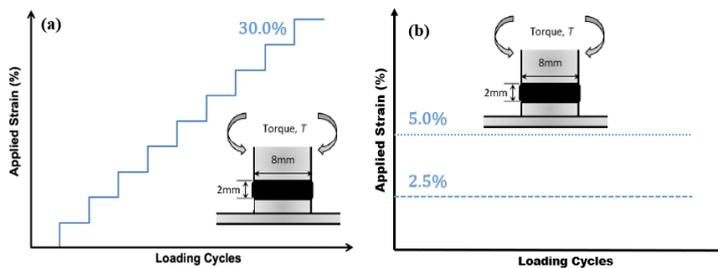
Figure 7.24 Fatigue test methods on bituminous materials

The simplified viscoelastic continuum damage (S-VECD) modelling [86] is adopted to analyze the LAS results. An internal parameter S is introduced to quantify the damaged state of bituminous materials:

$$\frac{ds}{dt} = (-\frac{\partial W^R}{\partial S})^{\propto} \tag{7.12}$$

where t refers to fatigue time, α shows a material constant related to the rate of damage accumulation, and W^R is the pseudo-strain energy density calculated as follows:

$$W^R = \frac{1}{2}C(S)(\gamma^R)^2 \tag{7.13}$$

The C function represents the pseudo stress quantitatively describing material integrity, defined as the ratio of peak stress τ_p and pseudo strain amplitude γ^R. In addition, the γ^R parameter is defined as below:

$$\gamma^R = \frac{(\gamma_p \cdot G^*_{LVE})}{G_R} \tag{7.14}$$

where γ_p shows the strain amplitude in a fatigue cycle, G_R and G^*_{LVE} are the arbitrary reference modulus and linear viscoelastic shear modulus. Thus, the C function can be rewritten as:

$$C(S) = \frac{\tau_p \cdot G_R}{(\gamma_p \cdot G^*_{LVE})} \tag{7.15}$$

Meanwhile, the damage state parameter S can be derived as follows:

$$S(t) = \sum_{i=1}^{N} \left[\frac{1}{2} (\gamma^R)^2 (C_{i-1} - C_i) \right]^{\frac{\alpha}{\alpha+1}} \cdot (t_i - t_{i-1})^{\frac{1}{\alpha+1}} \tag{7.16}$$

where N and i are the load cycles and the cycle number. A power law model is adopted to describe the correlation between the material integrity C and damage parameter S shown in **Eq.7.17**. The C_1 and C_2 are the constants.

$$C(S) = 1 - C_1 \cdot S^{C_2} \tag{7.17}$$

Based on the above equations, the fatigue life N_f of bituminous material can be predicted from the strain amplitude γ_p using **Eq.7.18**.

$$N_f = \frac{f \cdot 2^\alpha \cdot S_f^{1-\alpha C_2 + \alpha}}{(1 - \alpha C_2 + \alpha)(C_1 C_2)^\alpha (\gamma_p \cdot G^*_{LVE})^{2\alpha}} \tag{7.18}$$

where f refers to the fatigue frequency, and S_f is the damage at a failure point calculated as:

$$S_f = \left(\frac{1 - C_f}{C_1}\right)^{\frac{1}{C_2}} \tag{7.19}$$

The C_f is the C parameter at the failure point reaching the peak stress. For simplification, the **Eq.7.18** can be rewritten as follows:

$$N_f = A(\gamma_p)^B \tag{7.20}$$

where B=-2α and A represent the term displayed in **Eq.7.21**, k=1-αC$_2$+α.

$$A = \frac{f \cdot 2^\alpha \cdot S_f^k}{k(C_1 C_2)^\alpha (G^*_{LVE})^{2\alpha}} \tag{7.21}$$

7.5.2.3 Time sweep (TS) test

From **Figure 7.24(b),** 2.5% and 5.0% constant strain levels are applied to perform the TS tests at 20°C. The frequency is 10Hz, and the DSR specimen size is the same as the LVE test. At least two parallel specimens are measured for all LVE, LAS, and TS tests to ensure data reliability.

During the fatigue life, three stages of material integrity variation contain (i) No damage; (ii) Crack initiation; and (iii) Crack propagation. The cumulative dissipated energy ratio (DER) can clearly distinguish these three stages, calculated as **Eq.7.22**.

$$DER_n = \frac{\sum_{i=1}^{n} W_i}{W_n} \tag{7.22}$$

where W_i and W_n are the dissipated energies (DE) at the i and n fatigue cycles. And **Eq.7.23** is used to calculate the DE value.

$$W_i = \pi\tau_{0,i}\gamma_{0,i}\sin(\delta_i) \tag{7.23}$$

where $\tau_{0,I}$ and $\gamma_{0,I}$ are the stress and strain amplitudes in the ith cycle.

In the TS test, the variations of shear modulus G^* and DER values of bitumen as a function of the loading cycle are detected to measure the fatigue life. The N_{p20} parameter is always used as a failure criterion, defined as the number of loading cycles when the DER value is 20% higher than the corresponding point on the equality line. In addition, the N_{p20} shows an exponential relationship with the initial DE (W_0) values, as displayed in **Eq.7.24**.

$$N_{p20} = K_2\left(\frac{1}{W_0}\right)^{K_1} \tag{7.24}$$

where K_1 and K_2 are the fitting parameters, and it should be noted that the N_{p20} parameter corresponds to the demarcation point between the No damage and Crack initiation stages without considering the Crack propagation part. **Table 7.7** summarizes the test conditions and evaluation indicators of bitumen fatigue performance adopted in this dissertation.

To quantitatively estimate the rejuvenation efficiency of various rejuvenators on the fatigue properties of aged bitumen, a fatigue rejuvenation percentage index (FR) is introduced and calculated as follows:

$$FR = \frac{F_{aged} - F_{rejuvenated}}{F_{aged} - F_{virgin}} * 100 \tag{7.25}$$

where FR is the fatigue rejuvenation percentage, and F represents the fatigue indices in **Table 7.7**. Moreover, the F_{virgin}, F_{aged}, and $F_{rejuvenated}$ are the fatigue indices of the virgin, aged, and rejuvenated binders, respectively.

Table 7.7 Test conditions and evaluation indices of bitumen fatigue performance

Item	Fatigue tests	Conditions	Parameters
1	LVE test	Frequency sweep at 15 °C and 0.005 rad/s	G-R
		Frequency sweep from 10^{-2}-10^2 rad/s at 0, 10, 20, 30, and 40 °C	$G^*\sin\delta$, Fatigue failure temperature
2	LAS test	Linear amplitude sweep at 20°C and 10 Hz with the strain increasing linearly from 0.1% to 30%	τ-γ curves (f_{se}, ε, f_{sr}, E, G_{se}, G_{sl}, and G_{st}); C-S curves (C_1 and C_2); N_f; N_f-γ_p curves (α, k, $G^*\sin\delta_{initial}$, S_f, A, and B)
3	TS test	Strain-controlled time sweep with 2.5% and 5% strain levels at 20°C and 10 Hz	G^*-N curves ($N_{p50\%}$ and δ_{peak}); DER-N curves (N_{p20} and W_0); Crack width C-N curves (C_{500}, C_{1500}, C_{3000})

7.5.3 Linear viscoelastic parameters

7.5.3.1 G-R parameter

The G-R results of virgin and aged bitumen are displayed in **Figure 7.25**. The G-R values increase exponentially as the aging degree deepens, especially for the LAB80 binder. The increment in complex modulus G^* and decrease of phase angle δ result in the high G-R value of aged bitumen. The exponential correlation formula between the G-R and aging time with a high R^2 value of 0.999 can predict the G-R values of aged binders with other aging levels.
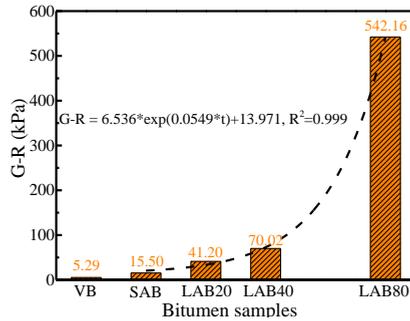
Figure 7.25 The variation of the G-R parameter of bitumen

The G-R-based rejuvenation percentages (G-RR) of rejuvenated binders are presented in **Figure 7.26**. A higher rejuvenator dosage leads to a larger G-RR value of rejuvenated bitumen. An exponential relationship between the G-RR and C parameters is observed for all rejuvenation cases. It indicates that the positive effect of rejuvenator content on G-R recovery of aged bitumen reduces gradually as more rejuvenator is added. The rejuvenator type and aging degree significantly affect the G-RR values and its variation trend versus rejuvenator dosage. The bio-oil and aromatic-oil show the strongest and smallest rejuvenation efficiency on the G-R value of aged bitumen. The engine-oil and naphthenic-oil rejuvenators have similar effects. Meanwhile, a high aging degree of bitumen results in a low rejuvenation efficiency on G-R value. Interestingly, the G-RR values of AORB and NORB binders are much closer in LAB80, indicating that aromatic-oil exhibits a significant rejuvenation efficiency in restoring the G-R value of aged bitumen with severe aging degrees.
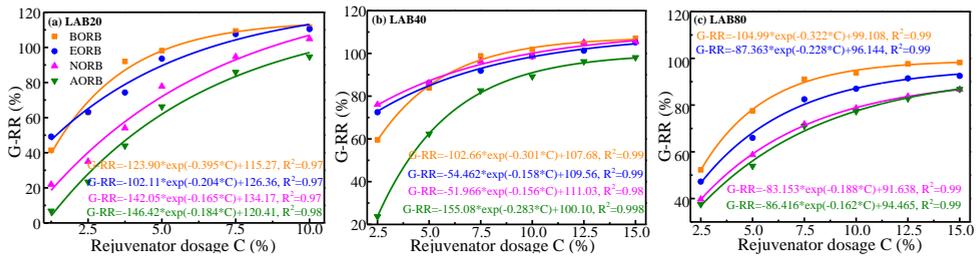
Figure 7.26 Influence of rejuvenator dosage on G-RR value of rejuvenated bitumen

7.5.3.2 G*sinδ parameter

The LVE fatigue parameter G*sinδ results of virgin and aged bitumen are displayed in **Figure 7.27(a)** at different temperatures.
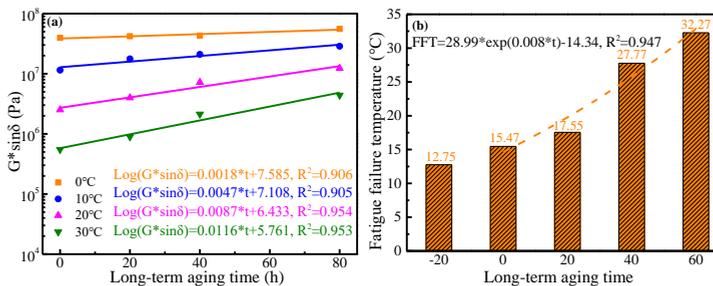
Figure 7.27 Aging effect on LVE fatigue characteristics of bitumen

It is obvious that long-term aging promotes the increase in G*sinδ of bitumen and reduces its temperature sensitivity. The Log(G*sinδ) of bitumen shows a linearly increasing trend as the aging level extends, and its sensitivity to the long-term aging time enlarges as the temperature rises. The fatigue failure temperatures (FFT) are defined as one temperature when the G*sinδ value equals 5000kPa, as presented in **Figure 7.27(b)**. As the aging time is prolonged, the FFT value of bitumen increases exponentially, implying that the fatigue resistance of bitumen deteriorates during the long-term aging time [51].

The G*sinδ-based rejuvenation percentages (FPR) of rejuvenated binders are illustrated in **Figure 7.28**. The FPR parameters for all rejuvenated bitumen samples exhibit a linear increase in response to the dosage of the rejuvenator. This trend indicates that all rejuvenators have a rejuvenating effect on enhancing the fatigue performance of aged bitumen. However, the efficiency of this rejuvenation is significantly influenced by both the type of rejuvenator and the degree of bitumen aging. The order of FPR values for all rejuvenated binders is as follows: AORB < NORB < EORB < AORB. This ranking implies that the addition of bio-oil results in the most substantial regeneration of the fatigue performance of aged bitumen, followed by engine-oil and naphthenic-oil rejuvenators. In contrast, the rejuvenation efficiency of the aromatic-oil rejuvenator is the lowest.

As the aging level increases, the sensitivity of FPR to the rejuvenator dosage diminishes, leading to a decrease in the FPR values of the rejuvenated binders. This suggests that the rejuvenation efficiency of the rejuvenators on the fatigue parameters weakens as the degree of aging becomes more pronounced. Furthermore, the ranking of the rejuvenation efficiency of the four rejuvenators to the fatigue parameter remains consistent regardless of aging level or rejuvenator dosage. This underscores the effectiveness of G*sinδ as a reliable metric for quantitatively assessing and distinguishing the rejuvenation efficiency of rejuvenators in restoring the fatigue performance of aged bitumen.
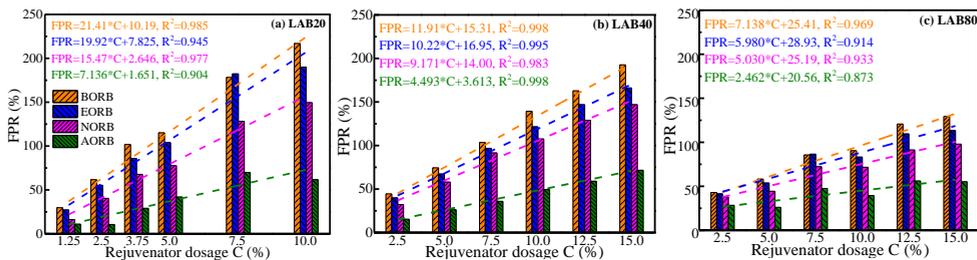
Figure 7.28 Influence of rejuvenator dosage on FPR value of rejuvenated bitumen

7.5.3.3 Fatigue failure temperature (FFT)

The FFT-based rejuvenation percentages (FFTR) of all rejuvenator-aged bitumen blends are drawn in **Figure 7.29**. The linear variation law of FFTR to the rejuvenator dosage is similar to the FPR parameter. Regardless of rejuvenator dosage and aging grade, the ranking of FFTR values of rejuvenated binders is AORB < NORB < EORB < BORB. Similar to the G*sinδ, the roles of rejuvenator type/dosage and aging degree of bitumen in affecting the rejuvenation efficiency on the fatigue performance can be recognized with the FFT index. Although the G-R value of aged bitumen can be restored by adding rejuvenators, the magnitude of G-RR for four rejuvenators varies greatly versus the rejuvenator content and aging degree of bitumen. Thus, the G-R fails to be a critical LVE index for rejuvenation efficiency evaluation on fatigue property. The G*sinδ and FFT parameters meet the requirement, but choose one of them because of high similarity. Due to the temperature independence, the FFT is recommended as the evaluation index for the LVE fatigue performance of various rejuvenator-aged bitumen systems.
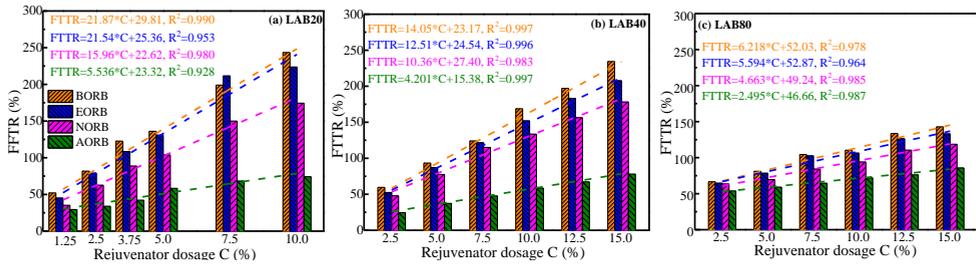
Figure 7.29 Influence of rejuvenator dosage on FFTR value of rejuvenated bitumen

7.5.4 LAS test parameters

7.5.4.1 Shear stress-strain curves and derived parameters

The shear stress-strain curves of virgin and aged bitumen during the LAS tests are shown in **Figure 7.30(a)**. As the shear strain rises from 0.1% to 30%, the corresponding stress increases to a maximum point and decreases gradually. Long-term aging significantly affects the stress-strain response of bitumen. As the aging degree extends, the stress-strain curve of bitumen becomes narrower and taller. The increased maximum stress of bitumen is associated with the high stiffness of aged bitumen, and a high aging degree promotes the strain sensitivity of the shear stress. Although the peak value of bitumen stress is enhanced, a high aging degree accelerates fatigue damage of bitumen. To quantitatively reflect the effects of aging and rejuvenation on the stress-strain response of bitumen, the stress-strain curve is divided into three pieces: the elastic stage, the stress accumulation stage, and the localized cracking [87], illustrated in **Figure 7.30 (b)**. These evaluation indices derived from the strain-stress curve are the f_{se}, f_{sr}, ε_{se}, ε_{sr}, E, G_{se}, G_{ss}, and G_{sl}. The f_{se} and ε_{se} are the maximum elastic stress and strain in the elastic stage, and the E parameter refers to the elastic modulus ($E = f_{se}/\varepsilon_{se}$). Moreover, the f_{sr} and ε_{sr} represent the peak stress and strain. The fracture energies at different stages are derived as follows:

$$
\left[
\begin{aligned}
G_{se} &= \int_0^{\varepsilon_{se}} f(\varepsilon)\, d\varepsilon \\[2mm]
G_{ss} &= \int_{\varepsilon_{se}}^{\varepsilon_{sr}} f(\varepsilon)\, d\varepsilon \\[2mm]
G_{sl} &= \int_{\varepsilon_{sr}}^{\varepsilon_{st}} f(\varepsilon)\, d\varepsilon
\end{aligned}
\right.
\tag{7.26}
$$
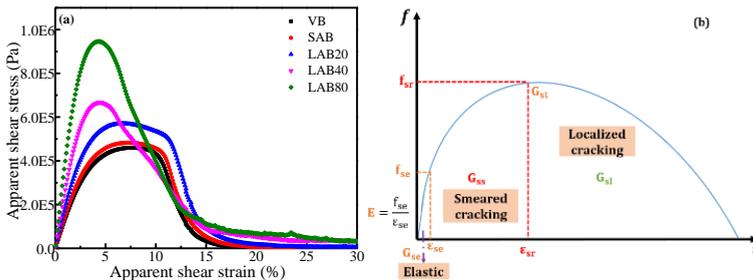
Figure 7.30 The stress-strain (f-ε) curves of virgin/aged bitumen (a) and evaluation indicators (b)

The effects of long-term aging time on the stress-strain curve parameters of bitumen are shown in **Figure 7.31**. Linear relationships between the aging time with these parameters are observed, which can be used to predict the aged bitumen's stress-strain curves with various aging degrees. As the aging level deepens,

the $Log(f_{se})$ and $Log(f_{sr})$ values tend to increase linearly, and the f_{se} parameter shows greater sensitivity to the aging time. The ε_{se} of all virgin and aged bitumen are similar, but the ε_{sr} value reduces linearly as the aging time extends. It indicates that long-term aging does not influence the elastic region but weakens the bitumen's stress accumulation capacity. Moreover, the elastic modulus E of bitumen significantly enlarges due to the increased aging level. Further, the fracture energies G_{se} and G_{sl} of bitumen show a distinct increasing trend as aging time prolongs, but the G_{ss} value decreases linearly. It suggests that long-term aging improves the elastic performance and local fracture energy but shortens the cracking time. Due to the low sensitivity of ε_{se} and G_{ss} to aging, these two parameters will not be considered while evaluating the rejuvenation effects on the stress-strain curve of aged bitumen.
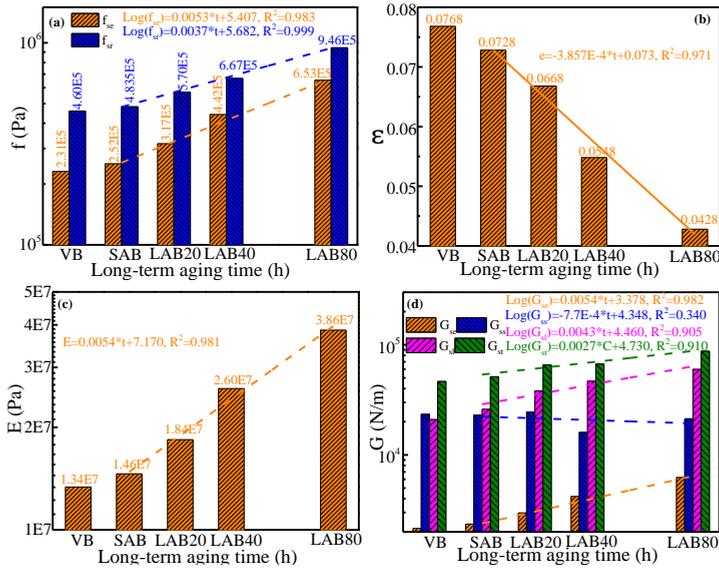
Figure 7.31 Effects of long-term aging on stress-strain curve parameters

The stress-strain curve parameters-based rejuvenation percentages of LAB40 rejuvenated bitumen are plotted in **Figure 7.32**, showing a linear increasing trend as the rejuvenator content increases. It indicates that these four rejuvenators can restore all aged bitumen stress-strain curve parameters, but the rejuvenator and evaluation index types affect the rejuvenation efficiency. The bio-oil and aromatic-oil rejuvenated binders exhibit the largest and smallest rejuvenation percentages. Meanwhile, the engine-oil and naphthenic-oil show moderate rejuvenation efficiency, much better than the aromatic-oil. However, some overlap sections in the f_{sr}R-C and G_{se}R-C curves of BORB and EORB at high rejuvenator dosages and the G_{sl}R-C curves of EORB and NORB are observed. Therefore, these parameters are not the first choice for evaluating and distinguishing the rejuvenation efficiency of various rejuvenators on the stress-strain response. Conversely, the f_{se}, ε_{sr}, and E parameters work well. Various rejuvenators have different rejuvenation percentages on these parameters. The percentage regions for f_{se}, ε_{sr}, f_{sr}, E, G_{se}, and G_{sl} of all rejuvenator-aged bitumen blends are 0-310%, 0-600%, 0-400%, 0-320%, 0-300%, and 0-200%, respectively. The ε_{sr}R scope is much wider than the others, and the f_{se}R and ER ranges are similar to the other parameters. Overall, the ε_{sr}, f_{se}, and E parameters derived from the stress-strain curves can effectively evaluate the rejuvenation efficiency of various rejuvenators on the fracture potential of all rejuvenator-aged bitumen systems.
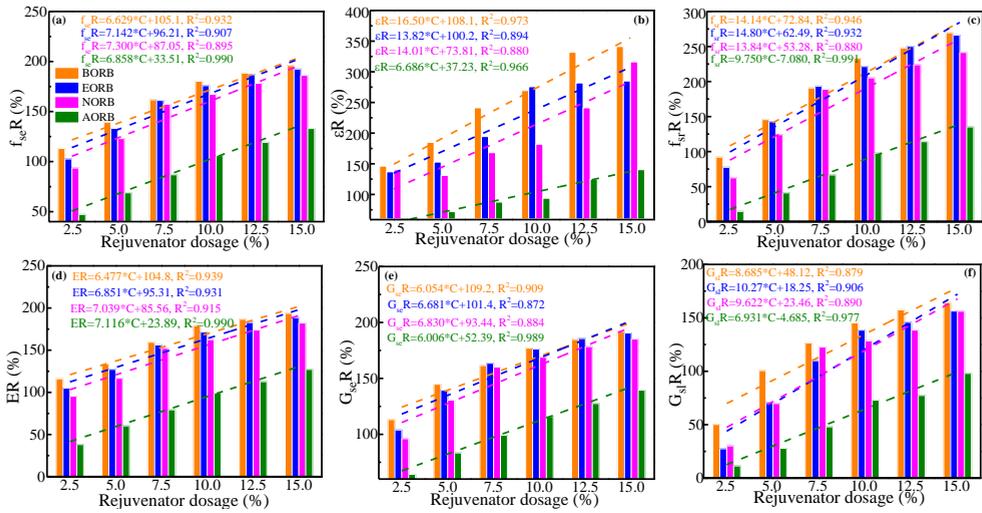
Figure 7.32 Rejuvenation effect on strain-stress parameters of aged bitumen

7.5.4.3 C-S curves and derived parameters

The C-S curves and correlation formulas of virgin and aged bitumen are presented in **Figure 7.33(a)**. As the damage intensity S rises, the C value decreases gradually. A high aging degree accelerates the reduction trend of the C parameter. It shows that the deterioration level of bitumen intensifies as the long-term aging time is prolonged. The influence of aging on the constants C_1 and C_2 of C-S curves is depicted in **Figure 7.33(b)**. As the aging time extends, the C_1 value rises, but the C_2 parameter declines linearly. It implies that a high aging degree intensifies the deterioration rate of material integrity but relieves its sensitivity to the damage intensity S of bitumen, revealing that the aging degree enlarges the destruction threshold but promotes the damage rate.
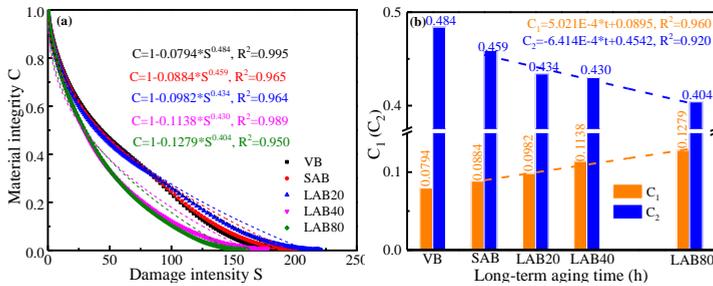
Figure 7.33 Aging effect on C-S curves and model parameters

The C_1 and C_2 values and their rejuvenation percentages (C_1R and C_2R) of rejuvenated bitumen are displayed in **Figure 7.34**, showing linear relationships with the rejuvenator dosage. C_1 and C_2 correlate negatively and positively with increased rejuvenator content. This variation trend is the opposite of the aging case, indicating that including rejuvenators dramatically improves the C-S response of aged bitumen. The rejuvenation efficiency of various rejuvenators on C_1 and C_2 parameters are different. In detail, the magnitude of C_1R values is BORB > NORB > EORB > AORB, while the order of the C_2R parameter follows BORB > AORB > NORB > EORB. Therefore, neither one can fully reflect the rejuvenation efficiency of different rejuvenators on the C-S curve of aged bitumen.
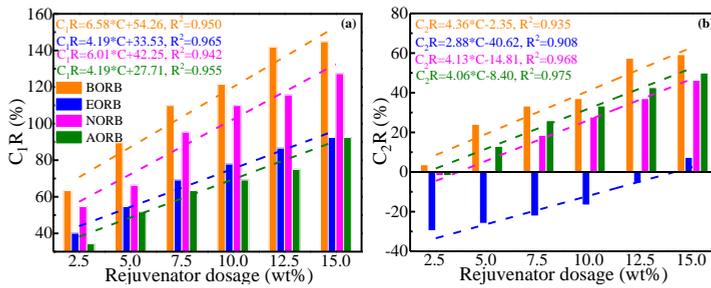
Figure 7.34 The rejuvenation effect on C-S curve model parameters

7.5.4.4 Fatigue life N_f and rejuvenation percentage

The N_f and N_fR values are calculated, and the results of virgin and aged bitumen are shown in **Figure 7.35**. The relationship between the N_f of bitumen and strain level agrees well with **Eq.7.20**, and the Log(N_f) value decreases linearly as the logarithmic value of shear strain increases. There is no consistent influence law of long-term aging time on the N_f values of bitumen in the entire strain region. At low strains (1%-2%), the N_f value of bitumen tends to increase as the aging level deepens, presenting an opposite trend when strain is higher than 4%. Based on the correlation equations, the aging degree promotes the enlargement in the initial N_f value of bitumen, increasing the reduction rate of the N_f parameter to the strain level. To keep consistent with the following sweep (TS) test, the N_f parameters at two strain levels of 2.5% and 5% are considered to assess the fatigue life of bitumen with different aging and rejuvenation conditions. To the N_f parameter at 2.5% strain ($N_{f2.5}$), the short-term aging shows a positive effect, slightly reducing after 20h long-term aging. However, the $N_{f2.5}$ values of LAB40 and LAB80 continue to rise, even larger than the virgin bitumen.
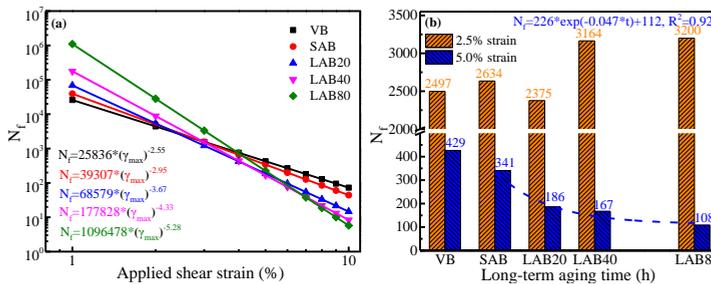
Figure 7.35 Influence of long-term aging on N_f values of bitumen
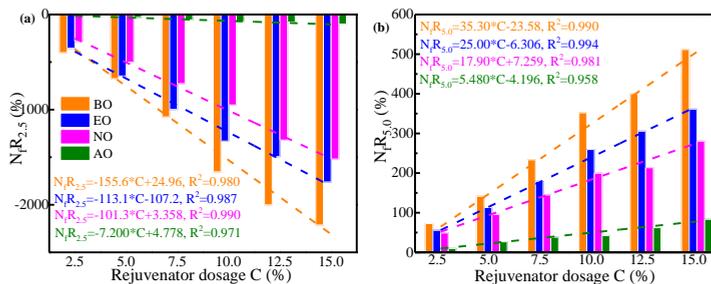
Figure 7.36 Influence of rejuvenator dosage on N_fR value of LAB40 rejuvenated bitumen

The N_f and N_fR values at 2.5% and 5% strains of LAB40 rejuvenated bitumen are displayed in **Figure 7.36**. Regardless of strain level, the N_f values of rejuvenated binders increase linearly as the rejuvenator dosage rises. It suggests that incorporating rejuvenators improves fatigue resistance and extends the service life of aged bitumen. As expected, the N_{f5} values are lower than the $N_{f2.5}$. The apparent difference in the enhancement level of four rejuvenators on the N_f of aged bitumen shows BORB > EORB > NORB > AORB. It further signifies that the bio-oil maximally enhances the fatigue life of aged bitumen, followed by engine-oil and naphthenic-oil, whereas the aromatic-oil has the lowest fatigue life extension capacity. The difference in N_f values of rejuvenated binders with various rejuvenators indicates that the N_f is an effective indicator to evaluate and discriminate the fatigue life of different rejuvenator-aged bitumen blends.

As the rejuvenator dosage increases, the N_fR_5 increases linearly, but the $N_fR_{2.5}$ shows a linearly decreasing trend. The reason for the negative $N_fR_{2.5}$ values is that the N_f of aged bitumen at 2.5% strain is higher than the virgin bitumen, and the inclusion of rejuvenators continues to enlarge the $N_{f2.5}$ value of aged bitumen. Thus, the $N_{f2.5}$ results violate the rejuvenation definition and fail to assess the rejuvenation efficiency of rejuvenators on the fatigue performance of aged bitumen. On the contrary, the N_fR_5 values can effectively and quantitatively estimate the rejuvenation efficiency of various rejuvenators on fatigue life, and the scope of N_fR_5 values (0-550%) is much wider than the stress-strain curve and C-S curve parameters. The aging level of bitumen remarkably influences the fatigue life and corresponding rejuvenation percentage. Furthermore, the ranking of N_{f5} and N_fR_5 is invariable as BORB > EORB > NORB > AORB.

7.5.5 TS test parameters

7.5.5.1 Aging influence on TS fatigue parameters

The G*-N curve is the main output from the time sweep test, and **Figure 7.37(a)** shows the G*-N curves of virgin and aged bitumen at two stresses of 2.5% and 5%. Different important evaluation parameters can be derived from the G*-N curves, such as the fatigue life with 50% residue G* ($N_{50\%}$) and phase angle at the peak point (δ_{peak}). Meanwhile, the dissipated energy ratio (DER) variation as introduced in **section 7.5.2.3** versus load cycles (illustrated in **Figure 7.37(b)**) can be used to determine two parameters (fatigue life N_{p20} and initial dissipated energy W_0). As the load cycle prolongs, the G* value of bitumen decreases gradually, which is more significant at high strain. Moreover, the descent rate of the G* value becomes faster after long-term aging. High strain level results in a large δ_{peak} value of bitumen, decreasing significantly due to aging.
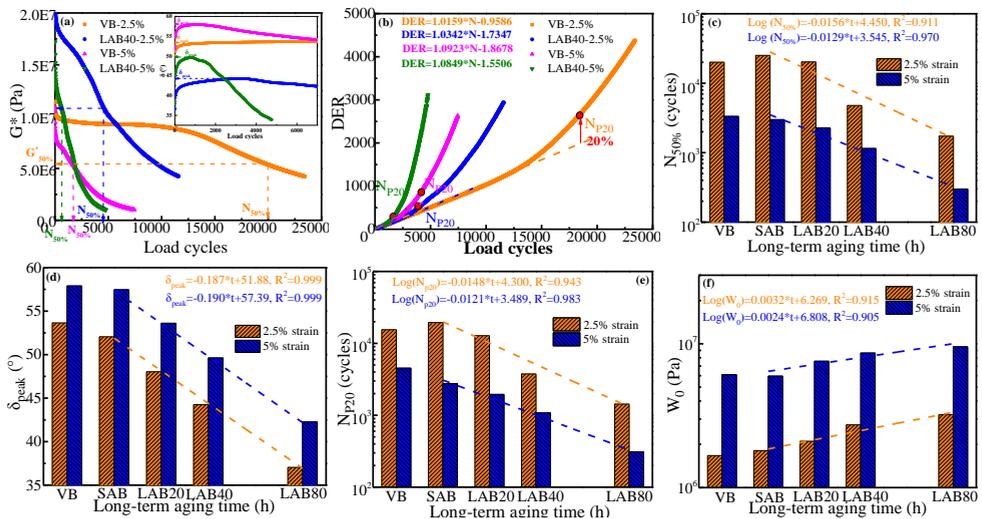
Figure 7.37 The TS fatigue parameters of virgin and aged bitumen

Regarding the DER-N curves, the high strain and aging intensify the increasing rate of DER curves dramatically, reducing the derived N_{p20} value of bitumen. Regardless of the strain levels, the linear relationships between the aging time with parameters $N_{50\%}$, δ_{peak}, N_{p20}, and W_0. Long-term aging reduces the $N_{50\%}$, δ_{peak}, and N_{p20} values but increases the W_0 parameter of bitumen. It suggests that a high aging level significantly shortens the fatigue life, enlarges the elastic ratio, and increases the energy dissipation of bitumen. Further, the high strain decreases the $N_{50\%}$ and N_{p20} and expands the δ_{peak} and W_0 values of bitumen, which weakens the sensitivities of $N_{50\%}$, N_{p20}, and W_0 parameters to the aging time.

7.5.5.2 TS fatigue parameters of rejuvenated bitumen

The $N_{50\%}$, δ_{peak}, and their rejuvenation percentage ($N_{50\%}R$ and $\delta_{peak}R$) of rejuvenated bitumen are shown in **Figure 7.38**. As the rejuvenator dosage increases, the $N_{50\%}$ and δ_{peak} values of rejuvenated bitumen enlarge, showing the opposite trend to the aging effect. It means that the inclusion of rejuvenators improves fatigue life and restores the viscoelastic property of aged bitumen. Like the LAS results, the strain level strongly affects the $N_{50\%}$ and $N_{50\%}R$ values of rejuvenated bitumen. When the strain level is 2.5%, the $N_{50\%}$-C (and $N_{50\%}R$-C) curves of EORB and NORB binders almost overlap, resulting in huge difficulty in differentiating the rejuvenation efficiency of engine-oil and naphthenic-oil rejuvenators on fatigue life. At 5% strain, the magnitude of $N_{50\%}R$ for rejuvenated binders is EORB > NORB > BORB > AORB. Additionally, the δ_{peak} and $\delta_{peak}R$ values of AORB are the highest, while the NORB shows the lowest values. Nevertheless, the sequence in δ_{peak} and $\delta_{peak}R$ of BORB and EORB inverts as the strain level changes from 2.5% to 5%.
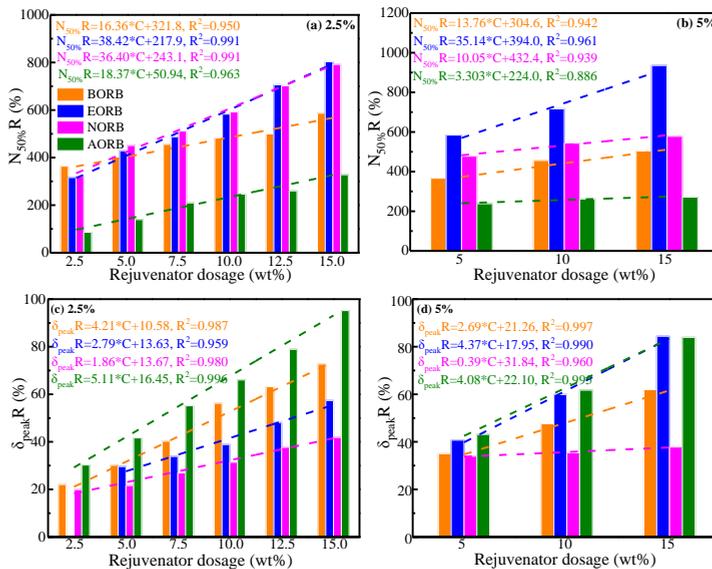
Figure 7.38 The $N_{p50\%}R$ and $\delta_{peak}R$ values of rejuvenated bitumen

The results of N_{p20} and W_0 parameters of rejuvenated binders are displayed in **Figure 7.39.** Similar to $N_{50\%}$, several intersections in N_{p20}-C and $N_{p20}R$-C curves of BORB with EORB and NOBR binders at a low strain of 2.5%. The variation law of N_{p20} and $N_{p20}R$ versus rejuvenator dosage and type at 5% strain is similar to the $N_{50\%}$ and $N_{50\%}R$ results. However, the ranking of $N_{50\%}R$ and $N_{p20}R$ of rejuvenated binders (EORB > NORB > BORB > AORB) from the TS test differs from N_f from the LAS test (BORB > EORB > NORB > AORB). The reason may be that the $N_{50\%}$ and N_{p20} parameters are determined from G*-N curves without considering the phase angle variation during the TS fatigue test. With the W_0 parameter, the rejuvenation efficiency of rejuvenators can be evaluated and distinguished, which completely agrees with the LVE and LAS fatigue results. However, it should be mentioned that the Wo represents the initial dissipated energy without considering the entire

fatigue cracking process. These four parameters fail to distinguish the rejuvenation efficiency of various rejuvenator-aged bitumen blends. The crack-based parameters derived from the TS test will be discussed further in the following subsection.
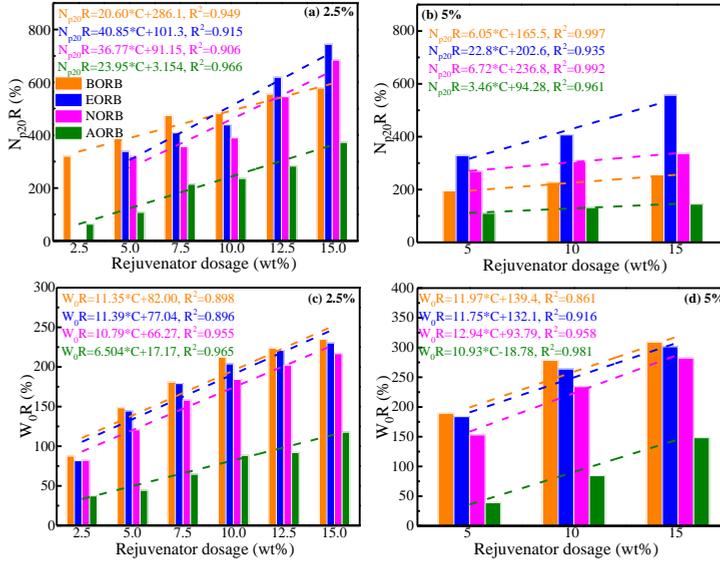
Figure 7.39 The $N_{p20}R$ and W_0R values of rejuvenated bitumen

7.5.5.3 Influence of aging on fatigue crack width of bitumen

The dissipated strain energy (DSE) density is popular to quantify the fatigue potential of bituminous materials, which is defined as the loop area of a stress-strain curve [88]. The DSE density at a given radial position r of undamaged bitumen follows:

$$DSE_0(r) = \int_{t_0}^{t_0+\frac{2\pi}{\omega}} \tau(t)d\gamma(t) = \pi\tau_0(r)\gamma_0(r)\sin\delta_0 = \pi\tau_0(r)^2 \frac{\sin\delta_0}{G_0^*} \tag{7.27}$$

where τ and γ refer to the shear stress and strain; τ_0 and γ_0 are the strain amplitude and stress amplitude; t is the loading time; G_0^* and δ_0 represent the complex shear modulus and phase angle of undamaged bitumen.

Similarly, the DSE density at the Nth load cycle (DSE_N) of a damaged bitumen can be calculated using **Eq.7.28**.

$$DSE_N(r) = \int_{(N-1)\frac{2\pi}{\omega}}^{N\frac{2\pi}{\omega}} \tau_N(t)d\gamma_d(t) = \pi\tau_N(r)\gamma_d(r)\sin\delta_N = \pi\tau_N(r)^2 \frac{\sin\delta_N}{G_N^*} \tag{7.28}$$

where G_N^* and δ_N are the complex shear modulus and phase angle of damaged bitumen at the Nth load cycle.

At the same time, the torque amplitude (T_0 and T_N) on undamaged and damaged bitumen specimens are defined as follows:

$$T_0 = \int_0^{r_0} (\tau_0 \cdot 2\pi r \cdot r)dr = \int_0^{r_0} (\frac{r}{r_0} \cdot \tau_{0max} \cdot 2\pi r \cdot r)dr = \frac{\pi r_0^3}{2}\tau_{0max} \tag{7.29}$$

$$T_N = \int_0^{r_0} (\tau_N \cdot 2\pi r \cdot r)dr = \int_0^{r_0} \left(\frac{r}{r_0} \cdot \tau_{Nmax} \cdot 2\pi r \cdot r\right)dr = \frac{\pi r_0^3}{2}\tau_{Nmax} \tag{7.30}$$

where r and r_0 are the radius position and the whole bitumen radius; τ_{0max} and τ_{Nmax} represent the maximum shear amplitude of undamaged and damaged samples at the Nth load cycle, respectively.

Based on the torque amplitude equilibrium principle, the T_N value of damaged bitumen at the Nth load cycle is equivalent to the T_0 of undamaged bitumen with an effective radius r_E, displayed as:

$$\frac{\pi r_0^3}{2}\tau_{Nmax} = \frac{\pi r_E^3}{2}\tau_{Emax} \tag{7.31}$$

where r_E and τ_{Emax} are the effective radius and maximum stress amplitude for the undamaged configuration.

The dissipated strain energy (DSE_N) is equivalent to the effective dissipated strain energy (DSE_E), shown in **Eqs.7.31** and **7.32**.

$$\iiint DSE_N(r)dV_0 = \iiint DSE_E(r)dV_E \tag{7.32}$$

$$\int_0^{r_0} (\pi\tau_N(r)^2 \frac{\sin\delta_N}{G_N^*} \cdot 2\pi r \cdot h)dr = \int_0^{r_E} (\pi\tau_E(r)^2 \frac{\sin\delta_0}{G_0^*} \cdot 2\pi r \cdot h)dr \tag{7.33}$$

where V_0 and V_E are the whole volume of undamaged bitumen and the effective volume of damaged bitumen; h shows the height of the bitumen specimen. Solving **Eqs.7.31** and **7.33**, the crack length c at the Nth load cycle can be calculated as follows:

$$c = r_0 - r_E = \left[1 - \left(\frac{\frac{G_N^*}{\sin(\delta_N)}}{\frac{G_0^*}{\sin(\delta_0)}} \right)^{\frac{1}{4}} \right] r_0 \tag{7.34}$$
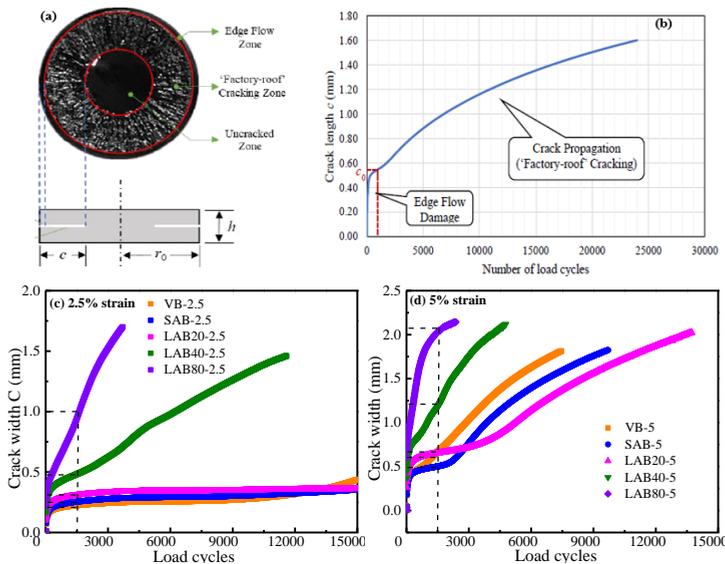
Figure 7.40 Fatigue crack characteristics of virgin and aged bitumen

The crack morphology and width variation versus load cycles are displayed in **Figure 7.40(a)** and **(b)**. After fatigue tests, three regions are detected for damaged bitumen: edge flow, factory-roof, and uncracked zones [89], also reflected by the C-N curve. This study compares the C-N curves of virgin/aged and

rejuvenated binders with variable rejuvenator conditions. The crack width-based rejuvenation percentage CR is adopted to quantitatively reflect the impacts of rejuvenator type/dosage and aging level on the fatigue cracking of rejuvenated bitumen.

The C-N curves of virgin and aged bitumen at 2.5% and 5% strain levels are depicted in **Figure 7.40(c)** and **(d)**, respectively. As the load cycle increases, the crack width of bitumen prolongs. The crack growth rate of bitumen increases significantly as the aging degree deepens. In other words, the higher the aging degree of bitumen, the earlier its fatigue failure occurs, especially when the aging level changes to LAB40 and LAB80. Meanwhile, bitumen's crack width and growth rate enlarge as the fatigue strain level increases from 2.5% to 5%. At the 5% strain, the crack width of the LAB80 binder increases to 2 mm when the load cycle is 1500, which reaches the halfway point of the specimen radius (4mm). In this thesis, the crack width values of virgin/aged and rejuvenated binders at the load cycles of 500, 1500, and 3000 are measured to estimate the aging and rejuvenation effects on the cracking potential of bitumen.

7.5.5.4 Crack width-based rejuvenation percentage (CR)

The crack width-based rejuvenation percentages of different rejuvenated binders are calculated and illustrated in **Figure 7.41**. All CR values of rejuvenated bitumen show linearly increasing correlations with the rejuvenator dosage. The variation trends of CR-C curves at different load cycles are similar. Thus, one crack width parameter is enough to evaluate the rejuvenation efficiency of rejuvenators on cracking potential. The $C_{500}R$ values can reflect the difference in the rejuvenation effectiveness of these four rejuvenators on the crack width of aged bitumen in the entire dosage range. Thus, it is recommended as an effective indicator for crack width-based fatigue performance evaluation of different rejuvenator-aged bitumen systems. Based on the $C_{500}R$ values, the ranking of crack width reduction efficiency of four rejuvenators is bio-oil > engine-oil > naphthenic-oil > aromatic-oil, which completely agrees with the conclusions from LVE and LAS tests.
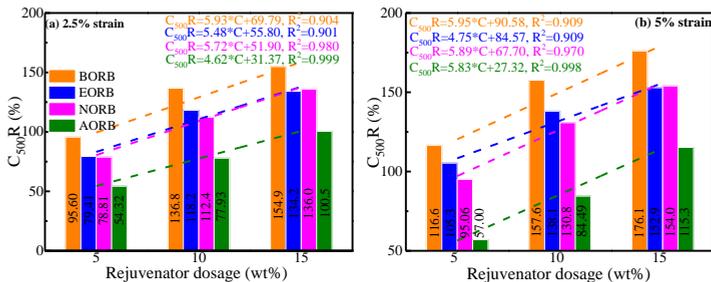
Figure 7.41 Crack width-based rejuvenation percentage of rejuvenated bitumen
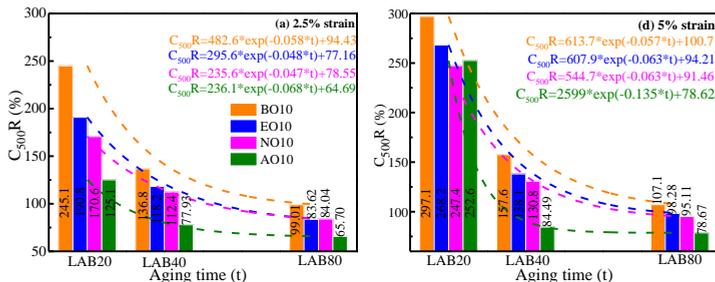
Figure 7.42 Influence of aging level on CR value of rejuvenated bitumen

As shown in **Figure 7.42**, the CR values of rejuvenated binders strongly depend on the aging degree of bitumen. All CR parameters tend to decrease exponentially as the aging level of bitumen increases. It means that the rejuvenation efficiency of all rejuvenators on preventing the fatigue crack of aged bitumen weakens

becomes smaller to an aged bitumen after severe aging. However, the aging degree does not influence the rejuvenation efficiency ranking on crack width reduction of these four rejuvenators. The correlations between the CR values and aging time are beneficial to predicting the crack width of rejuvenated bitumen with other aging degrees. According to the results, the C_{500} parameter is preferred to assess the rejuvenation efficiency on crack width restoration of different rejuvenator-aged bitumen blends.

7.5.6 Critical fatigue evaluation indicators and correlations

From the LVE test, the fatigue failure temperature (FFT) parameter is proposed as an effective LVE fatigue indicator. In the LAS test, the effective indicators are N_{f5}, ε_{sr}, and E parameters. In the TS test, the crack width (C) findings are consistent with conclusions from LVE and LAS tests. Overall, the proposed indicators for effectively evaluating and discriminating the rejuvenation efficiency of rejuvenators on fatigue performance are FFT from LVE, N_{f5}, ε_{sr}, E from LAS, and C_{500} from the TS test.

Exploring the potential connections between these critical evaluation indicators from different fatigue tests is interesting. **Figure 7.43** depicts the correlation curves between the C_{500} with FFT, N_{f5}, ε_{sr}, and E parameters. The crack width connects well with these parameters, and thus the crack width can be predicted with these correlation equations without conducting the time-consuming time sweep test. As the crack width increases, the FFT values of virgin/aged and rejuvenated binders enlarge while the N_{f5} and ε_{sr} decrease exponentially. Additionally, the elastic modulus E derived from the LAS stress-strain curve behaves in a linearly positive relationship with the C_{500} parameter.
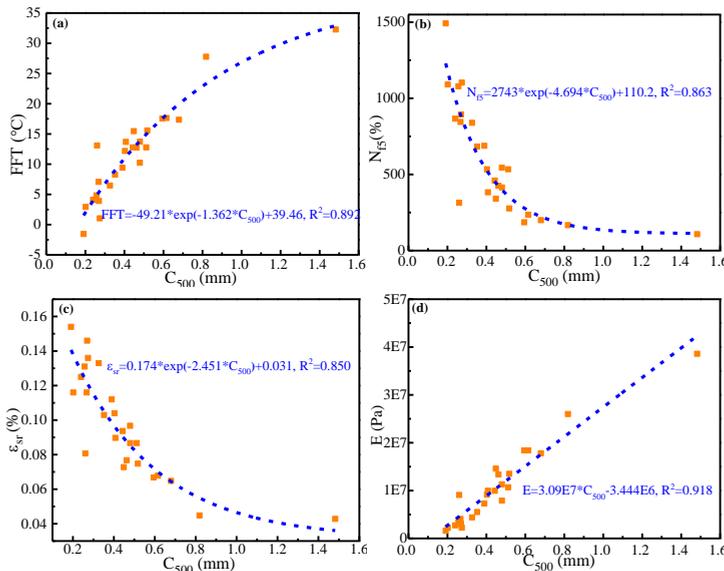
Figure 7.43 Correlations between the critical fatigue evaluation indicators

7.5.7 Summary

This subchapter proposes critical indicators for effectively evaluating and differentiating the rejuvenation efficiency of various rejuvenators on the fatigue behavior of aged bitumen. Moreover, the potential connections between these proposed fatigue indicators from different fatigue measurements are explored. The main conclusions and some recommendations are as follows:

(i) The bio-oil exhibits the greatest rejuvenation efficiency in improving the fatigue life of aged bitumen, followed by engine-oil, naphthenic-oil, and aromatic-oil rejuvenators. Meanwhile, the rejuvenation percentages on fatigue parameters enhance significantly with increased rejuvenator dosage but weaken as the aging level deepens.

(ii) From the LVE test, the fatigue parameter ($G^*\sin\delta$) can better reflect and distinguish the rejuvenation efficiency of various rejuvenators on the LVE fatigue performance of aged bitumen than the G-R parameter, but it shows a limitation of high-temperature dependence. The fatigue failure temperature (FFT) parameter is proposed as an effective LVE fatigue indicator.

(iii) In the LAS test, the effective indicators are fatigue life (N_{f5}), peak strain (ε_{sr}), and elastic modulus (E) parameters.

(iv) In the TS test, the parameters $N_{50\%}$ and N_{p20} derived from G*-N and DER-N curves fail to completely distinguish the rejuvenation effects of all rejuvenator-aged bitumen systems due to the negligence of variation in viscoelastic proportion. However, the crack width (C) findings are consistent with conclusions from LVE and LAS tests.

(v) The crack width C_{500} parameter shows great correlations with other critical indicators and can be predicted with these correlation equations without conducting the time-consuming time sweep test.

7.6 Discussion on rejuvenation efficiency indices of rejuvenated bitumen systems

The key objective of this chapter is to propose the critical indicators for effectively evaluating the rejuvenation efficiency of various rejuvenators on the chemical characteristics, rheological properties, high-temperature rutting performance, low-temperature cracking potential, and fatigue cracking resistance of aged bitumen. **Table 7.8** lists these critical evaluation indicators proposed based on the broad but limited results in this thesis.

Table 7.8 Critical indicators for effectively evaluating the rejuvenation efficiency

	Properties	Critical evaluation indicators				
1	High-temperature rutting performance (from LVE, flow, and MSCR)	Rutting failure temperature (RFT)	Zero-shear viscosity (ZSV)	Recovery percentage ($R_{3.2}$)	Creep compliance ($J_{nr0.1}$, $J_{nr3.2}$)	Stress sensitivity ($J_{nrslope}$)
2	Low-temperature cracking potential (from relaxation)	Shear stress (τ_{50s})	Relaxation time ($t_{25\%}$)	Relaxation model parameter A	-	-
3	Fatigue cracking resistance (from LVE, TS, and LAS)	Fatigue failure temperature (FFT)	Fatigue life (N_{f5})	Peak shear strain (ε_{sr})	Elastic modulus (E)	Crack width (C_{500})

      The rutting failure temperature (RFT) measured from the linear viscoelastic test can estimate the high-temperature performance of rejuvenated bitumen. Moreover, the zero-shear viscosity (ZSV) from the flow test, recovery percentage ($R_{3.2}$), creep compliance ($J_{nr0.1}$, $J_{nr3.2}$), and stress sensitivity ($J_{nrslope}$) from multiple stress creep and recovery (MSCR) of rejuvenated bitumen can be concentration points, which show great correlations with RFT parameter. The relaxation test assesses the low-temperature cracking potential of rejuvenated bitumen, and the shear stress (τ_{50s}), relaxation time ($t_{25\%}$), and relaxation model parameter A are recommended as the critical evaluation indicators. Lastly, different fatigue tests (linear viscoelastic LVE, time sweep TS, and linear amplitude sweep LAS) are carried out to evaluate the fatigue performance of rejuvenated binders. By analyzing and comparing the sensitivity of these fatigue parameters to rejuvenator

type/dosage and aging level of bitumen, the fatigue failure temperature (FFT), fatigue life (N_{f5}), peak shear strain (ε_{sr}), elastic modulus (E), and crack width (C_{500}) parameters are proposed as critical fatigue indicators of different rejuvenator-aged bitumen blends. It is important to propose these essential evaluation indicators for assessing and comparing the rejuvenation efficiency of various rejuvenator-aged bitumen systems.

7.7 References

[1] A. Eltwati, A. Mohamed, M. Hainin, E. Jusli, M. Enieb. Rejuvenation of aged asphalt binders by waste engine oil and SBS blend: physical, chemical, and rheological properties of binders and mechanical evaluations of mixtures. Construction and Building Materials. 2022, 346, 128441.

[2] M. Elkashef, J. Podolsky, R. Williams, E. Cochran. Preliminary examination of soybean oil derived material as a potential rejuvenator through Superpave criteria and asphalt bitumen rheology. Construction and Building Materials. 2017, 149, 826- 836.

[3] S. Nizamuddin, H. Baloch, M. Jamal, S. Madapusi, F. Giustozzi. Performance of waste plastic bio-oil as a rejuvenator for asphalt binder. Science of the Total Environment. 2022, 828, 154489.

[4] H. Dhasmana, K. Hossain, A. Karakas. Effect of long-term ageing on the rheological properties of rejuvenated asphalt binder. Road Materials and Pavement Design. 2019, 1686051.

[5] H. Ziari, S. Bananezhad, A. Bananezhad, M. Ziari. Immediate and long-term characteristics of recycling agents in the restoration of chemical properties of aged asphalt binder. Journal of Materials in Civil Engineering. 2022, 34(2), 04022318.

[6] M. Guo, X. Liu, Y. Jiao, Y. Tan, D. Luo. Rheological characterization of reversibility between aging and rejuvenation of common modified asphalt binders. Construction and Building Materials. 2021, 301, 124077.

[7] X. Xu, J. Yu, L. Xue, B. He, W. Du, H. Zhang, Y. Li. Effect of reactive rejuvenating system on physical properties and rheological characteristics of aged SBS modified bitumen, Construction and Building Materials. 2018, 176, 35-42.

[8] H. Jahanbakhsh, M. Karimi, H. Naseri, F. Nejad. Sustainable asphalt concrete containing high reclaimed asphalt pavements and recycling agents: Performance assessment, cost analysis, and environmental impact. Journal of Cleaner Production. 2020, 244, 118837.

[9] M. Zaumanis, R. Mallick. Review of very high-content reclaimed asphalt use in plant-produced pavements: state of the art. International Journal of Pavement Engineering. 2015,16(1), 39-55.

[10] C. Hettiarachchi, X. Hou, J. Wang, F. Xiao. A comprehensive review on the utilization of reclaimed asphalt material with warm mix asphalt technology. Construction and Building Materials. 2019, 227, 117096.

[11] P. Cong, X. Guo, L. Mei. Investigation on rejuvenation methods of aged SBS modified asphalt binder. Fuel. 2020, 279, 118556.

[12] A. Abdelaziz, E. Masad, A, Martin, E. Mercado, A. Bajaj. Multiscale characterization of aging and rejuvenation in asphalt binder blends with high RAP contents. Journal of Materials in Civil Engineering. 2021, 33(10), 04021287.

[13] Y. Sun. B. Huang, J. Chen, X. Jia, Y. Ding. Characterizing rheological behavior of asphalt binder over a complete range of pavement service loading frequency and temperature. Construction and Building Materials. 2016, 123, 661-672.

[14] M. Chen, F. Xiao, B. Putman, B. Leng, S. Wu. High temperature properties of rejuvenating recovered binder with rejuvenator, waste cooking and cotton seed oils. Construction and Building Materials. 2014, 59, 10-16.

[15] X. Yang, Z. You. High temperature performance evaluation of bio-oil modified asphalt binders using the DSR and MSCR tests. Construction and Building Materials. 2015, 76, 380-387.

[16] D. Wang, J. Zhu, L. Porot, A. Falchetto, S. Damen. Multiple stress creep and recovery test for bituminous binders-influence of several key experimental parameters. Road Materials and Pavement Design. 2023, 2180992.

[17] K. Shi, Z. Fu, F. Ma, J. Liu, R. Song, J. Li, J. Dai, C. Li, Y. Wen. Development on the rheological properties and micromorphology of active reagent-rejuvenated SBS-modified asphalt. ACS Sustainable Chemistry & Engineering. 2022, 10, 16734-16751.

[18] D. Daryaee, M. Habibpour, S. Gulzar, B. Underwood. Combined effect of waste polymer and rejuvenator on performance properties of reclaimed asphalt binder. Construction and Building Materials. 2021, 268, 121059.

[19] M. Ansari, K. Khatri, R. Vishnu, V. Chowdary. Performance evaluation of rejuvenated recycled asphalt blends at high and intermediate pavement temperatures. International Journal of Pavement Engineering. 2022, 23(12), 4112-4124.

[20] L. Zhang, I. Hoff. X. Zhang, C. Yang. Investigation of the self-healing and rejuvenating properties of aged asphalt mixture containing multi-cavity Ca-alginate capsules. Construction and Building Materials. 2022, 361, 129685.

[21] Ncat, NCAT researchers explore multiple user of rejuvenators asphalt technology news. 2014, 26(1), 1-16.

[22] H. Zhang, Z. Chen, G. Xu, C. Shi. Evaluation of aging behaviors of asphalt binders through different rheological indices. Fuel. 2018, 221, 78-88.

[23] S. Kabir, E. Fini. Investigating aging and rejuvenation mechanism of biomodified rubberized bitumen. Journal of Materials in Civil Engineering. 2021, 33(7), 04021142.

[24] D. Oldham, A. Rajib, K. Dandamudi, Y. Liu, S. Deng, E. Fini. Transesterification of waste cooking oil to produce a sustainable rejuvenator for aged asphalt. Resources, Conservation & Recycling. 2021, 168, 105297.

[25] L. Rzek, M. Tusar, L. Perse. Modelling rheological characteristics of rejuvenated aged bitumen. International Journal of Pavement Engineering. 2022, 23(4), 1282-1294.

[26] W. Zeiada, H. Liu, G. Al-Khateeb, A. Shanableh, M. Samarai. Evaluation of test methods for measurement of zero shear viscosity (ZSV) of asphalt binders. Construction and Building Materials. 2022, 325, 126794.

[27] A. Behnood. Application of rejuvenators to improve the rheological and mechanical properties of asphalt binders and mixtures: A review. Journal of Cleaner Production. 2019, 231, 171-182.

[28] M. Zahoor, S. Nizamuddin, S. Madapusi, F. Giustozzi. Sustainable asphalt rejuvenation using waste cooking oil: A comprehensive review. Journal of Cleaner Production. 2021, 278, 123304.

[29] H. Liu, W. Zeiada, G. Al-Khateeb, A. Shanableh, M. Samarai. Characterization of the shear-thinning behavior of asphalt binders with consideration of yield stress. Materials and Structures. 2020, 53, 105.

[30] Y. Wang, K. Zhao, F. Li, Q. Gao, K. Lai. Asphaltenes in asphalt: Direct observation and evaluation of their impacts on asphalt properties. Construction and Building Materials. 2021, 271, 121862.

[31] P. Hajikarimi, M. Rahi, F. Nejad. Comparing different rutting specification parameters using high temperature characteristics of rubber-modified asphalt binders. Road Materials and Pavement Design. 2015, 16(4), 751-766.

[32] F. Dong, X. Yu, B. Xu, T. Wang. Comparison of high temperature performance and microstructure for foamed WMA and HMA with RAP binder. Construction and Building Materials. 2017, 134, 594-601.

[33] K. Zhang, F. Huchet, A. Hobbs. A review of thermal processes in the production and their influences on performance of asphalt mixtures with reclaimed asphalt pavement (RAP). Construction and Building Materials. 2019, 206, 609-619.

[34] S. Ren, X. Liu, W. Fan, C. Qian, G. Nan, S. Erkens. Investigating the effects of waste oil and styrene-butadiene rubber on restoring and improving the viscoelastic, compatibility, and aging properties of aged asphalt. Construction and Building Materials. 2021, 269, 121338.

[35] L. Porot, J. Zhu, D. Wang, A. Falchetto. Multiple stress creep recovery test to differentiate polymer modified bitumen at high temperature. 2022. Journal of Testing and Evaluation. https://doi.org/10.1520/JTE20220306

[36] G. Skronka, M. Blascik, O. Vacin, M. Jasso. Impact of shear stress levels on validity of MSCR tests. Road Materials and Pavement Materials. 2022, 2106293.

[37] A. Sharma, G. Naga, P. Kumar, S. Raha. Rheological characterization of recycled asphalt binders and correlating the zero shear viscosity to the Superpave rutting parameter. Journal of Materials in Civil Engineering. 2022, 34(9), 04022218.

[38] A. Sharma, G. Naga, P. Kumar, S. Raha. Development of an empirical relationship between non-recoverable creep compliance & zero shear viscosity for wide-ranging stiffness of asphalt binders. Construction and Building Materials. 2022, 326, 126764.

[39] G. Li, Y. Tan, Y. Fu, P. Liu, C. Fu, M. Oeser. Density, zero shear viscosity and microstructure analysis of asphalt binder using molecular dynamics simulation. Construction and Building Materials. 2022, 345, 128332.

[40] X. Xu, A. Sreeram, Z. Leng, J. Yu, R. Li, C. Peng. Challenges and opportunities in the high-quality rejuvenation of unmodified and SBS modified asphalt mixtures: State of the art. Journal of Cleaner Production. 2022, 378, 134634.

[41] Z. Qasim, A. Abed, K. Almomen. Evaluation of mixing and compaction temperatures (MCT) for modified asphalt binders using zero shear viscosity and Cross-Williamson model. Case Studies in Construction Materials. 2019, 11, e00302.

[42] F. Kaseer, A. Martin, E. Arambula-Mercado. Use of recycling agents in asphalt mixtures with high recycled materials contents in the United States: A literature review. Construction and Building Materials. 2019, 211, 974-987.

[43] N. Saboo, P. Kumar. A study on creep and recovery behavior of asphalt binders. Construction and Building Materials. 2015, 632-640.

[44] K. Hofer, J. Mirwald, A. Bhasin, B. Hofko. Low-temperature characterization of bitumen and correlation to chemical properties. Construction and Building Materials. 2023, 366, 130202.

[45] P. Lin, X. Liu, P. Apostolidis, S. Erkens, S. Ren, S. Xu, T. Scarpas, W. Huang. On the rejuvenator dosage optimization for aged SBS modified bitumen. Construction and Building Materials. 2021, 271, 121913.

[46] D. Wang, A. Falchetto, C. Riccardi, J. Westerhoff, M. Wistuba. Investigation on the effect of physical hardening and aging temperature on low-temperature rheological properties of asphalt binder. Road Materials and Pavement Design. 2021, 22(5), 1117-1139.

[47] A. Mansourkhaki, M. Ameri, M. Habibpour, B. Underwood. Relations between colloidal indices and low-temperature properties of reclaimed binder modified with softer binder, oil-rejuvenator and polybutadiene rubber. Construction and Building Materials. 2020, 239, 117800.

[48] T. Wang, J. Wang, X. Hou, F. Xiao. Effects of SARA fractions on low temperature properties of asphalt binders. Road Materials and Pavement Design. 2021, 22(3), 539-556.

[49] L. Zhang, B. Hussain, Y. Tan. Effect of bio-based and refined waste oil modifiers on low temperature performance of asphalt binders. Construction and Building Materials, 2015, 86, 95-100.

[50] Y. Kumbargeri, J. Planche, J. Adams, M. Elwardany, G. King. Effect of binder chemistry and related properties on the low-temperature performance parameters of asphalt binders. Transportation Research Record. 2023, 1-19.

[51] S. Ren, X. Liu, P. Lin, S. Erkens, Y. Gao. Chemical characterizations and molecular dynamics simulations on different rejuvenators for aged bitumen recycling, Fuel. 2022, 324, 124550.

[52] J. Buchner, M. Wistuba, S. Miesem, M. Neliepp, M. Dietzsch, M. Sandor. Rheological characterisation of rejuvenator blending lines. Road Materials and Pavement Design. 2023, 2180994.

[53] R. Jing, A. Varveri, X. Liu, A. Scarpas, S. Erkens. Rheological, fatigue and relaxation properties of aged bitumen. International Journal of Pavement Engineering. 2020, 21(8), 1024-1033.

[54] L. Pang, K. Liu, S. Wu, M. Lei, Z. Chen. Effect of LDHs on the aging resistance of crumb rubber modified asphalt. Construction and Building Materials, 2014, 67, 239-243.

[55] W. Zheng, Y. Yang, Y. Chen, Y. Yu, N. Hossiney, G. Tebaldi. Low temperature performance evaluation of asphalt binders and mastics based on relaxation characteristics. Materials and Structures. 2022, 55, 204.

[56] B. Xing, W. Fan, Y. Lyu, J. Che, C. Zhuang. Influences of ball-milled limestone particle sizes and shapes on asphalt mastic stress relaxation behavior. Construction and Building Materials. 2020, 255, 119396.

[57] J. Buchner, D. Rys, S. Trifunovic, M. Wistuba. Development and application of asphalt binder relaxation test in different dynamic shear rheometers. Construction and Building Materials. 2023, 364, 129929.

[58] L. Zhang, M. Greenfield. Relaxation time, diffusion, and viscosity analysis of model asphalt systems using molecular simulation. The Journal of Chemical Physics. 2007, 127, 194502.

[59] K. Sonibare, G. Rucker, L. Zhang. Molecular dynamics simulation on vegetable oil modified model asphalt. Construction and Building Materials. 2021, 270, 121687.

[60] W. Sun, H. Wang. Molecular dynamics simulation of nano-crack formation in asphalt binder with different SARA fractions. Molecular Simulation. 2022, 48(9), 789-800.

[61] Y. Yaphary, Z. Leng, H. Wang, G. Ren, G. Lu. Characterization of nanoscale cracking at the interface between virgin and aged asphalt binders based on molecular dynamics simulations. Construction and Building Materials. 2022, 335, 127475.

[62] J. Xu, Z. Fan, J. Lin, P. Liu, D. Wang, M. Oeser. Study on the effects of reversible aging on the low temperature performance of asphalt binders. Construction and Building Materials. 2021, 295, 123604.

[63] L. Luo, P. Liu, S. Leischner, M. Oeser. Atomic insights into the nano-cracking behaviour of bitumen: considering oxidative aging effects. Road Materials and Pavement Design. 2023, 2180292.

[64] C. Liu, J. Du, C. Wu, K. Liu, K. Jiang. Low-temperature crack resistance of wood tar-based rejuvenated asphalt based on viscoelastic rheological method. International Journal of Pavement Research and Technology. 2022, 15, 1340-1353.

[65] Q. Fu, Y. Xie, D. Niu, G. Long, D. Luo, Q. Yuan, H. Song. Integrated experimental measurement and computational analysis of relaxation behavior of cement and asphalt mortar. Construction and Building Materials. 2016, 120, 137-146.

[66] T. Lopez-Montero, R. Miro, R. Botella, F. Perez-Jimenez. Obtaining the fatigue laws of bituminous mixtures from a strain sweep test: Effect of temperature and aging. International Journal of Fatigue. 2017, 100, 195-205.

[67] S. Mangiafico, C. Sauzeat, H. Benedetto, S. Pouget, F. Olard, L. Planque. Complex modulus and fatigue performance of bituminous mixtures with reclaimed asphalt pavement and a recycling agent of vegetable origin. Road Materials and Pavement Design. 2017, 18(2), 315-330.

[68] X. Cao, H. Wang, X. Cao, W. Sun, H. Zhu, B. Tang. Investigation of rheological and chemical properties asphalt binder rejuvenated with waste vegetable oil. Construction and Building Materials. 2018, 180, 455-463.

[69] M. Elkashef, R. Williams. Improving fatigue and low temperature performance of 100% RAP mixtures using a soybean-derived rejuvenator. Construction and Building Materials. 2017, 151, 345-352.

[70] A. Ali, Y. Mehta, A. Nolan, C. Purdy, T. Bennert. Investigation of the impacts of aging and RAP percentages on effectiveness of asphalt binder rejuvenators. Construction and Building Materials. 2016, 110, 211-217.

[71] M. Zaumanis, R. Mallick, L. Poulikakos, R. Frank. Influence of six rejuvenators on the performance properties of reclaimed asphalt pavement (RAP) binder and 100% recycled asphalt mixtures. Construction and Building Materials. 2014, 71, 538-550.

[72] F. Santos, A. Faxina, S. Soares. Soy-based rejuvenated asphalt binders: impact on rheological properties and chemical aging indices. Construction and Building Materials. 2021, 300, 124220.

[73] M. Alae, L. Xu, Z. Cao, X. Xu, F. Xiao. Fatigue and intermediate-temperature cracking performance of rejuvenated recycled asphalt binders and mixtures: A review. Journal of Cleaner Production. 2023, 384, 135587.

[74] H. Chen, H. Bahia. Modelling effects of aging on asphalt binder fatigue using complex modulus and the LAS test. International Journal of Fatigue. 2021, 146, 106150.

[75] R. Hajj, A. Bhasin. The search for a measure of fatigue cracking in asphalt binders - a review of different approaches. International Journal of Pavement Engineering. 2018, 19(3), 205-219.

[76] M. Elkashef, R. Williams, E. Cochran. Investigation of fatigue and thermal cracking behavior of rejuvenated reclaimed asphalt pavement binders and mixtures. International Journal of Fatigue. 2018, 108, 90-95.

[77] G. Guduru, A. Goli, S. Matolia, K. Kuna. Chemical and performance characteristics of rejuvenated bituminous materials with high reclaimed asphalt content. Journal of Materials in Civil Engineering. 2021, 33(1), 04020434.

[78] Z. Zhou, X. Gu, Q. Dong, F. Ni, Y. Jiang. Rutting and fatigue cracking performance of SBS-RAP blended binders with a rejuvenator. Construction and Building Materials. 2019, 203, 294-303.

[79] A. Mirhosseini, S. Tahami, I. Hoff, S. Dessouky, C. Ho. Performance evaluation of asphalt mixtures containing high-RAP binder content and bio-oil rejuvenator. Construction and Building Materials. 2019, 227, 116465.

[80] B. Asadi, N. Tabatabaee, R. Hajj. Use of linear amplitude sweep test as a damage tolerance or facture test to determine the optimum content of asphalt rejuvenator. Construction and Building Materials. 2021, 300, 123983.

[81] Y. Luo, P. Guo, J. Gao, J. Meng, Y. Dai. Application of design-expert response surface methodology for the prediction of rejuvenated asphalt fatigue life. Journal of Cleaner Production. 2022, 379, 134427.

[82] K. Yang, R. Li, C. Castorena, B. Underwood. Correlation of asphalt binder linear viscoelasticity (LVE) parameters and the ranking consistency related to fatigue cracking resistance. Construction and Building Materials. 2022, 322, 126450.

[83] W. Cao, Y. Wang, C. Wang. Fatigue characterization of bio-modified asphalt binders under various laboratory aging conditions. Construction and Building Materials. 2019, 208, 686-696.

[84] K. Zhao, W. Wang, L. Wang. Fatigue damage evolution and self-healing performance of asphalt materials under different influence factors and damage degrees. International Journal of Fatigue. 2023, 171, 107577.

[85] C. Yan, L. Yuan, X. Yu, S. Ji, Z. Zhou. Characterizing the fatigue resistance of multiple modified asphalts using time sweep test, LAS test and elastic recovery test. Construction and Building Materials, 2022, 322, 125806.

[86] H. Wang, X. Liu, M. van de Ven, G. Lu, S. Erkens, A. Skarpas. Fatigue performance of long-term aged crumb rubber modified bitumen containing warm-mix additives. Construction and Building Materials. 2020, 239, 117824.

[87] Z. Shi, Q. Su, F. Kavoura, M. Veljkovic. Uniaxial tensile response and tensile constitutive model of ultra-high performance concrete containing coarse aggregate (CA-UHPC). Cement and Concrete Composites. 2023, 136, 104878.

[88] Y. Gao, L. Li, Y. Zhang. Modelling crack initiation in bituminous binders under a rotational shear fatigue load. International Journal of Fatigue. 2020, 139, 105738.

[89] Y. Gao. Multiscale modelling of bonding performance of bituminous materials. PhD Thesis. Aston University. 2019.

8

MD simulations exploring the rejuvenation mechanisms of rejuvenated bitumen

This section delves into the efficaciousness of distinct rejuvenators concerning the molecular-scale attributes of aged bitumen, utilizing molecular dynamics simulations. A suite of thermodynamic metrics of rejuvenated bitumen models will be measured and compared to understand the difference in the efficacy of rejuvenators. Furthermore, this study will propose efficient atomic-level indicators for appraising and discriminating rejuvenation efficacy. These encompass physical indices, energetic parameters, dynamic behaviors, volumetric indicators, and interface characteristics. A key aspect of this chapter is linking the critical high-temperature, low-temperature, and fatigue indicators discussed in **Chapter 7** *with thermodynamic properties derived from MD simulations of virgin, aged, and rejuvenated binders. This approach aims to establish a comprehensive multiscale evaluation framework for rejuvenated bitumen.*

8.1 Introduction

In the Netherlands, the Sustainable Road Pavement Transition Path proposes to work on climate-neutral and 100% circular, with high-quality reuse of all materials and halving the use of primary raw materials, but with the high-quality standard that we are used to [1]. The concept of sustainable circulation expects that about 70% of reclaimed porous asphalt "waste" materials will be reused by 2030 [2]. To ensure the satisfactory engineering performance of recycled asphalt pavement with a high RAP ratio, the rejuvenators must be adopted [3, 4]. Thus, it is essential to develop high-efficiency rejuvenation technologies, but challenges still exist, especially for inconsistent rejuvenation efficiency evaluation methods and unclear rejuvenation mechanisms between different rejuvenators and aged binders [5]. It is also the main objective of the whole thesis, and **Chapter 7** has proposed several critical evaluation indicators on high-and-low temperature performance and fatigue behavior of rejuvenated bitumen from rheological measurements. These experimental parameters are beneficial to accelerating the establishment of uniform experimental methods for rejuvenation efficiency evaluation.

However, it is insufficient to build a comprehensive design-production-evaluation framework on rejuvenator-aged bitumen blends only based on macroscopic tests [6, 7]. The resource and component diversity of both rejuvenator and aged bitumen will lead to extensive rheological and mechanical tests [8, 9]. Therefore, it is necessary to fundamentally understand the rejuvenation mechanisms of variable rejuvenator-aged bitumen systems and exploit a multiscale evaluation framework. To this end, researchers have carried out molecular-scale characterizations and simulations on different rejuvenated bitumen systems [10, 11]. The molecular dynamics (MD) simulations are popularly utilized to fundamentally explore the rejuvenation efficiency and mechanism of various rejuvenated bitumen.

Although the rejuvenator type, influence factors, and evaluation indicators involved in various MD simulation studies are different, the general conclusion was drawn that the involvement in rejuvenator molecules would enhance these thermodynamic indicators and molecular distribution (especially for asphaltene clusters [12, 13]) of aged bitumen more or less. However, current MD simulation studies were only implemented to detect whether the addition of rejuvenator molecules would restore the thermodynamic and structural parameters of the aged bitumen model, and explain the molecular-scale rejuvenation mechanism. Limited work has been conducted to systematically investigate the influence of rejuvenator type/dosage and aging level of bitumen on MD simulation results, and the effective thermodynamic indices for rejuvenation efficiency evaluation of different rejuvenated bitumen models are still inconsistent and unclear. Meanwhile, MD simulation studies are always implemented solely with fewer connections with experimental rheological and mechanical properties of rejuvenated bitumen. Consequently, MD simulations on rejuvenated bitumen are only at the research stage with fewer benefits to guiding rejuvenator evaluation, optimization, and exploitation.
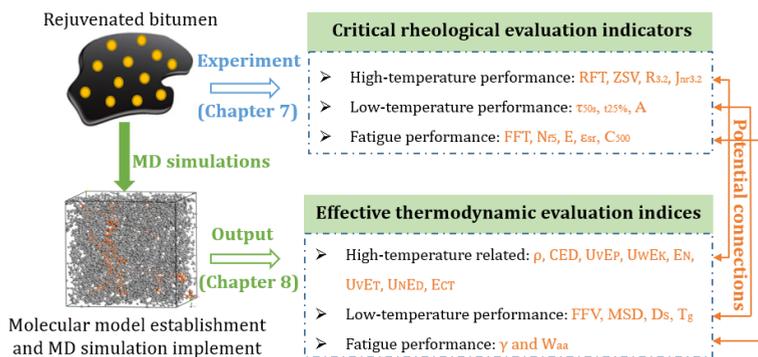
Figure 8.1 Flowchart of research structure

The main objective of this chapter is to fundamentally understand the rejuvenation efficiency and mechanism between different rejuvenators and aged bitumen at the molecular scale. It is expected to propose effective thermodynamic indices outputted from MD simulations for rejuvenation efficiency evaluation, closely related to macroscale critical rheological indicators measured from experiments. The research structure of this chapter and its connection with **Chapter 7** are illustrated in **Figure 8.1**. The molecular models of rejuvenated bitumen will be established by involving the rejuvenator molecules in the aged bitumen model based on **Chapters 3** and **4**. After MD equilibrium simulations, various thermodynamic properties of these rejuvenated bitumen models will be predicted.

8.2 Molecular models' establishment of rejuvenated bitumen

To mitigate any potential impact stemming from the MD simulation protocol, the procedure for generating rejuvenated bitumen aligns with that utilized for aged binders as outlined in **Chapter 3**. Illustrated in **Figure 8.2(a)**, the integration of rejuvenator molecules (depicted in orange) occurred through random dispersion amongst aged bitumen molecules (depicted in grey). Subsequently, an initial model geometry optimization was executed to achieve energy minimization and configuration stabilization. **Figure 8.2** presents a selection of overarching outcomes.
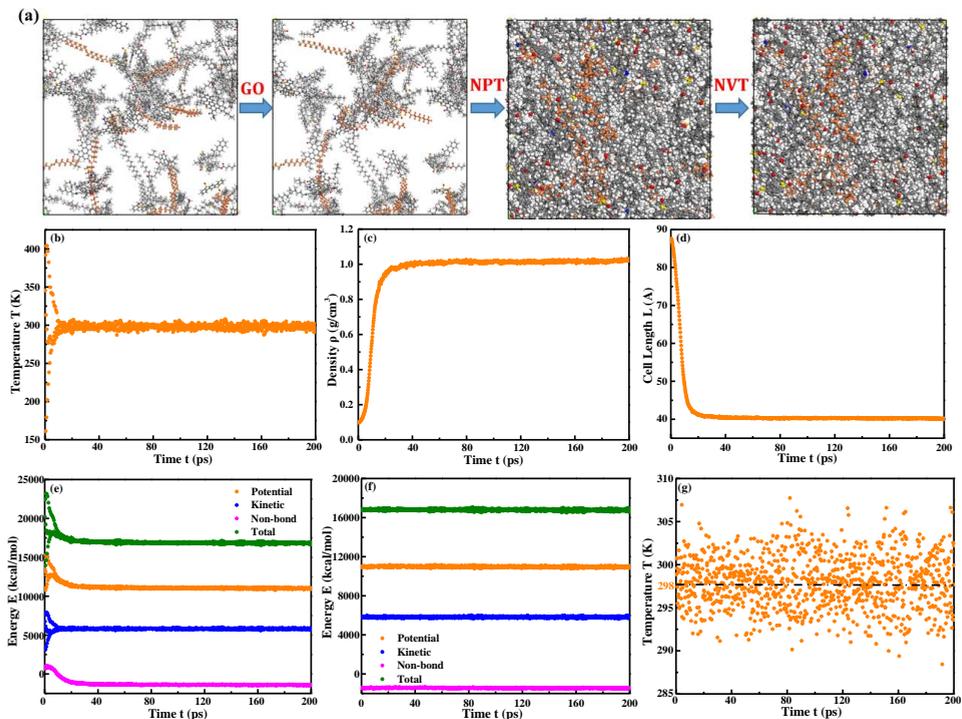
Figure 8.2 Graph illustration of MD model establishment of rejuvenated bitumen and thermodynamic parameters' variations during MD simulations (a) MD simulation process; (b)-(e) thermodynamic parameters during NPT; (f)(g) Energy and temperature during NVT

In the NPT simulation, equilibrium states for temperature (T = 298K), density (ρ), cell length (L), and energetic parameters (potential, kinetic, non-bond, and total energies) were promptly achieved. This substantiates the stability and precision of the MD simulation protocol. Similarly, the NVT simulation

exhibited constant energetic parameters along with temperature stability within a fluctuation range of ±10K. The fixed volume inherent to the NVT process resulted in unchanging density and cell length [14].

Within this thesis, 28 rejuvenated bitumen samples with variable rejuvenator type, dosage, and aging degree of bitumen were subjected to the MD simulations, and their MD simulation protocols were the same as discussed above. The investigation encompasses three aging degrees (1P, 2P, and 4P) of bitumen as expounded in **Chapter 3**. The average molecular structures of rejuvenators are introduced in **Chapter 4**, including the bio-oil (B), engine-oil (E), naphthenic-oil (N), and aromatic-oil (A). For 2P-aged bitumen, five rejuvenator dosages (5%, 7.5%, 10%, 12.5%, and 15%) of four rejuvenators are considered. In contrast, 1P and 4P aged binders involve only the 10% dosage, affording insight into the interplay between aging level and rejuvenated bitumen properties. The detailed model information is elucidated in **Table 8.1**.

Table 8.1 Molecular information of rejuvenated bitumen models

Models	No.B	No.R	No.C	No.H	No.N	No.O	No.S	No.M	Mw	V/Å³
VB	76	0	2441	3284	8	22	31	76	34032	56564.1
SAB	76	0	2462	3300	8	25	32	76	34380	56955.4
LAB20	75	0	2486	3301	11	51	32	75	35127	57453.8
LAB40	75	0	2480	3172	12	112	34	75	35980	56757.8
LAB80	75	0	2520	3006	14	217	37	75	38098	58652.0
1P10B	75	13	2733	3769	11	77	32	88	38975	64716.8
1P10E	75	13	2772	3873	11	51	32	88	39131	65383.9
1P10N	75	10	2746	3781	11	51	32	85	38727	64374.8
1P10A	75	9	2756	3861	11	51	32	84	38927	64342.6
2P5B	75	6	2594	3388	12	124	34	81	37756	61062.7
2P7.5B	75	10	2670	3532	12	132	34	85	38940	63165.3
2P10B	75	13	2727	3640	12	138	34	88	39828	65223.6
2P12.5B	75	17	2803	3784	12	146	34	92	41012	67642.2
2P15B	75	21	2879	3928	12	154	34	96	42196	69957.3
2P5E	75	6	2612	3436	12	112	34	81	37828	61515.2
2P7.5E	75	9	2678	3568	12	112	34	84	38752	63881.0
2P10E	75	13	2766	3744	12	112	34	88	39984	66322.0
2P12.5E	75	17	2854	3920	12	112	34	92	41216	69120.1
2P15E	75	20	2920	4052	12	112	34	95	42140	70980.0
2P5N	75	5	2610	3412	12	112	34	80	37780	60903.3
2P7.5N	75	8	2688	3556	12	112	34	83	38860	63102.3
2P10N	75	11	2766	3700	12	112	34	86	39940	65211.1
2P12.5N	75	14	2854	3844	12	112	34	89	41020	67427.0
2P15N	75	17	2922	3988	12	112	34	92	42100	69480.7
2P5A	75	5	2683	3372	12	112	34	80	37980	60971.0
2P7.5A	75	7	2690	3452	12	112	34	82	38780	62363.7
2P10A	75	10	2780	3572	12	112	34	85	39980	64932.2
2P12.5A	75	13	2870	3692	12	112	34	88	41180	66974.8
2P15A	75	16	2960	3812	12	112	34	91	42380	69368.0
4P10B	75	14	2786	3510	14	245	37	89	42242	65914.1
4P10E	75	13	2806	3578	14	217	37	88	42102	66173.1
4P10N	75	11	2806	3534	14	217	37	86	42058	66388.3
4P10A	75	10	2820	3406	14	217	37	85	42098	65498.9

Note: B-bitumen, R-rejuvenator, C-carbon, H-hydrogen, N-nitrogen, O-oxygen, S-sulfur, M-molecule, Mw-molecule weight, V-model volume

The ultimate equilibrium structures of 2P rejuvenated bitumen at 298K are presented in **Figure 8.3**, featuring varying rejuvenator dosages of 5%, 10%, and 15%. Notably, the distribution of rejuvenator molecules in aged bitumen is uneven, influenced by both rejuvenator type and dosage. This thesis mainly focuses on the thermodynamic property prediction of rejuvenated binders, and the structural parameters and molecular distribution of rejuvenator and aged bitumen molecules will not be examined.
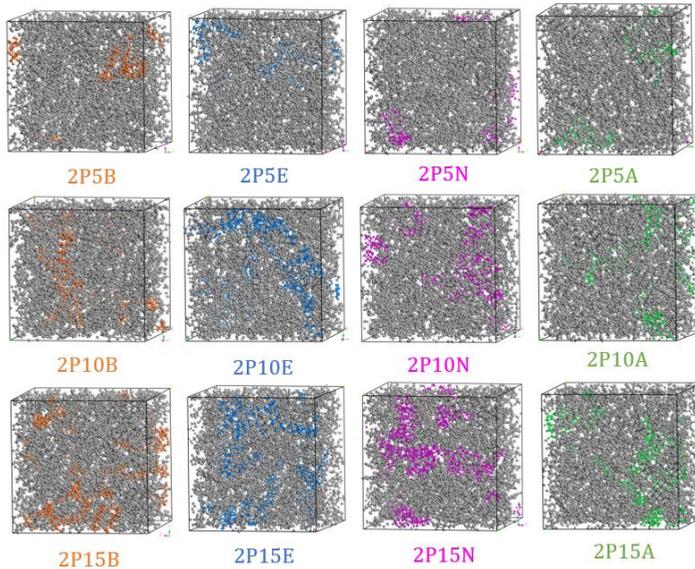
Figure 8.3 Bulk molecular models of 2P5, 2P10, and 2P15 rejuvenated bitumen at 298K
Grey: aged bitumen; Orange: bio-oil; Blue: engine-oil; Pink: naphthenic-oil; Green: aromatic-oil
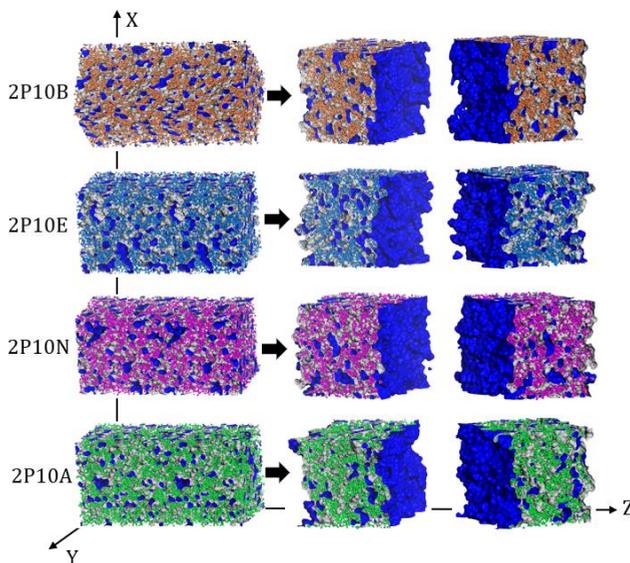
Figure 8.4 Bulk (left) and Confined (right) molecular models of 2P10 rejuvenated bitumen

In addition to the bulk molecular models, a distinct set of confined models has been established for all rejuvenated bitumen models to assess their surface characteristics, including surface energy and work of cohesion. The chemical constituents and MD simulation protocols used in the confined models mirror those of the corresponding bulk models for rejuvenated bitumen [15]. The primary distinction between these confined and bulk models lies in the boundary condition applied along the Z-axis. While the bulk models of rejuvenated bitumen feature a periodic boundary condition in all directions, the confined models only exhibit a periodic boundary condition along the X and Y directions. Along the Z-axis, a confined vacuum layer is introduced, as illustrated in **Figure 8.4**. As there is no boundary along the Z-axis in the confined model, two additional confined surfaces are created in this direction, as indicated in blue.

8.3 Molecular-scale evaluation indicators from MD simulations

The key molecular-scale assessment parameters for rejuvenated bitumen models, as presented in **Figure 8.5**, are used to gauge the impact of different rejuvenators on various thermodynamic properties of aged bitumen, as predicted through MD simulations. These thermodynamic properties encompass a wide range of aspects, including physical characteristics (such as density and glass transition temperature), intermolecular forces (cohesive energy density), energetic attributes, dynamic behavior (self-diffusion capacity), volumetric parameters, and surface properties (surface free energy). Subsequent sections provide detailed explanations of the definitions and methodologies applied to compute these comprehensive thermodynamic properties. The definitions and calculation equations for these thermodynamic indicators were previously introduced in **Chapters 3** and **4**. This section exclusively introduces a variety of energetic parameters.
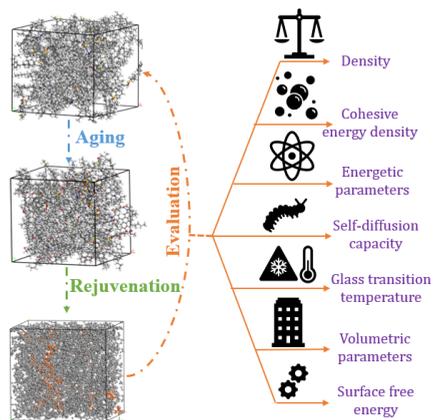
Figure 8.5 Graph illustration on molecular-scale evaluation indicators of bitumen models

At the atomic level, the energetic parameters are the basic for calculating various thermodynamic properties of bitumen models [16]. With the COMPASSII force field, energetic indices show the relationships as:

$$E_T = E_P + E_K = (E_V + E_N) + E_K = [(E_D + E_{CT}) + E_N] + E_K \tag{8.1}$$

where E_T is the total energy and is composed of potential energy E_P and kinetic energy E_K. Two elements of potential energy are valence energy E_V and non-bond energy E_N. The valence energy is divided into diagonal energy E_D and cross-terms energy E_{CT}.

Due to the heterogeneity characteristic of bitumen molecular distribution, the energetic parameters in a bitumen model are uneven. Thus, several unit energetic parameters are introduced: energy per volume U_VE (**Eq.8.2**), energy per weight U_WE (**Eq.8.3**), and energy per number U_NE (**Eq.8.4**).

$$U_V E = \frac{E}{V} \tag{8.2}$$

$$U_W E = \frac{E}{W} \tag{8.3}$$

$$U_N E = \frac{E}{N} \tag{8.4}$$

where E is the energetic parameter; V, W, and N refer to the model volume, molecular weight, and molecular number, respectively. The unit of $U_V E$ is kcal/(mol·Å³), while the unit of $U_W E$ and $U_N E$ is the same as kcal/mol.

Like the rejuvenation percentage based on rheological indices in **Chapter 7**, the thermodynamic-based rejuvenation percentage TRP of rejuvenated bitumen models is calculated as:

$$TRP = \frac{T_{aged} - T_{rejuvenated}}{T_{aged} - T_{fresh}} * 100 \tag{8.5}$$

where T represents a set of thermodynamic parameters encompassing density, cohesive energy density, energetic parameters, fractional free volume, self-diffusion coefficient, glass transition temperature, surface free energy, and work of cohesion. Moreover, T_{aged}, $T_{rejuvenated}$, and T_{fresh} denote the thermodynamic properties of aged, rejuvenated, and fresh bitumen, respectively.

8.4 MD simulation results and discussion

8.4.1 Rejuvenation effect on density (ρ)

The density-based rejuvenation percentage DRP values of these rejuvenated bitumen models at variable temperatures are shown in **Figure 8.6**. Regardless of temperature and rejuvenator dosage, the EORB binders exhibit the highest DRP values due to the lower ρ value of the engine-oil rejuvenator than the others. That's why the incorporation of an engine-oil rejuvenator regenerates the density of aged bitumen. However, the aromatic-oil with the highest ρ value shows the lowest restoration effect on the density of aged bitumen.
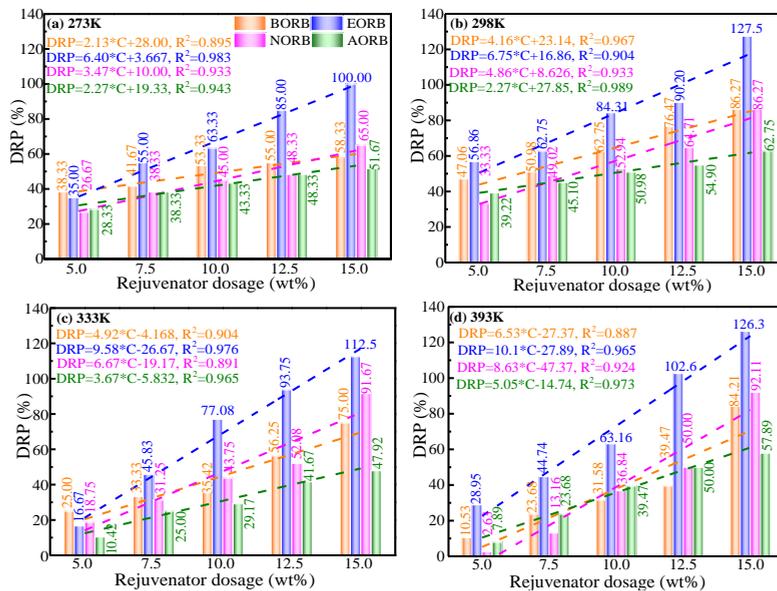
Figure 8.6 DRP values of rejuvenated bitumen

It is noticed that the DRP values of all simulated rejuvenated bitumen models are distributed in 0-130%, agreeing well with the rejuvenation efficiency range based on rheological properties in **Chapter 7**. Meanwhile, all DRP values of BORB, NORB, and EORB binders are lower than 100% even through the rejuvenator dosage reaches 15%. It implies that bio-oil, naphthenic-oil, and aromatic-oil rejuvenators fail to completely restore the ρ value of aged bitumen to virgin bitumen level. On the other hand, the ρ value of EORB binders is lower than virgin bitumen when the EO dosage exceeds 12.5% (273K, 298K, and 333K) or 10% (393K). The positive and linear correlation law between DRP values of rejuvenated bitumen and rejuvenator dosage is observed, and the magnitude of slope value for different rejuvenated bitumen is EORB > NORB > BORB > AORB, which is independent of rejuvenator dosage and temperature. Interestingly, the naphthenic-oil has a higher ρ value than bio-oil (see **Chapter 4**), but NORB shows a higher DRP value than BORB. It may be speculated that the own ρ value of the rejuvenator and its interaction level with aged bitumen both determine the final density of rejuvenated bitumen. According to the slope values, it is discerned that high temperatures hasten the rejuvenation efficiency of rejuvenators on density recovery of aged bitumen.

The aging degree influence on density recovery of aged bitumen by adding rejuvenators is investigated and the DRP results are displayed in **Figure 8.7**. With the elongation of aging duration, the DRP values of rejuvenated bitumen manifest an exponential attenuation. This observation underscores that heightened bitumen aging substantially diminishes the capacity of rejuvenators to induce recovery in the density attribute of aged bitumen [14]. Remarkably, irrespective of aging degree and temperature, the most pronounced DRP values are demonstrated by EORB binders. Notably, the magnitude of DRP values within BORB, NORB, and AORB binders is subject to the modulation introduced by aging duration and temperatures.
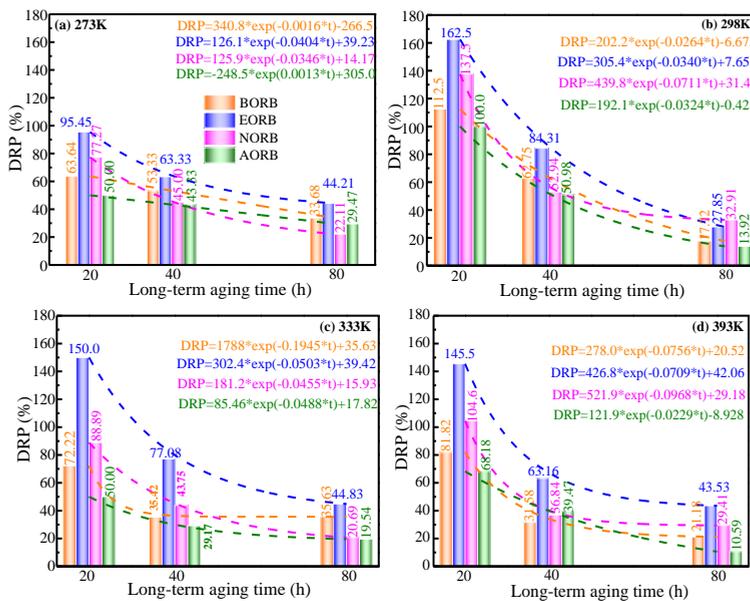
Figure 8.7 Influence of aging degree on DRP of rejuvenated bitumen

8.4.2 Rejuvenation effect on cohesive energy density (CED)

The CED-based rejuvenation percentages CEDR values of different rejuvenated bitumen are calculated and displayed in **Figure 8.8**. The CEDR values of all rejuvenated bitumen enlarge linearly as the rejuvenator dosage increases. Regardless of temperature and rejuvenator dosage, the CEDR values of BORB and AORB are lower than EORB and NORB binders. It means that the aromatic-oil rejuvenator shows the lower regenerating effect on the CED parameter of aged bitumen, while the naphthenic-oil rejuvenator has the largest CEDR

values. Meanwhile, the rejuvenation efficiency of bio-oil and engine-oil on CED recovery of aged bitumen is in the middle, and the engine-oil influence is more significant than the bio-oil rejuvenator.
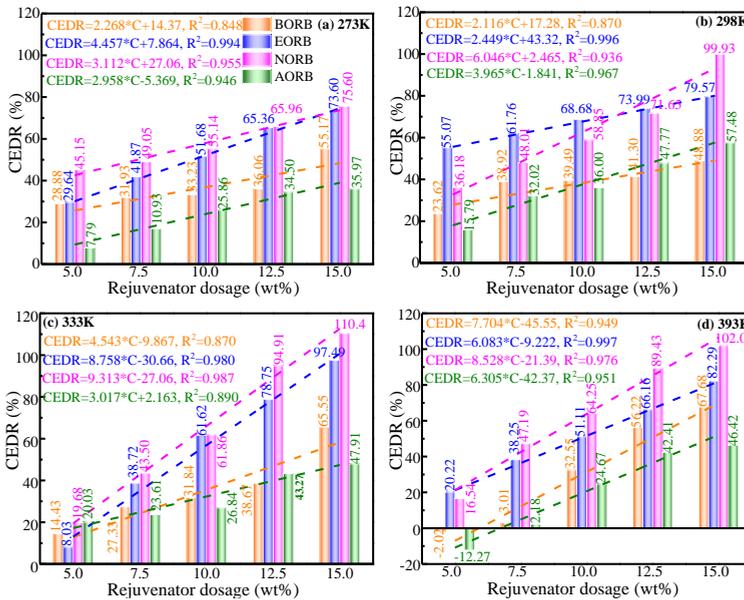
Figure 8.8 The CEDR values versus rejuvenator dosage of different rejuvenated bitumen
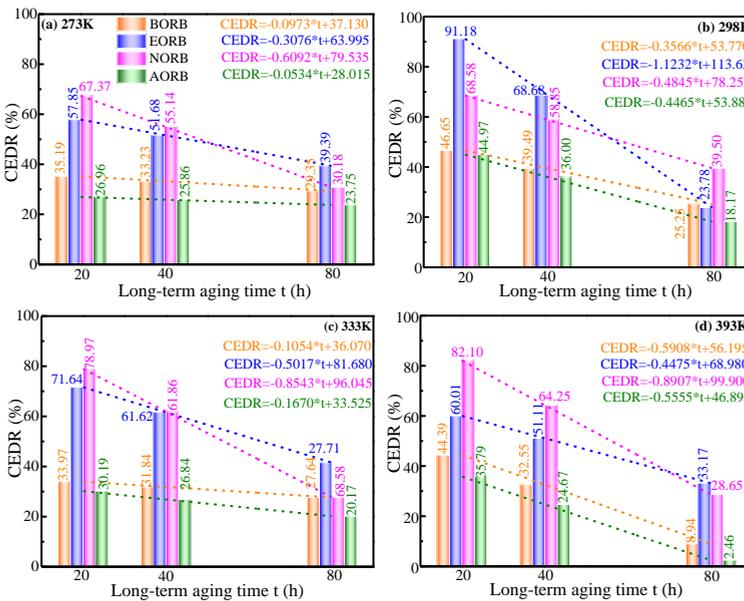
Figure 8.9 Aging effect on CEDR values of rejuvenated bitumen

Temperature shows a positive impact on enlarging the CEDR values of rejuvenated bitumen. At both 273K and 298K, all CEDR values are lower than 100%, indicating that all rejuvenators fail to regenerate the

CED value of aged bitumen to virgin bitumen level. Within all temperature and rejuvenator dosage regions, the CEDR values of engine-oil, bio-oil, and aromatic-oil rejuvenated bitumen are lower than 100%. Therefore, most rejuvenators cannot completely restore the cohesive energy density of aged bitumen even through their rejuvenator content reaches 15%. Overall, the CED parameter is effective in distinguishing the rejuvenation efficiency of aromatic-oils and others. Although the difference in CEDR of different rejuvenated bitumen is observed, the magnitude of CEDR values of bio-oil, engine-oil, and naphthenic-oil rejuvenators are converse to their order in high-temperature properties from experimental tests. The CED parameter can affect but only partially reflect the rejuvenation effectiveness of various rejuvenators on the macroscale high-temperature performance of aged bitumen.

The CEDR values of rejuvenated bitumen with variable aging degrees are shown in **Figure 8.9**. As the long-term aging level deepens, the CEDR parameter of rejuvenated bitumen declines linearly and distinctly. It manifests that the rejuvenation effect of rejuvenators on CED recovery of aged bitumen with higher aging levels becomes lower. Regardless of aging degree, the AORB binders have the smallest CEDR values, followed by BORB. However, the sequence in CEDR values of EORB and NORB binders is dependent on temperature and aging degree of bitumen.

8.4.3 Rejuvenation effect on energetic parameters

This thesis tries to explore the possibility of different energetic parameters outputted from MD simulations as effective indicators for reflecting the rejuvenation efficiency of various rejuvenators on aged bitumen. The flexibility of various energetic parameters as effective indicators for evaluating the rejuvenation efficiency of different rejuvenators is discussed. **Table 8.2** summaries the aging and rejuvenation effect on these energetic parameters of bitumen. Regardless of evaluation size, all potential energy indicators (E_P, $U_V E_P$, $U_W E_P$, and $U_N E_P$) can evaluate the rejuvenation effectiveness of bio-oil, engine-oil, and naphthenic-oil rejuvenators, but fail to assess the aromatic-oil. The E_K and $U_W E_K$ indices are applicable to estimate the rejuvenation effect on the kinetic energy of aged bitumen. Regarding the non-bond energy, the E_N is an effective evaluation parameter, while the others cannot succeed in the aromatic-oil rejuvenated binder. Meanwhile, it is not possible to use the E_T index for rejuvenation efficiency evaluation on the total energy of aged bitumen. The three average parameters ($U_V E_T$, $U_W E_T$, and $U_N E_T$) show the limitation in assessing the aromatic-oil rejuvenated bitumen. In addition, the diagonal energy is in the same situation as the total energy and only E_{CT} can reflect the rejuvenation work on cross-term energy. Overall, the effective energetic parameters for all rejuvenators are E_K ($U_W E_K$), E_N, and E_{CT}. The other three energetic parameters (potential, total, and diagonal) are also important to determine the thermodynamic and mechanical properties of rejuvenated bitumen, and the only issue for them is their application restriction in aromatic-oil case. Thus, this thesis will discuss the effective potential, total, and diagonal energetic parameters for bio-oil, engine-oil, and naphthenic-oil rejuvenated binders.

Table 8.2 Summary of aging and rejuvenation effects on different energetic parameters of bitumen

Energetic parameters		E_P	E_K	E_N	E_T	E_D	E_{CT}
E	Aging	+	-	+	+	+	+
	Rejuvenation	-, +(AO)	+	-	+	+ (BO, AO)	-
$U_V E$	Aging	+	-	+	+	+	+
	Rejuvenation	-, +(AO)	-	-, +(AO)	-, +(AO)	-, +(AO)	+
$U_W E$	Aging	+	-	+	+	O*	+
	Rejuvenation	-, +(AO)	+	-, +(AO)	-, +(AO)	-, +(AO)	+
$U_N E$	Aging	+	-	+	+	+	+
	Rejuvenation	-, +(AO)	-	-, +(AO)	-, +(AO)	-, +(AO)	+

Note: "+" and "-" mean the increasing effect and decreasing effect, respectively. O* shows no variation law.

8.4.3.1 Potential energy (E_P)

The potential energy-based rejuvenation percentages of rejuvenated bitumen are calculated and listed in **Table 8.3**. All E_PR values of AORB binders are negative, indicating that the addition of aromatic-oil fails to restore the potential energy of aged bitumen. Conversely, the other three rejuvenators (bio-oil, engine-oil, and naphthenic-oil) exhibit a positive rejuvenation function, and their E_PR values enlarge significantly as the rejuvenator dosage increases. However, the E_PR values of rejuvenated bitumen are lower than U_VE_PR, U_WE_PR, and U_NE_PR values. The reason is that the amount of rejuvenator molecules is lower than the whole aged bitumen molecules, and its influence on the whole potential energy is limited.

The rejuvenation efficiency of rejuvenator molecules on aged bitumen per volume, weight, and number is more significant. The E_PR values of BORB are negative due to the strong intermolecular interaction between polar groups in bio-oil with aged bitumen molecules, but the positive effect of bio-oil on unit potential energy is observed. Regardless of rejuvenator dosage and unit potential energy type, engine-oil has the largest rejuvenation efficacy, followed by NORB, BORB, and AORB. Further, the U_WE_PR values are higher than U_VE_PR and U_NE_PR, and the latter two are close, which are higher than the rejuvenation percentages based on critical high-temperature indicators. To this end, it is recommended to use the U_VE_PR index with the lowest values to evaluate the rejuvenation effectiveness on the potential energy of BORB, EORB, and NORB binders.

Table 8.3 Potential energy-based rejuvenation percentages of rejuvenated bitumen

E_PR	BORB	EORB	NORB	AORB	U_VE_PR	BORB	EORB	NORB	AORB
5%	-10.56	4.69	1.54	-90.72	5%	54.64	65.28	52.69	-33.11
7.5%	-6.63	8.08	2.05	-124.8	7.5%	76.27	98.34	87.99	-46.63
10%	-5.52	11.79	2.11	-178.6	10%	112.60	141.06	113.53	-56.35
12.5%	-4.40	14.21	5.73	-230.7	12.5%	144.68	175.29	148.0	-66.70
15%	-3.91	18.53	6.34	-280.6	15%	175.88	204.10	183.94	-72.12
U_WE_PR	BORB	EORB	NORB	AORB	U_NE_PR	BORB	EORB	NORB	AORB
5%	74.89	93.51	86.64	-70.60	5%	58.37	65.55	53.74	-24.74
7.5%	113.95	138.73	131.71	-92.86	7.5%	89.48	95.66	81.46	-31.96
10%	159.28	194.37	176.23	-129.3	10%	118.90	131.99	108.09	-44.33
12.5%	202.63	244.58	224.41	-160.8	12.5%	148.87	164.20	135.71	-54.53
15%	249.41	284.39	262.34	-186.9	15%	178.92	188.38	157.97	-62.41

8.4.3.2 Kinetic energy (E_K)

The kinetic energy-based rejuvenation percentages E_KR of rejuvenated bitumen are shown in **Table 8.4.** It further reveals the unsuitability of U_VE_K and U_NE_K indices for rejuvenation efficiency evaluation based on negative U_VE_KR and U_NE_KR values. Besides, the E_KR values are much higher than the U_WE_KR, and the former (400-1700%) seriously deviated from the sequence order of rejuvenation percentages based on critical macroscale performance presented in **Chapter 7**.

Table 8.4 Kinetic energy-based rejuvenation percentages of rejuvenated bitumen

E_KR	BORB	EORB	NORB	AORB	U_VE_KR	BORB	EORB	NORB	AORB
5%	448.50	513.28	480.96	456.42	5%	29.49	31.20	67.52	24.36
7.5%	733.12	761.14	759.21	630.98	7.5%	5.13	25.21	59.40	12.82
10%	942.92	1089.1	1034.7	892.93	10%	-9.40	12.39	55.13	-8.97
12.5%	1226.4	1417.7	1311.3	1157.6	12.5%	-29.91	2.99	43.16	-26.50
15%	1511.2	1669.3	1588.9	1417.3	15%	-39.74	-8.97	1.71	-54.27
U_WE_KR	BORB	EORB	NORB	AORB	U_NE_KR	BORB	EORB	NORB	AORB
5%	17.09	26.32	22.14	10.22	5%	-3050	-1505	15.33	-577.2
7.5%	25.02	36.94	32.59	12.57	7.5%	-5171	-2379	-216.7	-977.1
10%	30.06	49.91	42.08	15.96	10%	-6716	-3508	-493.5	-1539
12.5%	37.03	62.18	51.13	19.62	12.5%	-8540	-4523	-730.5	-2003
15%	43.82	71.84	59.92	22.23	15%	-10186	-5125	-928.2	-2542

The U_WE_KR acts as the critical index for assessing the rejuvenation efficiency of different rejuvenators on the kinetic energy of aged bitumen. By comparing the magnitude of different E_KR, the influence level of rejuvenation on E_K and U_NE_K is more significant than the U_VE_K and U_WE_K. All U_WE_KR values of rejuvenated bitumen are lower than 100%, indicating the U_WE_K of aged bitumen cannot be fully regenerated by rejuvenators even when the rejuvenator dosage reaches 15%. The sequence of U_WE_KR values of rejuvenated bitumen follows EORB > NORB > BORB > AORB.

8.4.3.3 Non-bond energy (E_N)

Only E_N parameter can reflect the rejuvenation work of all rejuvenators on non-bond energy of aged bitumen, while other unit E_N parameters fail to evaluate the rejuvenation efficiency of aromatic-oil rejuvenated bitumen. This finding is further verified based on the rejuvenation percentages results presented in **Table 8.5**. The U_VE_NR, U_WE_NR, and U_NE_NR values of all rejuvenated binders are located in -20-20%, lower than the E_NR region (0-51%). It manifests that the influence degree of rejuvenation on the average non-bond energy per volume, weight, and number is limited and lower than potential and kinetic energy. The E_NR values of rejuvenated bitumen are reasonable although it is smaller than the rheological-based rejuvenation percentages in **Chapter 7**. Similar to U_WE_K, the E_N value of aged bitumen does not return to the virgin bitumen level by adding rejuvenators with dosages varying from 5% to 15%. The BORB shows the highest E_NR value, followed by EORB and NORB, while aromatic-oil exhibits the lowest rejuvenation efficacy on non-bond energy.

Table 8.5 Non-bond energy-based rejuvenation percentages of rejuvenated bitumen

E_NR	BORB	EORB	NORB	AORB	U_VE_NR	BORB	EORB	NORB	AORB
5%	14.43	17.37	13.29	3.43	5%	2.65	4.93	-4.20	-7.39
7.5%	15.35	20.32	16.00	6.77	7.5%	4.74	-2.37	-1.46	-7.66
10%	35.17	25.09	24.28	8.44	10%	8.94	-1.46	-0.36	-13.05
12.5%	43.01	36.44	30.47	9.96	12.5%	10.95	0.18	0.82	-15.60
15%	50.73	41.40	33.45	19.81	15%	13.05	1.64	2,46	-17.70
U_WE_NR	BORB	EORB	NORB	AORB	U_NE_NR	BORB	EORB	NORB	AORB
5%	4.47	3.77	3.43	-5.41	5%	-1.27	-8.37	-6.63	-8.48
7.5%	6.31	5.06	1.14	-5.91	7.5%	-0.13	-5.73	-4.46	-9.71
10%	12.21	6.60	3.33	-9.14	10%	3.20	-4.09	-3.08	-14.51
12.5%	15.69	7.50	3.77	-12.26	12.5%	4.19	-1.42	-2.20	-16.29
15%	18.87	7.55	1.84	-9.19	15%	5.00	2.69	1.12	-19.12

8.4.3.4 Total energy (E_T)

The total energy-based rejuvenation percentages of rejuvenated binders are displayed in **Table 8.6**. All rejuvenation percentages of AORB binders show a decreasing trend as the aromatic-oil dosage increases, but the positive U_VE_TR, U_WE_TR, and U_NE_TR values of AORB binders are observed. It implies that the incorporation of aromatic-oil can restore the total energy of aged bitumen, which weakens as the AO dosage increases.

Table 8.6 Total energy-based rejuvenation percentages of rejuvenated bitumen

E_TR	BORB	EORB	NORB	AORB	U_VE_TR	BORB	EORB	NORB	AORB
5%	26.88	29.37	29.04	-21.29	5%	77.21	81.38	72.76	28.79
7.5%	13.31	22.62	19.08	-46.14	7.5%	87.54	99.81	93.06	20.70
10%	8.97	13.27	9.82	-84.95	10%	109.79	124.55	105.50	17.45
12.5%	-1.67	3.18	2.54	-122.9	12.5%	128.6	143.28	125.08	12.91
15%	-10.33	-3.17	-7.44	-159.5	15%	146.26	159.77	148.08	11.66
U_WE_TR	BORB	EORB	NORB	AORB	U_NE_TR	BORB	EORB	NORB	AORB
5%	106.33	112.65	110.55	37.22	5%	77.25	79.37	70.88	27.70
7.5%	123.02	131.57	129.45	25.62	7.5%	97.28	97.29	86.67	24.16
10%	143.73	154.91	148.37	6.77	10%	115.65	119.01	101.91	17.93
12.5%	162,81	175.75	169.21	-9.74	12.5%	134.67	138.29	117.66	12.79
15%	183.62	192.31	185.12	-23.31	15%	153.51	152.56	130.36	9.05

It is different from the potential energy result that aromatic-oil cannot restore all potential energy terms of aged bitumen. The $E_T R$ values of AORB binders are negative, indicating aromatic-oil shows a negative effect on the total energy. Similar to potential energy, the $U_V E_T$, $U_W E_T$, and $U_N E_T$ indicators can evaluate the rejuvenation efficiency of bio-oil, engine-oil, and naphthenic-oil on the total energy of the aged bitumen model. The $U_W E_T R$ values are higher than the $U_V E_T R$ and $U_N E_T R$, and larger than the rejuvenated-based rejuvenation efficiency. The influence level of these rejuvenators on the $U_W E_T$ is more significant than the volume-average and number-average ones. Moreover, the $U_V E_T R$ and $U_N E_T R$ values are similar, and the $U_V E_T$ parameter is selected as an evaluation index for the total energy term to be consistent with potential energy. The order of $U_V E_T R$ values of rejuvenated bitumen is EORB > NORB ≈ BORB > AORB.

8.4.3.5 Diagonal energy (E_D)

The diagonal energy-based rejuvenation percentages $E_D R$ of rejuvenated bitumen are summarized in **Table 8.7**. The $E_D R$ and $U_W E_D R$ values of BORB, EORB, and NORB binders decrease remarkably as the rejuvenator dosage increases. Thus, the E_D and $U_W E_D$ parameters are not considered effective evaluation energetic indicators. With the $U_V E_D$ and $U_N E_D$ indices, the rejuvenation efficiency of bio-oil, engine-oil, and naphthenic-oil rejuvenators on the diagonal energy can be evaluated, but they fail to assess the effectiveness of aromatic-oil because the $U_V E_D R$ and $U_N E_D R$ values of AORB have a negative correlation with aromatic-oil dosage, although low aromatic-oil content (5%, 7.5%, and 10%) can restore the $U_V E_D$ and $U_N E_D$ values of aged bitumen to a certain degree. Interestingly, it is observed that the order of magnitude for $U_V E_D R$, $U_W E_D R$, and $U_N E_D R$ is larger than $E_D R$, indicating the rejuvenation effect on unit diagonal energy of the aged bitumen model is more significant than the whole model. This phenomenon is opposite to the non-bond energy case. The $U_V E_D R$ and $U_N E_D R$ values of BORB. EORB and NORB are much higher than their rejuvenation percentages on critical high-temperature properties (0-200%). To narrow the gap, the smaller one ($U_N E_D$) parameter is proposed as an effective index for estimating the diagonal energy of BORB, EORB, and NORB binders.

Table 8.7 Diagonal energy-based rejuvenation percentages of rejuvenated bitumen

$E_D R$	BORB	EORB	NORB	AORB	$U_V E_D R$	BORB	EORB	NORB	AORB
5%	56.66	90.19	93.53	-145.2	5%	294.05	341.68	308.40	49.77
7.5%	57.92	107.78	82.58	-232.6	7.5%	401.53	474.20	430.08	20.61
10%	34.81	86.20	76.16	-382.6	10%	493.13	598.02	516.79	2.44
12.5%	13.33	78.25	68.39	-522.3	12.5%	596.49	711.60	623.97	-14.05
15%	6.11	98.11	68.13	-686.9	15%	700.76	827.94	762.29	-47.18
$U_W E_D R$	BORB	EORB	NORB	AORB	$U_N E_D R$	BORB	EORB	NORB	AORB
5%	-300.5	-357.9	-357.5	-30.57	5%	198.35	220.87	198.85	36.56
7.5%	-433.3	-484.6	-460.0	0.34	7.5%	291.67	301.67	262.71	30.42
10%	-494.3	-581.7	-563.3	70.46	10%	341.23	372.99	324.99	9.78
12.5%	-583.9	-691.4	-659.3	122.64	12.5%	407.49	446.18	382.24	-3.16
15%	-687.4	-803.6	-760.3	204.48	15%	476.89	511.81	440.20	-30.08

8.4.3.6 Cross-terms energy (E_{CT})

The rejuvenation percentages based on cross-terms energy of rejuvenated bitumen $E_{CT} R$ are demonstrated in **Table 8.8**. It is detected that the $U_V E_{CT} R$, $U_W E_{CT} R$, and $U_N E_{CT} R$ values of all rejuvenated binders are negative, implying that the involvement of all rejuvenators has no rejuvenation work on the volume, weight, and number-average cross-terms energy of aged bitumen. However, the $E_{CT} R$ index exhibits an opposite result, and thus E_{CT} parameter is the only valid indicator to appraise the rejuvenation efficacy of different rejuvenators on cross-terms energy on aged bitumen. Further, the $E_{CT} R$ values of all rejuvenated binders are lower than 25%, showing that these rejuvenators (even with a 15% rejuvenator dosage) have restricted recoverable effects on the cross-terms energy of aged bitumen. The sequence of $E_{CT} R$ values of rejuvenated bitumen is AORB > BORB > EORB > NORB.

Table 8.8 Cross-terms energy-based rejuvenation percentages of rejuvenated bitumen

$E_{CT}R$	BORB	EORB	NORB	AORB	$U_VE_{CT}R$	BORB	EORB	NORB	AORB
5%	6.55	4.33	2.34	4.67	5%	-2.69	-5.05	-5.38	2.35
7.5%	6.76	6.81	4.67	11.89	7.5%	-6.90	-7.40	-8.75	-0.59
10%	11.61	7.58	5.95	15.37	10%	-7.49	-12.95	-11.44	-3.36
12.5%	14.55	9.44	9.14	19.53	12.5%	-10.34	-14.13	-13.54	-4.96
15%	17.77	12.41	11.81	24.88	15%	-12.53	-20.61	-17.24	-5.80
$U_WE_{CT}R$	BORB	EORB	NORB	AORB	$U_NE_{CT}R$	BORB	EORB	NORB	AORB
5%	-0.65	-2.74	-4.22	0.23	5%	-5.14	-7.27	-7.37	-1.92
7.5%	-3.34	-3.76	-5.85	-0.93	7.5%	-11.96	-10.22	-10.49	-4.11
10%	-4.36	-7.06	-8.22	-1.53	10%	-12.53	-16.09	-14.35	-5.10
12.5%	-4.83	-9.38	-9.01	-2.14	12.5%	-16.21	-20.30	-16.28	-5.55
15%	-5.94	-11.98	-10.12	-2.97	15%	-19.35	-24.74	-18.52	-7.04

8.4.3.7 Discussion on critical energetic parameters

Eventually, the critical energetic indicators for effectively evaluating the rejuvenation efficiency are proposed: U_VE_P, U_WE_K, E_N, U_VE_T, U_NE_D, and E_{CT}. These rejuvenation percentages based on critical energetic parameters of different rejuvenated bitumen with 15% rejuvenator dosage are plotted in **Figure 8.10**. These critical energetic indicators can reflect the rejuvenation effectiveness of all rejuvenators on atomic-level energetic characteristics of aged bitumen, except for the U_NE_D and U_VE_P parameters in aromatic-oil rejuvenated bitumen cases. The rejuvenator effects on various critical energetic parameters are different. For bio-oil, engine-oil, and naphthenic-oil rejuvenators, their influence levels on these energetic parameters follow the sequence of U_NE_D > U_VE_P > U_VE_T > U_WE_K > E_N > E_{CT}. Thus, the rejuvenation efficiency is affected not only by molecular type/dosage, but also by the evaluation parameter size (entire, per volume, per weight, or per molecule). For aromatic-oil rejuvenated bitumen, the E_CT_R, U_VE_T, E_N, and U_WE_K values are all lower than 25%, indicating that the aromatic-oil rejuvenator has a limited rejuvenation effect on these critical energetic indices. It is expected that these critical energetic indicators still work in other rejuvenator cases, which should be further validated and optimized. Furthermore, these essential energetic parameters of virgin, aged, and rejuvenated binders will be connected with their corresponding critical high-temperature indicators from experiments (proposed in **Chapter 7**) to establish a multi-scale evaluation framework on the rejuvenation efficiency of rejuvenators.
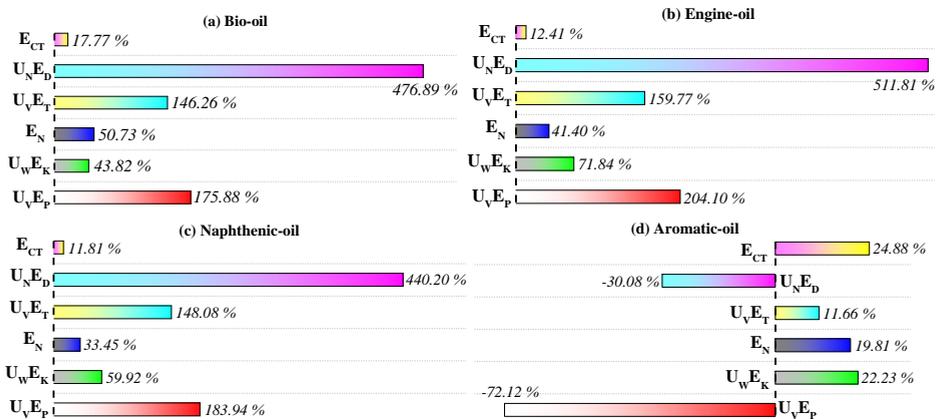
Figure 8.10 Comparison in energetic parameter-based rejuvenation percentages

The critical energetic parameter-based rejuvenation percentages of rejuvenated bitumen are displayed in **Figure 8.11** with variable rejuvenator types and dosages. All energetic rejuvenation percentages show linear relationships with rejuvenator content. Apart from the U_VE_PR, U_VE_TR, and U_NE_DR values of AORB, the increased rejuvenator dosage promotes the increment in energetic rejuvenation percentages of all

rejuvenated binders. Besides, the energetic rejuvenation percentages and their sensitivity levels to rejuvenator dosage are strongly affected by the rejuvenator type. The engine-oil rejuvenator exhibits the largest rejuvenation efficiency on potential, kinetic, total, and diagonal energies of aged bitumen, followed by the naphthenic-oil and bio-oils, while the aromatic-oil has the lowest rejuvenation effect on these energetic parameters. Moreover, bio-oil rejuvenator presents the highest rejuvenation efficacy on non-bond energy, followed by engine-oil, naphthenic-oil, and aromatic-oil rejuvenators. These findings agree well with the conclusion from **Chapter 7** that bio-oil and engine-oil show the highest rejuvenation percentages on high-temperature performance recovery of aged bitumen, followed by naphthenic-oil, whereas the aromatic-oil preserves the high-temperature rutting resistance of aged bitumen to the greatest extent. Nevertheless, it is worth noting that none of these essential energetic parameters exhibit the same rejuvenation percentage as those based on rheology. This suggests that the rheological performance of rejuvenated bitumen results from the collective influence of various molecular-scale energetic parameters.
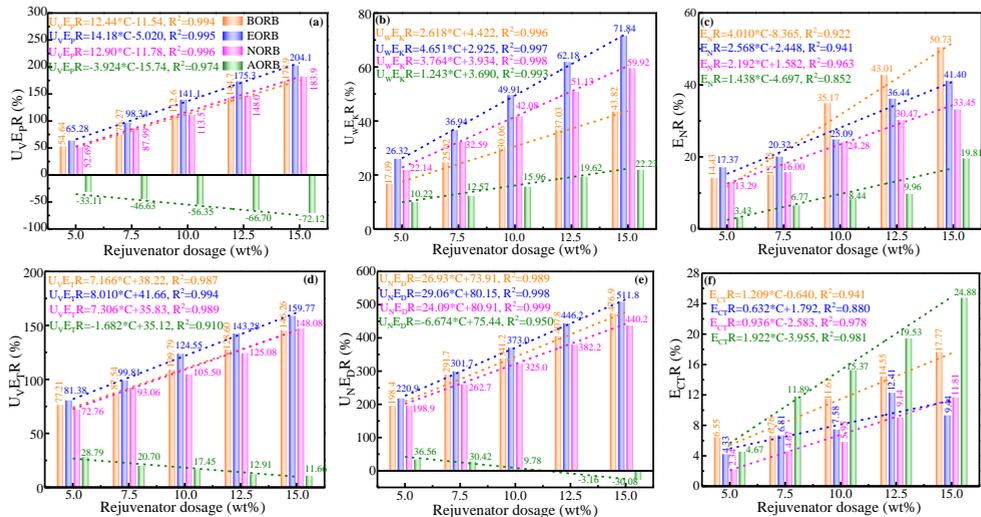
Figure 8.11 Critical energetic parameter-based rejuvenation percentages of rejuvenated bitumen

Interestingly, the magnitude of $E_N R$ values of rejuvenated bitumen is the same as the order of rejuvenation percentages based on critical high-temperature indicators in **Chapter 7** (BORB > EORB > NORB > AORB). There is speculation that the recovery of non-bond energy may serve as a primary rejuvenation mechanism for these rejuvenators; however, further verification is necessary. Furthermore, it is noteworthy that aromatic-oil demonstrates the most significant rejuvenating effect on the cross-terms energy of aged bitumen, in contrast to experimental observations. This implies that cross-terms energy might have a less pronounced impact on the macroscopic high-temperature properties of rejuvenated bitumen. This speculative hypothesis will be examined by assessing the correlation potentials between cross-terms energy and critical high-temperature indicators in the forthcoming **Section 8.5**.

8.4.4 Rejuvenation effect on fractional free volume (FFV)

It was reported that rejuvenators show a positive effect on restoring the free volume of aged bitumen [17]. The volumetric characteristics of rejuvenated bitumen with LAB40 aging degree and 10% rejuvenator dosage at different temperatures are illustrated in **Figure 8.12**. As the temperature rises, the free volume of rejuvenated bitumen increases gradually. To quantitatively assess the rejuvenation effectiveness of rejuvenators on free volume, the fractional free volume (FFV) of all rejuvenated binders is exported.
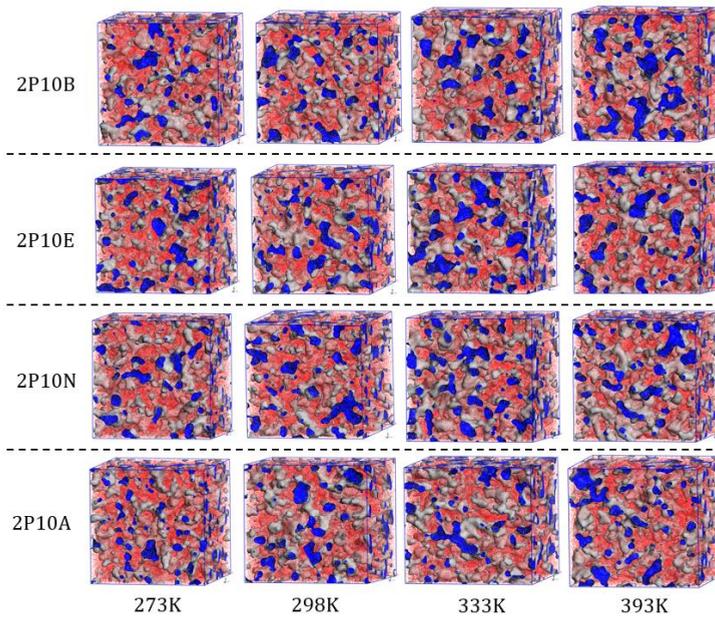
Figure 8.12 Volumetric illustration of rejuvenated bitumen versus temperature (White: molecular volume; Blue: isosurface; Red: free volume)

The FFV-based rejuvenation percentages of rejuvenated bitumen are calculated to investigate the feasibility of the FFV parameter as an effective index for evaluating the rejuvenation efficiency of different rejuvenators. The results are displayed in **Figure 8.13**. The FFVR values exhibit a positive and linear relationship with rejuvenator dosage, indicating more rejuvenator dosage would show more rejuvenation effectiveness on FFV recovery of aged bitumen. Meanwhile, the increment in temperature tends to enlarge the FFVR values of rejuvenated bitumen. The FFVR ranges are -15-120%, 0-360%, 0-210%, and 0-280% at 273K, 298K, 333K, and 393K, respectively. The magnitude of FFVR values is reasonable but higher than the rejuvenation percentage range based on relaxation parameters. Therefore, it is easier for rejuvenators to regenerate the free volume ratio of aged bitumen at the molecular level than the macroscale low-temperature relaxation performance. The reason may be that the low-temperature property of bitumen is related to not only free volume but also molecular motion and intermolecular interaction. The EORB binders show the highest FVVR values, showing that engine-oil addition can mostly improve the free volume ratio in aged bitumen. However, there is no general conclusion obtained on the FFVR order of BORB, NORB, and AORB binders, strongly dependent on the temperature and rejuvenator dosage. On the whole, the BORB and NORB have a higher FFVR than the AORB at both low temperatures (273K and 298K) and high temperatures (393K).

In addition, the aging effect on FFV values of rejuvenated bitumen is illustrated in **Figure 8.14**. As the aging degree deepens, the FFV values decrease gradually, showing that it is more difficult for rejuvenators to create new free volumes in a more aged bitumen. The variation trend of FFV and the long-term aging time t of rejuvenated bitumen depends on the rejuvenator type. For BORB, NORB, and AORB, their FFV values decline exponentially as the aging time prolongs, while the FFV parameter of the EORB binder shows a linear decreasing trend. Based on the MD results in **Chapter 4**, the engine-oil rejuvenator has a low molecular weight and polarity, and high molecular mobility. The low intermolecular interaction between engine-oil and aged bitumen as well as the high molecular movement both contribute to the large free volume ratio in EORB binders. For other rejuvenators, the increment in the aging degree of bitumen enhances the intermolecular interactions between rejuvenators with polar functional groups (bio-oil and aromatic-oil) and weakens their

functions on enlarging the free volume. The insufficient molecular mobility of naphthenic-oil molecules and the high molecular compactness of aged bitumen molecules both reduce the FFV value of NORB binder.
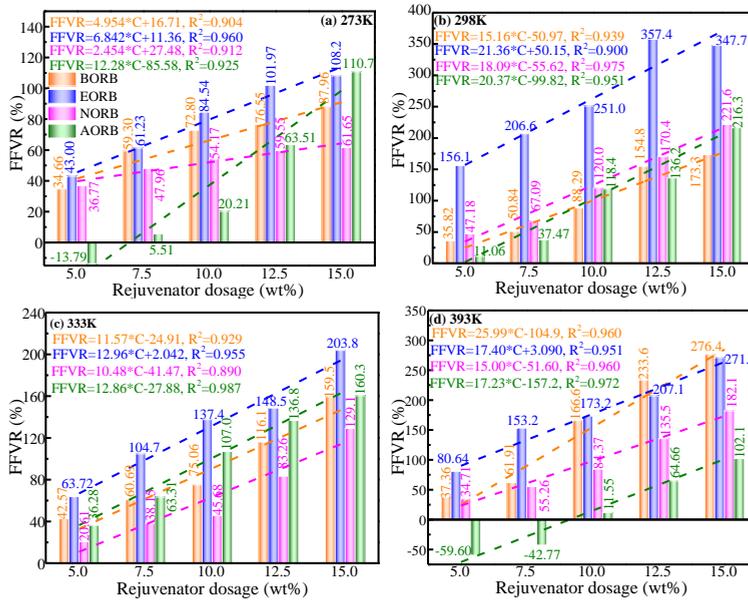
Figure 8.13 FFVR values versus rejuvenator dosage of different rejuvenated bitumen
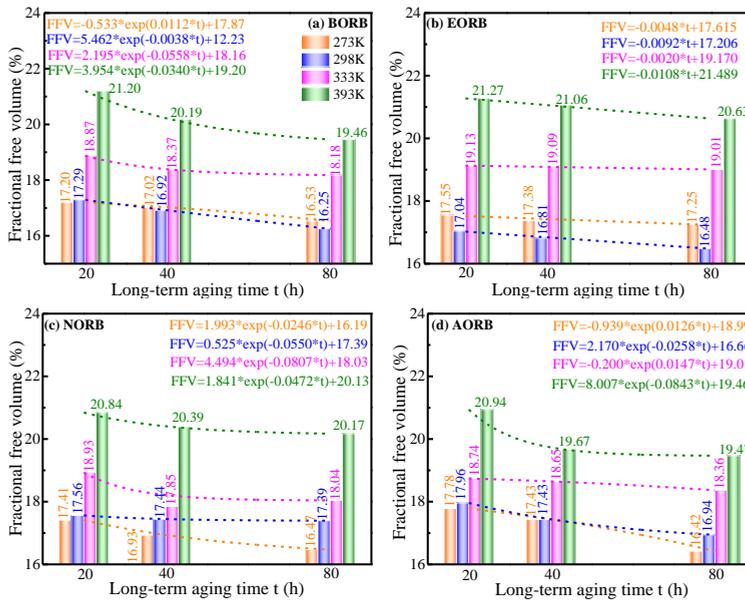
Figure 8.14 Influence of aging time on FFV value of rejuvenated bitumen

8.4.5 Rejuvenation effect on self-diffusion coefficient (D_s)

The rejuvenations also affect the molecular mobility of the bitumen model, thus resulting in the variation in rheological performance [18]. The self-diffusion coefficient (D_s) of rejuvenated binders is outputted from MD simulations to show the kinetic behaviors of various rejuvenated binders. The D_s-based rejuvenation percentage DR values of rejuvenated bitumen are calculated for quantitatively assessing the rejuvenation efficiency of different rejuvenators on the dynamic behavior of aged bitumen (displayed in **Figure 8.15**). All DR values of rejuvenated bitumen show a linear and positive correlation with rejuvenator dosage, indicating high rejuvenator dosage would promote the recovery and enhancement of molecular mobility of aged bitumen molecules. Moreover, the DR values become larger as the temperature rises. For all rejuvenated bitumen, the DR ranges at 273K, 298K, 333K, and 393K are 0-220%, 0-250%, 0-500%, and 140-1600%. It means that a small rejuvenator dosage would result in a huge rejuvenation percentage on molecule kinetics at high temperatures (333K and 393K).
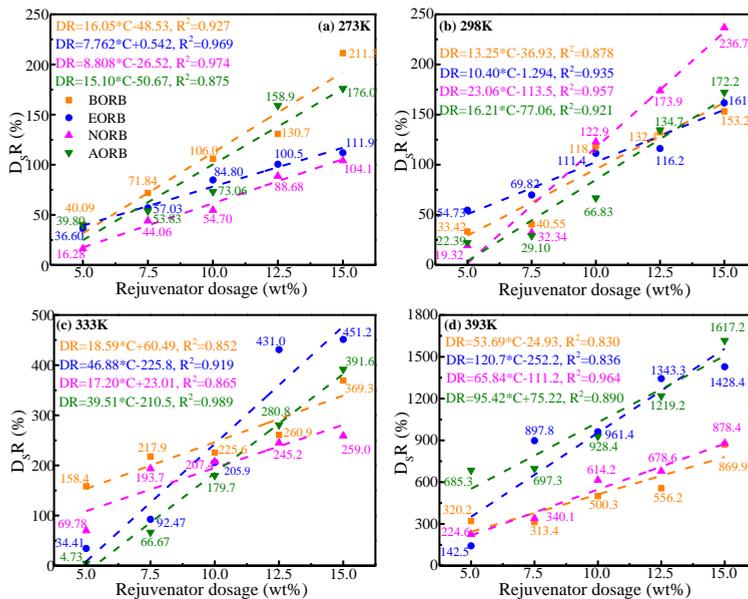
Figure 8.15 Diffusion-based rejuvenation percentage DR of rejuvenated bitumen

From **Figure 8.16**, the corresponding self-diffusion coefficient D_s values of rejuvenated binders are strongly affected by the aging degree of bitumen. As the long-term aging time extends from 20h to 40h and 80h, the D_s values of rejuvenated bitumen decline exponentially. The strong intermolecular interactions between aged bitumen molecules with high aging degrees hinder the molecular movement of bitumen molecules and further weaken the stress relaxation capacity of rejuvenated binders at low-temperatures. However, there is no explicit conclusion drawn regarding the effect of rejuvenator type on the variation trend of D_s-t curves of various rejuvenated binders because of the difference in intermolecular interactions between rejuvenators and aged bitumen molecules with variable aging levels. Therefore, it is necessary to develop an advanced analytic method to connect the D_s parameter of rejuvenated bitumen with variable influence factors.
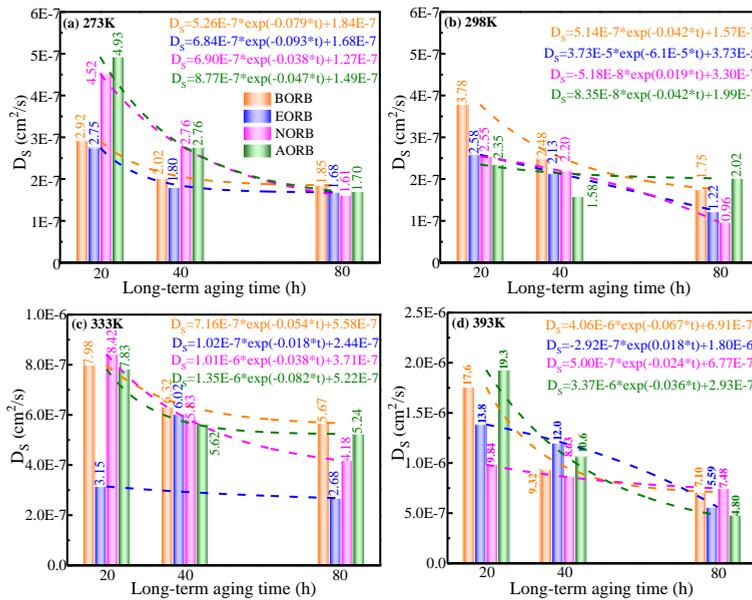
Figure 8.16 Influence of aging time on Ds values of rejuvenated bitumen

8.4.6 Rejuvenation effect on glass transition temperature (T_g)

In general, the T_g value of a material is determined by the turning point of temperature sensitivity of various thermodynamic properties, such as heat capacity, heat flow, and density [19]. In MD simulations, the predicted T_g values of rejuvenated binders are determined based on the variation curves of non-bond energy (E_N) and free volume FV versus temperatures owing to their high-temperature sensitivity. The T_g-based rejuvenation percentages T_gR values of rejuvenated bitumen are calculated and shown in **Figure 8.17**.
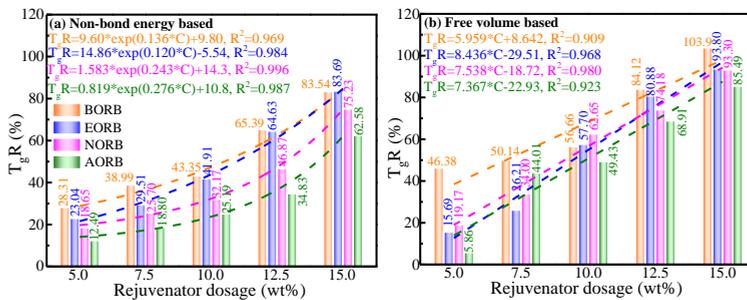
Figure 8.17 The T_g-based rejuvenation percentage T_gR of rejuvenated bitumen

Due to the positive effect of rejuvenators on T_g recovery, all T_gR values of rejuvenated bitumen increase as the rejuvenator dosage rises. However, the variation trend of T_gR-C curves depends on the determination way of the T_g parameter. For E_N-based T_g, the corresponding T_gR shows an exponential trend versus rejuvenator dosage, while the T_gR based on FV linearly correlates with rejuvenator dosage. Furthermore, all E_N-based T_gR of rejuvenated bitumen is lower than 100%, indicating that the addition of rejuvenators even with the dosage of 15% fails to completely restore the T_g value of aged bitumen to the virgin bitumen level. For FV-based T_gR values, the same finding is observed, except for the BORB sample with 15% bio-oil.

Interestingly, the magnitude of E_N-based T_gR for rejuvenated bitumen (BORB > EORB > NORB > AORB) is independent of rejuvenator dosage, while it is difficult to rank the FV-based T_gR values of EORB and NORB binders. Thus, the E_N-based T_g index is more appropriate to be an effective indicator for rejuvenation efficiency evaluation than the FV-based T_g index.

The effect of aging degree on the T_g values of rejuvenated bitumen is also investigated, and the results are shown in **Figure 8.18**. All T_g values of rejuvenated binders tend to increase significantly as the long-term aging time of bitumen deepens from 20 to 40 and 80 hours. It is noticed that most T_g values of rejuvenated bitumen show an exponentially positive connection with long-term aging time, except for the FV-based T_g of NORB and AORB binders. The E_N-based T_g ranking of rejuvenated bitumen (BORB < EORB < NORB < AORB) remains constant, while the FV-based T_g order depends on the aging level of bitumen. Eventually, the E_N-based T_g is recommended as an evaluation index, which will be connected with macroscale low-temperature indicators in the following subsection. It is interesting to note that the aging effect on the T_g value of bitumen decreases as the aging level deepens, while the influence of rejuvenator dosage on T_g becomes more significant at high rejuvenator contents.
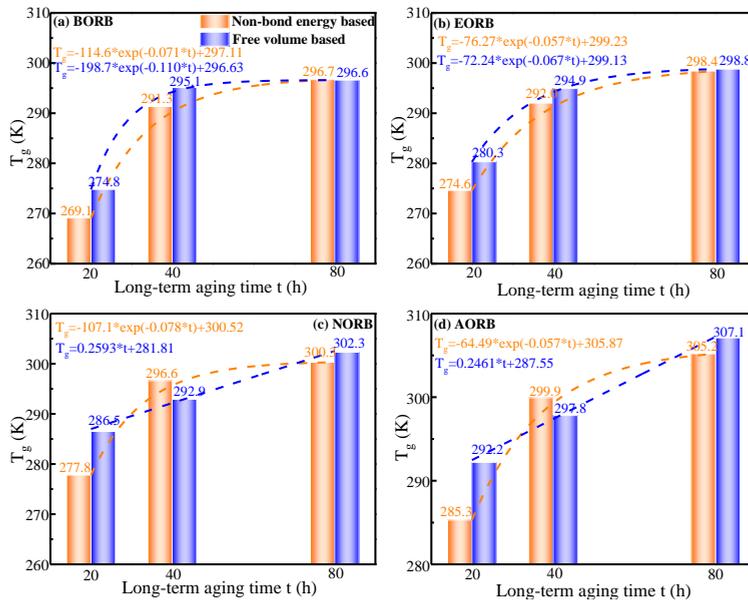
Figure 8.18 Aging influence on T_g values of rejuvenated bitumen

8.4.7 Rejuvenation effect on surface free energy (γ)

It was reported that the surface free energy and work of cohesion could reflect the cohesive cracking resistance of bituminous materials [20]. The surface free energy (γ) values of rejuvenated bitumen are predicted to investigate the rejuvenation efficiency of various rejuvenators on the cohesion fracture property. The γ-based rejuvenation efficiency values γR of rejuvenated bitumen are calculated following **Eq.8.11**, and the results are demonstrated in **Figure 8.19**. The γR values of rejuvenated bitumen show a linearly increasing trend as the rejuvenator dosage rises with an increasing slope of 4.314, 1.438, 1.353, and 1.033 for BORB, EORB, NORB, and AORB binders, respectively. It manifests that the bio-oil rejuvenator exhibits the greatest benefit in improving the cohesive cracking resistance of aged bitumen. With the long-term aging time t prolongs, the γR values of rejuvenated bitumen decline gradually. However, the variation trends of γR-t curves of rejuvenated bitumen depend on the rejuvenator type. For BORB and EORB binders, the γR-t curves have an exponentially decreasing trend, while the γR values of NORB and AORB binders reduce linearly as an

increase in the aging degree of bitumen. The γR values of rejuvenated bitumen are in the region of 20-180%, depending on the rejuvenator type/dosage and aging degree. Meanwhile, the magnitude of γR (BORB > EORB > NORB > AORB) is independent of the rejuvenator dosage and aging level of bitumen. Therefore, the surface free energy γ is an effective index to evaluate the rejuvenation efficiency of various rejuvenators on the cohesive cracking potential of aged bitumen.
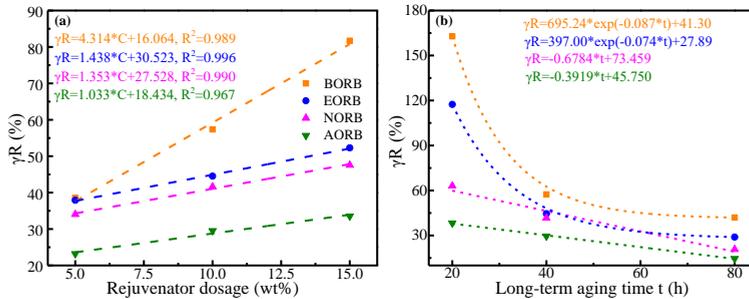
Figure 8.19 γ-based rejuvenation efficiency γR of rejuvenated bitumen

8.5 Connections between thermodynamic and rheological properties

This section sought to explore the potential connections between thermodynamic properties predicted by MD simulations and critical rheological indices of virgin, aged, and rejuvenated bitumen. These correlations will bridge the molecular-scale parameters to the macroscale performance. Only in this way can the MD simulation play a stronger role in molecular design and performance prediction of bituminous materials. More novel and efficacious rejuvenators will be developed and applied with the proposed multi-scale evaluation method.

8.5.1 High-temperature performance correlation

Based on the findings from **Chapter 7**, the critical indicators for effectively evaluating rejuvenation efficiency on high-temperature performance of rejuvenated bitumen are rutting failure temperature (RFT), zero-shear viscosity (ZSV), recovery percentage ($R_{3.2}$), and creep compliance ($J_{nr3.2}$). Their sensitivities to ρ, CED, Ds, U_VE_P, U_WE_K, E_N, U_VE_T, U_NE_D, and E_{CT} are analyzed herein.

8.5.1.1 Connections between critical rheological indices with ρ

The correlation curves between density ρ and RFT, ZSV, $R_{3.2}$, and $J_{nr3.2}$ values of virgin/aged and rejuvenated bitumen with variable rejuvenator types/dosages and aging degrees are depicted in **Figure 8.20**. It is observed that the density shows great linear relationships with these critical high-temperature performance indicators. As the increment in density ρ values, the RFT and $R_{3.2}$ parameters of bitumen tend to increase linearly with a correlation coefficient value of 0.840 and 0.847, respectively. Meanwhile, the Log(ZSV) values of all bitumen present a linear correlation with the ρ parameter, while the Log($J_{nr3.2}$) values exhibit a converse trend. All connection curves indicate that the bitumen with a high density would show a better high-temperature rutting resistance. It should be noted that the Log(ZSV) and Log($J_{nr3.2}$) parameters show a higher correlation level than the RFT and $R_{3.2}$ indicators. On the other hand, the influence degree of ρ on the $R_{3.2}$ value is the highest, followed by RFT, while the ZSV and $J_{nr3.2}$ parameters are the lowest and similar based on the absolute slope values of correlation equations. Overall, the ρ parameter exhibits a good connection with the high-temperature rheological and mechanical properties of all bitumen (all R^2 values are larger than 0.84), without the influence of aging level and rejuvenator type/dosage. Compared to RFT, $R_{3.2}$, and $J_{nr3.2}$, the ZSV index of bitumen greatly correlates with the predicted ρ value of the corresponding molecular model.
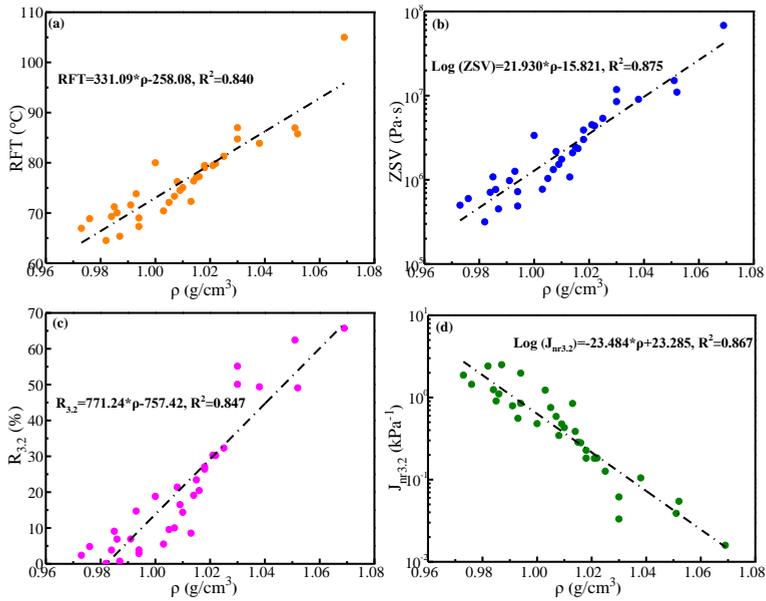
Figure 8.20 Connections between high-temperature critical parameters with density

8.5.1.2 Connections between critical rheological indices with CED

Different critical high-temperature performance indicators of all bitumen are connected with predicted CED values, shown in **Figure 8.21**.
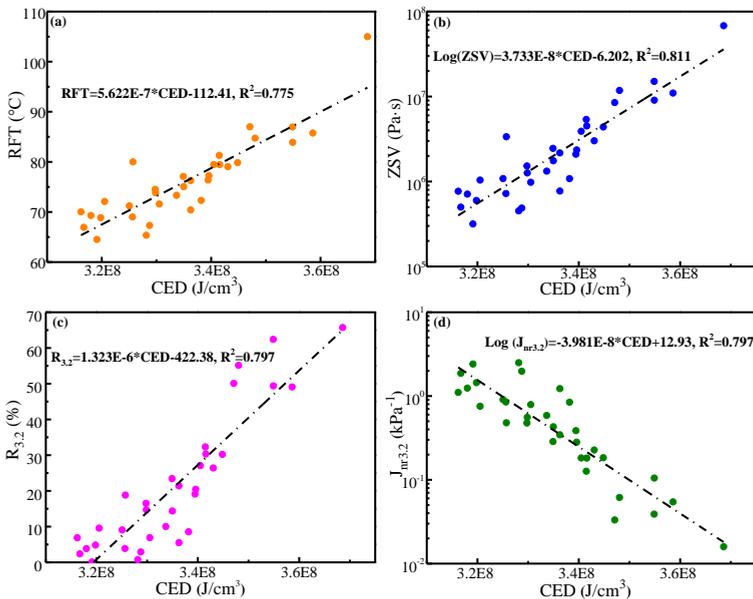
Figure 8.21 Connections between high-temperature critical parameters with CED

The variation trends of RFT-CED, ZSV-CED, $R_{3.2}$-CED, and $J_{nr3.2}$-CED curves are similar to their correlation curves with density. It implies that the CED parameter of bitumen is positively linked with high-temperature rutting resistance. Regarding the correlation level, the CED parameter is slightly worse than the ρ index according to the lower R^2 values. In addition, the ZSV index still has the best association effect with predicted CED values than the other critical measurement parameters. The ranking for the sensitivity level of these critical indicators to CED is the same as ρ case ($R_{3.2}$ > RFT > Log($J_{nr3.2}$) > Log(ZSV)). Therefore, the high-temperature deformation behavior of bituminous materials is significantly associated with intermolecular interaction level, and a larger CED value manifests the greater rutting resistance of bitumen. Although both ρ and CED indices link well with high-temperature properties, they show different explanations at the atomic level. The density index reflects the compactness of the whole bitumen model related to intermolecular force and distance, while the CED index incarnates the intermolecular interaction from the perspective of energy. Therefore, the density parameter can predict the high-temperature critical rheo-mechanical properties more accurately than the CED index.

8.5.1.3 Connections between critical rheological indices with D_s

The high-temperature deformation behavior of bituminous materials is not only affected by intermolecular interaction but also related to molecular mobility. The weakened intermolecular force and enhanced molecular movement both contribute to material distortion at high temperatures. Thus, the connections between the self-diffusion coefficient (D_s) at 60°C and these mechanical properties are examined, and the results are illustrated in **Figure 8.22**.
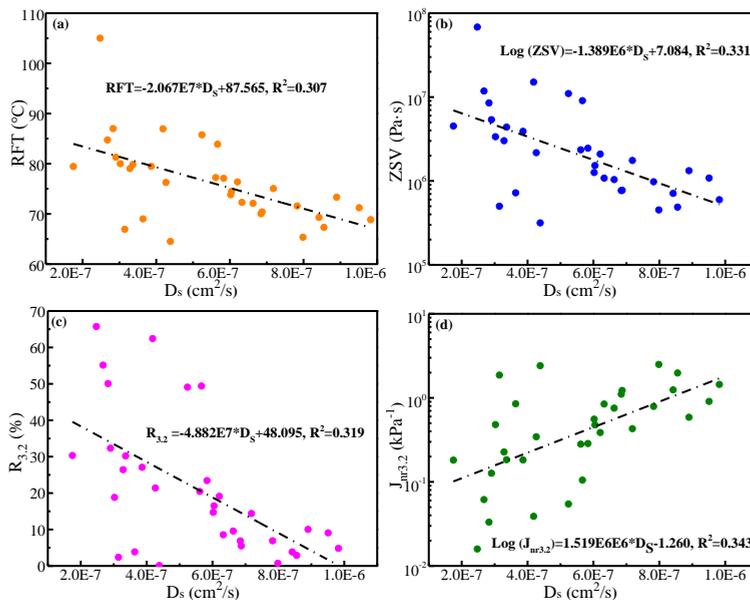
Figure 8.22 Connections between high-temperature critical parameters with self-diffusion coefficient

According to the low correlation coefficient R^2 values (< 0.4), it is concluded that the D_s parameter shows unsatisfactory connections with macroscale high-temperature properties of bitumen. Moreover, the influence of molecular mobility (D_s) on the high-temperature performance of virgin/aged and rejuvenated bitumen is smaller than the intermolecular interaction (CED). Additionally, as the D_s value increases, the RFT, ZSV, and $R_{3.2}$ parameters show decreasing trends, while the $J_{nr3.2}$ value tends to decrease gradually. A higher D_s value of the bitumen model means a more severe deformation potential, which is converse to the RFT, ZSV,

and $R_{3.2}$ indicators. Meanwhile, the D_s value presents a greater positive correlation with creep compliance $J_{nr3.2}$ than other parameters, indicating that the self-diffusion characteristic of bitumen molecules contributes to the creep behavior of bitumen at high temperatures. Overall, the self-diffusion capacity can reflect the high-temperature rutting potential of bitumen but is not decisive. It should be mentioned that the D_s parameter can explain the high-temperature and low-temperature properties from the perspective of molecular dynamics, simultaneously. The potential connections between D_s and low-temperature relaxation parameters will be discussed in the following subsection.

8.5.1.4 Connections between critical rheological indices with energetic parameters

(i) Potential, total, and diagonal energy

The correlation curves between U_VE_P and RFT, ZSV, $R_{3.2}$, and $J_{nr3.2}$ indicators of rejuvenated bitumen are shown in **Figure 8.23**. All correlation curves of the AORB binder show the opposite trends to the others because the potential energy fails to evaluate the rejuvenation efficiency of the aromatic-oil rejuvenator. Apart from AORB binders, the RFT, ZSV, and $R_{3.2}$ indices increase linearly, while the $J_{nr3.2}$ tends to decline as the increment in U_VE_P value. It means that the potential energy contributes positively to the high-temperature performance of bitumen. Based on the R^2 values of correlation equations, the connection levels of RFT-U_VE_P, ZSV-U_VE_P, $R_{3.2}$-U_VE_P, and $J_{nr3.2}$-U_VE_P curves are between 0.70-0.81, which are similar to the CED but lower than ρ parameter. In addition, the correlation level of the AORB binder is lower than the others. Similar to ρ and CED cases, the ZSV index shows the highest correlation level with potential energy, followed by RFT, while the $R_{3.2}$ and $J_{nr3.2}$ from multiple stress creep and recovery (MSCR) tests show lower R^2 values. In a word, potential energy strongly affects the high-temperature rutting performance of bitumen with a high correlation coefficient. However, this correlation law does not match the aromatic-oil rejuvenated bitumen case, which needs to be considered separately. Notably, it is found the total and diagonal energy results are similar to the potential energy, and thus their correlation curves are not displayed here.
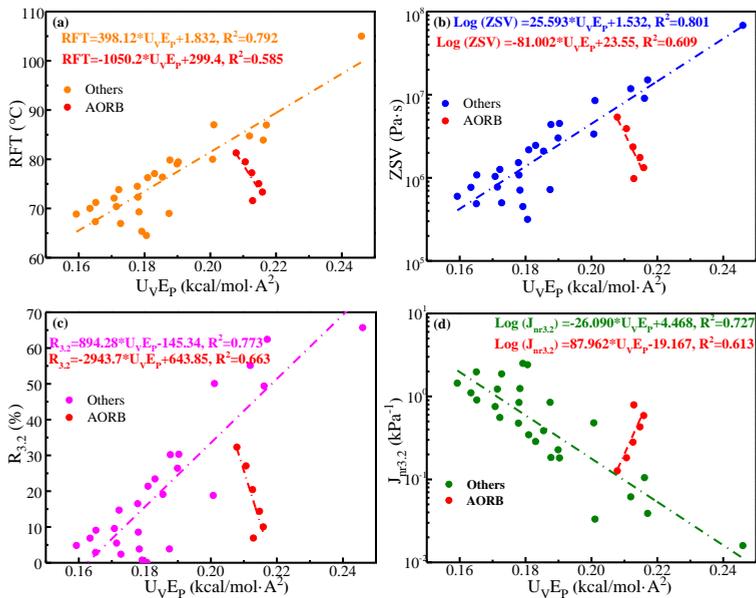
Figure 8.23 Connections between high-temperature critical parameters with potential energy

(ii) Kinetic energy

The correlation curves and corresponding equations between the kinetic energy parameter U_WE_K and four critical indicators are illustrated in **Figure 8.24**. The variation trends of RFT-U_WE_K, ZSV-U_WE_K, $R_{3.2}$-U_WE_K, and $J_{nr3.2}$-U_WE_K are the same as the self-diffusion coefficient (D_s) case because the kinetic energy is the basic of the molecular mobility of bitumen molecules. Nevertheless, the kinetic energy presents great connections with the macroscale properties with high correlation coefficient R^2 values higher than 0.8. As the U_WE_K value rises, the RFT, Log(ZSV), and $R_{3.2}$ values of virgin/aged and rejuvenated bitumen decline linearly, while the Log($J_{nr3.2}$) index increases linearly. It manifests that the bitumen with a lower kinetic energy would exhibit a greater high-temperature rutting resistance. It should be noted that the correlation law between the kinetic energy and macroscale indicators is appropriate to all rejuvenator cases, unlike the potential energy. Therefore, the kinetic energy term can succeed in predicting the RFT, ZSV, $R_{3.2}$, and $J_{nr3.2}$ indicators for evaluating and comparing the rejuvenation effectiveness of various rejuvenators on the high-temperature performance of rejuvenated bitumen. Based on the absolute slope values, the influence level of the $R_{3.2}$ index to U_WE_K value is the largest, followed by the RFT, while the ZSV and $J_{nr3.2}$ parameters are similar. Interestingly, the ZSV index still connects greatest to kinetic energy than others, which is also observed in ρ, CED, and U_VE_P cases.
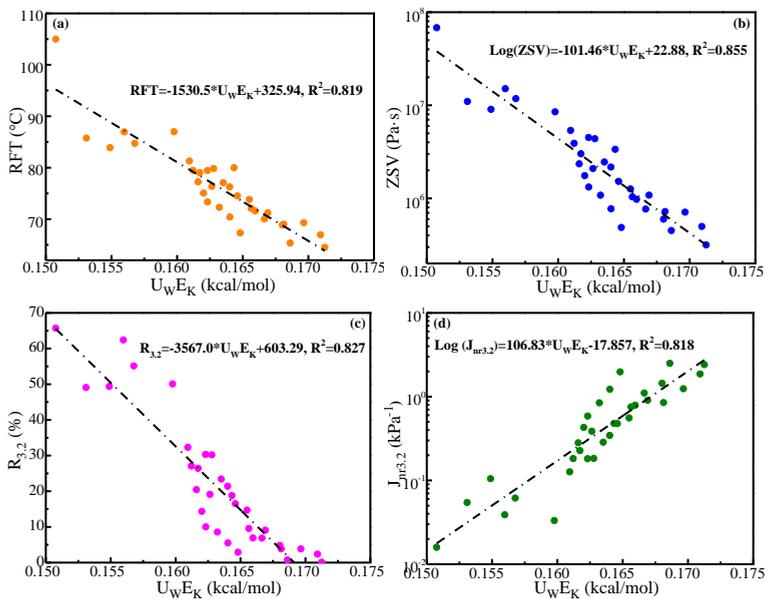
Figure 8.24 Connections between high-temperature critical parameters with kinetic energy

(iii) Non-bond and cross-terms energy

From the viewpoint of intermolecular interaction, the macroscale deformation at high temperatures of material is mainly associated with the non-bond energy without chemical reaction (bond breaking and formation) [21, 22]. **Figure 8.25** probes the potential relationships between the non-bond energy and critical indicators from experiments. Dissimilar to potential and kinetic energy, the correlation law of RFT-E_N, ZSV-E_N, $R_{3.2}$-E_N, and $J_{nr3.2}$-E_N curves are strongly dependent on the aging degree of bitumen. As the aging level deepens, the correlation curves of RFT-E_N, ZSV-E_N, and $R_{3.2}$-E_N move to the upper right, while the $J_{nr3.2}$-E_N curve tends to the bottom right. Thus, the general correlation law bridging the non-bond energy with macroscale indicators of various rejuvenated bitumen cannot be derived due to the large dependence on the aging level.
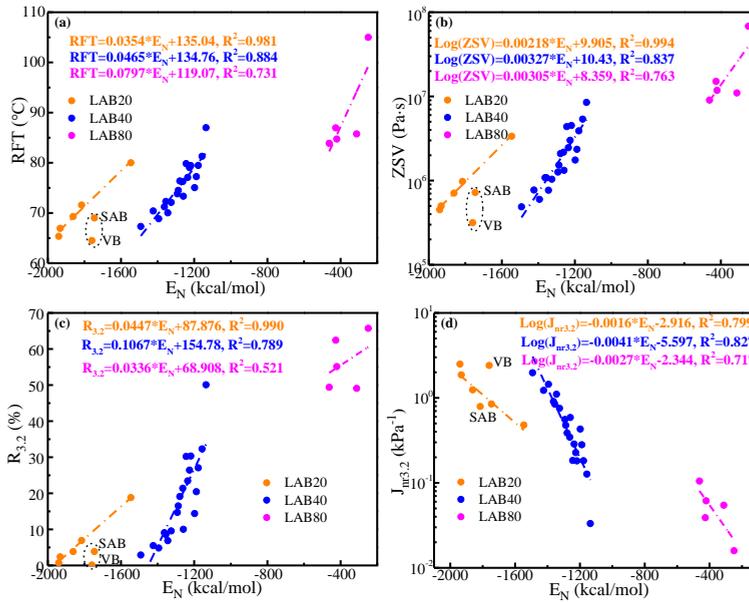
Figure 8.25 Connections between high-temperature critical parameters with non-bond energy

However, the linear correlations of rejuvenated bitumen with the same aging degree are observed. As the non-bond energy (E_N) rises, the RFT, Log(ZSV), and $R_{3.2}$ values enlarge linearly, whereas the Log($J_{nr3.2}$) decreases, indicating that the non-bond energy term is positively connected with high-temperature rutting resistance of bitumen. Therefore, the predicted E_N values can be used to predict the macroscale indicators, but the aging degree of bitumen should be mentioned specifically. Interestingly, the data points of virgin bitumen (VB) and short-term aged bitumen (SAB) are out of any correlation curves of rejuvenated bitumen because of the difference in aging degree. Some trend is observed in correlation curves of cross-terms energy.

Overall, it can be summarized that all energetic parameters contribute to the high-temperature performance of bituminous materials, and most of them show positive connections with rutting resistance, except for the kinetic energy term. The potential energy, total energy, and diagonal energy present similar correlation trends with these critical indicators, and the aromatic-oil rejuvenated bitumen has the opposite connections to the others and should be excluded. Moreover, the kinetic energy can connect well with the macroscale indices. Regarding the non-bond energy and cross-terms energy, the correlation curves are strongly affected by the aging degree of bitumen. The high-temperature properties of rejuvenated bitumen with a specified aging degree can be predicted by the non-bond energy, which cannot be achieved by the cross-terms energy due to the bad correlation levels. Thus, the kinetic energy term is the first choice to be an essential energetic index to predict the high-temperature critical indicators of various rejuvenated bitumen.

8.5.2 Low-temperature performance correlation

It is important to detect the potential connections between low-temperature critical indicators (shear stress τ_{50s}, relaxation time $t_{25\%}$, and A) proposed in **Chapter 7** and thermodynamic properties (self-diffusion coefficient D_s, fractional free volume FFV, and glass transition temperature T_g) predicted from MD simulations. The detailed correlation curves and equations are summarized in **Figure 8.26**.
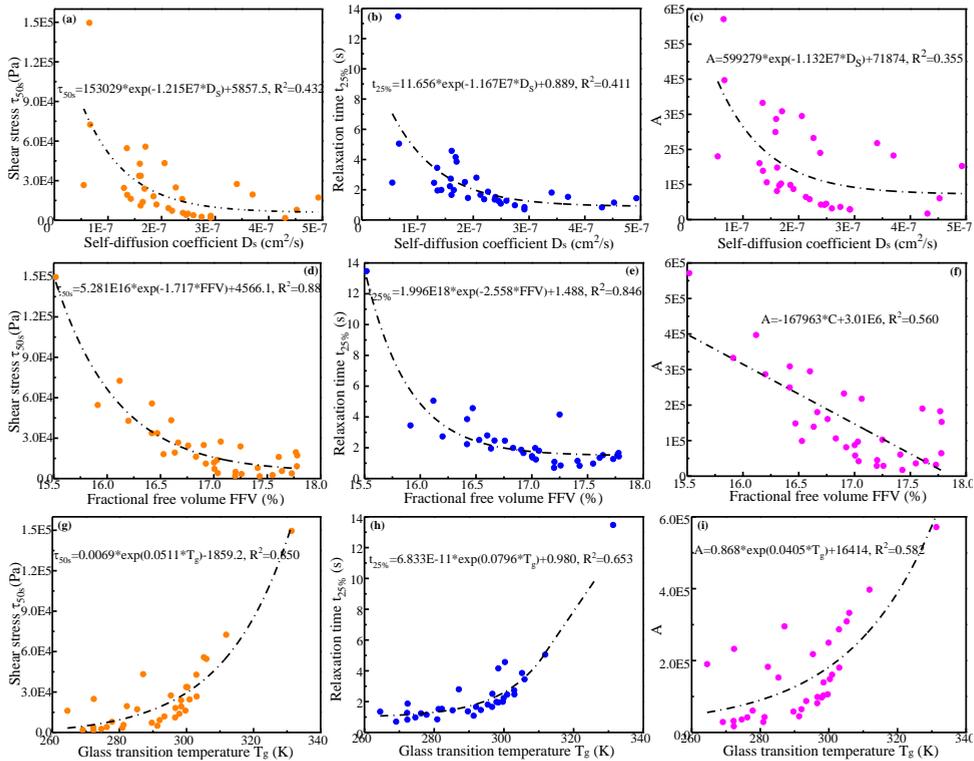
Figure 8.26 Connections between low-temperature critical parameters with thermodynamic indices

As the self-diffusion coefficient D_s increases, all relaxation indicators (τ_{50s}, $t_{25\%}$, and A) tend to decrease exponentially. Moreover, the shear stress τ_{50s} and relaxation time $t_{25\%}$ values decline exponentially as a function of fractional free volume FFV, while the A index decreases linearly. It means that the increased D_s and FFV values can reduce the relaxation stress and time, thus improving the relaxation capacity of bituminous materials. It agrees well with the knowledge that molecular mobility and free volume are the two key factors for material relaxation [23]. Additionally, the T_g index shows positive and exponential relationships with relaxation parameters, showing that the bitumen with a higher T_g value would show the worse relaxation performance at low temperatures.

Regarding the correlation degree, the R^2 values of τ_{50s}-D_s, $t_{25\%}$-D_s, and A-D_s curves are located in 0.3-0.5, suggesting that the self-diffusion coefficient D_s parameter shows unsatisfactory connections with critical relaxation indicators. The reason may be that the relaxation behavior of bitumen is complex, and the diffusion capacity of a molecule can affect but not completely determine the relaxation behavior of bitumen. On the contrary, the FFV parameter connects well with the τ_{50s} and $t_{25\%}$ indices based on the high correlation coefficient R^2 values of 0.875 and 0.846, respectively. However, the association effect of the FFV-A curve is poor with a low R^2 of 0.560. Lastly, the R^2 values of τ_{50s}-T_g, $t_{25\%}$-T_g, and A-T_g curves are 0.850, 0.653, and 0.582, respectively.

Overall, the relaxation model parameter A fails to connect well with all thermodynamic parameters. Meanwhile, the shear stress τ_{50s} shows greater connections with thermodynamic indices than the relaxation time $t_{25\%}$. On the other hand, the D_s have a lower association effect with critical relaxation indicators than the FFV and T_g indices. Furthermore, the FFV parameter exhibits a greater correlation with τ_{50s} and $t_{25\%}$ than T_g.

Therefore, it is recommended to predict the relaxation properties of different rejuvenated bitumen by the fractional free volume parameter from MD simulation. Eventually, the best correlation is the FFV-τ_{50s}, which can be adapted to evaluate the rejuvenation efficiency of various rejuvenators on low-temperature relaxation behaviors of aged bitumen.

It was reported that there were internal relationships between the thermodynamic indices (D_s, FFV, and T_g) [24]. **Figure 8.27** illustrates the initial connections of FFV-T_g, D_s-T_g, and D_s-FFV curves of virgin, aged, and rejuvenated bitumen. It is found that the T_g index shows a negative correlation with the FFV and D_s parameters, indicating that low free volume and molecular mobility would increase the T_g value of bitumen. This finding was also detected during the long-term aging of bitumen. Conversely, the incorporation of rejuvenators results in the increment in free volume ratio and molecular diffusion capacity, thus reducing the T_g value and improving the low-temperature cracking resistance of bitumen. Based on the absolute slope values of correlation equations, the D_s index shows a more significant effect on the T_g value of bitumen than the FFV parameter. However, the correlation level of the FFV-T_g curve is greater than the D_s-T_g curve. Interestingly, the D_s index has a positive connection with the FFV parameter of bitumen. The large free volume in bitumen would promote the enhancement of molecular mobility. Therefore, the T_g value of bitumen is affected by both free volume ratio (FFV) and molecular mobility (D_s), while the FFV and D_s indices are interactive at the atomic level.
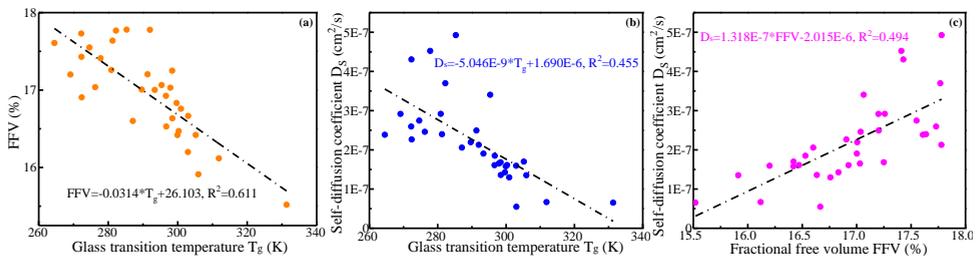
Figure 8.27 Potential Connections between Tg, FFV, and Ds values of bitumen

8.5.3 Fatigue cracking performance correlation

It was reported that the surface free energy (γ) was strongly associated with the cohesive cracking of materials [25]. The potential correlations between the γ values predicted from MD simulations and critical fatigue parameters (fatigue failure temperature FFT, fatigue life N_{f5}, elastic modulus E, peak strain ε_{sr}, and crack width C_{500}) proposed in **Chapter 7** are explored to link the results from different scales. The results are illustrated in **Figure 8.28**. It is observed that all critical fatigue parameters of rejuvenated bitumen link well to the surface free energy index. As the γ values increase, the FFT, E, and C_{500} indicators of rejuvenated bitumen tend to decrease exponentially, whereas the N_{f5} and C_{500} values rise gradually. It suggests that the surface free energy exhibits a positive correlation with the fatigue resistance of bitumen. Thus, these fatigue indicators of rejuvenated bitumen can be forecasted through their correlations with predicted γ values.

However, it should be noticed that the correlation curves of rejuvenated bitumen extremely rely on the aging level of bitumen, and the variations of FFT-γ, N_{f5}-γ, E-γ, ε_{sr}-γ, and C_{500}-γ curves of rejuvenated binders with a variable aging level of bitumen behave differently. In general, these correlation curves tend to move left as the aging status of bitumen changes from LAB20 to LAB40 and LAB80. It shows that when the critical fatigue indicators of rejuvenated bitumen with various aging levels are the same, their surface free energy γ values vary significantly. The reason may be that rejuvenation is a physical process without transforming the aged bitumen molecules back to their virgin status. From the viewpoint of macroscale rheology, the rejuvenator added can soften the aged bitumen and enhance its fatigue performance. Nevertheless, the effect of the rejuvenator on restoring the surface free energy of aged bitumen is much lower than the macroscale indicators. Additionally, the data points of virgin bitumen and short-term aged bitumen

are out of any correlation curves, which results from the difference in the aging degree of bitumen. A similar finding was observed in the chemical functional group case from FTIR tests discussed in **Chapter 7**, as well as the aforementioned non-bond energy and cross-terms energy. In a word, although these rejuvenators can regenerate the macroscale rheological properties of aged bitumen, their roles in restoring the chemical characteristics (such as functional group, and surface free energy) are limited.
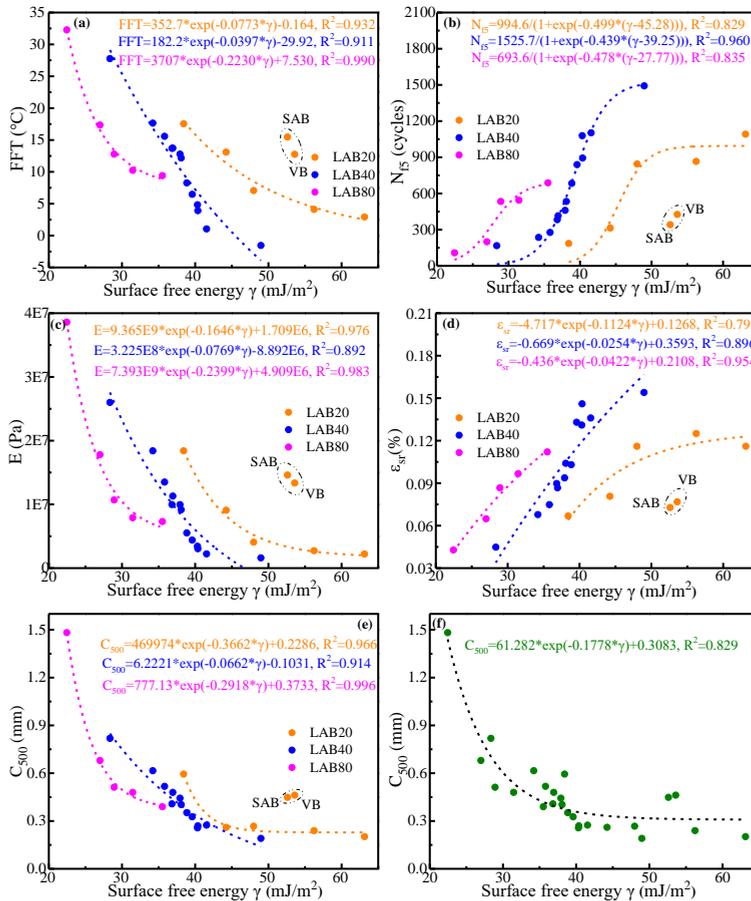
Figure 8.28 Connections between fatigue critical parameters with surface free energy

To date, it is recommended to specify the aging degree of bitumen in rejuvenated binders when these correlation laws between the surface free energy and critical fatigue indicators are adopted to predict the rejuvenation effectiveness of various rejuvenators on the fatigue performance of aged bitumen. Interestingly, it is noticed that the influence level of aging degree on the C_{500}-γ curves is smaller than other correlation curves. The reason is that the crack width C_{500} index is out of the rheological scope, which is a physical parameter during the fatigue damage of bituminous material. Therefore, the general correlation curve between the C_{500} and γ parameters is created and shown in **Figure 8.28(f)**. It is observed that the C_{500} index associates well with the γ values of virgin, aged, and rejuvenated bitumen with a correlation coefficient R^2 value of 0.829. It means that the relationship between the C_{500} index measured from experiments and γ value predicted from MD simulations of bitumen is independent of the rejuvenator type/dosage and aging degree

of bitumen, which can be utilized in other rejuvenated bitumen cases. However, the sensitivity of the C_{500}-γ correlation curve to bitumen type/components should be further explored in future work.

8.6 Summary

This chapter delves into the intricate interplay of rejuvenator type/dosage and aging level on the molecular-scale attributes of rejuvenated bitumen, a realm meticulously explored through the prism of MD simulations. The establishment of distinctive molecular models for various rejuvenated bitumen configurations sets the stage for a comprehensive evaluation of thermodynamic properties. These properties, subjected to comparison and scrutiny, offer a foundation for the formulation of effective atomic-level indicators. These indicators, in turn, facilitate the discernment and assessment of rejuvenator efficacy in the rejuvenation process. To construct a comprehensive multiscale framework elucidating the rejuvenation efficiency and its mechanistic nuances, the linkage between diverse thermodynamic properties of virgin, aged, and rejuvenated binders with their pivotal critical high-temperature rutting resistance, low-temperature relaxation behavior, and fatigue indicators, as proposed in **Chapter 7**, is established. Key insights gleaned from this chapter are as follows:

- The addition of all rejuvenators can restore the density and cohesive energy density of aged bitumen towards virgin bitumen, and the temperature influence is more significant than rejuvenator dosage. The incorporation of an engine-oil rejuvenator significantly regenerates the density of aged bitumen. However, the aromatic-oil with the highest ρ value shows the lowest restoration effect on the density of aged bitumen. The increment in the aging level of bitumen significantly weakens the rejuvenation effectiveness of rejuvenators. All rejuvenators fail to regenerate the CED value of aged bitumen to virgin bitumen level.

- The U_VE_P, U_WE_K, E_N, U_VE_T, U_NE_D, and E_{CT} are proposed as critical atomic-level energetic indicators for rejuvenation effectiveness evaluation, except for the U_NE_D and U_VE_P in the aromatic-oil case. The engine-oil rejuvenator exhibits the largest rejuvenation efficiency on potential, kinetic, total, and diagonal energies of aged bitumen, followed by the naphthenic-oil and bio-oil, while the aromatic-oil has the lowest effect on these energetic parameters. Moreover, bio-oil rejuvenator presents the highest rejuvenation efficacy on non-bond energy, followed by engine-oil, naphthenic-oil, and aromatic-oil rejuvenators. The magnitude of E_NR values is the same as the order of rejuvenation percentages based on critical high-temperature indicators (BORB > EORB > NORB > AORB).

- The bio-oil and engine-oil rejuvenated bitumen exhibit larger FFV values than the naphthenic-oil and aromatic-oil rejuvenated bitumen, At the atomic level, the coupled effects of rejuvenator type, dosage, and temperature on the free volume ratio of rejuvenated bitumen are complex. It is more difficult for rejuvenators to create new free volume in a severe-aged bitumen, and low intermolecular interaction and high molecular movement both contribute to the large free volume ratio in EORB binders.

- All rejuvenators play a positive role in restoring the molecule kinetics of aged bitumen. The bio-oil exhibits the strongest effect, while aromatic-oil is more effective in improving the molecular mobility of severely-aged bitumen.

- Adding rejuvenators can significantly restore the T_g parameter, and the efficiency ranking is BO > EO > NO > AO. However, the addition of rejuvenators even with the dosage of 15% fails to completely restore the T_g value of aged bitumen to the virgin level. The E_N-based T_g index is more appropriate to be an effective indicator for rejuvenation efficiency evaluation than the FV-based one.

- When the rejuvenator dosage is the same, the magnitude of γ values for rejuvenated binders is BORB > EORB > NORB > AORB. The aging degree harms the cohesive cracking resistance of rejuvenated bitumen but does not influence the order of γ values. Overall, the surface free energy γ is an effective index to evaluate the rejuvenation efficiency of rejuvenators on the cohesive cracking potential of aged bitumen.

- The ρ and CED parameters exhibit a good connection with the high-temperature rheological and mechanical properties of all bitumen without the influence of aging level and rejuvenator type/dosage. Compared to RFT, $R_{3.2}$, and $J_{nr3.2}$, the ZSV index of bitumen greatly correlates with ρ and CED. Regarding the correlation level, the CED parameter is slightly worse than the ρ, but much better than the D_s index.

- All energetic parameters contribute to the high-temperature performance of bituminous materials, and most of them show positive connections with rutting resistance, except for the kinetic energy term. The potential energy, total energy, and diagonal energy present similar correlation trends with these critical indicators, and the aromatic-oil rejuvenated bitumen has the opposite connections to the others and should be excluded. Moreover, the kinetic energy can connect well with the macroscale indices. Regarding the non-bond energy and cross-terms energy, the correlation curves are strongly affected by the aging degree of bitumen. Thus, the kinetic energy term is the first choice to be an essential energetic index to predict the high-temperature critical indicators of various rejuvenated bitumen.

- The shear stress τ_{50s} shows greater connections with thermodynamics indices than the relaxation time $t_{25\%}$. Moreover, the FFV parameter exhibits a greater correlation with τ_{50s} and $t_{25\%}$ than T_g. Thus, it is recommended to predict the relaxation properties of rejuvenated bitumen using the FFV index, with the best correlation between FFV and τ_{50s}.

- The extent of bitumen aging notably influences the relationships between surface free energy and crucial fatigue indicators in rejuvenated binders. The connection between the C_{500} index and the γ value remains consistent regardless of rejuvenator type, dosage, or aging degree, making it a valuable bridge for conducting a multiscale evaluation of the fatigue performance of rejuvenated bitumen.

8.7 References

[1] Road Pavement Transition Path. https://www.duurzame-infra.nl/roadmaps-uitvoering/transitiepad-wegverharding.

[2] Towards climate-neutral and circular government infrastructure projects. Ministry of Infrastructure and Water Management. https://www.duurzame- infra.nl.

[3] A. Rajib, A. Samieadel, A. Zalghout, K. Kaloush, B. Sharma, E. Fini. Do all rejuvenators improve asphalt performance? Road Materials and Pavement Design. 2022, 23(2), 358-376.

[4] X. Yang, H. Zhang, W. Zheng, Z. Chen, C. Shi. A novel rejuvenating method for structural and performance recovery of aged SBS-modified bitumen. ACS Sustainable Chemistry & Engineering. 2022, 10(4), 1565-1577.

[5] K. Schwettmann, N. Nytus, S. Weigel, M. Radenberg, D. Stephan. Effects of rejuvenators on bitumen ageing during simulated cyclic reuse: A review. Resources, Conservation and Recycling. 2023, 190, 106776.

[6] R. Moraes, F. Yin, C. Rodezno. Laboratory performance and compositional evaluation of bio-based recycling agents. Transportation Research Record. 2023, 1-13.

[7] E. Bocci, E. Prosperi, P. Marsac. Evolution of rheological parameters and apparent molecular weight distribution in the bitumen from reclaimed asphalt with rejuvenation and re-ageing. Road Materials and Pavement Design. 2022, 23(S1), S16-S35.

[8] S. Shariati, S. Aldagari, E. Fini. Bio-modifier: a sustainable suturing technology at the bitumen-aggregate interface. ACS Sustainable Chemistry & Engineering. 2023, 11(24), 8908-8915.

[9] A. Rajib. Structure-property relationships to understand comprehensive rejuvenation mechanisms of aged asphalt binder. Doctoral dissertation. 2020.

[10] H. Yu, J. Ge, G. Qian, C. Zhang, W. Dai, P. Li. Evaluation on the rejuvenation and diffusion characteristics of waste cooking oil on aged SBS asphalt based on molecular dynamics method. Journal of Cleaner Production. 2023, 406, 136998.

[11] S. Yan, Q. Dong, X. Chen, X. Zhao, X. Wang. Performance evaluation of waste cooking oil at different stages and rejuvenation effect of aged asphalt through molecular dynamics simulations and density functional theory calculations. Construction and Building Materials. 2022, 350, 128853.

[12] C. Bao, C. Zheng, Y. Xu, L. Nie, Y. Wang. Role of rejuvenator properties in determining the activation effects on aged asphalt based on molecular simulations. Journal of Cleaner Production. 2023, 405, 136970.

[13] D. Li, Y. Ding, J. Wang, Y. Shi, Z. Cao, G. Sun, B. Huang. Multiscale molecular simulations on the rejuvenation of recycled asphalt mixture: an insight into molecular impact of rejuvenators in aged binders. Journal of Cleaner Production. 2023, 414, 137621.

[14] S. Ren, X. Liu, P. Lin, S. Erkens, Y. Xiao. Chemo-physical characterization and molecular dynamics simulation of long-term aging behaviors of bitumen. Construction and Building Materials. 2021, 302, 124437.

[15] B. Cui, X. Gu, D. Hu, Q. Dong. A multiphysics evaluation of the rejuvenator effects on aged asphalt using molecular dynamics simulations. Journal of Cleaner Productions. 2020, 259, 120629.

[16] X. Zhang, X. Zhou, L. Chen, F. Lu, F. Zhang. Effects of poly-sulfide regenerant on the rejuvenated performance of SBS modified asphalt-binder. Molecular Simulation. 2021, 47(17), 1423-1432.

[17] X. Qu, D. Wang, Y. Hou, M. Oeser, L. Wang. Influence of paraffin on the microproperties of asphalt binder using MD simulation. Journal of Materials in Civil Engineering. 2018, 30(8), 04018191.

[18] K. Sonibare, G. Rucker, L. Zhang. Molecular dynamics simulation on vegetable oil modified model asphalt. Construction and Building Materials. 2021, 270, 121687.

[19] H. Ding, H. Wang, X. Qu, A. Varveri, J. Gao, Z. You. Towards an understanding of diffusion mechanism of bio-rejuvenators in aged asphalt binder through molecular dynamics simulation. Journal of Cleaner Production. 2021, 299, 126927.

[20] M. Alae, L. Xu, Z. Cao, X. Xu, F. Xiao. Fatigue and intermediate-temperature cracking performance of rejuvenated recycled asphalt binders and mixtures: A review. Journal of Cleaner Production. 2023, 384, 135587.

[21] M. Zadshir, D. Oldham, S. Hosseinnezhad, E. Fini. Investigating bio-rejuvenation mechanisms in asphalt binder via laboratory experiments and molecular dynamics simulation. Construction and Building Materials. 2018, 190, 392-402.

[22] M. Gong, B. Jiao. Thermodynamic properties analysis of warm-mix recycled asphalt binders using molecular dynamics simulation. Road Materials and Pavement Design. 2023, 2199883.

[23] R. Jing, D. Lin, Y. Roos, S. Miao. Glass transition, structural relaxation and stability of spray-dried amorphous food solids: A review. Drying Technology. 2019, 37(3), 287-300.

[24] A. Thran, G. Kroll, F. Faupel. Correlation between fractional free volume and diffusivity of gas molecules in glassy polymers. Journal of Polymer Science Part B: Polymer Physics. 1999, 37(23), 3344-3358.

[25] M. Yalghouzaghaj, A. Sarkar, G. Hamedi, P. Hayati. Application of the surface free energy method on the mechanism of low-temperature cracking of asphalt mixtures. Construction and Building Materials. 2021, 268, 121194.

9

Conclusions and recommendations

This chapter presents the key conclusions from this dissertation regarding the chemical characteristics and molecular models of both aged bitumen and rejuvenators, the diffusion and compatibility behavior of rejuvenator-aged bitumen blends, as well as the rejuvenation efficiency evaluation and molecular-scale mechanism of rejuvenated bitumen. Meanwhile, some insights and recommendations for both future research and industrial applications are provided based on the results obtained from this thesis.

9.1 Conclusions

This dissertation is committed to developing a multi-scale approach aimed at appraising the rejuvenation effectiveness in rejuvenated bitumen while unraveling the intricate interaction mechanisms between rejuvenators and aged binders. It converges molecular dynamics (MD) simulations with empirical characterizations to anticipate and authenticate the compatibility and diffusion dynamics of rejuvenators within aged bitumen. It also appraises the impact of rejuvenators on the chemo-thermo-rheological properties of aged bitumen, all the while accounting for diverse factors such as the type of rejuvenator, rejuvenator dosage, and bitumen aging degree.

As mentioned in **Chapter 1**, the main objectives of this thesis are to: (i) establish and authenticate molecular models for both aged bitumen and rejuvenators for comprehending variations in nanoscale properties; (ii) develop multiscale methodology for exploring the compatibility and diffusion behavior of rejuvenators within aged bitumen; (iii) propose essential evaluation criteria for determining the effectiveness of rejuvenating agents from both aspects of rheological and thermodynamic properties. Based on all the analyses and discussions, the main conclusions of this dissertation are described as follows:

9.1.1 Chemical characterization and molecular models' establishment for aged bitumen and rejuvenators

In **chapter 3**, the variation in the chemical components of bitumen during long-term aging. Representative molecular models of different aged binders with variable aging levels were proposed based on existing bitumen models, experimental results, and literature. Using these models, several thermodynamic properties of these aged binders were predicted based on the MD simulations to see the performance variation.

- For a used bitumen type, prolonged aging led to a reduction in its aromatic content and an increase in both resin and asphaltene fractions. Additionally, it resulted in the growth of sulfoxide and carbonyl functional groups, with sulfur oxidation proving to be more facile than carbon oxidation. These observations are necessary to determine the molecular models of aged bitumen. As introduced in **section 3.5.1**, the molecular model for virgin bitumen containing sulfoxide functional group was built and verified. Meanwhile, molecular models for aged bitumen were created by introducing varying levels of oxygen-containing functional groups (C=O and S=O) and adjusting the mass ratio of SARA fractions (see **section 3.5.2**).

- MD simulations were able to explore the long-term aging influence on the thermodynamic properties of bitumen. Aging significantly increased the cohesive energy density, solubility parameter, and activation energy of bitumen. However, it led to a decline in surface free energy, work of cohesion, and molecular mobility.

- Examining the aging kinetics of bitumen is a method that can be employed to assess chemical variations, facilitating the development of representative molecular models for bitumen at various aging levels. Section 3.7.1 indicated that the Zero-order model effectively described the long-term aging reaction kinetics of C=O and S=O groups in bitumen with a reaction rate constant ranging from $0.7*10^{-4}$ to $3.3*10^{-4}$ (mol·L^{-1}·h^{-1}). Concerning SARA variation (see **section 3.7.2**), the conversion of aromatics into resins and subsequently into asphaltenes followed a two-step reaction model. The most optimum kinetics model for aromatics was the Third-order reaction model with a k_1 value of 0.02 (mol·L^{-1})$^{-2}$(h)$^{-1}$. Meanwhile, converting resins to asphaltenes was the controlling step in the whole consecutive reaction model. The aging reaction kinetics of asphaltenes were well-fitted by the Zero-order model with a reaction rate constant k_2 of 3.85E-4 mol·(L·h)$^{-1}$.

In addition, **Chapter 4** aimed to identify typical molecular structures for various rejuvenators, to facilitate the development of their molecular models. Chemical tests were conducted to ascertain the chemical attributes of these rejuvenators and average and multi-component molecular models were developed for the

various rejuvenator types on the basis of these tests. Subsequently, MD simulations were used to assess the thermodynamic properties of both the average and multi-component rejuvenator models. Comparing the predictions to the measured properties and considering the requirements of the models, it was found that the average model was most suitable for the rejuvenators.

- From a functional group perspective (**section 4.4.2**), the ester groups existed in bio-oil (BO), while the other petroleum-based rejuvenators (engine-oil EO, naphthenic-oil NO, and aromatic-oil AO) primarily consisted of hydrocarbons with fewer heteroatom groups. Moreover, engine-oil and aromatic-oil had the lowest and highest degrees of unsaturation because the latter consisted of hydrocarbons with aromatic rings. With regard to molecular components, the alkane, naphthenic, and aromatic molecules were the main chemical components of EO, NO, and AO rejuvenators, differing in carbon-chain length, and the number of naphthenic and aromatic rings. Specifically, bio-oil rejuvenator mainly comprised methyl oleate, linoleate, and methyl palmitate (see **section 4.4.4**).

- Based on chemical characteristics, the average chemical formula for BO, EO, NO, and AO were determined as $C_{19}H_{36}O_2$, $C_{22}H_{44}$, $C_{26}H_{48}$, and $C_{30}H_{40}$, respectively. In detail, bio-oil consisted of a straight-chain monoalkene with 19 carbon atoms with one ester group, and the engine-oil molecule consisted of one cyclohexane and two saturated n-octane chains. Moreover, naphthenic-oil mainly had saturated tricyclic alkanes connected to n-hexane and n-heptane alkyl substituents, and aromatic-oil exhibited a polycyclic aromatic hydrocarbon structure with a central linkage to saturated straight-chain and monocyclic alkanes (see **section 4.5.1**).

- As shown in **section 4.6.3**, the predicted density ranking of rejuvenators based on average and multi-component models was AO > NO > BO > EO, which is consistent with measured values. The overall ranking for the potential energy, cohesive energy density (CED), and solubility parameter (δ) in the multi-component simulation cases aligned with the average models: AO > BO > NO > EO. Meanwhile, the fractional free volume (FFV) parameters of multi-component molecular models followed the order: EO > BO > NO > AO, consistent with the average models (see **section 4.7**).

- The average molecular model was more suitable than the multi-component model of aromatic-oil according to the unexpected self-diffusion coefficient and viscosity values. It indicated that the GC-MS method was not suited for aromatic-oil rejuvenator due to the undetected heavy-weight polycyclic aromatic molecules.

9.1.2 Compatibility and diffusion exploration of rejuvenated bitumen

In **chapter 5**, thermodynamic parameters and intermolecular binding energy were predicted from MD simulations to assess the compatibility behaviors of different rejuvenators in aged binders. Meanwhile, experimental thermal storage tests were implemented on rejuvenated binders to examine the difference in thermal storage stability and validate the compatibility findings from MD simulations.

- The thermodynamic parameters, namely $\Delta\delta$, χ, and ΔG_m, effectively estimated the compatibility potential of various rejuvenators with aged bitumen. It showed that the compatible capacity ranking of these four rejuvenators was AO > BO > NO > EO. The experimental finding is based on separation index (SI) values aligned with MD simulations.

- From the intermolecular binding energy ($E_{binding}$) results in **section 5.4.3**, it was found that aromatic-oil and engine-oil molecules exhibited the strongest and weakest interaction strengths with aged bitumen molecules, respectively. It verified the compatibility predictions based on thermodynamic parameters.

- In addition, increasing the aging degree of bitumen led to higher $\Delta\delta$ and SI values and increased intermolecular attraction. This implied that the severely-aged bitumen exhibited worse compatibility and thermal phase stability when reused.

Chapter 6 aimed to quantify and compare the diffusion behaviors of four rejuvenators in aged binders. Different interfacial rejuvenator-aged bitumen diffusion models were built and MD simulations were implemented to monitor the diffusive process of rejuvenator molecules in the aged bitumen matrix. Moreover, the experimental diffusion tests together with rheological characterizations were conducted to validate the simulation outputs. The synergetic effects of rejuvenator type, aging degree of bitumen, and temperature on the diffusive capacity were explored.

- At the molecular-scale, mutual but partial interfacial diffusion behaviors between rejuvenator and aged bitumen molecules were observed from MD simulations. The diffusion levels of all rejuvenators were improved by higher temperatures and longer diffusion times. The concentration distribution of rejuvenator molecules in the aged bitumen matrix under different diffusion conditions followed Fick's Second Law. The diffusion coefficient (D) of four rejuvenators varied from 10^{-11} to 10^{-10} m^2/s and strongly relied on the rejuvenator type, temperature, and bitumen aging level.

- In most cases, the order for the diffusive capacity of four rejuvenators was BO > EO > NO > AO. The experimental results regarding the magnitude and order of D parameters agree well with the MD simulation outputs, although the predicted D values at 160°C of all rejuvenators were approximately 3-6 times larger than the measured values (see **section 6.6.2**).

- From the results in **section 6.7**, engine-oil displayed a higher D value than bio-oil at low temperatures (25 and 60 °C). Furthermore, the diffusion behavior of bio-oil showed higher temperature sensitivity than the other three rejuvenators. Meanwhile, the diffusion capacity of BO, EO, and NO rejuvenators was negatively affected by the increased aging degree of bitumen, while the D value of the aromatic-oil molecule increased.

9.1.3 Critical indicators for rejuvenation efficiency evaluation

Chapter 7 investigated the coupled effects of rejuvenator type/dosage and aging degree of bitumen on the high-temperature rutting, low-temperature relaxation, and fatigue performance of rejuvenated binders. Meanwhile, it was expected to propose the critical rheological indicators for effectively evaluating the rejuvenation efficiency of various rejuvenators.

- From the rheological results in **section 7.3**, the BO significantly restored the high-temperature rutting, flow, and creep performance of aged bitumen, followed by EO, NO, and AO rejuvenators. Based on current samples and tests, the rutting failure temperature (RFT) and zero-shear viscosity (ZSV) parameters were effective in evaluating and distinguishing the rejuvenation efficiency of various rejuvenators. Additionally, the parameters $R_{3.2}$, $J_{nr0.1}$ or $J_{nr3.2}$, and $J_{nrslope}$ are recommended for estimating the elastic performance, creep potential, and stress sensitivity of rejuvenated bitumen. Among these, the RFT parameter was particularly critical for evaluating and distinguishing the rejuvenation effectiveness of various rejuvenators on the high-temperature performance of aged bitumen. Furthermore, the RFT index demonstrated strong connections with other effective high-temperature indicators.

- In **section 7.4**, the shear stress (τ), relaxation time (t), and residue stress ratio (R) values of bitumen increased with long-term aging but tended to decrease to the virgin bitumen level when rejuvenators were added. Among rejuvenators, the BO exhibited the highest rejuvenation efficiency, followed by the EO and NO, while the AO demonstrated the lowest effectiveness. Further, a high aging level of bitumen weakened the rejuvenation efficiency of rejuvenators on relaxation performance recovery. Besides, the relaxation model parameter A decreased and n increased as rejuvenator dosages increased. Ultimately, the parameters τ_{50s}, $t_{25\%}$, and A were recommended as critical indicators for evaluating the rejuvenation efficiency of these four rejuvenators on the relaxation performance of aged bitumen.

- The BO exhibited the greatest rejuvenation efficiency in improving the fatigue life of aged bitumen, followed by EO, NO, and AO rejuvenators. Compared to the G-R index, the fatigue parameter (G*sinδ)

proved to be a better indicator for reflecting the rejuvenation efficiency of rejuvenators on LVE fatigue performance. Considering high-temperature dependence, the fatigue failure temperature (FFT) parameter was proposed as an effective indicator for LVE fatigue performance evaluation. In the LAS test, the fatigue life (N_{f5}), peak strain (ε_{sr}), and elastic modulus (E) parameters were optimized as effective fatigue indicators. Furthermore, in the TS test, the crack width (C) results were consistent with the conclusions drawn from the LVE and LAS tests, showing strong correlations with other critical fatigue indicators (see **section 7.5**).

Chapter 8 delves into the intricate interplay of rejuvenator type/dosage and aging level on the molecular-scale attributes of rejuvenated bitumen, a realm meticulously explored through the prism of MD simulations. The establishment of distinctive molecular models for various rejuvenated bitumen configurations sets the stage for a comprehensive evaluation of thermodynamic properties. To construct a comprehensive multiscale framework elucidating the rejuvenation efficiency and its mechanistic nuances, the linkage between diverse thermodynamic properties of virgin, aged, and rejuvenated binders with their pivotal critical high-temperature rutting resistance, low-temperature relaxation behavior, and fatigue indicators is established. In sum, this chapter brings to light the complex and multifaceted relationships between rejuvenator attributes, bitumen properties, and aging conditions.

- Based on MD outputs in **sections 8.4.1** and **8.4.2**, all rejuvenators can restore the density and cohesive energy density of aged bitumen towards virgin bitumen. The engine-oil rejuvenator significantly regenerates the density but the aromatic-oil with the highest ρ value shows the lowest restoration effect on the density of aged bitumen. The increment in the aging level of bitumen significantly weakens the rejuvenation effectiveness of rejuvenators. All rejuvenators fail to regenerate the CED value of aged bitumen to virgin bitumen level. Compared to RFT, $R_{3.2}$, and $J_{nr3.2}$, the ZSV index of bitumen greatly correlates with ρ and CED. Regarding the correlation level, the CED parameter is slightly worse than the ρ, but much better than the D_s index (see **sections 8.5.1.1** and **8.5.1.2**).

- From **section 8.4.3**, the $U_V E_P$, $U_W E_K$, E_N, $U_V E_T$, $U_N E_D$, and E_{CT} are proposed as critical atomic-level energetic indicators for rejuvenation effectiveness evaluation, except for the $U_N E_D$ and $U_V E_P$ in aromatic-oil case. The EO rejuvenator exhibits the largest rejuvenation efficiency on potential, kinetic, total, and diagonal energies of aged bitumen, followed by the NO and BO, while the AO has the lowest effect on these energetic parameters. Moreover, bio-oil rejuvenator presents the highest rejuvenation efficacy on non-bond energy, followed by engine-oil, naphthenic-oil, and aromatic-oil rejuvenators. The magnitude of ENR values is the same as the order of rejuvenation percentages based on critical high-temperature indicators (BO > EO > NO > AO). The kinetic energy term was found to be the best energetic index to predict the high-temperature critical indicators of various rejuvenated bitumen with bio-oil, engine-oil, naphthenic-oil, and aromatic-oil rejuvenators (see **section 8.5.1.4**).

- The BO and EO rejuvenated bitumen exhibit larger FFV values than the NO and AO rejuvenated bitumen. Moreover, all rejuvenators play a positive role in restoring the molecule kinetics of aged bitumen. The BO exhibits the strongest effect, while AO is more effective in improving the molecular mobility of severely-aged bitumen. Further, adding rejuvenators can significantly restore the T_g parameter, and the efficiency ranking is BO > EO > NO > AO. However, the addition of rejuvenators even with the dosage of 15% fails to completely restore the T_g value of aged bitumen to the virgin level. The E_N-based T_g index is more appropriate to be an effective indicator for rejuvenation efficiency evaluation than the FV-based one. According to correlation results in **section 8.5.2**, it is recommended to predict the relaxation properties of rejuvenated bitumen using the FFV index, with the best correlation between FFV and τ_{50s}.

- From **section 8.4.7**, when the rejuvenator dosage is the same, the magnitude of γ values for rejuvenated binders is BO > EO > NO > AO. Overall, the surface free energy γ is an effective index to evaluate the rejuvenation efficiency of rejuvenators on the cohesive cracking potential of aged bitumen (see **section 8.5.3**). Most correlations notably depend on the bitumen aging level, but the connection between the

C_{500} index and the γ value remains consistent regardless of rejuvenator type, dosage, or aging degree, making it a valuable bridge for conducting multiscale evaluation on fatigue performance of rejuvenated bitumen.

9.2 Recommendations

Bitumen rejuvenation is a complex field that draws upon a range of multidisciplinary knowledge, encompassing aspects of physical (thermodynamic compatibility and kinetic diffusion), chemical (intermolecular interaction), and mechanical behavior. This dissertation contributes to the establishment of a multi-scale method for assessing the efficiency and mechanisms of rejuvenation in various blends of bitumen and rejuvenators. However, there remains a wealth of research not covered in this dissertation that holds significance in advancing the development of rejuvenation and recycling technologies for reclaimed asphalt (RA) materials. Drawing from the findings and insights of this thesis, some recommendations for future research are offered.

i. The incorporation of rejuvenators holds the potential to play a pivotal role in revitalizing the colloidal structure of bitumen components and alleviating the aggregation of asphaltene clusters. While this thesis provides some insights into the microstructure of different rejuvenated bitumen, additional research is necessary to explore the rejuvenation mechanism from a structural performance perspective. Specifically, the study will utilize the density functional theory (DFT) methodology for an in-depth investigation into the intermolecular interactions and deagglomeration potential of aged bitumen following the introduction of rejuvenator molecules.

ii. Although some potential connections are detected between thermodynamics parameters obtained from molecular dynamics (MD) simulations and critical macroscopic performance indicators observed in experiments of various rejuvenator-aged bitumen blends, the one-to-one correlation method has limitations. This is because, in many cases, multiple thermodynamic parameters can be linked to a single macroscale performance of bituminous materials. Thus, more advanced data analysis techniques, such as artificial neural networks, can be employed to establish chemo-thermodynamics-rheological models of variable rejuvenated bitumen.

iii. This thesis concentrated exclusively on evaluating the rejuvenation efficiency concerning the high-temperature rutting resistance, low-temperature relaxation, and fatigue performance of aged bitumen. Further research will investigate the aging, self-healing, and re-recycling potential of various rejuvenated binders to assess their durability performance.

iv. To validate the blending degree between rejuvenators and aged bitumen, additional experimental assessments are warranted to fine-tune the outputs of MD simulations. This calibration should consider different temperatures and aging levels of bitumen.

v. This thesis primarily concentrates on evaluating the performance and analysing the mechanisms of bitumen binders (cohesion). It is essential to examine the rejuvenation effectiveness on the adhesion performance of aged bitumen. The interfacial adhesion between the rejuvenated bitumen (mastic/mortar) and aggregates can be investigated through the thermodynamic adhesion parameters and experimental mechanical properties. In addition, the moisture sensitivity of adhesion performance of rejuvenated bitumen-aggregate systems can be studied to optimize the rejuvenator components.

vi. This thesis primarily addressed the binder level, and future research should emphasize the assessment of the rejuvenation effectiveness of different rejuvenators on the performance of asphalt mastic, mortar, and mixtures. It is essential to devise suitable critical evaluation methods and indicators at these scales because the most effective rejuvenator on the bitumen level might not be the most effective on the mixture level. Investigating potential correlations between critical evaluation indicators for rejuvenated bitumen and those of asphalt mastic, mortar, and mixtures can facilitate the prediction of rejuvenation efficiency across various scales of rejuvenator-aged bitumen blends. Moreover, mixture-scale tests

should be carried out to evaluate the influence of various rejuvenation conditions on the blending degree of recycled asphalt mixtures.

vii.   The rejuvenation technique is widely recognized for its economic and environmental benefits. To assess the sustainability of rejuvenated asphalt pavements, a life cycle assessment (LCA) methodology should be employed. The LCA outputs can guide decision-making processes regarding the optimization of rejuvenator types and rejuvenation conditions.

viii. Dutch contractors aim to transition to half-warm production (with temperatures not exceeding 140°C) by 2025. The shift in temperature, moving from hot-mix to warm-mix, will impact the blending, compatibility, and rejuvenation efficiency of rejuvenators in aged binders. It is imperative to explore the repercussions of temperature reduction on rejuvenator selection for future applications.

ix.   RA binders derived from diverse sites exhibit distinct performances owing to variations in virgin sources, service environment, and aging characteristics. It is essential to assess crucial chemical properties (SARA fractions, element analysis, and functional group distribution) and pivotal rheological properties (as proposed in this dissertation) across high, intermediate, and low temperatures. By integrating these properties with the objective of performance recovery, the most suitable rejuvenator from the database will be determined.

Appendix A

GC-MS information of engine-oil, naphthenic-oil, and aromatic oil rejuvenators

In this thesis, three rejuvenators (engine-oil, naphthenic-oil, and aromatic-oil) are derived from crude oil refinery processing, and their chemical components are composed of different hydrocarbons. This appendix summaries the detailed GC-MS information (including the retention time (RT), name, chemical formula, peak area percentage, molecular weight, density, and boiling point) of all chemical compositions in each petroleum-based rejuvenator (engine-oil: **Table A.1**; *naphthenic-oil:* **Table A.2**; *aromatic-oil:* **Table A.3**). *In addition, the discussion on these GC-MS results can be found in* **Chapter 4**.

Table A.1 GC-MS analysis on chemical components of the engine-oil rejuvenator

RT	Components	Chemical formula	CAS	Area pct.	Molecular weight
43.6568	Octadecane	$C_{18}H_{38}$	000593-45-3	5.9882	254.494
48.6687	Eicosane	$C_{20}H_{42}$	000112-95-8	5.0794	282.547
46.2186	n-Nonadecane	$C_{19}H_{40}$	000629-92-5	4.8650	268.521
40.9599	n-Heptadecane	$C_{17}H_{36}$	000629-78-7	4.3354	240.468
38.1279	Hexadecane	$C_{16}H_{34}$	000544-76-3	4.1847	226.441
25.0842	Dodecane	$C_{12}H_{26}$	000112-40-3	3.8404	170.335
51.0072	n-Heneicosane	$C_{21}H_{44}$	000629-94-7	3.4796	296.574
55.3845	Tricosane	$C_{23}H_{48}$	000638-67-5	2.7514	324.627
21.3297	n-Undecane	$C_{11}H_{24}$	001120-21-4	2.5129	156.31
4.9956	N-Hexane	C_6H_{14}	000110-54-3	2.2321	86.175
17.3871	Decane	$C_{10}H_{22}$	000124-18-5	1.7918	142.282
31.9821	Tetradecane	$C_{14}H_{30}$	000629-59-4	1.6146	198.388
28.633	n-Tridecane	$C_{13}H_{28}$	000629-50-5	1.6056	184.361
23.7504	2-methyl-Undecane	$C_{12}H_{26}$	007045-71-8	1.5719	170.335
20.1898	3-methyl-Decane	$C_{11}H_{24}$	013151-34-3	1.5259	156.308
19.9311	2-methyl-Decane	$C_{11}H_{24}$	006975-98-0	1.5121	156.308
25.5953	2,6-dimethyl-Undecane	$C_{13}H_{28}$	017301-23-4	1.4576	184.361
24.0031	3,8-dimethyl-Decane	$C_{12}H_{26}$	017312-55-9	1.4373	170.335
30.0079	2,2-Isopropylidenebis (tetrahydrofuran)	$C_{11}H_{20}O_2$	089686-69-1	1.4329	184.275
18.7797	1-methyl-2-pentyl-Cyclohexane	$C_{12}H_{24}$	054411-01-7	5.7143	168.319
18.6504	Limonene	$C_{10}H_{16}$	000138-86-3	1.5586	136.234
30.6307	2,4,4,6,6,8,8-Heptamethyl-1-nonene	$C_{16}H_{32}$	015796-04-0	0.9231	224.425
24.8609	5-methylundec-4-ene	$C_{12}H_{24}$	143185-91-5	0.3600	168.319
28.6846	4-methyl-4-Undecene	$C_{12}H_{24}$	061142-40-3	0.3576	168.32
30.2488	1-cyclohexene-1-carboxylic acid	$C_7H_{10}O_2$	000636-82-8	0.3504	126.153
17.0581	Myrcene	$C_{10}H_{16}$	000123-35-3	0.2082	136.234
33.5567	2,6-Di-tert-butylphenol	$C_{14}H_{22}O$	000128-39-2	11.0478	206.324
53.2281	2,4,6-Tri-tert-butylphenol	$C_{18}H_{30}O$	000732-26-3	4.3828	262.43
25.7601	Butylated hydroxytoluene	$C_{15}H_{24}O$	000128-37-0	4.3370	220.35

5.9827	1-Butanol	$C_4H_{10}O$	000071-36-3	1.7796	74.122
8.609	1-Pentanol	$C_5H_{11}DO$	014848-79-4	1.7217	88.148
16.6586	Phenol	C_6H_6O	000108-95-2	1.5619	94.111
31.3005	Butyl benzoate	$C_{11}H_{14}O_2$	000136-60-7	1.2864	178.228
49.4736	Octadecahydro-6-octylchrysene	$C_{26}H_{46}$	056247-68-8	0.9389	358.64
8.3388	4-Methyl-2-pentanol	$C_6H_{14}O$	000108-11-2	0.9150	102.175
51.1423	Isophyllocladene	$C_{20}H_{32}$	000511-85-3	0.8279	272.47
12.7455	n-Butyl ether	$C_8H_{18}O$	000142-96-1	0.7508	130.228
40.7308	butyl-cyclohexylmethyl-malonic acid diethyl ester	$C_{18}H_{32}O_4$	085211-25-2	0.5938	312.444
50.6781	1-Methyl-3-methoxy-7,9-dihydroxy-6H-dibenzo pyran-6-ketone	$C_{15}H_{12}O_5$	0056771-85-8	0.5843	272.253
7.7571	2-Methyl-1-butanol	$C_5H_{12}O$	001565-80-6	0.5575	88.148
18.527	2-ethyl-Hexanol	$C_8H_{18}O$	000104-76-7	0.5430	130.228
35.6014	2,4-di-tert-butylphenol	$C_{14}H_{22}O$	000096-76-4	0.4970	206.324
41.1773	6-Ethoxy-3,6-dihydro-2H-pyran-2-carbonxylic acid butyl ester	$C_{12}H_{20}O_4$	025556-20-1	0.4276	228.285
24.5965	5-Methyl-1-heptanol	$C_8H_{18}O$	007212-53-5	0.3713	130.228
24.9138	3,7-dimethyl-1-octanol	$C_{10}H_{22}O$	000106-21-8	0.3692	158.281
31.0713	4-tert-Butylphenol	$C_{10}H_{14}O$	000098-54-4	0.3444	150.218
13.7267	Propanoic acid butyl ester	$C_7H_{14}O_2$	000590-01-2	0.3298	130.185
53.4631	N-Ethyllysergamide	$C_{18}H_{21}N_3O$	000478-99-9	0.3125	295.379
5.3716	Isobutyl alcohol	$C_4H_{10}O$	000078-83-1	0.2780	74.122
24.1264	Isobutyl carbonate	$C_9H_{18}O_3$	000539-92-4	0.2774	174.237
31.6472	Methyl cinnamate	$C_{10}H_{10}O_2$	000103-26-4	0.2529	162.185
25.5189	2,6,8- trimethyl-4-Nonanone	$C_{12}H_{24}O$	000123-18-2	0.2413	184.318
7.0814	Methyl methacrylate	$C_5H_8O_2$	000080-62-6	0.2197	100.116
33.2982	Thiophosphoric acid triisopropyl ester	$C_9H_{21}O_3PS$	002464-03-1	0.1770	240.3
49.5911	1,5-Dihydroxy-6-methoxyxanthone	$C_{14}H_{10}O_5$	020081-69-0	0.1743	258.226
18.1801	2-Acetylthiazole	C_5H_5NOS	024295-03-2	0.1283	127.164

Table A.2 GC-MS analysis on chemical components of the naphthenic-oil rejuvenator

RT	Components	Chemical formula	CAS	Area pct.	Molecular weight
43.9156	2,6,10,14-tetramethyl-Hexadecane	$C_{20}H_{42}$	000638-36-8	2.1160	282.547
4.9958	Hexane	C_6H_{14}	000110-54-3	2.0324	86.175
46.6512	Octadecane	$C_{18}H_{18}$	000593-45-3	1.6758	254.494
48.663	Eicosane	$C_{20}H_{42}$	000112-95-8	1.4035	282.547
31.9823	Tetradecane	$C_{14}H_{30}$	000629-59-4	1.3985	198.388
46.2188	Nonadecane	$C_{19}H_{40}$	000629-92-5	1.2876	268.521
40.9602	Heptadecane	$C_{17}H_{36}$	000629-78-7	1.0855	240.468
53.2284	Docosane	$C_{22}H_{46}$	000629-97-0	1.0797	310.601
51.0015	Heneicosane	$C_{21}H_{44}$	000629-94-7	1.1065	296.574
28.6332	Tridecane	$C_{13}H_{28}$	000629-50-5	1.0147	184.361
25.0844	Dodecane	$C_{12}H_{26}$	000112-40-3	0.8521	170.335
17.3991	Decane	$C_{10}H_{22}$	000124-18-5	0.8236	142.282
9.6845	Octane	C_8H_{18}	000111-65-9	0.7128	114.229
13.4038	Nonane	C_9H_{20}	000111-84-2	0.6866	128.255
21.3299	Undecane	$C_{11}H_{24}$	001120-21-4	0.6676	156.31
40.7545	Perhydroyrene	$C_{16}H_{26}$	002435-85-0	1.8140	218.378
24.5673	Decahydro-1,5-dimethyl Naphthalene	$C_{12}H_{22}$	066552-62-3	0.4939	166.303
36.4125	Polymethylphenanthrene	$C_{15}H_{12}$	078869-40-6	4.6797	192.256
22.5931	9-methyl-trans-decahydronaphthalene	$C_{11}H_{20}$	002547-27-5	0.7780	152.276
33.2984	Hexahydro-1,1,4a-trimethyl-2(1H)-Naphthalenone	$C_{13}H_{20}O$	004668-61-5	3.7424	192.297
28.2396	2-Ethyl-1-methylbutylidene-cyclohexane	$C_{13}H_{24}$	074810-41-6	0.5792	180.33
30.8895	Dodecahydro-1H-phenalene	$C_{13}H_{22}$	002935-07-1	2.0312	178.14
21.9468	Decahydro-2-methylnaphthalene	$C_{11}H_{20}$	002958-76-1	1.1128	152.276
24.0561	Decahydro-2,3-dimethyl-Naphthalene	$C_{12}H_{22}$	001008-80-6	1.2033	166.303
34.6557	Tetradecahydro-anthracene	$C_{14}H_{24}$	006596-35-6	3.0884	192.34
12.2991	p-Xylene	C_8H_{10}	000106-42-3	1.3862	106.165
39.0506	Diphenylamine	$C_{12}H_{11}N$	000122-39-4	3.0076	169.222
17.358	Ethyl Caproate	$C_8H_{16}O_2$	000123-66-0	0.5305	144.211
20.8657	2-phenyl-2-propanol	$C_9H_{12}O$	000617-94-7	0.5241	136.191
30.8424	2-octylfuran	$C_{12}H_{20}O$	004179-38-8	0.8993	180.287
31.2949	Benzoate Butyl	$C_{11}H_{14}O_2$	000136-60-7	0.7689	178.228

29.779	2,5-dibutylfuran	$C_{12}H_{20}O$	072636-53-4	0.6613	180.287
50.6784	7,9-dihydroxy-3-methyl-6H-benzo chromen-6-ketone	$C_{15}H_{12}O_5$	056771-85-8	0.7759	272.253
33.0752	N,Ń-Diisopropyl-phenylenediamine	$C_{12}H_{20}N_2$	004251-01-8	1.2380	192.301
36.342	2,6-di-tert-butyl-benzoquinone	$C_{14}H_{20}O_2$	000719-22-2	1.4949	220.307
42.3762	2,4-dipentyl-phenol	$C_{16}H_{26}O$	000138-00-1	2.4649	234.377
35.5664	2,6-bis (2-methylpropylodene)-cyclohexanone	$C_{22}H_{22}O_3$	053376-38-8	1.3808	334.408
37.188	2-methyl-5-phenyl-thiazole	$C_{10}H_9NS$	019968-60-6	2.3855	175.25
42.8169	3-(6-methoxy-3-methyl-2-benzofuranyl) propionic acid	$C_{13}H_{14}O_4$	010410-30-7	3.8412	234.248

Table A.3 GC-MS analysis on chemical components of the aromatic-oil rejuvenator

RT	Components	Chemical formula	CAS	Area pct.	Molecular weight
38.1223	Hexadecane	$C_{16}H_{34}$	000544-76-3	1.2551	226.441
43.6570	Octadecane	$C_{18}H_{38}$	000593-45-3	1.8353	254.494
28.6332	Tridecane	$C_{13}H_{38}$	000629-50-5	0.2696	184.361
12.0048	Octane	C_8H_{18}	000111-65-9	0.2687	114.229
46.2129	Nonadecane	$C_{19}H_{40}$	000629-92-5	1.5368	268.521
41.1364	2,6,10-trimethyl-pentadecane	$C_{18}H_{38}$	003892-00-0	0.8662	254.494
40.9601	Heptadecane	$C_{17}H_{36}$	000629-78-7	1.4363	240.468
48.6572	Eicosane	$C_{20}H_{42}$	000112-95-8	1.3748	282.547
43.9097	Phytane	$C_{20}H_{42}$	000638-36-8	0.5404	282.547
53.2283	Docosane	$C_{22}H_{46}$	000629-97-0	1.0312	310.6
50.9956	Heneicosane	$C_{21}H_{44}$	000629-94-7	1.0233	296.574
25.0844	Dodecane	$C_{12}H_{26}$	000112-40-3	0.5099	170.335
27.9751	5-Ethyl-5-methyldecane	$C_{13}H_{28}$	017312-74-2	0.4802	184.361
21.4356	3,6-dimethyl-decane	$C_{12}H_{26}$	017312-53-7	0.4689	170.335
31.9764	Tetradecane	$C_{14}H_{30}$	000629-59-4	0.4497	198.388
19.7082	2,6-Dimethyldecane	$C_{12}H_{26}$	013150-81-7	0.3932	170.335
11.1828	2,4-Dimethyl-1-heptene	C_9H_{18}	019549-87-2	1.6574	126.239
17.0583	Myrcene	$C_{10}H_{16}$	000123-35-3	0.5055	136.234
32.9576	2,7-dimethyl-Naphthalene	$C_{12}H_{12}$	000582-16-1	3.7650	156.224
32.4758	1,6-dimethyl-Naphthalene	$C_{12}H_{12}$	000575-43-9	3.4700	156.224
33.0693	2,6-dimethyl-Naphthalene	$C_{12}H_{12}$	000581-42-0	3.3360	156.224

28.7507	2-methyl-Naphthalene	$C_{11}H_{10}$	000091-57-6	3.2910	142.197
29.3500	1-methyl-Naphthalene	$C_{11}H_{10}$	000090-12-0	3.1179	142.197
36.4418	1,4,6-trimethyl-Naphthalene	$C_{13}H_{14}$	002131-42-2	2.9639	170.25
36.2832	2,3,6-trimethyl-Naphthalene	$C_{13}H_{14}$	000829-26-5	2.4384	170.25
36.9354	1,2,6-trimethyl-Naphthalene	$C_{13}H_{14}$	003031-05-8	2.2797	170.25
37.4524	2-methyl-1-propyl-naphthalene	$C_{14}H_{16}$	054774-89-9	2.2736	184.277
33.6039	1,3-dimethyl-Naphthalene	$C_{12}H_{12}$	000575-41-7	2.1336	156.224
37.0235	1,3,6-trimethyl-Naphthalene	$C_{13}H_{14}$	003031-08-1	1.9070	170.25
33.7214	1,7-dimethyl-Naphthalene	$C_{12}H_{12}$	000575-37-1	1.8874	156.224
35.6134	1,6,7-trimethyl-Naphthalene	$C_{13}H_{14}$	002245-38-7	1.8861	170.25
41.5947	2-methyl-Fluorene	$C_{14}H_{12}$	001430-97-3	0.7974	180.245
32.1057	2-ethyl-Naphthalene	$C_{12}H_{12}$	000939-27-5	1.7937	156.224
33.2220	Hexamethyl-benzene	$C_{12}H_{18}$	000087-85-4	0.2831	162.271
37.5230	2-Isopropyl-naphthalene	$C_{13}H_{14}$	002027-17-0	1.7726	170.25
37.9812	2,3,6,7-tetramethyl-naphthalene	$C_{14}H_{16}$	001134-40-3	1.7308	184.277
24.7671	Naphthalene	$C_{10}H_8$	000091-20-3	1.7033	128.171
34.1092	1,4-dimethyl-naphthalene	$C_{12}H_{12}$	000571-58-4	1.6961	156.224
36.1716	1,4,5-trimethyl-naphthalene	$C_{13}H_{14}$	002131-41-1	1.6838	170.25
40.5489	1,4,5,8-tetramethyl-naphthalene	$C_{14}H_{16}$	002717-39-7	1.5945	184.227
23.5038	1,2,3,5-tetramethyl-benzene	$C_{10}H_{14}$	000527-53-7	0.5762	134.218
36.1187	1,1,4,5,6-pentamethyl-2,3-dihydro-1H-indene	$C_{14}H_{20}$	016204-67-4	0.4091	188.3086
42.3585	3, 3-dimethylbiphenyl	$C_{14}H_{14}$	000612-75-9	0.4056	182.261
32.0410	1,1,3-trimethyl-2,3-dihydro-1H-indene	$C_{12}H_{16}$	002613-76-5	0.3480	160.255
41.0189	Chamazulene	$C_{14}H_{16}$	000529-05-5	0.4353	184.277
38.4689	1,4-dimethyl-vinylazulene	$C_{14}H_{14}$	0321732-25-6	1.9788	182.26
38.1986	4,6,8-trimethylazulene	$C_{13}H_{14}$	000941-81-1	1.9313	170.25
10.9242	Furfural	$C_5H_4O_2$	000098-01-1	26.1233	96.084
11.6822	Furfuryl alcohol	$C_5H_6O_2$	000098-00-0	1.0236	98.1
15.9651	5-methyl furfural	$C_6H_6O_2$	000620-02-0	0.2836	110.111
39.0388	Diphenylamine	$C_{12}H_{11}N$	000122-39-4	1.1024	169.222
18.5272	2-ethyl-Hexanol	$C_8H_{18}O$	000104-76-7	1.0563	130.228
36.6886	2,5,7-trimethyl-benzothiophene	$C_{11}H_{12}S$	016587-65-8	0.5925	176.278

Summary

The increasing popularity of sustainable asphalt pavement stems from its advantageous attributes, such as cost-saving, environmental protection, and reductions in energy and material consumption. Although there is a desire to maximize the reuse of reclaimed asphalt (RA) waste materials in road construction, this is hindered by the poor performance of aged bitumen. In response, rejuvenation technology has been developed to restore the cohesive and adhesive properties of aged binders. To effectively select appropriate rejuvenators for aged bitumen derived from diverse RA sources and showing varying chemo-mechanical properties, it is crucial to establish an evaluation method that can assess and differentiate the rejuvenation efficiency of different rejuvenator-aged bitumen blends. Furthermore, it is essential to gain a fundamental understanding of the underlying mechanisms responsible for the variations.

This dissertation aims to develop a comprehensive and multi-scale approach for assessing the rejuvenation efficiency and mechanisms of various rejuvenator-aged bitumen blends. The combination of molecular dynamics (MD) simulations prediction and experimental validation is throughout the whole thesis to evaluate the compatibility potential and diffusive capacity of rejuvenators within aged bitumen, as well as their rejuvenation effectiveness in the chemo-thermodynamic-rheological performance. Additionally, the intermolecular interactions occurring between the rejuvenator and aged bitumen molecules are visualized and quantified by MD simulations.

The accurate construction of molecular models for aged bitumen is crucial for investigating the fundamental effects of aging on bitumen behavior at the molecular scale. To accomplish this, the long-term aging influence on the chemical characteristics of bitumen was assessed through Saturate, Aromatic, Resin, and Asphaltene (SARA) fractionation, Fourier Transform Infrared Spectroscopy (FTIR) test, and element analysis method. The chemical information obtained served as a foundation for determining the molecular structures of bitumen models. Various thermodynamic parameters of both virgin and aged bitumen were predicted to fundamentally evaluate the aging effect on bitumen properties. Lastly, functional group and SARA-based long-term aging reaction kinetics models were proposed to anticipate the chemical characteristics of aged bitumen with different aging degrees, thereby establishing the corresponding molecular models without the need for additional experimental procedures.

Simultaneously, novel average and multi-component molecular models for various rejuvenators (bio-oil BO, engine-oil EO, naphthenic-oil NO, and aromatic-oil AO) were established. The average models were based on the average chemical characteristics, such as functional group distribution, element component, and average molecular weight. On the other hand, multi-component models were derived from molecular component distribution in rejuvenators through Gas Chromatography-Mass spectrometry (GC-MS) analysis. Both models were validated by comparing MD outputs with experimental results. It was found that the average models provided more accurate predictions regarding the glass transition temperatures, especially for the aromatic-oil. Additionally, a range of thermodynamic parameters for the rejuvenators were predicted and compared. Finally, the average structures of rejuvenators were adopted to construct subsequent molecular models of rejuvenated binders.

The consideration of compatibility between the rejuvenator and aged bitumen is crucial due to the potential phase separation. In this thesis, different thermodynamic parameters, such as solubility parameter difference $\Delta\delta$, Flory-Huggins parameter χ, and mixing free energy ΔG_m were predicted and calculated using MD simulations for various rejuvenated bitumen systems. The predicted compatibility ranking for four rejuvenators was AO > BO > NO > EO, aligned with the experimentally measured thermal stability results. Moreover, separation index (SI) parameters based on rheological and chemical indices were available to assess the thermal stability of rejuvenated bitumen.

Furthermore, a comprehensive investigation was implemented to explore the effects of rejuvenator type, temperature, and aging degree of bitumen on the diffusion behavior of rejuvenators in aged binders at

multiple scales. The molecular dynamics (MD) simulation method was employed to detect the molecular-level diffusion characteristics of rejuvenators and predict their diffusion coefficient (D) parameters. At the atomic scale, it was observed that there was a mutual but partial interfacial diffusion feature between rejuvenators and aged bitumen molecules. Meanwhile, the concentration distribution of rejuvenator molecules in aged bitumen was well described by Fick's Second Law. The calculated D values for the four rejuvenators ranged from 10^{-11} to 10^{-10} m^2/s, and the diffusive capacities followed the order of BO > EO > NO > AO. To verify the MD simulation outputs, diffusion tests and dynamic shear rheometer (DSR) characterizations were conducted. The experimental results regarding the magnitude and order of the D values were in good agreement with the MD simulation findings. Lastly, it was observed that an increased aging degree of bitumen harmed the molecular diffusivity of BO, EO, and NO rejuvenators, whereas the D value of AO molecules enlarged as the aging level deepened.

A series of measurements were conducted to estimate the combined effects of rejuvenator type/dosage and aging degree of bitumen on the rheological properties of rejuvenated bitumen. Importantly, several critical indicators were identified that effectively assess and differentiate the rejuvenation efficiency of different rejuvenators on aged bitumen performance. In terms of high-temperature performance, parameters rutting failure temperature (RFT) and zero-shear viscosity (ZSV) from the linear viscoelastic (LVE) and flow tests were found to be useful. Additionally, parameters $R_{3.2}$, $J_{nr0.1}$ or $J_{nr3.2}$, and $J_{nrslope}$ were recommended for estimating the elastic performance, creep potential, and stress sensitivity of rejuvenated bitumen. Among these, the RFT parameter played a crucial role in evaluating and distinguishing the rejuvenation effectiveness of various rejuvenators on the high-temperature performance of aged bitumen. For the low-temperature relaxation property, parameters τ_{50s}, $t_{25\%}$, and A were proposed as critical indicators. Regarding fatigue life improvement, BO demonstrated the highest rejuvenation effectiveness, followed by EO, NO, and AO rejuvenators. The fatigue failure temperature (FFT) parameter was identified as an effective indicator for fatigue performance evaluation in LVE tests. In linear amplitude sweep (LAS) tests, the fatigue life (N_{f5}), peak strain (ε_{sr}), and elastic modulus (E) parameters were optimized as effective fatigue indicators. Nonetheless, crack width (C) results were consistent with conclusions drawn from LVE and LAS tests. Particularly, the crack width C_{500} parameter showed strong correlations with other critical fatigue indicators, and its prediction could be achieved using correlation equations without time-consuming TS tests.

At the atomic-level evaluation, several key thermodynamic properties of variable rejuvenated bitumen models were outputted by molecular dynamics (MD) simulation. The rejuvenation effectiveness of different rejuvenators on the thermodynamic indices of aged bitumen was estimated and compared. Importantly, the potential connections between these essential nanoscale parameters and critical macroscale indicators in terms of high-and-low temperature performance and fatigue behaviors of rejuvenated binders were explored. It was revealed that the addition of rejuvenators inherently catalyzed a restoration of density and cohesive energy density (CED) values toward those of virgin bitumen. A suite of indicators, including U_VE_P, U_WE_K, E_N, U_VE_T, U_NE_D, and E_{CT}, are introduced as critical energetic parameters, each reflecting rejuvenator efficacy on atomic-level energetic features, except for specific cases involving aromatic-oil rejuvenated binders. Meanwhile, it is recommended to predict the relaxation properties of different rejuvenated bitumen by the fractional free volume parameter from MD simulation. The surface free energy (γ) emerges as a dependable index for assessing the rejuvenation efficacy of the cohesive cracking potential of aged bitumen. The linkage between surface free energy and critical fatigue indicators (except for C_{500}), when gauging rejuvenation effectiveness, necessitates the specification of bitumen's aging degree in rejuvenated binders.

In summary, a multiscale evaluation framework of rejuvenated bitumen was proposed and developed in this dissertation, together with a full understanding of the difference in rejuvenation efficiency and mechanism between various rejuvenators on chemo-thermodynamic-rheological performance restoration of aged bitumen. The outcomes of this thesis would be beneficial to promoting the formation of classification standards of rejuvenator additives, development of advanced multifunctional rejuvenators, and improvement of all-round evaluation method on rejuvenated binder.

Samenvatting

De toenemende populariteit van duurzaam asfalt komt voort uit de voordelen op het gebied van kostenbesparing, milieubescherming en vermindering van energie- en materiaalverbruik. Alhoewel er een wens is om het hergebruik van gerecycled asfaltmateriaal in wegenbouw te maximaliseren, wordt dit bemoeilijkt door de slechte prestaties van verouderd bitumen. Als reactie hierop is er verjongingstechnologie ontwikkeld om de cohesie- en adhesie-eigenschappen van verouderde bindmiddelen te herstellen door lichtgewicht componenten, ook wel verjongingsmiddelen of recyclingmiddelen genoemd, toe te voegen. Om geschikte verjongingsmiddelen te selecteren voor verouderd bitumen afkomstig van verschillende RA-bronnen en met verschillende chemo-mechanische eigenschappen, is het cruciaal om een evaluatiemethode te ontwikkelen die de verjongingsefficiëntie van verschillende mengsels van door verjongingsmiddelen verouderd bitumen kan beoordelen en onderscheiden. Bovendien is het van vitaal belang om een fundamenteel begrip te krijgen van de onderliggende mechanismen die verantwoordelijk zijn voor de variaties.

Dit proefschrift heeft als doel een uitgebreide en multi-scale aanpak te ontwikkelen voor het beoordelen van de efficiëntie en mechanismen van verschillende mengsels van verouderd bitumen met verjongingsmiddel. Gedurende het hele proefschrift wordt gebruik gemaakt van voorspellingen op basis van moleculaire dynamica (MD) simulaties en experimentele validatie om het compatibiliteitspotentieel en de diffusiecapaciteit van verjongingsmiddelen in verouderd bitumen te evalueren, evenals hun effectiviteit in het verbeteren van de chemo-thermodynamische reologische prestaties. Bovendien worden de intermoleculaire interacties tussen de moleculen van het verjongingsmiddel en verouderd bitumen gevisualiseerd en gekwantificeerd met behulp van MD-simulaties.

Het nauwkeurig construeren van moleculaire modellen voor verouderd bitumen is cruciaal voor het onderzoeken van de fundamentele effecten van veroudering op het gedrag van bitumen op moleculaire schaal. Hiertoe werden de langetermijneffecten van veroudering op de chemische eigenschappen van bitumen beoordeeld aan de hand van Saturate, Aromatic, Resin, and Asphaltene (SARA)-fractie, Fourier Transform Infrared Spectroscopy (FTIR)-test, en de elementanalyse-methode. De verkregen chemische informatie diende als basis voor het bepalen van de moleculaire structuren van de bitumenmodellen. Diverse thermodynamische parameters van zowel vers als verouderd bitumen werden voorspeld om de invloed van de verouderingsgraad op de bitumeneigenschappen fundamenteel te beoordelen. Ten slotte werden modellen voorgesteld voor de functionele groepen en de kinematica van lange-termijn verouderingsreactie gebaseerd op SARA, om de chemische eigenschappen van verouderd bitumen met verschillende verouderingsgraden te anticiperen, waardoor de bijbehorende moleculaire modellen kunnen worden opgesteld zonder verdere experimenten uit te voeren.

Tegelijkertijd werden nieuwe gemiddelde en meer-componenten moleculaire modellen voor verschillende verjongingsmiddelen (bio-olie BO, motorolie EO, nafta-olie NO, aromatische olie AO) voor het eerst opgesteld. De gemiddelde modellen waren gebaseerd op gemiddelde chemische eigenschappen, zoals de verdeling van functionele groepen, element component en gemiddeld moleculair gewicht. Aan de andere kant werden de meer-componenten modellen afgeleid van de distributie van moleculaire componenten in de verjongingsmiddelen door middel van Gas Chromatography-Mass spectrometry (GC-MS) analyse. Beide modellen werden gevalideerd door de MD-uitvoer te vergelijken met experimentele resultaten. Het bleek dat de gemiddelde modellen nauwkeurigere voorspellingen gaven met betrekking tot de glasovergangstemperaturen, vooral voor de aromatische olie. Bovendien werden diverse thermodynamische parameters voorspeld en vergeleken voor de verjongingsmiddelen. Tenslotte werden de gemiddelde structuren van de verjongingsmiddelen gebruikt voor het construeren van volgende moleculaire modellen van geregenereerde bindmiddelen.

Het overwegen van de compatibiliteit tussen het verjongingsmiddel en verouderd bitumen is cruciaal vanwege het mogelijke faseafscheidingseffect. In dit proefschrift werden verschillende thermodynamische parameters, zoals het verschil in oplosbaarheidsparameter $\Delta\delta$, Flory-Huggins parameter χ en de mengvrije energie ΔG_m, voorspeld en berekend met behulp van MD-simulaties voor verschillende systemen van verjongd bitumen. De voorspelde compatibiliteitsorde voor vier verjongingsmiddelen was AO > BO > NO > EO, wat overeenkwam met de experimenteel gemeten thermische stabiliteit. Bovendien waren er scheidingsindex (SI)-parameters op basis van reologische en chemische indices beschikbaar om de thermische stabiliteit van verjongd bitumen te beoordelen.

Bovendien werd een uitgebreid onderzoek uitgevoerd om de effecten van het type verjongingsmiddel, temperatuur en verouderingsgraad van bitumen op het diffusiegedrag van verjongingsmiddelen in verouderde bindmiddelen op verschillende schalen te verkennen. De methode van moleculaire dynamica (MD-simulatie) werd toegepast om de diffusiekenmerken van verjongingsmiddelen op moleculair niveau te detecteren en hun diffusiecoëfficiënten (D-waarden) te voorspellen. Op atomair niveau werd waargenomen dat er een wederzijdse, maar gedeeltelijke interface diffusie plaatsvond tussen verjongingsmiddelen en verouderde bitumenmoleculen. Ondertussen werd de concentratiedistributie van verjongingsmiddelmoleculen in verouderd bitumen goed beschreven door de tweede wet van Fick. De berekende D-waarden voor de vier verjongingsmiddelen varieerden van 10^{-11} tot 10^{-10} m²/s, en de diffusiecapaciteiten volgden de volgorde BO > EO > NO > AO. Om de uitvoer van de MD-simulatie te verifiëren, werden diffusietests en karakteriseringen met een dynamische afschuifreometer (DSR) uitgevoerd. De experimentele resultaten met betrekking tot de grootte en volgorde van de D-waarden kwamen goed overeen met de bevindingen van de MD-simulatie. Tenslotte werd waargenomen dat een verhoogde verouderingsgraad van bitumen een negatieve invloed had op de moleculaire diffusie van de verjongingsmiddelen BO, EO en NO, terwijl de D-waarde van AO-moleculen toenam naarmate het verouderingsniveau dieper werd.

Er werden een reeks metingen uitgevoerd om de gecombineerde effecten van het type/dosering van het verjongingsmiddel en de verouderingsgraad van bitumen te beoordelen op de reologische eigenschappen van verjongd bitumen. Belangrijk is dat verschillende kritieke indicatoren werden geïdentificeerd die de verjongingsefficiëntie van verschillende verjongingsmiddelen op de prestaties van verouderd bitumen effectief kunnen beoordelen en differentiëren. Voor de prestaties bij hoge temperaturen bleken de parameters rutting failure temperature (RFT) en de zero-shear viscosity (ZSV) uit de lineaire visco-elastische (LVE) en flow tests nuttig te zijn. Daarnaast werden de parameters $R_{3.2}$, $J_{nr0.1}$ of $J_{nr3.2}$, en $J_{nrslope}$ aanbevolen voor het schatten van de elastische prestatie, kruipvermogen en stressgevoeligheid van verjongd bitumen. Onder deze parameters speelde de RFT-parameter een cruciale rol bij het evalueren en onderscheiden van de effectiviteit van verschillende verjongingsmiddelen op de prestaties bij hoge temperaturen van verouderd bitumen. Voor de eigenschappen bij lage temperaturen werden parameters τ_{50s}, $t_{25\%}$ en A voorgesteld als kritieke indicatoren. Wat betreft het verbeteren van de vermoeiingslevensduur toonde BO de hoogste verjongingseffectiviteit, gevolgd door EO, NO en AO olieverjongingsmiddelen. De vermoeiingsfaaltemperatuur (FFT) werd geïdentificeerd als een effectieve indicator voor vermoeiingsprestatiebeoordeling in LVE-tests. In lineaire amplitude sweep (LAS) tests werden de parameters vermoeiingslevensduur (N_{f5}), piekvervorming (ε_{sr}) en elastische modulus (E) geoptimaliseerd als effectieve vermoeiingsindicatoren. Desondanks waren de resultaten van de scheurbreedte (C) consistent met conclusies die werden getrokken uit LVE en LAS tests. Met name de scheurbreedteparameter C_{500} vertoonde sterke correlaties met andere kritieke vermoeiingsindicatoren, en de voorspelling ervan kon worden gedaan met behulp van correlatievergelijkingen zonder dat tijdrovende TS-tests nodig waren.

Bij de evaluatie op atomaire schaal werden verschillende belangrijke thermodynamische eigenschappen van verschillende gemodificeerde bitumenmodellen geëxtraheerd door middel van moleculaire dynamica (MD) simulatie. De effectiviteit van verschillende verjongingsmiddelen op de thermodynamische indices van verouderd bitumen werd geschat en vergeleken. Belangrijk is dat de potentiële verbindingen tussen deze essentiële nanoschaal parameters en kritieke macroschaal-indicatoren wat betreft prestaties bij hoge en lage temperaturen en vermoeiingsgedrag van verjongde bindmiddelen

werden onderzocht. Het werd ontdekt dat het toevoegen van verjongingsmiddelen intrinsiek leidde tot herstel van de dichtheid en cohesie-energiedichtheid (CED) naar waarden vergelijkbaar met die van vers bitumen. Een reeks indicatoren, waaronder $U_V E_P$, $U_W E_K$, E_N, $U_V E_T$, $U_N E_D$ en E_{CT}, werd geïntroduceerd als cruciale energetische parameters die elk de effectiviteit van het verjongingsmiddel op atomair niveau weerspiegelen, behalve in specifieke gevallen van bindmiddelen verjongd met aromatische olie. Ook wordt aanbevolen om de relaxatie-eigenschappen van verschillende verjongde bitumen te voorspellen aan de hand van de parameter voor fractioneel vrij volume uit MD-simulatie. De oppervlakte vrije energie (γ) komt naar voren als een betrouwbare index voor het beoordelen van de effectiviteit van verjonging op het cohesie-scheurpotentieel van verouderd bitumen. Het verband tussen oppervlakte vrije energie en kritieke vermoeiingsindicatoren (behalve C_{500}), bij het beoordelen van de effectiviteit van verjonging, vereist de specificatie van de mate van veroudering van het bitumen in verjongde bindmiddelen. Deze ontdekkingen bieden een diepgaand begrip van de ingewikkelde verjongingsmechanismen en banen de weg voor het ontwerp van geoptimaliseerde bindmiddelformuleringen.

Samengevat werd in deze dissertatie een evaluatiekader op meerdere schalen voor verjongd bitumen voorgesteld en ontwikkeld, samen met een volledig begrip van het verschil in verjongingsefficiëntie en -mechanisme tussen verschillende verjongingsmiddelen met betrekking tot het herstellen van de chemo-thermodynamisch-reologische prestaties van verouderd bitumen. De resultaten van deze dissertatie zouden gunstig zijn voor het bevorderen van de vorming van classificatiestandaarden voor verjongingsmiddel-additieven, de ontwikkeling van geavanceerde multifunctionele verjongingsmiddelen en verbetering van een alomvattende evaluatiemethode voor verjongde bindmiddelen.

Curriculum vitae

Shisong Ren

任施松

Jan. 1995   Born in Nantong, Jiangsu Province, China

EDUCATION

Sep. 2012 - Aug. 2016   BSc Student in Applied Chemistry

School of Chemical Engineering

China University of Petroleum (East China), China

Sep. 2016 – Aug. 2019   MSc Student in Chemical Engineering

School of Chemical Engineering

China University of Petroleum (East China), China

Sep. 2019 – Nov. 2023   PhD candidate

Section of Pavement Engineering

Delft University of Technology, the Netherlands

Dec. 2023 – Present   Postdoc researcher

Section of Pavement Engineering

Delft University of Technology, the Netherlands

List of Publications

I. Journal Publications (In thesis)

1. Shisong Ren[*], Xueyan Liu, Sandra Erkens. (2024). Role of thermodynamic relaxation on effectiveness of recycling agents on properties of aged bitumen. Fuel. Revision submitted.

2. Shisong Ren[*], Xueyan Liu, Sandra Erkens. (2024). Exploring the recovery capacity of recycling agents on atomic-scale energy properties of aged bitumen and their potential correlations with high temperature performance. Materials & Design. Revision submitted.

3. Shisong Ren[*], Xueyan Liu, Michèle van Aggelen, Peng Lin, Sandra Erkens. (2024). Do different chemical and rheological properties act as effective and critical indicators for efficiency evaluation of rejuvenated bitumen? Construction and Building Materials. 411, 134774.

4. Shisong Ren[*], Xueyan Liu, Aikaterini Varveri, Sadaf Khalighi, Ruxin Jing, Sandra Erkens. (2023). Aging and rejuvenation effects on the rheological response and chemical parameters of bitumen. Journal of Materials Research and Technology. 25, 1289-1313.

5. Shisong Ren[*], Xueyan Liu, Sandra Erkens. (2023). Insight into the critical evaluation indicators for fatigue performance recovery of rejuvenated bitumen under different rejuvenation conditions. International Journal of Fatigue. 175, 107753.

6. Shisong Ren[*], Xueyan Liu, Sandra Erkens. (2023) Towards critical low-temperature relaxation indicators for effective rejuvenation efficiency evaluation of rejuvenator-aged blends. Journal of Cleaner Production. 426, 139092.

7. Shisong Ren[*], Xueyan Liu, Sandra Erkens. (2023). Unraveling the critical indicators for evaluating the high-temperature performance of rejuvenator-aged bitumen blends. Case Studies in Construction Materials. 19, e02522.

8. Shisong Ren, Xueyan Liu, Yangming Gao[*], Ruxin Jing, Peng Lin, Sandra Erkens, Haopeng Wang. (2023). Molecular dynamics simulation and experimental validation on the interfacial diffusion behaviors of different rejuvenator in aged bitumen. Materials & Design. 226, 111619.

9. Shisong Ren[*], Xueyan Liu, Peng Lin, Yangming Gao, Sandra Erkens. (2022) Review on the transport and interfacial performance of sustainable bituminous

materials: From a perspective of molecular dynamics simulation. Journal of Molecular Liquids. 366, 120363.

10. Shisong Ren, Xueyan Liu, Yangming Gao, Peng Lin, Sandra Erkens. (2022) Insight into the compatibility behaviors between various rejuvenators and aged bitumen: Molecular dynamics simulation and experimental validation. Materials & Design. 223, 111141.

11. Shisong Ren, Xueyan Liu, Peng Lin, Sandra Erkens, Yangming Gao*. (2022) Molecular dynamics simulation on bulk bitumen systems and its potential connections to macroscale performance: Review and discussion. Fuel. 328C, 125382.

12. Shisong Ren*, Xueyan Liu, Sandra Erkens, Peng Lin, Yangming Gao. (2022). Multi-component analysis, molecular model construction and thermodynamics performance prediction on various rejuvenators of aged bitumen. Journal of Molecular Liquids. 360, 119463.

13. Shisong Ren*, Xueyan Liu, Peng Lin, Sandra Erkens, Yangming Gao. (2022). Chemical characterizations and molecular dynamics simulations on different rejuvenators for aged bitumen recycling. Fuel. 324, Part A, 124550.

14. Shisong Ren*, Xueyan Liu, Peng Lin, Ruxin Jing, Sandra Erkens. (2022). Towards the long-term aging influence and novel reaction kinetics models of bitumen. International Journal of Pavement Engineering. DOI: 10.1080/10298436.2021.2024188

15. Shisong Ren, Xueyan Liu, Peng Lin, Sandra Erkens, Yue Xiao. (2021). Chemo-physical characterization and molecular dynamics simulation of long-term aging behaviors of bitumen. Construction and Building Materials. 302, 124437.

II. Journal Publications (Out of thesis)

1. Shisong Ren, Xueyan Liu, Ruxin Jing, Yangming Gao*, Peng Lin, Sandra Erkens. (2023). Investigating the rheological properties, aging resistance, and compatibility of RET/PE and WR/CR/SBS compound-modified bitumen. Road Materials and Pavement Design. DOI:10.1080/14680629.2023.2221347

2. Shisong Ren, Xueyan Liu, Peng Lin, Sandra Erkens. (2022). Influence of the swelling-degradation degree on rheological properties and thermal pyrolysis behaviors of waste crumb rubber modified bitumen. Construction and Building Materials. 337, 127555.

3. Shisong Ren, Xueyan Liu, Yi Zhang, Peng Lin, Panos Apostolidis, Sandra Erkens, Mingliang Li, Jian Xu. (2021). Multi-scale characterization of lignin modified bitumen using molecular dynamics simulation. Construction and Building Materials. 287, 123058.

4. Shisong Ren, Xueyan Liu, Jian Xu, Peng Lin. (2021). Investigating the role of swelling-degradation degree of crumb rubber on CR/SBS modified porous asphalt binder and mixture. Construction and Building Materials. 300, 124048.

5. Shisong Ren, Xueyan Liu, Peng Lin, Haopeng Wang, Weiyu Fan, Sandra Erkens. (2021). The continuous swelling-degradation behaviors and chemo-rheological properties of waste crumb rubber modified bitumen considering the effect of rubber size. Construction and Building Materials. 307, 124966.

6. Shisong Ren, Xueyan Liu, Haopeng Wang, Weiyu Fan, Sandra Erkens. (2020). Evaluation of rheological behaviors and anti-aging properties of recycled asphalts using low-viscosity asphalt and polymers. Journal of Cleaner Production. 253, 120048.

7. Shisong Ren, Xueyan Liu, Mingliang Li, Weiyu Fan, Jian Xu, Sandra Erkens. (2020). Experimental characterization of viscoelastic behaviors, microstructure and thermal stability of CR/SBS modified asphalt with TOR. Construction and Building Materials. 261, 120524.

8. Shisong Ren, Xueyan Liu, Weiyu Fan, Chengduo Qian, Guozhi Nan, Sandra Erkens. (2020). Investigating the effects of waste oil and styrene-butadiene rubber on restoring and improving the viscoelastic, compatibility, and aging properties of aged asphalt. Construction and Building Materials. 121338.

9. Shisong Ren, Xueyan Liu, Weiyu Fan, Haopeng Wang and Sandra Erkens. (2019). Rheological Properties, Compatibility, and Storage Stability of SBS Latex-Modified Asphalt. Materials. 12, 3683.

10. Yi Zhang, Chundi Si, Taotao Fan, Yuefeng Zhu, Song Li, **Shisong Ren***, Peng Lin. (2023). Research on the optimal dosage of bio-oil/lignin composite modified asphalt based on rheological and anti-aging properties. Construction and Building Materials. 389, 131796.

11. Peng Lin, Xueyan Liu, **Shisong Ren***, Jian Xu, Yi Li, Mingliang Li. (2023). Effect of bitumen thickness on the aging behavior of high-content polymer-modified asphalt mixture. Polymers. 15, 2325.

12. Peng Lin, Xueyan Liu, **Shisong Ren***, Yi Li, Jian Xu, Mingliang Li. (2023). Unraveling the influence of fibers on aging susceptibility and performance of high

content polymer modified porous asphalt mixtures. Case Studies in Construction Materials. 18, e02211.

13. Haopeng Zhang, **Shisong Ren**[*], Yanjun Qiu. (2023). Balancing the sustainable component of ethylene-vinyl acetate for achieved better compatibility improvement of wax-based warm mix additives in bitumen. Colloids and Surfaces A: Physicochemical and Engineering Aspects. 2023, 675, 132054.

14. Mingliang Li, **Shisong Ren**[*], Xueyan Liu, Haopeng Zhang, Weiyu Fan, Jian Xu. (2022). Characterizing the rheological properties, compatibility and aging resistance of rejuvenated bitumen with different compound rejuvenators. Materials. 15, 5458.

15. Yi Zhang, Xueyan Liu, **Shisong Ren**[*], Ruxin Jing, Peng Lin, Panos Apostolidis, Sandra Erkens, Natascha Poeran, Tom Scarpas. (2021). Effect of bio-oil on rheology and chemistry of organosolv lignin modified bitumen. Journal of Materials in Civil Engineering. DOI: 10.1061/(ASCE)MT.1943-5533.0004140

III. Conference Proceedings and Presentations

1. Shisong Ren, Xueyan Liu, Peng Lin, Sandra Erkens. Use of waste oil/styrene-butadiene-rubber blends as rejuvenators for aged bitumen. The 6th Chinese European Workshop on Functional Pavement Design, Nanjing, China, 2020.

2. Shisong Ren, Xueyan Liu, Peng Lin, Sandra Erkens. The influence of long-term aging on the chemical properties of bitumen. The 5th International Symposium on Frontiers of Road and Airport Engineering (iFRAE), Delft, The Netherlands, 2021.

3. Shisong Ren, Xueyan Liu, Peng Lin, Ruxin Jing, Sandra Erkens. Towards a novel consecutive model for the long-term aging reaction kinetics of bitumen. The 101th TRB Annual Meeting, 2022. Poster presentation.

4. Shisong Ren, Xueyan Liu, Sandra Erkens. Insight into the compatibility behaviors between various rejuvenators and aged bitumen: Molecular dynamics simulation and experimental validation. The 59th Petersen Asphalt Research Conference. 2022. Presentation.

5. Shisong Ren, Xueyan Liu, Yangming Gao, Sandra Erkens, Peng Lin. Insights into the diffusion performance of rejuvenators in aged bitumen with molecular dynamics simulation. The 3rd Advances in Materials and Pavement Performance Prediction (AM3P). Hong Kong, 2023.